

Studies in Rhythm Engineering

Anirban Bandyopadhyay
Kanad Ray
Editors

Rhythmic Oscillations in Proteins to Human Cognition



Springer

Studies in Rhythm Engineering

Series Editors

Anirban Bandyopadhyay, Senior Researcher, ANCC, National Institute for Materials Science, Tsukuba, Ibaraki, Japan

Kanad Ray, Amity School of Applied Sciences, Amity University Rajasthan, Jaipur, Rajasthan, India

Chi-Sang Poon, Department of Health Sciences and Technology, Massachusetts Institute of Technology, Cambridge, MA, USA

This is a multi-disciplinary book series, ranging from astrophysics to biology, chemistry, mathematics, geophysics and materials science. Its primary scope is the fundamental science and associated engineering wherever cyclic and rhythmic oscillations are observed.

Time neither being an entity nor a process is unmeasurable and undefined, although a clock only measures the passage of time. The clock drove recurring processes are observed in the biological rhythms, astrophysical and geophysical environments. Always, the clocks are nested, arranged in a geometric shape to govern a phenomenon in nature. These clocks are made of atoms, molecules, their circuits, and complex networks. From biology to astrophysics, the clocks have enriched the science and engineering and the series would act as a catalyst and capture the forthcoming revolution of time cycles expected to unfold in the 21st Century. From the cyclic universe to the time crystal, the book series makes a journey through time to explore the path that time follows.

The series publishes monographs and edited volumes.

More information about this series at <http://www.springer.com/series/16136>

Anirban Bandyopadhyay · Kanad Ray
Editors

Rhythmic Oscillations in Proteins to Human Cognition



Springer

Editors

Anirban Bandyopadhyay
National Institute for Materials Science
Tsukuba, Ibaraki, Japan

Kanad Ray
Amity University Rajasthan
Jaipur, Rajasthan, India

ISSN 2524-5546

Studies in Rhythm Engineering
ISBN 978-981-15-7252-4
<https://doi.org/10.1007/978-981-15-7253-1>

ISSN 2524-5554 (electronic)

ISBN 978-981-15-7253-1 (eBook)

© The Editor(s) (if applicable) and The Author(s), under exclusive license to Springer Nature Singapore Pte Ltd. 2021

This work is subject to copyright. All rights are solely and exclusively licensed by the Publisher, whether the whole or part of the material is concerned, specifically the rights of translation, reprinting, reuse of illustrations, recitation, broadcasting, reproduction on microfilms or in any other physical way, and transmission or information storage and retrieval, electronic adaptation, computer software, or by similar or dissimilar methodology now known or hereafter developed.

The use of general descriptive names, registered names, trademarks, service marks, etc. in this publication does not imply, even in the absence of a specific statement, that such names are exempt from the relevant protective laws and regulations and therefore free for general use.

The publisher, the authors and the editors are safe to assume that the advice and information in this book are believed to be true and accurate at the date of publication. Neither the publisher nor the authors or the editors give a warranty, expressed or implied, with respect to the material contained herein or for any errors or omissions that may have been made. The publisher remains neutral with regard to jurisdictional claims in published maps and institutional affiliations.

This Springer imprint is published by the registered company Springer Nature Singapore Pte Ltd. The registered company address is: 152 Beach Road, #21-01/04 Gateway East, Singapore 189721, Singapore

Preface

On the eve of our first book in the series of Studies in Rhythm Engineering, SRE by Springer Nature, we would like to convey the readers that we are open to all topics, wherever, periodic events are there. Our objective is to explore and document fundamental research carried out globally from astrophysics to particle physics, from stock market to economic theories, and from plant biology to consciousness—we do not want to leave any stone unturned. In many years to come, the book series would answer a fundamental query to this universe, “Are all events in the universe, periodic, random and linear events are illusion, due to poor understanding of the phenomena?”

The current book emphasizes biophysics and biochemistry. Soon we would release its second part, since it was not possible to compile all chapters in one book. We have rigorously edited, and all authors have worked extremely hard to complete the theme in meticulous details. Readers would find a pattern in selecting the topics, a periodic feature. Let us briefly explain how eight writers have envisioned periodicity in their distinct domains of works.

Chapter 1 is written by Irena Cosic and Drasko Cosic on the protein vibrations. Irena has been developing mechanisms to build a proper theoretical model that could explain how protein vibrates to deliver key life functions. Protein is the key device for life forms.

Chapter 2 is written by Enrico Prati. There exists a scientific view that space exists and time is secondary. Based on that view, Enrico is reviewing the argument if the time or periodicity that we see is an illusion. It is a nice contrary addition to the concept explored here.

Chapter 3 is written by Danko D. Georgiev. Brain’s cognition is a rhythmic process. Membrane firing is time tuned for human thoughts. What could be its origin? Deep inside neuron, there could be rhythms in the filaments, regulating the membrane above. Danko details the theory.

Chapter 4 is written by Pathik Sahoo and Subrata Ghosh. They have carried out an extensive search whether if chemical clocks are nested to regulate life. Current biology is all about highly interconnected chemical reactions. It is a new outlook to resolve rhythmic pathways.

Chapter 5 is written by Correna et al on the visual cognitive system. This chapter addresses a fundamental feature of cognition, bio-inspired visual devices, and associated technologies. Human cognition could be achieved via bionic eyes connected to higher-level intelligent devices.

Chapter 6 is written by M. V. Altaisky and N. E. Kaputkina on quantum neural network. Quantum properties are those features that add new information to the classical understanding of a phenomenon. A neuron being a classical device could harness quantum technologies. Authors have built a rigorous and robust theory for that.

Chapter 7 is written by Iain Pinder and Jonathan J. Crofts. They have addressed synchronization of periodic oscillations and clocks in a neural network. Human brain is intelligent because neurons edit time gap between spikes extremely precisely. Origin of that technology is explored here.

Chapter 8 is written by Dirk K. F. Meijer et al. He has proposed a new way of looking into the proposition of quantum consciousness. Normally, we try to add additional properties in a classical neural network property to proclaim quantum features in the brain. However, Meijer proposes that thoughts and consciousness emerge from quantum superfluids, where all information is poured in. A fantastic journey to end the book.

We hope eight completely different topics, all related to different distinct perspectives of biophysics and biochemistry would trigger a new generation of debates.

Jaipur, India
Tsukuba, Japan

Kanad Ray
Anirban Bandyopadhyay

Contents

1 Macromolecular Resonances	1
Irena Cosic and Drasko Cosic	
2 Reformulating Physics Without Time	37
Enrico Prati	
3 Electric and Magnetic Fields Inside Neurons and Their Impact upon the Cytoskeletal Microtubules	51
Danko D. Georgiev	
4 Time Crystal Engineering in Catalytic Reaction Cycles	103
Pathik Sahoo and Subrata Ghosh	
5 Blue Light Spectroscopy from Electronic Visual Displays	135
N. Correa, E. Spezzia, R. Doti, J. Faubert, and J. E. Lugo	
6 Quantum Neural Networks and Quantum Intelligence	165
M. V. Altaisky and N. E. Kaputkina	
7 Oscillations and Synchrony in a Network of Delayed Neural Masses	187
Iain Pinder and Jonathan J. Crofts	
8 Biophysics of Consciousness: A Scale-Invariant Acoustic Information Code of a Superfluid Quantum Space Guides the Mental Attribute of the Universe	213
Dirk K. F. Meijer, Igor Jerman, Alexey V. Melkikh, and Valeriy I. Sbitnev	

About the Editors

Dr. Anirban Bandyopadhyay is a Senior Scientist at the National Institute for Materials Science (NIMS), Tsukuba, Japan. He completed his Ph.D. in Supramolecular Electronics at the Indian Association for the Cultivation of Science (IACS), Kolkata, 2005. From 2005 to 2008, he was an independent Researcher, as an ICYS Research Fellow at the International Center for Young Scientists (ICYS), NIMS, Japan, where he worked on the brain-like bio-processor building. In 2008, he joined as a Permanent Scientist at NIMS, working on the cavity resonator model of human brain and design synthesis of brain-like organic jelly. From 2013 to 2014, he was a Visiting Scientist at the Massachusetts Institute of Technology (MIT), USA. He has received several honors, such as the Hitachi Science and Technology Award 2010, Inamori Foundation Award 2011–2012, Kurata Foundation Award, Inamori Foundation Fellow (2011–), and Sewa Society international member, Japan. He has patented ten inventions (i) a time crystal model for building an artificial human brain, (ii) geometric-musical language to operate a fractal tape to replace the Turing tape, (iii) fourth circuit element that is not memristor, (iii) cancer & alzheimers drug, (iv) nano-submarine as a working factory & nano-surgeon, (vi) fractal condensation-based synthesis, (vii) a thermal noise harvesting chip, (viii) a new generation of molecular rotor, (ix) spontaneous self-programmable synthesis (programmable matter), and (x) fractal grid scanner for dielectric imaging. He has also designed and built multiple machines and technologies, (i) THz-magnetic nano-sensor (ii) a new class of fusion resonator antenna, etc. Currently, he is building time crystal-based artificial brain using three ways, (i) knots of darkness made of fourth circuit element, (ii) integrated circuit design, and (iii) organic supramolecular structure.

Dr. Kanad Ray is a Professor and Head of the Department of Physics at the Amity School of Applied Sciences Physics Amity University Rajasthan (AUR), Jaipur, India. He has obtained M.Sc. and Ph.D. degrees in Physics from Calcutta University and Jadavpur University, West Bengal, India. In an academic career spanning over 22 years, he has published and presented research papers in several national and international journals and conferences in India and abroad. He has

authored a book on the Electromagnetic Field Theory. Professor Ray's current research areas of interest include cognition, communication, electromagnetic field theory, antenna & wave propagation, microwave, computational biology, and applied physics. He has served as Editor of Springer Book Series such as AISC and LNEE and an Associated Editor of Journal of Integrative Neuroscience published by IOS Press, Netherlands. He has established an MOU between his University and University of Montreal, Canada, for various joint research activities. He has also established MOU with National Institute for Materials Science (NIMS), Japan, for joint research activities and visits NIMS as a Visiting Scientist. He had been Visiting Professor to Universiti Teknologi Malaysia (UTM) and Universiti Teknikal Malaysia Melaka (UTeM), Malaysia. He had organized international conference series such as SoCTA, and ICOEVCI as General Chair. He is a senior member of IEEE and an Executive Committee member of IEEE Rajasthan. He has visited Netherlands, Turkey, China, Czechoslovakia, Russia, Portugal, Finland, Belgium, South Africa, Japan, Malaysia, Thailand, Singapore, etc., for various academic missions.

Chapter 1

Macromolecular Resonances



Irena Cosic and Drasko Cosic

1 Introduction

Constant changes are everywhere in the nature. Majority of them are rhythmic, meaning regular recurrence or pattern in time that can apply to wide variety of cyclical natural phenomena having periodicity or frequency of anything from fraction of seconds to several minutes, even hours or at most extreme over many years. Besides natural rhythms, there are also man made rhythms, where the music is the well-known example. Rhythms also play crucial role in biology including: circadian rhythm (daily physiological changes), heart activity within the frequency range of 0.5 Hz, brain activity within the frequency range of 1–100 Hz, muscular activity about 100 Hz and resonances within cellular and molecular elements ranging from MHz to THz, where biological damage occurs at frequencies higher than PHz. Here, we concentrate on rhythms and resonances within biological macromolecules, particularly those resonances relevant to macromolecular biological functions.

Over last few decades, we have discovered that crucial driving force for macromolecules (protein, DNA and RNA) activation and interaction is resonant electromagnetic energy transfer at specific frequency unique for specific activation and interaction. Based on this finding, we have developed Resonant Recognition Model (RRM) [3, 4], which is able to calculate these frequencies from periodicities within the distribution of energy of delocalised electrons along protein, DNA and/or RNA molecules using charge velocity through these macromolecules. We have applied this concept on number of proteins, DNA and/or RNA examples [1, 3–5], as well as

I. Cosic (✉) · D. Cosic
AMALNA Consulting, Black Rock, Melbourne, VIC 3193, Australia
e-mail: icosic@amalnaconsulting.com

I. Cosic
College of Science, Engineering and Health, RMIT University, Melbourne, VIC 3000, Australia

on some medical conditions like: Crigler–Najjar syndrome [6], pain [7] and influence of environmental light to health [8]. This concept has been also experimentally tested by predicting the electromagnetic frequencies for activation of l-lactate dehydrogenase [9] and has been tested independently on experimental measurements of photon emission from dying melanoma cells [10], on photon emission from lethal and non-lethal Ebola strains [11], as well as on differentiation of osteoblasts stem cells [12].

These findings could be used, not only to understand biological processes and resonances in biomolecules, but also to influence these processes using either radiation or design of related molecules and conductive particles. Thus, the RRM model is promising tool for design and development of new techniques in pharmacology, drug design, biotechnology, medicine and even electronics.

2 Resonant Recognition Model (RRM)

Proteins and DNA/RNA are the main macromolecules in any living organism that are crucial for control and execution of majority biological processes within any living organism. Proteins are the main work forces, while DNA keeps all information about any biological organism and transfers this information through RNA to proteins. The Resonant Recognition Model (RRM) represents whole new view to biomolecular interactions, in particular protein–protein and protein–DNA interactions [3, 4].

The RRM is based on the finding that certain periodicities (frequencies) within distribution of energies of delocalised electrons along a protein molecule are critical for protein biological function and/or interaction with its target. The RRM enables these frequency characteristics to be calculated. These findings can be applied to the:

- (a) Definition of protein or DNA functions;
- (b) Definition of protein or DNA targets and analysis of their mutual recognition;
- (c) Prediction of amino acids in the protein or nucleotides in the DNA which are mostly important for the function of the macromolecule;
- (d) Prediction of functionally relevant mutations in proteins and/or DNA;
- (e) Design of a completely new peptides or DNA fragments with desired spectral characteristics and consequently corresponding biological activities been designed.

All these RRM applications have been experimentally tested on number of examples including de novo design of Fibroblast Growth Factor (FGF) analogues [13], Human Immunodeficiency Virus (HIV) envelope mimicking peptides [14–16], and Myxoma virus analogues [17, 18].

2.1 *Resonances in Proteins and DNA/RNA as Calculated by RRM Model*

All proteins and DNA/RNA can be considered as linear sequence of their constitutive elements, i.e. amino acids or nucleotides and their biological function is determined primarily by the linear sequence of their constitutive elements. The Resonant Recognition Model (RRM) interprets this linear information by transforming macromolecular sequence into a numerical series and then into the frequency domain using digital signal processing methods, the Fourier transform.

In the RRM model, the protein primary structure is presented as numerical series by assigning a physical parameter value relevant to the protein's biological activity to each amino acid. Although a number of amino acid indices have been found to correlate in some ways with the biological activity of the whole protein, our investigations have shown that the best correlation can be achieved with parameters which are related to the energy of delocalised electrons of each amino acid [19, 20]. These findings can be explained by the fact that the electrons delocalised from the particular amino acid have the strongest impact on the electronic distribution of the whole protein. Within the RRM, the energy of delocalised electrons is calculated as the electron–ion interaction pseudopotential (EIIP) of each amino acid residue using the following semiempirical formula as developed by Veljkovic [21, 22]:

$$\langle k + q | w | k \rangle = 0.25Z \sin(\pi 1.04Z)/2\pi \quad (\text{v})$$

where q is change of momentum of delocalised electron in the interaction with potential w , while Z is average valence number over the whole amino acid residue. The resulting numerical series represents the distribution of the free electron energies along the protein molecule.

At the second stage, the numerical series are analysed by digital signal analysis methods, using Fourier transform, in order to extract information pertinent to the biological function. The average distance between amino acid residues in a polypeptide chain is about 3.8 Å and it can be assumed that the points in the numerical sequence derived are equidistant. For further numerical analysis, the distance between points in these numerical sequences is set at an arbitrary value $d = 1$. Therefore, the maximum frequency in the spectrum is $F = 1/2d = 0.5$. The total number of points in the sequence influences the resolution of the spectrum only. Therefore, for N -point sequence, the resolution in the spectrum is equal to $1/N$. The n -th point in the spectral function corresponds to the frequency $f = n/N$.

In order to extract common spectral characteristics of sequences having the same or similar biological function, the cross-spectral function is used. Peak frequencies in the amplitude cross-spectral function define common frequency components of the two sequences analysed. To determine the common frequency components for a group of protein sequences, we have calculated the absolute values of multiple cross-spectral function coefficients for the whole group.

Peak frequencies in such multiple cross-spectral function present common frequency components for all sequences analysed. Signal-to-noise ratio S/N for each peak is defined as a measure of similarity between sequences analysed. The S/N is calculated as the ratio between the signal intensity at the peak frequency and the mean value over the whole spectrum. Previous research results have shown that the value of S/N ratio of at least 20 can be considered as significant [3, 4]. The multiple cross-spectral function of large group of sequences with the same biological function is called “consensus spectrum”. The presence of a peak frequency with the significant signal-to-noise ratio in a consensus spectrum implies that all the analysed sequences within the group have one frequency component in common. This frequency is related to the biological function provided the following criteria are met:

- (a) one peak only exists for a group of protein sequences sharing the same biological function
- (b) no significant peak exists for biologically unrelated protein sequences
- (c) peak frequencies are different for different biological functions.

Above criteria have been implemented throughout the sequence databases [3, 4] and the following fundamental conclusion was drawn:

Each specific biological function within protein or DNA is characterised by one frequency.

The comprehensive analysis done so far confirms that all protein sequences with the common biological function have common frequency component, which is specific feature for the observed function/interaction [1, 3–8, 23–25]. In order to understand the meaning of the characteristic frequency, it is important to clarify what is meant by the biological function of proteins. Each biological process is driven by proteins that selectively interact with other proteins, DNA regulatory segment or small molecules. These interactive processes that involve energy transfer between the interacting molecules are highly selective. How is this selectivity achieved? In the RRM, it is assumed that the selectivity is defined within the amino acid sequence. It has been shown that proteins and their targets share the same characteristic frequency [3, 4, 23, 24], as presented in case of leptin–leptin receptor interaction in Fig. 1. However, there is opposite phase (phase difference close to 3.14 rad) at this characteristic frequency for each pair of interacting macromolecules, as presented in case of leptin–leptin receptor interaction in Fig. 2.

Having all above in mind, we conclude that RRM characteristic frequencies represent proteins’ general functions, as well as mutual recognition between protein and its target (receptor, ligand, etc.). These results from matching of periodicities within the distribution of energies of free electrons along the interacting proteins, can be regarded as the resonant recognition. Therefore, it has been proposed that interacting molecules “communicate” with each other, i.e. recognise each other at the distance, based on the same/similar characteristic frequency. Thus, these frequencies must represent oscillations of some physical field which can transmit through water dipoles. One of the possibilities is that this field is electromagnetic in nature [1, 3–5].

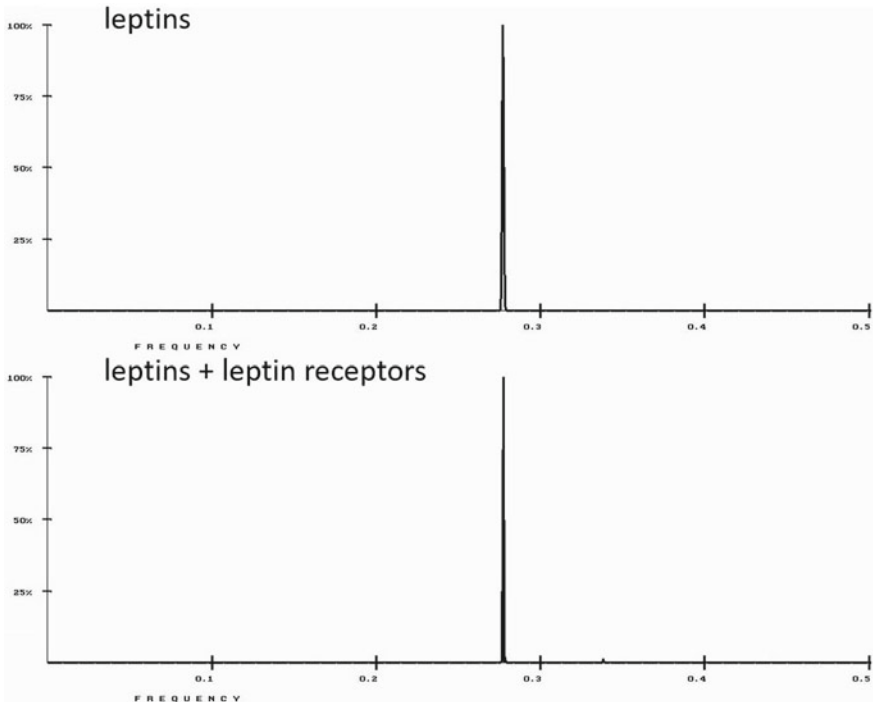


Fig. 1 Cross-spectrum of leptins and leptin-leptin receptors identifying the common characteristic RRM frequency of 0.2764 [24]

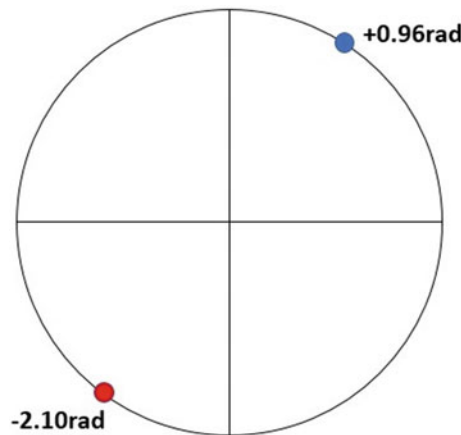


Fig. 2 Phase circles at RRM frequency of 0.2764 for human leptin protein (+0.96 rad) in blue and human leptin receptor protein (-2.10 rad) in red. It can be easily observed that these phases are opposite to each other, supporting the RRM approach that protein and protein receptors should have opposite phases at RRM frequency characterising their recognition and interaction. Phases at leptin-leptin receptor characteristic RRM frequency approximately opposite with phase difference of 3.06 rad [24]

2.2 Electromagnetic RRM Resonances Relevant to Biomolecular Biological Functions

The RRM proposes that protein and DNA/RNA activations and interactions entail mechanism of resonant energy transfer between involved macromolecules at the frequency specific for each observed function/interaction [3, 4]. This proposal is based on the findings that certain periodicities within the distribution of energy of delocalized electrons along protein molecule are critical for protein biological function and/or interaction with their targets [3, 4]. If charge transfer through these macromolecules is introduced, then charge moving through macromolecular backbone can produce electromagnetic radiation, absorption and resonance with spectral characteristics corresponding to the energy distribution [3, 4].

Since there is evidence that proteins and DNA have certain conducting or semi-conducting properties, charge moving through the macromolecular backbone and passing different energy stages, caused by different amino acid or nucleotide side groups, can produce sufficient conditions for a specific electromagnetic radiation or absorption. The frequency ranges of this field depend on the charge velocity. The charge velocity through protein backbone could be estimated from potential difference between COOH and NH₂ ends of protein. According to the EIIP pseudopotential theory [21, 22], this potential energy difference is:

$$W = W(\text{COOH}) - W(\text{NH}_2) = 0.13 \text{ Ry}$$

This energy difference allows for maximum velocity of charge, which is equal to:

$$V_{\max} = \sqrt{(2eW/m)}$$

where e represents the electron charge and m represents the electron mass. Therefore:

$$V < 7.87 \times 10^5 \text{ m/s}$$

Thus, the RRM proposes that the charge is travelling through the macromolecular backbone at the estimated velocity $V = 7.87 \times 10^5 \text{ m/s}$ [1, 3, 4]. For this velocity and with the distance between amino acids along the protein backbone $d = 3.8 \text{ \AA}$, the maximum frequency that could be emitted during this electron transfer is $F_{\max} = V/(2d) \approx 10^{15} \text{ Hz}$, while the minimum frequency that could be emitted depends on the length of the protein $F_{\min} = 2F_{\max}/N$, where N is the total number of amino acids within the protein. For example, for protein of 200 amino acids in length, the minimum frequency is $F_{\min} \approx 10^{13} \text{ Hz}$. Thus, the frequency range of protein interactions was estimated to be in the range between 10^{13} Hz and 10^{15} Hz [1, 3, 4], including far infra-red, infra-red and visible up to ultra-violet light spectrum. To support this idea, we compared our computational predictions with number of published experimental results [3, 4]:

- Laser light growth promotion of cells, by using the particular frequencies of light to produce the similar effect to that of growth factor proteins;
 - Chymotrypsin activation (increase of enzyme activity) achieved by laser light radiation in a range of 850–860 nm;
 - Activation of highly homologous plant photoreceptors which, although being very homologous, absorb different wavelengths of light;
 - Photoactivated proteins, e.g. rhodopsin, flavodoxin, etc.

These comparisons have shown a strong linear correlation between frequencies, as calculated using the RRM method and experimentally measured characteristic frequencies, with the slope factor of $K = 201$ [3, 4]. This finding parallels with the frequency range previously associated with the RRM numerical frequency spectrum that has been calculated from the charge velocities through the protein backbone. This correlation can be represented as following:

$$\lambda = K/f_{\text{rrm}}$$

where λ is the wavelength of light irradiation in nm, which can influence a particular biological process, f_{rrm} is RRM numerical frequency and K is coefficient of this linear correlation.

We applied this concept on number of proteins and DNA-selective interactions, biological processes and pathways in living cells. In our previous work, we calculated large number of specific frequencies for different protein and DNA biological functions and interactions [1, 3–5, 8, 24, 25], as presented in Fig. 3. In addition, although biological processes are currently looked as large number of different events, we have shown that they are grouped in relatively small number of general functions (functional super families) enabling the simpler approach to understanding macro-molecular interactions, biological functions and related health effects [8, 24, 25]. Functional super families are differently coloured and labelled in Fig. 3.

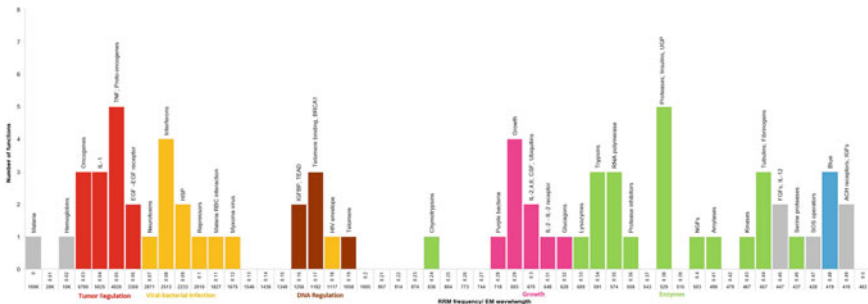


Fig. 3 Number of functional groups within each Resonant Recognition Model (RRM) frequency range of 0.01. X-axis represents RRM frequency in steps of 0.01, as well as corresponding electromagnetic frequency in nm. Y-axis represents the number of functional groups. Names of functional groups are written on the top of each bar. Functional super families are differently coloured and labelled below the X-axis

The RRM concept, proposing that specific frequencies of electromagnetic radiation are critical for macromolecular activities and interactions, has been experimentally tested on electromagnetic frequencies activating l-lactate dehydrogenase [9], photon emission from dying melanoma cells [10], photon emission from lethal and non-lethal Ebola strains [11], JAK-STAT signalling pathway [26], as well as more recently on osteoblastic differentiation of stem cells by photobiomodulation [12]. Even more, the RRM model, for the first time, explains how and why external blue light can be used in treatment of Crigler–Najjar syndrome [6]. This means that, by radiating the whole body with specific RRM frequency, the desired health and medical effects can be achieved.

Keeping all this in mind, we propose that the RRM concept is excellent predictor for proteins and DNA/RNA selective interactions, biological processes and pathways in living cells.

2.3 Electromagnetic RRM Resonances Relevant in Electronics

So far, we have presented above the possibility of electromagnetic resonances within protein, DNA and/or RNA relevant for their biological functions. These resonances are based on charge velocity through macromolecular backbone of $V = 7.87 \times 10^5$ m/s [3, 4] and consequently producing electromagnetic radiation within range of far infra-red, infra-red and visible up to ultra-violet light spectrum. However, there are additional possible electromagnetic resonances in proteins that can be related, not only to their biological function, but also to some other properties of proteins, which can be important for some technological applications. Such resonances could be within different frequency ranges of electromagnetic radiation based on different charge velocity, but with the same distribution of free electron energies along the protein. We have examined these possibilities on example of tubulin [1].

Tubulin and microtubules have been extensively researched in two directions. One direction is towards an idea that these macromolecules are essential element of brain cells processing information as proposed by Hameroff [27]. He proposes that microtubules quantum states of decoherence are essential element for neuro-physiological effects. However, there is no agreement on velocity and frequency of this decoherence in regard to velocity of neurological effects. While Tegmark proposes that these processes are in order of decoherence time of 10^{-13} s [28], Hameroff argues that these processes are much slower [27].

Consequently, there has been a proposal that “microtubules can act as macromolecular computer with phonon-coupled tubulin dipole states functioning as bits interacting/computing with neighbouring tubulin bit states in microtubule (cellular) bit automata” [29]. For this purpose, it is important to investigate resonances in tubulin [30].

The second direction of research is towards the understanding tubulin biological function in cells other than the brain cells and in particular tubulin's possible role in cell division in relation to division of cancer cells. Interest in tubulin structure and function increased when taxol, which binds to microtubules, was found to be effective treatment for a number of cancers. By binding to microtubules and causing them to become more stable, taxol prevents cell division and thus blocks cancer growth [31].

To analyse all possible resonances for both directions of tubulin research, we have applied the RRM model for different possible velocities of charge transfer along protein. As described above, the RRM method is based on the finding that certain periodicities (frequencies) within distribution of energies of delocalized electrons along protein molecule are critical for protein biological function and/or interaction with its target [3, 4]. If protein conductivity was introduced, then charge moving through protein backbone can produce electromagnetic irradiation or absorption with spectral characteristics corresponding to energy distribution along the protein. The RRM method enables these spectral characteristics to be calculated. These frequencies depend on charge velocity. Initially, charge velocity was considered to travel only through the protein backbone when the frequencies were found to be in the range from far infra-red, infra-red and visible up to ultra-violet light spectrum [1, 3–5, 8, 12]. When different charge movement modalities (velocities) were applied to the whole protein 3D structure (not backbone only), other possible resonant frequency ranges were identified [1]. We applied the charge velocity in the forms of solitons, excitons and phonons, which may travelled through the 3D structure of proteins, in particular through the alpha helix. In these instances, protein resonant frequencies have much wider spectrum, ranging from KHz to THz [1]. This enabled completely new view to protein resonances that could be particularly relevant to tubulin activity as quantum information communication system (macromolecular computer).

As shown above, the RRM characteristic frequencies calculated from protein sequence can be related to their electromagnetic frequencies if there is charge travelling along the protein sequence. Initially, we proposed that charge (most probably electrons) is travelling through protein backbone with the velocity of 7.87×10^5 m/s. For this velocity and the distance between amino acids in a protein molecule, which is 3.8 Å, the frequency range obtained for protein interactions was estimated to be in the range between 10^{13} and 10^{15} Hz.

However, if we take into account the complex structure of proteins and in particular, alpha helices, the charge transfer is also possible to occur through these 3D structures, different charge transfer modalities can be applied, and the range of possible resonant frequencies can be extended. We considered the following charge transfer modalities: solitons (Davydov [32, 33], Hayman [34], Sinkala [35]), excitons (Davydov [32, 33], Sinkala [35], Pang [36], Yomosa [37]) and phonons (Pang [36], Yomosa [37], Ichinose [38]). These other forms of charge transfers are at different velocities ranging from 10^5 m/s for solitons and some excitons to the speed of sound and small fractions of speed of sound for phonons. Therefore, with the same numerical characteristic frequencies calculated using the RRM method, different modalities of charge transfer can produce different resonant electromagnetic frequencies, which

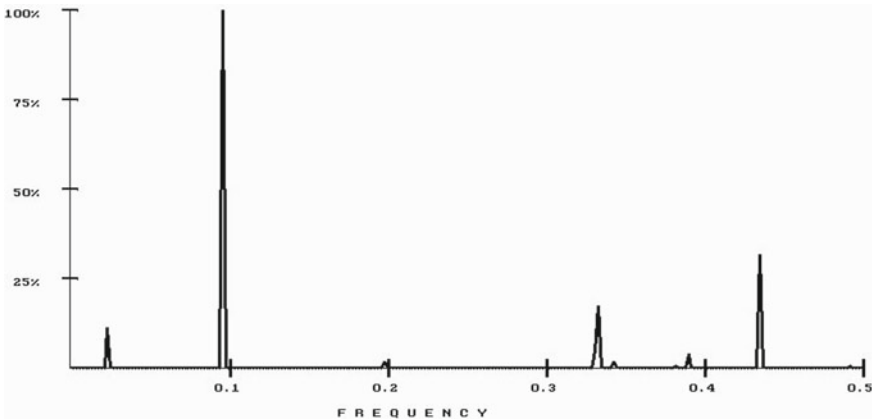


Fig. 4 Cross-spectrum for mammalian tubulin alpha and beta chains together calculated using the RRM method [1]

are not necessarily related to the protein biological function but could be related to protein resonances in general. When numerical cross-spectra RRM calculations have been applied to alpha and beta tubulins, the main common frequency was found to be at 0.0957, as presented in Fig. 4 [1].

This frequency of 0.0957 represents the characteristic periodicity in distribution of energies of free electrons along protein for all analysed tubulins. With the same periodicity of energy distribution, but different velocities due to different modalities of charge transfer, the different resonant frequencies have been obtained as presented in Table 1.

These results have shown that possible resonant frequencies in tubulin molecules can be within different frequency ranges (THz, GHz, MHz and even KHz) depending on mechanism and charge velocity within the protein structure.

These results have been viewed in the light of the theory proposed by Hameroff and Tuszynski et al. [39–41] where they compare coherent energy transfer between aromatic rings in tubulin and microtubules to quantum conductance through photosynthesis. Such process is explained by mechanical vibration in microtubules. Microtubules appear to have their own set of mechanical vibrations as proposed by Anirban Bandyopadhyay [42, 43] which are called “Bandyopadhyay coherence—BC”. Bandyopadhyay is suggesting that quantum effects occurred in microtubules as electronic conductance along microtubules became extremely high, close to quantum conductance, at certain specific resonant frequencies. These resonances are consistent with the intra-tubulin aromatic ring pathways in THz ranges, as well as quantum effects proposed by Bandyopadhyay which occur in GHz, MHz and KHz ranges and are particularly prominent in low MHz range (e.g. 8.9 MHz) [42, 43]. When compared with our results [1], these mechanical vibrations could be particularly related to phonon velocities as proposed by Ichinose [38]. In addition, Bandyopadhyay suggested that there is the whole range of resonances in a single microtubule

Table 1 Different resonant frequencies for different charge transfer modalities [1]

RRM frequency	Velocity RRM 7.78×10^5 m/s	Velocity Yomosa 3.2 m/s	Velocity Yomosa 1.2×10^5 m/s	Velocity Pang 68 m/s	Velocity Davydov 170 m/s	Velocity Ichinose 0.34 m/s	Velocity Ichinose 5×10^{-4} m/s
0.0957	97-101 THz	392-411 MHz	14-16 THz	8-9 GHz	21-22 GHz	40-42 MHz	60-62 KHz

from 1 kHz to 1.3 GHz with the most prominent peaks at: (a) around 15 kHz, (b) within range of 9–30 MHz and (c) within range of 86–228 MHz [42]. These results are again comparable with our results for velocities of phonons [1], as proposed by Ichinose [38]. However, our results extend to much higher frequencies in GHz and THz ranges. This suggests that these higher frequencies, which are not related to phonon velocities, but are related to velocities of solitons and excitons, are not mechanical, but pure electromagnetic in nature.

3 RRM Bioresonances in Biology and Medicine

There is much evidence of existence of electromagnetic resonances within biological macromolecules, particularly proteins and DNA/RNA. The whole area of biophotonics is related to ultra-weak photon emission from biological systems [44], particularly within the range of UVA, visible and infra-red spectrum. In addition, there is also evidence of biomolecular resonances in much lower frequency ranges including KHz, MHz and GHz. However, so far there is no evidence or theory, how and if these macromolecular resonances are related to biological activity of macromolecules.

Here we present, the Resonant Recognition Model (RRM), which can explain that such emission, and particularly its specific frequencies, are critical for resonant activation of proteins and DNA/RNA. The RRM is based on the findings that certain periodicities within the distribution of energy of delocalized electrons along protein (DNA/RNA) molecule are critical for their biological function and/or interaction with their targets [3, 4, 23, 24]. If charge transfer through these macromolecules is introduced, then charge moving through macromolecular backbone can produce electromagnetic radiation, absorption and resonance with spectral characteristics corresponding to energy distribution. The frequency range of this radiation depends on charge velocity [3, 4]. We applied this concept on number of proteins and DNA/RNA examples, as well as on some medical conditions like: Crigler–Najjar syndrome [6], pain and influence of environmental light to health [8]. This concept has been also experimentally tested by predicting the electromagnetic frequencies for activation of l-lactate Dehydrogenase [9]. The concept has also been tested independently on experimental measurements of photon emission from dying melanoma cells [10], as well as on photon emission from lethal and non-lethal Ebola strains [11].

These findings could be used, not only to understand biological processes and resonances in biomolecules, but also to influence these processes using either radiation or design of related molecules. Thus, the RRM approach is promising tool for design and development of new techniques in pharmacology, drug design, biotechnology and medicine.

3.1 *Interactions Between Proteins and DNA/RNA*

The RRM is unique model that is capable to analyse directly activities and interactions of proteins, DNA and RNA by identifying their characteristic frequencies. One example is analysis of interaction between telomere (DNA), telomerase (protein) and telomerase binding region (RNA), all of which are involved in cellular ageing process. Biological ageing at the cellular level was always puzzling scientists. It is well known that any mature cell can divide only certain number of times before stop dividing and eventually die. The main part in this process is due to telomeres, which are made up of many kilo bases of DNA repeats (TTAGGG) at the end of each chromosome and, bound and protected by telomere binding protein [45, 46]. Each time when cell divides, the chromosomes of the new cell are shorter at the ends making telomeres shorter. When telomeres get too short, the cell can no longer divide, becomes inactive and dies. If there would not be telomeres at all, the main genetic information in chromosomes will become shorter with each cell division and the genetic information will be then lost and corrupted [45, 46].

In contrast to process of shortening telomeres, enzyme telomerase can add nucleotides to the end of telomeres. Telomerase is composed of reverse transcriptase (TERT) and an RNA component (TERC) that serves as template for telomere elongation [45, 46]. In somatic cells, there is not enough telomerase to keep telomeres from eventual wearing down producing cells ageing, inactivity and eventual death [45, 46]. In cancer cells, which divide much more often than normal cells, telomeres get very short. However, these cells very often produce telomerase enzyme which prevents telomeres to get too short and thus prevents cell from dying [45, 46].

By applying the RRM model, we have investigated interactions between participants in process of telomere shortening and/or elongation including telomeres, telomerase and telomere binding proteins [5, 47]. When human telomeres (DNA) from different human chromosomes were compared the common RRM characteristic frequency is at 0.1875 within wide spectrum range of 0.17–0.19, as presented in Fig. 5 top.

Interestingly when all participants in telomeres activity binding and elongation were compared, no matter if they are proteins, DNA or RNA as possible by the RRM model, the same common characteristic frequency was obtained at 0.1875 within wider spectrum range of 0.17–0.19, as presented in Fig. 5 bottom.

This result is significant showing that all participants in telomere related cellular ageing are having common RRM characteristic frequency. This result can be significant in further understanding of cellular ageing. In addition, this is excellent example demonstrating capability of RRM model to analyse and compare activities and interactions of proteins, DNA and RNA.

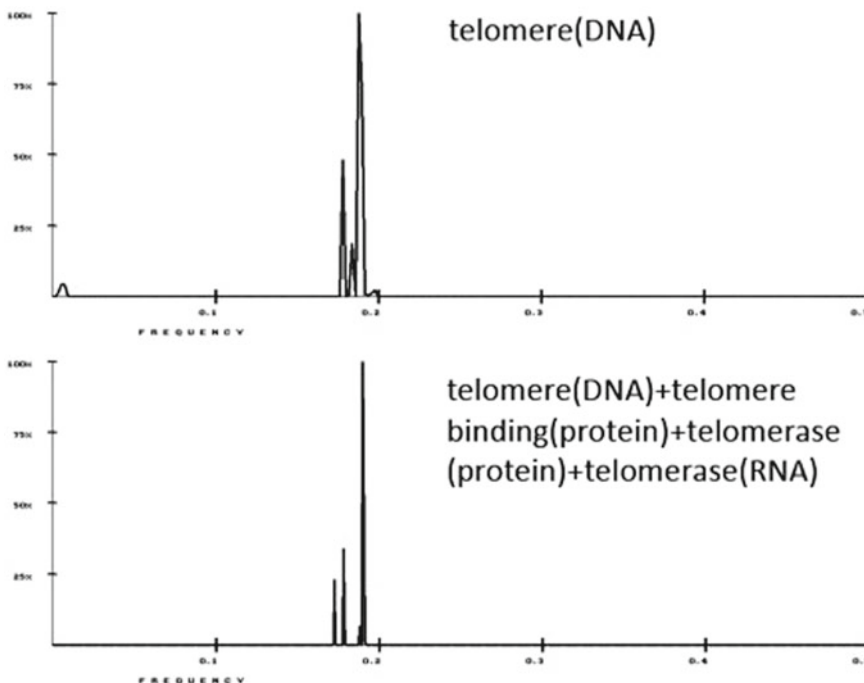


Fig. 5 Top: RRM cross-spectrum for human telomere (DNA); Bottom: RRM cross-spectrum for telomere (DNA), telomere binding protein (protein), telomerase (protein) and telomerase (RNA). The common RRM characteristic frequency for telomeres and telomere related macromolecules has been identified at 0.1875

3.2 Drug Design

There is large multi-billion biotechnology industry mostly developing new drugs for various diseases that are not yet successfully treated. These developments are usually based on testing of large number of compounds/molecules without complete understanding of their activity, specificity and side effects. As such tapping in the dark developments are time consuming, expensive and very often do not lead to desired results, there is need for better understanding of biomolecular activity and specificity. The most important group of biomolecules are proteins, which are the main biomolecular forces that are involved in controlling most biological processes in living cells, tissues and organisms. They exhibit their biological functions through selective interactions with other molecules, which could also be proteins and/or DNA. The most complex protein interactions are interactions between proteins and their receptors, which are proteins or complexes of proteins that selectively drive specific biological pathways. Currently, the selectivity of interactions between proteins and their receptors is investigated mostly using 3D matching between interacting proteins, which

is not explicit enough to explain the high specificity of these interactions. Experimentally, protein–receptor interactions are investigated by number of techniques including X-ray, MRI, spectroscopy, etc. However, all these techniques are very expensive and time consuming. Thus, there is need for biophysical approach that can investigate protein–receptor interactions with more specificity than 3D matching. The RRM model is capable to analyse activity and specificity of protein interactions by calculating characteristic frequency and phase for each specific biological interaction and activity. Once when we know that each biological function/interaction is characterised with RRM frequency and phase, we can use this parameter to analyse protein biological function, predict key amino acids (“hot spots”) for the particular function and even design de novo peptides/proteins with the desired biological function or interaction ability.

Knowing the characteristic frequency of a particular protein function creates the possibility to predict which amino acids prevail in the sequence and predominantly contribute to this frequency and consequently to the observed function. This could be achieved by small alternations of amplitude in single protein spectrum at characteristic frequency and then observing which amino acids are mostly sensitive to this alternation [3, 4, 23, 48–50]. These sensitive amino acids (“hot spots”) are related to characteristic frequency and consequently to the corresponding biological function. The “hot spots” predictions, using the RRM, have been applied already to a number of protein and DNA examples including interleukin-2, SV40 enhancer, epidermal growth factor EGF, Ha-ras p21 oncogene product, glucagons, haemoglobins, myoglobins and lysozymes [3, 4, 23, 48–50].

It has been experimentally documented at the example of influenza virus that such predicted amino acids denote residues crucial for protein function [51]. In addition, these “hot spots” amino acids are found to be spatially clustered in the protein tertiary structure and to be positioned in and around the protein active site [48–50].

Once the characteristic biological function of the protein is identified, it is possible to design new proteins with desired frequency components and consequently with desired biological functions [3, 4, 13–15, 52–55]. The process of bioactive peptides design is as follows:

1. Determination of RRM characteristic frequency using multiple cross-spectral function for a group of protein sequences that share common biological function (interaction);
2. Determination of phases for the characteristic frequencies of a particular protein which is selected as the parent for agonist/antagonist peptide;
3. Calculation using inverse Fourier transform of the signal with characteristic frequency and phase. The minimal length of the designed peptide is defined by the characteristic frequency f as $1/f$;
4. Determination of resulting amino acid sequence using tabulated EIIP parameter values.

This approach has been already successfully applied and experimentally tested in design of FGF [13], HIV envelope protein analogue [14–16] and peptide to mimic myxoma virus oncolytic function [17, 18].

For example, in the case of Fibroblast Growth Factors, two characteristic frequencies were identified: one related to receptor recognition and another related to “growth activity”. The aim of that project was to design peptide which can competitively bind to the FGF receptor but without inducing growth. Using only receptor recognition frequency, the 16-mer peptide was designed, experimentally tested and indeed had receptor recognition activity without inducing growth [13].

In the case of HIV virus, the one common RRM frequency was identified for all HIV envelope protein despite their high variability. This frequency was used to design peptide that can immunologically mimic all HIV isolates and thus could be a good candidate for vaccine [14–16].

Similar idea as described above was used to mimic myxoma virus oncolytic function. Myxoma virus (MV) is a rabbit-specific poxvirus pathogen that also exhibits a unique tropism for human tumour cells and is dramatically oncolytic for human cancer xenografts. The RRM characteristic frequency for MV proteins was identified and used to design peptides that were experimentally shown to mimic myxoma virus oncolytic function [18].

It is important to note that de novo designed peptides/proteins do not have any significant homology with the original protein but have the same RRM characteristic frequency and related biological function. This is like in music, when you can recognise the same melody even when written with different notes.

3.3 Photobiomodulation in Medicine

There is much evidence that electromagnetic radiation can influence human health and wellbeing. As RRM model proposes that electromagnetic radiation can influence protein activity, we propose that biomodulation health effects are based on selective activation of proteins. One example is treatment of Crigler–Najjar syndrome by blue light. The Crigler–Najjar syndrome is extremely rare genetic disease affecting the metabolism of bilirubin, resulting in a form of non-haemolytic jaundice [56]. This disease is caused by lack of expression of UDP glucuronosyltransferase 1-A1. Hence, there is no response to treatment with phenobarbital. The only available treatment is phototherapy, which involves radiation of patients with the blue light for an extensive time every day, usually whole night. Similar treatment is used for jaundice in newborn babies.

Here, we have investigated: how and why, the specific blue light radiation can mimic activity of UDP glucuronosyltransferase 1-A1 [6]. For that purpose, we used Resonant Recognition Model and we found that specific RRM frequency for UDP glucuronosyltransferase 1-A1 biological function is within the blue light frequency range [6]. This finding explicitly explains, why the blue light can mimic and replace activity of UDP glucuronosyltransferase 1-A1.

We have analysed six HUMAN UDP glucuronosyltransferase proteins using the RRM and it has been revealed that the common frequency for all analysed sequences is at frequency of 0.3799, as presented in Fig. 6.

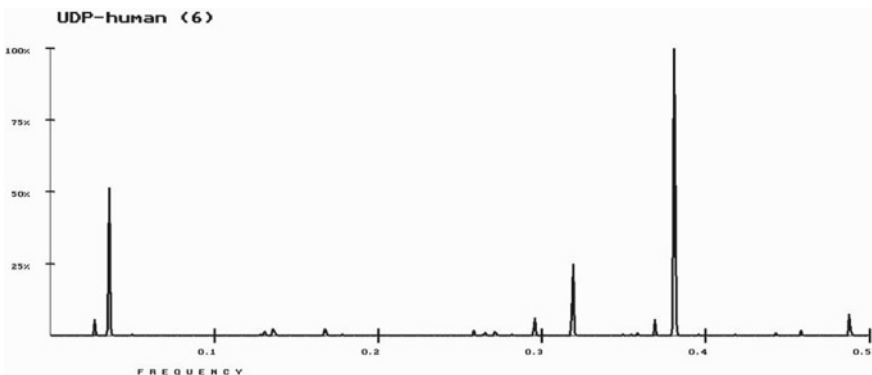


Fig. 6 Spectrum for six human UDP proteins showing prominent common peak at frequency of 0.3799

To make sure that this frequency is related to UDP function in bilirubin metabolism, we have also compared these six human UDP's with beta-barrel protein (angja) that binds bilirubin with high affinity. The result is the more prominent peak at frequency of 0.3799, as presented in Fig. 7. This confirms that frequency of 0.3799 is common to UDP's and angja proteins. According to RRM principles this numerical frequency is related to electromagnetic radiation of 529 nm, which is within blue visible light spectrum [6].

As it can be seen from the results above, using the RRM model we have found that specific RRM frequency for UDP glucuronyltransferase 1-A1 biological function is within the blue light frequency range [6]. This finding explicitly explains, why the blue light can mimic and replace activity of UDP glucuronyltransferase 1-A1.

Along these lines, we propose that number of other diseases and syndromes could be treated by electromagnetic frequencies calculated specifically for activation of

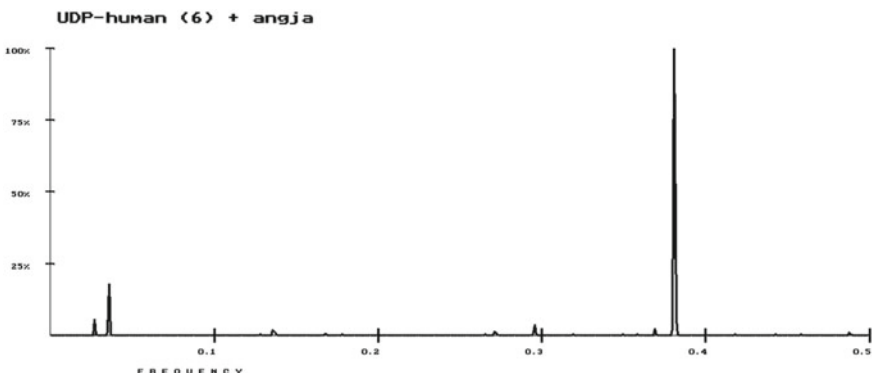


Fig. 7 Spectrum for six human UDP proteins together with angja protein showing single prominent peak at frequency of 0.3799 (529 nm)

proteins critical for those diseases and syndromes. For example, we propose that cystic fibrosis, which is genetic disease caused by mutation in CFTR protein, could be treated by electromagnetic radiation wavelength of 4527 nm corresponding to RRM frequency of 0.0444, which is mimicking healthy CFTR protein [57].

The other example is treatment of obesity by electromagnetic radiation wavelength of 727 nm corresponding to RRM frequency of 0.2764, which characterise leptin proteins that are critical for hunger control and energy balance within the body [24].

There is also possibility for cancer treatment using electromagnetic radiation predicted by the RRM model. As already established that there are two different computationally calculated RRM frequencies for oncogenes at $f_o = 0.0322$ corresponding to wavelength of 6242 nm and for proto-oncogenes at $f_p = 0.0537$ corresponding to wavelength of 3743 nm [25], as presented in Fig. 8.

It has been also shown that number of proteins involved in anticancer activity and apoptosis, like TNF and TNF receptor, are also having the RRM characteristic frequency within the range of RRM frequencies characterising proto-oncogenes f_p [23]. Thus, it is proposed that electromagnetic radiation within far infra-red spectrum related to RRM frequency f_p can induce cytotoxic effects on cancer cells. It has been shown in number of in vitro experiments that light exposure within the far infrared range of 3500–6400 nm can induce significant cytotoxic effect on cancer cells, while the same exposure regime does not show substantial effect on normal cells

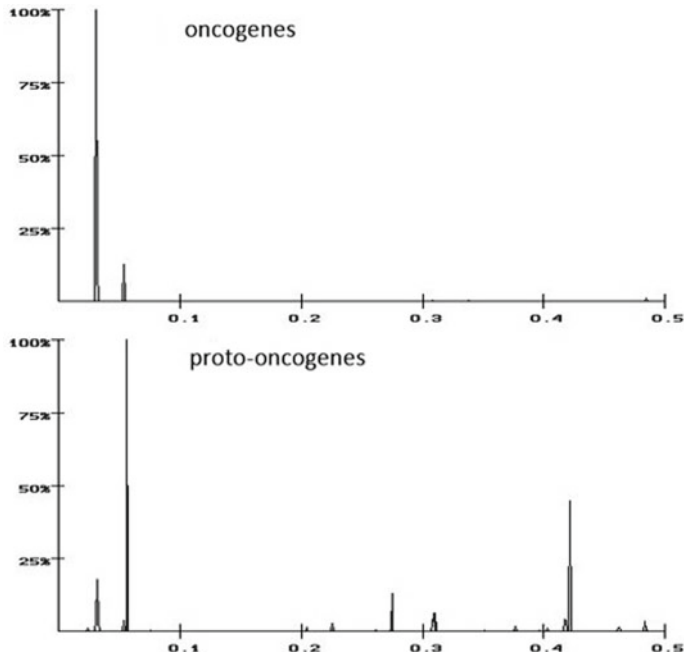


Fig. 8 RRM frequencies for oncogenes at $f_o = 0.0322$ corresponding to wavelength of 6242 nm and for proto-oncogenes at $f_p = 0.0537$ corresponding to wavelength of 3743 nm

[58]. Thus, findings from that study validate the proposed hypothesis that the RRM calculated frequencies within far infra-red spectrum can induce cytotoxic activity on cancer cells opening new path for treatment of cancer.

3.4 Stem Cell Differentiation Using Electromagnetic Radiation

There is an emerging need to use tissue engineering based on living cells as an alternative to tissue or organ transplantation. The main interest is differentiation of stem cells into osteoblasts for bone regeneration, bone healing and bone transplantation. Parathyroid hormone (PTH) is involved in the stimulation of bone remodelling and in the induction of differentiation of bone marrow mesenchymal stromal/stem cells by enhancing bone morphogenetic protein signalling [59].

The PTH is the principal regulator of calcium homeostasis in the human body and capable to influence and expand the bone marrow stem cell niche with both self-renewal and differentiation. As it has been shown that the population of pluripotent stem cells highly express parathyroid hormone type 1 receptors, it was postulated that parathyroid hormone has similar action as stromal cell-derived factor-1 (SDF-1 α), which is crucial for the recruitment of stem cells to number of diseased organs [60].

Moreover, it has been shown that photobiomodulation (PBM) of specific blue and green light wavelengths initiates osteoblastic differentiation of human adipose-derived stem cells [61]. The research described in reference [61] presents the effect of PBM on both proliferation and differentiation of osteogenic stem cells. The effects of four different wavelengths (420, 540, 660 and 810 nm) were measured and it has been shown that wavelengths of 420 and 540 nm were more efficient in stimulating osteoblast differentiation compared to wavelengths of 660 and 810 nm [61].

Here, we hypothesised that stimulation of osteoblast differentiation by specific blue and green light wavelengths is related to activation of proteins involved in osteoblast differentiation like PTH and SDF-1 α . For this purpose, we have utilised the RRM model, which proposes that protein activation and function are based on specific wavelengths (frequencies) of electromagnetic radiation within far infra-red, infra-red and visible up to ultra-violet light spectrum. Thus, by using the RRM, we have analysed the parathyroid hormone, its receptor and stromal self-derived factor with the aim to predict the characteristic wavelengths (frequencies) related to parathyroid hormone activities, particularly differentiation of stem cells into osteoblasts [12].

When PTH proteins and SDF-1 α proteins have been analysed together, using the RRM model, the prominent common RRM frequency was calculated at 0.3975 as presented in Fig. 9, characterising their common biological function, i.e. stem cells differentiation into osteoblasts. This RRM frequency corresponds to electromagnetic radiation wavelength of 502 nm [12].

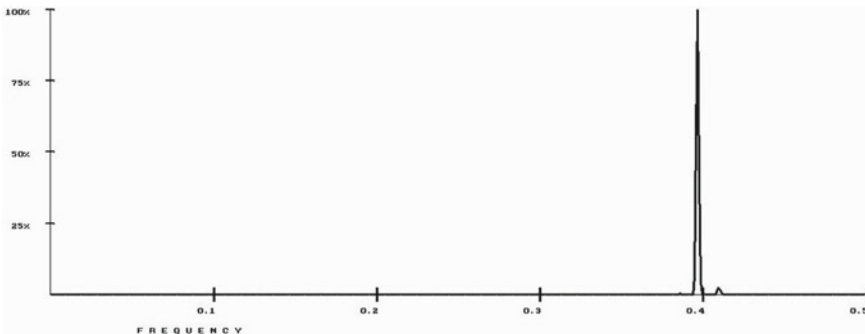


Fig. 9 RRM cross-spectrum of PTH proteins and SDF-1 α proteins. The prominent common characteristic frequency is at 0.3975, which represents an electromagnetic radiation wavelength of 502 nm [12]

The presented results show that characteristic frequency for the activity of parathyroid hormone (PTH) and stromal cell-derived factor-1 (SDF-1 α) related to differentiation of stem cells is at 0.3975 with corresponding electromagnetic radiation wavelength of 502 nm [12]. It is important to observe that wavelength of 502 nm is exactly between the wavelengths of 420 nm and 540 nm, which in previous experiment was found to be effective in stimulating osteoblast differentiation [61]. This indicates that specificity of wavelengths, which stimulate osteoblast differentiation, could be explained by photoactivation of proteins involved in osteoblast differentiation, as predicted by the RRM model. Even more, as the RRM model predicts that the most effective wavelength would be 502 nm [12], which is in between the already tested wavelengths of 420 and 540 nm [61], we propose that wavelength of 502 nm would induce even more efficient stimulation of osteoblast differentiation. Thus, the findings of this research can be used in development of improved techniques for differentiation of stem cells using the electromagnetic radiation of specific wavelength of 502 nm. Future research should involve validation of these results by experimental testing of stem cell differentiation.

3.5 Environmental Radiation

It is well known that the life on Earth originated and has been sustained by the electromagnetic energy from the sun light. In primitive organisms and plants, the sun light directly influences biological processes, while in more complex organisms, it has more indirect role. In these organisms, due to their more complex structure, the sun light cannot penetrate into each cell, therefore they have to create their own “internal sun” energy to drive selectivity of biological processes in their cells, in the same manner as it was originally initiated by the sun light [44, 62].

The meaning and influence of light to biomolecular interactions and consequently to health has been analysed using the RRM model, which proposes that macromolecular selective interactions are based on electromagnetic resonant energy transfer between macromolecules in the range of far infra-red, infra-red and visible up to ultra-violet light spectrum. This energy transfer then could mimic specificity enabled by different frequencies (wavelengths) of the sun light [8]. The RRM model is capable to identify relevant frequencies of this resonant energy transfer critical for activation of specific biological activities of proteins and DNA/RNA [1, 3–6, 8, 9].

As shown previously [8] and presented in Fig. 3, it can be observed that the whole spectrum of frequencies, as predicted by RRM to be relevant for biological activity of proteins and DNA, is also covering the same spectrum as the spectrum of the sun light on the Earth's surface, as presented with the yellow line in Fig. 10 [63]. This finding was as expected, since the sun light is the source of all life processes on the Earth. This implies that protein and DNA activity is mimicking the role of the sun within the biological functions of the cells [8].

It is also important to note that all biological processes in living cells occur in water medium, which is only transparent for electromagnetic frequencies in the spectrum encompassing mostly visible light, just as predicted by RRM. This means the water medium enables electromagnetic radiation of these frequencies to be transferred between macromolecules without loss of energy and therefore maximising the efficiency of these interactions [8].

The frequency range for biological functions has been found using RRM to be the same as the frequency range of the sun light on the Earth, as described above. This reinforces the fact that the life has originated on the Earth and is sourced by the energy from the sun light. This also means that the environmental sun light is natural source for the life on the Earth. However, humans are spending more and more time under the artificial light, which may not have the same spectral characteristics as the sun light and therefore may induce debalance in some biological functions. The spectrum of some artificial light sources has been presented in Fig. 10 [63]. It is interesting to note that the incandescent light, as presented with the purple line, has similar spectrum shape as the sun light. In contrast, the LED light, as presented with the blue line and the CFL light, as presented with the green line, has the distinct peaks at certain frequencies within the spectrum, while they are missing many of the other frequencies from the sun light spectrum.

We have compared the spectrum of LED and CFL artificial lights with the frequencies for biological functions, as calculated by the RRM model [8]. It can be observed that the artificial lights have strong radiation relevant for enzyme and control growth activity, while they are missing frequencies related to the tumour regulation and viral–bacterial infections. This finding could lead to possibility that under such artificial light's tumour regulation could be diminished leading to formation and growth of some tumours. In addition, lack of light frequencies in the range of bacterial and viral infection control could lead to higher susceptibility to these infections. Although the majority of biological functions within the human organism are protected from electromagnetic radiation within observed spectrum by skin and clothes, these artificial lights might still cause some distortions to biological functions due to the lack of full

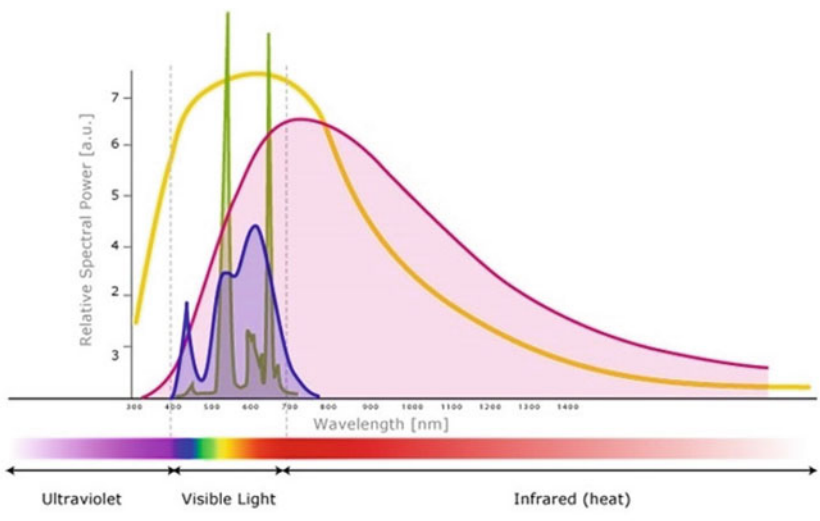


Fig. 10 Diagram of the spectrum a LED lamp (blue), a CFL (green) and an incandescent (purple) superimposed the solar spectrum (yellow) [63]

spectrum of sun light on humans. For example, there is the experimental evidence that specific photon energies of weak magnetic field of LED wavelength pulses are stored in malignant cells [64].

The environmental light electromagnetic radiation was investigated as source and influence of biomolecular interactions, related biological functions and consequent health effects. The relationship between our theoretical model, the RRM, and sun light, as origin of life, gives the possible explanation on how life processes have evolved and are controlled in more complexed organisms, where the sun light could not penetrate all cells and cellular processes.

3.6 Titanium Salt Patches and Nanophotonic Particles

Besides using RRM characteristic frequencies for bioactive peptide design or direct radiation with predicted electromagnetic wavelength producing desired biological and health effects, it is possible to use RRM identified frequencies to predict resonances between conductive elements like titanium salt and nanophotonic particles on one side with biological tissue also producing desired biological and health effects. It has been shown that titanium salt-infused patches with specific resonant characteristics are for example able to remediate pain, autism and attention deficit disorders when properly designed and applied [7, 65, 66]. The frequencies in such patches are produced with titanium salt-infused imprints and are passively transmitted through

the skin contact. This type of imprinting technology is not new and is used often in electronics by imprinting microchips with different frequencies.

Pain, both acute and chronic, is debilitating medical condition that is major cause of suffering in the general population and has significant economic impact. Often, only the pain symptoms could be treated, but not the cause. Currently, the pharmaceutical approach is used, which is costly and very often cause multiple side effects. In recent studies, it has been shown that the titanium in pico-nanometre scale and soluble form has beneficial effect on reduction of pain [66]. TERP patches are the silicon-based titanium salt-infused adhesive patches, which when directly applied to the pain areas, have been able to diminish pain, as shown in preliminary clinical studies [7]. Pain is very complex biochemical and electrical process involving sensory part, nerve transmission and brain perception of pain [67]. Pain is travelling along the nerves (axons) in shape of action potential going to doors root ganglia's, where it is processed in spinal dorsal horn and it is transferred through spinal nerves to brain where perception of pain is processed [67]. We have concentrated on the nerve transmission which is in fact electrical signal along the nerve (axon). This electrical signal is formed by complex activation (opening and closing) of specific pain related ion channels and the redistribution of electrically charged ions at nerve cell membrane. Ion channels are made of number of proteins that are involved and control these complex processes of opening and closing ion channels [68]. Activity of sodium ion channels is the most critical for pain transmission along nerves, while there is specific role for calcium ion channels in pain transfer along the nerve in the similar manner [67]. Acute, inflammatory and neuropathic pain can all be decreased or diminished by applying the local treatment of sodium ion channel blockers, which could be neurotoxins [69]. Therefore, the neurotoxins have recently been considered as the bases for development of new and more potent pain killer drugs. We have analysed both sodium and calcium ion channel proteins and neurotoxins proteins using the RRM model to identify characteristic electromagnetic frequency of the pain related to ion channel activation and consequently propose that the TERP patches conductive imprint can interfere with this frequency [7]. Our findings could explain mechanisms of TERP patches for relieving the pain through the resonances with pain related ion channels [7]. This would mean that TERP patches could mimic similar activity as toxin-based pain killers, but without side effects.

Autism is mental disorder, diagnosable from early childhood, characterised by impaired communication and socialisation, and repetitive behaviours. Along with the learning difficulties and limitations present in intellectually disabled, these characteristics may pose large burden on parents of disabled children. While there is no known cure for autism, certain behaviours may be managed by adherence to strict routines, regular consultations with healthcare professionals, and focus on alleviating the most detrimental symptoms [70–72]. The Autism Spectrum Disorder (ASD) is hereditary and is associated with malfunction of development and functioning of neuro synapses due to mutations within proteins responsible for proper functioning of nerve cells synapses [70–73], while Attention Deficit Hyperactivity Disorder (ADHD) is not well understood. Preliminary clinical results are indicative that titanium salt-infused patches can improve condition of patients with behavioural

disorders including autism and attention deficit [65]. Motivated by these results, we have investigated here the mechanisms of titanium salt-infused patches remediation of autism and attention deficit disorders at molecular level [65]. To achieve this goal, we have analysed synaptic proteins resonant frequencies using the RRM model and have investigated possibility of these frequencies to resonate with frequencies imprinted within titanium salt-infused patches. That work represents innovative approach to study mechanisms of titanium salt-infused patches effects to ASD and ADHD at cellular and molecular level. The results of that study could explain benefits of titanium salt-infused patches for ASD and ADHD patients through electromagnetic resonances between titanium salt-infused patches and synaptic proteins and can establish new treatments without using drugs and their negative side effects.

Similarly, to titanium salt-infused patches, it is possible to achieve resonances between nanophotonic particles and proteins at specific RRM electromagnetic wavelengths. Such resonance can activate selectively targeted proteins to achieve desired biological function. Nanophotonic particles that resonate with RRM characteristic frequency are being tested to demonstrate ability to stimulate both plant and fish growth. One example is application of nanophotonic particles for activation of chlorophyll binding proteins with the aim to improve plant growth. The main proteins within cascade of light harvesting in plants are Photosystem I (PSI) and Photosystem II (PSII) and the RRM model identified characteristic frequency for PSI at $f_1 = 0.3672$, which represents electromagnetic radiation wavelength of 547 nm and characteristic frequency for PSII at $f_2 = 0.0293$, which represents electromagnetic wavelength of 6860 nm, as presented in Fig. 11.

Some preliminary experiments on plant growth, based on nanophotonic particles designed via the RRM approach, have yielded fascinating results, as can be observed with the photograph of tomatoes, presented in Fig. 12 [74].

4 Bioresonances and Temperature

It is well known that temperature plays significant role in biological functioning of living organisms. Besides the fact that most of proteins important for controlling the living processes cannot function above temperature of about 44 °C due to protein denaturalisation, many other temperature related biological processes are not well understood. For example, it is not yet well understood why mammalian organisms need specific temperature of about 37 °C to function and grow properly, why sex of reptile eggs is very finely defined by environmental temperature or why function of faulty CFTR protein with deletion at F508 can be restored at specific temperature of about 28 °C, among other examples. As on one hand, temperature is important for activation of certain biological processes, and on the other hand, we found that certain wavelengths of electromagnetic radiation are also important for activation of proteins and related biological processes, we made here an attempt to correlate biologically important temperatures with related RRM frequencies (electromagnetic wavelengths). We have analysed the certain number of examples where temperature

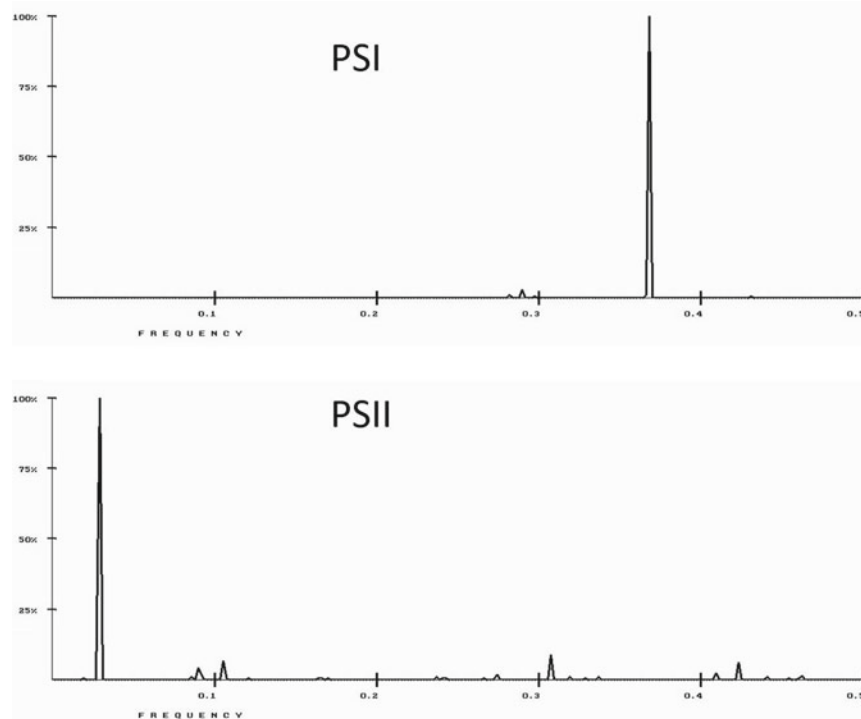


Fig. 11 RRM cross-spectrum of chlorophyll binding and light harvesting proteins related to Photosystem I (PSI) showing characteristic frequency is at $f_1 = 0.3672$, which represents electromagnetic radiation wavelength of 547 nm and RRM cross-spectrum of Photosystem II (PSII) related proteins showing characteristic frequency at $f_2 = 0.0293$, which represents electromagnetic radiation wavelength of 6860 nm

is critical for activation of biological processes and compared them with characteristic RRM frequencies for the same processes [2].

4.1 Cystic Fibrosis

The cystic fibrosis is genetic disease characterised by build-up of thick mucus in the lungs, which causes difficulties in breathing [75]. This disease is caused by mutations in CFTR proteins. The most common mutation that causes the cystic fibrosis is deletion of amino acid, phenylalanine (F) at 508th position of the CFTR protein [75]. However, the number of experiments in cell cultures have shown that specific temperature of about 28 °C can restore effect of F508 deletion in CFTR proteins [76–78]. The fact that temperature can restore the function of mutated proteins gave us an idea that activity of CFTR proteins can be manipulated by energy levels in



Fig. 12 The four tomatoes at the bottom were picked from the plant that was sprayed with nanophotonic particles and the one at the top was from the plant that was not sprayed. The top tomato is about 7 cm in diameter. All plants were grown under the same environmental parameters, soil and watering conditions. Nanophotonic particles were sprayed three times per week on the leaves of the plant, yielding the four tomatoes shown at the bottom [74]

the environment, which might be done using electromagnetic radiation. To understand such process, we analysed CFTR proteins and their mutants using the RRM model [57].

When we have analysed healthy CFTR proteins the most prominent common frequency was found at $f_1 = 0.0444$ with high signal-to-noise ratio of 863, as

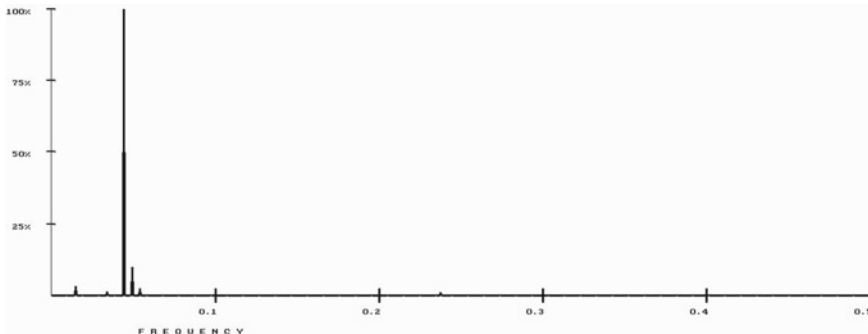


Fig. 13 RRM cross-spectrum of healthy CFTR proteins. The common characteristic frequency is at $f_1 = 0.0444$, with signal-to-noise ratio of 863. Frequency f_1 represents electromagnetic radiation wavelength of 4527 nm

presented in Fig. 13. This result indicates that frequency f_1 is characterising CFTR protein's healthy activity. According to conversion formula between numerical RRM frequency into the electromagnetic wavelength in nanometres (nm), the frequency f_1 corresponds to electromagnetic radiation of 4527 nm, which is within far infra-red spectrum.

When we have analysed same CFTR proteins, but with deletion F508, the same most prominent common frequency has been found at $f_1 = 0.0444$, but with much smaller signal-to-noise ratio of 686. This result indicates that mutated proteins have much lower amplitude at RRM characteristic frequency f_1 , indicating lower activity in mutated proteins and thus could explain why CFTR protein with F508 deletion is malfunctioning.

All these results are indicating that frequency f_1 is critical for normal healthy functioning of CFTR proteins. As specific temperature of about 28 °C can restore the healthy function of mutated CFTR protein with F508 deletion, we propose that this temperature is related to RRM characteristic frequency for healthy functioning of CFTR proteins at $f_1 = 0.0444$ (4527 nm) [57].

4.2 Sex Determination in Alligators

Some reptiles including alligators have temperature dependant sex determination, where environmental temperature of the developing eggs determines the sex of newborn babies. In the case of American alligators, eggs incubation at 33 °C produces mostly males, while incubation at 30 °C produces mostly females. It has been found that thermo-sensitive protein TRPV4 is crucial for male sex determination pathway at molecular level during thermal sex determination of the alligators [79]. Alligator TRPV4 protein is responsive to temperatures near to mid-thirties and by

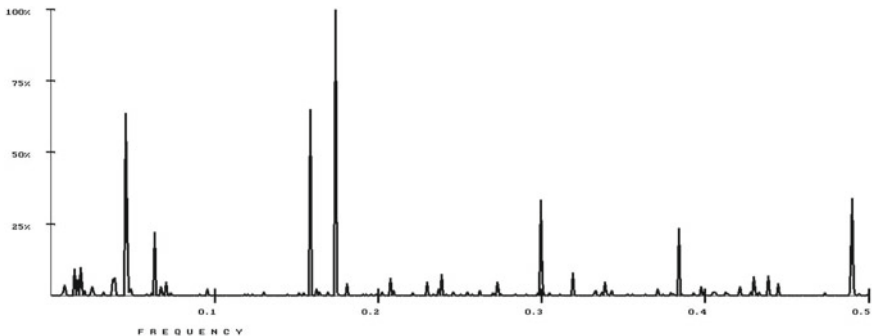


Fig. 14 RRM cross-spectrum of alligator TRPV4 protein as tetramer. The common characteristic frequency is at $f_2 = 0.1738$. Frequency f_2 represents electromagnetic radiation wavelength of 1156 nm [2]

inducing calcium ion influx can activate cell signalling, which is important for male development within the developing eggs [79].

To find out if there is relationship between sex determination temperature in alligators and corresponding RRM characteristic frequency for TRPV4 proteins, we have analysed alligator TRPV4 protein in tetramer form, as its active structure. When we have analysed alligator TRPV4 protein as tetramer from reference [79], we found the most prominent common frequency at $f_2 = 0.1738$, as presented in Fig. 14. According to conversion formula between numerical RRM frequency into the electromagnetic wavelength in nanometres (nm), the frequency f_2 corresponds to electromagnetic radiation of 1156 nm, which is within infra-red spectrum [2].

Thus, we propose that frequency $f_2 = 0.1738$ (1156 nm) is characterising temperature related sex determination and can be correlated to temperature of 33 °C.

4.3 Heat Shock Proteins

The heat shock proteins (HSPs) are essential factor for cellular responses to hyperthermia and other environmental stressors. The transcription of HSPs is mainly controlled by heat shock transcription factor 1 (HSF1). It has been shown experimentally in cell culture that heat shock factors are produced using heat shock treatment at 43 °C in water bath [80].

When we have analysed HSF1 proteins as trimers which is their active form [80], we have found the most prominent common frequency at $f_3 = 0.4144$, as presented in Fig. 15. According to conversion formula between numerical RRM frequency into the electromagnetic wavelength in nanometres (nm), the frequency f_3 corresponds to electromagnetic radiation of 485 nm, which is within violet light spectrum [2].

Thus, we propose that frequency $f_3 = 0.4144$ (485 nm) is characterising activation of heat shock proteins by HSF1 proteins and can be correlated to temperature of 43 °C.

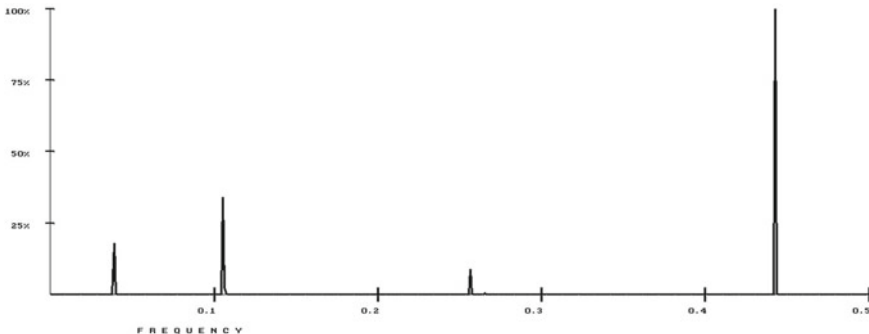


Fig. 15 RRM cross-spectrum of HSF1 proteins as trimers. The common characteristic frequency is at $f_3 = 0.4144$. Frequency f_3 represents electromagnetic radiation wavelength of 485 nm [2]

4.4 Growth Factor

In our previous extensive work [3, 4, 8, 25], we have identified RRM characteristic frequency of $f_4 = 0.2929$ as the main characteristic frequency for the number of growth factors, and thus, we proposed that it is characterising general growth function in mammalian cells. This frequency f_3 corresponds to electromagnetic radiation of 686 nm, which is within red light spectrum. It is also well known that temperature of about 37 °C is optimal temperature for biological processes within mammalian cells, particularly for their growth. Thus, the temperature of 37 °C can be related to general RRM characteristic frequency of $f_4 = 0.2929$ (686 nm) for mammalian cell growth.

4.5 Skin Temperature in Mammals

There is general relationship between different electromagnetic radiation frequencies and temperature, so called Wien's displacement law, which states that the peak wavelength of electromagnetic radiation is inversely proportional to temperature, and the peak frequency of electromagnetic radiation is directly proportional to temperature [81]. We used this proportionality to find the relationship between RRM frequency characterising the different protein biological functions and temperature that can influence these functions. According to Wien's displacement law, one of the examples is that mammals with skin temperature of about 300 °K (27 °C) emit pick radiation at around 10,000 nm within the far infra-red spectrum [81]. According to RRM conversion formula between wavelength of electromagnetic radiation and RRM frequency, as described in methods, this wavelength corresponds to RRM frequency of $f_5 = 0.0201$.

4.6 Temperature of Protein Denaturalisation

It is well known that proteins cannot naturally function above temperature of about 44 °C due to protein denaturalisation. This temperature could be considered as the maximum for protein natural activity, without help of any chaperones and thus could be related to the maximum frequency of RRM spectrum, which is $f_{\max} = 0.5$.

4.7 Correlation Between Temperature and RRM Frequencies

So far, we have presented number of very different biological processes that are related to temperature, including recovery of critical mutation within CFTR proteins related to cystic fibrosis, temperature induced sex determination in alligators, heat shock protein temperature characteristics, temperature induced growth, mammal skin temperature electromagnetic radiation, as well as temperature of protein denaturalisation [2]. All these examples are related to RRM characteristic frequencies, either through RRM characteristics of relevant proteins or through electromagnetic radiation that can be related to RRM. When those biologically relevant temperatures are correlated with related RRM characteristic frequencies, the striking linear correlation was found with correlation coefficient of over 0.99 and slope factor of 36.2 as presented in Table 2 and Fig. 16 [2].

Such striking correlation can support the idea that RRM frequencies are related to biologically relevant temperatures, possibly through electromagnetic radiation that is related to protein functions and interactions. This relationship can explain why certain temperatures have specific effect on certain biological activities. If this relationship is universally true, it would mean that biological functions of proteins can be influenced, not only by electromagnetic radiations of specific frequencies, as has been shown previously within RRM model, but also by specific temperatures. Such findings can introduce completely new view into how biological functions of proteins can be influenced by not only electromagnetic radiation, but also temperature. This finding could open whole new area in treatment of diseases and health conditions.

Table 2 Correlation between temperature and RRM frequencies [2]

RRM frequency	Temperature (°C)	Biological effect
0.0444	28	CFTR proteins (cystic fibrosis)
0.1738	33	Alligator sex determination (TRPV4)
0.4414	43	Heat shock proteins (HSF1)
0.2929	37	Mammalian cell growth
0.0201	27	Maximum skin temperature
0.5000	44	Maximum RRM frequency/maximum protein functional temperature

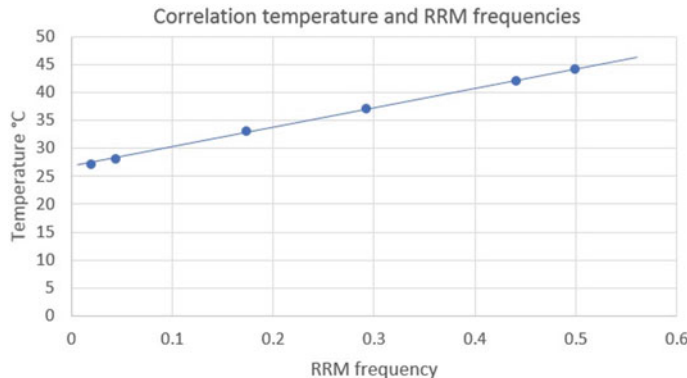


Fig. 16 Graphical presentation of correlation between temperature and RRM frequencies [2]

5 Conclusion

Oscillations and rhythms exist everywhere from cosmos to Earth and all the way down to electrons and even smaller particles and they are essence of matter and energy. Within this chapter, we have investigated only very small range of oscillations related to biological macromolecules, which are very little understood, but essential for living world. We have discovered that resonant electromagnetic energy transfer between interacting biological macromolecules is crucial for their biological function, which is characterised by specific frequency (wavelength) for each function/interaction. Based on this discovery, we have developed the so-called Resonant Recognition Model (RRM), which can identify resonant frequency characterising each biological function/interaction. The RRM model is completely changing the paradigm of understanding living processes at macromolecular level. We have also found striking correlation between temperature and RRM identified electromagnetic resonant frequencies relevant for specific biological functions of macromolecules. Although this correlation is surprising, it is logical as temperature plays significant role in number of biological processes. Within this chapter, we have presented the RRM model, its biophysical bases and possible applications in biotechnology, pharmacology, medicine, agriculture and even in electronics. Having all this in mind, we can conclude that the Resonant Recognition Model (RRM) is powerful tool in understanding and analysis of macromolecular biological activities, which are based on resonant electromagnetic energy transfer and can have huge impact, both scientific and commercial in biotechnology, pharmacology, medicine, and agriculture.

References

1. Cosic I, Lazar K, Cosic D (2015) Prediction of tubulin resonant frequencies using the Resonant Recognition Model (RRM). *IEEE Trans Nanobiosci* 12:491–496. <https://doi.org/10.1109/TNB.2014.2365851>
2. Cosic I, Cosic D (2020) Roll of temperature in living systems analysed using the resonant recognition model. *Int J Sci* 9(04):40–44
3. Cosic I (1994) Macromolecular bioactivity: is it resonant interaction between macromolecules?-theory and applications. *IEEE Trans Biomed Eng* 41:1101–1114
4. Cosic I (1997) The resonant recognition model of macromolecular bioactivity: theory and applications. Birkhauser Verlag, Basel
5. Cosic I, Cosic D, Lazar K (2015) Is it possible to predict electromagnetic resonances in proteins, DNA and RNA? *Nonlinear Biomed Phys* 3. <https://doi.org/10.1140/s40366-015-0020-6>
6. Cosic I, Cosic D (2016) The treatment of crigler-najjar syndrome by blue light as explained by resonant recognition model. *EPJ Nonlinear Biomed Phys* 4(1)
7. Cosic I, Cosic D Influence of tuning element relief patches on pain as analyzed by the resonant recognition model. *IEEE Trans Nanobiosci* 16(8):822–827
8. Cosic I, Cosic D, Lazar K (2016) Environmental light and its relationship with electromagnetic resonances of biomolecular interactions, as predicted by the resonant recognition model. *Int J Environ Res Public Health* 13(7):647. <https://doi.org/10.3390/ijerph13070647>
9. Vojisavljevic V, Pirogova E, Cosic I (2009) The effect of electromagnetic radiation (550 – 850 nm) on L-Lactate dehydrogenase kinetics. *Int J Radiat Biol* 83(4):221–230
10. Dotta BT, Murugan NJ, Karbowski LM, Lafrenie RM, Persinger MA (2014) Shifting wavelengths of ultraweak photon emissions from dying melanoma cells: their chemical enhancement and blocking are predicted by Cosic's theory of resonant recognition model for macromolecules. *Naturwissenschaften* 101(2):87–94
11. Murugan NJ, Karbowski LM, Persinger MA (2015) Cosic's resonance recognition model for protein sequences and photon emission differentiates lethal and non-lethal ebola strains: implications for treatment. *Open J Biophys* 05(01):35–43
12. Cosic I, Paspaliaris V, Cosic D (2019) Explanation of osteoblastic differentiation of stem cells by photo biomodulation using the resonant recognition model. *Appl Sci* 9(10):1979
13. Cosic I, Drummond AE, Underwood JR, Hearn MTW (1994) In vitro inhibition of the actions of basic FGF by a novel 16 amino acid peptide. *Mol Cell Biochem* 130(1):1–9
14. Krsmjanovic V, Biquard JM, Sikorska-Walker M, Cosic I, Desgranges C, Trabaud MA, Whitfield JF, Durkin JP, Achour A, Hearn MTW Investigations into the cross-reactivity of rabbit antibodies raised against nonhomologous pairs of synthetic peptides derived from HIV-1 gp120 proteins. *J Pept Res* 52(5):410–420
15. Hearn MTW, Biquard JM, Cosic I, Krsmjanovic V (2001) Peptides immunologically related to proteins expressed by a viral agent, having a sequence of amino acids ordered by means of protein informational method. US Patent 6, 294, 174
16. Achour A, Biquard JM, Krsmjanovic V, M'Bika JP, Ficheux D, Sikorska M, Cozzzone AJ, Unutmaz D (2007) Induction of human immunodeficiency virus (HIV-1) envelope specific cell-mediated immunity by a non-homologous synthetic peptide. *PLoS ONE* 2(11):e1214
17. Almansour NM, Pirogova E, Coloe PJ, Cosic I, Istivan TS (2012) Investigation of cytotoxicity of negative control peptides versus bioactive peptides on skin cancer and normal cells: a comparative study. *Future Med Chem* 4(12):1553–1565
18. Istivan TS, Pirogova E, Gan E, Almansour NM, Coloe PJ, Cosic I, Fernandez-Fuentes N (2011) Biological effects of a De Novo designed myxoma virus peptide analogue: evaluation of cytotoxicity on tumor cells. *PLoS ONE* 6(9):e24809
19. Pirogova E, Cosic I (2002) The use of ionisation constants of amino acids for protein signal analysis within the RRM – application to proteases. *Mol Simul* 28(8-9):845–851
20. Pirogova E, Simon GP, Cosic I (2003) Investigation of the applicability of dielectric relaxation properties of amino acid solutions within the resonant recognition model. *IEEE Trans Nanobiosci* 2(2):63–69

21. Veljković V, Slavić I (1972) Simple general-model pseudopotential. *Phys Rev Lett* 29(2):105–107
22. Veljković V (1973) The dependence of the fermi energy on the atomic number. *Phys Lett A* 45(1):41–42
23. Cosic I, Cosic D, Lazar K (2016) Analysis of tumor necrosis factor function using the resonant recognition model. *Cell Biochem Biophys* 74(2):175–180
24. Cosic I, Paspaliaris V, Cosic D (2019) Analysis of protein–receptor interactions on an example of leptin–leptin receptor interaction using the resonant recognition model. *Appl Sci* 9(23):5169
25. Cosic I, Cosic D, Lazar K (2017) Cancer related BRCA-1 and BRCA-2 mutations as analysed by the resonant recognition model. *J Adv Mol Biol* 1(2)
26. Karbowski LM, Murugan NJ, Persinger MA (2015) Novel cosic resonance (standing wave) solutions for components of the JAK-STAT cellular signaling pathway: a convergence of spectral density profiles. *FEBS Open Bio* 5(1):245–250
27. Hameroff SR (2007) The brain is both neurocomputer and quantum computer. *Cogn Sci* 31(6):1035–1045
28. Tegmark M (2000) Importance of quantum decoherence in brain processes. *Phys Rev E* 61(4):4194–4206
29. Hameroff S (1987) Ultimate computing-biomolecular consciousness and nanotechnology. Elsevier, North Holland
30. Saha AA, Craddock TJA, Tuszyński JA (2012) An investigation of the plausibility of stochastic resonance in tubulin dimers. *Biosystems* 107(2):81–87
31. Nogales E, Wolf SG, Downing KH (1998) Structure of the $\alpha\beta$ tubulin dimer by electron crystallography. *Nature* 391(6663):199–203
32. Davydov AS (1987) Excitons and solitons in molecular systems. *Int Rev Cytol* 106:183–225
33. Davydov AS (1979) Influence of electron-phonon interaction on the motion of an electron in a one-dimensional molecular system. *Theor Math Phys* 40(3):831–840
34. Hyman JM, McLaughlin DW, Scott AC (1983) On Davydov's Alpha-Helix Solitons, long-time prediction in dynamics. John Wiley & sons 367–394
35. Sinkala Z (2006) Soliton/exciton transport in proteins. *J Theor Biol* 241(4):919–927
36. Pang XF (2007) Theory of bio-energy transport in protein molecules and its experimental evidences as well as applications (I). *Front Phys China* 2(4):469–493
37. Yomosa S (1963) The exciton in protein. *J Phys Soc Jpn* 18(10):1494–1498
38. Ichinose S (1991) Soliton excitations in alpha-helical protein structures. *Chaos, Solitons Fractals* 1(6):501–509
39. Hameroff S, Penrose R (2014) Consciousness in the universe. *Phys Life Rev* 11(1):39–78
40. Craddock TJA, Tuszyński JA, Hameroff S, Bernroider G (2012) Cytoskeletal signaling: is memory encoded in microtubule lattices by CaMKII phosphorylation?. *PLoS Comput Biol* 8(3):e1002421
41. Ayoub AT, Craddock TJA, Klobukowski M, Tuszyński J (2014) Analysis of the strength of interfacial hydrogen bonds between tubulin dimers using quantum theory of atoms in molecules. *Biophys J* 107(3):740–750
42. Sahu S, Ghosh S, Ghosh B, Aswani K, Hirata K, Fujita D, Bandyopadhyay A (2013) Atomic water channel controlling remarkable properties of a single brain microtubule: correlating single protein to its supramolecular assembly. *Biosens Bioelectron* 47:141–148
43. Sahu S, Ghosh S, Hirata K, Fujita D, Bandyopadhyay A (2013) Multi-level memory-switching properties of a single brain microtubule. *Appl Phys Lett* 102(12):123701
44. Cifra M, Pospišil P (2014) Ultra-weak photon emission from biological samples: definition, mechanisms, properties, detection and applications. *J Photochem Photobiol B* 139:2–10
45. Blackburn EH, Greider CW, Szostak JW (2006) Telomeres and telomerase: the path from maize, tetrahymena and yeast to human cancer and aging. *Nat Med* 12(10):1133–1138
46. Meyne J, Ratliff RL, Moyzis RK (1989) Conservation of the human telomere sequence (TTAGGG) n among vertebrates. *Proc Nat Acad Sci* 86(18):7049–7053
47. Cosic I, Lazar K, Cosic D (2014) Cellular ageing- telomere, telomerase and progerin analysed using resonant recognition model. *MD-Medical Data* 6(3):205–209

48. Cosic I, Hearn MTW (1991) Hot spot amino acid distribution in Ha-ras Oncogene product p21: relationship to guanine binding site. *J Mol Recognit* 4:57–62
49. COSIC I, HEARN MTW (1992) Studies on protein-DNA interactions using the resonant recognition model. Application to repressors and transforming proteins. *Eur J Biochem* 205(2):613–619
50. COSIC I, HODDER AN, AGUILAR MI, HEARN MTW (1991) Resonant recognition model and protein topography. Model studies with myoglobin, hemoglobin and lysozyme. *Eur J Biochem* 198(1):113–119
51. Schmier S, Mostafa A, Haarmann T, Bannert N, Ziebuhr J, Veljkovic V, Dietrich U, Pleschka S (2015) In silico prediction and experimental confirmation of HA residues conferring enhanced human receptor specificity of H5N1 influenza a viruses. *Sci Rep* 5(1)
52. Pirogova E, Istivan T, Gan E, Cosic I (2011) Advances in methods for therapeutic peptide discovery, design and development. *Curr Pharm Biotechnol* 12(8):1117–1127. Bentham Science Publishers Ltd, Netherlands, ISSN: 1389-2010
53. Cosic I, Pirogova E (2007) Bioactive peptide design using the resonant recognition model. *Nonlinear Biomed Phys* 1(1)
54. Cosic I, Paspaliaris V, Cosic D, Kolios G (2019) Analysis of Interleukin-12 and Interleukin-23 pathways to distinguish between immune activation and inflammation functions, MD-Medical Data 11(1):007–014
55. Pirogova E, Istivan T, Gan E, Coloe P, Cosic I (2009) Computationally designed Interleukin-like peptide as a candidate for cancer treatment. In: Dössel O, Schlegel WC (eds) IFMBE Proc. 25/IV, world congress on medical physics and biomedical engineering, Springer, Berlin, pp 1973–1976
56. Jansen PLM (1999) Diagnosis and management of Crigler-Najjar syndrome. *Eur J Pediatr* 158(S2):S089–S094
57. Cosic I, Paspaliaris V, Cosic D (2019) Biophysical insights into cystic fibrosis based on electromagnetic resonances in CFTR proteins. *Int J Sci* 8(09):1–8
58. Peidaee P, Almansour NM, Pirogova E (2016) In vitro evaluation of low-intensity light radiation on murine melanoma (B16F10) cells. *Med Biol Eng Comput* 54(2–3):325–332
59. Yu B, Zhao X, Yang C, Crane J, Xian L, Lu W, Wan M, Cao X (2012) Parathyroid hormone induces differentiation of mesenchymal stromal/stem cells by enhancing bone morphogenetic protein signaling. *J Bone Miner Res* 27(9):2001–2014
60. Wang F, Du L, Ge S (2016) PTH/SDF-1 α cotherapy induces CD90+CD34– stromal cells migration and promotes tissue regeneration in a rat periodontal defect model. *Sci Rep* 6(1)
61. Wang Y, Huang YY, Wang Y, Lyu P, Hamblin MR (2016) Photobiomodulation (blue and green light) encourages osteoblastic-differentiation of human adipose-derived stem cells: role of intracellular calcium and light-gated ion channels. *Sci Rep* 6(1)
62. Cifra M, Brouder C, Nerudová M, Kučera O (2015) Biophotons, coherence and photocount statistics: a critical review. *J Lumin* 164:38–51
63. Katz B (2016) How to light art glass—lighting art guide. Available online: <https://bernardkatz.com>
64. Karbowski LM, Murugan NJ, Persinger MA (2016) Experimental evidence that specific photon energies are “Stored” in malignant cells for an hour: the synergism of weak magnetic Field-LED wavelength pulses. *Biol Med* 8:1–8
65. Cosic I, Cosic D, Uzelac B, Brasovan S (2018) Possible mechanism of titanium salt infused patches remediation of autism and attention deficit disorders. MD-Medical Data 10(2):097–102
66. Rowlands D, Shultz S, Ogawa T, Aoi W, Korte M (2014) The effects of uniquely-processed titanium on biological systems: implications for human health and performance. *J Funct Biomaterials* 5(1):1–14
67. Bourinet E, Altier C, Hildebrand ME, Trang T, Salter MW, Zamponi GW (2014) Calcium-permeable ion channels in pain signaling. *Physiol Rev* 94(1):81–140
68. Bagal SK, Chapman ML, Marron BE, Prime R, Storer RI, Swain NA (2014) Recent progress in sodium channel modulators for pain. *Bioorg Med Chem Lett* 24:3690–3699

69. Wood JN, Boorman JP, Okuse K, Baker MD (2004) Voltage-gated sodium channels and pain pathways. *J Neurobiol* 61(1):55–71
70. Chaste P, Leboyer M (2012) Autism risk factors: genes, environment, and gene-environment interactions. *Dialogues Clin Neurosci* 14:281–292
71. Ornoy A, Weinstein-Fudim L, Ergaz Z (2015) Prenatal factors associated with autism spectrum disorder (ASD). *Reprod Toxicol* 56:155–169
72. Levy SE, Mandell DS, Schultz RT (2009) Autism. *The Lancet* 374(9701):1627–1638
73. Chen J, Yu S, Fu Y, Li X (2014) Synaptic proteins and receptors defects in autism spectrum disorders. *Front Cell Neurosci* 8
74. Cosic I, Paspaliaris V, Cosic D (2018) Decoding protein/DNA functions through frequencies and resonances. *Research Gate November* 1–4
75. O'Sullivan BP, Freedman SD (2009) Cystic fibrosis. *The Lancet* 373(9678):1891–1904
76. Gomes-Alves P, Neves S, Coelho AV, Penque D (2009) Low temperature restoring effect on F508del-CFTR misprocessing: a proteomic approach. *J Proteomics* 73(2):218–230
77. Wilke M, Bot A, Jorna H, Scholte BJ, De Jonge HR, Neeraj Vij (2012) Rescue of murine F508del CFTR activity in native intestine by low temperature and proteasome inhibitors. *PLoS ONE* 7(12):e52070
78. Reynolds J, Boyaka PN, Bellis SL, Cormet-Boyaka E (2008) Low temperature induces the delivery of mature and immature CFTR to the plasma membrane. *Biochem Biophys Res Commun* 366(4):1025–1029
79. Yatsu R, Miyagawa S, Kohno S, Saito S, Lowers RH, Ogino Y, Fukuta N, Katsu Y, Ohta Y, Tominaga M, Guillette Jr LJ, Iguchi T (2016) TRPV4 associates environmental temperature and sex determination in the American alligator. *Sci Rep* 5(1)
80. Wang HY, Fu JCM, Lee YC, Lu PJ (2013) Hyperthermia stress activates heat shock protein expression via propyl isomerase 1 regulation with heat shock factor 1. *Mol Cell Biol* 33(24):4889–4899
81. Walker J (2008) Fundamentals of Physics. 8th ed. John Wiley and Sons

Chapter 2

Reformulating Physics Without Time



Enrico Prati

1 A Path Towards Timeless Physics

The concept of time has been naturally embedded in spoken language from ancient times. A trained brain has a physical structure correlated with the outside world, a property that we call memory [1]. It exhibits the capability of generalizing, extrapolating, and formulating predictions by applying the induction. The correspondent description of the outside world that arises from how the brain organizes the knowledge by categories—including time—can be formalized by compact empirical laws. Such laws describe the usual behavior of macroscopic objects. It is therefore efficient to export to scientific language common words such as *period*, *before*, *after*, *later* and all the time-related concepts in general. Such description proves extremely effective for macroscopic objects. After the definition of scientific method by Galileo, increasingly refined clocks have been employed by the scientists. As a consequence, the uncertainty on the measurement of time has been reduced from hours to minutes to seconds and in the modern era to fractions of a second thanks to atomic clocks. Scientists exported the terminology related to time used in natural language to formal definitions and by implicit assumptions. If one considers experiments involving macroscopic objects, GPS systems, and to predict time evolution of systems with dynamics, the standard conceptual framework in which time is treated as a fundamental quantity is not critical, even if recasted in a special relativistic framework. Instead, including time among the independent variables forming the ontology of nature [2–6] cannot be naively and implicitly assumed when analyzing nature at a fundamental level. Unfortunately, many key concepts employed in physics such as causality, locality, or the definition of a space-time background in theories including some versions of quantum gravity [7] are based on time.

Many distinct contributions around the nature of time start from hidden assumptions about the nature of time itself. Several authors introduce the concept of arrow of time in a heavily tautological conceptual framework, for instance, as follows:

E. Prati (✉)

Istituto di Fotonica e Nanotecnologie, Consiglio Nazionale delle Ricerche, Piazza Leonardo da Vinci 32, 20133 Milano, Italy

e-mail: enrico.prati@cnr.it

the experience of the time flow is assumed, so there is a *before* and an *after*, so the plan is to find way to explain this fundamental difference with respect to space along which, instead, an observer can move in both directions. This is the case for instance of the topological perspective of Kiehn [8] which assumes the concept of both reversible and irreversible evolutions itself in its axioms as a primitive concept, just to mention one example among many. The issue is that, in order to examine the concept of time, we should instead rely on a wording which is totally purified from any time-related concept. At a deeper sight, words such as *before* and *after* hide the use of time itself as it means that an object has some properties related to a previous time (i.e., registered in a memory device and labeled with a lower real number by a clock device) or to a future time (i.e., whose existence is postulated to occur and to be labeled with a higher real number by a clock device). Using verbs in the past form, using words such as *change*, *evolution*, *during*, *when*, *previous*, *later*, *caused*, and so on, makes the analysis corrupted by tautologies, returning an empty meaning to the reasoning. The main source of contradictions is that time is not an entity to be captured by a definition, but a simplified category which performs very well when applied to describe macroscopic bodies, not extendable to intervals below those that can be experimentally resolved. The issue is therefore how to create a conceptual framework enabling us to take into account for the experience of time, the usefulness of clocks, the success of time evolution equations in physics, and to grant that the reasoning on ultimate reality is fully timeless so to enable consistent findings at a fundamental level of nature. In the past, I have developed two complementary arguments to support fundamental timelessness of Physics. The first one [9] to reformulate the definition of atomic clocks—the paramount operative definition of time, so to reduce it to bare elements by showing that we can formulate it avoiding all the time-related concepts. Consequently, we do not have any experimental evidence that time is something fundamental. The other one [9] to reformulate Hamiltonian dynamics without any mention to time. In other words, if one eliminates all the hidden references to time from the natural language during the construction of the theoretical framework of atomic clocks and of dynamics, it results that we can describe Physics without time. On the other hand, this fact matches the experimental evidence that we do not need to make any use of it as from the previous remark. Apparently, despite such reasoning is fully consistent, it generates a discrepancy from our common experience. In order to reconnect such common experience and fundamental timelessness of nature, I have suggested to define generalized clocks [5], where the ill-defined tautological concept of period is replaced with the more relaxed concept of cycle in the phase space. To summarize, the reasoning leads to discover that time is a variable which holds only when describing a system which includes a macroscopic object, and that the attempt to extend the concept of time to sub-period intervals (shorter than single period oscillations of an atomic clock) is a hidden assumption not supported experimentally. Consequently, discussing about a postulated arrow of time or considering time scales such as the Plank time are unjustified extrapolations based on theory-dependent concepts, not logically connected with the fundamental description of nature.

In order to discriminate speakable and unspeakable in physics of time, the single-ion optical atomic clock and the double time-slit experiments can be considered. Their description clarifies that temporal quantities such as time and frequency are fundamentally unspeakable, while speakable is only related to ratios between wavelengths and to boundary conditions of stationary light beams. In addition, time intervals lower than the minimum period realized by the experimental apparatus are an unjustified extrapolation out of the domain of definition.

The following sections are devoted to show both that time is not necessary to describe experiments involving atomic clocks, which are used to define time in Physics, and it is also not necessary to formulate a mathematical construction of dynamics. First, I describe two experiments believed to involve time at a fundamental level (Sects. 2 and 3, which turn out instead not connected to time. Such experiment concerns the single-Hg-atom atomic clock [10] and a double time-slit experiment [11], respectively. Such experiments are used to discern speakable and unspeakable. By rigorously analyzing their arrangement, it emerges that time and frequency quantities are artificially introduced with recursive definitions during the construction, and they are *unspeakable*. Indeed, the bare description of the experiments is based on wavelengths. A toy model of definitions related to time and frequency is defined in Sect. 4. It is found that the source of the self-recursivity is hidden in the definitions of time and frequency, respectively. Indeed, they are generated by time-related concepts introduced by an unjustified extrapolation from the natural language, making implicit use of concepts such as *duration* and *repetitive* events. On the other hand, in Sect. 5, I show that Hamiltonian dynamics itself can be defined without the use of time. The bridge between fundamental timelessness and the success of metrology based on clocks lies in its ability to provide a good approximation of the natural parametrization of trajectories in phase space for which equations of motion look simple.

2 Experiment 1: Describing a Reference Atomic Clock by a Timeless Approach

Atomic clocks are the most precise instruments used to define time intervals thanks to their accuracy and stability. In the following, the analysis of single-atom atomic clock clarifies at which point of the operative definition time arises. The implementation realized in 2001 at NIST by an Hg atom [10] provides the guide for the discussion. A single-ion clock requires a device producing supposedly periodic events (clock ticks), a counter to accumulate and display, and the resonance of a well-isolated atomic transition. The Hg atom clock mentioned above is based on an optical transition at a much higher frequency and a specialized frequency divider (frequency chain). The apparatus consists of a self-referenced all-optical clock in which a femtosecond laser with repetition rate $f_r = 1 \text{ GHz}$ is locked to the frequency of a single-atom oscillator. Such femtosecond laser delivers the beam to a microstructure fiber which operates

a spectral broadening and produces a set of frequencies in the visible/near infrared. The low-frequency portion of the set is frequency-doubled and heterodyned against the high-frequency portion in a photodetector. The offset frequency f_0 common to all modes of the set is extracted. A specific frequency is heterodyned with the optical standard laser oscillator ($f_{\text{Hg}} = 532 \text{ THz}$), locked to the clock transition frequency of the single $^{199}\text{Hg}^+$ ion, by the photodetector PD2, returning a beat frequency f_b . By employing two phase-locked loops (PLL) on f_0 and f_b , the spacing f_r of the two is phase-locked to the Hg^+ standard. The output of the clock is the microwave domain frequency f_r , detected by the photodetector PD3, which is employed to generate the time standard. In this system, there are two implicit assumptions. One is that for a light beam $c = \lambda f$ where c is a constant (which we call speed of light), while the second is that the locked frequencies are operated in stationary conditions. Therefore, let us investigate how this conversion from lengths to frequency is realized: the optical components such as the photodetectors and phase locked loops work thanks to interferometry in space: for instance the phase-locked loop PLL2 changes the cavity length of the fs laser with a piezo mirror such that $f_r = af_0$. Here is where the time-related description of frequency sets in. If we limit ourselves to the description of the mere facts about the clock, it is based on space boundary conditions. Indeed, the description of the atomic clock is based on a stationary equipment. The control of boundary conditions in space is rephrased in terms of *frequency chain*. From one hand, the description of all the PLLs is done in terms of ratios between the wavelength of different light beams, and on the other hand, different frequencies are attributed to photons of different wavelengths, by giving a meaning to the constant c in terms of speed. The latter is a time-related concept, so it should not contribute to definition of itself. If one limits to express the experiment in terms of the space boundary conditions of the stationary waves only, there is technically no reason to employ an alternative set of definitions or concepts like *time*, *time evolution* and *period*. The only speakable in science of atomic clock experiment is ratios between wavelengths.

3 Experiment 2: Deconstructing the Interpretation of Double Time-Slit Experiments at Subwavelength Timescale

There is another conceptual framework in which the use of the concept of time is meaningless. It consists of the extension of the definition of time below a single period—one should better say a single cycle in experiments involving double time slit setups, such as from Ref. [11, 12]. Such setup is ordinarily used for attosecond time scale molecular dynamics [13]. The pulses, because of their short duration, are said *sub-cyclic*. Intense pulses of radiation on the femtosecond scale show phenomena attributed to the opening of time slits for time intervals shorter than the period itself, at the attosecond scale. Such scheme is referred to as double-slit experiments operated in the time–energy domain. The role of the slits is said to be played by windows in a

time of attosecond duration. Slits can be opened and closed by changing the temporal evolution of the field of a few cycles-laser pulse, so at any given time, there is only a single particle in the double-slit. I first summarize the experiment of Ref. [11] and next I comment about the consistency of the standard wording used to describe it. Argon atoms are ionized by an intense few-cycle 760 nm laser pulses. The electrons are detected by two opposite detectors. The laser field is horizontally polarized, i.e., parallel to an axis defined by the electron detectors. The experimental observation consists of fringe pattern in the energy domain as time and energy are conjugated variables, attributed to the interference of temporally separated wave packets. By using phase-controlled few-cycle laser pulses, the temporal evolution of the field is manipulated, by gradually opening or closing the slits at different time. Therefore, depending on the field, one or two half-cycles—or anything in between—contribute to the electron amplitude for a given direction and electron energy. The experimenter shifts a glass wedge into the beam so the envelope of the pulse with respect of the carrier is delayed, achieving different conditions of self-interference. For the case of sine pulses, the effect is attributed to two slits with no which-way information in one direction of the emission (said positive, in the right direction R), and one slit with complete which-way information in the opposite direction (L). Each argon atom emits at most one electron, which creates interference depending on the trajectories which contribute to its final state. The interpretation looks at the conservation of the momentum in presence of the vector potential $A(t)$. As the momentum before the interaction of the electron bound to the atom is zero, then $\mathbf{p} - e\mathbf{A}(t_0) = 0$, and the final result comes from the interference of all trajectories of momentum \mathbf{p} . Each slit is, according to the standard interpretation, a pair of slits. The time separation of such sub-slits depends on the electron energy, which in turn is the quantity measured by the equipment. By inverting the energy-time relation, the experimental data provide a measurement of the time difference of the two sub-slits of about 500 as. In the simple's man model, the interpretation of the experiment is based on the assumption that the same electron is ionized twice in time. After the first time, the electron re-enters through the second slit and it re-exits [14]. This view approximates the result of the path integral approach [15], for which all the paths contribute to the final result. The questions is whether we can attribute the meaning of a time interval to such process below the time duration of a single period or cycle. Does a temporal interpretation of the process below the period of a single cycle have something do to with the real process, if the equipment is unable to resolve such process? Time duration is defined in terms of counting of periods, so the employment of the concept of time interval here is out of the domain of definition. As the system provides a minimum period thanks to the laser frequency, the sub-cycle *time slit separation* is an extrapolation, whose value is calculated indirectly. Implicitly, one extends the concept of time interval below the duration of a single cycle, but there is neither direct measurement nor evidence that some ordered time according to the atomic-clock standard definition, which, as said, operates in stationary conditions thanks to space-related boundary conditions. The notion of time is defined by a clock apparatus, and the concept or duration of a narrow pulse below a single cycle is an arbitrary extrapolation of the same concept, with the further issue that it is not supported by any evidence when it is employed to interpret

the experiment in terms of interval duration between time slits. While time duration is unspeakable as it consists only in a rephrasing of the same experiment (atomic clock) with other words (previous paragraph), time intervals of duration below a single cycle are unspeakable as they extend the previous (unspeakable) concept out of the domain of definition itself. We cannot skip the observation that Planck time precisely falls into this double inconsistency.

4 Debunking the Definition of Time by the *clack* Toy system

In order to make evident the origin of the inconsistency of the definition of time and frequency, and the abuse of natural language when we apply it in fundamental physics, I introduce a toy system based on a fantasy atom synthesized by a civilization from another planet. This system is based on $^{666}\text{frigerium}$ and it is employed to define a new quantity, the *quid*. The operative definition of the quid is based on the description of the instrument to measure it: the *clack*. The clack is an instrument designed to measure the *quid* intervals—a postulated physical quantity, which is measured in this units *quix*. By definition, one *quix* is a quid interval which consists of the duration of 1.000.000 of *quods* of the radiation corresponding to the transition between two hyperfine levels of the ground state of the $^{666}\text{frigerium}$ atom. Conversely, the *douq* is defined as the rate of occurrence of a repetitive event. If Q is the quod of a repetitive event, then the douq is the reciprocal $1/Q$. To complete the system, the quod is a quid interval expressed in quixes. The issue for a human is to provide some meaning to this set of definitions. The reading above fails to suggest what is a clack and what does it measure in terms of quixes. If one examines naively the definitions, he gets immediately that they consist of a set of mutually crossed definitions P_1 , P_2 , P_3 and P_4 :

1. quid = $P_1(\text{clack})$
2. clack = $P_2(\text{quid}, \text{quix})$
3. quix = $P_3(\text{quods}, \text{quid})$
4. quod = $P_4(\text{quix}, \text{quid})$

The information provided by these definitions is insufficient to capture their meaning. As we really want to understand their true meaning, we examine more deeply the other words implicitly used in the definitions. We may ask if the problem comes from the concept of *repetitive event*. We rule out the issue by saying that a repetitive event is an event which occurs with a multiplicity in quid. Next, we may ask if the problem comes from the concept of *duration*. We can easily recognize that the *duration* in quid is its extension, given by the number of standard quods in a quid interval. There is only one possible source of issues remaining, which is the only reference of something connected to our experience, which is the *quod of the radiation*. We may

agree to experimentally obtain the quod of the radiation from λ/k where λ is the wavelength and k is a constant in [m][quix] $^{-1}$. This completes the picture, so now the Definitions 1 and 2 are completed as follows:

3. quix = $P_3(\text{quods}, \text{quid}, \text{quod of a radiation})$
4. quod = $P_4(\text{quix}, \text{quid})$
5. quod of a radiation = $P_5(\text{wavelength}, \text{quid}, \text{quix})$

In other words, the toy model consists of a set of definition based on a reference atom and the concept of space. Excluding mass, radiation beams, and space, there is no reason to suspect the existance of further independent quantities on that planet and to give any ontological status to the quid independently from the space. The real problem for us, on Earth, is that this toy model which proves totally useless on the hypothetical planet, coincides with the definition of clock (the clack), time (quid), second (quix) and period (quod), if only one replaces frigerium with cesium and k with c [16]. As already said, at this stage, the latter constant is not informative, as the notion of speed is implicitly related to that of time, which is the object of the tentative construction. The toy system highlights how the use of natural language applied to time in physics implicitly extends to scientific instruments our common sense. Therefore, as implicitly adopt specific words connected to the concept of time to give more general attributes: *extension of an interval* is said *duration*, and *multiplicity* with respect to something is said *repetitive*. Unfortunately, duration and repetitive are unspeakable, as they are used to define the same concept on which they are partially grounded. In the definition of time, clock, and period, an abuse of language based on the concept of *duration* and *repetitivitiy* erroneously supports the idea that time is an independent quantity, which refers to something real and ontologically distinct. We must accept that the definition of time, if any, would need to be purified from time-related words and re-expressed by a neutral speakable language, not implicitly involving time. The issue is that there is currently no alternative to capture time by a timeless definition.

5 Natural Time Parameter Generated by the Hamiltonian Timeless Scenario

In this Section, I summarize the derivation of the natural time parameter by imposing a variational principle. The purpose is to build dynamics from a timeless framework [5]. Indeed, the Maupertuis action principle generates the dynamics without explicitly using time [17]. The focus concerns closed systems, so the Hamiltonian is independent from parameters. The approach consists of expressing the variational principle, the Hamiltonian, and the generalized coordinates in a timeless framework. The consequence of imposing both the variational principle and the stationarity of the Hamil-

tonian is to induce a natural parametrization among all the possible parametrizations, which turns out to be the one commonly used to describe dynamics. Such parameter is indicated by σ . It corresponds to τ of Ref. [18] and to parameter time t or ix_0 in ordinary Hamiltonian theory. To define Hamiltonian mechanics without the concept of time requires consequently that some additional hypotheses are assumed in order to provide a consistent definition of clock time useful when dealing with macroscopic objects.

5.1 Natural Time Parameter in Timeless Classical Mechanics

In the following, I summarize the approach I proposed in Ref. [5]. The Hamilton equations are expressed in timeless formalism by starting from a variational principle on asynchronous-varied trajectories. The time independent Hamiltonian $H(\mathbf{p}, \mathbf{q})$ is a function of the generalized three-dimensional coordinates \mathbf{p} and \mathbf{q} . The independence of H from time reduces the degrees of freedom to $2n - 1$. It is necessary to assume that it exists a set of trajectories in the coordinates space μ for which H is constant.

In order to determine the parametrization imposed by the stationarity of the action, a generic parametrization of the points of the trajectories is initially assumed. Such arbitrary parametrization λ gives $q_i = q_i(\lambda)$ and $p_i = p_i(\lambda)$ where all the functions belong to C^2 on the interval $[\lambda_A, \lambda_B] \in \mathcal{R}$. The Hamiltonian $H(\mathbf{p}, \mathbf{q})$ does not depend explicitly on λ . In order to impose a variational principle on the trajectory, it is now considered a variation that is normally used to impose asynchronous varied trajectories in canonical formalism to derive Hamilton equation from the Maupertuis principle. A new parametrization σ of the generalized coordinates and of λ is now defined, under the condition that $\frac{d\lambda}{d\sigma} \neq 0$ on $[\sigma_A, \sigma_B]$.

Such distinction between λ and σ represents a subtle point and technical difference from the approach of Refs.[2, 19]. Let us impose the stationarity of the action:

$$A = \int p_i dq_i \quad (1)$$

where the Einstein summation on the repeated indexes is adopted and $i = 1, 2, 3$. The Maupertuis variational principle reads

$$\delta A = \delta \int p_i dq_i = 0 \quad (2)$$

The imposition of the stationarity of the action is given by the variation of the trajectories. Neglecting as usual second-order perturbations and integrating by parts where necessary, one has:

$$d\sigma = \left(\frac{\partial H}{\partial p_i} \right)^{-1} dq_i = - \left(\frac{\partial H}{\partial q_i} \right)^{-1} dp_i \quad (3)$$

under the hypothesis that $\left(\frac{\partial H}{\partial p_i}\right) \neq 0$ and $\left(\frac{\partial H}{\partial q_i}\right) \neq 0$. Such equations differ from the Hamilton equations since σ does not represent the macroscopic clock time. On the contrary, it only represents the natural parameterization of the system imposed by the energy conservation. Let us clearly remark that σ is not the quantity measured by clocks.

5.2 Natural Time Parameter in Quantum Field Theory

Let us now recast the previous discussion by quantum formalism. The most convenient formalism to extend the action principle to general relativity and to quantum mechanics is the extended presymplectic approach [3]. There, dynamics is expressed on the unparameterized curve γ in the relativistic configuration space $C = \mathcal{R} \times C_0$, where C_0 is the m -dimensional space of coordinates q^i , which extremizes the integral

$$A[\gamma] = \int_{\gamma} \theta \quad (4)$$

where

$$\theta = p_i dq^i + p_t dt \quad (5)$$

is the natural one-form defined on the cotangent space T^*C and the constraint

$$H(q^i, t, p_i, p_t) = 0 \quad (6)$$

where H is the relativistic Hamiltonian. In the extended presymplectic formalism, the variational principle reads:

$$\delta A[\gamma] = \delta \int_{\gamma} \theta = 0 \quad (7)$$

Such principle allows a quantum extension, which goes beyond the scopes of this analysis. Both the Lagrangian and the extended presymplectic formalism consider time as a part of the manifold where physics is defined. Time t or x_0 assumes a role comparable to that of space, even when starting with an unparameterized curve as it happens in presymplectic approach. Technically, since the action admits invariance under reparameterization of time (spacetime in relativistic domain), it does not represent a problem. In the following, in order to avoid the use of the concept of time, the configuration space is only C_0 instead of $C = \mathcal{R} \times C_0$ and the extended configuration space will only include fields and their conjugate momenta (generalized fields).

A Hamiltonian operator $H = \int d^3x \mathcal{H}$ is given, where \mathcal{H} is the Hamiltonian density. The Hamiltonian operator H acts as a constraint for quantum field dynamics.

The action, in terms of a quantum fields $\psi_i(x)$ and the conjugate coordinates $\pi_i(x)$, can be re-expressed as:

$$A = \int d^3x \int d\psi_i \pi_i \quad (8)$$

where the Einstein summation on the repeated indexes is adopted. The roman index spans on the space dimensions 1, 2, and 3. To define time as the natural parameterization of change in the generalized coordinate space μ_Q , the points of the trajectories $f(q_i, p_i) = 0$ are replaced in QFT by space configurations of the generalized field $Q = (\psi_i(\mathbf{x}), \pi_i(\mathbf{x}))$ in μ_Q . In the classical case neighboring, position and momentum states are associated to the parameter σ , while in QFT σ labels the generalized field with support in \mathcal{R}^3 . Two arrays of fields vibrate the quantum fields and their conjugate fields, respectively. As in the previous case, the extremality of the action is obtained under the condition that:

$$d\sigma = \left(\frac{\delta \mathcal{H}}{\delta \pi_i} \right)^{-1}_{\psi_i} d\psi_i(\mathbf{x}) = - \left(\frac{\delta \mathcal{H}}{\delta \psi_i} \right)^{-1}_{\pi_i} d\pi_i(\mathbf{x}) \quad (9)$$

The parameter σ belongs to \mathcal{R} by construction. The parameterization of the field distribution is locally achieved by tagging neighboring configurations with the parameter σ .

6 Recovering Generalized Clock Time

The advantage of the discussion above is that clock time is never used. Therefore, one may ask how such derivation can be useful to describe physical world, where the experience of time makes it the most useful quantity to describe dynamics. The last step of the reasoning consists of explaining how it is possible to operatively define clock time by starting from the natural time parameter defined above. As already said, the parameter σ has the property of providing a natural parameterization suitable for describing dynamics, but it is not an observable quantity. In order to explain the macroscopic experience of time in complex systems, an observable quantity T is built as follows. The quantity T provides by construction an experimentally measurable discrete approximation of σ . Let us now stress the following remark: since time is operatively defined by clock standards based on the period of an oscillator, *it is only defined in such systems complex enough to contain a subsystem acting as the clock*. As said, the definition of periodicity implicitly assumes that an external time is available in order to compare a period with the next one, which is meaningless in a timeless framework. Consequently, the concept of *period* is here relaxed by re-expressing it in timeless wording by the concept of *cycle* in the phase space μ or in μ_Q . Defining the *clock time* T , measured, for example, by atomic clocks, corresponds to label simultaneous occurrences in the phase space of two or more subsystems where one

is identified as the clock. The clock corresponds to the cyclic subsystem, as defined below. The dynamics of the i -th observable O_i will consequently be expressed by the simple law involving σ :

$$O_i(T) \cong O_i(\sigma) \quad (10)$$

Let us consider a Hamiltonian system S separable by two independent subsystems S_1 and S_2 , so that all the states are represented by factorized (eigen)states of their respective Hamiltonian $\psi_1 \otimes \psi_2 \in H_1 \otimes H_2$ where H_1 and H_2 are the Hilbert spaces of the subsystems 1 and 2, respectively. As from above, the system S owns a unique natural time parameter σ which is consistently defined also separately for the two subsystems by construction. In the following, the properties required by the system S_1 to act as a clock in S are defined in order to describe dynamics in S_2 . For a given $\bar{\sigma}$, a state $\psi \in H_1 \otimes H_2$ consists of the tensor product of the state $\psi_1(\bar{\sigma}) \in H_1$ and the state $\psi_2(\bar{\sigma}) \in H_2$. We define $\bar{\psi}_1$ as the multiplicity κ_{AB} on the interval (σ_A, σ_B) if there are κ_{AB} values of $\tilde{\sigma}_i \in (\sigma_A, \sigma_B)$ (Fig. 1) such that $\psi_1(\tilde{\sigma}_i) = \bar{\psi}_1$ where $i \in (0, \kappa_{AB})$. By definition, the subsystem S_1 is cyclic in the phase space if

1. its path in the phase space is closed,
2. its velocity $|dQ/d\sigma| \neq 0$ and it is smooth,
3. the multiplicity κ_{AB} of a state vector in the System 1 monotonically grows with the interval (σ_A, σ_B) and it tends to infinity when $\sigma_A \rightarrow -\infty \wedge \sigma_B \rightarrow +\infty$.

The second requirement grants that the realizations of two contiguous states occur along the σ axis according to the order of the parameter σ . The third requirement that the clock never stops and its velocity in the phase space is enough to grant that the number of cycles is not finite.

Given the interval (σ_A, σ_B) , it is now defined the set $\Omega(\sigma_A, \sigma_B) \subset H_2$:

$$\Omega(\sigma_A, \sigma_B) = \{\psi_2(\sigma) \in H_2 | \sigma \in (\sigma_A, \sigma_B)\} \quad (11)$$

An arbitrary origin σ_0 is fixed for the natural time parameter. We associate to such origin the arbitrary initial states $\bar{\psi}_1 = \psi_1(\sigma_0)$ and $\bar{\psi}_2 = \psi_2(\sigma_0)$. Macroscopic time duration $T^{(S_1)}$ of the interval (σ_A, σ_B) measured by the cyclic subsystem S_1 is given by the number k_{AB} of states $\psi_2(\sigma) \in \Omega$ so that $\psi_1(\sigma) = \bar{\psi}_1$. More explicitly, one has

$$T_{AB}^{(S_1)} \equiv k_{AB} \quad (12)$$

Let us go back to the science and technology of clock standards to remind that a clock is evaluated according to two figures of merit. The first property is the *stability* (small standard deviation) and the second one is the *accuracy* (high Q factor of the

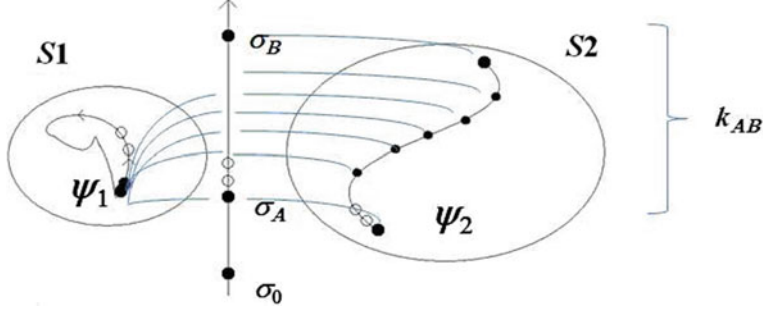


Fig. 1 Representation of the generalized clock in phase space. A cyclic system $S1$ allows to count k_{AB} correspondences of the same state ψ_1 with different points of the phase space of $S2$, thanks to the common parametrization σ induced by the Hamiltonian constraint and the variational principle on the action. Under suitable stability conditions, $S1$ acts as generalized clock for $S2$, so motion described in terms of σ is well approximated by motion as a function of the clock time $T = \alpha k_{AB}$ where α is a scaling factor. Reproduced with permission from Ref. [9]

resonance associated to the clock) [20, 21]. Since the accuracy refers to the arbitrary resonance frequency of the time standard (e.g., the Cesium resonance frequency) and in order to fulfill the timeless approach in the following, we can consider only the requirement of stability. Given a target standard deviation Σ required in an experiment performed on the subsystem $S2$ in the interval (σ_A, σ_B) and for an integration time τ , the *generalized clock* has to fulfill the following prescription:

$$\epsilon \equiv E^2 \left[T_{i,i+1}^{(S1)} \right] < \Sigma \quad (13)$$

where E^2 is the standard deviation and

$$\sigma_{i+1} = \sigma_i + \tau \quad (14)$$

where $i = 0, \dots, N_{AB}$ with $N_{AB} = (\sigma_B - \sigma_A)/\tau$. Consequently, the definition of clock time loses of validity for time intervals $T^{(S1)}$ comparable with the clock period, and for shorter time intervals. Under such hypothesis, dynamics of observables in the interval (σ_A, σ_B) is approximated by the discrete-valued equations:

$$x_\rho(T_i) \cong x_\rho(\sigma_i \pm \epsilon) = x_\rho(\sigma_i) \pm O_{x\rho}[\sigma_i, \epsilon] \quad (15)$$

$$p_\rho(T_i) \cong p_\rho(\sigma_i \pm \epsilon) = p_\rho(\sigma_i) \pm O_{p\rho}[\sigma_i, \epsilon] \quad (16)$$

where $\rho = 1, 2, 3$, and $O_{x\rho}[\sigma, \epsilon]$ and $O_{p\rho}[\sigma, \epsilon]$ are higher order quantities in ϵ . Such equations provide the bridge between natural time parameter of Hamiltonian timeless formalism, and the experimentally defined clock time experienced by observers.

7 Conclusion

I have shown that, despite time is not a fundamental quantity in physics and it can be only effectively defined to describe systems involving macroscopic objects, it is possible to provide the connection between fundamental timelessness of physics in the microscopic domain, and clock time of metrology. Since clock time is by definition fundamentally discrete and it depends on the specific fabrication of the clock, a measurement of time below one cycle (period) is meaningless. It implies for example that Planck time scale is an extrapolation not grounded on experimental evidence, consisting of an extension of the concept of clock time beyond its field of definition. On the other hand, an explicit Hamiltonian framework, entirely developed without the concept of time, can be defined. To explain and restore the usefulness of clocks, the time and frequency metrology is mapped through equations of motion expressed as a function of the parameter obtained in the timeless framework used as time. It is made possible by defining cyclic subsystems capable to account for the discrete definition of clock time. Such framework accounts for the timelessness of nature at a fundamental level and it explains how clock time can be defined in metrology and experiments, consistently with the dynamics described by relations between variables and the Hamiltonian parametrization.

References

1. Prati E (2016) Atomic scale nanoelectronics for quantum neuromorphic devices: comparing different materials. *Int J Nanotech* 13(7):509–523
2. Barbour JB (1994) The timelessness of quantum gravity: II. The appearance of dynamics in static configurations *Class Quantum Gravity* 11:2875, 2898
3. Rovelli C (2006) Quantum gravity. Cambridge University Press, Cambridge
4. Callender C (2010) Is Time an Illusion? *Sci Am* 302:58–65
5. Prati E (2011) Generalized clocks in timeless canonical formalism. *J Phys: Conf Ser* 306:012013
6. Zenczykowski P (2009) The Clifford algebra of nonrelativistic phase space and the concept of mass. *J Phys A: Math Theor* 42:045204
7. De Witt BS (1967) Quantum theory of gravity. I *Phys Rev* 160:1113
8. Kiehn RM (2003) Thermodynamic irreversibility and the arrow of time. In: Buccheri R et al (eds) *The nature of time: geometry, physics and perception*. Springer, Dordrecht, pp 243–250
9. Prati E (2013) Speakable and unspeakable in physics of time. *EPJ Web Conf* 58:01019
10. Diddams et al (2001) An optical clock based on a single trapped $^{199}\text{Hg}^+$ ion. *Science* 293:825
11. Lindner et al (2005) Attosecond double-slit experiment. *Phys Rev Lett* 95:040401
12. Palacios A (2009) Two-electron time-delay interference in atomic double ionization by attosecond pulses. *Phys Rev Lett* 103:253001
13. Niikura H (2002) Sub-laser-cycle electron pulses for probing molecular dynamics. *Nature* 417:917–922
14. Linden HBV et al (2001) Multiphonon processes studies in modern optics, vol 8. Cambridge University Press, Cambridge, p 25
15. Salieres P et al (2002) Feynman's path-integral approach for intense-laser-atom interactions. *Science* 292:902

16. Sydenham PH, Thorn R (2005) Handbook of measuring system design. Definition of time, time interval and frequency. Wiley, p 1341
17. Landau LD, Lifshitz EM, Mechanics, vol 1
18. Arnold VI (1989) Mathematical methods of classical mechanics. Chap IX, 2ed. Springer, Berlin
19. Barbour JB (1994) The timelessness of quantum gravity: II. The appearance of dynamics in static configurations. *Class Quantum Gravity* 11:2898
20. Levine (1999) Invited Review Article: The statistical modeling of atomic clocks and the design of time scales. *Rev Sci Instrum* 70(6):2567
21. Heavner P, Jefferts SR, Donley EA, Shirley JH, Parker TE (2005) NIST-F1: recent improvements and accuracy evaluations. *Metrologia* 42(5):411

Chapter 3

Electric and Magnetic Fields Inside Neurons and Their Impact upon the Cytoskeletal Microtubules



Danko D. Georgiev

1 Introduction

The brain consists of electrically excitable nerve cells called neurons [1]. Neurons utilize electric signals to input sensory information, to process or integrate the sensory information with previously stored memories, and to output motor information for execution of muscle action [2]. All of these processes were extensively characterized down to the level of individual membrane-bound protein ion channels with their respective ionic fluxes, which are subject to intensive research by molecular neuroscience [3–7]. The electric currents are relevant stimuli for eliciting conscious experiences, such as recollections of past events, [8–10] and are used to restore the visual image perception in blind patients via implanted in the occipital cortex electrodes connected to bionic eye-camera [11]. There are some speculations, however, that the electric activity of neurons may not provide the full picture of the information flow in the nervous system, instead intracellular microtubules, which are an integral part of the neuronal cytoskeleton, are supposed to be somehow involved in the processing of sensory information and provide the seat of consciousness [12]. In this work, we assess whether microtubules are capable of inputting sensory information carried by the membrane electric signals that enter into the brain cortex, followed by processing of this information to control the electric signals that are eventually sent to α -motor neurons in the spinal cord in view of commanding skeletal muscle contraction.

Different scenarios for interaction between the electromagnetic field and the cytoskeletal microtubules have been put forward such as the ferroelectric model of microtubules [13–19], the Penrose–Hameroff orchestrated objective reduction (Orch OR) model [12], and Porter’s topological anyon microtubule model [20, 21]. Careful consideration of the electromagnetic field strength in neurons reveals, however,

D. D. Georgiev (✉)

Institute for Advanced Study, 30 Vasilaki Papadopulu Str., Varna 9010, Bulgaria

e-mail: danko.georgiev@mail.bg

© The Editor(s) (if applicable) and The Author(s), under exclusive license

to Springer Nature Singapore Pte Ltd. 2021

A. Bandyopadhyay and K. Ray (eds.), *Rhythmic Oscillations in Proteins to Human Cognition, Studies in Rhythm Engineering*,

https://doi.org/10.1007/978-981-15-7253-1_3

that none of these models is biologically feasible. First, the ferroelectric microtubule model requires extremely high electric field strength in order to polarize microtubules and does not take into account that the suggested $\alpha \leftrightarrow \beta$ electron hopping leads to conformational transitions that may disassemble the microtubule. Second, the same $\alpha \leftrightarrow \beta$ electron hopping problem is found in the Orch OR model where additionally it is required that the microtubules are shielded from the surrounding electromagnetic field for prolonged 25 ms periods of time in order to prevent quantum decoherence. Third, Porter's model predicting topologically stabilized quantum states and anyons require extreme magnetic field strength for the generation of putative quantum Hall effect in the two-dimensional cylindrical microtubule wall. This latter idea faces serious problems due to the minute magnetic field strength of $\approx 10^{-9}$ T generated by individual electric spikes and the apparent necessity of temperatures near absolute zero for sustaining the quantum Hall effect. In addition, there is no biologically known mechanism by which the tubulin conformations inside microtubules could control the electric spiking of neurons in order to output motor information to skeletal muscles. Taken together the presented results suggest that any claims for possible microtubule processing of information should be viewed with caution.

2 Neurobiology

2.1 Brain Cortex Structure

The brain cortex is the anatomical seat of consciousness [2, 22, 23]. All sensory stimuli are consciously experienced only when they reach the brain cortex and not before that, as it can be determined by clinical data from patients with neurological deficits due to trauma or cerebrovascular accidents [24].

The evolutionary development of the neocortex could be outlined as follows [25]: Amphibians lack a cortical formation. Reptiles have a simple three-layered cortex in their pallium [26]. Mammals have a six-layered neocortex, which is flanked by two three-layered cortical structures, namely the prepiriform cortex and the hippocampus. The neocortex is small in marsupials and insectivores, but attains amazing dimensions in anthropoids (simians, monkeys, and apes) and cetaceans (whales and dolphins).

Cortical neurons can be allocated to one of two basic categories: pyramidal and non-pyramidal cells. The pyramidal neurons form the principal excitatory units in the cortical circuitry, accounting for at least 70% of the total cortical population. The evolutionary development of the pyramidal neurons can be traced from simple, extraverted neurons in the amphibian pallium, via pyramid-like neurons in the reptilian cortex to the fully developed neocortical pyramidal neurons denoted by Ramón y Cajal as “psychic cells” [27].

The pyramidal neurons constitute the sole output and the largest input system of the neocortex [25]. The neurons from different layers communicate via axo-dendritic synapses, which are chemical informational junctions that transfer information via

neuromediator molecules. The neuromediator molecules released from the axonal terminal under membrane depolarization (due to incoming electric impulse) enter into the synaptic cleft where they diffuse to bind postsynaptic (dendritic) ligand-gated ion channels, modulate their ionic conductivity, and generate again electric impulses. Thus, electric processes are essential in neuronal functioning, including transfer and processing of information.

2.2 *Electric Sensory Input to the Cortex*

Experiments with implanting of electrodes directly into the brain cortex of human patients suggest that the brain cortex is the seat of conscious experience. In a ground-breaking surgical procedure, William Dobelle was able to restore vision of a blind man using electrodes implanted into the occipital cortex and connected to a tiny charge-coupled device (CCD) camera mounted on a pair of glasses [11]. Although the patient did not see in the conventional sense, he was able to make out the outlines of objects, read large letters or numbers on a contrasting background, and use direct digital input to operate a computer.

The patient, who was identified only as Jerry, has been blind after a blow to the head since age of 36 in 1973. He then volunteered for the study and got a brain implant at the age of 41 in 1978. There has been no infection or rejection of the implant. At age of 62 in 1999 Jerry was enabled to use the implant as a primitive visual system supported by newly developed computer software [11]. Jerry's bionic eye consisting of the CCD camera sent the captured images for processing by a small computer, carried on his hip. The computer system was upgraded to use a 233 MHz processor, 32 MB of RAM, and a 4 GB hard disk to detect edges using Sobel filters and black/white reversal. The processed image signal was then relayed to an array of 68 small platinum electrodes on the surface of Jerry's brain, through wires entering his skull behind his right ear. The electrodes stimulated cortical neurons making Jerry perceive dots of light called phosphenes. Through the experience of white phosphenes on a black background, Jerry was able to walk across a room, pull a ski hat off a wall and correctly put the hat on the head of a mannequin. Jerry's bionic vision even allowed him to navigate in unfamiliar environments including the New York City subway system.

Another functionally relevant clinical observation is that lesions in the primary visual cortex may lead to cortical amaurosis—a condition with decreased visual acuity or even blindness, but with normal pupillary reactions, that is although there is subcortical neural processing of visual information, the visual image is not consciously experienced because it does not enter into the brain cortex [2].

Taken together, the above clinical results imply that the relevant sensory stimulus for the cortical neurons is the transmembrane potential, which needs to be converted into specific conformational states if microtubules are indeed relevant for consciousness.

2.3 Neuronal Morphology

The morphology of pyramidal neurons resembles a tree (Fig. 1). Each pyramidal neuron has a cell body called soma and two types of projections: apical or basal dendrites that input electric information and an axon branching into axonal collaterals that output information via neuromediator release (exocytosis) upon electric firing (membrane depolarization). When cortical pyramidal cells are stained using immunohistochemical methods, microscopic observations reveal that long apical dendrites are extended toward the superficial cortical layer and basal dendrites are

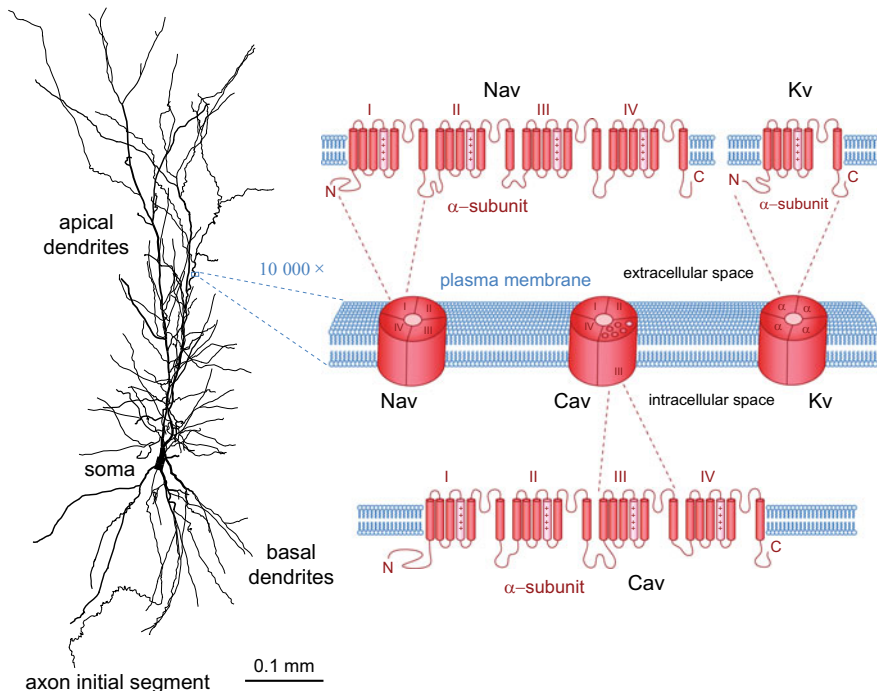


Fig. 1 Morphology of a hippocampal CA1 pyramidal neuron from a 1-month-old male Wistar rat (NeuroMorpho.org NMO_49823) with structural representation of voltage-gated ion channels in a patch of the electrically excitable plasma membrane. The pyramidal neuron receives excitatory or inhibitory synaptic inputs applied at the apical and basal dendrites or the soma. If the summated synaptic electric currents depolarize the axon initial segment over the threshold value of -55 mV , the neuron discharges an action potential, which propagates down the axon and initiates the release of neurotransmitter from terminal axonal boutons onto target neurons. The electric activity of the neuron is mainly driven by ionic fluxes through sodium (Nav), potassium (Kv), and calcium (Cav) voltage-gated ion channels. Individual Nav and Cav channels are composed of α -subunits with four protein domains (I–IV) each, whereas Kv channels have disjoint protein domains into separate α -subunits. Each transmembrane channel domain is formed by six α helices bundled in parallel. The electrically charged voltage sensor that gates the ion channel is located within the 4th α -helix of each domain. Modified from Ref. [28]

extended in all directions in the area adjacent to the soma. Dendrites can be thought of as extensions of the cell body with maximal length $\approx 1\text{--}2$ mm in the largest neurons [29], which provide increased surface area at much lower cell volumes. For example, the dendrites of cat motor neurons have $3.7 \times 10^5 \mu\text{m}^2$ of surface area while occupying only $3 \times 10^5 \mu\text{m}^3$ [30]. To provide an equivalent surface, a spherical cell body should be 343 μm in diameter and would have a volume of $2 \times 10^7 \mu\text{m}^3$. The fact that $\approx 80\%$ of the surface area of proximal dendrites of motor neurons are covered with synapses [31] supports the conclusion that the increased surface area provided by dendrites is indeed valuable for increasing the number of inputs to a neuron.

Dendrites in rat CA1 pyramidal neuron are characterized by different parameters depending on the dendritic type [32]. Typically, there are five basal dendrites whose proximal diameter is 1 μm , distal diameter is 0.5–1 μm , and dendrite extent is 130 μm with 30 branch points. There is a single apical dendrite that extends in stratum radiatum whose proximal diameter is 3 μm , distal diameter is 0.25–1 μm , and dendrite extent is 110 μm with 30 branch points. Additionally, in stratum moleculare there are another 15 branch points of dendrites with distal diameter of 0.25–1 μm and dendrite extent of 500 μm [32].

Spines are synaptic specializations of dendrites of pyramidal neurons. Simple spines are protrusions from the dendrite of usually no more than 2 μm , often ending in a bulbous head attached to the dendrite by a narrow stalk or neck [32]. Spine heads usually have diameter $\approx 0.6 \mu\text{m}$; when this diameter is exceeded the spines are referred to as mushroom spines. The spines are usually pedunculated (that is they have narrow neck) but sessile spines with no neck are also known. For a single CA1 pyramidal neuron, the total spine length is 0.2–2 μm , neck diameter is 0.04–0.5 μm , neck length is 0.1–2 μm , total spine volume is 0.004–0.6 μm^3 , total surface area of a single spine is 0.1–4 μm^2 , and the postsynaptic density area is 0.01–0.5 μm^2 [32].

Neurons are classified as spiny, sparsely spiny, and non-spiny (or smooth) according to the density of simple spines on their dendrites [33]. This classification is complicated by the fact that widely different spine densities may be exhibited by different dendrites of a single neuron [34]. Moreover, the spine densities can vary widely even along the length of a single dendritic segment [32].

The cytoskeleton of neural projections (dendrites or axons) is composed of microtubules, neurofilaments, and actin filaments. Microtubules are long, hollow cylindrical structures, approximately 25 nm in diameter, oriented to the longitudinal axis of the neural projection. In regions of the dendrite that lack large organelles, microtubules are spaced 80–200 nm apart in a regular array at a density of $50\text{--}150 \mu\text{m}^{-2}$ [32]. In axons, microtubules are packed even tighter. For an axon with length of 56 μm , the total microtubule length measured by electron microscopy was 5750 μm [35], which results in microtubule density of $130\text{--}160 \mu\text{m}^{-2}$ for varying axon diameter in the range 0.9–1.0 μm (where smaller diameter results in higher density) [36]. Microtubules serve as the railroad tracks of the cell for transport of mitochondria and other organelles by motor proteins [37].

The cell body (soma) is the trophic center of the neuron and in CA1 neuron has diameter $\approx 21 \mu\text{m}$. The soma contains the nucleus (with DNA genes) and the principal protein synthetic machinery of the neuron including rough endoplasmic

reticulum and polyribosomes. Basic dyes such as cresyl violet stain heavily neuronal cell bodies due to the large concentrations of ribosomes [38]. The clumps of heavily stained material by cresyl violet are called Nissl bodies, which represent the stacks of rough endoplasmic reticulum visible at the electron microscopic level. The intensity of Nissl staining is an indication of the protein synthetic activity of the neuron. Nissl staining is decreased under conditions that lead to decreases in protein synthesis such as during axotomy (when the axon of the neuron is cut or otherwise severed from the soma).

Axons lack the ability to synthesize protein, because they do not contain ribosomes or significant amounts of messenger RNA (mRNA). Consequently, axons depend entirely on proteins produced in the cell body, which are transported into the axon by motor proteins walking over the microtubules. Dendrites do contain small amounts of both mRNA and ribosomes, and this protein synthetic machinery could play an important role in synaptic plasticity and memory formation [39]. Nevertheless, most of the proteins that are located in dendrites are also transported from the cell body.

The axon is the output projection of the neuron that branches into axonal collaterals that reach distant dendrites of target neurons. Study of CA3→CA1 axo-dendritic synapses shows that the synapses are formed at $2.7 \mu\text{m}$ intervals along the axons, the axonal shafts are $1.4 \pm 1.2 \mu\text{m}$ long and the varicosities have oblong form and length of $1.1 \pm 0.7 \mu\text{m}$ [40]. Axo-axonal electric synapses known as gap junctions could also be present and may account for ultrafast (200Hz) signaling between neurons [41].

2.4 *The Neuronal Cytoskeleton*

The neuronal cytoskeleton is a protein lattice composed of actin filaments, intermediary filaments and microtubules. Microtubules are hollow cylindrical tubes with outer diameter of 25 nm and inner diameter of 14 nm. The microtubule walls are polymerized from two globular protein monomers known as α and β tubulin, which bind into a stable structural unit referred to as $\alpha\beta$ tubulin dimer [42]. The $\alpha\beta$ tubulin dimers assemble into longitudinal strings called protofilaments. Lateral alignment of 13 parallel protofilaments forms the complete microtubule [43]. The α and β tubulin monomers are similar in shape and oriented in the same way within the protofilaments. In the polymerized state of the microtubule, one monomer consists of $\approx 40\%$ α -helix, $\approx 31\%$ β -sheet and $\approx 29\%$ random coil. The size of each monomer is about $4 \text{ nm} \times 4 \text{ nm} \times 4 \text{ nm}$, and its mass is contributed by about 500 amino acids [44]. Each $\alpha\beta$ tubulin dimer behaves like an electric dipole, with the negative end oriented toward the α monomer and the positive end toward the β monomer. The dipole character of the dimer originates from the 18 Ca^{2+} ions bound within each β monomer. An equal number of negative charges required for the electrostatic balance are localized near the neighboring α monomer [45].

The cytoplasmic organization of neurons is regulated by cytoskeletal microtubules, which may undergo assembly or disassembly. Microtubule assembly consists of two stages: nucleation and elongation.

The nucleation of microtubules requires α and β tubulins, Mg^{2+} ions and guanosine triphosphate (GTP). This stage is relatively slow until the microtubule is initially formed. In a solution of purified tubulin subunits, microtubule nucleation can occur spontaneously or it can be stimulated by addition of seeds [43]. The crucial event in microtubule nucleation appears to be the formation of a two-dimensional polymer, which grows to form the microtubule wall. Noteworthy, a third type of tubulin subunit called γ tubulin is also important for nucleation [43]. The γ tubulin forms a cap-like ring with 13-fold microtubule symmetry that extends into a microtubule by direct assembly of $\alpha\beta$ tubulin dimers [46].

The elongation of microtubules proceeds much more rapidly. The $\alpha\beta$ tubulin dimers attach to other dimers to elongate the growing protofilaments. Each $\alpha\beta$ dimer carries two GTP molecules: one attached to α tubulin and one attached to β tubulin. The GTP bound to α tubulin is occluded by the adjacent β tubulin and cannot be further hydrolyzed [47]. However, the GTP that is bound to β tubulin could be hydrolyzed. When an $\alpha\beta$ tubulin dimer is added to the microtubule, the GTP of preceding β tubulin is hydrolyzed to GDP and the released energy is stored as an elastic strain in the microtubule wall [48]. The microtubule wall is closed by lateral assembly of 13 protofilaments. The tubulin assembly into microtubules proceeds optimally at a temperature of 37 °C, but it is halted at 4 °C.

In the cell, microtubules are nucleated from a microtubule organizing center referred to as the centrosome, which is built from two centrioles arranged in a T-shape [49]. The centrosomal microtubules are unstable and undergo intense dynamics. Microtubules are polar with a plus end (fast growing) and a minus end (slow growing). Usually the minus end is the anchor point in the centrosome. The plus end is capped by a single layer of GTP molecules, which may be hydrolyzed to GDP [50]. Hydrolysis is not necessary, however, for microtubule assembly to proceed. Experiments have shown that microtubules will form normally with a non-hydrolyzable GTP analog molecules attached, however they will not be able to depolymerize [51–53].

Much of the dynamic nature of microtubules is attributed to regulated growth and shrinkage of the polymer plus ends (dynamic instability) or to the addition of subunits at the plus end while they are simultaneously lost from the minus end (treadmilling). Noteworthy, microtubule severing in neurons by specific enzyme called katanin [54] is important for the production of non-centrosomal microtubules, which are subsequently integrated into the cytoskeleton of axons or dendrites. In fact, neurons require a large number of non-centrosomal microtubules for the growth and maintenance of their cable-like axonal or dendritic projections [55]. For example, injection of an anti-katanin antibody into neurons leads to an accumulation of centrosomal microtubules and a loss of neuronal projections, which indicates that centrosomal katanin is important for the production of non-centrosomal microtubules primarily through

severing of the microtubules near the centrosome. In neurons, the microtubule minus ends might be capped, which would enhance the stability of centrosome-free microtubules [56].

Computational study of microtubules has revealed a positively charged core sandwiched between two negatively charged inner and outer surfaces [57]. This result was used to argue in favor of possible anyon formation within the microtubule inner or outer two-dimensional electron layers. Anyons have been found in nature and were speculated to be harnessed by microtubules [20, 21]. Anyons are two-dimensional quasiparticles with partial spin made out of groups of electrons, which are suitable candidates for fault-tolerant quantum computation [58, 59]. According to Porter [20], there are four ways in which the microtubule has what it takes to be an anyonic medium: it is two-dimensional, which is necessary for anyons; it is a cylinder rather than a plane, which should turn useless abelian anyons into useful nonabelian anyons; it is a hexagonal array of qubits, which could form domain walls and anyonic defects; and the Fibonacci numbers define the geometry of the microtubule, hence quantum computation with anyons could make use of the golden ratio that is embedded in the Fibonacci numbers. The topological anyon model, however, critically depends on the magnetic field strength and putative quantum Hall effect in neurons. To assess whether the neuronal microtubules could act as subneuronal processors of information (and possibly quantum computers) [12–17, 20, 21, 60, 61], next we will focus our attention on the interaction between the microtubules and the local electromagnetic field.

3 Electrodynamics

3.1 Right-Handed Coordinate Systems

For proper assessment of the electromagnetic field structure, it is appropriate to be acquainted with the basic physical postulates in electrodynamics [62]. Physical quantities could be represented mathematically by scalars or vectors. Scalars are quantities, which are fully described by a magnitude alone. Vectors are quantities, which are fully described by both a magnitude and a direction [63]. Because, we will work mostly with vectors it would be helpful to define what is a right-handed coordinate system, what is a positive direction of a given contour ℓ , and what is a positive normal to a given surface s (Fig. 2).

Definition 1 Right-handed coordinate system O_{xyz} is a system in which if the z -axis points toward your face the counterclockwise rotation of the O_x axis to the O_y axis has the shortest possible path.

Definition 2 The positive direction of the contour ℓ is the direction in which the rotation of x -axis to the y -axis has the shortest possible path.

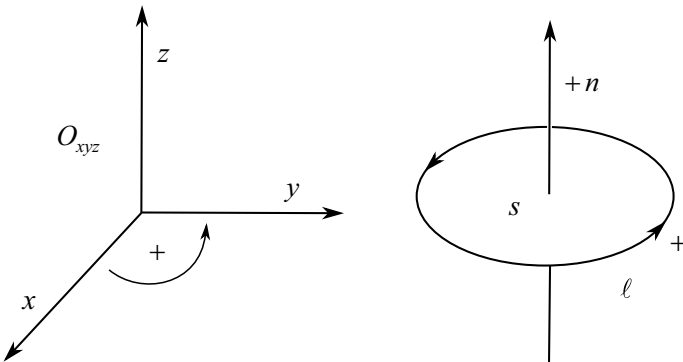


Fig. 2 Right-handed coordinate system O_{xyz} , positive direction of contour ℓ , and positive normal $+n$ of a surface s

Definition 3 The positive normal $+n$ of given surface s closed by contour ℓ is collinear with the O_z axis of right-handed coordinate system O_{xyz} whose x - and y -axis lie in the plane of the surface.

3.2 Vectors

Multiplication of vectors could be performed in several different ways. Two physically useful definitions of vector multiplication include the dot product and the cross product.

Definition 4 The dot product of two vectors is the magnitude of one vector times the projection of the other along the first. Since this product has magnitude only, it is also known as the scalar product

$$\vec{A} \cdot \vec{B} = AB \cos \theta \quad (1)$$

where θ is the angle between the two vectors.

Definition 5 The cross product of two vectors is the area of the parallelogram between them. Since this product has magnitude and direction, it is also known as the vector product

$$\vec{A} \times \vec{B} = AB \sin \theta \vec{n} \quad (2)$$

where the vector \vec{n} is a unit vector perpendicular to the plane formed by the two vectors. The direction of \vec{n} is determined by the right-hand rule.

Definition 6 The right-hand rule states that if you hold your right hand out flat with your fingers pointing in the direction of the first vector and orient your palm so that

you can fold your fingers in the direction of the second vector, then your thumb will point in the direction of the cross product.

3.3 Electric Field

The electromagnetic field is composed from electric and magnetic field. The electric field could be described via vector field of electric intensity \vec{E} . The electric intensity is defined as the ratio of the electric force \vec{F}_E acting upon charged body and the charge q of the body

$$\vec{E} = \lim_{\Delta q \rightarrow 0} \frac{\Delta \vec{F}_E}{\Delta q} = \frac{d\vec{F}_E}{dq} \quad (3)$$

The electric field is a potential field, that is the work W along a closed contour ℓ is zero

$$W_\ell = \oint_\ell dW = \oint_\ell \vec{F}_E \cdot d\vec{l} = 0 \quad (4)$$

where l is the length of the contour ℓ [63].

Every point from the electric field has an electric potential V defined with the specific (for unit charge) work needed to carry a charge from this point to infinity. The electric potential of point c of given electric field \vec{E} has potential V defined by

$$V = \int_c^\infty \vec{E} \cdot d\vec{l} + V_\infty \quad (5)$$

where the potential at infinity is $V_\infty = 0$. The electric potential difference between two points x_1 and x_2 defines voltage ΔV (synonyms: electric potential, electromotive force, potential, potential difference, potential drop)

$$\Delta V = \int_{V_1}^{V_2} dV = \int_{x_1}^{x_2} \vec{E} \cdot d\vec{l} \quad (6)$$

The link between the electric intensity \vec{E} and the gradient of the voltage ∇V is

$$\vec{E} = -\nabla V \quad (7)$$

where the gradient is a vector operator denoted ∇ called Del or nabla [64–66]

$$\nabla f \equiv \text{grad}(f) \quad (8)$$

The gradient vector is pointing toward the higher values of V , with magnitude equal to the rate of change of values. The direction of ∇f is the orientation in which the directional derivative has the largest value and $|\nabla f|$ is the value of that directional

derivative. The directional derivative $\nabla_u f(x_0, y_0, z_0)$ is the rate at which the function $f(x, y, z)$ changes at a point (x_0, y_0, z_0) in the direction u

$$\nabla_u f \equiv \nabla f \frac{u}{|u|} = \lim_{h \rightarrow 0} \frac{f(x + h\vec{u}) - f(x)}{h} \quad (9)$$

where \vec{u} is a unit vector.

Another vector that describes the electric field is the vector of electric induction \vec{D} , which for isotropic dielectric is defined as

$$\vec{D} = \varepsilon \cdot \vec{E} \quad (10)$$

where ε is the electric permittivity of the dielectric. The electric permittivity of the vacuum is $\varepsilon_0 \approx 8.854 \times 10^{-12} \text{ F m}^{-1}$.

3.4 Physical and Vector Fluxes

Maxwell's law for the electric flux Φ_D of the vector of electric induction \vec{D} states that Φ_D through any closed surface s is equal to the charge q exciting the electric field that is located in the space region enclosed by s . This is expressed mathematically as

$$\Phi_D = \iint_s \vec{D} \cdot d\vec{s} = q \quad (11)$$

If the normal $+n$ of the surface s and the vector \vec{D} form an angle θ (Fig. 3), the flux Φ_D is defined as

$$\Phi_D = \iint_s \vec{D} \cdot d\vec{s} = \vec{D} \cdot \vec{s} = D s \cos \theta \quad (12)$$

$$d\Phi_D = \vec{D} \cdot d\vec{s} = D \cdot ds \cos \theta \quad (13)$$

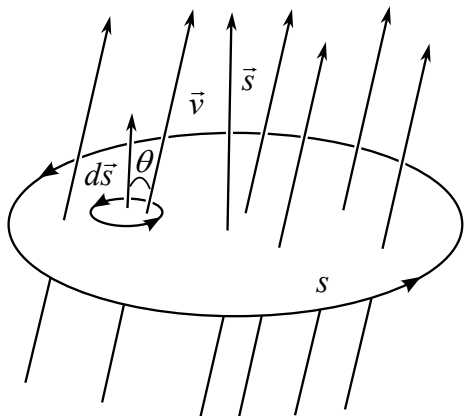
From Maxwell's law we could derive Gauss' theorem

$$\Phi_E = \iint_s \vec{E} \cdot d\vec{s} = \frac{q}{\varepsilon} \quad (14)$$

where Φ_E is the flux of the vector of electric intensity \vec{E} through the closed surface s . In the case when the full electric flux Φ_D is concentrated only in small region Δs of the closed surface s , we could approximate

$$\Phi_D = \iint_{\Delta s} \vec{D} \cdot d\vec{s} = q \quad (15)$$

Fig. 3 Flux Φ_D of the vector of electric induction \vec{D} through surface s . If the surface s is closed then $\Phi_D = q$



In other cases when the electric field is not concentrated in such small region but we are interested to know the partial electric flux $\Delta\Phi_D$ through partial surface Δs for which is responsible electric charge Δq , it is appropriate to use the formula

$$\Delta\Phi_D = \iint_{\Delta s} \vec{D} \cdot d\vec{s} = \Delta q \quad (16)$$

3.5 Electric Current

The electric current i representing the flux of physical charges can be defined using both scalar and vector quantities

$$i = \lim_{\Delta t \rightarrow 0} \frac{\Delta q}{\Delta t} = \frac{dq}{dt} = \iint_s \vec{J} \cdot d\vec{s} = \Phi_J \quad (17)$$

where \vec{J} is the density of the electric current.

As a scalar quantity, the current density J is defined as

$$J = \lim_{\Delta s_n \rightarrow 0} \frac{\Delta i}{\Delta s_n} = \frac{di}{ds_n} \quad (18)$$

where s_n is the cross section of the current flux Φ_J . Usually with i is denoted the flow of positive charges. The flow of negative charges could be replaced with positive current with equal magnitude but opposite direction. To underline the nature of the charges in the current, vectors with indices \vec{i}_+ or \vec{i}_- could be used in which the direction of the vectors coincides with the direction of charge motion.

Given a cable with current i flowing through it, Ohm's law states that the current i is proportional to the voltage V and conductance G and inversely proportional to the resistance R as follows

$$i = \frac{V}{R} = VG \quad (19)$$

$$R = \rho \frac{l}{s} \quad (20)$$

$$G = \gamma \frac{s}{l} \quad (21)$$

where ρ is the specific resistance for the media, γ is the specific conductance, l is the length of the cable, and s is its cross section.

3.6 Magnetic Field

The magnetic field is described by the vector of magnetic induction \vec{B} (also known as: magnetic field strength or magnetic flux density) that is perpendicular to the vector of electric intensity \vec{E} . The magnetic field acts only on moving charges and manifests itself via electromagnetic force \vec{F}_M acting upon flowing currents inside the region where the magnetic field is distributed. Laplace's law states that the electromagnetic force \vec{F}_M acting upon cable with electric current $i \cdot \vec{l}$, which is inside magnetic field with magnetic induction \vec{B} , is equal to the vector product of the two vectors

$$\vec{F}_M = i \cdot \vec{l} \times \vec{B} \quad (22)$$

$$d\vec{F}_M = i \cdot d\vec{l} \times \vec{B} \quad (23)$$

For a magnetic dipole, the direction of the vector of magnetic induction is from the south pole (S) to the north pole (N) inside the dipole and from N to S outside the dipole.

The magnetic field can be excited either via changes in existing electric field \vec{E} or by flowing electric current i .

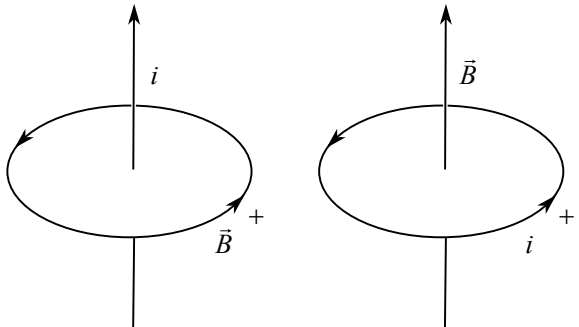
In the first case, the magnetic induction \vec{B} is defined by Ampere's law

$$\oint_{\ell} \vec{B} \cdot d\vec{l} = \mu_0 \varepsilon_0 \frac{d\Phi_E}{dt} \quad (24)$$

In the second case, if we have a cable with current i it will generate magnetic field with induction \vec{B} whose lines have the direction of rotation of right-handed screw when it penetrates in the direction of the current i (Fig. 4)

$$\oint_{\ell} \vec{B} \cdot d\vec{l} = \mu_0 i \quad (25)$$

Fig. 4 Direction of the lines of magnetic induction \vec{B} around axis with current i (left) and along the axis of a contour with current i (right). The current i by convention denotes the flux of positive charges



The composite electromagnetic field manifests itself with a resultant electromagnetic force \vec{F}_{EM} defined by the Coulomb–Lorentz formula

$$\vec{F}_{EM} = q(\vec{E} + \vec{v}_i \times \vec{B}) \quad (26)$$

where \vec{v}_i is the velocity of the charge q given by

$$\vec{v}_i = \frac{d\vec{l}}{dt} = \frac{dq \cdot d\vec{l}}{dt \cdot dq} = \frac{i \cdot d\vec{l}}{dq} \quad (27)$$

For a magnetically isotropic media, we could define another vector describing the magnetic field called magnetic intensity \vec{H} given by

$$\vec{H} = \frac{\vec{B}}{\mu} \quad (28)$$

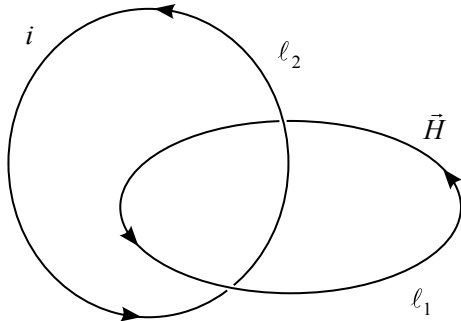
where μ is the magnetic permeability of the media. The magnetic permeability of the vacuum is $\mu_0 \approx 4\pi 10^{-7} \text{ H m}^{-1}$.

The circulation of the vector of magnetic intensity \vec{H} along closed contour ℓ_1 with length l , which interweaves contour ℓ_2 with flowing current i through it (Fig. 5), is given by

$$\oint_{\ell_1} \vec{H} \cdot d\vec{l} = i \quad (29)$$

The magnetic field is a non-potential field because the lines of magnetic field intensity \vec{H} are closed and always interweave the contour with the excitatory current i . The circulation of the vector \vec{H} will be zero only along those closed contours that do not interweave any current i .

Fig. 5 Circulation of the vector of magnetic intensity \vec{H} along the closed contour ℓ_1 equals the current i flowing through the interwoven contour ℓ_2



3.7 Electromagnetic Induction

The flux Φ_B of the vector of magnetic induction \vec{B} is given by

$$\Phi_B = \iint_S \vec{B} \cdot d\vec{s} \quad (30)$$

The change in the magnetic flux generates induced voltage V_Φ according to Lenz's law

$$V_\Phi = -\frac{d\Phi_B}{dt} \quad (31)$$

$$\oint_{\ell} \vec{E} \cdot d\vec{l} = -\frac{d\Phi_B}{dt} \quad (32)$$

Thus, Lenz's law states that there will be induced current if there is a static cable inside a changing magnetic field

$$V_\Phi = -\iint_S \frac{\partial \vec{B}}{\partial t} \cdot d\vec{s} \quad (33)$$

or if the cable is moving inside a static magnetic field

$$V_\Phi = -[\vec{v} \times \vec{B}] \cdot \vec{l} \quad (34)$$

The full magnetic flux Φ_L of the self-induced magnetic field \vec{B} by contour with current i is called self-induced flux. The self-induced flux is a linear function of the current

$$\Phi_L = L \cdot i \quad (35)$$

where L is a scalar called self-inductance, which depends only on the magnetic permittivity μ of the media and the geometric parameters that determine the size and the shape of the contour.

Self-induced voltage V_L appears in an electric cable whenever there is a change of the current i and this self-induced voltage opposes the change of current

$$V_L = -L \cdot \frac{di}{dt} \quad (36)$$

3.8 Maxwell's Equations

The basic principles of electromagnetism could be summarized in four equations known as Maxwell's equations. These equations were originally derived in 1861 by Maxwell in an equivalent form, but were later recast in modern vector notation by Heaviside in 1884.

3.8.1 Integral Form in the Absence of Magnetic or Polarizable Media

Gauss' law for electricity

$$\oint\!\oint \vec{E} \cdot d\vec{s} = \frac{q}{\varepsilon_0} \quad (37)$$

Gauss' law for magnetism

$$\oint\!\oint \vec{B} \cdot d\vec{s} = 0 \quad (38)$$

Faraday's law of induction

$$\oint \vec{E} \cdot d\vec{l} = -\frac{d\Phi_B}{dt} \quad (39)$$

Ampere's law

$$\oint \vec{B} \cdot d\vec{l} = \mu_0 i + \frac{1}{c^2} \frac{\partial}{\partial t} \oint \vec{E} \cdot d\vec{l} \quad (40)$$

3.8.2 Differential Form in the Absence of Magnetic or Polarizable Media

Gauss' law for electricity

$$\nabla \cdot \vec{E} = \frac{\rho}{\varepsilon_0} = 4\pi k\rho \quad (41)$$

where ρ is the charge density and $k = \frac{1}{4\pi\varepsilon_0}$ is Coulomb's constant.

Gauss' law for magnetism

$$\nabla \cdot B = 0 \quad (42)$$

Faraday's law of induction

$$\nabla \times E = -\frac{\partial B}{\partial t} \quad (43)$$

Ampere's law

$$\nabla \times B = \frac{J}{\varepsilon_0 c^2} + \frac{1}{c^2} \frac{\partial E}{\partial t} \quad (44)$$

3.8.3 Differential Form with Magnetic And/or Polarizable Media

Gauss' law for electricity

$$\nabla \cdot D = \rho \quad (45)$$

$$D = \varepsilon_0 E + P \quad (46)$$

where P denotes the polarization. For free space, we have $D = \varepsilon_0 \cdot E$ and for isotropic linear dielectric $D = \varepsilon \cdot E$. In the absence of an electric field, polar molecules are randomly oriented inside a dielectric material. Application of an external electric field, however, will polarize the dielectric material by orienting the dipole moments of polar molecules. Consequently, the presence of dielectric material between two charged plates will decrease the effective electric field between the plates.

Gauss' law for magnetism

$$\nabla \cdot B = 0 \quad (47)$$

Faraday's law of induction

$$\nabla \times E = -\frac{\partial B}{\partial t} \quad (48)$$

Ampere's law

$$\nabla \times H = J + \frac{\partial D}{\partial t} \quad (49)$$

$$B = \mu_0(H + M) \quad (50)$$

where M denotes the magnetization. For free space, we have $B = \mu_0 \cdot H$ and for isotropic linear magnetic medium $B = \mu \cdot H$. In the absence of a magnetic field, the orbital motion of electrons in diamagnetic materials generates randomly oriented atomic current loops with their corresponding magnetic fields. Application of an external magnetic field, however, will orient the atomic current loops in such a

way that their magnetic fields oppose the applied magnetic field. This response is a manifestation of Lenz's law at the atomic scale, namely induced magnetic fields tend to oppose the change, which created them [67].

The three basic physical constants in electromagnetism: the electric permittivity of vacuum, the magnetic permeability of vacuum, and the velocity of light in vacuum are linked by the equation

$$\varepsilon_0 \mu_0 c^2 = 1 \quad (51)$$

Equipped with the basic physical laws of electrodynamics, we are ready to assess the intracellular electromagnetic field strength in different compartments of the neural cells—dendrites, soma, and axons.

4 Electromagnetic Fields in Vivo

4.1 Neuronal Membranes as Excitable Units

The physiologically relevant signal that delivers information to the nervous system is the difference in electrical potential between the interior of a neuron and the surrounding extracellular medium [68]. The ionic concentration gradients across the plasma membrane and the membrane permeability to these ions determine the membrane potential. The plasma membrane is a lipid bilayer, which is impermeable to most ions. Electrically, the membrane acts as a capacitor separating the charges residing along its inner and outer surface. While the resistance of the lipid bilayer by itself is quite high, the resistance of the membrane may be significantly reduced by opening of protein ion channels that traverse the membrane [69].

The ion flow into and out of the cell is controlled by forces resulting from the voltage and concentration gradients. Without external stimuli, these different forces drive the neuron to an equilibrium point referred to as the resting membrane potential V_m . Under resting conditions, the electrical gradient and the ionic concentration gradient balance each other for each of the ion types. The potential on the inner side of the plasma membrane (resulting from the accumulation of charges on the membrane) is about -70 mV relative to the potential of the surrounding extracellular matrix and the cell is said to be polarized.

Positive ions (Na^+ , Ca^{2+}) that enter the cytosol decrease the electronegativity of the membrane potential and depolarize the membrane. Conversely, negative ions (Cl^-) entering the cytosol increase the electronegativity of the membrane potential and hyperpolarize the membrane. The flow of ions from the extracellular space toward the cytosol is called influx, while the opposite flow is called efflux. Certain ion channels and ion pumps extrude ions from the cytosol toward the extracellular space. The efflux of positive ions (K^+) leads to membrane hyperpolarization, whereas efflux of negative ions (HCO_3^-) leads to membrane depolarization. Under physiological

conditions, the neuronal membrane potential varies over a range from about -90 mV to $+50$ mV.

The protein ion channels in the neuronal membranes are of two types: ligand-gated or voltage-gated. Ligand-gated ion channels are sensitive to neuromediator molecules, which bind to specific receptor sites to open the ion channel gate causing flux of ions. Voltage-gated ion channels are sensitive to the voltage across the membrane and their gates may open or close depending on even minor membrane potential changes. Thus, electric signals triggered by ionic fluxes through ligand-gated ion channels could be significantly amplified by concerted opening of voltage-gated ion channels.

4.2 Cable Equation and Dendritic Modeling

The main communication between pyramidal neurons is achieved via axo-dendritic synapses located at the top of dendritic spines. Released excitatory neurotransmitter (glutamate) molecules bind to receptors in the dendritic postsynaptic membranes, which generate postsynaptic electric currents through influx of Na^+ and Ca^{2+} ions. The positively charged ions entering into the dendritic cytosol depolarize the membrane potential.

Dendrites could be modeled as electric cables in which the electric impulses decay as they are transmitted at a distance. The neuronal membrane could be modeled with an electric circuit diagram that takes into account only the passive properties of the membrane (Fig. 6).

The passive biophysical parameters listed in Table 1 are linked according to the following equations

$$R_a = r_i l = \frac{4l}{\pi d^2} R_A \quad (52)$$

$$R_m = \frac{r_m}{l} = \frac{R_M}{\pi dl} \quad (53)$$

$$C_m = c_m l = \pi dl C_M \quad (54)$$

where d is the diameter of the neural projection and l is its length.

The specific biophysical parameters have been experimentally measured for real neurons. The specific axial resistance R_A is $0.6\text{--}1 \Omega \text{ m}$ [70–72]. The value of the specific membrane resistance R_M is $0.5\text{--}10 \Omega \text{ m}^2$ [71] and for the specific membrane capacitance C_M it is 0.01 F m^{-2} [71]. For hippocampal CA1 neurons, the specific membrane capacitance C_M is 0.01 F m^{-2} at the soma and 0.016 F m^{-2} at dendrites to account for dendritic spines [73], R_M is $7 \Omega \text{ m}^2$ at soma, $1 \Omega \text{ m}^2$ at distal dendrites [74] and $53 \Omega \text{ m}^2$ for myelinated axon [75], R_A is $1.39\text{--}2.18 \Omega \text{ m}$ [74] or $2.52 \Omega \text{ m}$ [73].

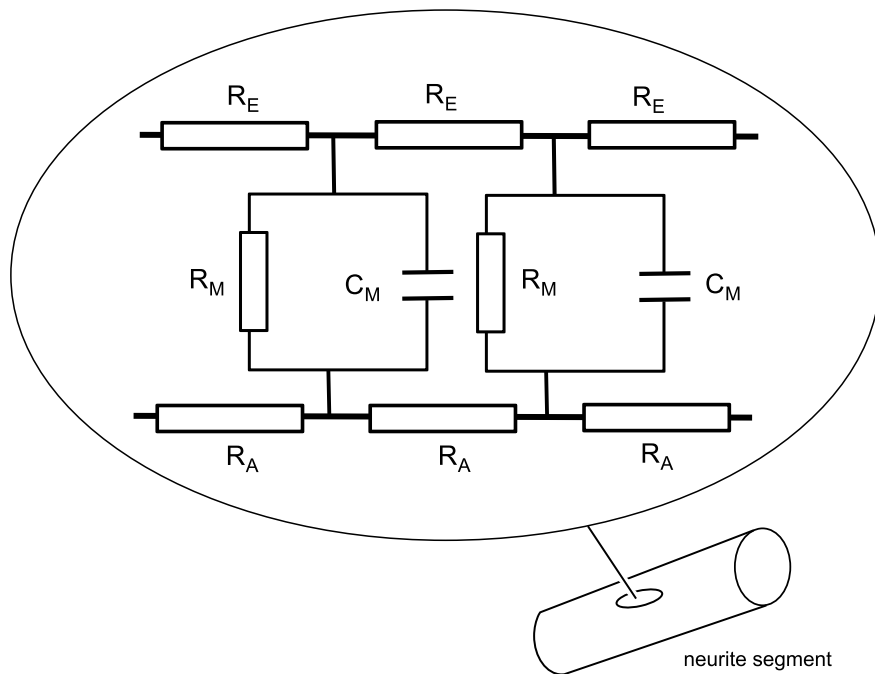


Fig. 6 Electric circuit diagram of passive neuronal membrane

Table 1 Units of the passive membrane

Symbol	SI units	Physical meaning	Notes
R_a	Ω	Axial (intracellular) resistance	For a segment of cable with a fixed length and fixed diameter
R_e	Ω	Extracellular resistance	
R_m	Ω	Membrane resistance	
C_m	F	Membrane capacitance	
r_i	$\Omega \text{ m}^{-1}$	Cytoplasmic resistivity	For unit length of cable with fixed diameter
r_e	$\Omega \text{ m}^{-1}$	Extracellular resistivity	
r_m	$\Omega \text{ m}$	Membrane resistivity	
c_m	F m^{-1}	Membrane capacitance	
R_A	$\Omega \text{ m}$	Specific axial resistance	For unit length and unit diameter (i.e., unit volume or surface area of cable)
R_E	$\Omega \text{ m}$	Specific extracellular resistance	
R_M	$\Omega \text{ m}^2$	Specific membrane resistance	
G_M	S m^{-2}	Specific membrane conductance	
C_M	F m^{-2}	Specific membrane capacitance	
V_m	V	Transmembrane voltage	

If we introduce a localized electric impulse onto a passive dendrite, the voltage V across the membrane will change according to the cable equation

$$-\lambda^2 \frac{\partial^2 V}{\partial x^2} + \tau \frac{\partial V}{\partial t} + V = 0 \quad (55)$$

where the time constant τ is

$$\tau = r_m c_m = R_m C_m = R_M C_M \quad (56)$$

and the square of the space constant λ is

$$\lambda^2 = \frac{r_m}{r_i + r_e} \quad (57)$$

Because in neurons $r_i \gg r_e$, we can write [76]

$$\lambda = \sqrt{\frac{r_m}{r_i}} = \sqrt{\frac{d}{4} \frac{R_M}{R_A}} \quad (58)$$

The cable equation describes the distribution of the membrane potential in space and time if hyperpolarizing or depolarizing impulse is applied. The time constant τ and the space constant λ have the meaning, respectively, of time and distance for which the electric voltage V drops $e \approx 2.72$ times [77].

The time constant τ depends on the membrane resistance that changes in time because ion channels may close and open. Dendritic membrane resistivity obeys a sigmoidal function [78]. The time constant depends on the channel conductances [79] and varies in the range from 10 to 100 ms. For CA1 pyramidal neuron, the membrane time constant τ is 38–44 ms [74].

The space constant depends on the geometry of the neuronal projection and particularly on its diameter (Eq. 58). For a distal dendrite with diameter $d = 0.25\text{--}1 \mu\text{m}$, $R_M = 1 \Omega \text{ m}^2$ and $R_A = 1.39\text{--}2.52 \Omega \text{ m}$, the space constant λ varies in the range 157–424 μm . For a proximal dendrite with diameter $d = 0.5\text{--}1 \mu\text{m}$, $R_M = 7 \Omega \text{ m}^2$ and $R_A = 1.39\text{--}2.52 \Omega \text{ m}$, the space constant λ varies in the range 589–1943 μm .

4.3 Electric Field in Dendrites

Evoked excitatory postsynaptic potentials (EPSPs) measured at the soma of impaled CA1 neurons could be recorded by inducing single electric spike (firing) of the presynaptic terminal of a connected CA3 neuron. Statistical analysis of 71 unitary EPSPs evoked in CA1 pyramidal neurons by activation of single CA3 pyramidal neurons revealed that the peak amplitudes of these EPSPs ranged from 0.03 to 0.665 mV with a mean of 0.131 mV [80]. Later experiments with CA1 neurons also confirmed

that the somatic single EPSP magnitude is ≈ 0.2 mV [81]. It needs to be taken into account, however, that EPSPs at the dendrite are much larger than somatic EPSPs. To counteract the significant EPSP decay due to dendritic leakage associated with the transport at a distance, remote synapses produce larger EPSPs, or in other words they speak louder than the proximal synapses [82]. In fact, the reversal potential for excitatory synapses with AMPA receptors is $E_{\text{AMPA}} = 0$ mV, which means that the local amplitude of EPSPs at the dendrite under active spines could reach 70 mV [83–85].

To obtain the distribution of the voltage along the dendrite in time and space, we could solve the cable equation through separation of variables, namely the solution is sought in the form $V(x, t) = V_1(x)V_2(t)$. Plugging this into the cable equation (55) results in

$$\tau \frac{\partial V_2(t)}{\partial t} V_1(x) = \lambda^2 \frac{\partial^2 V_1(x)}{\partial x^2} V_2(t) - V_1(x)V_2(t) \quad (59)$$

Dividing both sides by $V_1(x)V_2(t)$ gives

$$\tau \frac{\partial V_2(t)}{\partial t} \frac{1}{V_2(t)} = \lambda^2 \frac{\partial^2 V_1(x)}{\partial x^2} \frac{1}{V_1(x)} - 1 \quad (60)$$

The left side is a function only of time t , whereas the right side is a function only of space x . The two sides can only be equal if they are equal to a constant, which we will denote as $-k^2$. Thus, from (60), we obtain a system of equations

$$\tau \frac{\partial V_2(t)}{\partial t} = -k^2 V_2(t) \quad (61)$$

$$\lambda^2 \frac{\partial^2 V_1(x)}{\partial x^2} = (1 - k^2) V_1(x) \quad (62)$$

The solution of (61) is

$$V_2(t) = C_0 e^{-\frac{k^2 t}{\tau}} \quad (63)$$

Similarly, the solution of (62) is

$$V_1(x) = C_1 e^{\frac{-\sqrt{1-k^2}x}{\lambda}} + C_2 e^{\frac{\sqrt{1-k^2}x}{\lambda}} \quad (64)$$

Imposing boundary conditions allows for unambiguous determination of the integration constants. For an infinitely long cable, in the middle of which at $x = 0$ is injected current for a long time followed by sudden cessation of the current injection at $t = 0$, the solution is given by [86]

$$V(x, t) = \frac{1}{2} V_0 \left\{ e^{-\frac{x}{\lambda}} \left[1 + \operatorname{erf} \left(\frac{x\tau - 2t\lambda}{2\lambda\sqrt{t\tau}} \right) \right] - e^{\frac{x}{\lambda}} \left[1 - \operatorname{erf} \left(\frac{x\tau + 2t\lambda}{2\lambda\sqrt{t\tau}} \right) \right] \right\} \quad (65)$$

where V_0 is the potential at the point of injection $x = 0$ at $t = 0$. This solution is transient, which means that for $t \rightarrow \infty$ the potential goes to zero everywhere.

Taking the limit as $t \rightarrow 0$, the solution (65) reduces to the well-known time-independent case [77]

$$V(x, 0) = V_0 e^{-\frac{x}{\lambda}} \quad (66)$$

From the distribution of the voltage spread $V(x)$ along the dendritic axis, we could find the electric intensity along the dendrite after differentiation with respect to space

$$\vec{E} = -\nabla V = -\frac{\partial V(x)}{\partial x} = \frac{1}{\lambda} V_0 e^{-\frac{x}{\lambda}} \quad (67)$$

The maximal electric field intensity at $x = 0$ for a single EPSP at a distal dendrite with magnitude of $V_0 = 70$ mV and space constant $\lambda = 157$ μm is $E \approx 446$ V m^{-1} . At a distance of 400 μm away the electric field intensity is $E \approx 35$ V m^{-1} , and at 957 μm away, it drops to $E \approx 1$ V m^{-1} . These results are consistent with previous estimates of the intracellular electric field in the range 1–10 V m^{-1} [87].

EPSPs carry information from the presynaptic axonal boutons to the dendritic spines, and this information has to be decoded by the underlying microtubules if these subneuronal structures are supposed to host consciousness. The dendritic spine consists of a spine head (where the synapse is formed) and a spine stalk (a narrowing of the spine diameter raising the stalk resistance up to 800 M Ω [71]). From passive models of the spine head membrane, previous studies have concluded that the efficacy of a synapse onto a spine head would be less than or equal to the efficacy of an identical synapse directly onto the parent dendrite [88, 89]. However, models with active spine head membrane suggest that the spines might act as synaptic amplifiers [71]. This implies that the ion channels located in the spine stalk are voltage-gated and the EPSP propagation exhibits nonlinear properties. In other words, when the voltage in the spine stalk reaches a certain voltage threshold, a large fraction of the voltage-gated channels open and amplify the synaptic input.

If we consider that microtubules have acquired mechanisms for translating the information from the electric impulses into specific quantum states then it is demanded to find out a possibility for a microtubule to recognize from which synapse (dendritic spine) the impulse is generated, i.e., the geometric structure of the dendritic tree must have specific meaning for microtubules. The vector of electric intensity under the firing dendritic spines is not collinear with the axis of the parent dendrite, therefore \vec{E} is not collinear with the microtubule z -axis in the parent dendrite and an angle θ will be formed. Thus, the electric field may be a carrier of information about specific bifurcation points in the dendritic tree geometry. The \vec{E} vector becomes collinear with the z -axis of microtubules in the areas between two firing stalks including the space under silent dendritic spines.

4.4 Electric Currents in Dendrites

From Ohm's law, we could calculate the axial current i_a if we know the applied voltage V_0 upon the dendritic projection

$$i_a = \frac{\partial V}{\partial l} \cdot \frac{1}{r_i} = \vec{E} \cdot \frac{1}{r_i} \quad (68)$$

where l is the direction along the axis of the dendrite. The same equation is valid for the axial current outside the dendrite; the only difference is that we should use the r_e value. The currents flowing along the dendrite under applied depolarizing or hyperpolarizing impulses are known as local currents. If we have depolarizing impulse, there is a positive current \vec{i}_+ flowing from the excited area toward the non-excited regions inside the cytoplasm, while outside of the dendrite the positive currents flow toward the place of excitation.

From (52) we find $r_i = \frac{4R_A}{\pi d^2}$ and after substitution

$$\vec{i}_a = \frac{\partial V}{\partial l} \cdot \frac{\pi d^2}{4R_A} = \vec{E} \cdot \frac{\pi d^2}{4R_A} \quad (69)$$

Calculation of the current through the dendrite after applied EPSP with a momentary electric field $E \approx 446 \text{ V m}^{-1}$ gives

$$i_a = \frac{446 \text{ V m}^{-1} \times 3.14 \times (0.5 \times 10^{-6})^2 \text{ m}^2}{4 \times 2.52 \Omega \text{m}} \approx 35 \text{ pA} \quad (70)$$

This result is consistent with the registered excitatory postsynaptic currents (EPSCs) in CA1 neurons of $\approx 22 \text{ pA}$ [90] or evoked inhibitory postsynaptic currents (IPSCs) whose amplitude varies from 20 to 100 pA [91–93]. Noteworthy, giant EPSCs in CA3 neurons of $\approx 1700 \text{ pA}$ have also been observed [94].

The current density J through the cross section of the neuronal projection could be calculated from

$$\vec{J} = \frac{\vec{i}_a}{\vec{s}} = \frac{\partial V}{\partial l} \cdot \frac{1}{R_A} = \vec{E} \cdot \frac{1}{R_A} = \frac{446 \text{ V m}^{-1}}{2.52 \Omega \text{m}} \approx 177 \text{ A m}^{-2} \quad (71)$$

4.5 Magnetic Field in Dendrites

The postsynaptic currents are experimentally measured to be from 20 to 100 pA for GABAergic synapses [93]. Using the formula

$$\oint_{\ell} \vec{H} \cdot d\vec{l} = Hl = i$$

we can find the average magnetic intensity H for a contour ℓ with length $l = \pi d$ that interweaves the whole current i_A . For a dendrite with diameter of 1 μm conducting a current of 100 pA, we obtain $H \approx 31.8 \times 10^{-6} \text{ A m}^{-1}$.

Since water has a unit relative magnetic permeability $\mu_r = \frac{\mu}{\mu_0} = 1$, the maximal magnitude of the magnetic induction \vec{B} in the dendrite is

$$B = \mu_r \mu_0 H = \mu_r \mu_0 \frac{i}{\pi d} \quad (72)$$

For a dendrite with diameter of 1 μm conducting a current of 100 pA, we obtain $B \approx 4 \times 10^{-10} \text{ T}$. Even for the giant EPSCs of $\approx 1700 \text{ pA}$ observed in CA3 neurons [94], the magnetic field strength is only $6.8 \times 10^{-9} \text{ T}$. For comparison, the strength of Earth's magnetic field is about half a Gauss ($5 \times 10^{-5} \text{ T}$), where Gauss is a unit (10^{-4} T) used for measuring weak magnetic fields. Thus, it is evident that the magnetic field generated by individual dendritic currents cannot be used as an informational signal because the noise resulting from the Earth's magnetic field will suffocate it.

4.6 Electromagnetic Field in Soma

From a computational point of view, the neuronal soma integrates dendritic inputs. The passive properties of dendrites lead to decrement of EPSPs and IPSPs that reach the soma. But this also allows for EPSPs and IPSPs to summate over space and time so that whenever a critical threshold of about -55 mV in the soma is reached, an electric spike will be initiated in the axon initial segment. Because the soma has a large diameter of 15–20 μm , it will have a large space constant λ . Consequently, the magnetic and electric field strengths are expected to be similar to those in dendrites with maximal magnetic strength of $\approx 10^{-9} \text{ T}$ and maximal electric strength of $\approx 100 \text{ V m}^{-1}$.

4.7 Axonal Electrophysiology

Neurons output information via long projections called axons. Typically, the diameter of axons is about 1 μm in humans. Axons with small diameter could be non-myelinated. However, the larger axons in the central nervous system are ensheathed by multiple membrane layers known as myelin. Myelin is produced by supportive glial cells called oligodendrocytes. Oligodendrocytic membrane rotates around the axon and forms multiple-layered phospholipid structure that insulates the axon from the surrounding environment. One axon is insulated by numerous oligodendrocytes; however, there are tiny places where the axonal membrane is non-myelinated. They are located between two oligodendrocytic membranes and are called nodes of Ranvier. In the peripheral nervous system, the myelin is produced by Schwann cells.

The generation of an action potential by axons is an all-or-none event. When the transmembrane voltage in the axonal hillock reaches a threshold potential of about -55 mV, the action potential is initiated. The axonal membrane depolarizes due to opening of sodium gates allowing Na^+ ions to rush into the cell through voltage-gated Na^+ channels. When the inner side of the membrane is depolarized to $+40$ mV, the sodium gates are closed and potassium gates open. Subsequently, K^+ ions rush out through open potassium gates (at this time the sodium gates are closed and inactive). The axonal membrane repolarizes and even may be hyperpolarized briefly (overshoot). Refractory period occurs while the sodium gates of the voltage-gated Na^+ channels remain closed. The membrane will not respond again until the sodium gates are activated again.

The ion currents in axons are larger than the currents in dendrites and electric spikes propagate without decrement. This is due to the fact that the ion channels in the axonal membrane are voltage-gated and the current propagation is nonlinear. In the myelinated axons, the electric spike jumps from one node of Ranvier to another (so-called saltatory conduction). The myelin sheath is not permeable for ions and prevents the ion leakage across the membrane. As a result, the sodium and potassium channels are clustered at the nodes of Ranvier, which leads to a significant increase of the conducting velocity. Greater intensity of stimuli applied upon the nerve cell is reflected in increased frequency of impulses, not in higher voltages of individual impulses, i.e., all action potentials appear to be similar in shape and duration. The speed of propagation of the action potential for mammalian myelinated motor neurons is $10\text{--}120 \text{ m s}^{-1}$, whereas for non-myelinated sensory neurons, the speed is about $5\text{--}25 \text{ m s}^{-1}$.

4.8 The Hodgkin–Huxley Model

The Hodgkin–Huxley model of an active axonal membrane is based on an isopotential membrane patch or a single electrical compartment, that is there are no spatial effects on the potential [95–97]. The units of the model are per membrane unit area, from which it is straightforward to scale the model to a compartment of any desired membrane area. The current flow across the cell membrane depends on the capacitance of the membrane and the conductivity of ion channels (Fig. 7). The total ionic current is represented by the sum of the sodium current, potassium current, and a small leakage current. The leakage current represents the collective contribution of ions such as chloride and bicarbonate.

The total membrane current is the sum of the ionic currents and the capacitive current

$$I_m(t) = I_{\text{Na}}(t) + I_{\text{K}}(t) + I_L(t) + C_M \frac{dV(t)}{dt} \quad (73)$$

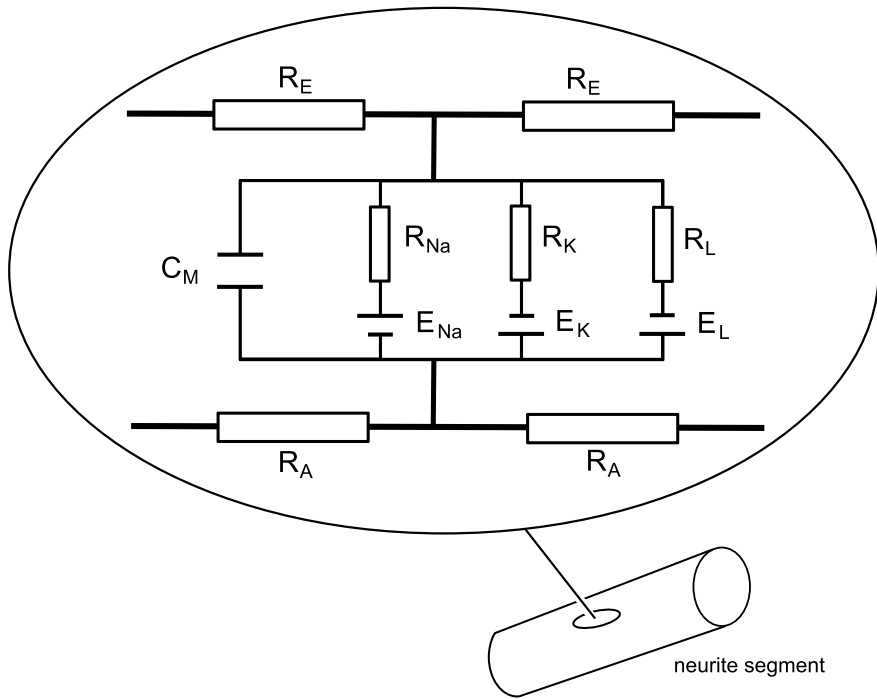


Fig. 7 Electric circuit diagram describing the ionic current flows across the cell membrane that are captured in the Hodgkin–Huxley model

where I_m is the membrane current density, I_{Na} is the sodium current density, I_K is the potassium current density, I_L is the leak current density, C_M is the membrane capacity per unit area, and V is the membrane voltage.

The individual ionic currents are linearly related to the membrane potential V according to Ohm's law

$$I_K(t) = G_K(V, t)[V(t) - E_K] \quad (74)$$

$$I_{Na}(t) = G_{Na}(V, t)[V(t) - E_{Na}] \quad (75)$$

$$I_L(t) = G_L(V, t)[V(t) - E_L] \quad (76)$$

where G_K , G_{Na} and G_L are the potassium, sodium, and leak conductances per unit area of the membrane and E_K , E_{Na} , and E_L are the corresponding reversal potentials of each of the ionic species (the potential at which the ionic concentration gradient is balanced by the electrical potential gradient, and there is no net flux of the ions of this type).

The reversal potential for a given ion is determined by Nernst equation

$$E_{\text{ion}} = \frac{RT}{FZ} \ln \frac{[\text{ion}]_e}{[\text{ion}]_i} \quad (77)$$

where $R = 8.314 \text{ J K}^{-1} \text{ mol}^{-1}$ is the gas constant, T is temperature, $F = 96,485 \text{ C mol}^{-1}$ is Faraday constant, Z is the ion valence, $[\text{ion}]_e$ and $[\text{ion}]_i$ are, respectively, the ion concentrations in the extracellular or intracellular space.

The voltage-dependent conductances $G_{\text{Na}}(t)$ and $G_{\text{K}}(t)$ are given by

$$G_{\text{Na}}(t) = G_{\text{Na}}^{\max} f_{\text{Na}}(t) \quad (78)$$

$$G_{\text{K}}(t) = G_{\text{K}}^{\max} f_{\text{K}}(t) \quad (79)$$

where G_{Na}^{\max} and G_{K}^{\max} are the peak sodium and potassium conductances per unit membrane area and $f_{\text{Na}}(t)$ and $f_{\text{K}}(t)$ are each the corresponding (instantaneous) fraction of the maximal conductance which is actually open (or active).

Thus, the equation that describes the membrane potential is a function of all the currents that flow across the membrane

$$\begin{aligned} C_M \frac{dV}{dt} = & G_{\text{Na}}^{\max} f_{\text{Na}}(t)[E_{\text{Na}} - V(t)] + G_{\text{K}}^{\max} f_{\text{K}}(t)[E_{\text{K}} - V(t)] \\ & + G_L^{\max} f_L(t)[E_L - V(t)] + I_{\text{injected}}(t) \end{aligned} \quad (80)$$

The values for the biophysical parameters are: $E_{\text{Na}} = +60 \text{ mV}$, $G_{\text{Na}}^{\max} = 120 \text{ mS cm}^{-2}$, $E_{\text{K}} = -93 \text{ mV}$, $G_{\text{K}}^{\max} = 36 \text{ mS cm}^{-2}$, $E_L = -60 \text{ mV}$ and $G_L^{\max} = 0.3 \text{ mS cm}^{-2}$.

The Hodgkin–Huxley model replicates the main features of spiking of the squid giant axon: the form, duration, and amplitude of a single electric spike, including its sharp threshold, the conduction velocity of the spike along the axon, the refractory period of the neuron, the impedance changes during the spike, anode-break excitation, accommodation, subthreshold response, and oscillations. Simulations with sustained injected stimulus currents demonstrate a discontinuous onset of repetitive firing with a high spiking frequency together with a limited bandwidth of the firing frequency. Some limitations of the model are that it does not provide a good description of the refractory behavior of the preparation in response either to sustained or periodic current pulse stimulation [98]. Also, the model does not account for after potentials and slow changes in the squid giant axon.

Nevertheless, the Hodgkin–Huxley model is the golden standard for studying neuronal excitability, and with minor modifications it serves as the backbone of most neuronal spiking models. The main reason is that the model captures correctly the essence of spiking through ionic currents, which enter and leave the cell through voltage-gated ion channels. Moreover, the model is compact and incorporates many of the features shared by different types of neurons. Further addition of appropriate currents for other channel types (usually using similar kinetic schemes) is easily done. In fact, the Hodgkin–Huxley model is the common choice of conductance-based modeling for computational studies.

4.9 Magnetic Field in Axons

The vector of magnetic induction \vec{B} will form closed loops around the axis of the neuronal projection and the direction will be defined by the right-hand screw rule (Fig. 4). In axons, the magnetic field is stronger than the magnetic field in dendrites because of the greater ion currents flowing inside the axoplasm. The nerve action potential has the form of a moving electric spike, which can be modeled as two opposing current dipoles driven by a potential change of the order of 110 mV. The peak current in cortical pyramidal neurons during action potential is ≈ 5.2 nA [99]. Axons reach gigantic size in squid of about 1 mm. For CA1 neurons in humans, however, the axon diameter is 3.92 ± 0.42 μm for the initial segment within 70 μm from the soma, but in the remaining distance it is much thinner ≈ 0.9 μm [100]. Calculation of the magnetic flux density in the axon of cortical pyramidal neuron with current of 5.2 nA and diameter of 0.9 μm gives $B = 2.3 \times 10^{-9}$ T. Although this result is an order of magnitude greater than the experimentally measured magnetic field of 1.2×10^{-10} T in frog sciatic nerve using SQUID magnetometer [101], it remains too weak in comparison with Earth's magnetic field, hence it will be suffocated.

4.10 Electric Field in Axons

The space constant λ in axons is an order of magnitude larger than the dendritic space constant. The space constant λ for an axonal projection with diameter $d = 0.9$ μm and specific axial resistance $R_A = 1 \Omega \text{ m}$ is large due to myelin enhancement of the specific membrane resistance to $R_M = 53 \Omega \text{ m}^2$ [75]

$$\lambda = \sqrt{\frac{d R_M}{4 R_A}} = \sqrt{\frac{0.9 \times 10^{-6} \text{ m} \times 53 \Omega \text{ m}^2}{4 \times 0.62 \Omega \text{ m}}} \approx 3.5 \text{ mm} \quad (81)$$

If the applied voltage V_0 is ≈ 110 mV (taking into account that the action potential varies the voltage from -70 mV to $+40$ mV), the electric intensity $E = V_0/\lambda$ reaches only ≈ 31 V m^{-1} . In essence, due to large λ , the electric field intensity in the axon is not greater than the electric field intensity in dendrites.

Noteworthy, axonal damage in multiple sclerosis appears to be initiated by increased membrane permeability followed by enhanced Ca^{2+} influx. Disruption of axonal transport alters the cytoskeleton and leads to axonal swelling, lobulation and, finally, disconnection [102]. Thus, a drastic change of the electric microenvironment may lead directly to microtubule dysfunction in neurons.

5 Implications for Microtubule Function

5.1 No Hall Effect in Microtubules

The Hall effect is a phenomenon leading to anisotropy of the electroconductivity in a conductor or semiconductor, which is caused by magnetic field whose induction \vec{B} is perpendicular to the vector representing the current density \vec{J} . In this case, the vector \vec{J} and the electric intensity vector \vec{E} are not collinear, but form an angle θ_H between them, called Hall angle (Fig. 8). Hall effect, discovered in 1879, is almost unnoticeable in metals but is much more pronounced in semiconductors.

Let us examine a metal lamina in which under the action of electric field \vec{E}_i is generated current i_- comprised of electrons with mean velocity $\vec{v}_- = \text{const}$. Suppose that there is also a constant magnetic field with induction $\vec{B} = \text{const}$, whose lines are perpendicular to the metal lamina. The vector of velocity \vec{v}_- is collinear with the vector of electron current \vec{i}_- . The vectors \vec{i}_- and \vec{B} define electrodynamic field \vec{E}_{md} given by

$$\vec{E}_{md} = \vec{v}_- \times \vec{B} \quad (82)$$

The electromagnetic force \vec{F}_M , which acts upon N moving electrons q_e , is

$$\vec{F}_M = q_e N \vec{v}_- \times \vec{B} \quad (83)$$

The electromagnetic force \vec{F}_M has the opposite direction of \vec{E}_{md} , thus the side M_- is polarized negatively, whereas the side M_+ is polarized positively. Between M_+ and M_- , there is an excited potential electric field with intensity \vec{E}_H . The vector \vec{E}_H has the opposite direction of \vec{E}_{md} . The respective force \vec{F}_H defined as

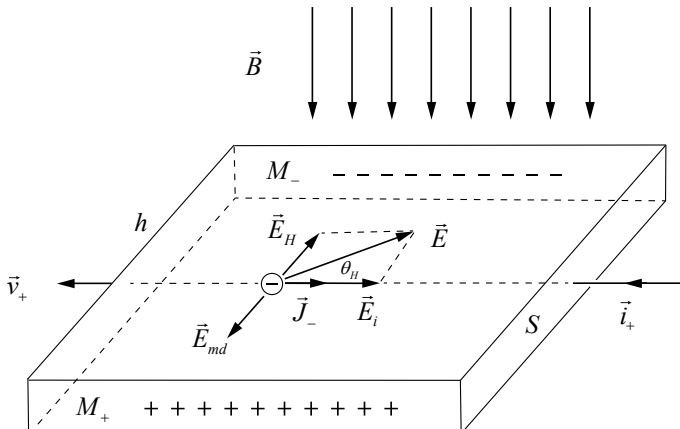


Fig. 8 Hall effect in a metal lamina with monotype carriers of negative charges (electrons)

$$\vec{F}_H = q_e N \vec{E}_H \quad (84)$$

is the opposite of \vec{F}_M . The polarization between M_+ and M_- is steady when the two forces \vec{F}_M and \vec{F}_H become equal. The current is still flowing but the vector \vec{J}_- and the resultant field \vec{E} are no more collinear, instead they form the Hall angle θ_H [63]. Then, Ohm's law $\vec{J}_- = \gamma \vec{E}$ is not valid (where γ is the specific conductivity of the metal).

The calculation of the angle θ_H is simple when we have monotype current carriers (in our case electrons). At equilibrium, the two forces balance each other

$$\vec{F}_M + \vec{F}_H = 0 \quad (85)$$

Taking into account the geometry of the Hall effect in the metal lamina, we obtain

$$\vec{E}_H = -\vec{v}_- \times \vec{B} = \vec{B} \times \vec{v}_- \quad (86)$$

$$\tan(\theta_H) = \frac{E_H}{E_i} = -\frac{v_-}{E_i} B \quad (87)$$

$$\theta_H = \arctan(k_n B) \quad (88)$$

where the electron mobility in the metal lamina is

$$k_n = -\frac{v_-}{E_i} \quad (89)$$

If we suppose that the electric polarizing field \vec{E}_H is constant, the electric voltage V_H between M_+ and M_- is given by

$$V_H = E_H h = h B v_- \sin \alpha \quad (90)$$

where α is the angle between \vec{B} and \vec{v}_- (for $\alpha = \frac{\pi}{2}$ the latter term becomes $\sin \alpha = 1$). The condition $\vec{E}_H = \text{const}$ is fulfilled if $\vec{v}_- = \text{const}$ and $\vec{B} = \text{const}$. The current density J_- through the surface S of the lamina is

$$J_- = \frac{i_-}{S} = v_- n q_e \quad (91)$$

$$v_- = R_H J_- \quad (92)$$

$$R_H = \frac{1}{n q_e} \quad (93)$$

where n denotes the number of the elementary charges q_e in unit volume, and R_H is called Hall coefficient. R_H can thus be measured to find the density of carriers in the material.

After substitution, we find that the voltage between the two sides M_+ and M_- is

$$V_H = hBR_H J_- \sin \alpha \quad (94)$$

The quantum Hall effect is a phenomenon occurring at low temperatures (millikelvin range) and when strong magnetic fields (1–15 T) are applied upon semiconductors. In the absence of a magnetic field, the density of states in two dimensions is constant as a function of energy. Alternatively, in the presence of a magnetic field, the available states clump into Landau levels separated by the cyclotron energy, with regions of energy between the Landau levels where there are no allowed states. As the magnetic field is swept the Landau levels move relative to the Fermi energy. When the Fermi energy lies in a gap between Landau levels, electrons cannot move to new states and so there is no scattering. Thus, the transport is dissipationless and the resistance falls to zero [103, 104].

Porter [20] proposed that in neurons there may be analogous situation where the local magnetic field produced by the neuronal currents acts upon the microtubules and that anyons could be formed via quantum Hall effect. However, the idea that the local magnetic field generated by neuronal currents inputs information to the brain microtubules via Hall effect and that this process is linked to our conscious experience is biologically untenable. Since the local magnetic flux density of individual spikes is less than 10^{-8} T, it cannot be a meaningful source of information—in fact, the brain is exposed to stronger magnetic fields such as Earth's magnetic field and no direct effects on consciousness are registered. Noteworthy, strong magnetic fields reaching flux density of 1 T are used in functional magnetic resonance imaging (fMRI). The visualization of the brain with fMRI, however, also has no impact on conscious experiences.

5.2 Microtubule Lattice Structure

In a list of 20 testable predictions, the Penrose–Hameroff Orch OR model [12] claims that the dendrites of cortical neurons should contain largely A lattice microtubules compared to B lattice microtubules (Fig. 9), because A lattice microtubules are preferable for information processing [13]. Indeed, there were old experimental data obtained via X-ray scattering [105] or electron microscopy with image reconstruction of microtubules [106–108] that in vitro assembled microtubules may have either A or B lattice. However, with the development of new technologies for production of recombinant motor proteins, decoration of microtubules with kinesin heads revealed that all brain microtubules have B lattice [109]. The possibility of A lattice to exist at all in vivo was seriously questioned and it was proposed that all in vivo assembled microtubules exhibit B lattice [109]. This meant that microtubules with 13 protofilaments, the most abundant in vivo, must have a seam where lateral contacts involve heterologous subunits. Such a seam has been directly visualized, both in vivo and in

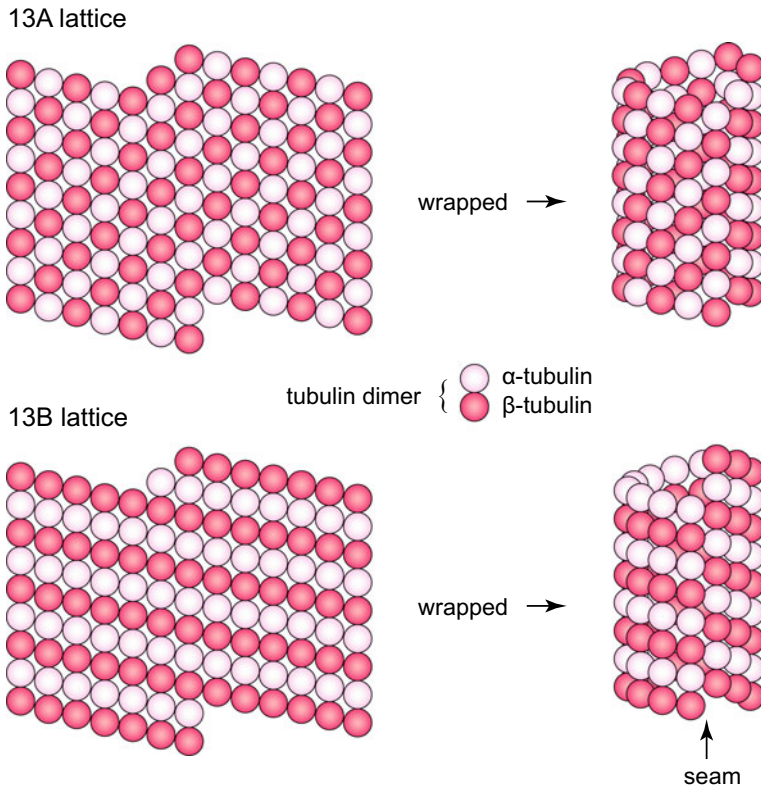


Fig. 9 Unfolded and wrapped 13A and 13B microtubule lattices. Brain microtubules *in vivo* possess 13B lattice and a seam

vitro, using freeze-fracture replicas [110]. Thus, it is hard to envision why Hameroff insisted on A lattice [12] and bet on experimentally disproved position.

Noteworthy, microtubules with B lattice possess a number of interesting properties. For example, the transition from ordered to paraelectric phase happens at higher temperatures in B lattice than in A lattice because of the existing seam [18]. Another difference lies in the attachment of microtubule-associated proteins (MAPs) to microtubules. MAPs attach to microtubules in periodic patterns and their function is to stabilize the assembly properties of the microtubule by preventing the conformational change of the tubulin dimer to which it is attached. This may be understood by viewing the fixed conformation dipoles as seeds of order. Also unlike the lattices that consist of even number of protofilaments (12 or 14), in 13B lattices, there are two different values of polarization that correspond to the antiferroelectric ground state: $-\frac{1}{13}$ when all dipoles in 6 rows point up and all dipoles in 7 rows point down and $+\frac{1}{13}$ when all dipoles in 7 rows point up and all dipoles in 6 rows point down. Computational simulations revealed that the $-\frac{1}{13}$ or $+\frac{1}{13}$ polarization depends on the MAP/microtubule ratio [18].

5.3 Problems in the Ferroelectric Model of Microtubules

The dipole moment of tubulin dimers is crucial for the proper assessment of microtubule sensitivity to external electric fields [18, 111, 112]. The ferroelectric model of microtubules considers each tubulin dimer as a two-level system whose dipole moment could be in \uparrow or \downarrow position. When the dipole is in \uparrow position, it is collinear with the microtubule z -axis, whereas when the dipole is in \downarrow position, it forms an angle $\phi \approx 29^\circ$ with the z -axis. The ferroelectric model is considered to be an improved version of the cellular automaton model developed by Hameroff [60, 61] where a discrete charge is associated with each tubulin dimer and can either be localized in the top monomer (α state) or bottom monomer (β state).

Unfortunately, the ferroelectric model leads to problematic results. The conformational states that are considered to represent single bits or qubits designated with \uparrow and \downarrow (or α and β) are in fact boundary conformations that may trigger disassembly of microtubules, hence cannot be used for computation by stable microtubules. In addition, computer simulations showed that normal electric fields inside the cell will not have an effect on the dipole ordering in microtubules, instead an applied external electric field will be effective only when it exceeds 10^5 V m $^{-1}$ in the cytosol [18].

To avoid microtubule catastrophe, the change in the dipole moment of the tubulin dimer could be supposed to result from electron hopping between the α and β tubulin, without an associated mechanical rotation of the dimer. Theoretical investigation of the biological electron conductance of microtubules and the associated electron hopping in the presence of applied external electric fields revealed that the energy for intradimer hopping is 0.4 eV and for interdimer hopping is 1.0 eV [17]. The microtubule is not insulator, but its conductivity depends on the lattice geometry (13B lattice has lower resistance) and the boundary conditions (whether the microtubule lattice is wrapped into a tube or not). The situation is compared to carbon nanotubes, where particular sets of boundary conditions produce a semiconducting nanotube while the appropriate choice of wrapping the nanotube gives rise to metallic conduction [113].

Straightforward calculations show, however, that the intraneuronal electric field could not supply the needed energy for the electron hopping. The work W (respectively the energy needed) for intradimer hopping could be assessed from the formula

$$W = \vec{F} \cdot \vec{l} = \vec{E} \cdot q_e \cdot \vec{l} \quad (95)$$

In the intradimer hopping model, the estimated value is $W = 0.4$ eV (6.4×10^{-20} J), the electron charge is $q_e = 1.6 \times 10^{-19}$ C and the hopping distance is $l \approx 4$ nm. Thus, we find that the needed electric intensity of the field is

$$E = \frac{W}{q \cdot l} = \frac{6.4 \times 10^{-20} \text{ J}}{1.6 \times 10^{-19} \text{ C} \times 4 \times 10^{-9} \text{ m}} = 10^8 \text{ Vm}^{-1} \quad (96)$$

This result is consistent with the reported prediction that normal electric fields inside the cell would not have an effect on the dipole ordering in microtubules [15, 16, 18, 111]. The electric fields start to be effective when they exceed intensity $10^4 - 10^5$ V m⁻¹, which cannot be attained in the cytosol of neurons.

The energy for the electron hopping between the α and β tubulin is equal to the energy released from hydrolysis of the GTP molecule attached to β tubulin. GTP hydrolysis releases approximately 0.4 eV per molecule and is accompanied by a conformational change [114]. This change has been modeled to result in 27° angle between the original line connecting the centers of the α and β monomers and the new center-to-center line [115]. These two conformational states and their associated dipole moments have been proposed as the basis for a binary system for information storage and manipulation [12, 19, 21, 45, 60, 61, 116–118]. This model is biologically flawed because the associated conformational change $\alpha \leftrightarrow \beta$ could not be used for computation as it leads to microtubule destabilization and subsequent disassembly [119]. Next, we will review in detail the mechanics of microtubule disassembly.

5.4 GTP Hydrolysis and Dynamic Instability

The main difference between α and β tubulins is in binding GTP. Noteworthy, α -bound GTP is effectively sequestered—it is not exchanged and not hydrolyzed [47]. In contrast, β -bound GTP is labile—it is exchangeable in the free dimer and hydrolyzed to (non-exchangeable) guanosine diphosphate (GDP) in the protofilament [120]. A significant amount of the free energy of this hydrolysis goes into the microtubule via a conformational change of the tubulin dimer [48]. Although the hydrolysis reaction is closely coupled to microtubule assembly [121, 122], its consequence is to destabilize the structure. Experiments indicate that unhydrolyzed GTP-tubulin is limited to the last layer of subunits at the end of a microtubule [50, 123, 124]. The usual interpretation is that this layer acts as a GTP-cap, keeping an otherwise unstable microtubule intact [125].

Microtubule dynamic instability arises from the hydrolysis of GTP bound to the β monomer of the tubulin dimer. The released energy of 0.4 eV from GTP hydrolysis triggers a conformational change in the tubulin molecule [51] that eventually destabilizes the aggregate [119] and causes microtubule disassemble into protofilaments of GDP-bound tubulin that curve away from the microtubule axis (Fig. 10). The unfolding of N-terminal tubulin domain called entropic bristle domain localized in the microtubule interior provides a biomolecular mechanism that leads to disassembly of the microtubule into protofilaments [126]. Such a change is able to destabilize the aggregate in a manner consistent with structural data [127]. The hypothesis not only explains the hydrolysis-associated change in microtubule supertwist [52] but also provides a unifying explanation for the effects of temperature [128] and glycerol [129] on microtubule disassembly rates.

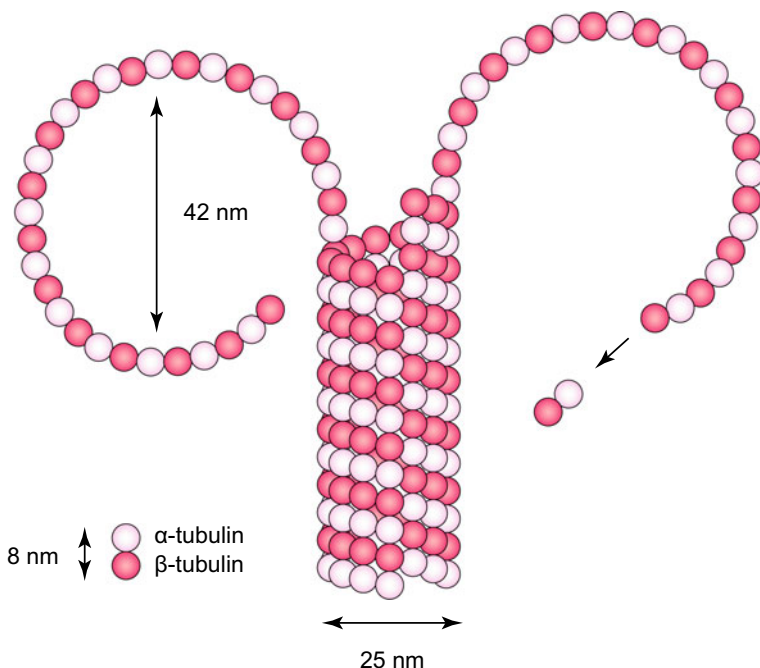


Fig. 10 Microtubule catastrophe following hydrolysis of the GTP cap with outward protofilament curling into rings and disassembly of individual $\alpha\beta$ tubulin dimers

At the ends of growing microtubules, protofilaments of different lengths are straight and closely associated. In shortening microtubules, protofilaments separate from one another and curl back, away from the microtubule axis, forming characteristic blunt blossoms at the microtubule ends [53, 119]. This observation is the basis for comments about the tubulin dimer adopting a “curved” or “kidney-bean shaped” conformation, held under tension in the microtubule lattice [119, 130]. Localization of the hydrolyzed nucleotide at the interdimer interface is highly suggestive, but which residues and how they shift to generate tension and weaken lateral bonds is an important subject of active research [131, 132].

Multiple tubulin conformational states may be separated by different energy barriers between them. Consequently, the putative computational states (representing bits or qubits) in stable non-centrosomal neuronal microtubules should be well chosen in order to achieve output tubulin states that are of biological importance and to avoid the risk of triggering microtubule disassembly.

5.5 The Importance of the Water Microenvironment

Nuclear magnetic resonance (NMR) evidence indicates that water inside cells possesses more structure than liquid water [133–135]. A substantial part of water molecules in the cell is in the form of hydration water bound to various macromolecules. This bound water has several exotic properties: it does not freeze at temperature of -35°C [136], it is a poor solvent for electrolytes [137], and it has a higher viscosity than normal water and exhibits dynamic correlations between individual water molecules [137]. Because cytoskeletal microtubules provide a large surface area inside and outside the tube, a significant fraction of intracellular water is expected to be bound to microtubules. Consequently, measured electret properties of bound water with associated nonlinearity, hysteresis effects and long relaxation times on the order of 1 s and activation energies of about $7\text{--}9\text{ kcal mol}^{-1}$ [138], could indicate the presence of long-range dipole order leading to the formation of internal electric fields or perhaps collective oscillations of electric fields [139].

The microtubule cavities with water in their vicinity have been modeled in the framework of quantum field theory revealing two important phenomena that could take place inside the cell: collective infrared photon emission by water molecules known as superradiance [140–143] and Rabi coupling between the water molecules inside the cavity of the microtubule and the tubulins that build up the microtubule walls [45, 116–118].

Abdalla and colleagues [144] suggested that the vicinal water of the brain microtubules generates electromagnetic sine-Gordon solitons propagating with velocity v_0 given by

$$v_0 = \frac{2p}{\pi\hbar} V = \frac{2p}{\pi\hbar} \int E \cdot dz \quad (97)$$

where z is the length of the microtubule, E is the electric field intensity, and p is the permanent electric of water ($p = 6.2 \times 10^{-30} \text{ C m}$). After substitution of the obtained value for $E \approx 100 \text{ V m}^{-1}$ and for microtubule with length $z = 50 \mu\text{m}$, we find the soliton velocity

$$v_0 = \frac{2 \times 6.2 \times 10^{-30} \text{ C m} \times 100 \text{ V m}^{-1} \times 50 \times 10^{-6} \text{ m}}{3.14 \times 1.055 \times 10^{-34} \text{ J s}} = 187 \text{ m s}^{-1} \quad (98)$$

This result is consistent with the previously reported velocity $v_0 \approx 140 \text{ m s}^{-1}$ [144] and suggests that dissipationless transport of energy could be achieved by collective water molecule dynamics. However, superradiance is not sufficient to explain microtubule function as this phenomenon is not microtubule specific. Indeed, proper connection with specific protein conformational states must be found for this transfer of energy to be biologically important [145–147]. From the presented experimental data and estimates of the intracellular electric intensities, we have seen that $\alpha \leftrightarrow \beta$ tubulin switches could not account for biologically feasible model of subneuronal processing of information [47]. This problem may be resolved if we focus our atten-

tion on the microtubule outer surface and the microtubule interaction with MAPs or motor proteins [145–147]. In this respect, tubulin C-terminal tails, which are highly acidic (hydrophilic) and flexible (allowing multiple conformations with low energy barrier heights), could control MAP attachment and motor protein activity.

5.6 *Tubulin C-Terminal Tails*

C-terminal ends of α - and β -tubulin known as tubulin tails are rich in acidic amino acid residues [148, 149]. Structurally, the C-terminal tails are highly flexible mobile random coils, susceptible to proteolysis, and exposed to the solvent [150, 151]. Because of their intense negative charge and high flexibility, the tubulin C-terminal tails could be sensitive to the local electric field and input information that is carried by the membrane potentials. This possibility is supported by the observation that the highly acidic tubulin C-terminal tails interact with motor proteins and microtubule-associated proteins (MAPs). In fact, experimental studies revealed that MAPs are able to directly bind α -tubulin at amino acid sequences Lys 430–Glu 441 and β -tubulin at amino acid sequences Tyr 422–Gly 434 [152].

Different biomolecular partners or pharmacological agents exhibit different binding preferences to microtubules. For example, the β -tubulin C-terminus binds microtubule-associated protein 2 (MAP-2) or tau, whereas the α -tubulin C-terminus binds these proteins only weakly [153]. The α -tubulin C-terminus determines colchicine binding properties [154] despite the fact that the binding site is located on β -tubulin [155, 156]. When colchicine is delivered directly to the brain or cerebrospinal fluid of experimental animals it causes significant cognitive impairments of learning and memory [157, 158]. The β -tubulin C-terminus enhances the polymerization response to vinblastine, while the removal of the β -tubulin C-terminus abolishes the inhibitory effect of oligoanions on vinblastine-induced polymerization [153]. The C-termini of tubulin also play a role in the dimer-polymer equilibrium [159], as attachment points for microtubule-associated proteins [152, 160] and cytoplasmic dynein [161], and as possible binding sites for calcium ions [162].

The amino acid sequences encoded by β -tubulin genes have revealed a high level of overall similarity, but significant divergence between their C-termini [163]. Differential expression patterns of β -tubulin genes have been observed in several different human cell lines. It appears that distinct human β -tubulin isotypes are encoded by genes whose exon size and number has been conserved evolutionary, but whose pattern of expression may be regulated either coordinately or uniquely [163].

Among the variety of tubulin C-termini functions is observed chaperon-like activity [150]. Within the cell, molecular chaperones help the proper protein folding of newly synthesized proteins. Chaperones are needed because polypeptides may fold in multiple ways, some of which are biologically useless (aggregation). Thus, there is always a kinetic competition between the correct folding and aggregation [164] and

the yield of the folded protein will depend upon the relative rate of the two processes. To enhance the probability of successful protein folding, chaperones minimize the rate of aggregation.

5.7 Post-translational Modification of Tubulin Tails

The tubulin C-terminal tails are prone to intense modification and regulation by different biochemical pathways inside neurons. In mammalian cells, both α - and β -tubulin occur as seven to eight different genetic variants, which also undergo numerous post-translational modifications [165–167]. The main control of the microtubule function is achieved via covalent modifications [168]. Indeed, in protists where identical α - and β -tubulins are expressed [169], post-translational modifications provide the only source of variation. Modifications such as acetylation, palmitoylation, phosphorylation, and polyglutamylation are post-translational modifications found on other proteins; others such as detyrosination and polyglycylation appear to be tubulin specific [170].

Tyrosination/detyrosination is one of the major post-translational modifications in which the C-terminal tyrosine residue in α tubulin is added or removed reversibly [168]. The tubulin tyrosination cycle involves the enzymatic removal of the C-terminal tyrosine residue present on some α -tubulin isotypes by a specific carboxypeptidase, and its subsequent restoration by a tubulin-tyrosine ligase [171]. Although the functional relevance of this modification is not always clear, highly stable microtubules such as those of the axoneme are detyrosinated, and this appears to reflect the length of time the individual α -tubulin substrate molecule has spent in a microtubule. Although tyrosination does not alter the assembly activity of tubulin in vitro, these two forms of tubulin have been found to be distributed differently in vivo and are also correlated with microtubule stability [172]. Detyrosination of tubulin also regulates interaction of microtubules with vimentin intermediate filaments by a kinesin-dependent mechanism [173]. Removal of the penultimate glutamate residue from the α -tubulin polypeptide produces $\Delta 2$ -tubulin, a derivative that is unable to act as a substrate for tubulin-tyrosine ligase, and this truncated protein is therefore removed from the tyrosination cycle. $\Delta 2$ -tubulin is particularly prevalent on microtubule structures such as the axonemes of flagella and cilia and also in mammalian brain cell microtubules.

The tubulin modifications polyglutamylation and polyglycylation involve the attachment of oligoglutamyl and oligoglycyl side chains of variable length to specific glutamate residues located near the C-terminus of both α - and β -tubulin. These side chains can be of considerable length for instance, axonemal tubulin of Paramecium is modified by up to 34 glycyl residues [174], and the microtubules of Trypanosoma brucei contain 15 glutamyl residues per α -tubulin subunit [175]. Polyglutamylation and polyglycylation are particularly associated with stable microtubule structures such as the axonemes of cilia and flagella.

Microtubules in the centriole appear to be polyglutamylated but not polyglycylated [176]. Polyglutamylation appears to be critical for the stability of centriole microtubules, since microinjection of monoclonal antibodies specific for polyglutamylated tubulin isotypes, results in the transient disappearance of centrioles in mammalian cells [177].

Polyglutamylation also represents the major post-translational modification of axonal tubulin in neuronal cells, where it appears to regulate the differential interaction between microtubules and microtubule-associated proteins (MAPs). For instance, MAPs such as tau and kinesin exhibit optimal binding to tubulin modified by ≈ 3 glutamyl residues, binding affinity decreasing with increased polyglutamyl chain length [178, 179]. In contrast, increasing polyglutamyl chain length does not appear to affect the binding affinity of MAP1A significantly [180]. Thus, differential binding of MAPs to polyglutamylated tubulin could facilitate their selective recruitment to distinct microtubule populations and thereby modulate the functional properties of microtubules [180].

Genetic mutations in tubulin C-terminal tail have been observed to result in cerebral pathology. For example, British type familial amyloidosis is an autosomal dominant disease characterized by progressive dementia, spastic paralysis, and ataxia. Amyloid deposits from the brain tissue of an individual who died with this disease have been characterized. Trypsin digestion and subsequent N-terminal sequence analysis yielded a number of short sequences, all of which are tryptic fragments of the C-termini of human α - and β -tubulin. Consistent with the definition of amyloid, synthetic peptides based on the sequences of these fragments formed fibrils in vitro, suggesting that the C-termini of both α - and β -tubulin are closely associated with the amyloid deposits of this type of amyloidosis [181].

5.8 Processing of Information by Brain Microtubules

Taking into account the experimental data from the molecular studies, we can construct a quantum model of microtubule processing of the electrophysiological information. Microtubule C-terminal tails are both intensely charged and flexible, so they could undergo conformational transitions separated by relatively low energy barriers when the strength and the direction of the electric field vector changes. They are also biochemically regulated via second messengers coupled to metabotropic G protein coupled receptors and have diverse intraneuronal effects. Quantum solitons could then transfer energy between the tubulin tails without dissipation. The solitons are nonlinear waves that do not disperse as they propagate [182, 183] and include kinks, antikinks, and different kind of breathers [184–187].

Subneuronal computation in brain microtubules could occur via solitons that are localized excitations propagating in a system with constant velocity and colliding with each other without change in their shapes [145–147, 188, 189]. During the collision of solitons, the solution cannot be represented as a linear combination of two soliton solutions. Remarkably, after the collision solitons recover their shapes

and the only result of collision is a phase shift. There are several equations whose solutions produce solitons [190]. One of the best studied is the sine-Gordon model described by Lagrangian

$$\mathcal{L} = \frac{1}{2} \frac{\partial^2}{\partial t^2} \phi(x, t) - \frac{1}{2} \frac{\partial^2}{\partial x^2} \phi(x, t) - (1 - \cos \phi(x, t)) \quad (99)$$

Static solutions to the sine-Gordon model are the kink and anti-kink

$$\phi = 4 \arctan e^{\pm x} \quad (100)$$

that have winding numbers ± 1 , respectively.

The kink is a localized lump of energy centered around $x = 0$. Other static solutions can be obtained by translating this solution and moving solutions can be obtained by Lorenz transform. If two of these kinks at different positions are superimposed and allowed to evolve, they will move away from each other [145, 146, 189]. The winding number guarantees that the kink cannot decay to the vacuum even if it is perturbed. Noteworthy, the kink–anti-kink solution also does not decay to the vacuum. Collision of a kink with an anti-kink does not lead to annihilation, instead the two solitons will pass through each other [187, 189]. Another oscillating solution known as a breather has a winding number zero and is stable, at least to small perturbations.

The water molecule superradiance [140–143] could contribute to microtubule processing of information if the conformational states of tubulin C-terminal tails are coupled with the dynamics of their hydration shells. In contrast to the intracavital soliton propagation [144], the C-terminal tails/water molecule solitons would be formed on the microtubule surface and could have direct intraneuronal effects such as control of MAP binding and motor protein mediated cargo trafficking. Thus, the flexible tubulin tails could provide means for electric sensitivity and could account for direct translation of the EPSPs and IPSPs into quantum states of microtubules. The model appears to be reasonable because the proposed microtubule solitons could have direct effect upon the presynaptic scaffold protein function and exocytosis [2, 28, 191–193] and because the tubulin tails are prone to extensive biochemical modification thereby providing link to intraneuronal signaling through biochemical second messengers [145, 166, 167, 194]. The only problem is that the tubulin C-terminal tails on microtubules do not appear to have physical means to affect back the electric fields generated by neurons. This one-directional flow of information suggests that microtubules may not be directly involved in the generation of conscious experiences.

5.9 Elastic and Piezoelectric Properties of Microtubules

The elasticity of microtubules is an important physical property of theoretical interest. Experimental measurement of microtubule flexural rigidity determined the Young's modulus of microtubules to be 1.2–1.4 GPa [195, 196]. The value of Young's modulus increases almost threefold under the stabilizing action of MAP tau or taxol [196]. Theoretical models of microtubule vibrations in water revealed interface elastic waves with frequencies up to the gigahertz range and acoustic waves with velocities from 200 to 600 m s⁻¹ [197].

Piezoelectric properties of biological matter also have been considered [198]. The word piezo is Greek for “push.” Piezoelectric crystals acquire an electric charge when compressed, twisted or distorted. Conversely, piezoelectric crystals mechanically contract or expand under the influence of applied electric field. The piezoelectric effect and its inverse provide means for interconversion between electrical and mechanical (elastic) oscillations. The biological importance of microtubule piezoelectric effect remains to be assessed [111].

6 Conclusion

Neuronal membranes support strong electric fields with intensity of $\approx 10^7$ V m⁻¹ [62]. These transmembrane electric fields act upon voltage-gated ion channels whose opening and closing determines the propagation of action potentials within the neural networks. Disturbances in the electric activity of neural networks in the brain lead to neurological or psychiatric diseases [199, 200]. In contrast, the intraneuronal electric field is at least four orders of magnitude weaker. In dendrites, the electric intensity is less than 500 V m⁻¹, which rules out any effect upon the putative ferroelectric state of microtubules. Similarly, intraneuronal magnetic flux density of individual action potentials is less than 10⁻⁸ T, which makes the magnetic field even worse source of sensory information as it will be suffocated by Earth's magnetic field. If cytoskeletal microtubules are somehow involved in the generation of our conscious experiences, then they should have developed mechanisms for converting the electric signals that bring sensory information to the brain cortex into tubulin conformational states. From a biological perspective, the most promising proposal for input of sensory information by microtubules is through tubulin C-terminal tails, which carry a large negative charge and may respond conformationally to local changes of the intraneuronal electric field. Whether the intraneuronal conditions are suitable for generation and propagation of solitons on the microtubule outer surface deserves a further study. The prospects of confirming that microtubules are nothing more than railroad tracks with primary structural function, however, are substantial. The estimated strength of electric and magnetic fields in different neuronal compartments favors voltage-gated ion channels as the main biomolecular substrates supporting consciousness [2, 22, 23].

References

1. Kandel ER, Schwartz JH, Jessell TM, Siegelbaum SA, Hudspeth AJ (2012) Principles of neural science, 5th edn. McGraw-Hill Professional, New York
2. Georgiev DD (2017) Quantum information and consciousness: a gentle introduction. CRC Press, Boca Raton. <https://doi.org/10.1201/9780203732519>
3. Johnston D, Wu SM-S (1995) Foundations of cellular neurophysiology. Bradford Books, MIT Press, Cambridge, MA
4. Sakmann B, Neher E (1995) Single-channel recording, 2nd ed. Springer, New York. <https://doi.org/10.1007/978-1-4419-1229-9>
5. Routh BN, Johnston D, Harris K, Chitwood RA (2009) Anatomical and electrophysiological comparison of CA1 pyramidal neurons of the rat and mouse. *J Neurophysiol* 102(4):2288–2302. <https://doi.org/10.1152/jn.00082.2009>
6. Tripathy SJ, Burton SD, Geramita M, Gerkin RC, Urban NN (2015) Brain-wide analysis of electrophysiological diversity yields novel categorization of Mammalian neuron types. *J Neurophysiol* 113(10):3474–3489. <https://doi.org/10.1152/jn.00237.2015>
7. Malik R, Dougherty KA, Parikh K, Byrne C, Johnston D (2016) Mapping the electrophysiological and morphological properties of CA1 pyramidal neurons along the longitudinal hippocampal axis. *Hippocampus* 26(3):341–361. <https://doi.org/10.1002/hipo.22526>
8. Penfield WG (1954) Some observations on the functional organization of the human brain. *Proc Am Philos Soc* 98(5):293–297
9. Penfield WG (1954) Studies of the cerebral cortex of man: a review and an interpretation. In: Delafresnaye JF (ed) Brain mechanisms and consciousness. Blackwell Publishing, Oxford, pp 284–309
10. Penfield WG (1955) The twenty-ninth Maudsley lecture: the role of the temporal cortex in certain psychical phenomena. *J Mental Sci* 101(424):451–65. <https://doi.org/10.1192/bj.101.424.451>
11. Dobelle WH (2000) Artificial vision for the blind by connecting a television camera to the visual cortex. *ASAIO J* 46(1):3–9. <https://doi.org/10.1097/00002480-200001000-00002>
12. Hameroff SR (1998) Quantum computation in brain microtubules? The Penrose-Hameroff ‘Orch OR’ model of consciousness. *Philos Trans R Soc Lond A* 356(1743):1869–1896. <https://doi.org/10.1098/rsta.1998.0254>
13. Tuszyński JA, Hameroff S, Sarić MV, Trpišová B, Nip MLA (1995) Ferroelectric behavior in microtubule dipole lattices: implications for information processing, signaling and assembly/disassembly. *J Theor Biol* 174(4):371–380. <https://doi.org/10.1006/jtbi.1995.0105>
14. Tuszyński JA, Trpišová B, Sept D, Brown JA (1997) Selected physical issues in the structure and function of microtubules. *J Struct Biol* 118(2):94–106. <https://doi.org/10.1006/jsbi.1997.3843>
15. Tuszyński JA, Sept D, Brown JA (1997) Polymerization, energy transfer and dielectric polarization of microtubules. *Phys Canada* 53(5):237–246
16. Tuszyński JA, BrownJA, Hawrylak P (1998) Dielectric polarization, electrical conduction, information processing and quantum computation in microtubules. Are they plausible? *Philos Trans R Soc Lond. Ser A: Math Phys Eng Sci* 356(1743):1897–1926. <https://doi.org/10.1098/rsta.1998.0255>
17. Tuszyński JA (2008) Molecular and cellular biophysics. Pure and applied physics. CRC Press, Boca Raton. <https://doi.org/10.1201/b21427>
18. Trpišová B, Brown JA (1998) Ordering of dipoles in different types of microtubule lattice. *Int J Mod Phys B* 12(5):543–578. <https://doi.org/10.1142/s0217979298000338>
19. Mershin A, Kolomenski AA, Schuessler HA, Nanopoulos DV (2004) Tubulin dipole moment, dielectric constant and quantum behavior: computer simulations, experimental results and suggestions. *BioSystems* 77(1–3):73–85. <https://doi.org/10.1016/j.biosystems.2004.04.003>
20. Porter MJ (2003) Topological stabilization of quantum states in the microtubule. paper presented at Quantum Mind II: “Consciousness, Quantum Physics & the Brain”

21. Hameroff S, Nip A, Porter MJ, Tuszyński JA (2002) Conduction pathways in microtubules, biological quantum computation, and consciousness. *BioSystems* 64(1–3):149–168. [https://doi.org/10.1016/S0303-2647\(01\)00183-6](https://doi.org/10.1016/S0303-2647(01)00183-6)
22. Georgiev DD (2013) Quantum No-Go theorems and consciousness. *Axiomathes* 23(4):683–695. <https://doi.org/10.1007/s10516-012-9204-1>
23. Georgiev DD (2020) Inner privacy of conscious experiences and quantum information. *Biosystems* 187:104051. <https://doi.org/10.1016/j.biosystems.2019.104051>
24. Ropper AH, Samuels MA, Klein J, Prasad S (2019) Adams and Victor's principles of neurology, 11th edn. McGraw-Hill, New York
25. Nieuwenhuys R (1994) The neocortex: an overview of its evolutionary development, structural organization and synaptology. *Anat Embryol* 190(4):307–337. <https://doi.org/10.1007/bf00187291>
26. Jarvis ED (2009) Evolution of the pallium in birds and reptiles. In: Binder MD, Hirokawa N, Windhorst U (eds) Encyclopedia of neuroscience. Springer, Berlin, pp 1390–1400. https://doi.org/10.1007/978-3-540-29678-2_3165
27. Goldman-Rakic PS (2002) The “psychic cell” of Ramón y Cajal. *Prog Brain Res* 136:427–434. [https://doi.org/10.1016/S0079-6123\(02\)36035-7](https://doi.org/10.1016/S0079-6123(02)36035-7)
28. Georgiev DD, Glazebrook JF (2014) Quantum interactive dualism: from Beck and Eccles tunneling model of exocytosis to molecular biology of SNARE zipping. *Biomed Rev* 25:15–24. <https://doi.org/10.14748/bmr.v25.1038>
29. Harris KM, Spacek J (2016) Dendrite structure. In: Stuart G, Spruston N, Häusser M (eds) Dendrites, 3rd ed. Oxford University Press, Oxford, pp 1–46. <https://doi.org/10.1093/acprof:oso/9780198745273.003.0001>
30. Ulvhake B, Kellerth JO (1981) A quantitative light microscopic study of the dendrites of cat spinal α -motoneurons after intracellular staining with horseradish peroxidase. *J Comp Neurol* 202(4):571–583. <https://doi.org/10.1002/cne.902020409>
31. Kellerth JO, Berthold CH, Conradi S (1979) Electron microscopic studies of serially sectioned cat spinal α -motoneurons. III. Motoneurons innervating fast-twitch (type FR) units of the gastrocnemius muscle. *J Comp Neurol* 184(4):755–767. <https://doi.org/10.1002/cne.901840408>
32. Fiala JC, Harris KM (1999) Dendrite structure. In: Stuart G, Spruston N, Häusser M (eds) Dendrites, 1st edn. Oxford University Press, Oxford, pp 1–34
33. Peters A, Jones EG (1984) Cerebral cortex, vol 1: Cellular components of the cerebral cortex. Plenum Press, New York
34. Feldman ML, Peters A (1978) The forms of non-pyramidal neurons in the visual cortex of the rat. *J Comp Neurol* 179(4):761–793. <https://doi.org/10.1002/cne.901790406>
35. Yu W, Baas PW (1994) Changes in microtubule number and length during axon differentiation. *J Neurosci* 14(5):2818–2829. <https://doi.org/10.1523/jneurosci.14-05-02818.1994>
36. Georgiev DD (2009) Remarks on the number of tubulin dimers per neuron and implications for Hameroff-Penrose Orch OR. *NeuroQuantology* 7(4):677–679. <https://doi.org/10.14704/nq.2009.7.4.261>
37. Overly CC, Rieff HI, Hollenbeck PJ (1996) Organelle motility and metabolism in axons vs dendrites of cultured hippocampal neurons. *J Cell Sci* 109(5):971–980
38. Steward O (2000) Functional neuroscience. Springer, New York. <https://doi.org/10.1007/978-1-4612-1198-3>
39. Martin KC, Zukin RS (2006) RNA trafficking and local protein synthesis in dendrites: an overview. *J Neurosci* 26(27):7131–7134. <https://doi.org/10.1523/jneurosci.1801-06.2006>
40. Shepherd GMG, Harris KM (1998) Three-dimensional structure and composition of CA3→CA1 axons in rat hippocampal slices: implications for presynaptic connectivity and compartmentalization. *J Neurosci* 18(20):8300–8310. <https://doi.org/10.1523/jneurosci.18-20-08300.1998>
41. Traub RD, Bibbig A (2000) A model of high-frequency ripples in the hippocampus based on synaptic coupling plus axon-axon gap junctions between pyramidal neurons. *J Neurosci* 20(6):2086–2093. <https://doi.org/10.1523/jneurosci.20-06-02086.2000>

42. Nogales E, Wolf SG, Downing KH (1998) Structure of the α/β tubulin dimer by electron crystallography. *Nature* 391(6663):199–203. <https://doi.org/10.1038/34465>
43. Erickson HP, Stoffler D (1996) Protofilaments and rings, two conformations of the tubulin family conserved from bacterial FtsZ to α/β and γ tubulin. *J Cell Biol* 135(1):5–8. <https://doi.org/10.1083/jcb.135.1.5>
44. Nanopoulos DV (1995) Theory of brain function, quantum mechanics and superstrings. <https://arxiv.org/abs/hep-ph/9505374>
45. Mavromatos NE, Mershin A, Nanopoulos DV (2002) QED-cavity model of microtubules implies dissipationless energy transfer and biological quantum teleportation. *Int J Mod Phys B* 16(24):3623–3642. <https://doi.org/10.1142/S0217979202011512>
46. Kollman JM, Polka JK, Zelter A, Davis TN, Agard DA (2010) Microtubule nucleating γ -TuSC assembles structures with 13-fold microtubule-like symmetry. *Nature* 466(7308):879–882. <https://doi.org/10.1038/nature09207>
47. Georgiev DD (2009) Tubulin-bound GTP cannot pump microtubule coherence in stable microtubules: towards a revision of microtubule based quantum models of mind. *NeuroQuantology* 7(4):538–547. <https://doi.org/10.14704/nq.2009.7.4.250>
48. Caplow M, Ruhlen RL, Shanks J (1994) The free energy for hydrolysis of a microtubule-bound nucleotide triphosphate is near zero: all of the free energy for hydrolysis is stored in the microtubule lattice. *J Cell Biol* 127(3):779–788. <https://doi.org/10.1083/jcb.127.3.779>
49. Baas PW (1996) The neuronal centrosome as a generator of microtubules for the axon. *Curr Top Dev Biol* 33:281–298. [https://doi.org/10.1016/S0070-2153\(08\)60341-5](https://doi.org/10.1016/S0070-2153(08)60341-5)
50. Drechsel DN, Kirschner MW (1994) The minimum GTP cap required to stabilize microtubules. *Curr Biol* 4(12):1053–1061. [https://doi.org/10.1016/S0960-9822\(00\)00243-8](https://doi.org/10.1016/S0960-9822(00)00243-8)
51. Hyman AA, Salser S, Drechsel DN, Unwin N, Mitchison TJ (1992) Role of GTP hydrolysis in microtubule dynamics: information from a slowly hydrolyzable analogue, GMPCPP. *Mol Biol Cell* 3(10):1155–1167. <https://doi.org/10.1091/mbc.3.10.1155>
52. Hyman AA, Chretien D, Arnal I, Wade RH (1995) Structural changes accompanying GTP hydrolysis in microtubules: information from a slowly hydrolyzable analogue guanylyl-(α,β)-methylene-diphosphonate. *J Cell Biol* 128(1–2):117–125. <https://doi.org/10.1083/jcb.128.1.117>
53. Müller-Reichert T, Chrétien D, Severin F, Hyman AA (1998) Structural changes at microtubule ends accompanying GTP hydrolysis: information from a slowly hydrolyzable analogue of GTP, guanylyl (α,β)-methylenediphosphonate. *Proc Nat Acad Sci* 95(7):3661–3666. <https://doi.org/10.1073/pnas.95.7.3661>
54. Quaranta L (2000) Cellular Samurai: Katanin and the severing of microtubules. *J Cell Sci* 113(16):2821–2827
55. Ahmad FJ, Yu W, McNally FJ, Baas PW (1999) An essential role for katanin in severing microtubules in the neuron. *J Cell Biol* 145(2):305–315. <https://doi.org/10.1083/jcb.145.2.305>
56. Rodionov V, Nadezhina E, Borisy G (1999) Centrosomal control of microtubule dynamics. *Proc Nat Acad Sci USA* 96(1):115–120. <https://doi.org/10.1073/pnas.96.1.115>
57. Baker NA, Sept D, Joseph S, Holst MJ, McCammon JA (2001) Electrostatics of nanosystems: application to microtubules and the ribosome. *Proc Nat Acad Sci* 98(13):10037–10041. <https://doi.org/10.1073/pnas.181342398>
58. Kitaev AY (2003) Fault-tolerant quantum computation by anyons. *Ann Phys* 303(1):2–30. [https://doi.org/10.1016/S0003-4916\(02\)00018-0](https://doi.org/10.1016/S0003-4916(02)00018-0)
59. Mochon C (2003) Anyons from nonsolvable finite groups are sufficient for universal quantum computation. *Phys Rev A* 67(2):022315. <https://doi.org/10.1103/PhysRevA.67.022315>
60. Hameroff SR, Watt RC (1982) Information processing in microtubules. *J Theor Biol* 98(4):549–561. [https://doi.org/10.1016/0022-5193\(82\)90137-0](https://doi.org/10.1016/0022-5193(82)90137-0)
61. Hameroff SR (1987) Ultimate computing: biomolecular consciousness and nanotechnology. North-Holland, Amsterdam
62. Georgiev DD (2004) The nervous principle: active versus passive electric processes in neurons. *Electroneurobiologia* 12(2):169–230

63. Zlatev MP (1972) Theoretical electrotechnics, vol 1. Tehnika, Sofia
64. Arfken G (1985) Mathematical methods for physicists, 3rd edn. Academic Press, San Diego
65. Kaplan W (2002) Advanced calculus, 5th edn. Addison Wesley, Reading, MA
66. Schey HM (2005) Div, grad, curl, and all that: an informal text on vector calculus, 4th edn. W. W. Norton & Company, New York
67. Nave CR (2017) HyperPhysics. Georgia State University, Atlanta, Georgia. <http://hyperphysics.phy-astr.gsu.edu/hbase/index.html>
68. Schneidman E (2001) Noise and information in neural codes. Ph.D. thesis
69. Georgiev DD (2015) Monte Carlo simulation of quantum Zeno effect in the brain. *Int J Mod Phys B* 29(7):1550039. <https://doi.org/10.1142/S0217979215500393>
70. Miller JP, Jacobs GA (1984) Relationships between neuronal structure and function. *J Exp Biol* 112(1):129–145
71. Miller JP, Rall W, Rinzel J (1985) Synaptic amplification by active membrane in dendritic spines. *Brain Res* 325(1–2):325–330. [https://doi.org/10.1016/0006-8993\(85\)90333-6](https://doi.org/10.1016/0006-8993(85)90333-6)
72. Fleshman JW, Segev I, Burke RB (1988) Electrotone architecture of type-identified α -motoneurons in the cat spinal cord. *J Neurophysiol* 60(1):60–85. <https://doi.org/10.1152/jn.1988.60.1.60>
73. Omori T, Aonishi T, Miyakawa H, Inoue M, Okada M (2006) Estimated distribution of specific membrane resistance in hippocampal CA1 pyramidal neuron. *Brain Res* 1125(1):199–208. <https://doi.org/10.1016/j.brainres.2006.09.095>
74. Golding NL, Mickus TJ, Katz Y, Kath WL, Spruston N (2005) Factors mediating powerful voltage attenuation along CA1 pyramidal neuron dendrites. *J Physiol* 568(1):69–82. <https://doi.org/10.1113/jphysiol.2005.086793>
75. Cohen CCH, Popovic MA, Klooster J, Weil M-T, Möbius W, Nave K-A, Kole MHP (2020) Saltatory conduction along myelinated axons involves a periaxonal nanocircuit. *Cell* 180(2):311–322. <https://doi.org/10.1016/j.cell.2019.11.039>
76. Holmes WR (2013) Cable equation. In: Jaeger D, Jung R (eds) Encyclopedia of computational neuroscience. Springer, New York, pp 1–13. https://doi.org/10.1007/978-1-4614-7320-6_478-1
77. Stoilov SP, Rusanov EM, Mitev DN, Genkov DN (1985) Biofizika. Medicina i Fizkultura, Sofia
78. Waldrop B, Glantz RM (1985) Synaptic mechanisms of a tonic EPSP in crustacean visual interneurons: analysis and simulation. *J Neurophysiol* 54(3):636–650. <https://doi.org/10.1152/jn.1985.54.3.636>
79. Mayer ML, Vyklicky L Jr (1989) Concanavalin A selectively reduces desensitization of Mammalian neuronal quisqualate receptors. *Proc Nat Acad Sci* 86(4):1411–1415. <https://doi.org/10.1073/pnas.86.4.1411>
80. Sayer RJ, Friedlander MJ, Redman SJ (1990) The time course and amplitude of EPSPs evoked at synapses between pairs of CA3/CA1 neurons in the hippocampal slice. *J Neurosci* 10(3):826–836. <https://doi.org/10.1523/jneurosci.10-03-00826.1990>
81. London M, Segev I (2001) Synaptic scaling in vitro and in vivo. *Nat Neurosci* 4(9):853–855. <https://doi.org/10.1038/nn0901-853>
82. Spruston N (2000) Distant synapses raise their voices. *Nat Neurosci* 3(9):849–851. <https://doi.org/10.1038/78734>
83. Geiger JRP, Lübke J, Roth A, Frotscher M, Jonas P (1997) Submillisecond AMPA receptor-mediated signaling at a principal neuron-interneuron synapse. *Neuron* 18(6):1009–1023. [https://doi.org/10.1016/S0896-6273\(00\)80339-6](https://doi.org/10.1016/S0896-6273(00)80339-6)
84. Kleppe IC, Robinson HP (1999) Determining the activation time course of synaptic AMPA receptors from openings of colocalized NMDA receptors. *Biophys J* 77(3):1418–1427. [https://doi.org/10.1016/S0006-3495\(99\)76990-0](https://doi.org/10.1016/S0006-3495(99)76990-0)
85. Li S, Liu N, Yao L, Zhang X, Zhou D, Cai D (2019) Determination of effective synaptic conductances using somatic voltage clamp. *PLoS Comput Biol* 15(3):e1006871. <https://doi.org/10.1371/journal.pcbi.1006871>

86. Hodgkin AL, Rushton WAH (1946) The electrical constants of a crustacean nerve fibre. Proc R Soc Lond. Ser B Biol Sci 133(873):444–479. <https://doi.org/10.1098/rspb.1946.0024>
87. Jaffe LF, Nuccitelli R (1977) Electrical controls of development. Ann Rev Biophys Bioeng 6(1):445–476. <https://doi.org/10.1146/annurev.bb.06.060177.002305>
88. Chang H-T (1952) Cortical neurons with particular reference to the apical dendrites. Cold Spring Harb Symp Quant Biol 17:189–202. <https://doi.org/10.1101/sqb.1952.017.01.019>
89. Coss RG, Globus A (1978) Spine stems on tectal interneurons in jewel fish are shortened by social stimulation. Science 200(4343):787–790. <https://doi.org/10.1126/science.644322>
90. Pankratov YV, Krishtal OA (2003) Distinct quantal features of AMPA and NMDA synaptic currents in hippocampal neurons: implication of glutamate spillover and receptor saturation. Biophys J 85(5):3375–3387. [https://doi.org/10.1016/S0006-3495\(03\)74757-2](https://doi.org/10.1016/S0006-3495(03)74757-2)
91. Kirischuk S, Veselovsky N, Grantyn R (1999) Relationship between presynaptic calcium transients and postsynaptic currents at single γ -aminobutyric acid (GABA) α ergic boutons. Proc Nat Acad Sci 96(13):7520–7525. <https://doi.org/10.1073/pnas.96.13.7520>
92. Akaike N, Murakami N, Katsurabayashi S, Jin Y-H, Imazawa T (2002) Focal stimulation of single GABAergic presynaptic boutons on the rat hippocampal neuron. Neurosci Res 42(3):187–195. [https://doi.org/10.1016/S0168-0102\(01\)00320-0](https://doi.org/10.1016/S0168-0102(01)00320-0)
93. Akaike N, Moorhouse AJ (2003) Techniques: applications of the nerve-bouton preparation in neuropharmacology. Trends Pharmacol Sci 24(1):44–47. [https://doi.org/10.1016/S0165-6147\(02\)00010-X](https://doi.org/10.1016/S0165-6147(02)00010-X)
94. Henze DA, McMahon DBT, Harris KM, Barrio Nuevo G (2002) Giant miniature EPSCs at the hippocampal mossy fiber to CA3 pyramidal cell synapse are monoquantal. J Neurophysiol 87(1):15–29. <https://doi.org/10.1152/jn.00394.2001>
95. Hodgkin AL, Huxley AF (1952) Currents carried by sodium and potassium ions through the membrane of the giant axon of Loligo. J Physiol 116(4):449–472. <https://doi.org/10.1113/jphysiol.1952.sp004717>
96. Hodgkin AL, Huxley AF (1952) The components of membrane conductance in the giant axon of Loligo. J Physiol 116(4):473–496. <https://doi.org/10.1113/jphysiol.1952.sp004718>
97. Hodgkin AL, Huxley AF (1952) The dual effect of membrane potential on sodium conductance in the giant axon of Loligo. J Physiol 116(4):497–506. <https://doi.org/10.1113/jphysiol.1952.sp004719>
98. Clay JR (1998) Excitability of the squid giant axon revisited. J Neurophysiol 80(2):903–913. <https://doi.org/10.1152/jn.1998.80.2.903>
99. Carter BC, Bean BP (2009) Sodium entry during action potentials of mammalian neurons: incomplete inactivation and reduced metabolic efficiency in fast-spiking neurons. Neuron 64(6):898–909. <https://doi.org/10.1016/j.neuron.2009.12.011>
100. Benavides-Piccione R, Regaldo-Reyes M, Fernaud-Espinosa I, Kastanauskaitė A, Tapia-González S, León-Espinosa G, Rojo C, Insausti R, Segev I, DeFelipe J (2019) Differential structure of hippocampal CA1 pyramidal neurons in the human and mouse. Cereb Cortex. <https://doi.org/10.1093/cercor/bhz122>
101. Wikswo JP, Barach JP, Freeman JA (1980) Magnetic field of a nerve impulse: first measurements. Science 208(4439):53–55. <https://doi.org/10.1126/science.7361105>
102. Neuhaus O, Archelos JJ, Hartung H-P (2003) Immunomodulation in multiple sclerosis: from immunosuppression to neuroprotection. Trends Pharmacol Sci 24(3):131–138. [https://doi.org/10.1016/S0165-6147\(03\)00028-2](https://doi.org/10.1016/S0165-6147(03)00028-2)
103. Leadley DR, Nicholas RJ, Maude DK, Utjuh AN, Portal JC, Harris JJ, Foxon CT (1997) Fractional quantum Hall effect measurements at zero g factor. Phys Rev Lett 79(21):4246–4249. <https://doi.org/10.1103/PhysRevLett.79.4246>
104. Leadley DR, van der Burgt M, Nicholas RJ, Gee PJ, Singleton J, Harris JJ, Foxon CT (1996) The unifying role of effective field in the composite fermion model of the fractional quantum Hall effect. Surf Sci 361–362:22–25. [https://doi.org/10.1016/0039-6028\(96\)00321-4](https://doi.org/10.1016/0039-6028(96)00321-4)
105. Mandelkow E, Thomas J, Cohen C (1977) Microtubule structure at low resolution by x-ray diffraction. Proc Nat Acad Sci USA 74(8):3370–3374. <https://doi.org/10.1073/pnas.74.8.3370>

106. Mandelkow E-M, Mandelkow E, Unwin N, Cohen C (1977) Tubulin hoops. *Nature* 265(5595):655–657. <https://doi.org/10.1038/265655a0>
107. Crepeau RH, McEwen B, Edelstein SJ (1978) Differences in α and β polypeptide chains of tubulin resolved by electron microscopy with image reconstruction. *Proc Nat Acad Sci USA* 75(10):5006–5010. <https://doi.org/10.1073/pnas.75.10.5006>
108. McEwen B, Edelstein SJ (1980) Evidence for a mixed lattice in microtubules reassembled in vitro. *J Mol Biol* 139(2):123–143. [https://doi.org/10.1016/0022-2836\(80\)90300-9](https://doi.org/10.1016/0022-2836(80)90300-9)
109. Song Y, Mandelkow E (1993) Recombinant kinesin motor domain binds to β -tubulin and decorates microtubules with b surface lattice. *Proc Nat Acad Sci* 90(5):1671–1675. <https://doi.org/10.1073/pnas.90.5.1671>
110. Kikkawa M, Ishikawa T, Nakata T, Wakabayashi T, Hirokawa N (1994) Direct visualization of the microtubule lattice seam both in vitro and in vivo. *J Cell Biol* 127(6):1965–1971. <https://doi.org/10.1083/jcb.127.6.1965>
111. Brown JA, Tuszyński JA (1999) A review of the ferroelectric model of microtubules. *Ferroelectrics* 220(1):141–155. <https://doi.org/10.1080/00150199908216213>
112. Faber J, Portugal R, Rosa LP (2006) Information processing in brain microtubules. *BioSystems* 83(1):1–9. <https://doi.org/10.1016/j.biosystems.2005.06.011>
113. Dresselhaus MS, Dresselhaus G, Eklund PC (1996) Science of fullerenes and carbon nanotubes: their properties and applications. Academic Press, San Diego
114. Audenaert R, Heremans L, Heremans K, Engelborghs Y (1989) Secondary structure analysis of tubulin and microtubules with Raman spectroscopy. *Biochimica et Biophysica Acta (BBA) - Protein Struct Mol Enzymol* 996(1):110–115. [https://doi.org/10.1016/0167-4838\(89\)90102-7](https://doi.org/10.1016/0167-4838(89)90102-7)
115. Melki R, Carlier MF, Pantaloni D, Timasheff SN (1989) Cold depolymerization of microtubules to double rings: geometric stabilization of assemblies. *Biochemistry* 28(23):9143–9152. <https://doi.org/10.1021/bi00449a028>
116. Mavromatos NE, Nanopoulos DV (1998) On quantum mechanical aspects of microtubules. *Int J Mod Phys B* 12(5):517–542. <https://doi.org/10.1142/s0217979298000326>
117. Mavromatos NE, Nanopoulos DV, Samaras I, Zioutas K (1999) Ferroelectrics and their possible involvement in biology. *Adv Struct Biol* 5:127–134. [https://doi.org/10.1016/S1064-6000\(98\)80009-4](https://doi.org/10.1016/S1064-6000(98)80009-4)
118. Mavromatos NE, Nanopoulos DV (1999) Quantum mechanics in cell microtubules: wild imagination or realistic possibility? *Adv Struct Biol* 5:283–318. [https://doi.org/10.1016/S1064-6000\(98\)80015-X](https://doi.org/10.1016/S1064-6000(98)80015-X)
119. Tran PT, Joshi P, Salmon ED (1997) How tubulin subunits are lost from the shortening ends of microtubules. *J Struct Biol* 118(2):107–118. <https://doi.org/10.1006/jsb.1997.3844>
120. Weisenberg RC, Deery WJ, Dickinson PJ (1976) Tubulin-nucleotide interactions during the polymerization and depolymerization of microtubules. *Biochemistry* 15(19):4248–4254. <https://doi.org/10.1021/bi00664a018>
121. Carlier MF, Pantaloni D (1981) Kinetic analysis of guanosine 5'-triphosphate hydrolysis associated with tubulin polymerization. *Biochemistry* 20(7):1918–1924. <https://doi.org/10.1021/bi00510a030>
122. Stewart RJ, Farrell KW, Wilson L (1990) Role of GTP hydrolysis in microtubule polymerization: evidence for a coupled hydrolysis mechanism. *Biochemistry* 29(27):6489–6498. <https://doi.org/10.1021/bi00479a022>
123. Voter WA, O'Brien ET, Erickson HP (1991) Dilution-induced disassembly of microtubules: relation to dynamic instability and the GTP cap. *Cell Motil Cytoskelet* 18(1):55–62. <https://doi.org/10.1002/cm.970180106>
124. Walker RA, Pryer NK, Salmon ED (1991) Dilution of individual microtubules observed in real time in vitro: evidence that cap size is small and independent of elongation rate. *J Cell Biol* 114(1):73–81. <https://doi.org/10.1083/jcb.114.1.73>
125. Mitchison T, Kirschner M (1984) Dynamic instability of microtubule growth. *Nature* 312(5991):237–242. <https://doi.org/10.1038/312237a0>

126. Fygenson DK (2001) A unifying hypothesis for the conformational change of tubulin. <https://arxiv.org/abs/physics/0101078>
127. Mandelkow E-M, Mandelkow E, Milligan RA (1991) Microtubule dynamics and microtubule caps: a time-resolved cryo-electron microscopy study. *J Cell Biol* 114(5):977–991. <https://doi.org/10.1083/jcb.114.5.977>
128. Fygenson DK, Braun E, Libchaber A (1994) Phase diagram of microtubules. *Phys Rev E* 50(2):1579–1588. <https://doi.org/10.1103/PhysRevE.50.1579>
129. Fygenson DK (1995) Microtubules: the rhythm of growth and evolution of form. Ph.D. thesis. Princeton University
130. Downing KH, Nogales E (1998) Tubulin and microtubule structure. *Curr Opin Cell Biol* 10(1):16–22. [https://doi.org/10.1016/S0955-0674\(98\)80082-3](https://doi.org/10.1016/S0955-0674(98)80082-3)
131. Davis A, Sage CR, Dougherty CA, Farrell KW (1994) Microtubule dynamics modulated by guanosine triphosphate hydrolysis activity of β -tubulin. *Science* 264(5160):839–842. <https://doi.org/10.1126/science.8171338>
132. Sage CR, Dougherty CA, Davis AS, Burns RG, Wilson L, Farrell KW (1995) Site-directed mutagenesis of putative gtp-binding sites of yeast β -tubulin: evidence that α -, β -, and γ -tubulins are atypical gtpases. *Biochemistry* 34(22):7409–7419. <https://doi.org/10.1021/bi00022a014>
133. Cope FW (1975) A review of the applications of solid state physics concepts to biological systems. *J Biol Phys* 3(1):1–41. <https://doi.org/10.1007/bf02308900>
134. Hazlewood CF, Nichols BL, Chamberlain NF (1969) Evidence for the existence of a minimum of two phases of ordered water in skeletal muscle. *Nature* 222(5195):747–750. <https://doi.org/10.1038/222747a0>
135. Hazlewood CF, Chang DC, Nichols BL, Woessner DE (1974) Nuclear magnetic resonance transverse relaxation times of water protons in skeletal muscle. *Biophys J* 14(8):583–606. [https://doi.org/10.1016/S0006-3495\(74\)85937-0](https://doi.org/10.1016/S0006-3495(74)85937-0)
136. Kuntz ID, Kauzmann W (1974) Hydration of proteins and polypeptides. *Adv Protein Chem* 28:239–345. [https://doi.org/10.1016/S0065-3233\(08\)60232-6](https://doi.org/10.1016/S0065-3233(08)60232-6)
137. Cooke R, Kuntz ID (1974) The properties of water in biological systems. *Ann Rev Biophys Bioeng* 3(1):95–126. <https://doi.org/10.1146/annurev.bb.03.060174.000523>
138. Mascarenhas S (1974) The electret effect in bone and biopolymers and the bound-water problem. *Ann N Y Acad Sci* 238(1):36–52. <https://doi.org/10.1111/j.1749-6632.1974.tb26778.x>
139. Del Giudice E, Doglia S, Milani M, Vitiello G (1986) Collective properties of biological systems. In: Gutmann F, Keyzer H (eds) Modern bioelectrochemistry. Springer, Boston, pp 263–287. https://doi.org/10.1007/978-1-4613-2105-7_9
140. Jibu M, Hagan S, Hameroff SR, Pribram KH, Yasue K (1994) Quantum optical coherence in cytoskeletal microtubules: implications for brain function. *BioSystems* 32(3):195–209. [https://doi.org/10.1016/0303-2647\(94\)90043-4](https://doi.org/10.1016/0303-2647(94)90043-4)
141. Jibu M, Yasue K (1995) Quantum brain dynamics and consciousness: an introduction, vol 3 of advances in consciousness research. John Benjamins, Amsterdam. <https://doi.org/10.1075/aicr.3>
142. Jibu M, Pribram KH, Yasue K (1996) From conscious experience to memory storage and retrieval: the role of quantum brain dynamics and boson condensation of evanescent photons. *Int J Mod Phys B* 10(13–14):1735–1754. <https://doi.org/10.1142/S0217979296000805>
143. Jibu M, Yasue K (1997) What is mind?—quantum field theory of evanescent photons in brain as quantum theory of consciousness. *Informatica (Slovenia)* 21(3):471–490
144. Abdalla E, Maroufi B, Melgar BC, Sedra MB (2001) Information transport by sine-Gordon solitons in microtubules. *Phys A* 301(1–4):169–173. [https://doi.org/10.1016/S0378-4371\(01\)00399-5](https://doi.org/10.1016/S0378-4371(01)00399-5)
145. Georgiev DD, Papaioanou SN, Glazebrook JF (2004) Neuronic system inside neurons: molecular biology and biophysics of neuronal microtubules. *Biomed Rev* 15:67–75. <http://doi.org/10.14748/bmr.v15.103>

146. Georgiev DD, Glazebrook JF (2007) Subneuronal processing of information by solitary waves and stochastic processes. In: Lyshevski SE (ed) Nano and molecular electronics handbook. Nano and microengineering series, Chap 17. CRC Press, Boca Raton, pp 1–41
147. Georgiev DD, Glazebrook JF (2007) Conformational dynamics and thermal cones of C-terminal tubulin tails in neuronal microtubules. *NeuroQuantology* 5(1):62–84. <http://doi.org/10.14704/nq.2007.5.1.119>
148. Krauhs E, Little M, Kempf T, Hofer-Warbinek R, Ade W, Ponstingl H (1981) Complete amino acid sequence of β -tubulin from porcine brain. *Proc Nat Acad Sci* 78(7):4156–4160. <https://doi.org/10.1073/pnas.78.7.4156>
149. Ponstingl H, Krauhs E, Little M, Kempf T (1981) Complete amino acid sequence of α -tubulin from porcine brain. *Proc Nat Acad Sci USA* 78(5):2757–2761. <https://doi.org/10.1073/pnas.78.5.2757>
150. Sarkar T, Manna T, Bhattacharyya S, Mahapatra P, Poddar A, Roy S, Pena J, Solana R, Tarazona R, Bhattacharyya B (2001) Role of the carboxy-termini of tubulin on its chaperone-like activity. *Proteins* 44(3):262–269. <https://doi.org/10.1002/prot.1091>
151. Wall KP, Pagratis M, Armstrong G, Balsbaugh JL, Verbeke E, Pearson CG, Hough LE (2016) Molecular determinants of tubulin's C-terminal tail conformational ensemble. *ACS Chem Biol* 11(11):2981–2990. <https://doi.org/10.1021/acschembio.6b00507>
152. Fujii T, Koizumi Y (1999) Identification of the binding region of basic calponin on α and β tubulins. *J Biochem* 125(5):869–875. <https://doi.org/10.1093/oxfordjournals.jbchem.a022362>
153. Rai SS, Wolff J (1998) The c terminus of β -tubulin regulates vinblastine-induced tubulin polymerization. *Proc Nat Acad Sci* 95(8):4253–4257. <https://doi.org/10.1073/pnas.95.8.4253>
154. Mukhopadhyay K, Parrack PK, Bhattacharyya B (1990) The carboxy terminus of the α subunit of tubulin regulates its interaction with colchicine. *Biochemistry* 29(29):6845–6850. <https://doi.org/10.1021/bi00481a013>
155. Uppuluri S, Knippling L, Sackett DL, Wolff J (1993) Localization of the colchicine-binding site of tubulin. *Proc Nat Acad Sci USA* 90(24):11598–11602. <https://doi.org/10.1073/pnas.90.24.11598>
156. Bai R, Pei X-F, Boye O, Getahun Z, Grover S, Bekiszi J, Nguyen NY, Brossi A, Hamel E (1996) Identification of cysteine 354 of beta-tubulin as part of the binding site for the A ring of colchicine. *J Biol Chem* 271(21):12639–12645
157. Bensimon G, Chermat R (1991) Microtubule disruption and cognitive defects: effect of colchicine on learning behavior in rats. *Pharmacol Biochem Behav* 38(1):141–145. [https://doi.org/10.1016/0091-3057\(91\)90602-X](https://doi.org/10.1016/0091-3057(91)90602-X)
158. Kolasa K, Jope RS, Baird MS, Johnson GVW (1992) Alterations of choline acetyltransferase, phosphoinositide hydrolysis, and cytoskeletal proteins in rat brain in response to colchicine administration. *Exp Brain Res* 89(3):496–500. <https://doi.org/10.1007/bf00229873>
159. Sackett DL, Bhattacharyya B, Wolff J (1985) Tubulin subunit carboxyl termini determine polymerization efficiency. *J Biol Chem* 260(1):43–45
160. Skiniotis G, Cochran JC, Mueller J, Mandelkow E, Gilbert SP, Hoenger A (2004) Modulation of kinesin binding by the C-termini of tubulin. *EMBO J* 23(5):989–999. <https://doi.org/10.1038/sj.emboj.7600118>
161. Serrano L, de la Torre J, Maccioni RB, Avila J (1984) Involvement of the carboxyl-terminal domain of tubulin in the regulation of its assembly. *Proc Nat Acad Sci USA* 81(19):5989–5993. <https://doi.org/10.1073/pnas.81.19.5989>
162. Solomon F (1977) Binding sites for calcium on tubulin. *Biochemistry* 16(3):358–363. <https://doi.org/10.1021/bi00622a003>
163. Lewis SA, Gilmartin ME, Hall JL, Cowan NJ (1985) Three expressed sequences within the human β -tubulin multigene family each define a distinct isotype. *J Mol Biol* 182(1):11–20. [https://doi.org/10.1016/0022-2836\(85\)90023-3](https://doi.org/10.1016/0022-2836(85)90023-3)
164. Zettlmeissl G, Rudolph R, Jaenicke R (1979) Reconstitution of lactic dehydrogenase. Non-covalent aggregation vs. reactivation. 1. Physical properties and kinetics of aggregation. *Biochemistry* 18(25):5567–5571. <https://doi.org/10.1021/bi00592a007>

165. Ludueña RF (1997) Multiple forms of tubulin: different gene products and covalent modifications. *Int Rev Cytol* 178:207–275. [https://doi.org/10.1016/S0074-7696\(08\)62138-5](https://doi.org/10.1016/S0074-7696(08)62138-5)
166. MacRae TH (1997) Tubulin post-translational modifications. Enzymes and their mechanisms of action. *Euro J Biochem* 244(2):265–278. <https://doi.org/10.1111/j.1432-1033.1997.00265.x>
167. Rosenbaum J (2000) Cytoskeleton: functions for tubulin modifications at last. *Curr Biol* 10(21):R801–R803. [https://doi.org/10.1016/s0960-9822\(00\)00767-3](https://doi.org/10.1016/s0960-9822(00)00767-3)
168. Banerjee A (2002) Coordination of posttranslational modifications of bovine brain α -tubulin: polyglycylation of $\delta 2$ tubulin. *J Biol Chem* 277(48):46140–46144. <https://doi.org/10.1074/jbc.m208065200>
169. Silflow CD (1991) Why do tubulin gene families lack diversity in flagellate/ciliate protists? *Protoplasma* 164(1):9–11. <https://doi.org/10.1007/bf01320810>
170. McKean PG, Vaughan S, Gull K (2001) The extended tubulin superfamily. *J Cell Sci* 114(15):2723–2733
171. Idriss HT (2000) Man to Trypanosome: the tubulin tyrosination/detyrosination cycle revisited. *Cell Motility Cytoskeleton* 45(3):173–184. [http://doi.org/10.1002/\(SICI\)1097-0169\(200003\)45:3<173::AID-CM1>3.0.CO;2-0](http://doi.org/10.1002/(SICI)1097-0169(200003)45:3<173::AID-CM1>3.0.CO;2-0)
172. Gundersen GG, Kalnoski MH, Bulinski JC (1984) Distinct populations of microtubules: tyrosinated and nontyrosinated alpha tubulin are distributed differently in vivo. *Cell* 38(3):779–789. [https://doi.org/10.1016/0092-8674\(84\)90273-3](https://doi.org/10.1016/0092-8674(84)90273-3)
173. Kreitzer G, Liao G, Gundersen GG (1999) Detyrosination of tubulin regulates the interaction of intermediate filaments with microtubules in vivo via a kinesin-dependent mechanism. *Mol Biol Cell* 10(4):1105–1118. <https://doi.org/10.1091/mbc.10.4.1105>
174. Bré MH, Redeker V, Vinh J, Rossier J, Levilliers N (1998) Tubulin polyglycylation: differential posttranslational modification of dynamic cytoplasmic and stable axonemal microtubules in Paramecium. *Mol Biol Cell* 9(9):2655–2665. <https://doi.org/10.1091/mbc.9.9.2655>
175. Schneider A, Plessmann U, Weber K (1997) Subpellicular and flagellar microtubules of trypanosoma brucei are extensively glutamylated. *J Cell Sci* 110(4):431–437
176. Million K, Larcher J, Laoukili J, Bourguignon D, Marano F, Tournier F (1999) Polyglutamylation and polyglycylation of α - and β -tubulins during in vitro ciliated cell differentiation of human respiratory epithelial cells. *J Cell Sci* 112(23):4357–4366
177. Bobiniec Y, Khodjakov A, Mir LM, Rieder CL, Eddé B, Bornens M (1998) Centriole disassembly in vivo and its effect on centrosome structure and function in vertebrate cells. *J Cell Biol* 143(6):1575–1589. <https://doi.org/10.1083/jcb.143.6.1575>
178. Boucher D, Larcher J-C, Gros F, Denoulet P (1994) Polyglutamylation of tubulin as a progressive regulator of in vitro interactions between the microtubule-associated protein tau and tubulin. *Biochemistry* 33(41):12471–12477. <https://doi.org/10.1021/bi00207a014>
179. Larcher J-C, Boucher D, Lazereg S, Gros F, Denoulet P (1996) Interaction of kinesin motor domains with α - and β -tubulin subunits at a τ -independent binding site. Regulation by polyglutamylation. *J Biol Chem* 271(36):22117–22124. <https://doi.org/10.1074/jbc.271.36.22117>
180. Bonnet C, Boucher D, Lazereg S, Pedrotti B, Islam K, Denoulet P, Larcher JC (2001) Differential binding regulation of microtubule-associated proteins MAP1A, MAP1B, and MAP2 by tubulin polyglutamylation. *J Biol Chem* 276(16):12839–12848. <https://doi.org/10.1074/jbc.m011380200>
181. Baumann MH, Wisniewski T, Levy E, Plant GT, Ghiso J (1996) C-terminal fragments of α - and β -tubulin form amyloid fibrils in vitro and associate with amyloid deposits of familial cerebral amyloid angiopathy, British type. *Biochem Biophys Res Commun* 219(1):238–242. <https://doi.org/10.1006/bbrc.1996.0211>
182. Dodd RK, Eilbeck JC, Gibbon JD, Morris HC (1982) Solitons and nonlinear wave equations. Academic Press, London
183. Fordy AP (1994) A historical introduction to solitons and bäcklund transformations. In: Fordy AP, Wood JC (eds) Harmonic maps and integrable systems. Aspects of mathematics. Vieweg, Wiesbaden, pp 7–28. https://doi.org/10.1007/978-3-663-14092-4_2

184. Dmitriev SV, Nauman LV, Wusatowska-Sarnek AM, Starostenkov MD (1997) Generation and annihilation of dislocations in the discrete Frenkel-Kontorova model. *Phys Status Solidi (b)* 201(1):89–96. [http://doi.org/10.1002/1521-3951\(199705\)201:1<89::AID-PSSB89>3.0.CO;2-E](http://doi.org/10.1002/1521-3951(199705)201:1<89::AID-PSSB89>3.0.CO;2-E)
185. Dmitriev SV, Shigenari T, Vasiliev AA, Miroshnichenko AE (1998) Effect of discreteness on a sine-Gordon three-soliton solution. *Phys Lett A* 246(1–2):129–134. [https://doi.org/10.1016/S0375-9601\(98\)00459-9](https://doi.org/10.1016/S0375-9601(98)00459-9)
186. Dmitriev SV, Miyachi T, Abe K, Shigenari T (2000) Kink-breather solution in the weakly discrete Frenkel-Kontorova model. *Phys Rev E* 61(5):5880–5885. <https://doi.org/10.1103/PhysRevE.61.5880>
187. Miroshnichenko AE, Dmitriev SV, Vasiliev AA, Shigenari T (2000) Inelastic three-soliton collisions in a weakly discrete sine-Gordon system. *Nonlinearity* 13(3):837–848. <https://doi.org/10.1088/0951-7715/13/3/318>
188. Georgiev DD, Glazebrook JF (2006) Dissipationless waves for information transfer in neurobiology - some implications. *Informatica (Slovenia)* 30(2):221–232
189. Georgiev DD, Papaioanou SN, Glazebrook JF (2007) Solitonic effects of the local electromagnetic field on neuronal microtubules. *NeuroQuantology* 5(3):276–291. <http://doi.org/10.14704/nq.2007.5.3.137>
190. Wadati M (2001) Introduction to solitons. *Pramana* 57(5–6):841–847. <https://doi.org/10.1007/s12043-001-0002-3>
191. Georgiev DD, Glazebrook JF (2010) SNARE proteins as molecular masters of interneuronal communication. *Biomed Rev* 21:17–23. <http://doi.org/10.14748/bmr.v21.43>
192. Georgiev DD, Glazebrook JF (2012) Quasiparticle tunneling in neurotransmitter release. In: Goddard III WA, Brenner D, Lyshevski SE, Iafrate GJ (eds) *Handbook of nanoscience, engineering, and technology*, 3rd ed. Electrical Engineering Handbook, Chap 30. CRC Press, Boca Raton, pp 983–1016
193. Georgiev DD, Glazebrook JF (2018) The quantum physics of synaptic communication via the SNARE protein complex. *Prog Biophys Mol Biol* 135:16–29. <https://doi.org/10.1016/j.pbiomolbio.2018.01.006>
194. Włoga D, Joachimiak E, Fabczak H (2017) Tubulin post-translational modifications and microtubule dynamics. *Int J Mol Sci* 18(10):2207. <https://doi.org/10.3390/ijms18102207>
195. Gittes F, Mickey B, Nettleton J, Howard J (1993) Flexural rigidity of microtubules and actin filaments measured from thermal fluctuations in shape. *J Cell Biol* 120(4):923–934. <https://doi.org/10.1083/jcb.120.4.923>
196. Mickey B, Howard J (1995) Rigidity of microtubules is increased by stabilizing agents. *J Cell Biol* 130(4):909–917. <https://doi.org/10.1083/jcb.130.4.909>
197. Sirenko YM, Stroscio MA, Kim KW (1996) Elastic vibrations of microtubules in a fluid. *Phys Rev E* 53(1):1003–1010. <https://doi.org/10.1103/PhysRevE.53.1003>
198. Athenstaedt H (1974) Pyroelectric and piezoelectric properties of vertebrates. *Ann N Y Acad Sci* 238(1):68–94. <https://doi.org/10.1111/j.1749-6632.1974.tb26780.x>
199. Lerche H, Jurkat-Rott K, Lehmann-Horn F (2001) Ion channels and epilepsy. *Am J Med Genet* 106(2):146–159. <https://doi.org/10.1002/ajmg.1582>
200. Georgiev D, Arion D, Enwright JF, Kikuchi M, Minabe Y, Corradi JP, Lewis DA, Hashimoto T (2014) Lower gene expression for KCNS3 potassium channel subunit in parvalbumin-containing neurons in the prefrontal cortex in schizophrenia. *Am J Psychiatry* 171(1):62–71. <https://doi.org/10.1176/appi.ajp.2013.13040468>

Chapter 4

Time Crystal Engineering in Catalytic Reaction Cycles



Pathik Sahoo and Subrata Ghosh

1 Introduction

A spontaneous symmetry breaking in a Hamiltonian system is a fundamental concept in modern physics [1] that attributes the findings like superconductors, (anti)ferromagnets, cosmology, Bose–Einstein condensates or high-energy physics theoretically. For example, time-reversal symmetry and spin symmetry breaking form the magnetically ordered materials [2, 3]. Likewise, breaking of global gauge symmetry generates Higgs boson/superfluids [4, 5].

Regarding crystals, breaking of spatial translational symmetry triggers the formation of spatial crystal and leads phase changing from liquid to solid state. Similarly, a breaking of translational symmetry in time creates ‘time crystal’ [6, 3] or space-time crystal, which is forbidden in thermal equilibrium [7, 8, 9]. In other words, a structure of time crystal gets repeated against both time and space synchronously [10], whereas sole spatial repetition generates spatial crystal. Time crystal does not convert the thermal energy into mechanical work as the overall energy is conserved, implies it does not break the laws of thermodynamics. Their ‘motion without energy’ does never represent the conventional kinetic energy in system [11]. Last few years witnessed the implications of time crystals from cyclic universe [2] to trapped ions

P. Sahoo (✉)

International Center for Materials Nanoarchitectonics, National Institute for Materials Science (NIMS), 1-1 Namiki, Tsukuba, Ibaraki 305-0044, Japan

e-mail: 2c.pathik@gmail.com

International Institute of Invincible Rhythms, Shimla, Himachal Pradesh 171006, India

S. Ghosh

Chemical Science & Technology Division, Academy of Scientific & Innovative Research, CSIR-North East Institute of Science & Technology, Jorhat, Assam, India

e-mail: ocsgin@gmail.com

[12]. This chapter will recapitulate the potential aspects of catalytic reaction cycles in finding geometrical pattern, kinetic effects, effect of breaking cycle, information processing, self-decisive cycles in exploring a new avenue in time crystal.

Considering each single reaction in a catalytic reaction cycle an event, some single events can also be composed of a set of other reactions. Herein, a time-dependent geometrical shape can be constructed by integrating the time associated several individual events inside a single event, which change with time and fed into events groups, namely phase prime metric. Generally, times associated between the tandem reactions are expected to be unequal which will make the arm lengths different in forming time crystal.

While constructing a time crystal, we consider each individual event as a single point, connected by time in building different geometric shapes classically. In case of catalytic reaction cycle, the events are happening through chemical reactions but represented as the connector between the two intermediates formed in the sequential or simultaneous reaction paths of a single reaction event. Thus, transforming a catalytic cycle in time crystal, every reaction stage should be presented as an event, connected by the time-consuming intermediates states. The fundamental difference in presenting time crystal and catalytic cycles are given in Fig. 1 [13].

Depending upon the numbers of secondary reactions inside a particular single reaction in a catalytic cycle, various virtual geometries like triangle, tetragon pentagon, hexagon, cube or sphere can be constructed. Some typical cases also arise where reaction cycle inside a reaction cycle appear and so on to construct a fractal clock while presenting such reaction cycles in time crystal schematically. A phase system travelling along the catalytic cycle would witness two different speeds in time flow (58, 91 in AB). The larger phase cycle with longer time period will be appeared

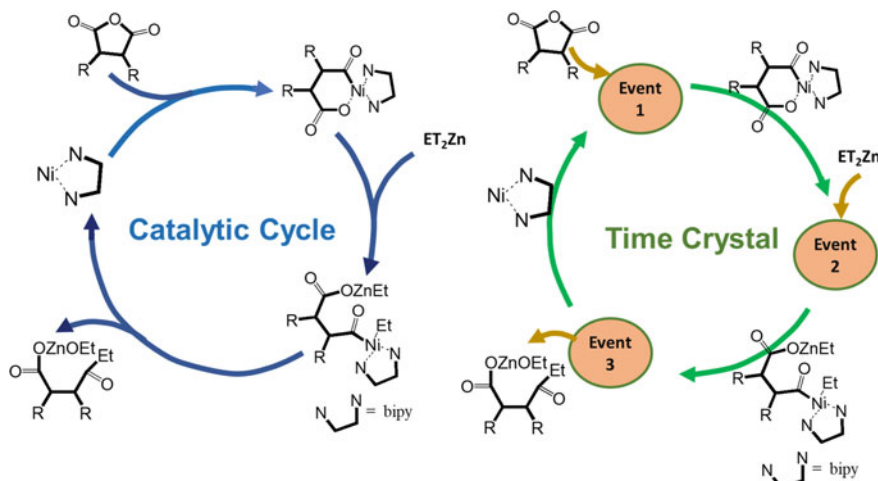


Fig. 1 Left: A catalytic cycle on alkylation of anhydrides with Et_2Zn in presence of $\text{Ni}(\text{COD})_2/\text{bipy}$ catalyst. Right: Time crystal of the corresponding catalytic cycle

as the primary time cycle hosting the smaller phase cycle in time crystal. However, schematic representation of primary catalytic cycles does not represent the longer time phase necessarily. A reconstruction of catalytic cycle into a cyclic time phase by assembling host-guest phase would generate a time crystal in chemical reacting system. Cyclic catalytic reactions might face limitation in constructing information structure with the limited fractal cycles, but the follows of same repetitive path can restore the information identical. The time crystals with certain geometric shape self-assembled to form clocking topology of phase. Some recent studies on the geometry of reaction cycles exhibit, the information processing and artificial intelligence by following the phase prime metric. In addition to secondary catalytic cycles (the cycles inside the primary cycle), another primary catalytic cycle could be nested with the first primary catalytic cycle to generate a complex geometrical catalytic pathway. While transforming such nested cycles into a time crystal, the longer time associated with the catalytic cycle will be the main clock to build the host time cycle.

Though all the homogeneous reactions take place in a same place, heterogeneous catalytic system may occur at two or more different places. In such cases, numerous heterogeneous catalytic sites are well separated by reaction vessel or cell wall but connected through a common solvent system or by a reaction channel.

Herein, the efficiency of a catalytic cycle can be determined by ratio of chemical potential to the chemical impedance, which is broadly known as turnover frequency (TOF). This TOF can be measured by number of reaction cycles performed per time unit and per catalyst concentration [14]

$$\text{TOF} = N/[C]t.$$

2 Geometric Patterns of Catalytic Cycles

Considering each chemical reaction in a catalytic cycle as event, every event is connected to a geometric shape in constructing time crystal. In practice, we never emphasize on relative sizes while drawing catalytic cycle, but while transforming it to time crystal we need to draw the cycles according to all the time associated between two successive events. The geometric shapes assembled here either ‘side by side’ or ‘one inside another’. The various geometric presentations of catalytic cycles will be discussed here.

a. Single Cycle

The single cycles are highly abundant among all the catalytic pathways. One of the most salient features here is the mechanism associated in such reactions are comparatively simple.

Wilkinson’s catalyst (Fig. 2), chloridotris(triphenylphosphane)rhodium(I) is widely used for hydrogenation at olefinic double bounds with molecular hydrogen.

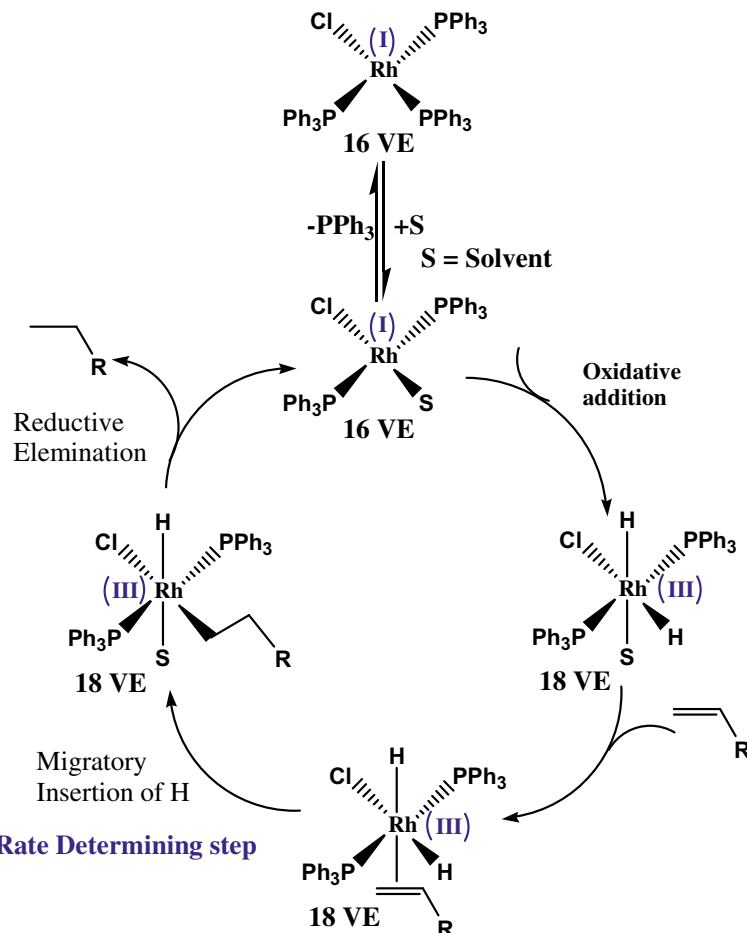
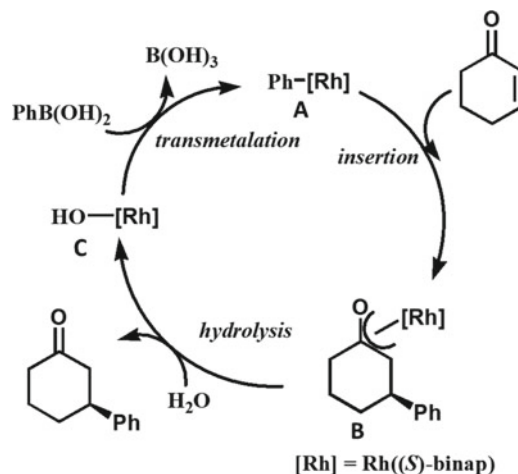


Fig. 2 Wilkinson's catalyst, chloridotris(triphenylphosphine)rhodium(I) for hydrogenation

It is a homogeneous catalyst with a slightly distorted square planar geometry. Rh(I) is a d⁸ system, where four ligands contribute another eight electrons to make it a 16-electron complex. While participating in hydrogenation, initially it leaves one or two triphenylphosphine ligands to transform into a 14- or 12-electron complexes. Thereafter it uptakes H₂ by oxidative addition and olefin by π-complexation to promote itself into a 18-electron system. Finally, after migratory insertion and reductive elimination it produces alkane. Notably, Wilkinson's catalyst does not participate in catalytic cycle directly rather it changes into a solvent(S) coordinated complex, (S)RhCl(PPh₃)₂. In true sense, it acts as a catalyst precursor.

Another rhodium-based catalyst used for 1,4-addition to produce highly enantioselective α, β-unsaturated ketones in the aqueous solvent is also generated from a catalyst precursor [RhCl(C₂H₄)₂] and (S)-binap, in tetrahydrofuran (THF) at 20 °C.

Fig. 3 An asymmetric 1,4-addition of $\text{PhB}(\text{OH})_2$ by rhodium based catalyst



The catalytic cycle mainly associated with three intermediates, phenylrhodium A, (oxa- π -allyl)rhodium B and hydroxorhodium C (Fig. 3) [15].

In organic chemistry, C–C bond formation is one of the most important tools for the organic synthesis. Yasuda et al. carried out one copper-catalysed coupling reactions between alkyl-9-BBN and allylicphosphate. They used triphenylphosphine ligand-based Cu complex to promote stereoselective Allyl–alkyl coupling reaction (Fig. 4) [16]. This allylic substitution was claimed as a first catalytic reaction with secondary alkylboron compound.

Prolinol–phosphine chiral ligand coordinated Copper (I) complex catalyses the coupling reaction between terminal alkynes and nitrones(Kinugasa reaction) to produce enantioselective 1,3,4-trisubstituted β -lactams in most effective way (Fig. 5) [17]. This synthetic root opens the new door for preparing β -lactam drug molecules as it has the high level of enantio selectivity with alkylacetylenes besides aryl- or alkenylacetylenes for manipulating alkyl group at the carbonyl α -position (C3).

The dinuclearnickel complex, $[\text{Ni}_2\text{L}^1](\text{ClO}_4)_4$ ($\text{L}^1=1,2\text{-bis}((5,7\text{-dimethyl}-1,4,8,11\text{-tetraazacyclotetradecan-6-yl)methyl})\text{benzene}$) exhibits an efficient electrocatalytic reduction of CO_2 to CO (Fig. 6) [18]. To envisage the contribution of dual centres, Cao et al. carried out Electrochemical experiments, coupled with density functional theory (DFT) calculations to establish the synergistic effect between two Ni centres.

Zhu et al. established an effective way of preparing propeller-like molecules through tandem Diels–Alder reactions via trapping of the o-quinodimethane (cyclic o-QDM) as intermediate. This catalytic cycle with mild reaction conditions and accommodability with wide range of functional groups withdraws a high interest in preparing propeller-like molecules (Fig. 7) [19]. They found that 1,3-dimesitylimidazol-2-ylidene(IMes) or 1,3-dimesitylimidazolin-2-ylidene (SIMes) supported gold(I) complex (IMes-AuCl, 92% or SIMes-AuCl, 97%) yielded comprehensively. **1** is AgOTf in reaction cycle.

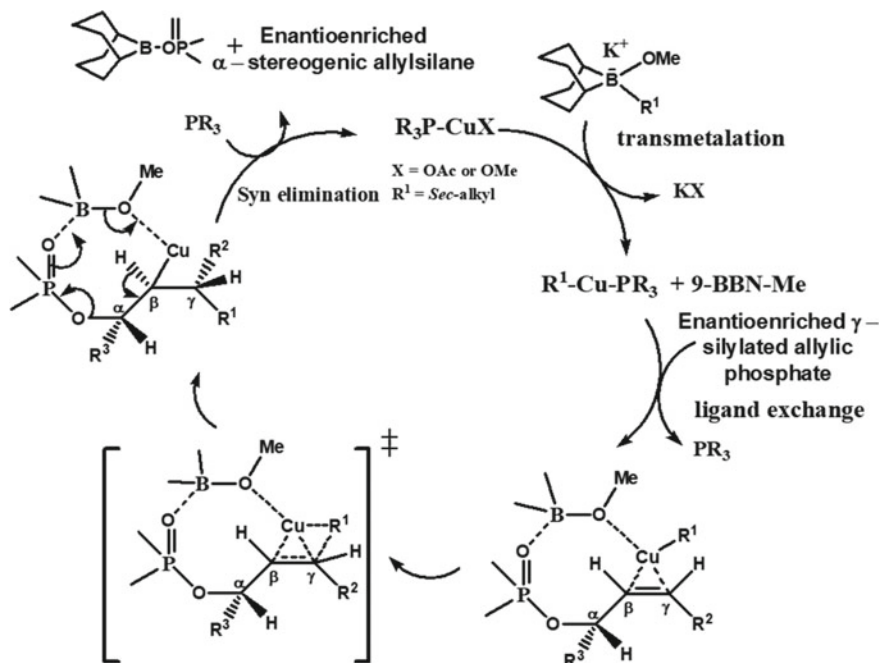


Fig. 4 The catalytic cycle for the γ -syn-selective Cu catalysed allylic cross-coupling reaction between secondary allylic phosphates and secondary alkylboranes

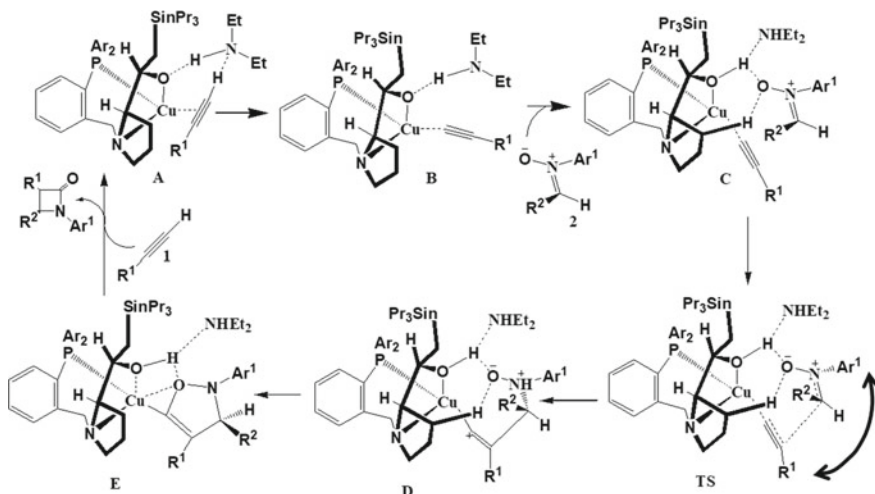


Fig. 5 The catalytic cycle of enantio controlled Kinugasa reaction

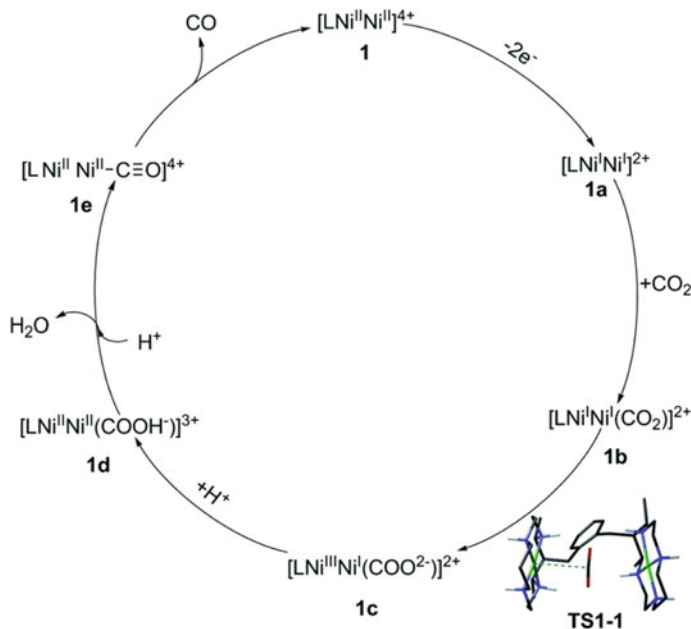


Fig. 6 A dinuclear nickel complex catalysed catalytic cycle for CO_2 to CO conversion

Palladium catalysts are well known in cross-coupling reactions [20], C–H bond activation [21] and C–C bond activation [22]. Ishitsuka et al. reported a Pd complex, $[\text{Pd}^0(\text{PPh}_3)_4]$ in cyanoesterification reaction on olefin to produce exclusive *exo*-product through C–C bond activation (Fig. 8) [23]. Theoretical calculation shows *exo* product is thermodynamically more stable than *endo* product. Notably, they isolated one of the intermediates *trans*- $[\text{Pd}^{\text{II}}(\text{CN})(\text{COOR})(\text{PPh}_3)_2]$ and solved the structure crystallographically.

In addressing renewable energy by splitting water, Wang et al. prepared a macrocyclic Ni complex and employed in electrocatalytic water oxidation process (Fig. 9) [24]. It exhibited high Faradaic efficiencies, catalytic currents with a reasonable stability at neutral aqueous medium. The steric effect from axially oriented methyl groups at macrocycle hinders the formation of $\text{Ni}^{\text{III}}\text{--phosphate}$, which enhance the catalytic performance.

Catalytic cycles in living systems are also omnipresent from photosynthesis to enzymatic reactions. In these systems, a metal atom coordinated by several organic ligands seats inside the supramolecular protein cavity to run the reaction cycle. Tetradeятate porphyrin coordinated to a metal centre is a commonly observed cofactor which exists in various bioinorganic complexes like cytochromes, haemoglobin, myoglobin or chlorophyll. A Fe based porphyrin is observed in cytochromes, haemoglobin and myoglobin, which is replaced by Mg coordinated porphyrin in chlorophyll.

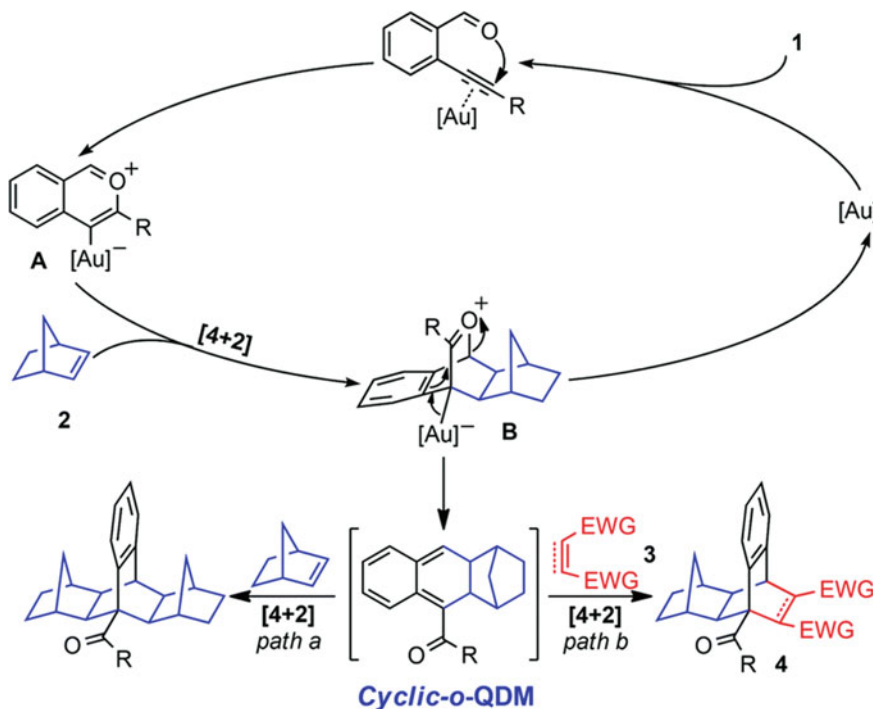


Fig. 7 Gold catalysed Diels–Alder reactions of enynals/enynones with alkenes

Guallar and Friesner studied the catalytic pathway on bacterial Cytochrome P450cam (works on camphor, [25] by a combined quantum and molecular mechanics method (Fig. 10) [26]. They demonstrated the proper role of protein part at different steps in enzymatic cycle. Initially the protein controls the energy difference between the high- and low-spin states while substrate (O_2) binding to suppress the reduction potential in heme cofactor. At next step, selective protonation occurred to the distal oxygen atom at ferric superoxo species by Thr252 to break the O–O bonding. Herein, a controlled long-distance protonation is promoted by the water channel in protein structure.

Porphyrin based chlorophyll a and chlorophyll b molecules carry out the photosynthesis reaction at chloroplast inside a plant cell. Chloroplast is one kind of organelle, where disc-shaped thylakoid stacked together to form grana inside the matrix, stroma. The total system is coated with two membranes. Photosynthesis occurred at two phases, namely light dependent step and light independent step. Light dependent phase happens in thylakoid membranes to produce ATP and NADPH by photosystem I (PS I) and PS II respectively. PS I was discovered earlier and hence designated as PS I after second photosystem (PS II) discovery. The main striking difference is, PS I with higher chlorophyll a/chlorophyll b ratio get excited at longer wave length (700 nm) to that of PS II (680 nm) [27]. In presence of light, PS II splits water into

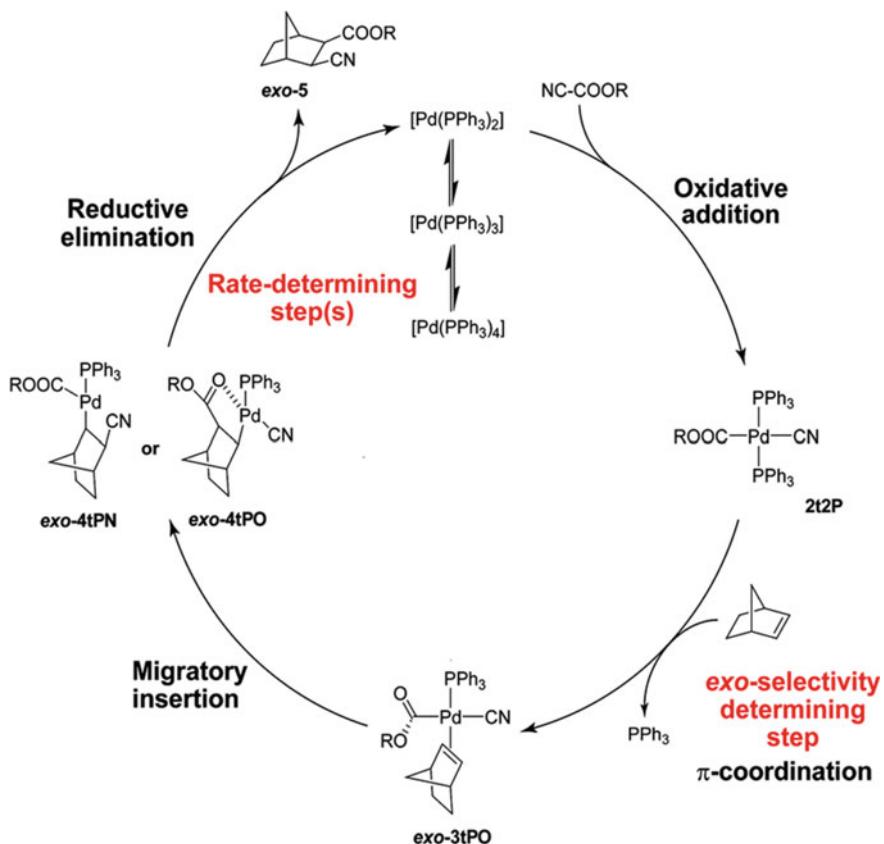


Fig. 8 The catalytic cycle of Pd-catalysed cyanoesterification onto norbornene

oxygen and protons and excited electron. This electron is transported ultimately to PS I and, therein it follows a cyclic path to under light.

Under light independent state, the tandem reactions consume the products (ATP and NADPH) from light dependent reaction and convert CO_2 and other compounds into glucose in a cyclic path way. This state occurred at stroma. Notably, this reaction cycle is also known in some different names, like Calvin cycle, Calvin–Benson–Bassham (CBB) cycle, reductive pentose phosphate cycle or C_3 cycle. The name C_3 denotes the 3 carbon atom based first product, namely phosphoglycerate in Calvin cycle.

Special case 1: Single Cycle with two different reaction cells

About 3% of plants (8100 species) use C_4 carbon fixation cycle, which is very efficient to prepare carbohydrate from CO_2 under draught, high temperature and lower CO_2 concentration. All these 8100 belongs to angiosperms category. If we further compare the C_4 cycles among angiosperms, 40% of monocots use the C_4

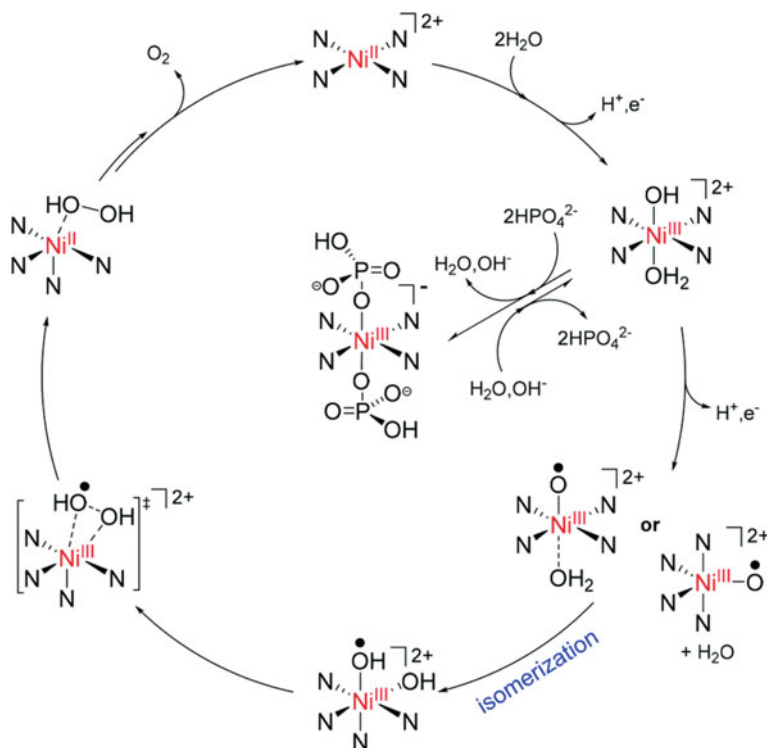


Fig. 9 The catalytic cycle of water oxidation by $[\text{Ni}^{\text{II}}(\text{MexL})](\text{ClO}_4)_2$ ($x = 4, 6$ or 8) through intramolecular HO–OH coupling

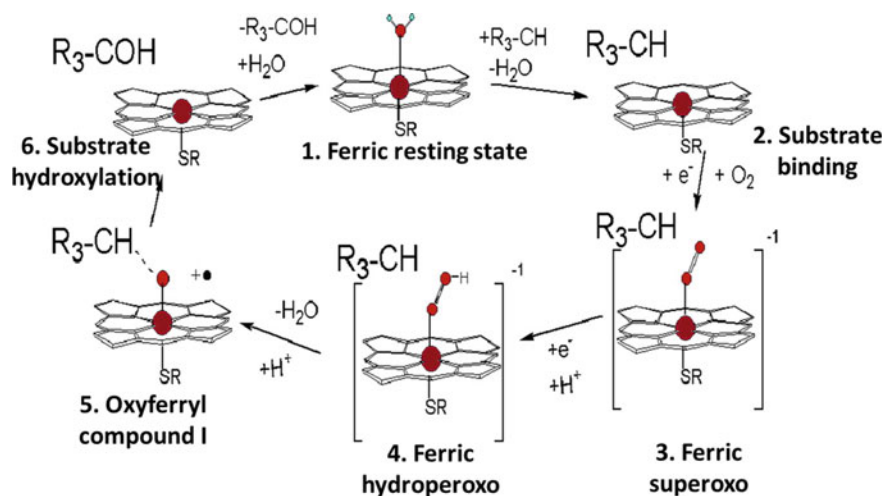


Fig. 10 Common catalytic cycle in cytochrome P450s

pathway over only 4.5% dicots. The name C₄ stands for the four-carbon atom based first product oxaloacetate in this carbon fixing cycle.

Interestingly, some part of C₄ cycle takes place in mesophyll cell and rest occurred in bundle sheath cell (Fig. 11) [28]. Herein, atmospheric CO₂ first diffuse into mesophyll cell and get reduced by carbonic anhydrase (CA). Phosphoenolpyruvate carboxylase (PEPC) then binds the bicarbonate and 3-carbon based compound phosphoenolpyruvate (PEP) to produce the four-carbon based oxaloacetate (OAA). Oxaloacetate is then reduced to malate (MAL) by the enzyme malate dehydrogenase and transported to bundle sheath through plasmodesmata. After reaching here, NADP-malic enzyme converts malate into pyruvate under decarboxylation procedure. The removed CO₂ get associated with Rubisco under C₃ cycle to produce sugars and the pyruvate returns to the mesophyll cell where it is phosphorylated by pyruvate phosphate dikinase (PPDK) to regenerate phosphoenolpyruvate (PEP). Herein, after completing a single event, the product reaches to the next reaction site and completes event with keeping the reaction sites geometrically fixed to build the clocking topology of phase. However, in case of homogeneous reactions the events never happen at geometrically fixed sites. All the biological reaction cycles are basically heterogeneous and are associated with geometrically fixed sites. All event occurs at dedicated geometrically fixed sites in photochemical heterogeneous catalytic cycles in either light or in dark phase to pursue photosynthesis.

Special case 2: Single cycle with additional loop

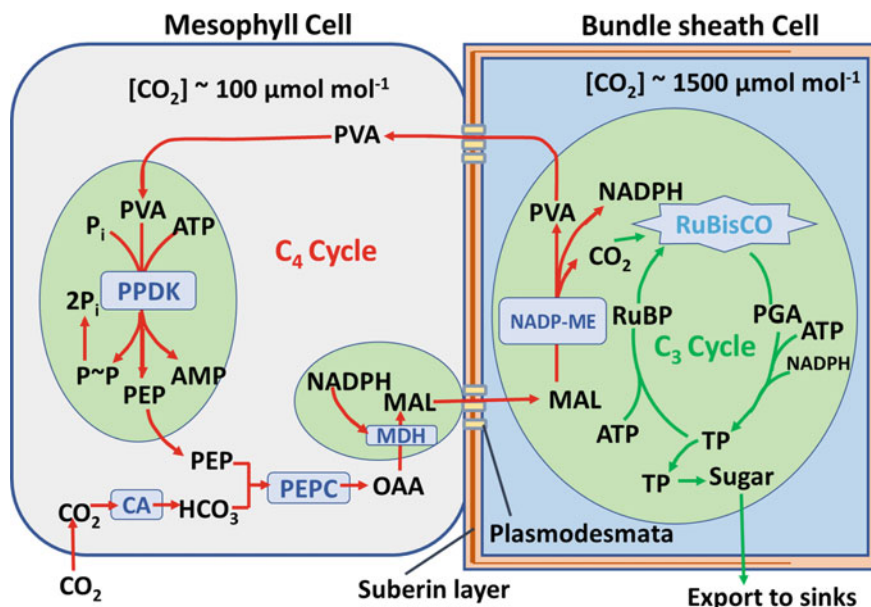


Fig. 11 Schematic presentation of C₄ cycle at two different cells

In some cases, one or few consecutive reactions might be replaced by an alternative pathway under some favourable reaction conditions to construct an additional loop in a reaction cycle [29]. Such loops cannot complete a full cycle, as all the reactions inside this discreet part do not follow the same direction.

For example, a methanol-to-olefin conversion reaction by zeotype material HSAPo-34 follows an addition loop in constructing reaction cycle [30] (Fig. 12). In short, they reinvestigated a methyl benzene based side chain hydrocarbon pool mechanism by DFT calculation with van der Waals correction. They established the methanol-to-olefin (MTO) conversion mechanism with energy profile diagram and demonstrated an alternative loop in the catalytic cycle as well. Notably, the additional loop is not an independent part here. It is also not indispensable part to complete reaction cycle.

Special case 3: Reversible cycle

Some of the reactions are reversible in nature. For example, enzyme catalysed reactions are reversible. However, often they follow some complex pathways (Fig. 21 and 22).

Conjugated 1,3-dienes are used as building blocks in synthesizing many organic and polymer materials. Enyne metathesis reactions are generally performed to develop such structural backbones. Ene–yne cross-metathesis reaction occurs in two

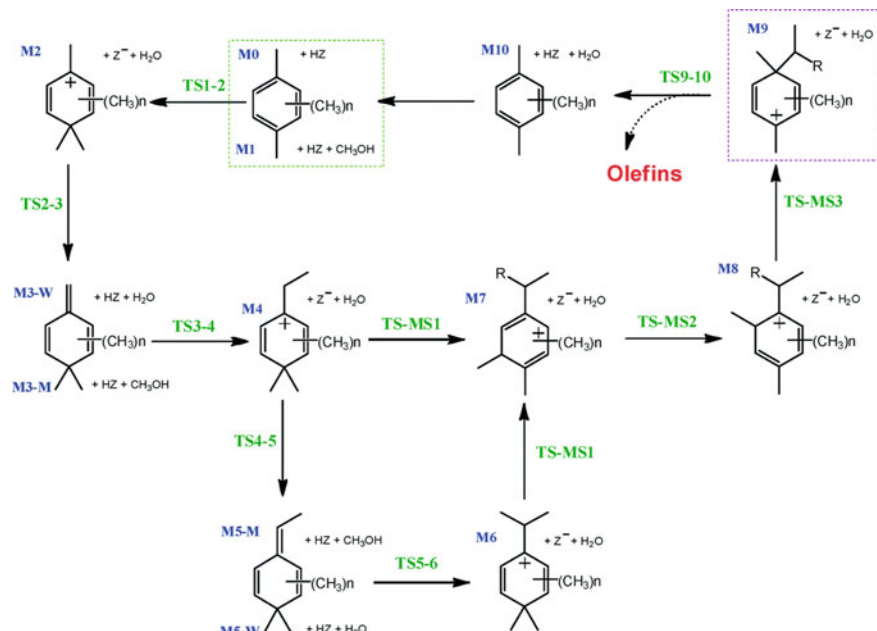


Fig. 12 methylbenzene based side chain hydrocarbon pool mechanism (where R = H/Me) with an additional loop at reaction cycle

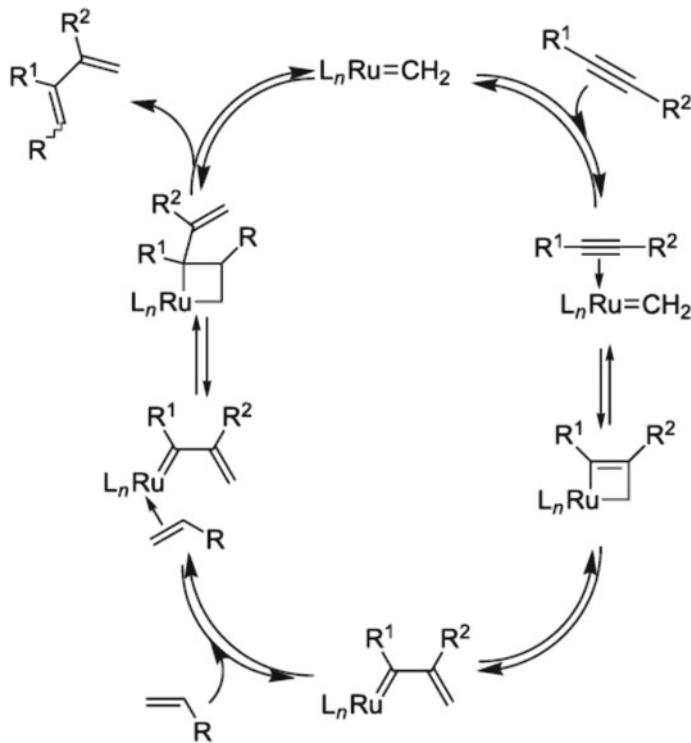


Fig. 13 Catalytic cycle with starting interaction of metal methylidene with a triple (from [23])

parallel pathways, (1) the interaction of an alkyne with a methylidene metal (Fig. 13) or (2) through an alkylidene metal intermediate. All the cycles are reversible [31].

Catalytic hydrogenation-dehydrogenations are extremely crucial from organic synthesis to spasmodic energy storage through chemical bonds. By employing bifunctional catalyst, the designing procedure can be simplified and certain bonds can be activated in chemical process of storing the energy. Bonitatibus Jr. et al. employed iron and iridium as catalytic sites for preparing carbonyl compounds from alcohols under reversible dehydrogenation process. They also showed, the plausible mechanism for iron-catalysed alcohol dehydrogenation (Fig. 14) [32].

Special case 4. Uncountable Colloidal Particle based Cycle

Colloidal nanoparticles follow an explicit time-dependent cyclic pathway like other catalytic reactions. The nanoparticles forms cluster in solution and acts as template simultaneously in forming other clusters. Zeravcic et al. [33] developed a simple templating rule based on cluster templated huge numbers of clusters formation (Fig. 15). This templating reactions produces other catalytic cycles exponentially like the Dyson's notion one exponential growing of metabolic cycles. To simplify the study on cluster dynamics, they have fixed the set of interactions and selected

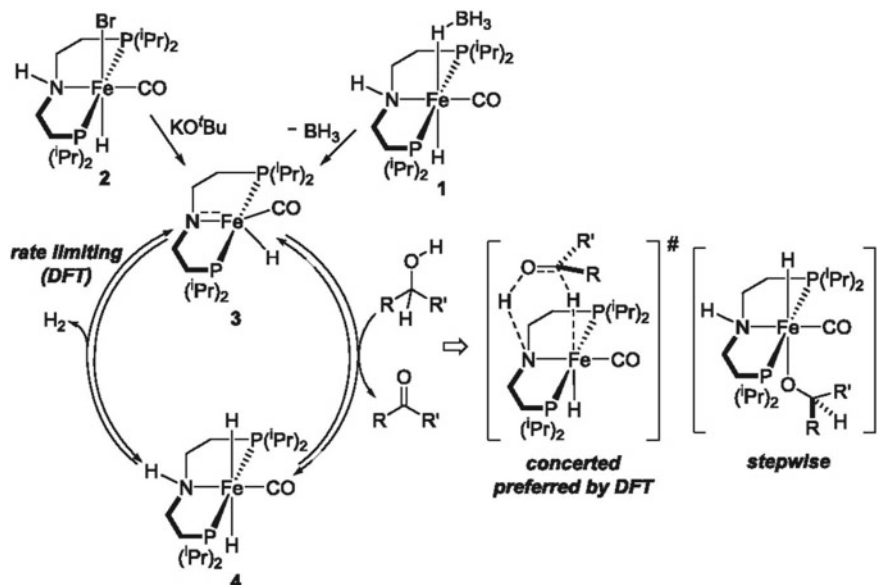
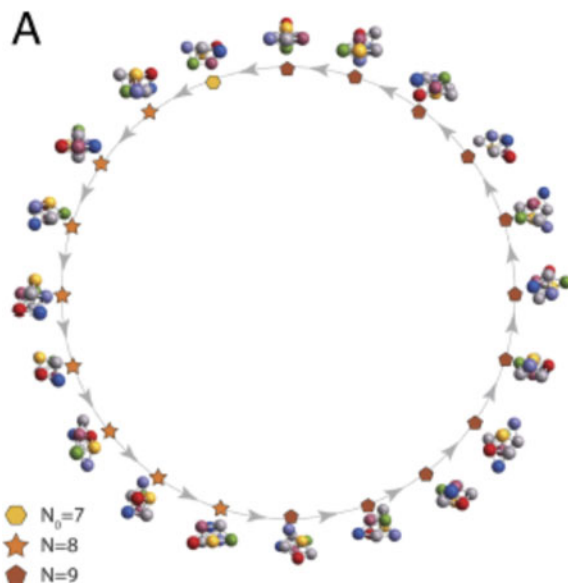


Fig. 14 Catalytic cycle with starting interaction of metal methyldene with a triple

Fig. 15 A catalytic cycle derived from 7 nanoparticle-based cluster system



the six-particle cluster from seven-particle cluster. None the less it generates a huge number of clusters made of 2–11 particles, which again form catalytic cycles in solution.

b. Nested cycles

Reaction cycles can be nested with one or few more reaction cycles frequently. This nesting process are observed either by sharing one or few successive reaction steps to fuse two reaction cycles or a reaction product from a cycle can construct another reaction cycle under a complicated path way. Interestingly, both the shared or connective reactions in the reaction cycles will be represented as a common event in between two time crystal clock.

i. Nested bi-cycle

Two independent or interdependent cyclic reactions with different mechanism fused together by a common step to produce bi-cyclic catalytic mechanism. As passing throw a common reaction step, the reaction cycles need to be presented schematically in opposite directions. Besides such fused bi-cycle, a single product from a reaction cycle can drive a different reaction cycle, the way C₄ reaction cycles do in plant (vide supra) to run two consecutive reaction cycles. However, such interlinked reaction cycles will not be discussed.

There may be two kinds of merging of cycles, (i) a merging by electron or molecular part exchange reactions and, (ii) merging by sharing common reactions.

(α) a merging by electron or molecular part exchange reaction

The fused nested cycles may represent completely two different types of reactions like organocatalytic and photocatalytic reactions [34] (Fig. 16). An enantioselective intermolecular α-alkylation reaction on aldehydes evidenced two fused reaction cycles through single-electron transfer (SET) mechanism. A photoredox catalyst Ru(bpy)₃Cl₂ and an imidazolidinone organo catalyst plays the individual role to drive the SET coupled nested reaction cycles.

Sonogashira coupling is an indispensable tool in organic chemistry for C–C bond formation. Initially the reaction was carried out by Pd complexes, however in presence of Cu salt based cocatalyst, another reaction cycle appeared. The acetylene moiety and the leaving group from Cu complex and the Pd complex are get exchanged to combine these two cycles (Fig. 17), [35].

(β) merging by sharing common reactions

Carbenium ions, namely heptamethylbenzenium cation and pentamethylcyclopentenyl cation ions associated in methanol-to-olefin reaction for the first time detected in Chabazite (CHA)-type zeolites from the reaction mixture by ¹³C MAS NMR and isotopic switch experiments [36] (Fig. 18). It implies two energetically feasible simultaneous reaction cycles, paring and side chain methylation, fused by only a single reaction step.

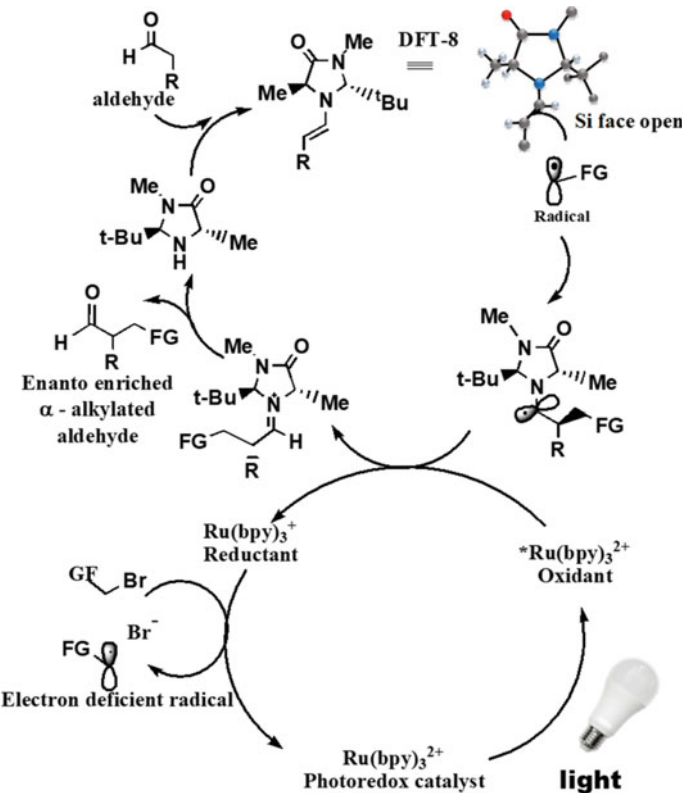


Fig. 16 Merging a photoredox catalytic cycle with an organocatalytic cycle by single-electron transfer process

There are many fused bi-cycles in literatures like palladium-mediated cross-coupling reactions for substituting halides by alkyl groups at aryl halide [37], vanadia- or titania-based catalyst for nitric oxide by ammonia reductions [38] and so on.

ii. Nested Tri-cycle

Three reaction cycles can be fused in such a way that three cycles can be presented linearly, or three cycles can be fused by a single reaction step to form a flower of cycles and product of one cycle can be fed to another cycle. *Desulfovibrio vulgaris* superoxide reductase (SOR) reduces superoxide at $[\text{Fe}(\text{His})_4(\text{Cys})]$ active site to H_2O_2 after receiving the electron from rubredoxin [39] (Fig. 19). This rubredoxin redox cycle receives electron from a NADPH oxidation reaction via another ferredoxin driven redox cycle.

iii. Nested Fractal Cycle (Cycle inside cycle inside cycle)

While retrieving the time crystal concept after 1972, Frank Wilczek did not introduce the guest cycle in 2012 (dada, ref 108). When the guest starts hosting a new guest, it

Fig. 17 Two different metal based two catalytic cycles nested together by exchanging molecular parts (R^1 = aryl, hetaryl, vinyl; X = I, Br, Cl, OTf)

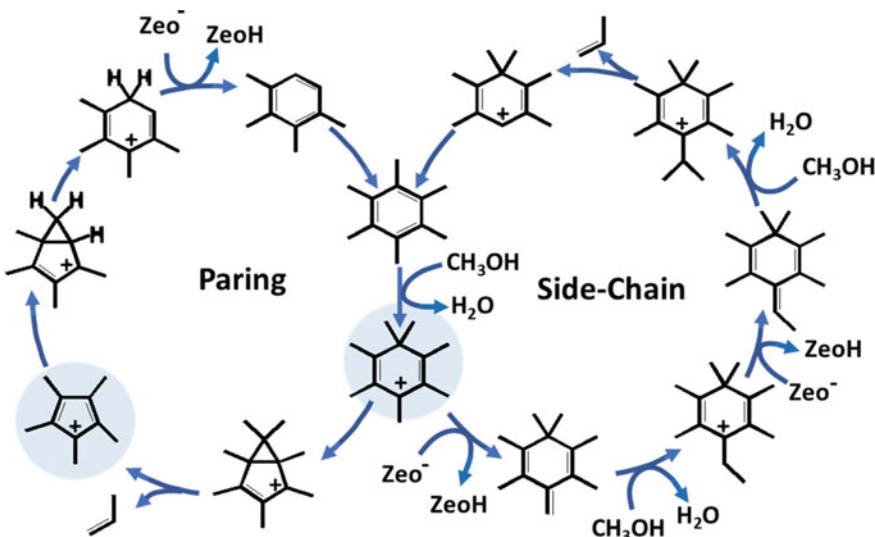
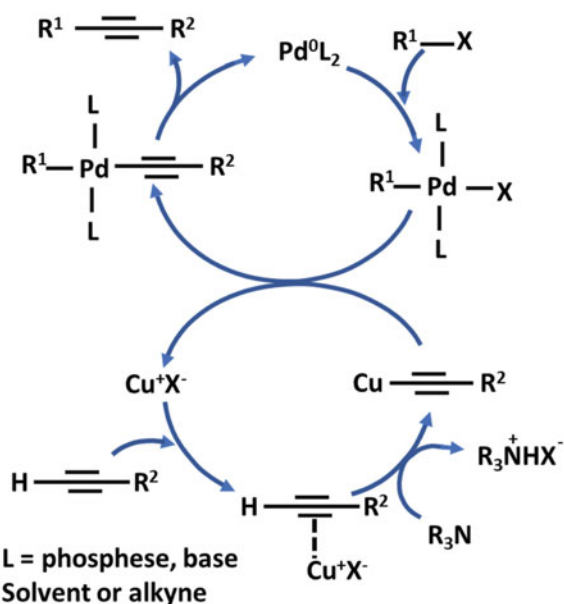


Fig. 18 The fusion of two catalytic cycles by sharing common reactions from paring and side chain catalytic cycles in MTO conversion. Herein, the calculated energy barriers are provided in kcal mol⁻¹

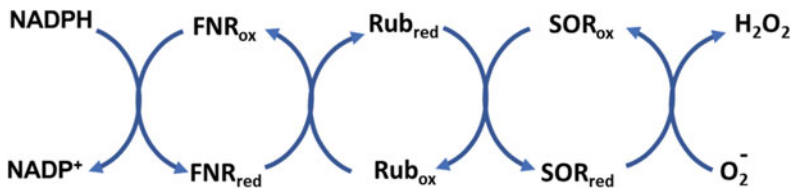


Fig. 19 Linearly nested superoxide reductase catalytic cycle

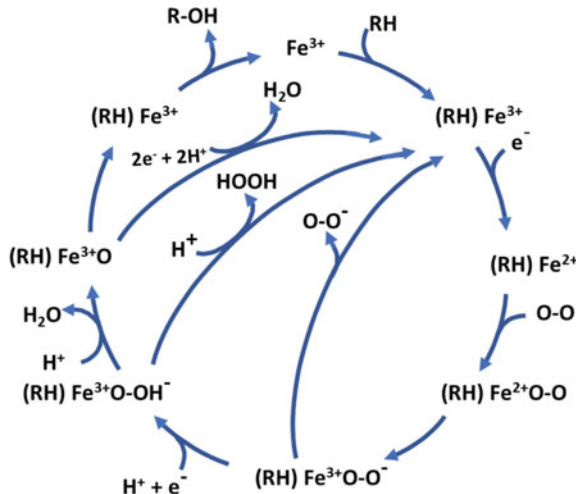
makes fractal time crystal. Such a phenomenon may also appear in catalytic reaction cycles, where smaller reaction cycles are nested inside a bigger or primary reaction cycle.

Metabolism of xenobiotics by cytochrome P450 enzymes generally needs at least NADPH and cytochrome P450 reductase (CPR) [40]. For elucidating the requirement of NADPH cofactor protein and redox transfer proteins CYP2C9 (Cytochrome P450 Family 2 Subfamily C Member 9) was coated over gold electrode. Cyclic voltammetry established the fast electron transfer between the heme iron and the gold electrode and depicts the metabolism of warfarin after applying electrical potential even in the absence of CPR or NADPH. In Fig. 20, inside the normal P450-mediated metabolism, steps 3a to 5a are shunt processes exhibiting alternative cyclic pathways to form fractal cycles.

A similar geometrical pattern also obtained in the catalytic cycle of cytochrome P450 [41] or in rhodium-biphephoscatalyst1-dodecene hydroformylation reaction [42].

2c. Cubes

Fig. 20 Metabolism of xenobiotics by cytochrome P450 enzymes



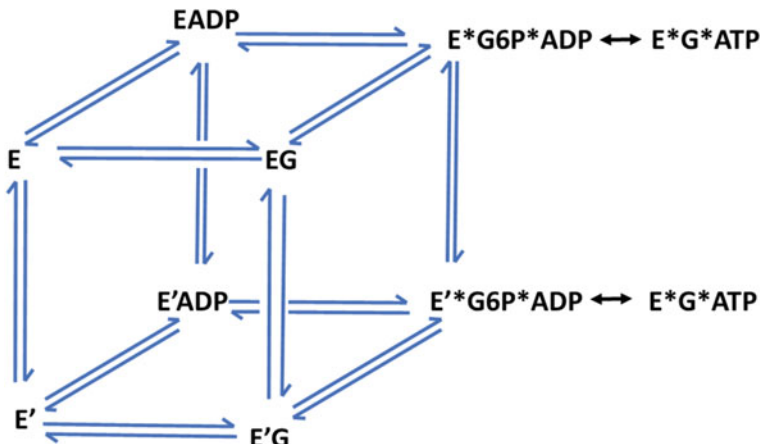


Fig. 21 Ligand induced slow transition model for regulating glucose levels in human blood

A monomeric enzyme, namely human pancreatic glucokinase controls regulation of blood glucose levels in our body (Fig. 21) [43]. One theoretical postulate, ligand-induced slow transition model (LIST) suggests a slower rate constant among two pre-existing enzymic interconversion than the turnover number. LIST model however can be well explained by global fit analyses on experimental glucose binding curves with a total four glucose-associated binary complexes. Herein, the kinetic model depicts the presence of multiple conformations in glucokinase in absence of ligands, which refrains from conformational changes even after the enzymic association with glucose molecule. This LIST model suggests two separate catalytic cycles involving two conformationally different species.

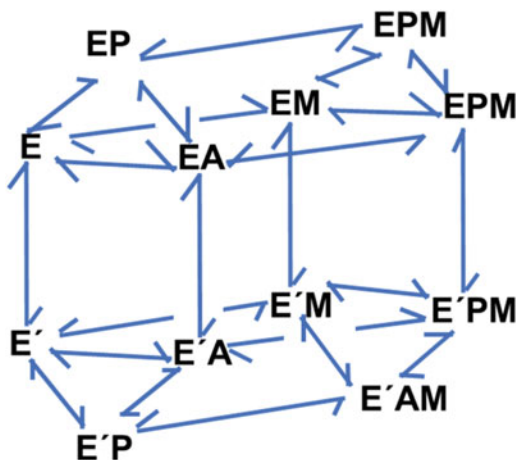
2d. Deformed hexagonal prism

When a monomeric single site enzyme reacts on a substrate (A) in presence of a modifier (M), a slow transient kinetics model is proposed to interpret the isomerisation of enzymes (E, E_t), a dissociation-association of binding modes of a catalytic deformed hexagonal prism in forming product (P) [44] (Fig. 22). Enzymes like Pyruvate kinase, n-Lactate dehydrogenase, Adenylate deaminase, Hexokinase works on their corresponding substrate to follow the reaction pathway.

3 Kinetic Study

Scrutinization of a catalytic reaction by Kinetic modelling becomes indispensable for studying reaction rate [45, 46] and reaction mechanism [47]. Kinetic modelling portrays a reaction profile by depicting all the parameter detailing like reaction rate or concentration that fingerprints a reaction batch qualitatively with quantitative

Fig. 22 The schematic presentation of Enzymatic reactions under deformed hexagonal prismatic pathway



specifications. Several kinds of models proposed to illustrate the reaction profile independently. Some of those models will be discussed here without any mathematical detailing. An intrinsic reaction kinetics and deduction of rate equation from a reaction profile elucidate the strategy in reaction engineering for designing a reactor (Chaudhari et al. 2001). Despite the informative nature in intrinsic kinetic approach, it is a time-consuming complex model to work with [48]. Herein, a mechanistic study can be performed either by experimental isolation of a reaction intermediate, followed by spectroscopic characterizations (IR, NMR) or theoretical computational modelling. Reaction calorimetry may also be employed to correlate the heat changes associated with reaction rate according to the equation $q^{\cdot} = \Delta H_{\text{rxn}} \cdot V \cdot r$. [49].

A fractional heat flow in a tandem reaction can also be detected by integrating a heat flow curve by

$$x = \frac{\int_{t_0}^{t_x} \dot{q} dt}{\int_{t_0}^{t_f} \dot{q} dt}$$

where \dot{q} = reaction heat flow; ΔH_{rxn} = heat of reaction; V = reaction volume; r = reaction rate; x = fractional heat flow; t_0 = reaction starting point; and t_f = reaction end time point.

In case the intermediate species possess a very short lifespan, low stability or poor concentration bellow the spectroscopic detection level, cannot be detected experimentally. To resolve this issue, an analysis of global kinetics on working catalytic cycle demonstrates the information like catalytic resting state, turnover limiting step and plausible intermediates most directly [49]. Regardless of the simplicity in a common expression for multi-step reaction pathway, the global kinetic model has the limited capability in predicting the system. A full story of a catalytic mechanism can be explicated by a time-dependent monitoring of reaction progress in comparison to a mere snapshot in classical kinetic methods.

In 2014, Stewart et al. showed, the combined intrinsic and global kinetic approach might be a better solution than any of its individual kinetic model [48]. The dual model even produces more data than global kinetic model.

Reaction progress kinetic analysis (RPKA) is another methodology to extract the maximum information through a time consequential graphical manipulation, derived from a minimal number of mathematically independent experimental inputs [50]. It can also be featured as fingerprint to the corresponding reaction profile.

The model developed by combining the two methods, namely kinetic-quantum chemical model aims to estimate TOF straightforwardly for a catalytic cycle. Kozuch et al. showed the *energetic span* (δE), i.e., apparent activation energy of the complete cycle is affected by the two different species, belonging to different energy levels [51]. The two species, namely the *TOF determining intermediate* (TDI) and the *TOF determining transition state* (TDTS) are not necessarily the contiguous states. This TDTS was earlier mentioned as RDTS (Rate Determining Transition State [52]).

4 Time Breathing

All these kinetic models of catalytic cycles with precise information like reaction rates, stability of intermediate scan be converted into time crystal. These time clocks can increase or decrease their diameters periodically under the time breathing process. The intermediates, connecting to consecutive chemical events in time crystal does never have some discrete life time, rather have the time ranges, within which they get consumed. While drawing a time crystal from a reaction cycle, the longer lifespan of intermediate generates an arc for a bigger cycle, and vice versa. This oscillation in radius will represent the time crystal in breathing mode. Even by changing the temperature of a reacting system, the exo and endo-thermic reactions will response differently to manipulate reaction rates. For example, by reducing the temperature of an exothermic system, reaction can proceed faster, which will be imparting the smaller radius in time crystals. Breathing is expected to be controlled by agitating the reaction temperature periodically. Like temperature, pressure also plays the same role according to Le Chatelier's principle. All the circles nested together oscillates by increasing or decreasing their diameters coherently under the time breathing process, which does not participate in information processing.

5 Engineering of Time Crystal

All the chemical events in a catalytic cycle assembled through time consuming intermediates in forming clocking topology releases a single product. Keeping the reaction clock unperturbed, different stereo isomers can be delivered by introducing additional stereospecific interaction in a reaction mechanism. Herein the different energy levels of the diastereomeric intermediates play this pivotal role to kinetically

control the product. Unfavourable conformations of reactant molecules suppress one isomer over other at the transition state. In biological system, a single option inside the supramolecular cavity releases only the biologically active single product.

Going from a simple single reaction cycle to a cycle assembled fractal pathways with different products at end, a certain pathway can be stimulated by employing a path-specific catalyst. This simple technique can selectively promote a desired product over other side products from a catalytic system. Herein, the fractal pathway is demonstrated by genetic engineering concept (vide infra).

a. Chemical System

The reaction under a strong basic condition, where anucleophile can be generated from a nitroalkane to condense with an electrophilic aldehyde molecule to produce β -nitroalcohol is called **Henry reaction**. Recently, by keeping the mechanism unchanged, some chiral catalysts have been introduced to promote certain enantiomer from the reaction product. Such nitroaldol reaction can be derived by many types of catalysts like organic or inorganic bases, quaternary ammonium salts, and different protic or aprotic solvents. Basically, the reaction conditions are selected by the functionality present in the molecules, but the excessive aldehyde may lead to aldol condensation reaction. For example, adinuclear Zn based catalyst have been used by Trost et al. to promote the asymmetric synthesis [53, 54]. White et al. introduced a new tetrahydrosalen based chiral ligand and prepared Cu(I) based complex in situ by reacting with $(\text{CuOTf})_2 \cdot \text{C}_6\text{H}_5\text{CH}_3$ to prepare the chiral catalyst for asymmetric synthesis [55] (Fig. 23, Right). This chiral reagent was able to produce the enantiomeric excess up to 98%. If this reaction is carried out by an inorganic base like LiAlH_4 , [56] same reaction cycle would have produced the racemic mixture of both the enantiomers (Fig. 23, left). By introducing the chiral catalyst, the interaction with the reactant molecule produces two parallel reaction pathways with two different diastereomeric transition states. The product related to the transition state

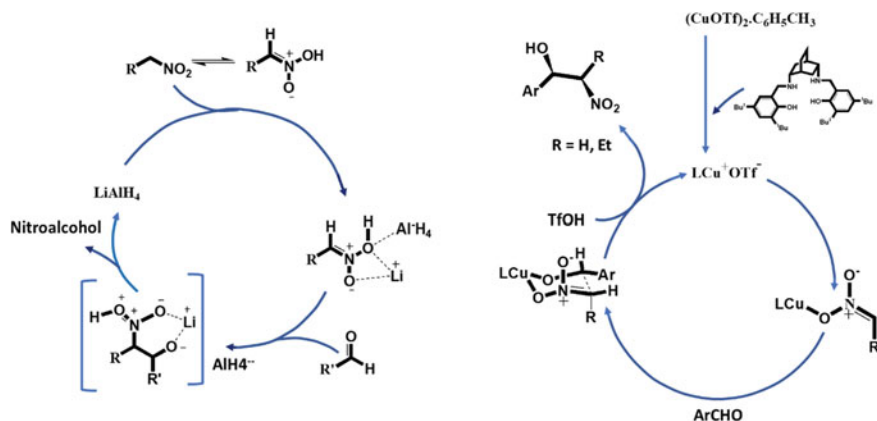


Fig. 23 left, with achiral inorganic base catalysed reaction. Right, Chiral catalyst-based reaction

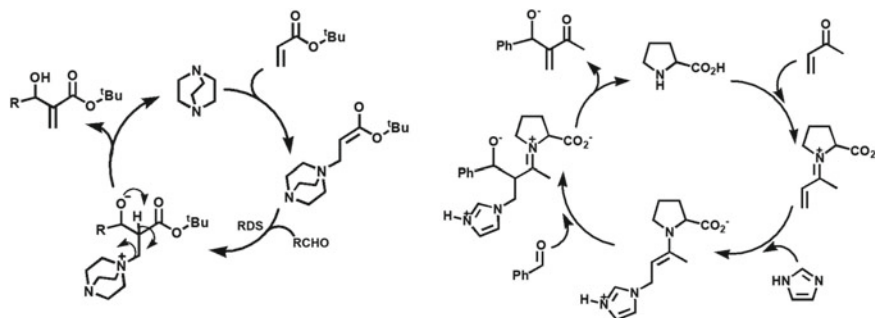


Fig. 24 Left: Common reaction cycle with DABCO catalyst. Right: with chiral catalyst

of lower energy level predominates over other product to end up with enantiomeric excess [57, 58].

Carbon-carbon bond formation is also carried out by **Baylis–Hillman Reaction**, where an α -carbon at activated double bonded is coupled with an electrophilic sp^2 carbon under certain catalytic condition [59]. Initially aldehyde functionality was selected to generate electrophilic centre but later extended to imine in carrying out aza Baylis–Hillman reaction [60]. The selection of base for preparing nucleophilic carbon is crucial as it is not supposed to exhibit nucleophilic nature. In this regard, the bases like different tertiary amines, phosphines are used as catalyst in Baylis–Hillman Reaction. DABC (1,4-diazabicyclo[2.2.2]octane) is widely used base, which cannot compete with the generated nucleophile in the reaction (Fig. 24 left) [61]. Besides this tertiary amine, quinuclidine, 3-hydroxyquinuclidine is also commonly used as catalyst for this reaction [60]. Aggarwal et al. used lewis acid to accelerate this reaction with DABCO catalyst. They used tert-butyl acrylate to react with DABCO by Michael-type nucleophilic addition at the activated double bond to produce enolate. This enolate reacted as nucleophile to aldehyde to pursue Baylis–Hillman Reaction.

In presence of chiral catalyst like L-proline with weak or strong Lewis base, the activated alkene methyl vinyl ketone can condense with arylaldehyde to give enantiomeric excess (<5%) [62]. Interestingly this experiment was carried out in different solvent to envisage the solvent effect on yield. Davies et al. found that water is a poor solvent but DMF:H₂O (9:1) is the best solvent to yield 80% product (Fig. 24 right) [63]. Aroyan et al. studied intramolecular Morita–Baylis–Hillman reaction by employing pipecolinic acid and N-methylimidazole as cocatalyst to obtain 98% enantiomeric excess [64]. Similarly, Raheem et al. selected several Chiral Thiourea Derivatives for carrying out highly enantioselective Aza-Baylis–Hillman Reactions [65]. However, a use of an ordinary DABCO would produce both the enantiomers equally. Without hampering the reaction cycle, certain product (enantiomer) can also be increased in Baylis–Hillman reactions.

Heck Coupling is the other way of C–C coupling between aromatic or alkene halides and activated alkenes by Pd catalyst under the basic condition. Imbos et al. carried out an intermolecular Heck reaction on cyclohexadienones

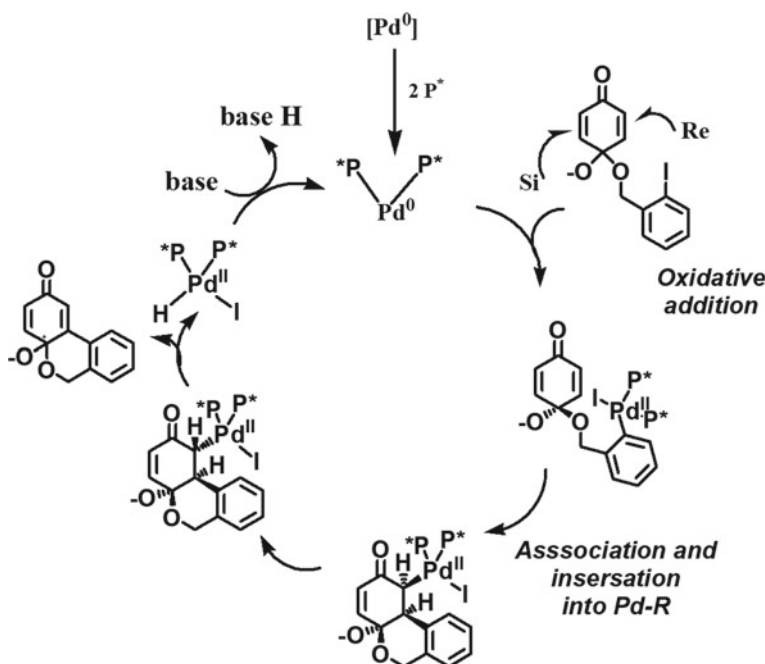


Fig. 25 96% enantiomeric excess in Heck coupling

by employing $\alpha,\alpha,\alpha',\alpha'$ -tetraaryl-2,2-disubstituted 1,3-dioxolane-4,5-dimethanol (TADDOL)-based mono- and bidentate phosphoramidites as chiral ligands (Fig. 25) [66] to produce up to 96% enantiomeric excess. In a similar way, by using the chiral ligand, Minatti et al. also prepared enantiomerically enriched (80%)3-substituted indanones [67]. A common Pd catalyst cannot selectively produce the certain isomers here.

b. Biological system

A highly complex reaction system, wherein the chemical events follow a fractal pathway through impregnating events inside a bigger event, can be controlled externally. The addition of a precise catalyst can trigger a particular fractal pathway to promote some desired product. Thus, a process by which a certain fractal pathway can be promoted to emphasize a desired product by employing a certain catalyst can be known as time crystal engineering. By time crystal engineering approach, by simple changing the catalyst, we can promote a desired product associated with a certain fractal pathway. Chemical reactions with multiple fractal pathways are not abundant till date. Oppositely, catalytic cyclic reactions cannot be represented schematically in genetic engineering where hundreds of event cycles are existed to follow a certain fractal pathway.

Transcription factors (TF) are the DNA sequence specific protein molecules in molecular biology, which controls the genetic information through the transcription

rate from a DNA to messenger RNA (mRNA) by binding to a precise DNA chain. Metabolic activity or phenotype can be changed by dynamically altering the transcriptome (the sum of mRNA units expressed from genes) with modifying a TF [68]. In consequence, transcriptional regulation plays a crucial role in controlling gene expression in biological system. Such regulated genes with the corresponding TF collectively called ‘regulon’. TFs often result in mutation to the informative phenotype and a number of TFs are identified as key regulators in various plant functions.

Though the TFs act either as activators or repressors mostly, Ikeda et al. demonstrated a bifunctional TF, namely WUSCHEL protein in *Arabidopsis thaliana* which controls the stem cell population at shoot meristems [69]. It basically behaves as a repressor and conserved among WOX genes. Nonetheless, it becomes an activator after involving in regulating the AGAMOUS (AG) gene. The C terminal part of WUSCHEL is active for some biological functions and associated with a WUS box, an acidic region, and an EAR like motif [70]. Ikeda et al. demonstrated here that WUS behaves as an active repressor. In addition, WUS box behaves as a repression domain, associated with the induction and conservation of shoot stem cell.

The two orthologous genes, CpAG1(AB548889) and CpAG2 (AB548890) of a winter blossoming perennial plant, *Cyclamen persicum* (cyclamen) was cloned by Tanaka and his co-workers [71] (Fig. 26). Those CpAG1 and CpAG2 are primarily expressed by stamen and carpel, respectively. Cyclamen flowers are comprised of 5 petals. With the expression of chimeric repressor, the stamens were converted to petals, resulting the Cyclamen flowers blossomed with 10 petals. However, CpAG2 reacted in different way, where the formation of both stamens and carpels were perturbed. Chimeric repressor gene-silencing technology (CRES-T) suppress the targeted genes of transcription factors to dominate in genetic expression. In this way

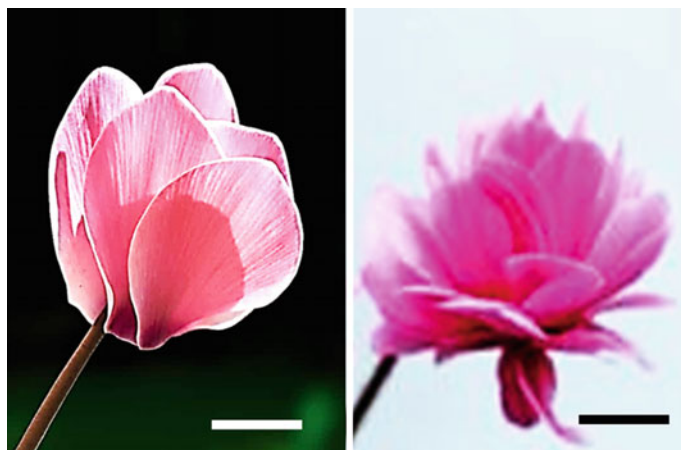


Fig. 26 A Wink Pink double-petal and a CpAG2 multi-petal flower (scale bar: 1 cm)

a multi-petal cyclamen can be generated by expressing two chimeric AG repressors, without changing the biological reaction pathways.

A structurally rigid plant tissue needs a robust secondary cell wall comprised with lignin, cellulose and hemicelluloses in a typical topology. Both cellulose and hemicellulose microfibrils are arranged parallel to construct individual layers but stacked diagonal to each other wherein lignin is impregnated. This secondary cell wall is located between plasma membrane and the primary cell wall [72]. The orthologous master regulators for secondary cell wall synthesis were identified both for dicots and monocots previously. However, the role of Master regulators in monocots were not studied extensively. Yoshida et al. demonstrated that the SECONDARY WALL NAC DOMAINPROTEINS, the transcription factor, are potentially useful in developing the secondary cell wall in monocots like rice (*Oryza sativa*) [73].

Root plasticity in distributing the roots spatially in soil against environmental stresses is a fundamental characteristic. Toda et al. demonstrated a rice nuclear factor, namely RICE SALT SENSITIVE3 (RSS3) exhibits root cell elongation to address the salinity [74]. Nuclear factor binds as dimer to a specific DNA sequences with high affinity. Losing of RSS3 function generally constrains the cell elongation under normal condition but stimulates a natural root cell swelling and inhibiting from root development under saline environments. RSS3 generally expressed at root tip and susceptible to bind to a transcription factor class-C basic helix-loop-helix (bHLH) and JASMONATE ZIM-DOMAIN proteins to form a ternary complex. The failing of rss3 allele released mutated protein in interacting with bHLH and the expressive upregulation of JA responsive genes in rss3 results in the expressive modulation of Jasmonate by RSS3 to elongate root cells in saline water.

6 Biological Effects of Cycle Breaking

Biological catalytic pathways are highly complex to present them schematically the way chemists do conventionally. Some cyclic reactions can be inhibited by some reactant blocking molecule to suppress the toxicity. For example, Alzheimer's disease (AD) is driven by the formation of amyloid- β peptide (A β 42), the senile plaques caused the neurodegenerative pathogenesis. Once the A β 42 peptides are formed, their surface starts catalysing the formation of neurotoxic oligomers to introduce AD. To prevent the AD, we need prevent the formation of neurotoxic oligomers by breaking the catalytic cycle. Cohen et al. in an in vitro experiment showed that this catalytic cycle can be selectively inhibited by the chaperone protein [75] to control the A β 42 toxicity [76]. Therein, the chaperon binds the surface of A β 42 fibrils to redirect the aggregation reaction into a different pathway that release minimal toxicity [77]. The mechanism was verified in mouse brain by carrying out electrophysiology and cytotoxicity experiments.

7 Self-activated Cycles

In all the living organism, the enzyme like DNA/RNA polymerase driven polymerization of DNA/RNA happens for genetic inheritance fundamentally. By employing the bioinformatics analysis, Genna et al. established that, an H-bond forms between the 3'-OH of an incoming nucleotide substrate and β -phosphate moieties while forming a Michaelis complex (Fig. 27) [78]. Such H-bonded complex was not discussed in all the earlier proposed mechanism. This study established that, this newly discovered H-bonded Michaelis complex promotes a unique self-activated mechanism to attribute the nucleotide addition derived in situ nucleophile formation and nucleic acid translocation synergistically. This self-activated mechanism drives the catalytic cycle, which was not explained previously. To further verify the mechanism, ab initio QM/MM simulations was carried out on a DNA repairing enzyme, the human DNA polymerase- η . It is mainly governed by five steps. (1) It begins with Michaelis-Menten complex, where pyrophosphate (PPi) transfer takes place by the two-metal-aided phosphoryl under S_N2 -type process. The nucleophilic oxygen is activated through deprotonation and marked in red colour. (2) At next state, products formed

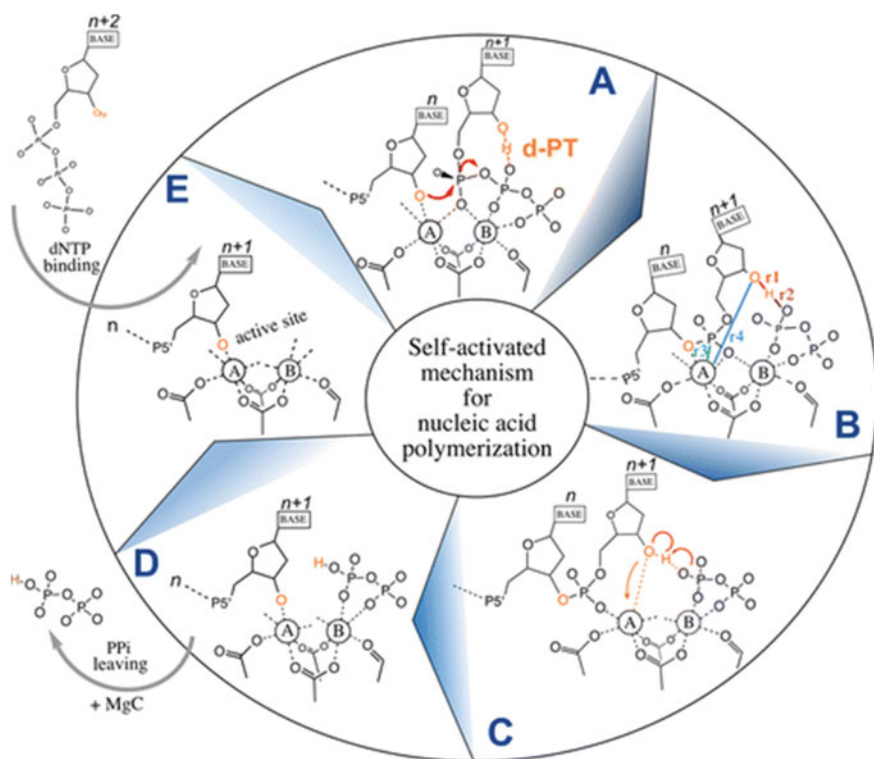


Fig. 27 Self-activated reaction cycle for nucleic acid polymerization

in nucleotide addition. Coloured lines are presenting the selected distances taken to investigate self-activated mechanism. (3) Then the nucleophile 3'-OH gets activated by deprotonating for leaving PPi r4 gets shortened to translocate the initial nucleic acid. (4) At the fourth stage, PPi is released from the catalytic site by transient third metal cation. (5) At the final stage, the enzyme is ready for the corresponding polymerization cycle through binding a new nucleotide.

8 Self-decisive Cycle

The immune system, comprised of some special proteins, cells, tissues, and organs (bone marrow, thymus and lymph nodes) acts over bacteria, viruses, parasites or toxins to protect us continuously. This system can modify itself in a given condition to fight against foreign body with time. Such adaptive immune system decorated with antigen receptors are produced by somatic recombination. Interestingly, the immune system is specific, yet versatile to fight against a wide range of pathogens with keeping the memory sharp. Some of the foreign bodies like varicella zoster virus (in chicken pox) cannot attack us multiple times as our immune system adapt against them. We also provide artificial memory in form of vaccine to encounter potential pathogens for the first time [79]. Artificial memory can also be imposed by triggering vaccination repeatedly against time in booster dose. This booster dose acts like time crystal on immune system to memorize the unencountered foreign bodies, which protects us from upcoming attack. However, facing the pathogens or virus for the first time without the availability of proper antibodies, immune system produces the target specific antigen by itself through the adaptive immunity process. While doing so, it changes its bio-chemical cycles intelligently in designing new antibody to fight against foreign bodies.

9 Conclusion

The physical properties like superconductors, (anti)ferromagnets, cosmology, Bose–Einstein condensates appear in a certain system by breaking certain symmetry in a Hamiltonian system. Extension of such fundamental concept in the breaking of time translational symmetry witnessed ‘time crystal’ in creating the clocking topology. Such clocks run without energy, as the overall energy is conserved. Until now, the time crystal perception has already been employed in attributing from Cyclic universe to trapped ions. As the catalytic reaction cycles are getting repeated against time, it is worth to extend the time crystal concept and explore the engineering part to trigger a certain reaction product from a reaction system. For better understanding, the patterns or physico-chemical properties of various reaction cycles are analysed here before transforming them into time crystals. Each catalytic cycle comprised of several cascade reactions to connect the intermediates with different reaction

kinetics. Considering every single reaction as event, we can fix the events as points on a cycle by connecting them with time-consuming intermediates to construct the time crystal. The reactions with transition state will be appeared inside the events only. In other words, the chemical reactions are drawn on arc between two pointed intermediated in catalytic cycle schematically but get reversed while constructing a time crystal. If a catalytic system produces two or more competitive products, by time crystal engineering approach, one of the products can be promoted without changing the catalytic cycles. This approach is shown here to trigger certain stereo isomers from same catalytic cycles and extended in genetic engineering as well. To enhance immunity, booster dose is administrated to a body at a certain time interval in immunizing certain antigen as well. Presently we are working to exploit this concept on a real catalytic system mathematically after solving the Hamiltonian on catalytic reaction cycle.

References

1. Sachdev S (1999) Quantum phase transitions. Cambridge University Press, Cambridge
2. Das P, Pan S, Ghosh S, Pal P (2018) Cosmological time crystal: cyclic universe with a small cosmological constant in a toy model approach. *Phy Rev D* 98:024004
3. Zhang J, Hess PW, Kyprianidis A, Becker P, Lee A, Smith J, Pagano G, Potirniche I-D, Potter A C, Vishwanath A, Yao NY, Monroe C (2017) Observation of a discrete time crystal. *Nature* 543:217
4. Else DV, Bauer B, Nayak C (2016) Floquet time crystals. *PRL* 117:090402
5. Lim CS (2014) The Higgs particle and higher-dimensional theories. *Prog Theor Exp Phys* 2014:02A101. <https://doi.org/10.1093/ptep/ptt083>
6. Wilczek F (2012) Quantum time crystals. *Phys Rev Lett* 109:160401
7. Bruno P (2013) Comment on “quantum time crystals”. *Phys Rev Lett* 110:118901
8. Bruno P (2013) Impossibility of spontaneously rotating time crystals: a no-go theorem. *Phys Rev Lett* 111:070402
9. Watanabe H, Oshikawa M (2015) Absence of quantum time crystals phys. *Rev Lett* 114:251603
10. Chandrashekaran MK (1974) Phase shifts in the *Drosophila Pseudoobscura* circadian rhythm evoked by temperature pulses of varying durations. *J Interdiscipl Cycle Res* 5:371–380
11. Reddy S, Sonker D, Sing P, Saxena K, Singh S, Chhajed R, Tiwari S, Karthik KV, Ghosh S, Ray K, Bandyopadhyay A (2018) A brain-like computer made of time crystal: could a metric of prime alone replace a user and alleviate programming forever? soft computing applications. Springer Nature Singapore Pte Ltd 761:1–43
12. Li T, Gong Z-X, Yin Z-Q, Quan HT, Yin X, Zhang P, Duan L-M, Zhang X (2012) Space-time crystals of trapped ions. *PRL* 109:163001(1)–163001(5)
13. Johnson JB, Bercot EA, Rowley JM, Coates GW, Rovis T (2007) Ligand-dependent catalytic cycle and role of styrene in nickel-catalyzed anhydride cross-coupling: evidence for turnover-limiting reductive elimination. *J Am Chem Soc* 129:2718–2725
14. Kozuch S, Shaik S (2011) How to conceptualize catalytic cycles? the energetic span model. *AccChem Res* 44:101–110
15. Tokunaga N, Yoshida K, Hayashi T (2004) Mechanistic studies on the catalytic cycle of rhodium-catalyzed asymmetric 1,4-addition of aryltitanate reagents to α, β -unsaturated ketones. *PNAS* 101:5445–5449
16. Yasuda Y, Nagao K, Shido Y, Mori S, Ohmiya H, Sawamura M (2015) Copper-catalyzed γ -selective and stereospecific allylic cross-coupling with secondary alkylboranes chem. *Eur J* 21:9666–9670

17. Takayama Y, Ishii T, Ohmiya H, Iwai T, Schwarzer MC, Mori S, Taniguchi T, Monde K, Sawamura M (2017) Asymmetric synthesis of b-lactams through copper-catalyzed alkyne-nitrone coupling with a prolinol-phosphine chiral ligand chem. *Eur J* 23:8400–8404
18. Cao L-M, Huang H-H, Wang J-W, Zhong D-C, Lu T-B (2018) The synergistic catalysis effect within a dinuclear nickel complex for efficient and selective electrocatalytic reduction of CO₂ to CO. *Green Chem* 20:798–803
19. Zhu S, Hu L, Jiang H (2014) Gold-catalyzed tandem Diels-Alder reactions of enynals/enynones with alkenes: generation and trapping of cyclic o-QDMs. *Org Biomol Chem* 12:4104–4111
20. Miyaura N, Suzuki A (1995) Palladium-catalyzed cross-coupling reactions of organoboron compounds. *Chem Rev* 95:2457–2483
21. Engle KM, Mei T-S, Wasa M, Yu J-Q (2012) Weak coordination as a powerful means for developing broadly useful C–H functionalization reactions. *Acc. Chem Res* 45:788–802
22. Waibel M, Cramer N (2010) Palladium-catalyzed arylation ring-opening reactions of norbornenols: entry to highly substituted cyclohexenes, quinolines, and tetrahydroquinolines. *Angew Chem Int Ed* 49:4455–4458
23. Ishitsuka T, Okuda Y, Szilagyi RK, Mori S, Nishihara Y (2016) The molecular mechanism of palladium-catalysed cyano-esterification of methyl cyanoformate onto norbornene. *Dalton Trans* 45:7786–7793
24. Wang J-W, Hou C, Huang H-H, Liu W-J, Ke Z-F, Lu T-B (2017) Further insight into the electrocatalytic water oxidation by macrocyclic nickel (II) complexes: the influence of steric effect on catalytic activity. *Catal Sci Technol* 7:5585–5593
25. Rydzewski J, Nowak W (2017) Thermodynamics of camphor migration in cytochrome P450cam by atomistic simulations. *Sci Rep.* <https://doi.org/10.1038/s41598-017-07993-0>
26. Guallar V, Friesner RA (2004) Cytochrome P450CAM enzymatic catalysis cycle: a quantum mechanics/molecular mechanics study. *J Am Chem Soc* 126:8501–8508
27. Ohtsuka T, Ito H, Tanaka A (1997) Conversion of chlorophyll b to chlorophyll a and the assembly of chlorophyll with apoproteins by isolated-chloroplasts. *Plant Physiol* 113:137–147
28. Sage RF, Sage TL, Kocacinar F (2012) Photorespiration and the evolution of C₄ photosynthesis. *Annu Rev Plant Biol* 63:19–47
29. Roy S, Sharma B, Pécaut J, Simon P, Fontecave M, Tran PD, Derat E, Artero V (2017) Molecular cobalt complexes with pendant amines for selective electrocatalytic reduction of carbon dioxide to formic acid. *J Am Chem Soc* 139:3685–3696
30. Wang C-M, Wang Y-D, Xie Z-K (2014) Verification of the dual cycle mechanism for methanol-to-olefin conversion in HSAP0-34: a methylbenzene-based cycle from DFT calculations. *Catal Sci Technol* 4:2631
31. Fischmeister C, Bruneau C (2011) Ene-yne cross-metathesis with ruthenium carbene catalysts, Beilstein. *J Org Chem* 7:156–166
32. Bonitatibus PJ Jr, Chakraborty S, Doherty MD, Siclovan O, Jones WD, Soloveichik GL (2015) Reversible catalytic dehydrogenation of alcohols for energy storage. *PNAS* 112:1687–1692
33. Zeravcic Z, Brenner MP (2017) Spontaneous emergence of catalytic cycles with colloidal spheres. *PNAS* 114:4342–4347
34. Nicewicz DA, MacMillan DWC (2008) Merging photoredox catalysis with organocatalysis: the direct asymmetric alkylation of aldehydes. *Science* 322:77–80
35. Chinchilla R, Nájera C (2007) The sonogashira reaction: a booming methodology in synthetic organic chemistry. *Chem Rev* 107: 874–922
36. Xu S, Zheng A, Wei Y, Chen J, Li J, Chu Y, Zhang M, Wang Q, Zhou Y, Wang J, Deng F, Liu Z (2013) Direct observation of cyclic carbenium ions and their role in the catalytic cycle of the methanol-to-olefin reaction over chabazite zeolites. *Angew Chem Int Ed* 52:11564–11568
37. Christmann U, Vilar R (2005) Monoligated palladium species as catalysts in cross-coupling reactions. *Angew Chem Int Ed* 44:366–374
38. Dumesic JA, Topsøe N-Y, Topsøe H, Chen Y, Slabiak T (1996) Kinetics of selective catalytic reduction of nitric oxide by ammonia over vanadia/titania. *Journal of Catal* 163:409–417
39. Emerson JP, Coulter ED, Phillips RS, Kurtz DM Jr (2003) Kinetics of the superoxide reductase catalytic cycle. *J Biol Chem* 278:39662–39668

40. Yang M, Kabulski JL, Wollenberg L, Chen X, Subramanian M, Tracy TS, Lederman D, Gannett PM, Wu N (2009) Electrocatalytic drug metabolism by CYP2C9 bonded to a self-assembled monolayer-modified electrode. *Drug Metabolism Disposition* 37:892–899
41. Barnaba C, Gentry K, Sumangala N, Ramamoorthy A (2017) The catalytic function of cytochrome P450 is entwined with its membrane-bound nature. *Food Res.* <https://doi.org/10.12688/f1000research.110151>
42. Kiedorf G, Hoang DM, Müller A, Jörke A, Markert J, Arellano-Garcia H, Seidel-Morgenstern A, Hamel C (2014) Kinetics of 1-dodecene hydroformylation in a thermomorphic solvent system using a rhodium-biphephoscatalyst. *Chem Eng Sci* 115:31–48
43. Larion M, Miller BG (2010) Global fit analysis of glucose binding curves reveals a minimal model for kinetic cooperativity in human glucokinase. *Biochemistry* 49:8902–8911
44. Ainslie GR, Shill JP Jr, Neet KE (1972) A slow transition model for relating transients and cooperative kinetics of enzymes. *J Biol Chem* 247:7088–7096
45. Santacesaria E (1999) Fundamental chemical kinetics: the first step to reaction modelling and reaction engineering. *Catal Today* 52:113–123
46. Smith JM (1981) Chemical engineering kinetics. McGraw-Hill, New York
47. Parshall GW (1980) Homogeneous catalysis. Wiley/Interscience, New York
48. Stewart J, Douglas R, Goguet A (2014) Integrating intrinsic and global kinetics as a dual kinetic model for automotive catalysis. *J Automob Eng* 228:285–294
49. Blackmond DG (2015) Kinetic profiling of catalytic organic reactions as a mechanistic tool. *J Am Chem Soc* 137:10852–10866
50. Blackmond DG (2005) Reaction progress kinetic analysis: a powerful methodology for mechanistic studies of complex catalytic reactions. *Angew Chem Int Ed* 44:4302–4320
51. Kozuch S, Shaik S (2008) Kinetic-quantum chemical model for catalytic cycles: the Haber-Bosch process and the effect of reagent concentration. *J Phys Chem A* 112:6032–6041
52. Kozuch S, Shaik SA (2006) Combined kinetic-quantum mechanical model for assessment of catalytic cycles: application to cross-coupling and heck reactions. *J Am Chem Soc* 128:3355
53. Trost BM, Yeh VSC (2002) A dinuclear Zn catalyst for the asymmetric nitroaldol (Henry) reaction. *Angew Chem Int Ed* 41:861–863
54. Trost BM, Yeh VSC (2002) Effect of ligand structure on the zinc-catalyzed Henry reaction. Asymmetric syntheses of (−)-denopamine and (−)-arbutamine. *Org Lett* 4:2621–2623
55. White JD, Shaw S (2012) A new catalyst for the asymmetric Henry reaction: synthesis of β-nitroethanols in high enantiomeric excess. *Org Lett* 14:6270–6273
56. Youn SW, Kim YH (2000) Facile synthesis of 2-nitroalkanols mediated with LiAlH₄ as catalyst. *Synlett* 6:880–882
57. Risgard T, Gothelf KV, Jorgensen K A (2003) Catalytic asymmetric Henry reactions of silyl nitronates with aldehydes. *Org Biomol Chem* 1:153–156
58. Sasai H, Tokunga T, Watanabe S, Suzuki T, Itoh N, Shibasaki M (1995) Efficient diastereoselective and enantioselective nitroaldol reactions from prochiral starting materials: utilization of La-Li-6,6'-disubstituted BINOL complexes as asymmetric catalysts. *J Org Chem* 60:7388–7389
59. Basavaiah D, Rao AJ, Satyanarayana T (2003) Recent advances in the Baylis-Hillman reaction and applications. *Chem Rev* 103:811–891
60. Declerck V, Martinez J, Lamaty F (2009) aza-Baylis-Hillman Reaction. *Chem Rev* 109:1–48
61. Aggarwal VK, Mereu A, Tarver GJ, McCague R (1998) Metal- and Ligand-accelerated catalysis of the Baylis-Hillman reaction. *J Org Chem* 63:7183–7189
62. Shi M, Jiang J-K, Li C-Q (2002) Lewis base and L-proline co-catalyzed Baylis–Hillman reaction of arylaldehydes with methyl vinyl ketone. *Tetrahedron Lett* 43:127–130
63. Davies HJ, Ruda AM, Tomkinson NCO (2007) Aminocatalysis of the Baylis-Hillman reaction: an important solvent effect. *Tetrahedron Lett* 48:1461–1464
64. Aroyan CE, Vasbinder MM, Miller SJ (2005) Dual catalyst control in the enantioselective intramolecular Morita-Baylis-Hillman reaction. *Org Lett* 7: 3849–3849–3851
65. Raheem IT, Jacobsen EN (2005) Highly enantioselective Aza-Baylis–Hillman reactions catalyzed by chiral thiourea derivatives. *Adv Synth Catal* 347:1701–1708

66. Imbos R, Minnaard AJ, Feringa BL (2002) A highly enantioselective intramolecular heck reaction with a monodentate ligand. *J Am Chem Soc* 124:184–185
67. Minatti A, Zheng X, Buchwald SL (2007) Synthesis of chiral 3-substituted indanones via an enantioselective reductive-heck reaction. *J Org Chem* 72:9253–9258
68. Mitsuda N, Ohme-Takagi M (2009) Functional analysis of transcription factors in arabidopsis. *Plant Cell Physiol* 50:1232–1248
69. Ikeda M, Mitsuda N, Ohme-Takagi M (2009) *Arabidopsis WUSCHEL* is a bifunctional transcription factor that acts as a repressor in stem cell regulation and as an activator in floral patterning. *Plant Cell* 21:3493–3505
70. Kieffer M, Stern Y, Cook H, Clerici E, Maulbetsch C, Laux T, Davies B (2006) Analysis of the transcription factor *WUSCHEL* and its functional homologue in *Antirrhinum* reveals a potential mechanism for their roles in meristem maintenance. *Plant Cell* 18:560–573
71. Tanaka Y, Oshima Y, Yamamura T, Sugiyama M, Mitsuda N, Ohtsubo N, Ohme-Takagi M, Terakawa T (2013) Multi-petal cyclamen flowers produced by AGAMOUS chimeric repressor expression. *Sci Rep.* 3:2641
72. Loix C, Huybrechts M, Vangronsveld J, Gielen M, Keunen E, Cuyper A (2017) Reciprocal interactions between cadmium-induced cell wall responses and oxidative stress in plants. *Front Plant Sci* 8:1867. <https://doi.org/10.3389/fpls.2017.01867>
73. Yoshida K, Sakamoto S, Kawai T, Kobayashi Y, Sato K, Ichinose Y, Yaoi K, Akiyoshi-Endo M, Sato H, Takamizo T, Ohme-Takagi M, Mitsuda N (2013) Engineering the *Oryza sativa* cell wall with rice NAC transcription factors regulating secondary wall formation. *Front Plant Sci* 4:383. <https://doi.org/10.3389/fpls.2013.00383>
74. Toda Y, Tanaka M, Ogawa D, Kurata K, Kurotani K-i, Habu Y, Ando T, Sugimoto K, Mitsuda N, Katoh E, Abe K, Miyao A, Hirochika H, Hattori T, Takeda S (2013) RICE SALT SENSITIVE3 forms a ternary complex with JAZ and Class-C bHLH factors and regulates jasmonate-induced gene expression and root cell elongation. *Plant Cell* 25:1709–1725
75. Willander H et al (2012) High-resolution structure of a brichos domain and its implications for anti-amyloid chaperone activity on lung surfactant protein c. *Proc Natl Acad Sci USA* 109:2325–2329
76. Allsop D, Mayes J (2014) Amyloid β -peptide and Alzheimer's disease. *Essays Biochem* 56:99–110
77. Cohen SIA et al (2015) A molecular chaperone breaks the catalytic cycle that generates toxic $A\beta$ oligomers. *Nat Struct Mol Biol* 22:207–213
78. Genna V, Vidossich P, Ippoliti E, Carloni P, Vivo MD (2016) A self-activated mechanism for nucleic acid polymerization catalyzed by DNA/RNA polymerases. *J Am Chem Soc* 138:14592–14598
79. Flajnik MF, Kasahara M (2010) Origin and evolution of the adaptive immune system: genetic events and selective pressures. *Nat Rev Genet* 11:47–59

Chapter 5

Blue Light Spectroscopy from Electronic Visual Displays



N. Correa, E. Spezzia, R. Doti, J. Faubert, and J. E. Lugo

1 Introduction

It is clear now the existence of physiological behaviors organized in periodic patterns [1]. Likely the most inescapable physiological rhythms are rhythms with periods of 24 h or circadian rhythms. The period is frequently just precise, yet on rare occasions precisely 24 h. That is, living things have internal patterns: circadian cadences or rhythms whose meaning is “approximately every day.” The detected circadian rhythms reveal the operation of a biological clock. “clock” given that it cyclically computes time, occasionally with incredible exactitude, with time spans around 24 h and “biological” since it is seemingly originated internally in the living things. We find these circadian rhythms in each important category of plants and animals [1].

The exposure to blue light during the day has some benefits to humans like the increase of focus, memory, and awareness [2–5]. This kind of light has been naturally provided by the sun since human beings exist on earth. A problem emerges when this kind of light is used or obtained away from its natural schedule by an artificial source [2–5]. The introduction of fluorescent bulbs and LED screen devices in our life that are used at a late hour at night are not just altering our circadian sleep cycle and eyestrain; they may also cause severe damage to the retina. Even though the light sends out by many LEDs seems white, LEDs have a bandwidth within the blue light range (400–490 nm). Currently, there are a vast number of studies showing that blue light is very sensible on the brain centers that limit circadian

N. Correa · E. Spezzia

Instituto de Energías Renovables, Universidad Nacional Autonóma de México, Privada Xochicalco S/N, 62580 Temixco, Morelos, Mexico

R. Doti · J. Faubert · J. E. Lugo (✉)

Faubert Lab, School of Optometry, Université de Montréal, C. P. 6128 Montreal, Quebec, Canada
e-mail: eduardo.lugo@gmail.com

rhythms and sleep, which is in agreement with the finding of the melanopsin as a photopigment [6]. In mammals, the population of melanopsin is small, only about 2% of the retinal ganglion cells. They are photosensitive and have absorption peaks around 470–480 nm. These cell axons produce a neural pathway, known as the retinohypothalamic tract. Such pathway communicates the retina and the master circadian clock which is situated within the hypothalamus in the suprachiasmatic nucleus. For example, from cone electroretinogram measurements if the melanopsin gene is lost, then there is a lack of control in the circadian clock [7]. In another research Brainard et al. [8] found that the maximum melatonin depletion in humans occurs at a wavelength around 460 nm, thus putting forward the idea that melanopsin is a crucial agent in the photic controlling of melatonin concentrations and consequently of the circadian rhythms and sleep.

The inhibition of serum melatonin concentrations caused by a short light subjection through the night is a proven approach to estimate the impact of different sources of light on the circadian network. In [6], the efficacy to block serum melatonin concentrations through the night using distinct wavelengths within a light source was tested. Eighteen rats, divided into three groups, were subjected to a color light pulse during 30 min at night. White, blue, or green colors were used, and the light intensity was $1 \times 10^{-1} \mu\text{W}/\text{cm}^2$. Six rats served as a controls group and were not subjected to any light. Blood samples were obtained, and melatonin was collected from the serum, and its concentration was estimated. Both white and blue lights were effective to inhibit melatonin concentrations. Exposure to green light did not have any significative influence of melatonin concentrations.

One may think of using these results to create new devices for light therapy to optimize melatonin levels. Nonetheless, we have to consider that blue light (420–460 nm) within the intensity range of natural light can produce retinal harm in humans [9–11]. Whence, it is serious about evaluating the wavelength spectra of LED-based displays or light sources to reduce the jeopardy related with blue light subjection [12, 13]. There are three known mechanisms of how light can induce retinal harm: photothermal, photomechanical, and photochemical. Photothermal harm happens when the retina and the retinal pigment epithelium (RPE) are subjected to a short-lasting (100 ms to 10 s) but considerable light that may raise tissues' temperature. Photomechanical harm may be due to a sharp amplification of captured energy by the RPE, which may create irrecoverable RPE harm and consequently photoreceptor injury. It has been demonstrated that this kind of retinal injury relies on how much energy has been absorbed regardless of the light spectral constitution [12, 13]. The photochemical harm usually happens as the eyes are subjected to the presence of light within the wavelength range between 390 and 600 nm (UV-VIS). Current research put forward [2] two different mechanisms of photochemical harm. The first one is related with short but noticeable subjection to light damaging the RPE, and the second mechanism is correlated with more prolonged but less noticeable light subjection, that may damage the photoreceptors external part. For instance, blue light exposures of less than 12 h may induce RPE damage in rhesus monkeys [14].

On the contrary, the other harm mechanism happens with lasting periods between 12 and 48 h but with less noticeable light subjection. This mechanism was first

observed in albino rats and another species [15]. In albino rats, subjected to blue light for four hours per day during 30 days, a light wavelength of 474 nm, an intensity of $1 \times 10^{-1} \mu\text{W}/\text{cm}^2$, the amount of melanopsin was reduced up to 20%. This result may have an impact on circadian rhythms.

Because it is not possible to change the primary composition of fluorescent and photoluminescent light, one of the simplest ways to overcome this issue is the use of some filters [5] and specialized software to reduce or even suppress the wavelength spectrum of the blue light at late hours. The questions that arise then are about how these types of applications suppress the wavelength range required, just as *f.lux*, one computer application that supposed to adjust the color temperature of a screen display that takes into account spatial position and time of day. This action is supposed to decrease the amount of blue light that input the eyes; consequently, reducing disturbance of sleep patterns.

In this chapter, we present a series of spectroscopy experiments to characterize the presence of blue light under different digital filtering conditions and screens. The work is divided into five sections; Sect. 2 describes the analysis of the wavelength spectra obtained from a laptop screen modified by *f.lux* software using a spectrometer. Section 3 narrates the analysis of the wavelength spectra from different display devices using the RGB control on Paint. Section 4 shows the light power characterization at different color temperatures and display devices. Finally, in Sect. 5, we wrap up the chapter by giving some conclusions.

2 Analysis of the Wavelength Spectra Obtained from a Laptop Screen Modified by Software Using a Spectrometer

In this experiment, wavelength spectra from a laptop screen were collected as the *f.lux* application was used to modify color temperature.

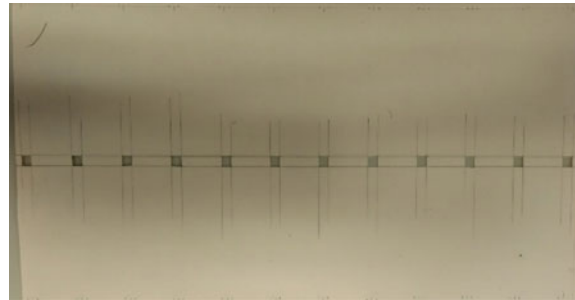
2.1 Methods

We downloaded and installed the software *f.lux* in a computer and also an image where all the color gamut was displayed. We used a fiber optic spectrometer (Stellarnet, Tampa, FL, USA) to obtain all the wavelength spectra.

A cardboard filter was made, using the wide and length of the screen ($26 \times 19 \text{ cm}$). In this cardboard were made 12 equidistant square holes. Each hole measures 0.5 cm per side (Fig. 1). This physical filter was used to select the specific sections of the image that were analyzed.

Once the image was set in the screen and the cardboard filter was placed on top, the next step was to put the metallic base of the spectrometer above the screen, so the

Fig. 1 Cardboard filter, where the square holes can be seen



optical fiber tip would be in a vertical position to measure the wavelength spectrum. The separation between the optical fiber tip and the screen was about 1.5 cm. In all measurements, the lights were off, and we placed one of the spectrometer optical fiber tips right on top of each square (Fig. 2), to guarantee that the spectrometer was receiving the optimal amount of light from the screen, and then the other extreme of the optical fiber was connected directly to the spectrometer.

The projection of the image was modified using *f.lux* software by setting color temperatures of 1900, 4200, and 6500 K. Wavelength spectra were taken on each of the 12 square holes at 6500 K, then at 4200 K and finally at 1900 K.

The laptop used was a LENOVO model: 1066AJU with an Intel(R) HD Graphics 3000 screen.

The image used was the one below (Fig. 3), and each region of the image that was analyzed along with its wavelength spectrum is shown below.

Fig. 2 Setup for the experiment

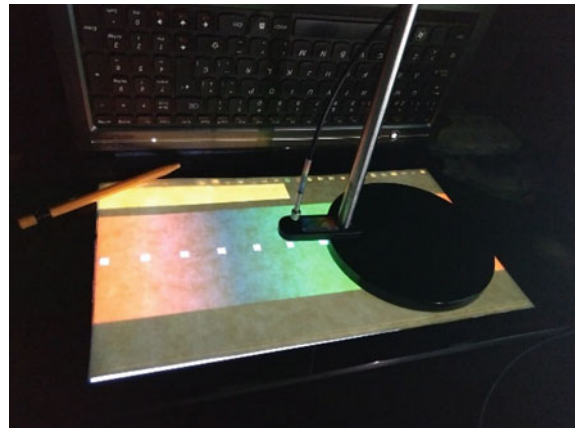




Fig. 3 Gamut color image

2.2 Results

In the following graphs, the ordinate axis displays counts (which are proportional to light intensity) and on the abscissa axis the wavelength (nm)

2.3 Discussion

None of the selected regions have shown a pure color; each square was given a combination of the intensities of the three RGB LEDs (red, green, blue) from each pixel on the screen. As the temperature of light projected on the screen is reduced, the amplitude of the maximum peak shown by the spectrometer decreased.

The application was not able to suppress the blue light completely, and it was observed that within the bandwidth from 400 to 500 nm a faster loss of intensity occurred. This loss can be seen in Fig. 4 overall in the bluish colors.

The use of this software alters the image seen on the screen, as it can be observed in Fig. 5 this perturbation on the image is caused by the alteration of the original gamut of colors.

3 Analysis of the Wavelength Spectra from Different Display Devices Using the RGB Control on Paint

In this case, the wavelength spectra of each RGB and white, “purest” colors from Paint, were measured from different screens; each measurement was done under the same conditions. The main objectives were: analyze the “purest” colors that different display devices can emit and analyze more in detail the white color, to see if it is the complete combination of the RGB gamut.

3.1 Methods

Five display devices were used for analysis, and Table 1 shows some characteristics of the utilized display devices.

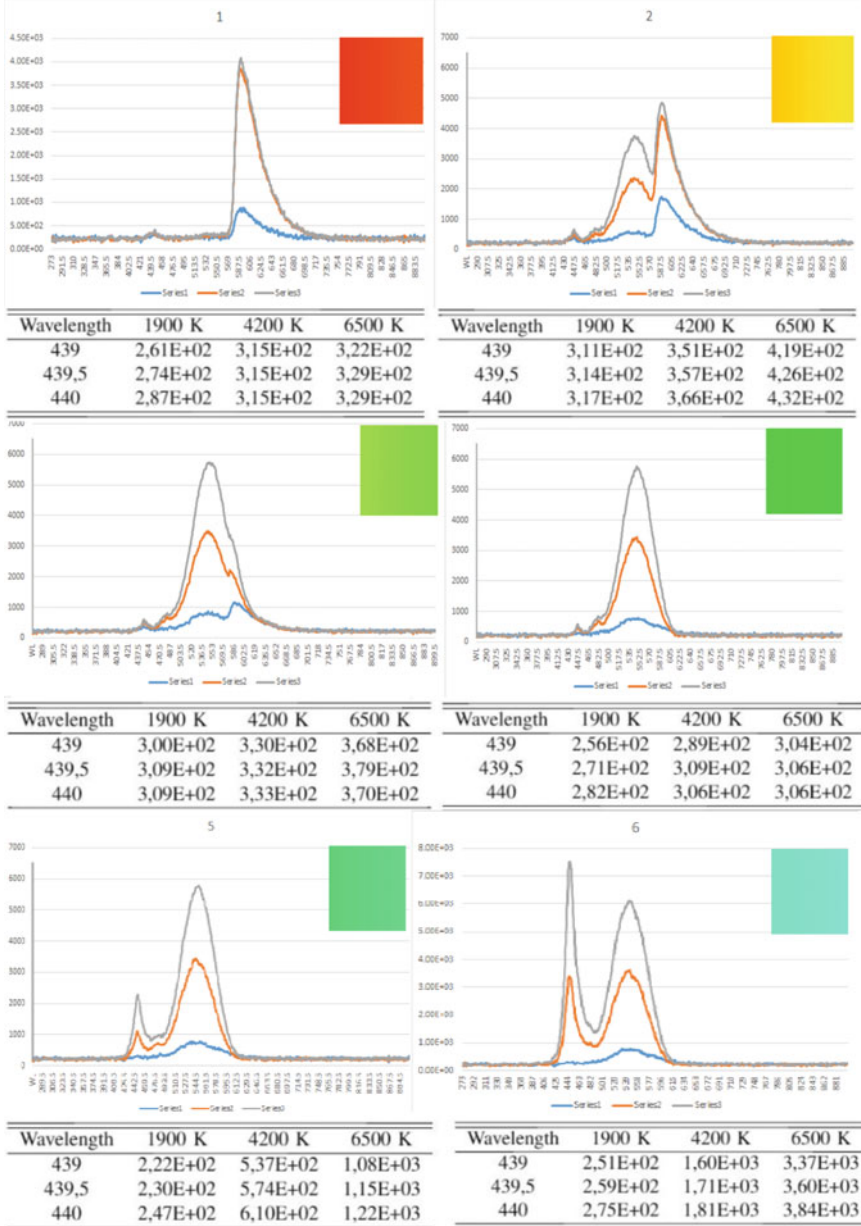


Fig. 4 The wavelength spectra from the 12 regions selected from Fig. 3. The gray line corresponds to 6500 K, orange line to 4200 K and blue line to 1900 K. The tables beneath each graph display intensity values, in arbitrary units, for three different wavelengths and color temperatures

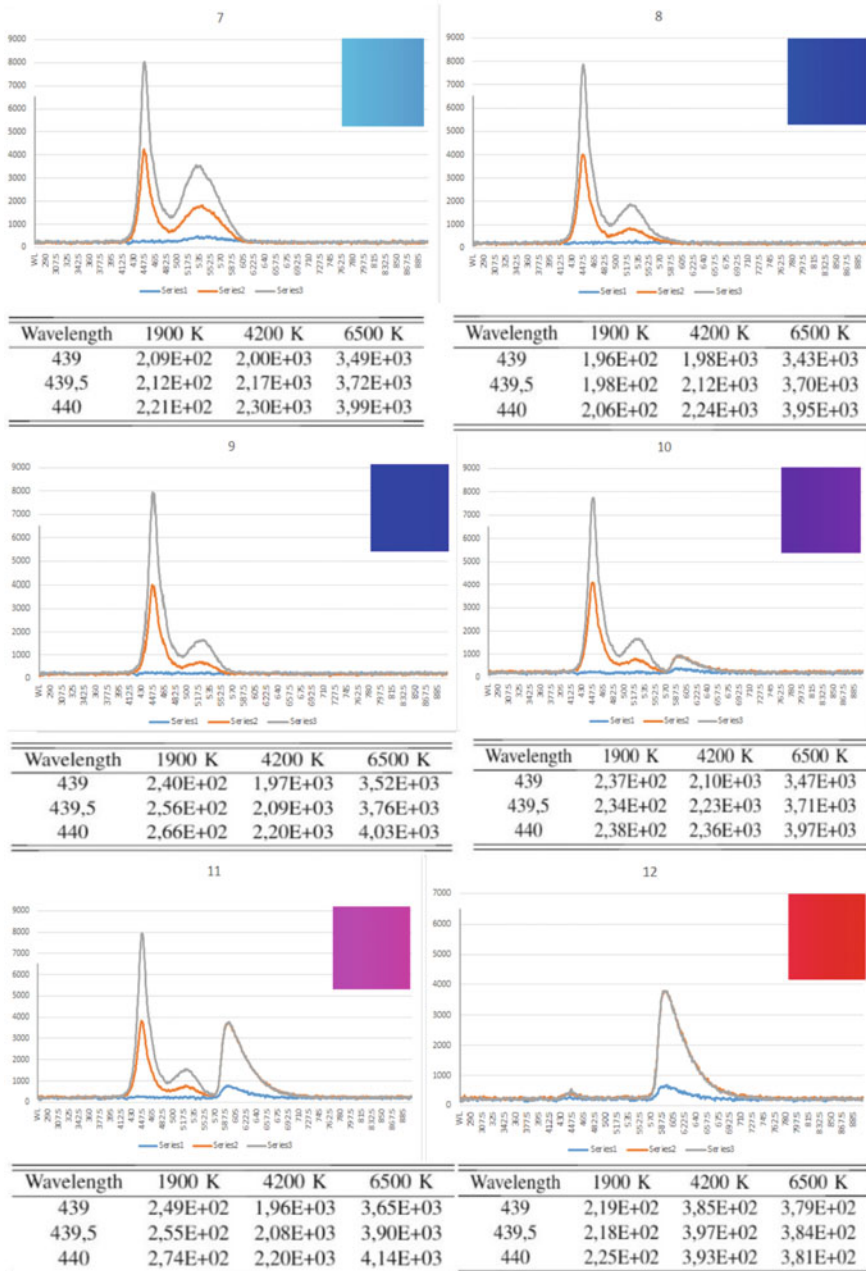
**Fig. 4** (continued)



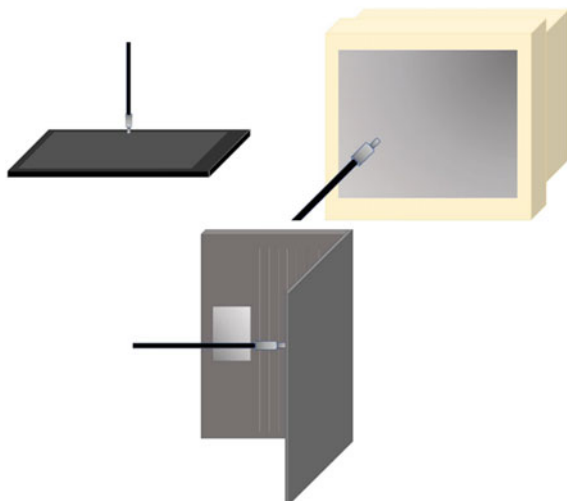
Fig. 5 A landscape image with different color temperature

Table 1 The display devices used here

Device	Brand	Model
Laptop	DELL	Inspiron 5558
CRT monitor	SAMSUNG	15GL CSR59987L
Filament projector	ViewSonic	PJD7383
LED projector	QUIMI	Pocket Q2-B
Cellphone	HUAWEI	QISCAM-L03

In order to mount the experiments, the optical fiber tip of the spectrometer was placed just above the screens, in the case of the cellphone, the laptop, and the CRT (Fig. 6), while in the case of the projector, the tip was positioned 20° off the projector lens optical axis (Fig. 7). The reason behind this tip position is to avoid the power saturation limit of the spectrometer that may damage the spectrometer optical sensors.

Fig. 6 Optical fiber tip position to measure wavelength spectra from different display devices



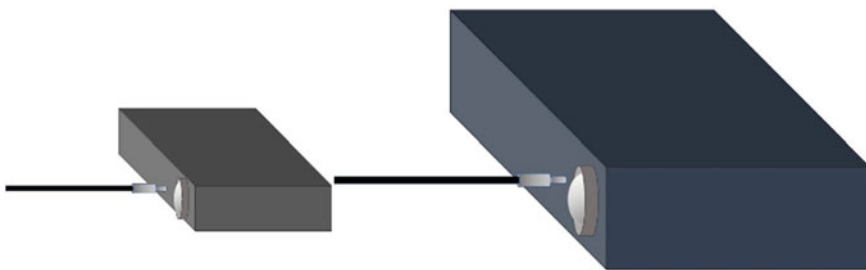


Fig. 7 Optical fiber tip position to measure wavelength spectra from the projector lens

Table 2 The measurement parameter values for the devices used in this experiment

Device	Integration time	Averaged scans
Laptop	400	1
CRT	200	10
Filament projector	1	10
LED projector	1	100
Cellphone	200	1

The light sources had different luminances, so for each one, a different integration time was defined, in a way that all data from each device could be analyzed in a space with equivalent characteristics.

The spectrometer was used along with the SpectraWiz software (Stellarnet, Tampa, FL, USA) to record data for its later analysis.

In order to set the RGB and white color data on one single graph for each device, it was necessary to set specific measurement parameter values on the SpectraWiz software, and in Table 2 these values are observed.

The RGB and white colors for the analysis were selected using Paint (Windows 10). Figures 8, 9, 10, and 11 display this color selection process. The luminance of RGB and white colors was kept constant.

3.2 Results

From Figs. 12, 13, 14, 15, and 16 the wavelength spectra for each color light source are displayed. The color of each curve represents the corresponding color projection using Microsoft Windows Paint.

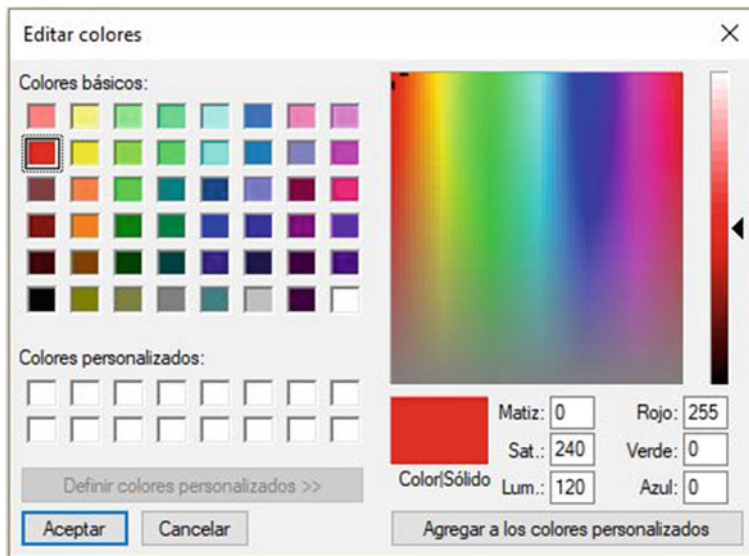


Fig. 8 Red color setup

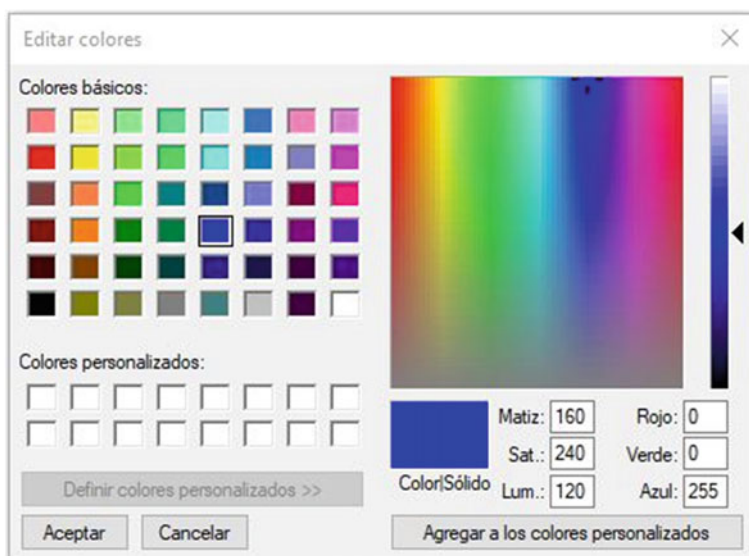


Fig. 9 Blue color setup

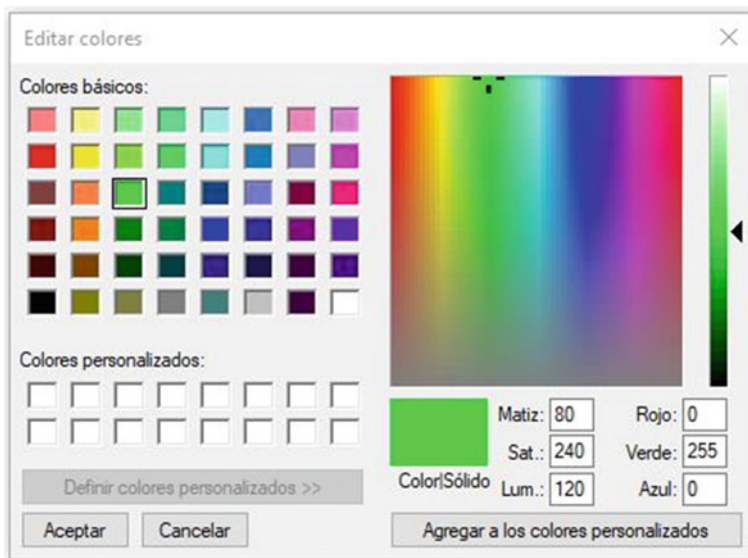


Fig. 10 Green color setup

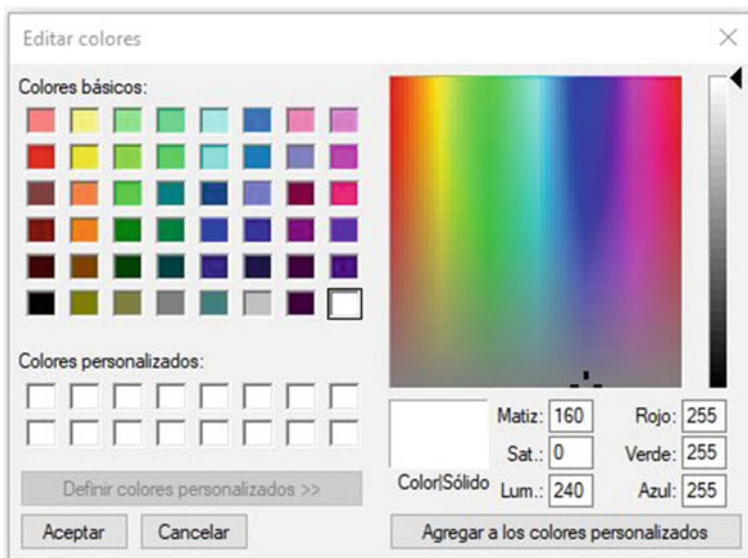


Fig. 11 White color setup

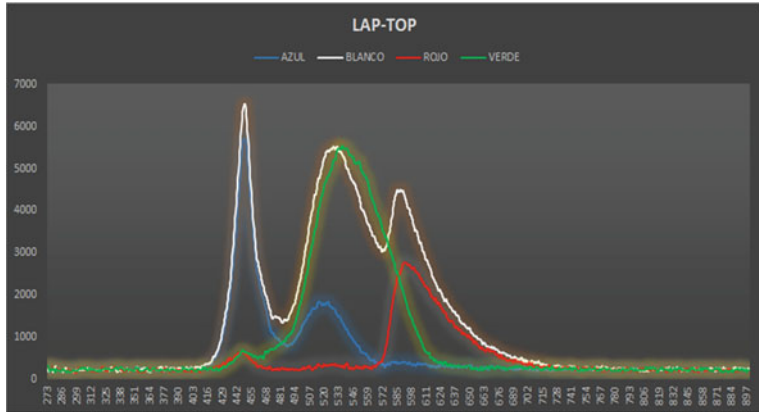


Fig. 12 Laptop results. The color of each curve represents the corresponding color projection using Microsoft Windows Paint

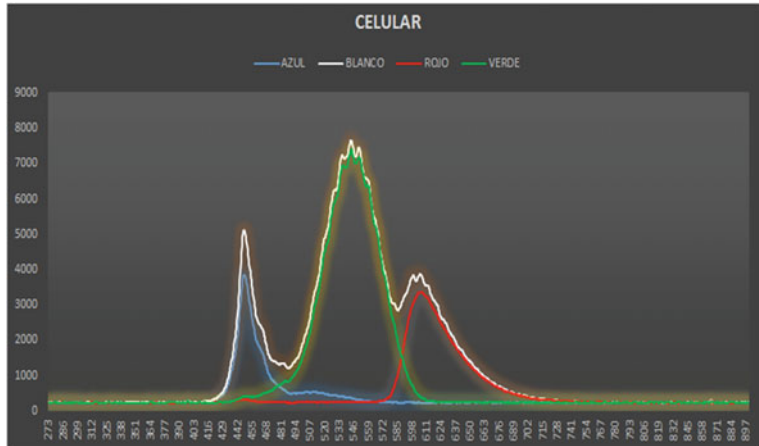


Fig. 13 Cellphone results. The color of each curve represents the corresponding color projection using Microsoft Windows Paint

3.3 Discussion

The device that showed the most balanced wavelength spectrum concerning the combination of its RGB components was the HUAWEI cellphone because its white spectrum takes precisely the shape and amplitude of the peaks of their RGB LEDs. However, their LEDs did not show a “pure” color; the supposedly pure colors showed wavelengths corresponding to another color, for example, a large amount of green within blue bandwidth. All the devices, except the LED projector, had this problem of lacking pure color wavelengths.

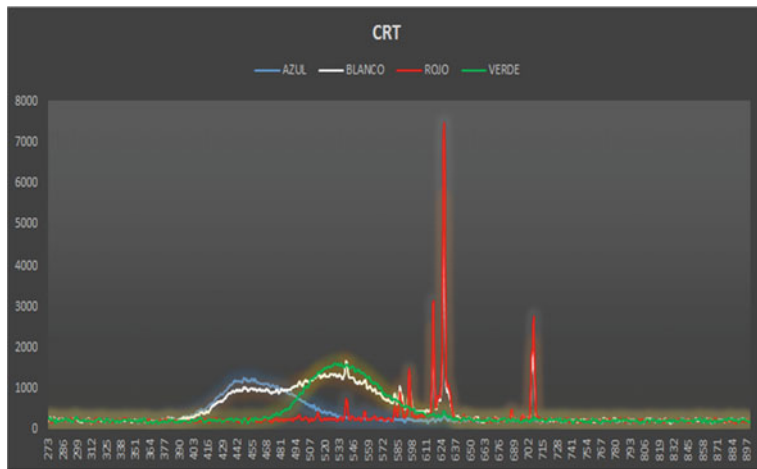


Fig. 14 CRT results. The color of each curve represents the corresponding color projection using Microsoft Windows Paint

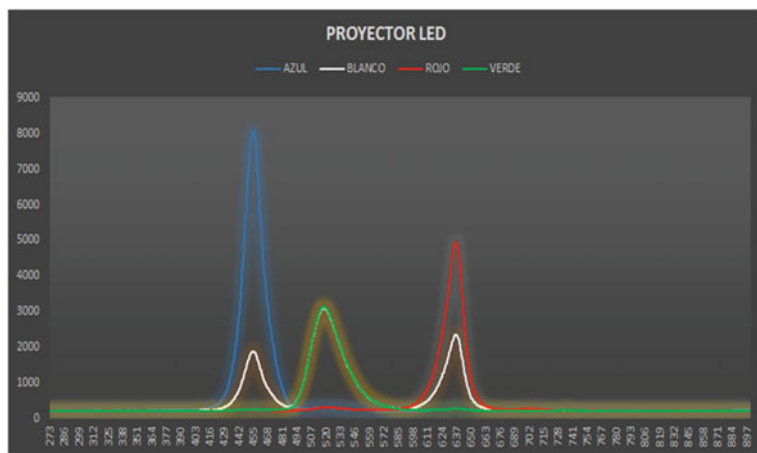


Fig. 15 LED projector results. The color of each curve represents the corresponding color projection using Microsoft Windows Paint

In the case of the CRT monitor, the blue and green bands have low-intensity powers; the red and infrared bands showed discrete peaks.

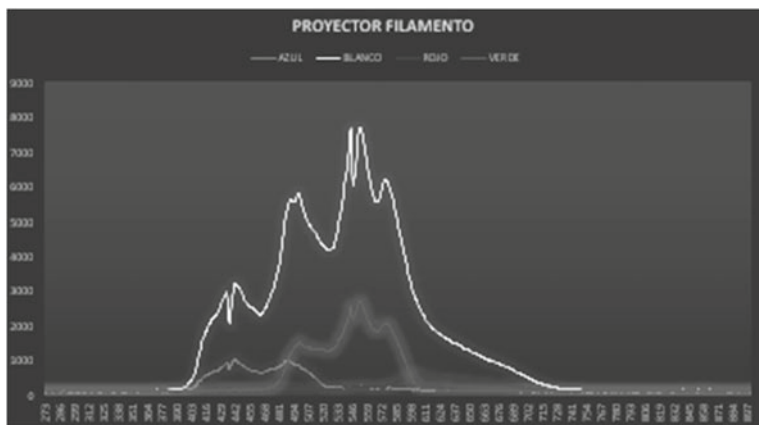


Fig. 16 Filament projector results. The color of each curve represents the corresponding color projection using Microsoft Windows Paint

4 Light Power Characterization at Different Color Temperatures and Display Devices

In this section, light power from different color images and displays devices was collected with the help of an optical power meter. The objectives were to measure emitted power by the previous sources of light in different wavelength bandwidths.

4.1 Methods

4.1.1 Wavelength Spectrum Characterization at Different Color Temperatures and Display Devices

Three physical filters (red, green, and blue) were used with the idea of finding a way to separate different wavelengths bandwidths from the rest of the visible frequency spectrum of light.

The utilized filters were installed on a plastic rotatory disk (see Fig. 17). First, the transmission of the filters was characterized. In Fig. 18, we can observe the experimental setup where the optic fiber tip was installed as close as possible from the filter surface without touching it.

As reference light to measure transmission, it used a tungsten halogen lamp. In one side of the filter, the tip of one optic fiber was placed connected to the spectrometer, and in the other side of the filter disk, the tip of another optic fiber was placed connected to the lamp.

From Figs. 19, 20, and 21, the transmission for each color filter is shown as a percentage in the ordinate axis and the wavelength (nm) in the abscissa axis. The

Fig. 17 The three color filters placed on the rotatory disk

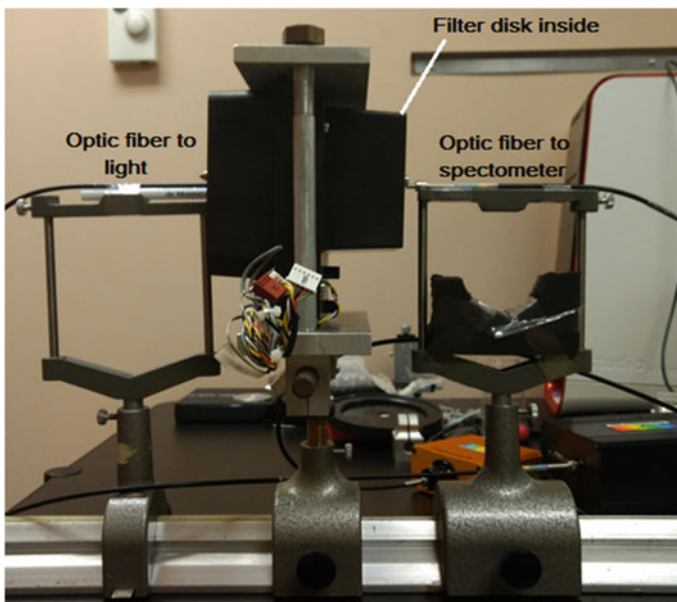
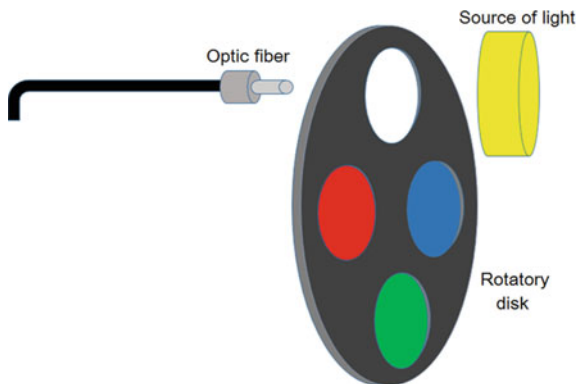


Fig. 18 Experimental setup to characterize the optical transmission of three color filters

red filter is a short wavelength filter, and the blue and green are bandpass filters. As it is shown, the filters did not block the infrared emitted light, and the blue filter transmitted on the 400–500 nm bandwidth. The transmission of the color filters could be useful in combination with an infrared filter to detect the presence of red, green, or blue light only.

For that reason, we decided to use an infrared filter along with the filters from the RGB filter wheel.

The first step was to obtain an infrared filter. In this case, a Webcam Logitech QuickCam Pro 3000 was disassembled to use its filter (see Fig. 22). Once the filter

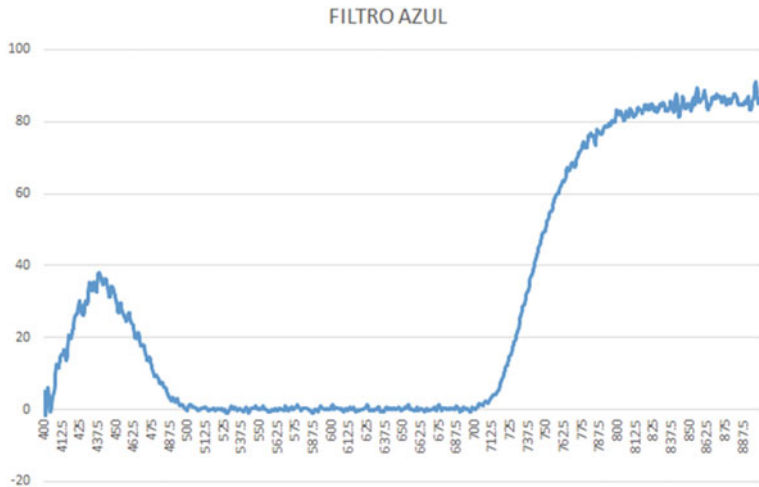


Fig. 19 Blue filter transmission. It has a maximum transmission of 38.5%

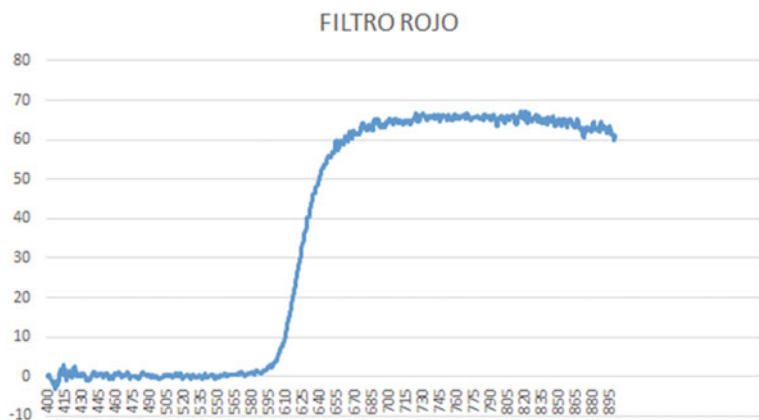


Fig. 20 Red filter transmission. It has a maximum transmission of 65%

was removed, it was added to the fiber optic tip that inputs the spectrometer and then the fiber was settled in front of the color filters (see Fig. 23). The procedure to obtain all wavelength spectra was as follows:

1. We displayed in the CRT screen one of the RGB or white colors.
2. Put the red filter and measure the red, green, blue, and white images first at 6500 K, then at 3850 K and finally, 1200 K. Measure the wavelength spectrum and save the data.
3. Repeat the process for the green, blue filter and without a filter.
4. Repeat again points one, two, and three but using the laptop screen instead of the CRT.

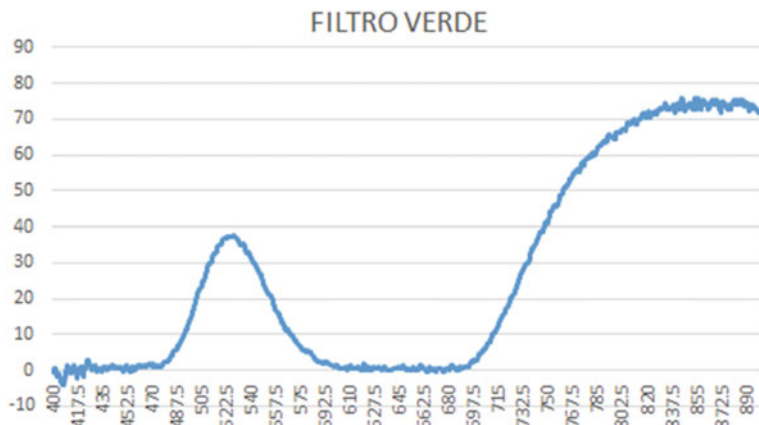


Fig. 21 Green filter transmission. It has a maximum transmission of 38.5%

Fig. 22 Logitech QuickCam Pro 3000 and its infrared filter



Fig. 23 A photograph of the optical fiber from the spectrometer attached to the infrared filter and then put it in front of the filters of the RGB filter wheel

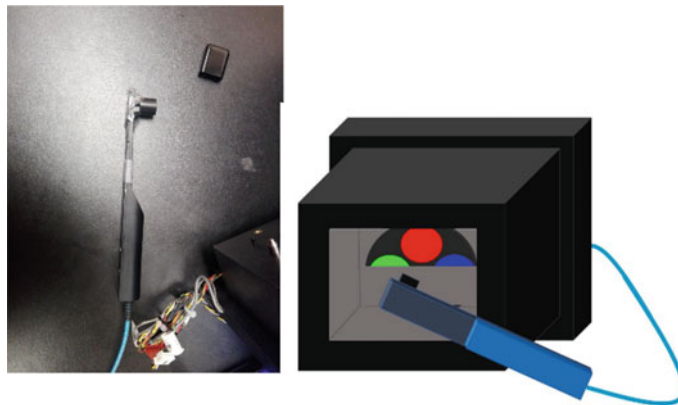


Fig. 24 Left, Photograph of the optical power meter attached to the infrared filter. Right, a diagram of the sensor located in the base of the filter box

4.1.2 Light Power Measurements

For power measurements, we used an optical power meter (Newport 843-R, Irvine, CA, USA).

Using the optical power meter and information obtained with the spectrometer from the preceding sections, we will analyze the optical power for each color. To make this, it was necessary to attach the infrared filter to the optical power meter sensor and then to put in front of the RGB filter box (Fig. 24)

4.2 Results

It was obtained four graphics per filter with the colors red, green, blue and white, and every graph also has its color temperature manipulated through software.

4.3 Discussion

4.3.1 Wavelength Spectrum Characterization at Different Color Temperatures and Display Devices

Using the RGB filter wheel, we obtained the transmission spectrum of each color filter. The green and blue filters were bandpass filters, and the red is a high-pass wavelength filter. The presence of infrared radiation was notorious in all transmission spectra. Since the idea of using the RGB color filters was to study the same color

images presented in Sect. 2 but within each color band, it was necessary to add an infrared filter to warrant the milestone as mentioned earlier.

For the laptop display (Figs. 25, 26, and 27), when the red image is analyzed without any filter, there were blue light wavelengths present at three different color temperatures, which it was changed digitally using *f.flux*. The same is also true for the green color image, and for the blue image, the presence of green wavelengths is notorious. When the red filter is used, the green and blue colors do not have any red wavelengths which optical power is embedded inside the noise floor. With the green filter, the blue color image contained a noticeable band of green wavelengths, when the color temperature was high, but when the color temperature was decreased, the blue wavelengths disappeared. The red color image did not contain any green wavelengths. When the blue filter is utilized, the red and green colors do not have any blue wavelengths which optical power are almost embedded inside the noise floor, and the blue color peak decreases as the color temperature decreases. Finally, when no RGB filter is used (Fig. 28), as it was seen in Sect. 2, we observed the red color contained some blue color wavelengths at all measured color temperatures. This result is problematic because even when we applied the digital filter by decreasing the color temperature of the image, the image may look red, but the presence of blue wavelengths is evident from these experiments.

For the CRT display (Figs. 29, 30, and 31) the red filter gave a pair of well-delimited peaks within the red color band, and when the color temperature was modified the peaks amplitudes almost were the same, the presence of green or blue wavelengths was not evident with this filter. With the green filter, colors blue and red are also present within that wavelength band. At 3850 K, almost all the blue and red wavelengths in the bandwidth of 500–600 nm disappeared and just the red peak and one green peak, due to white color remained at 1200 K. With the blue filter, it was seen that there was no interference from other wavelength color spectra. The color blue has a fast amplitude fall when the temperature decreased and disappeared entirely at 1200 K. Like in the laptop screen measurements the white color matches all the maximum curves and peaks.

When no RGB filter is used (Fig. 32), we observed that there was a small wavelength overlap between the green and blue colors. That is, the green contained some blue color wavelengths and vice versa. This behavior disappeared at 1200 K; at this color temperature only the red component of the white color prevailed. Thus, the digital filter technique would serve well its purpose when used along with a CRT display device. The red color image contained some green wavelength peaks as well.

4.3.2 Light Power Measurements

As we observed in the preceding section, the red color image contained some blue color wavelengths at all measured color temperatures. That is, even when we applied the digital filter by decreasing the color temperature of the image, the image may look red but the presence of blue wavelengths is evident from these results. Optical power peaks were obtained using the optical power meter considering that when the

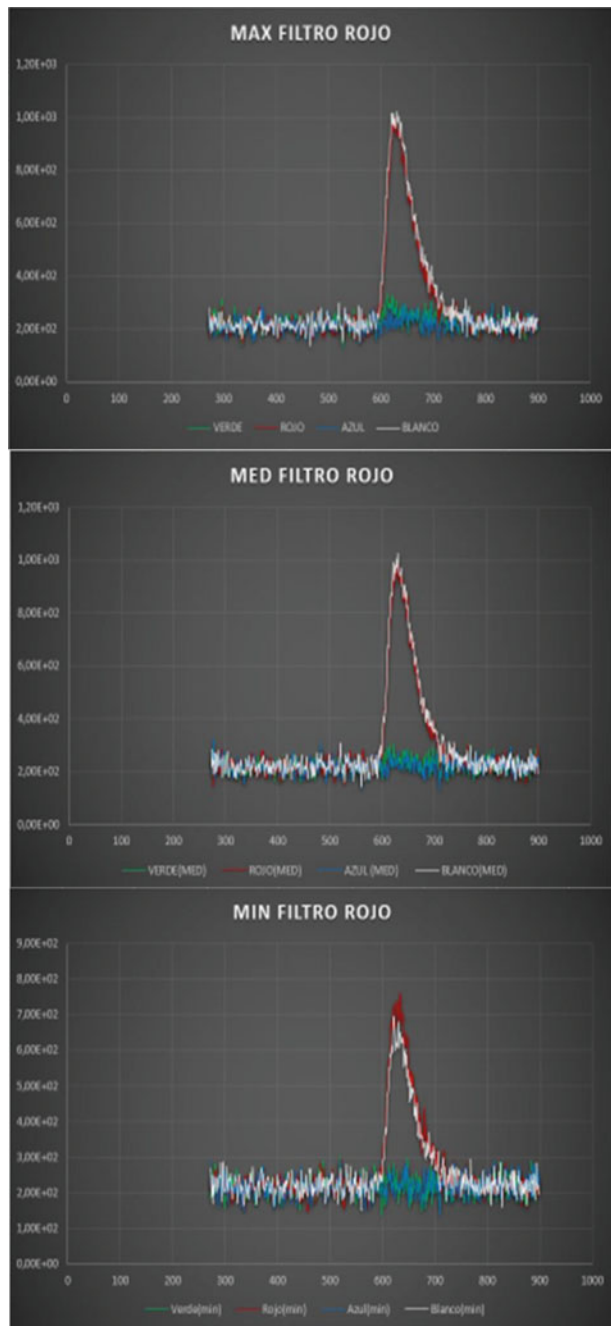
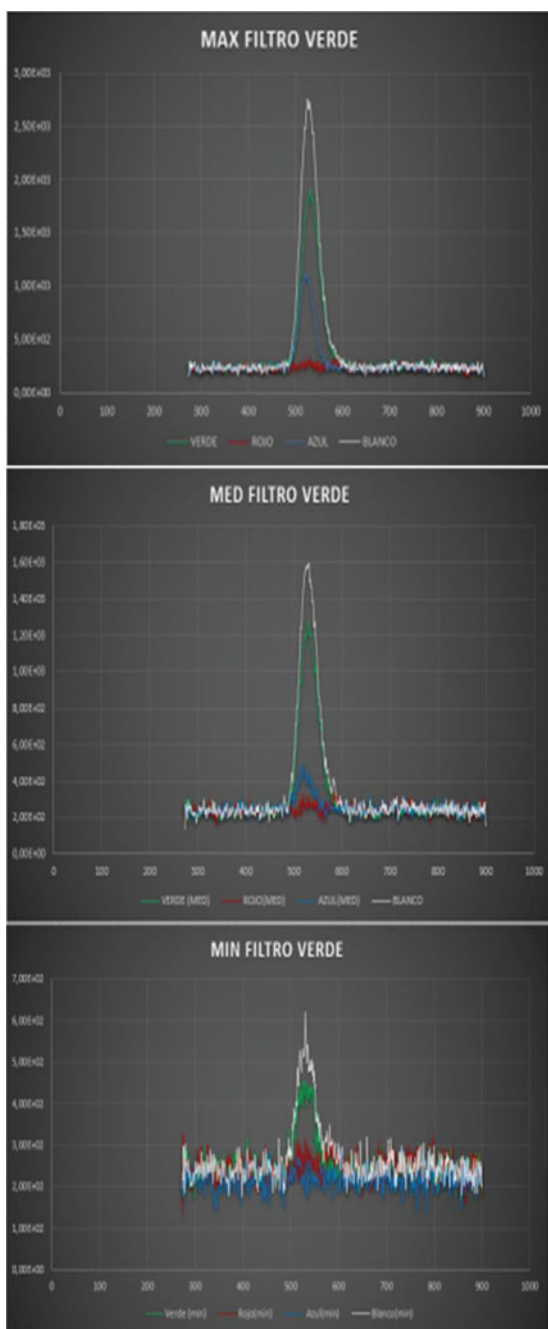


Fig. 25 The laptop red filter graph at three different color temperatures. 6500 K (Top); at 3850 K (Middle); and 1200 K (Bottom). The color of each curve represents the corresponding color projection using Microsoft Windows Paint

Fig. 26 The laptop green filter graph at three different color temperatures. 6500 K (Top); at 3850 K (Middle); and 1200 K (Bottom). The color of each curve represents the corresponding color projection using Microsoft Windows Paint



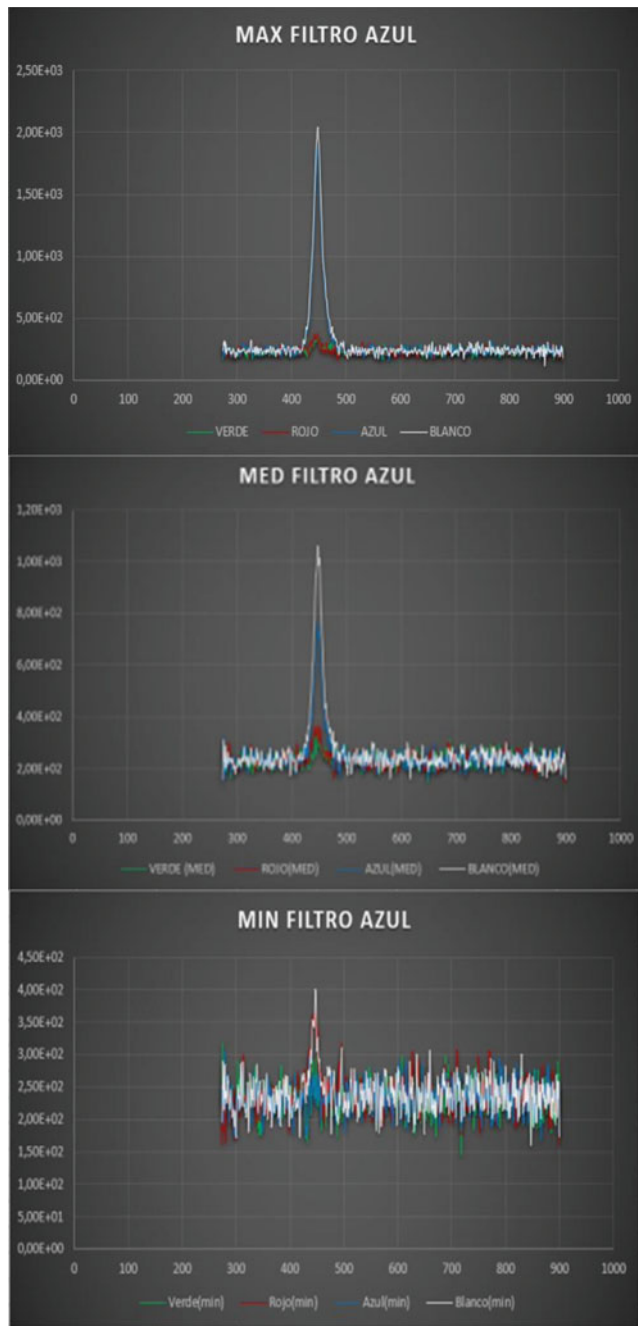


Fig. 27 The laptop blue filter graph at three different color temperatures. 6500 K (Top); at 3850 K (Middle); and 1200 K (Bottom). The color of each curve represents the corresponding color projection using Microsoft Windows Paint

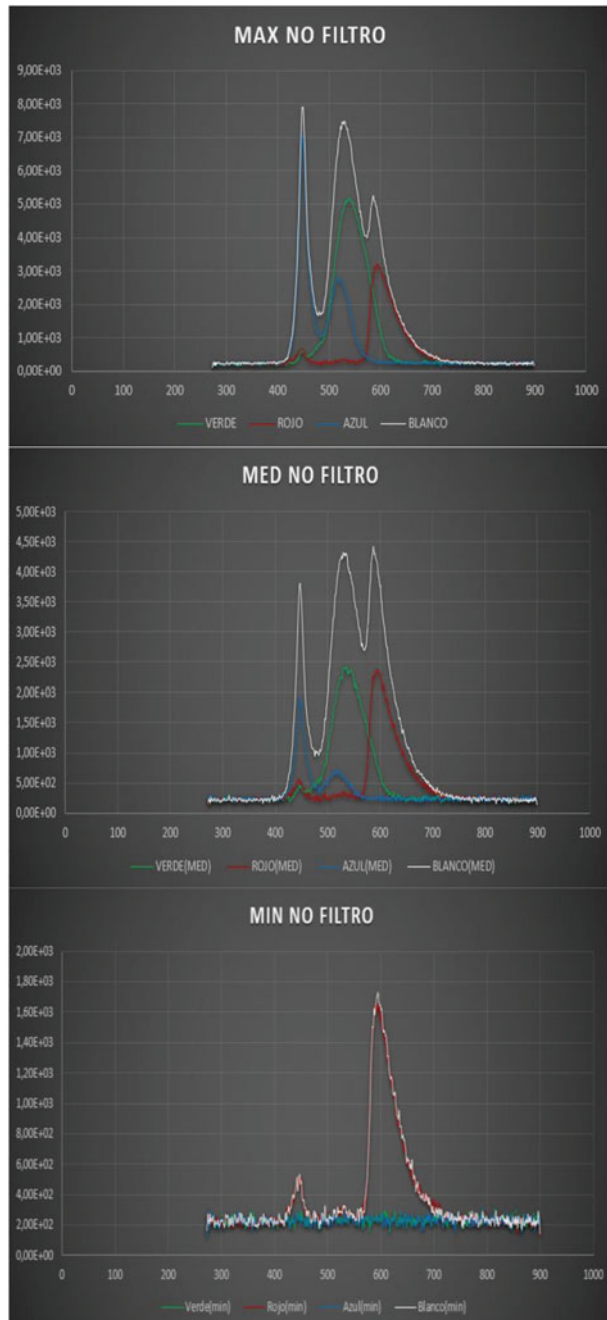


Fig. 28 The LAPTOP no RGB filter graph at three different color temperatures. 6500 K (Top); at 3850 K (Middle); and 1200 K (Bottom). The color of each curve represents the corresponding color projection using Microsoft Windows Paint

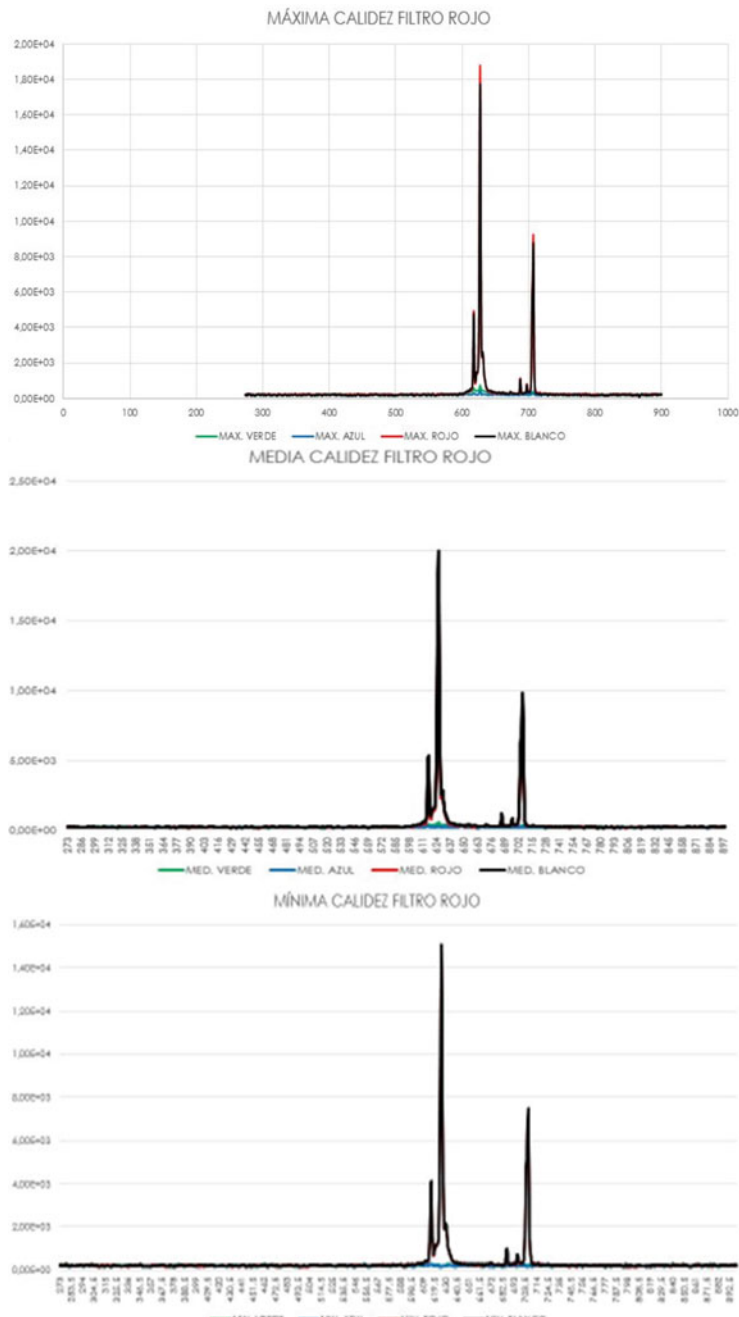


Fig. 29 The CRT red filter graph at three different color temperatures. 6500 K (Top); at 3850 K (Middle); and 1200 K (Bottom). The color of each curve represents the corresponding color projection (except white which is depicted in black) using Microsoft Windows Paint

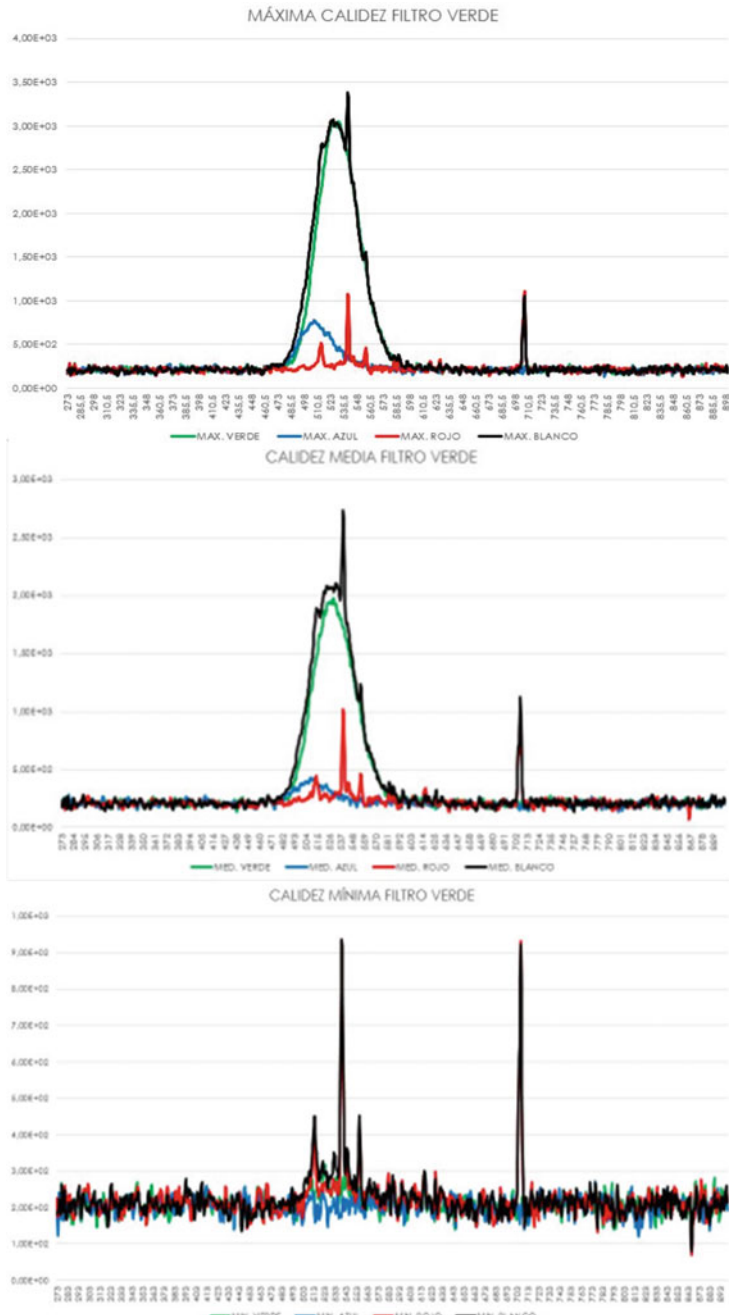


Fig. 30 The CRT green filter graph at three different color temperatures. 6500 K (Top); at 3850 K (Middle); and 1200 K (Bottom). The color of each curve represents the corresponding color projection (except white which is depicted in black) using Microsoft Windows Paint

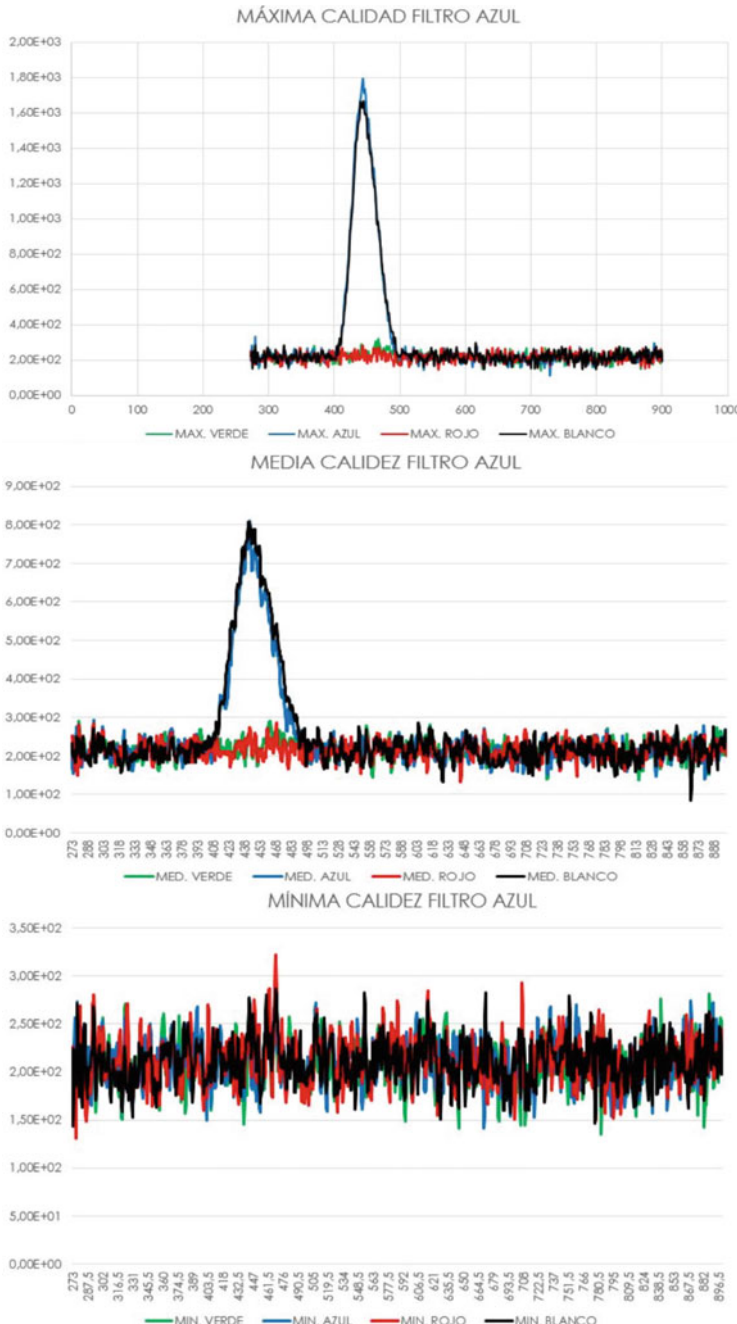


Fig. 31 The CRT blue filter graph at three different color temperatures. 6500 K (Top); at 3850 K (Middle); and 1200 K (Bottom). The color of each curve represents the corresponding color projection (except white which is depicted in black) using Microsoft Windows Paint

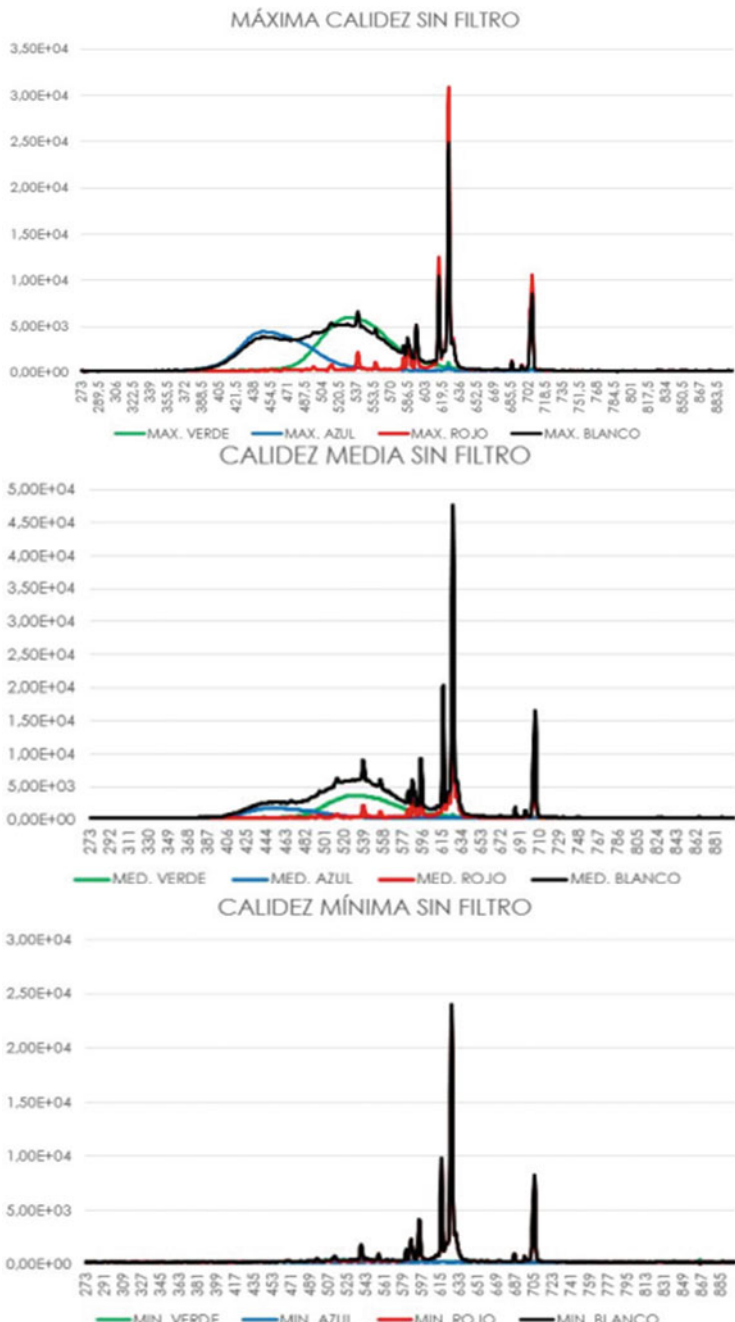


Fig. 32 The CRT no RGB filter graph at three different color temperatures. 6500 K (Top); at 3850 K (Middle); and 1200 K (Bottom). The color of each curve represents the corresponding color projection (except white which is depicted in black) using Microsoft Windows Paint

Table 3 The laptop power meter measurements using three RGB filters at three color temperatures. The last column shows the measured power without filters and the same three color temperatures

Red image			
Color Temperature (K)	Wavelenght(nm)	Power(microW) with red filter @ maximum	Power(microW) without filter @ maximum
6500	634	0,29	0,64
3850	634	0,29	0,63
1200	634	0,26	0,49
Green image			
Color Temperature (K)	Wavelenght(nm)	Power(microW) with green filter @ maximum	Power(microW) without filter @ maximum
6500	528	0,38	1,07
3850	528	0,32	0,91
1200	528	0,22	0,22
Blue image			
Color Temperature (K)	Wavelenght(nm)	Power(microW) with blue filter @ maximum	Power(microW) without filter @ maximum
6500	448	0,4	1,32
3850	448	0,26	0,83
1200	448	0,25	0,24

lecture was not stable, we took the average between the maximum and the minimum values. The noise floor value was estimated in $0.23 \pm 0.02 \mu\text{W}$. That is the noise floor level fluctuated between 0.22 and 0.25 μW .

The results obtained with the optical power meter with the laptop are shown in Table 3. Displaying the red color with the red filter gave a power value almost constant of $0.29 \mu\text{W}$ at 6500 K and $0.26 \mu\text{W}$ at 1200 K, but without the filter the optical power decreased from $0.64 \mu\text{W}$ at 6500 K to $0.49 \mu\text{W}$ at 1200 K. Taking into account that the red filter showed 65% transmission, we should have $0.45 \mu\text{W}$ ($0.29 \mu\text{W}/0.65$) of red wavelength power. Thus, the difference between $0.64 \mu\text{W}$ and $0.45 \mu\text{W}$ gives the amount of blue wavelength power (see Fig. 28) presented in the red image at 6500 K, that is $0.19 \mu\text{W}$. For 1200 K, the result is $0.09 \mu\text{W}$. The green image also contained some blue wavelengths which had an optical power of $0.08 \mu\text{W}$ at 6500 K and 3850 K. It was not possible to measure the optical power below that color temperature. Because the blue color contained only green wavelengths (lower energy than blue wavelength energy), we did not analyze this experimental case more profoundly. All these optical powers can be translated into irradiance values by dividing this power by the detector's surface area, which was 1 cm^2 .

On the CRT (Table 4), the red color image was the only color showing some significant power contribution when the green filter was applied. With this filter the optical power dropped, when the color temperature decreased, from $0.34 \mu\text{W}$ at 6500 K to $0.29 \mu\text{W}$ at 1200 K. Without the filter the optical power decreased from $0.56 \mu\text{W}$ at 6500 K to $0.48 \mu\text{W}$ at 1200 K. This means that approximately $0.04 \mu\text{W}$ comes from green wavelengths at 6500 K and $0.03 \mu\text{W}$ at 1200 K.

Table 4 The CRT power meter measurements using three RGB filters at three color temperatures. The last column shows the measured power without filters and the same three color temperatures

Red image			
Color Temperature (K)	Wavelenght(nm)	Power(microW) with red filter @ maximum	Power(microW) without filter @ maximum
6500	634	0,34	0,56
3850	634	0,33	0,58
1200	634	0,29	0,48
Green image			
Color Temperature (K)	Wavelenght(nm)	Power(microW) with green filter @ maximum	Power(microW) without filter @ maximum
6500	528	0,4	1,04
3850	528	0,34	0,89
1200	528	0,22	0,22
Blue image			
Color Temperature (K)	Wavelenght(nm)	Power(microW) with blue filter @ maximum	Power(microW) without filter @ maximum
6500	448	0,42	1,1
3850	448	0,32	0,84
1200	448	0,22	0,22

5 Conclusions

After this first attempt to study the blue light and the way the *f.lux* software tries to suppress it, it was necessary to show the purest colors from the screens, or in other words, each of the RGB LEDs working without the interference of the others. This procedure was done in order to analyze the change of the primary colors that recreate the gamut on different screen devices.

This experiment demonstrated how the composition of color for each source is different, and it was shown that blue light wavelengths are present within other colors images in different light sources without being perceived.

Thanks to the combination of the RGB filter box and the infrared filter, it was possible to control the bandwidth at which every color worked, and also to observe the mutual interference between the RGB color components in two display devices at different color temperatures.

The optical irradiance values of blue light within the red color image, displayed in the laptop screen, at three different temperatures seemed very low, from $0.19 \mu\text{W}/\text{cm}^2$ at 6500 K to $0.09 \mu\text{W}/\text{cm}^2$ at 1200 K. For the green color image, we found light wavelengths within the blue band having optical powers from $0.08 \mu\text{W}/\text{cm}^2$ at 6500 K to $0 \mu\text{W}/\text{cm}^2$ at 1200 K. So even though we might believe a red or green image does not contain any optical power within the blue band in a LED screen, our experiments shown otherwise. The blue wavelength peaks lay within the band of 440–480 nm and their associated optical power order of magnitude is the same as the one used in [15], where white and blue lights were effective to inhibit melatonin concentrations or reduced up to 20% the amount of melanopsin in rats, a result that could have an impact on circadian rhythms.

Moreover, according to references [5, 15], these irradiance values would be harmless to human photoreceptors.

Finally, the strategy using a digital filter to decrease the amount of blue light in a three LED-based display screen like the one used here is not the best solution. It

is better to use a CRT display along with the digital filter technique to avoid blue or green light power exposure.

Acknowledgements An NSERC discovery grant supported this work. N.C. and E.S. want to thank “Proyecto de Becas para Estancias Cortas de Investigación en el Extranjero UNAM-FUNAM-SEP 2017” for the scholarship that made possible their visit to Université de Montréal.

References

1. Winfree AT (1980) The geometry of biological time (Biomathematics; 8). Springer, New York. <https://doi.org/10.1007/978-3-662-22492-2>
2. Tosini G, Ferguson I, Tsubota K (2016) Effects of blue light on the circadian system and eye physiology. *Mol. Vis.* 22:61–72
3. Cajochen C, Chellappa SL, Schmidt C (2014) Circadian and light effects on human sleepiness–alertness. In: S. Garbarino et al (eds) Sleepiness and human impact assessment. Springer, Berlin. https://doi.org/10.1007/978-88-470-5388-5_2
4. Bonmati-Carrion MA, Arguelles-Prieto R, Martinez-Madrid MJ, Reiter R, Hardeland R, Rol MA, Madrid JA (2014) Protecting the melatonin rhythm through circadian healthy light exposure. *Int J Mol* 15:23448–23500. <https://doi.org/10.3390/ijms151223448>
5. Smick K, Villette T, Boulton ME, Brainard GC, Jones W, Karpecki P, Melton R, Thomas R (2013) Blue light hazard: new knowledge, new approaches to maintaining ocular health, report of a roundtable, New York City, NY, USA, sponsored by Essilor of America
6. Ferguson I, Melton A, Li N, Nicol D, Eun Hyun Park EH, Tosini G (2008) Imitating broadband diurnal light variations using solid state light sources. *Light Vis Environ* 32(2):63–68
7. Peirson S, Foster RG (2006) Melanopsin: another way of signaling light. *Neuron* 49:331–339.
8. Brainard GC, Hanifin JP, Greeson JM, Byrne B, Glickman G, Gemer E, Rollag MD (2001) Action spectrum for melatonin regulation in humans: evidence for a novel circadian photoreceptor. *J Neurosci* 21:6405–6412.
9. Wu J, Seregard S, Algvere PV (2006) Photochemical damage of the retina. *Surv Opth* 51:461–481
10. Margrain TH, Boulton M, Marshall J, Slaney DH (2004) Do blue light filters confer protection against age-related macular degeneration? *Ret Eye Res* 23:523–531
11. Mainster MA (2006) Violet and blue light blocking intraocular lenses: photoprotection versus photoreception. *Brit J Opth* 90:784–792
12. Wenzel A, Grimm C, Samardzija M, Reme CE (2005) Molecular mechanisms of light-induced photoreceptor apoptosis and neuroprotection for retinal degeneration. *Prog Retin Eye Res* 24:275–306
13. Organisciak DT, Vaughan DK (2010) Retinal light damage: mechanisms and protection. *Prog Retin Eye Res* 29:113–134
14. Ham WT, Ruffolo JJ, Mueller HA, Clarke AM, Moon ME (1978) Histologic analysis of photochemical lesions produced in rhesus retina by short-wavelength light. *Invest Ophthalmol Vis Sci* 17:1029–1035
15. Noell WK, Walker VS, Kang BS, Berman S (1966) Retinal damage by light in rats. *Invest Ophthalmol Vis Sci* 5:450–473

Chapter 6

Quantum Neural Networks and Quantum Intelligence



M. V. Altaisky and N. E. Kaputkina

1 Introduction

Quantum information processing and artificial intelligence (AI) are two approaches to the problems otherwise intractable for classical computers. The latter, having been revolutionizing our daily life with different intelligent services for quite some time, is expected to deliver even stronger results in near future, but being still implemented on classical hardware it has its own limitations. In this paper, we try to shed some new light on the problem of what we can expect from the convergence of artificial intelligence and quantum technologies.

The concept of quantum neural network (QNN) has emerged from the attempts to marry the models of neural networks (NN) with the ideas of quantum speedup of computations. While the latter was based on completely algorithmic ideas of quantum information processing, pioneered by Deutsch and Josza [1], the former was based on neurophysiological observations on functioning of the brain, which appears as a self-organized evolution of a complex system of identical elements, rather than algorithmic data processing by regular circuits. According to physiological observations of Hebb, the brain is a massively parallel system of identical cells, called neurons, which are connected to each other via synaptic contacts, the strengths of which gradually grow if the activity of corresponding neurons correlates (p. 62 of [2]):

When an axon of cell A is near enough to excite a cell B and repeatedly or persistently takes part in firing it, some growth process or metabolic changes take place in one or both cells such that A's efficiency as one of the cells firing B is increased.

McCulloch and Pitts proposed a mathematical model of neuron [3] as a linear adder of input signals followed by nonlinear transformation of the sum, with the weights

M. V. Altaisky (✉)
Space Research Institute RAS, Profsoyuznaya 84/32, Moscow 117997, Russia
e-mail: altaisky@rss.ru

N. E. Kaputkina
National University of Science and Technology ‘MISIS’, Leninsky av.4, Moscow, Russia
e-mail: kaputkina.ne@misis.ru

somehow learned from the data. This has further resulted in Rosenblatt's *perceptron* model [4], a linear classifier, the first model of neural network that was implemented artificially and has given offspring of all modern artificial neural networks (ANN), which now control face and speech recognition and drive autonomous vehicles.

ANN, or simply neural networks, can be considered as alternative to deterministic computers which maps input data to output data by executing some algorithm. In contrast to it, the neural networks, like the human brain, learn from data. A neural network can be considered as a black box that maps N -dimensional input data vector to M -dimensional output data vector. The internal state of NN is adaptive: it can be changed depending on the applied data. Changing the interneuron connections, the synaptic weights, randomly set at the beginning, the NN gradually tunes these weights to some optimal values, depending on which input-output mappings are rewarded and which are not. If there exists a *training set*, for which desired output is known, the learning process is known as *supervised learning*. Usually, the training, whatever simple or complex it is, demands not less than thousands of training vectors to learn the weights properly. The idea that both the learning of weights and the execution of the input-output mapping can be performed by a quantum system to effectuate the performance have been considered by different authors since the pioneering Feynman's paper on quantum simulators [5]. An essential step towards building of mathematical models for quantum neural networks was done in [6], assuming the potential of the Schrödinger equation, describing the quantum simulator, can be learned from data.

The term 'quantum neural network' was coined by Subhash Kak [7], substituting the inputs of NN by quantum states, the output of such network is determined by a quantum superposition of input states taking with appropriate complex weights. Each input state is, therefore, not only weighted in amplitude, but shifted in phase. The usage of the signal *phase* in neural network models is a brilliant mathematical finding. It can be related to the generalization of back-propagation algorithm, used for classical perceptron, to neural networks with complex weights [8]. In this sense (ignoring the nonlinear effects), the QNNs are identical to optical neural networks [9]. It should be also noted that possible importance of phase relations between quantum mechanical wave functions of certain elements of nervous fibre in human brain have been emphasized by Chavchanidze [10], long before the emergence of quantum computation concept.

The modern approach to the prospective QAI systems consists in exploiting quantum parallelism of information processing to speed up the learning and the classification procedures already known in classical machine learning, see e.g. [11]. This can be done either by facilitating the eigenproblem solution by using quantum computers instead of classical ones, or by direct physical transition of a model quantum system from its initial state to a final state, which represents solution of a given problem. Accordingly, the remainder of this paper is organized as follows. In Sect. 2, we remind some basics of neural networks and classical machine learning, then, in relation to tasks of intelligent agents, we present some basics of quantum information theory in Sect. 4, and turn to the existing models of quantum machine learning. We

pay special attention to prospective QAI systems interacting with a finite temperature environment. We conclude with the role of quantum measurement and the role of human consciousness in QAI to human interaction.

2 Neural Networks

2.1 Feedforward Networks

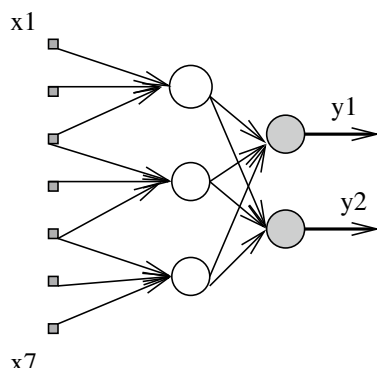
There are a lot of excellent books and review papers on neural networks and machine learning, see, e.g. [12–14]. Formally, a neural network can be considered as a directed graph mapping the N inputs of the network to M outputs, with the neurons being the vertices of the graph. The neurons connected neither to inputs nor to outputs are referred to as *hidden* neurons. The network, where the signals propagate in one direction, from input to output is a *feedforward* network. If the output signals are used for feedback of other neurons, the network is referred to as *recurrent* network. A typical graph of a feedforward network with one layer of hidden neurons is shown in Fig. 1.

According to McCulloch and Pitts model, each neuron in the graph Fig. 1 is a linear adder

$$u_k = \sum_{j=1}^N w_{jk}x_j + b_k, \quad (1)$$

followed by nonlinear transformation $y = \phi(u_k)$. The nonlinearity of $\phi(\cdot)$ is an essential property of classical neural networks: a single neuron, the scheme of which is shown in Fig. 2, can discriminate only linear separable subspaces in \mathbb{R}^N , the combination of neurons in a network with more than one layer can classify linearly inseparable subspaces, i.e. it can work as universal function approximator [15]. Historically, the

Fig. 1 Feedforward network with 7 input nodes, 3 hidden neurons, and 2 output neurons



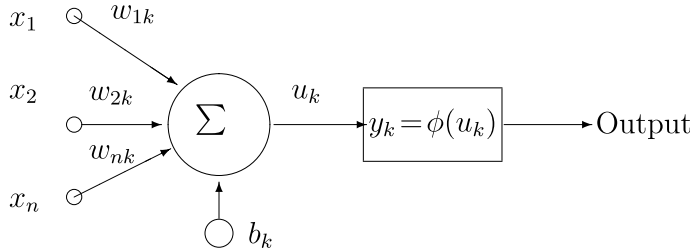


Fig. 2 McCulloch and Pitts mathematical model of neuron

Rosenblatt's perceptron used a step function $\theta(u)$ as nonlinearity. Latter, the $\tanh(u)$ and the logistic function $\phi(u) = \frac{1}{1+e^{-\beta u}}$, $\beta > 0$ were used. With the promotion of deep networks it was shown that the ReLU function $\phi(u) = \max(0, u)$ suffice for most applications—if the network is big enough [16].

The simplest learning rule is the mathematical formulation of Hebbian learning rule

$$\Delta w_{kj}^t = \eta y_k^t x_j^t, \quad (2)$$

where t is discrete instant of time. The Hebbian rule, in its primitive form (2), leads to unlimited growth of weights, and in all practical applications are subjected to some regularization.

For a supervised learning, when there exists a training set of vectors $\mathbf{x}_j \in \mathbb{R}^N$ for which the desired output values d_j are known, the weight learning process can be considered as a minimization of the mean squared error

$$E(\mathbf{w}) = \frac{1}{n} \sum_{j=1}^n (y_j(\mathbf{x}_j, \mathbf{w}) - d_j)^2, \quad (3)$$

where $y_j = y_j(\mathbf{x}_j)$ is the output of the network provided the j -th training vector is shown. The learning rule can be schematically written as gradient descent in discrete time t :

$$\mathbf{w}^{t+1} = \mathbf{w}^t - \eta \frac{\partial E(\mathbf{w}^t)}{\partial \mathbf{w}^t}, \quad (4)$$

to which different regularization terms can be added and sophisticated dependencies of the learning rate η from the data can be imposed [12].

Practically, the error functional (3) is just a simplest form of error functional, suitable for function approximation. The minimization of it for a network with significant number of hidden neurons can be computationally expensive even for modern computers. This is a point for application of quantum speedup of calculations, and also a point to think of how to solve the problem efficiently, possibly using some other criteria. It is quite common here to use statistical methods based on maximum likelihood to approximate the joint distribution of input and output vectors [13].

There is no unique recipe to choose a network architecture for a given problem. Referring the reader to special literature on the theory of classical neural networks, we just mention, that the learning of fully connected network is computationally hard, or even unfeasible, and for this reason deep learning methods applied to relatively sparse convolutional networks are becoming of common use [16].

2.2 Associative Memory

The use of feedforward networks is rather wide, say in medical diagnostics, exchange rate forecasting, autonomous vehicle control. The other common task for neural networks is to retrieve from memory a previously stored picture maximally close to the shown example. This is an associative memory problem. To memorize an image ξ of $n \times m$ pixels, a network can represent it as a vector of size $l = n \times m$, comprised of bits (0,1), or Ising spins (-1,+1), or whatever dichotomic states. For each image ξ the correlation matrix $J_{ij} = \frac{1}{l} \xi_i \xi_j$, $i, i = \overline{1, l}$ determines the minimum of energy functional

$$H = -\frac{1}{2} \sum_{i,j=1}^l J_{ij} \xi_i \xi_j \quad (5)$$

on this very image. If N different images of the same size should be remembered, the correlation matrix can be averaged over all images

$$J_{ij} = \frac{1}{l} \sum_{k=1}^N \xi_i^k \xi_j^k \quad (6)$$

Thus, different images can be generated by a Boltzmann machine with Hamiltonian (5) with different probabilities.

The correlation matrix J_{ij} requires resources quadratic in the image size, it can be considered as a projector, which transforms an input image into a sum of memorized images taken with different amplitudes. Such memory can be implemented, for instance, by a recurrent neural network, with outputs of the neurons feeding the inputs of other neurons, except for their own. The recurrent model seems to render more adequate description of real biological neural network than a feedforward model does and may result in a complex dynamical behaviour. If a recurrent network is supplied by certain weight-update rule (say, ‘winner takes all’), applied when each new sample is exposed to the network, such network can be used in classification problems without training set, i.e. in unsupervised learning for spontaneous data clustering.

Complex recurrent networks may contain no output neurons at all. Instead, they comprise a set of *interface neurons* that provide the exchange of information between network and its environment. The remaining core (hidden) neurons behaviour is affected by both the interface neurons and the bulk neurons of the network.

Schematically, the dynamics of such network can be described by a system of dynamical equations of the form

$$C_j \dot{u}_j(t) = -\frac{u_j(t)}{R_j} + \sum_{i,j=1}^N w_{ji} \phi_j(u_i(t)) + I_j, \quad (7)$$

where (C_j, R_j, I_j) are capacity, resistance, and current associated with the j -th neuron. The study of complex dynamic behaviour of a big system of equations of the type (7) can be substituted by thermodynamic description of the state vector system $\{x_j^{(k)}\}_k$ with the Lyapunov energy functional

$$E = -\frac{1}{2} \sum_{i,j=1}^N w_{ji} x_i x_j + \sum_{j=1}^N \frac{1}{R_j} \int_0^{x_j} \phi_j^{-1}(x) dx - \sum_{j=1}^N I_j x_j.$$

Such network can be used, for instance, as an associative memory, tuning the weights $w_{ij} = w_{ji}$ in such a way that the Boltzmann probability function

$$P(x) \propto e^{-\frac{\sum_{i,j} w_{ij} x_i x_j}{2T}}$$

yields different vectors x with the probabilities close to that found in experimental sample. The states that provide the minimum of energy will appear most frequently. This is so-called Boltzmann machine.

2.3 Deep Learning Revolution

A typical network aimed for image recognition may involve tenth of millions of weights w_{ij} to be found by gradient descent. Even for modern computers this seems to be a hard minimization problem. The progress has been achieved around years 2006–2009, when graphical processing units (GPU) have come into play and have speed the calculation up roughly 10–20 times [17]. Around the same time, it was found that for a network with sufficient number of hidden layers the piecewise linear function $\phi(z) = \max(0, z)$ can substantially overdue the commonly used logistic function and hyperbolic tangents. At earlier years of neural networks, a clever choice of network topology, first of all, the way how the input nodes are connected with first hidden layer neurons, and hence what features are extracted at the first level of abstraction, was half of the problem solution and was therefore more an art than a science. The invention of deep learning methods has led to representation learning, i.e. a deep network can learn itself what features are to be extracted at each hierarchy level [14].

3 Artificial Intelligence

The future of civilization is intimately related to the development of AI. Autonomous vehicles and automatic banking and automatic medical diagnostics, autonomous space apparatus for deep space missions should be capable of decision making with little or no human involved. AI is the execution of human thinking and decision making functions by artificial systems in situations, when the presence of human is ineffective or dangerous. The term ‘AI’ was coined at Dartmouth College conferences in 1956, which were organized to develop ideas about machines that can think [18]. Since the beginning of cybernetics [19], and up to now we still do not know how the brain works, and hence how we can substitute its functions by that of artificial devices. The first approach, the *computationalism* assumes that the thinking process is algorithmic, like a flow of logical operations in a Boolean processor [20]. The second approach, known as *connectionism* assumes that mental and behavioural phenomena are emergent properties of interconnected network of brain neurons. The first approach is evidently insufficient to describe the vast variety of mental phenomena. It is questionable whether the second approach can do it. Modern AI systems utilize both the logical processing and neural networking together.

Principle difference of AI from standard data processing is that an AI system learns from data rather than executes a prescribed algorithm. AI systems are designed to control the action of autonomous apparatus or *intelligent agents* (IA). AI can substitute a taxi driver in autonomous vehicle: it can drive you from prescribed point A to prescribed point B, but it cannot decide for you where to go. Its only goal is to minimize certain objective function prescribed by human.

Generally, an intelligent agent is an open system interacting with environment in a way shown in Fig. 3: it receives information from different sensors, processes it with AI system, typically a neural network, and executes produced commands by effectors, therefore, changing its own state and the state of environment. The scheme, as shown in Fig. 3, which also describes the functioning of living creatures [12], and seems trivial for classical information channels, may become nontrivial for open quantum systems.

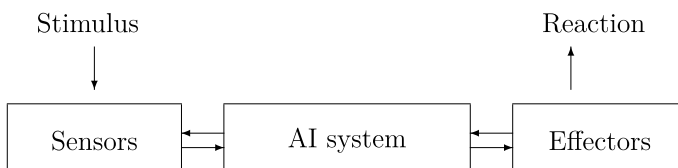


Fig. 3 Functioning of intelligent agent

4 Quantum Speedup

4.1 Quantum Information Processing

Classical computers operate with *bits*—physical systems that can be in one of two mutually exclusive states, designated as ‘1’ and ‘0’, for definiteness. Usual implementations of these states are the presence or absence of current in the electronic device, or two mutually orthogonal polarizations of light in case of optical devices. An uncertainty of qubit state in a register may result in calculation error, and should be avoided—either by duplication, or by using the error correction codes.

The miniaturization of computing hardware down to nanometre scales results in impossibility to describe physical systems which comprise one bit of information in classical terms. For proper description, the laws of quantum mechanics are required. This means, each physical bit can be in either of the states, ‘1’ or ‘0’, with probabilities different from zero and unity. For classical microprocessors, which operate according to Boolean logic, the difference of the output probability from unity is a spurious effect. The architecture of microprocessors is designed in a way to make this difference negligible. This can be achieved in hundred- and ten-nanometre technologies.

Descending to few-nanometre scales one can no longer neglect the quantum uncertainty, originating from the Heisenberg uncertainty principle. The state of each bit is then described by a vector of quantum state

$$|\psi\rangle = c_0|0\rangle + c_1|1\rangle, \quad |0\rangle, |1\rangle \in \mathcal{H}, c_0, c_1 \in \mathbb{C}, |c_0|^2 + |c_1|^2 = 1, \quad (8)$$

where \mathcal{H} is a Hilbert space of states, i.e. complex linear space with a scalar product $\langle \cdot | \cdot \rangle$. The probability of finding the bit in one of two mutually orthogonal quantum states, $\langle 0|0\rangle = 1 = \langle 1|1\rangle$, $\langle 0|1\rangle = 0$, is given by the modulus squared amplitude of those states:

$$P(|0\rangle) = |c_0|^2, P(|1\rangle) = |c_1|^2.$$

Such bit, the evolution of which obeys the Schrödinger equation

$$\imath \frac{\partial}{\partial t} |\psi\rangle = \hat{H} |\psi\rangle, \quad (9)$$

is called a quantum bit, or *qubit*.

The real situation is even more complicated: along with the quantum nature of qubit, one has to take into account its interaction with fluctuating environment, using for that the density matrix formalism of the open quantum system theory [21, 22]. But still the equation (8) itself allows for the generalization of classical information theory to the theory of *quantum information* [23].

The main idea of quantum information theory consists in a possibility to build a fast (polynomial-time) computer capable of solving a large class of problems, which

are exponentially hard to any classical computer, by using a *register of quantum bits* instead of the classical ones, and evolving this register quantum-mechanically instead of using Boolean logic. This computer is referred to as a quantum computer [24].

4.2 *Quantum Algorithms*

Quantum computers, as well as classical ones, can be built according to the Turing machine principles [25]. They can execute any prescribed sequence of operations with bits, either classical or quantum [26]. If the Boolean logic is executed the algorithm remains classical, regardless whether classical or quantum bits are processed. In this case, the processing operations are irreversible in the sense of quantum mechanics, keeping the elapsed resources and time more or less the same for both classical and quantum registers.

The superiority of quantum algorithms over conventional ones can be achieved using quantum evolution of the bit register instead of the Boolean operations. The bit register is then necessarily a register of quantum bits. The unitary evolution of quantum register (isolated from the environment) is a time-reversal evolution. All possible quantum states of the register can be processed in parallel by special devices, called *quantum gates*, or by other special equipment, which works according to the laws of quantum mechanics. A quantum algorithm, therefore, is an algorithm the execution of which essentially demands quantum computer.

There are two quantum algorithms most known to the present time: the Grover's unordered database search algorithm [27], and the Shor's factorization algorithm based on quantum Fourier transform [28]. Both algorithms are the idealizations: the initially prepared quantum state of the register is subjected to unitary evolution with a help of quantum gates, applied bitwise or pairwise to qubits in the register. The unitarity of the whole computation process—from initial state preparation to the final measurement of output—is secured by the isolation of the computer from fluctuating environment. The latter is merely an idealization: it is impossible to isolate a physical system from its environment completely. Therefore, besides well-established quantum schemes, which can be found in textbooks [23], we are to search for new schemes, capable of taking into account physical–physical interaction of quantum computer with its environment. This is being done based on open quantum system theory [21, 22].

4.2.1 Grover's Algorithm

Searching an unsorted database of N records in length, say, a subscriber name by phone number in a phone-book takes a classical search algorithm $N/2$ record views on average. In quantum language, it means that each of $N = 2^n$ records, labelled

by $|x\rangle$, written in n -qubit register, is subjected to the action of a certain operator \mathbf{O} (Oracle):

$$\mathbf{O}|x\rangle = (-1)^{f(x)}|x\rangle,$$

where the function $f(x)$ takes the value 1 if x satisfies the search condition and takes the value 0 otherwise. Thanks to quantum mechanics, we can prepare an equally-weighted superposition of all label states $|x\rangle$:

$$|\psi_0\rangle = \frac{1}{\sqrt{N}} \sum_{x=0}^{N-1} |x\rangle, \quad (10)$$

and then apply quantum operations not to records, but to their linear combination. The operator \mathbf{O} can alternate the sign of those terms in linear superposition (10) that satisfy the search condition $f(x) = 1$. Using the orthonormal state vectors, the algorithm can be designed so that each iteration step increases the norm of the term, which satisfies the search condition, but decreases the norm of all other terms. Referring the reader to the standard literature for the details of the Grover's algorithm [23, 24, 27], we are to note that a search of desired record by Grover's algorithm usually takes $\sim \sqrt{N}$ iterations on an average, instead of $N/2$ iterations of classical search.

4.3 Quantum Machine Learning

The general idea of quantum information processing and that of neural computing seems to be the same—to process all data in parallel. However, the physics of circuit-based quantum computers and that of classical neural networks is essentially different. The former are based on unitary evolution (unless a readout of the final result is being performed), and hence are time-reversal and do not dissipate $\sim kT \ln 2$ of energy per operation, the latter are fully dissipative nonlinear systems, learning by interaction with environment. It is not a trivial task to marry these two approaches, for direct application of quantum mechanics does not allow for nonlinearity.

Quantum-inspired neural networks—Initiated by the proposal of S. Kak to feed NN with quantum states [7], first regular suggestion of quantum speedup for supervised machine learning was presented by Menneer and Narayanan [29], who suggested to consider an ensemble of neural networks, each of those taught on only one vector of the training set, and then construct a single neural network, the weights of which are linear quantum superpositions of the weights of the considered network ensemble. Definitely, processing the training set in parallel would dramatically reduces the learning time, but since there are no practical means to implement such network, they called their model a *quantum-inspired neural network*.

Associative memory—Another early model of a quantum neural network was an optically-inspired *quantum associative memory* model proposed by Vlasov [30]. The Hopfield network correlation matrix (6) turns to be a sum of projectors

$$\hat{J} = \sum_{i=1}^M |i\rangle\langle i|,$$

if the vectors are considered in a Hilbert space of states. This practically makes the Hopfield network into an optical network, which separates input image into M input channels, each of those supplied with the corresponding mask (filter) $|i\rangle\langle i|$, corresponding to the i -th image. The functioning of this network consists in determination of the channel with greatest amplitude of the output signal, see Fig. 4. All channels in optical network, as well as in quantum network, work in parallel, i.e. simultaneously.

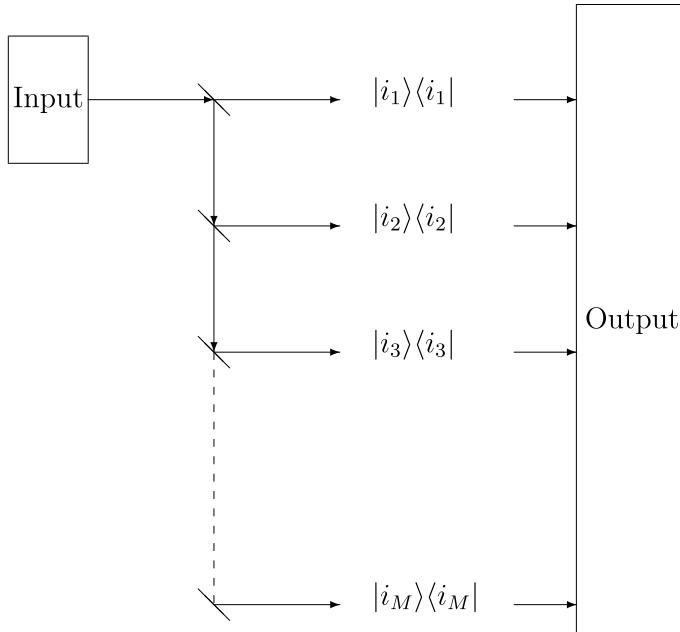


Fig. 4 Implementation of quantum associative memory based on optical interference (scheme from [30]). The input quantum state $|\chi\rangle$, to be classified in either of M classes, is splitted in M channels supplied with projectors $\hat{J}_i = |i\rangle\langle i|$. The classification is performed according to the maximum of light intensity $I_i = \frac{I_0}{M} |\langle \chi | i \rangle|^2$

4.4 Quantum Neural Technology

The main obstacle hampering the creation quantum machine learning devices of industrial scope is the same as in circuit-based quantum computing—the problem of decoherence. Same as in quantum computing, different types of qubits have been tried. Those are: ion in traps, nuclear magnetic resonance in fluids, quantum dots, optical networks with waveguides and photonic crystals. In all cases, the decoherence time decreases with the increase of qubit number. The quantum neural networks have their own peculiarities. The direct addressability of each qubit, neuron, is not strictly required: only input neurons, output neurons and the weights to be tuned should be accessible. On the other hand, the time-reversibility of the whole network is not required either. The ultimate goal of massively parallel neural network is to provide a correct input→output mapping. In the mapping process, some of the huge bulk of degrees of freedom of the network may live in the decoherence-free subspaces, while the others are allowed to interact with thermal environment, working as a fridge for *decoherence-free subspaces*, according to the Zanardi and Rasetti idea [31]. At the same time, the interaction with environment, which decoherences some of degrees of freedom, introduces nonlinearity into a system of quantum neurons, which is essential for the network functioning. For these reasons, the creation of a scalable technology for quantum neural networks seems to be easier than that for a circuit-based quantum computers.

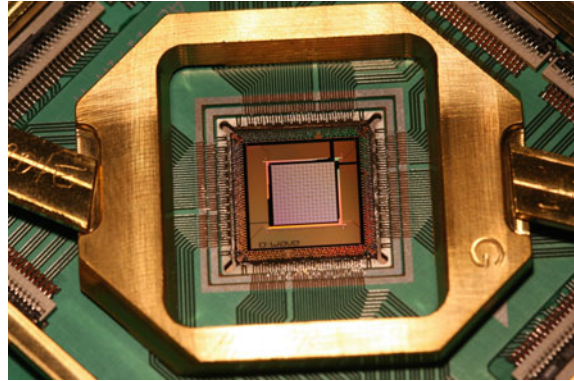
First, commercial quantum neural technology was implemented by D-Wave Systems Inc. for a SQUID-based quantum annealing processor aimed for constrained binary optimization in an Ising model [32]. This method, often referred to as *quantum annealing* [33], consists in solution of optimization problems by means of quantum evolution of the Ising spin system from the initially prepared quantum state, to the state which corresponds to the minimum energy of the quadratic Hamiltonian

$$\mathcal{H}_P = - \sum_i h_i \sigma_i^z - \sum_{i < j} J_{ij} \sigma_i^z \sigma_j^z. \quad (11)$$

The qubits in this system are implemented by Ising spins, taking two values $\sigma_i^z = \{-1, +1\}$ after the measurement. In D-Wave machines, the Ising spins are represented by quantized magnetic fluxes of SQUIDs [34]. The spins are confined to a d -dimensional lattice \mathbb{Z}^d . The conditions of the optimization problem are determined by the matrix J_{ij} , the elements of which in quantum case assume only two discrete values $J_{ij} \in \{0, 1\}$. The solution of the optimization problem turns to be a search for the spin configuration $\{\sigma_i^z\}_{i \in \mathbb{Z}^d}$ that provides a minimum to the Hamiltonian \mathcal{H}_P at a given set of parameters $\{h_i, J_{ij}\}$.

Since a SQUID-based qubit has a classical size (from micrometre to millimetre range), and the probability of a spontaneous reversal of the magnetic flux direction is negligibly small, the system of SQUIDs with inductive couplings is a reliable implementation of the scalable quantum register. This register is brought into the ground state using the quantum annealing method, which combines the classical annealing

Fig. 5 Photograph of the D-Wave systems 1000 qubit processor based on SQUIDS. Taken from website <http://www.dwavesys.com>



method and the quantum tunnelling [35]. The picture of the D-wave Systems Inc. quantum annealing processor for 1000 qubits is shown in Fig. 5.

To execute quantum annealing, additionally to magnetic field h_z , which defines the direction the spins are measured along, an extra magnetic field Δ is applied along the direction x . This results in addition of a new magnetic term to the Hamiltonian:

$$\mathcal{H}(t) = -\Gamma(t) \sum_{i=1}^n \Delta_i \sigma_i^x + \Lambda(t) H_P. \quad (12)$$

The factor $\Gamma(t)$ monotonically decreases with time from 1 to 0, and $\Lambda(t)$ monotonically increases from 0 to 1 as time tends to infinity. At the initial instant of time $t = 0$, $\Lambda(0) = 0$, the ground state of the system corresponds to the orientation of all spins along the x axis. If $\Gamma(t)$ decreases quite slowly, and so increases $\Lambda(t)$, the system of spins adiabatically passes into the ground state of the Hamiltonian H_P [36].

While the classical annealing probability of passing over the potential barrier of height ΔE is proportional to $e^{-\Delta E/T}$, the quantum annealing probability of tunnelling under a barrier of height ΔE and length L is proportional to $e^{-L\sqrt{\Delta E}/\Gamma}$, where Γ is the quantum annealing constant. This means, the quantum annealing will overdo the classical annealing in effectiveness if the barriers are large in height, but small in width [37]. Actual equivalence of the quantum annealing method to the standard circuit-based quantum computing was proved in [38].

An alternative model of quantum Hopfield network, described by the same Hamiltonian (11), have been built in Japan on the base of optical parametric oscillators: each ‘spin’ is represented by the phase shift $\{0, \pi\}$ relatively to the phase of the pumping laser [39]. The set of degenerated optical parametric oscillators (OPO) is generated in a closed long fibre cavity. The oscillators are kept equidistant during the run. The spin-spin coupling matrix J_{ij} is implemented with mutual injections of OPO light using delay interferometers [39]. The total length of the fibre guide may exceed a few kilometres, providing the circulation of ten thousand of ‘spins’. The

computation is being finalized when the system of OPOs equilibrates into its ground state having completed significant number of cycles in the optical fibre cavity, typically ($\sim 10^2$). For instance, the equilibration time for a system of 100 OPO, running in a 1 km fibre, is less than a millisecond [40]. An evident advantage of this scheme is the use of standard optical fibre technology, providing such systems operate at room temperature and keeps the price low. The potential shortcoming of the closed-loop optical scheme may be the use of quasi-one-dimensional space, an optical waveguide, as a computational space. In combination with usage of classical electronic controller, which monitors the optical interferometer, the use of one-dimensional array of oscillators makes rather dim its prospects for scalability and speed of big data processing.

The model system (11) of Ising type is used in different problems of combinatorial optimization, implemented in magnetic [34], and optical [40] models. Something similar to it could be built on the base of other quantum systems with two mutually orthogonal quantum states. The use of the excited and the ground state of a quantum dot as a qubit seems perspective in this respect. The idea of using QDs as qubits in a circuit-based quantum computer have been proposed by Loss and DiVincenzo [41], the idea of building a quantum neural network based on quantum dots was put forward in [42].

Quantum dots ('artificial atoms') are small regions of a semiconductor heterostructure, from nanometers to micrometers in size, with precisely controlled number electrons [43, 44]. Potential advantages of a QNN made of quantum dots are the small qubit size, typically less than 100 nm, the availability of a scalable technology for the production of quantum dot arrays, the possibility of tuning QD parameters by applying external electric and magnetic fields. The correlations between given QDs in an array may be controlled by imposing electric or optical junction between them. The model elements of a quantum dot neural network have been described in [45, 46].

5 How the Brain Works?

5.1 Biological Coherence

Quantum effects that are important for such functions as single-photon perception and DNA replication are known in biology for quite a long time, may be starting from the Schrödinger's book 'What is life?' [47]. However, the application of quantum mechanics to life sciences is not restricted to quantum chemistry only.

It was suggested long time ago, but detected experimentally rather recently that large biological macromolecules can absorb light quanta as a whole—not by inter-level transitions of certain atoms—and then coherently transfer the absorbed energy to utmost macroscopic distances to the reaction centres, where it is utilized by chemical reactions [48, 49]. This mechanism, which is used by photosynthetic plants, gives

significant biological advantage, if compared to diffusive energy transfer. Photosynthesis is a source of energy for utmost all life on the Earth. The photons from the Sun are absorbed by light-harvesting antennas in the form of electronic excitations. The excitations are then transported in the form of excitons to the reaction centre, where they create a long-lived forms of chemical energy.

The other biologically important quantum effect is the navigation of higher organisms, migrating birds first of all, using the Earth magnetic and electric fields—the so-called avian compass. The exact mechanism of birds navigation is not yet known for sure. It is known, however, that quantum transitions between atomic levels depend on the strength of the magnetic and the electric fields, hence, the brain can learn the direction of motion from the rates of such transitions. One of the recent hypotheses is the magnetic field sensitivity of the radical pair reactions, where a pair of electrons may be in either triplet or in singlet state [50].

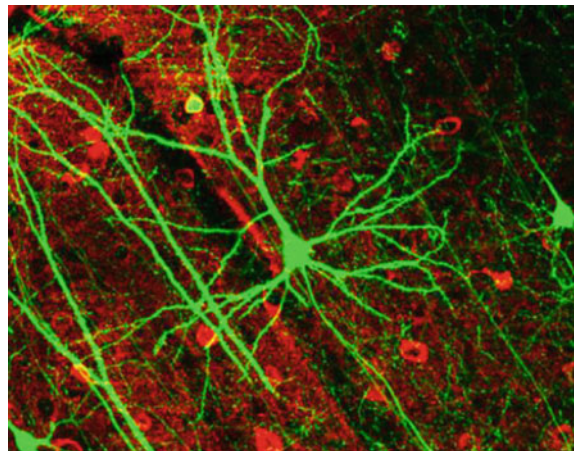
The work of the brain is a special issue. According to classical theory of neuron firing, each operation (firing) is of about 10^{-16} J energy expense [12], which is much worse than that of classical computers. Definitely, a real brain spends much less energy for thinking process.

5.2 Brain Functioning

The function of the human brain is to receive the sensory information, perceive it, and make appropriate decisions. Morphologically, the brain is represented by a network of special cells—neurons—linked to each other by synaptic connections between axon of one neuron and dendrites of the others. Being known from fundamental works of Lapicque [51] and Cajal [52], the functional portray of neuron have been unchanged for more than hundred years. The neuron is ‘widely believed to be a balloon filled with cytoplasma’, which if fed with neurotransmitters, penetrating the membrane, can integrate the signals of all dendrites and fire—if the threshold is achieved. The learning in such network is believed to take place solemnly by metabolic growth of synaptic bonds between particular neurons that correlate their firing [2]. The typical operating frequency of electrochemically signalling neurons lies in kHz range, which is at least six orders of magnitude below that of modern computers. Still, due to massive parallelism of about 8.6×10^{10} neurons [53], the brain often outperforms computer in such tasks as image and speech recognition.

It was suggested by Beck and Eccles [54] that since the exocytosis process occurs with probability much less than one, on arrival of the nerve impulse, the process should be described quantum-mechanically, by Schrödinger equation. This, however, does not answer the question, how the barrier—the potential of the Schrödinger equation—is controlled, and whether the phases of the input signals, or only the amplitude of their sum matter. The standard widely accepted theory of neuron firing also does not shed light on the role of mitochondria in launching of exocytosis. The analysis presented by Tegmark [55] shows that the process of exocytosis, when launched, due to the large number of involved particles and a short decoherence time

Fig. 6 Image of pyramidal neurons in mouse cerebral cortex expressing green fluorescent protein.
Photograph from [56]



($10^{-20} \div 10^{-13}$ s), can indeed be considered in a classical framework. This does not preclude any quantum effects taking place *before* the avalanche process to be the cause of this process. Similarly, the classical nature of a chemical bomb explosion does not preclude a wave nature of electromagnetic radiation used to communicate the ignition.

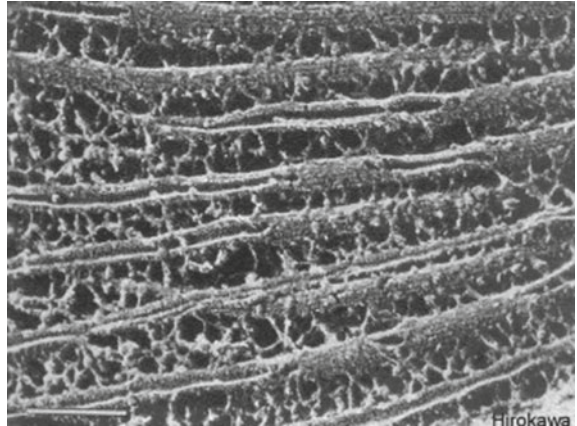
The importance of quantum wave processes for brain functioning has been suggested by Chavchanidze [10], long before the Feynman ideas of quantum simulation. The work of Chavchanidze just declares the propagation of coherent waves in jelly-like brain media, consisting of neurons and glial cells.

No arguments were given for the possibility to keep these ways free of decoherence. It is not so easy to imagine and understand the mechanism of coherent wave propagation in a highly irregular neuron structure, see Fig. 6. The wave properties of neuron, beyond the electrochemical mechanism of nerve pulse propagation, have become the object of experimental studies rather recently [57, 58]. Although there is a good deal of theoretical ideas on biophoton propagation in axon [59], the experimental verification of optical signalling in brain remains a hard problem.

There are also other models relating the brain functioning to a quantum neural computer. One of the first developed models was the quantum information processing by the brain microtubules [60]. The microtubules are major components of cytoskeleton that help the cell to maintain its shape. The microtubules form a lattice-like structure, see Fig. 7.

The microtubules are hollow cylinders about twenty nanometres in diameter made up of 13 filaments that are stung together out of proteins known as tubulin dimers. According to [60], two conformations of these dimers, α and β , can serve as two qubit states. These dimers can take transitions between α and β states, which differ in the values of electric dipole moment. The moving excitation of kink-like type can produce a propagation of dipole moment along the tubulin axis, but the estimation of this wave speed is rather low—about 1 m/s [60]. Speculatively, the tubulin dimers can

Fig. 7 Immunoelectron micrograph of dendritic microtubules interconnected by microtubule-associated proteins. Scale bar at lower left represents 100 nm.
Image from the book [61]



be considered as both the quantum processing units and the mean of communication. However, the model of [60] seems to be highly controversial, and the estimation of the maximum coherence time of ~ 1 s order, provided by quantum gravity only, seems not realistic. It was criticized in [55, 62] on the base of the ion collision mechanism to be 10 or 20 orders of magnitude shorter.

Instead of polarization wave propagation in microtubules, or other mechanisms, similar to phonon propagation, it seems much likely, that axons, or even microtubules, serve as waveguides for biophotons. The biophotons, produced in mitochondria, in their turn can be in quantum superpositions and form entangled states, like in QED cavity networks [63]. In that case, the axon of a neuron carrying a miillin shield is an efficient optical waveguide rather than a pipe for ion flows. In that case, the avalanche process of neuron firing may be the readout process performed on the ensemble of biophotons that harness the quantum computation. This process may take place with the active participation of the nuclear spin of the phosphorous nuclei [64].

More formally, as described by Tegmark [55], the quantum mechanical description of the learning process, taking place in the neural network of brain, should necessarily include three parts:

Object (O): from which, the Brain learns.

Subject (S): degrees of freedom of the brain, directly subjected to changes in the process of learning. Most likely these are represented by pointer states [65].

Environment (E): fluctuating thermal environment, which interacts with ‘S’ by means of the Hamiltonian H_{SE} and with the ‘O’ by means of the Hamiltonian H_{SO} .

The collection of all three parts is described by the total density matrix ρ , which obeys the von Neumann master equation

$$i\hbar \frac{\partial \rho}{\partial t} = [H, \rho], \quad (13)$$

where $H = H_S + H_O + H_E + H_{SE} + H_{OE} + H_{SO}$ is the total Hamiltonian of the system. The goal of learning is then to establish maximal mutual information I_{SO} between the subject and the object, tracing out all degrees of freedom of the environment.

$$I_{SO} = S_S + S_O - S \quad (14)$$

where $S = -\text{Tr}\rho \log \rho$ is the total entropy of the system. $S_O = -\text{Tr}_{ES}\rho \log \rho$. $S_S = 0$ according to [55], but it may be a problem with it—for it is not known how the pointer states of the brain are measured. We can only believe that the final observer is Consciousness, but we cannot define it in an unambiguous way. Depending on particular type of interaction H_{SO} and typical time scales of the Hamiltonian H_S , the learning process can be either classical or quantum. So, depending on particular task, both the wave mechanisms based on biophotons [66] and the widely accepted chemical mechanism may be important. Very recently, an interesting idea was put forward: the learning in a randomly connected network may happen by means of making entanglement in randomly chosen neighbours using two-mode non-coherent light [67].

6 Conclusion

The aim of this short paper was to emphasize some principles and mathematical models of quantum neural networks, which can be important for both quantum artificial intelligent systems and the functioning of biological brain. We have touched neither technological details of commercial quantum neural networks, or more precisely the adiabatic quantum computers produced by www.dwavesys.com on the base of SQUIDs, nor the blooming field of quantum optical technologies [39]. For more formal mathematical introduction to the methods of quantum machine learning implemented on quantum computers, we should refer the reader to a monograph [11].

References

1. Deutsch D, Jozsa R (1992) Rapid solution of problems by quantum computation. Proc Roy Soc Lond A 439:553–558
2. Hebb DC (1949) Organization of behavior. Wiley, New York
3. McCulloch WS, Pitts W (1943) A logical calculus of the ideas immanent in nervous activity. Bull Math Biophys 5:115–133
4. Rosenblatt F (1958) The perceptron: a probabilistic model for information storage and organization in brain. Psychol Rev 65(6):386–408
5. Feynman R (1982) Simulating physics with computers. Int J Theor Phys 21:467–488
6. Behera L, Kar I, Elitzur AC (2005) A recurrent quantum neural network model to describe eye tracking of moving targets. Found Phys Lett 18(4):357–370
7. Kak S (1995) On quantum neural computing. Inf Sci 83:143–160

8. Nitta T (1997) An extension of the back-propagation algorithm to complex numbers. *Neural Networks* 10(8):1397–1415
9. Shariv I, Friesem AA (1989) All-optical neural network with inhibitory neurons. *Opt Lett* 14(10):485–487
10. Chavchanidze V (1970) On spatial-temporal processes in neural networks, Soobshch. AN Gruzinskoi SSR 59(1):37–40
11. Schuld M, Petruccione F (2018) Supervised learning with quantum computers. Springer, Berlin
12. Haykin S (2009) Neural networks and learning machines. Pearson Education, London
13. Murphy KP (2012) Machine learning: a probabilistic perspective. MIT Press, Cambridge
14. Goodfellow I, Bengio Y, Courville A (2016) Deep learning. MIT Press, Cambridge
15. Hornik K, Stinchcombe M, White H (1989) Multilayer feedforward networks are universal approximators. *Neural networks* 2(5):359–366
16. LeCun Y, Bengio Y, Hinton G (2015) Deep learning. *Nature* 521:436–444
17. Raina R, Madhavan A, Ng AY (2009) Large-scale deep unsupervised learning using graphics processors. In: Proceedings of the 26th annual international conference on computer vision and pattern recognition, pp 873–880
18. Russel S, Norvig P (2009) Artificial intelligence: a modern approach, 3d edn. Prentice Hall, Upper Saddle River
19. Wiener N (1948) Cybernetics: or control and communication in the animal and the machine, 2d edn. MIT Press, Cambridge
20. Piccinini G (2004) Functionalism, computationalism and mental contents. *Canad J Phil* 34:375–410
21. Feynman RP, Vernon FL Jr (1963) The theory of a general quantum system interacting with a linear dissipative system. *Ann Phys* 24:118–173
22. Breuer HP, Petruccione F (2002) The theory of open quantum systems. Oxford University Press, Oxford
23. Nielsen MA, Chuang IL (2000) Quantum computation and quantum information. Cambridge University Press, New York
24. Stoltz J, Suter D (2008) Quantum computing: a short course from theory to experiment. Wiley-VCH, Weinheim
25. Bernstein E, Vazirani U (1997) Quantum complexity theory. *SIAM J Comput* 26:1411–1473
26. Deutch D (1985) Quantum theory, the Church-Turing principle and the universal quantum computer. *Proc R Soc Lond A400:97–117*
27. Grover LK (1997) Quantum mechanics helps in searching for a needle in a haystack. *Phys Rev Lett* 79:325–328
28. Shor P (1994) Polynomial-time algorithm for prime factorization and discrete logarithms on a quantum computer. In: Proceedings of 35th annual symposium on foundations of computer science, Piscataway, NJ. IEEE Press, New York
29. Menneer T, Narayanan A (1995) Quantum-inspired neural networks. In: NIPS'95, Denver, Colorado
30. Vlasov AY (1997) Quantum computations and images recognition. [arxiv.org:quant-ph/9703010](https://arxiv.org/abs/quant-ph/9703010)
31. Zanardi P, Rasetti M (1997) Noiseless quantum codes. *Phys Rev Lett* 79(17):3306
32. Neven H, Denchev VS, Rose G, Macready WG (2009) Training a large scale classifier with the quantum adiabatic algorithm. [arxiv.org \(0912.0779\)](https://arxiv.org/abs/0912.0779)
33. Aeppli G, Rosenbaum TF (2007) In: Das A, Chakrabarti K (eds) Quantum annealing and related optimization methods, volume 679 of Lecture notes in physics. Springer, Heidelberg, pp 159–169
34. Johnson MW et al (2011) Quantum annealing with manufactured spins. *Nature* 473:194–198
35. Martoňák R, Santoro GE, Tosatti E (2002) Quantum annealing by the path-integral Monte Carlo method: the two-dimensional random ising model. *Phys Rev B* 66:094203
36. Fahri E et al. (2001) A quantum adiabatic evolution algorithm applied to random instances of NP-complete problem. *Science* 292:472–475
37. Das A, Chakrabarti BK (2008) Colloquium: quantum annealing and analog quantum computation. *Rev Mod Phys* 80:1061–1081

38. Mizel A, Lidar DA, Mitchell M (2007) Simple proof of equivalence between adiabatic quantum computation and the circuit model. *Phys Rev Lett* 99:070502
39. Inagaki T, Inaba K, Hamerly R, Inoue K, Yamamoto Y, Takesue H (2016) Large-scale Ising spin network based on degenerate optical parametric oscillators. *Nat Photonics* 10:415
40. McMahon PL, Marandi A, Haribara I, Hamerly R, Langrock C, Tamate S, Inagaki T, Takesue H, Utsunomiya S, Aihara K, Byer RL, Fejer MM, Mabuchi H, Yamamoto Y (2016) A fully programmable 100-spin coherent Ising machine with all to all connections. *Science* 354(6312):614
41. Loss D, DiVincenzo DP (1998) Quantum computation with quantum dots. *Phys Rev A* 57(1):120–126
42. Behrman EC, Nash LR, Steck JE, Chandrashekhar VG, Skinner SR (2000) Quantum dot neural networks. *Inf Sci* 128:257
43. Reimann SM, Manninen M (2002) Electronic structure of quantum dots. *Rev Mod Phys* 74:1283–1342
44. Kastner MA (2005) Prospects for quantum dot implementation of adiabatic quantum computers for intractable problems. *IEEE Proc* 93(10):1765–1771
45. Altaisky Mikhail V, Zolnikova Nadezhda N, Kaputkina Natalia E, Krylov Victor A, Lozovik Yurii E, Dattani Nikesh S (2016) Towards a feasible implementation of quantum neural networks using quantum dots. *Appl Phys Lett* 108(10)
46. Altaisky MV, Zolnikova NN, Kaputkina NE, Krylov VA, Lozovik YE, Dattani NS (2017) Entanglement in a quantum neural network based on quantum dots. *Photonics Nanostruct Fundam Appl* 24:24–28
47. Schrödinger E (1992) What is life?. Cambridge University Press, Cambridge
48. Lee H, Cheng Y-C, Fleming GR (2007) Coherence dynamics in photosynthesis: protein protection of excitonic coherence. *Science* 316:1462–1465
49. Ringsmuth AK, Milburn GJ, Stace TM (2012) Multiscale photosynthetic and biomimetic excitation energy transfer. *Nat Phys* 8:562–567
50. Schulten K, Swenberg CE, Weller AA (1978) Biomagnetic sensory mechanism based on magnedic field modulated coherent electron spin motion. *Z Phys Chem* 111:1–5
51. Lapicque L (1907) Recherches quantitatives sur l'excitation électrique des nerfs traitée comme une polarisation. *J Physiol Pathol Gen* 9:620–635
52. Ramon Cajal S (1911) Histologie du Systems Nerveux de l'homme et des vertebres. Maloine, Paris
53. Herculano-Houzel S (2009) The human brain in numbers: a linearly scaled-up primate brain. *Front Hum Neurosci* 3:31
54. Beck F (1992) Quantum aspects of brain activity and the role of consciousness. *PNAS J Eccles* 89:11357–11361
55. Tegmark M (2000) Importance of quantum decoherence in brain processes. *Phys Rev E* 61(4):4194–4206
56. Lee W-CA, Huang H, Feng G, Sanes JR, Brown EN, So PT, Nedivi E (2006) Dynamic remodeling of dendritic arbors in GABAergic interneurons of adult visual cortex. *PLoS Biol* 4(2):e29
57. Ghosh S, Sahu S, Agrawal L, Shiga T, Bandyopadhyay A (2016) Inventing a co-axial atomic resolution patch clamp to study a single resonating protein complex and ultra-low power communication deep inside a living neuron cell. *J Integr Neurosci* 15(3):1–31
58. Agrawal L, Sahu S, Ghosh S, Shiga T, Fujita D, Bandyopadhyay A (2016) Inventing atomic resolution scanning dielectric microscopy to see a single protein complex operation live at resonance in a neuron without touching or adulterating the cell. *J Integr Neurosci* 15(4):435–462
59. Kumar S, Boone K, Tuszyński J, Barclay P, Simon C (2016) Possible existence of optical communication channels in the brain. *Sci Rep* 6:36508
60. Hagan S, Hameroff SR, Tuszyński JA (2002) Quantum computation in brain microtubules: decoherence and biological feasibility. *Phys Rev E* 65:061901
61. Hirokawa N (1991) In: Burgoyne R (ed) The Neuronal Cytoskeleton. Wiley, New York
62. Rosa LP, Faber J (2004) Quantum models of the mind: Are they compatible with environment decoherence? *Phys Rev E* 70:031902

63. Orszag M, Ciobanu N, Coto R, Eremeev V (2015) Quantum correlations in cavity qed networks. *J Mod Opt* 62(8):593–607
64. Fisher MPA (2015) Quantum cognition: The possibility of processing with nuclear spins in the brain. *Ann Phys* 362:593–602
65. Zurek WH (1981) Pointer basis of quantum apparatus: Into what mixture does the wave packet collapse? *Phys. Rev. D* 24:1516–1525
66. Tang R, Dai J (2014) Spatiotemporal imaging of glutamate-induced biophotonic activities and transmission in neural circuits. *PLoS ONE* 9(1):e85643
67. Ghosh S, Opala A, Matuszewski M, Paterek T, Liew TCH (2019) Quantum reservoir processing. *npj Quantum information* 5:35

Chapter 7

Oscillations and Synchrony in a Network of Delayed Neural Masses



Iain Pinder and Jonathan J. Crofts

1 Introduction

Network neuroscience provides a general framework in which to study the type of large-scale brain networks that naturally arise from modern neuroimaging methodologies [1–3]. Patterns of oscillation across the brain emerge because of structural connections between brain regions, and understanding the mechanisms underlying the synchronisation and propagation of neural activity is a key aim of network neuroscience [4–6]. A recent approach used to understand structure–function relations in the brain is to employ brain network models (BNM), which combine detailed anatomical connectivity with simulated neural activity in order to replicate large-scale *functional connectivity* [7–10]. The advantage of such an approach is that one can perform *in silico* experiments which can be used for predictive purposes as well as to test a range of experimental scenarios—such methods have the potential to lead to personalised treatments in neuroscience [10–14].

Brain networks are organised over multiple temporal and spatial scales and so employing network theory to model the brain requires the choice of a scale relevant to the study at hand, which, depending upon the scientific problem, can range from the microscopic scale (i.e., single neurons) to the meso/macroscopic scale (i.e., cortical columns/brain regions) [15, 16]. Here, we focus on large-scale brain network models in which network nodes describe cortical regions and connections can be one of two types: *anatomical connections* that represent neuronal axons, or more typically collections of axons known as fibre bundles; or *functional connections*, which refers to connectivity inferred from synchronisation of neural activity across brain regions. Note that a third type of connectivity exists, namely *effective connectivity* [17], which describes the influence that cortical regions have over each other; however, we shall not consider effective connectivity in this work.

I. Pinder · J. J. Crofts (✉)
Nottingham Trent University, Nottingham NG11 8NS, UK
e-mail: jonathan.crofts@ntu.ac.uk

Another important aspect of neural systems that any physiologically accurate BNM should account for is the time delays that arise due to finite conduction velocities of neurons and their interconnections [18–21]. When considering large-scale BNMs as we do here, there are two main sources of delay: *internodal* delays, which typically occur between excitatory populations of neurons; and within population, or *intranodal*, delays, which can either describe delayed self-interactions and/or cross-interactions. Note that the majority of BNMs that incorporate delays restrict to internodal delays, typically using a constant delay for all interconnections despite the variation in length of long-distance pathways in the brain – although a number of recent studies have considered delay times that are distant-dependent (see, e.g., [22, 23]). Recently, the authors in [24] considered the effects of inter- and intra-delays on a system of coupled neural masses [2, 25] via a numerical simulation. Deploying a range of model topologies, such as a ring network, a path network and a lattice network, they found that when coupled with neural delays, network structure had the ability to both regularise or deregularise network dynamics, depending upon the networks heterogeneity. One of the main goals of this work is to further explore some of these ideas by simulating neural dynamics on a range of topologies, including both artificial and experimental architectures.

In this chapter, we deploy an idealised neural mass network to understand the influence of network structure on neural activity in the presence of time delays. We start by introducing the mathematical model of interest in the case without delay and discuss its dynamic behaviour via a bifurcation analysis. We then extend this model to a BNM and discuss how such a model is naturally extended to a network of delayed differential equations, thus accounting for naturally occurring delays in neural systems. Using numerical simulations, we investigate the role of network structure on the resulting dynamics for a range of toy model structures as well as experimentally obtained cortical structures. We finish with a brief summary and some suggestions for possible future work in this area.

1.1 The Wilson–Cowan Model

In this work, we deploy the population model due to Wilson and Cowan [26]. The model considers two populations of excitatory and inhibitory neurons, and neural activity is described by the following system

$$\begin{aligned} \frac{du}{dt} &= -u(t) + f(au(t) + bv(t) + P), \\ \frac{dv}{dt} &= -v(t) + f(cu(t) + dv(t) + Q). \end{aligned} \tag{1}$$

Here, u and v represent the synaptic activity of the two populations, the architecture of the network is given by the weights a , b , c and d , while the parameters, P and Q , are control parameters that represent the basal input to each population. The population firing rate is determined by the sigmoid function

$$f(x) = \frac{1}{1 + e^{-\beta x}}. \quad (2)$$

Here, the parameter β controls the gradient of the sigmoid function at $x = 0$.

Importantly, the system in (1) can be shown to exhibit both steady-state solutions and stable oscillations, the latter of which is the brains natural resting state since it is continually active [27]. To see this one can perform a bifurcation analysis to determine bifurcation sets of the system in (1) as the control parameters P and Q are varied.

The Jacobian matrix for the model in (1) is given by

$$J = \begin{pmatrix} -1 + af'(P + au + bv) & bf'(P + au + bv) \\ cf'(Q + cu + cv) & -1 + df'(Q + cu + dv) \end{pmatrix}, \quad (3)$$

which can be more conveniently represented by noting that at a fixed point (u^*, v^*) we have

$$\begin{aligned} u^* &= f(P + au^* + bv^*) \\ v^* &= f(Q + cu^* + dv^*), \end{aligned} \quad (4)$$

and moreover, that the firing rate function f satisfies the Riccati equation

$$f' = \beta f(1 - f). \quad (5)$$

Using the above, we can write the Jacobian matrix in the simplified form

$$J = \begin{pmatrix} -1 + a\beta u^*(1 - u^*) & b\beta u^*(1 - u^*) \\ c\beta v^*(1 - v^*) & -1 + d\beta v^*(1 - v^*) \end{pmatrix}. \quad (6)$$

Bifurcation sets can then be determined using the usual conditions. For example, the saddle-node bifurcation set is given for values of P and Q satisfying $\det J = 0$ (see the bold curve in Fig. 1); whilst the Hopf bifurcation set (dashed curve in Fig. 1) is given by

$$\text{Tr } J = -2 + a\beta u^*(1 - u^*) + d\beta v^*(1 - v^*) = 0 \quad \text{and} \quad \det J > 0. \quad (7)$$

In Fig. 1, we choose $a = -b = c = 10$ and $d = 2$ as in [28]. Note that the reader interested in the details of the above bifurcation analysis should see the excellent book by Hoppensteadt and Izhikevich [29].

Fig. 1 Bifurcation sets for a single Wilson–Cowan node with $a = 10$, $b = -10$, $c = 10$, $d = 2$ and $\beta = 1$. Bold curve denotes the saddle-node bifurcation set and the dashed curve the Hopf bifurcation set

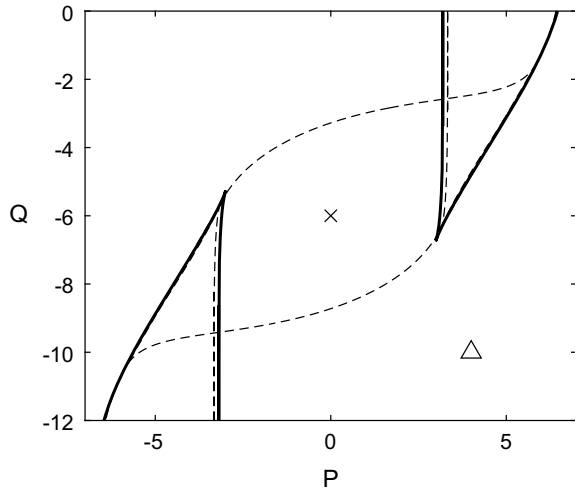


Figure 2 shows the results of numerical simulations of Eq. (1) for two different sets of control parameters (P, Q) (the remaining parameter values were taken the same as in [28]). Figure 2(a, b) shows the phase plane and time courses, respectively, for parameter values for which a stable limit cycle solution exists (parameter values are indicated by a cross in Fig. 1); whilst Fig. 2(c, d) shows the phase plane and time course, respectively, for parameter values (see the triangle in Fig. 1) for which a steady state solution exists. Importantly, as can be seen from the bifurcation diagram in Fig. 1, the system in (1) exhibits one of only two behaviours: It either tends to a steady state or it oscillates. Note that whilst the Wilson–Cowan model is a relatively simple neural oscillator model, it provides a convenient and compelling method for highlighting differences imparted by the different network structures considered later on. In principle, more physiologically realistic models such as those proposed by Jansen and Ritt [30], Liley et al. [31] or Coombes and Byrne [32] that more reliably replicate EEG and fMRI signals could be deployed for more detailed simulations.

1.2 Prerequisites in Complex Networks

Networks of neural masses, such as the Wilson–Cowan model introduced in the previous section, consist of a set of nodes $V = \{v_1, \dots, v_N\}$ representing different cortical regions and a set of edges $E = \{e_1, \dots, e_M\}$ representing structural (i.e., anatomical) connectivity. Such networks are said to be *undirected* if an edge exists between nodes i, j if and only if an edge exists between j, i , otherwise it is *directed*. Note, that whilst brain networks are inherently directed [1], experimental limitations means that most studies ignore the effect of directionality—see the recent paper by Kale et al. [33] for a discussion on the reliability of network studies on undirected connectomes.

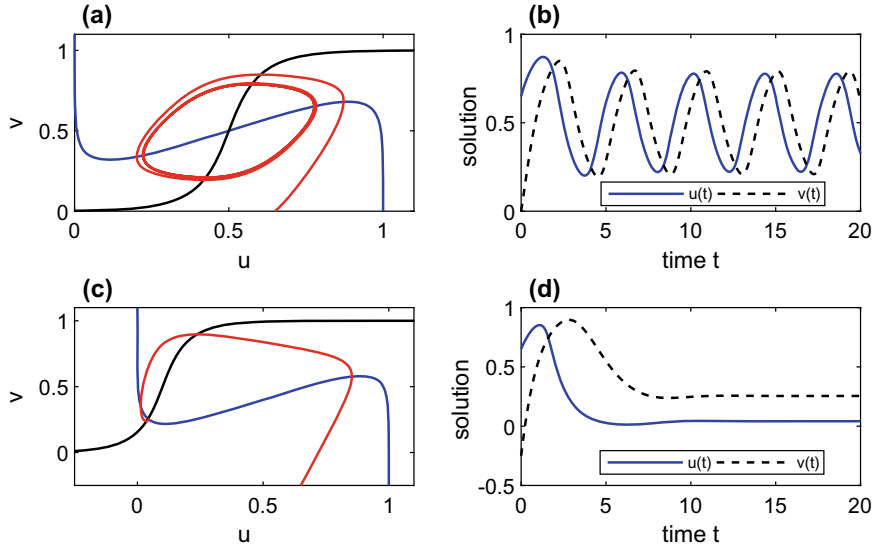


Fig. 2 Numerical simulations of a single Wilson–Cowan node. **a** and **b** display phase plane and time courses for oscillatory solutions of the model in (1) with $P = 0$, $Q = -6$. **c** and **d** display phase plane and time courses for steady-state solutions with $P = 4$, $Q = -10$. The remaining parameter values are set as $a = -b = c = 10$ and $d = 2$. In figures **(a)** and **(c)** we also plot the nullclines of the system in (1) for the respective choices of P and Q

A simple way to represent a network is via its *adjacency matrix*, which is the $N \times N$ matrix defined as

$$A = \begin{cases} 1 & i \sim j, \\ 0 & \text{otherwise.} \end{cases} \quad (8)$$

Here, \sim denotes that nodes i and j are connected. Given the adjacency matrix of a network, many network statistics can be computed; for example, the *network degree* of the i th node, that is the number of nodes adjacent to node i , is given by

$$k_i = \sum_j a_{ij}. \quad (9)$$

The mean degree

$$\langle k \rangle = \frac{1}{N} \sum_i k_i = \frac{2M}{N}, \quad (10)$$

where here, $M = |E|$ is the number of edges in the network. A related quantity is that of *network density*, which tells us what proportion of a networks edges are present and is given by

$$\rho = \frac{M}{N(N-1)/2} = \frac{\langle k \rangle}{N-1}. \quad (11)$$

Degree heterogeneity refers to deviations from regularity in the degrees of a network [34]. A number of recent studies have found that for certain classes of networks increasing the density, which is akin to reducing network heterogeneity, can have an enhancing effect on network synchronisation [35–37]. Typically, degree heterogeneity is accounted for by studying the networks *degree distribution*, $P(k)$, which for a given network provides the probability that a randomly chosen node has degree k . However, the question of how to compare heterogeneity of different networks based on degree distributions can only be answered in a few special cases (such as networks with scale-free degree distributions); thus, a more quantitative approach is desirable. Such an approach was recently forwarded by Estrada [38] in the form of the following heterogeneity index:

$$\sigma = \frac{1}{N - 2\sqrt{N-1}} \sum_{(i,j) \in E} \left(\frac{1}{\sqrt{k_i}} - \frac{1}{\sqrt{k_j}} \right)^2. \quad (12)$$

Importantly, the above measure is maximised for starlike networks (i.e., $\sigma = 1$) and minimised for regular networks (i.e., $\sigma = 0$).

A *path* of length k in the network is defined as a set of nodes $\{i_1, i_2, \dots, i_{k+1}\}$ such that for all $1 \leq l \leq k$, the nodes i_l and i_{l+1} are adjacent and no nodes are repeated except if the path is closed in which case $i_1 = i_{k+1}$. We say that the network is *connected* if a path exists between all node pairs. The *distance* (or *path-length*) d_{ij} between nodes i and j is defined as the shortest path connecting them, and the average distance is given by

$$\langle l \rangle = \frac{1}{N(N-1)} \sum_{i=1}^N \sum_{j=1}^N d_{ij}. \quad (13)$$

The *diameter* of a network is defined as the maximum of all shortest path distances between node pairs in the network.

Another important concept in network science is that of *local clustering* as introduced by Watts and Strogatz [39]. The clustering coefficient of the i th node is given by

$$C_i = \frac{2t_i}{k_i(k_i-1)}. \quad (14)$$

Here t_i denotes the number of closed paths of length three, or triangles, centred on node i . A global measure of clustering is then provided by the average

$$\langle C \rangle = \frac{1}{N} \sum_{i=1}^N C_i,$$

although a related global measure of clustering known as the *transitivity* index is also common in the literature and is preferable in some circumstances [34, 40].

Networks that are characterised by dense local clustering (or cliquishness of links between neighbouring nodes) and a small average path-length due to the presence of ‘shortcuts’ arising from the existence of a small number of long-range connections play a special role in network science and are known as *small-world* networks. Brain networks, in particular, have been shown to display small-world topologies, both in their anatomical and functional architectures [1, 41], and these structures are believed to be both universal and of great functional relevance in nervous systems across a range of species [42]. Small-world networks have been studied intensively, including a number of investigations into the effect of such structures on the synchronisation of network dynamics [35, 43, 44] both with and without delay.

Brain network models without delay The BNMs we consider are coupled via the excitatory nodes only [7, 45], as is the case in the brain. In the non-delay case, this results in a system of equations of the following form

$$\begin{aligned}\frac{du_i}{dt} &= -u_i + f(au_i + bv_i + P + \epsilon \sum_j w_{ij}u_j), \\ \frac{dv_i}{dt} &= -v_i + f(cu_i + dv_i + Q),\end{aligned}\tag{15}$$

for $i = 1, \dots, N$. Here, u_i and v_i denote synaptic activity of the i th population, the firing rate function is as in (2), and the coupling strength is given by ϵ . All other parameters are as described for Eq. (1). The matrix W in the coupling term is given by

$$W = D^{-1}A,\tag{16}$$

where D is the diagonal matrix of degrees, i.e.,

$$D = \begin{pmatrix} k_1 & & \\ & \ddots & \\ & & k_N \end{pmatrix}.$$

Importantly, the above normalisation ensures that all nodes receive a similar input.

Recently, the model in (15) has been used to explore the relationship between structural and functional connectivity in the brain [7, 45]. Structural brain connectivity in both studies was defined by the known anatomical structure of the Macaque monkey, which for these particular studies consisted of 47 cortical regions and some 505 anatomical connections, and is freely available via the CoComac website [46]. Figure 3 shows a plot of the structural connectivity of the Macaque monkey (LHS) and the results of a numerical simulation (RHS) for $P = 0$, $Q = -8$ and $\epsilon = 1$. Note that despite the relatively large coupling strength the system does not synchronise since a small amount of white noise ($\sigma = 0.01$) was added to the excitatory variable of each node. The resulting system was integrated using the Euler–Maruyama [47]

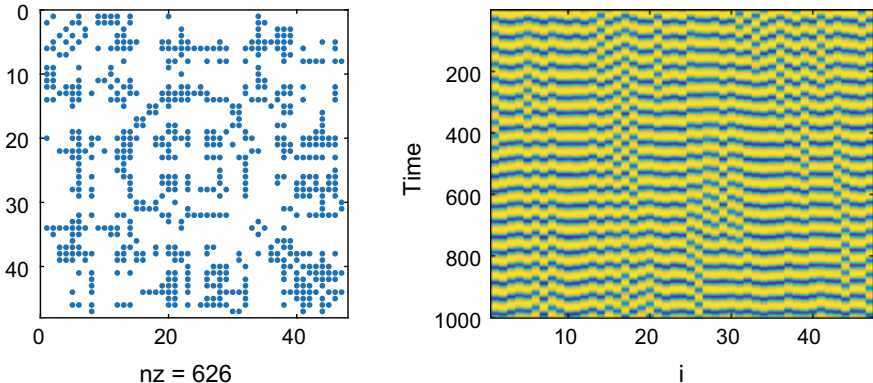


Fig. 3 LHS: brain anatomical connectivity data for the Macaque monkey. RHS: example time series of the excitatory variable, $u(t)$, for the system in (15) coupled via the Macaque connectivity data

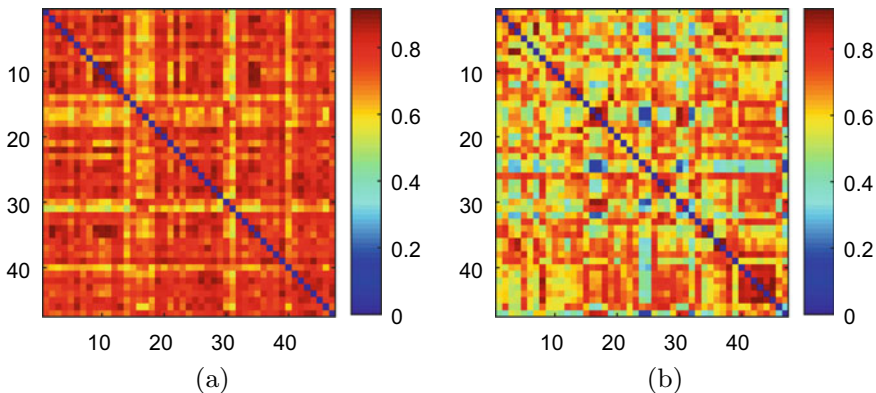


Fig. 4 Comparison of functional connectivity values for two different realisations of Eq. (15): **a** $P = 0, Q = -6$; and **b** $P = 1, Q = -8$

method with time-step $dt = 0.1$. Also, we note that the Macaque structural connectivity data is directed since it is collated from tract-tracing studies, which can infer both the location and direction of fibre tracts; however, for simplicity we ignore directionality in our simulations.

Given a time series describing neural activity, such as that shown in Fig. 3, a functional connectivity network can be constructed by calculating Pearson's correlation coefficient of the time series of all cortical areas. To obtain a binary functional connectivity matrix, the resulting correlation matrix should be thresholded; for example, by keeping a certain percentage of links (35% is often cited in the neuroscience literature), or by matching the number of functional and structural links. In Fig. 4(a, b), we display heat maps of functional connectivity matrices that were obtained from different realisations of Eq. (15), with (P, Q) values chosen, respectively, to be either

far from the Hopf boundary (dashed curve in Fig. 1) or close to the Hopf boundary. Note that both sets of (P, Q) values result in oscillatory solutions; however, those close to the Hopf boundary (Fig. 4b) result in a functional connectivity matrix that much more closely resembles the structural connectivity matrix—see Fig. 3.

The above result is in agreement with a growing body of evidence (see, e.g., [5, 48, 49]) that structure–function relations are considerably increased at critical points of the underlying neural model. Indeed, these results are likely a manifestation of the so-called *critical brain hypothesis* [50], which states that the brain operates at, or close to, a phase transition. Interestingly, in [45] a multiplex network approach was deployed to simultaneously model structure–function relations in the brain with the authors finding that multiplex network measures were heightened in regions of parameter space both close to and far away from criticality, suggesting that the form of structure–function relations can differ significantly depending on the specific dynamical regime of the neural system.

2 Time Delays in Neural Systems

In this section, we consider the role of time delays in neural systems. Note that there are several sources of delay that can arise [19], such as the time for an action potential to propagate along the axon, or depending upon the location of the synapse relative to the cell body, the delay associated with the propagation of the action potential along the dendrite. The simplest way to incorporate the effect of such delays on the propagation of action potentials is to include a time delay in the coupling term.

Such a system can be described by the initial value problem

$$\frac{dx}{dt} = \mathbf{f}(\mathbf{x}(t), \mathbf{x}(t - \tau_1), \dots, \mathbf{x}(t - \tau_d)), \quad \mathbf{x}(t) \in \mathbb{R}^n, t \geq 0, \quad (17)$$

with initial (or history) function

$$\mathbf{x}(t) = \phi(t), \quad t \leq 0.$$

Note that in this chapter, we restrict to constant delays for simplicity, despite the growing number of studies that consider time-dependent delays $\tau_j(t)$ as well as state-dependent delays $\tau_j(t, y(t))$. For a discussion on these and other aspects of delay differential equations see, for example, [51–53] and references therein.

2.1 Stability Analysis for Delay Differential Equations

Next, we briefly discuss the linear stability analysis of a delay differential equation of the form

$$\frac{d\mathbf{x}}{dt} = \mathbf{f}(\mathbf{x}(t), \mathbf{x}(t - \tau_1), \mathbf{x}(t - \tau_2)). \quad (18)$$

In our case, the state variable $\mathbf{x} = (u_1, \dots, u_N, v_1, \dots, v_N)^T$, where N is the number of neural masses. We describe the linear stability analysis for the two delay case as it is most relevant to our studies; the extension to larger numbers of delays is similar but the analysis becomes more challenging.

As with ordinary differential equations, a linear stability analysis requires the linearisation of Eq. (17) about an equilibrium solution \mathbf{x}^* :

$$\frac{d\mathbf{x}}{dt} = A\mathbf{x}(t) + B\mathbf{x}(t - \tau_1) + C\mathbf{x}(t - \tau_2). \quad (19)$$

Here, A is the Jacobian of $\mathbf{f}(\mathbf{x}, \mathbf{y}, \mathbf{z})$ with respect to \mathbf{x} , B the Jacobian of $\mathbf{f}(\mathbf{x}, \mathbf{y}, \mathbf{z})$ with respect to \mathbf{y} , and C the Jacobian of $\mathbf{f}(\mathbf{x}, \mathbf{y}, \mathbf{z})$ with respect to \mathbf{z} , that is

$$A = \frac{\partial f_i}{\partial x_j}, \quad B = \frac{\partial f_i}{\partial y_j} \quad \text{and} \quad C = \frac{\partial f_i}{\partial z_j}.$$

To determine the stability of the equilibrium solution \mathbf{x}^* , we assume Eq. (19) admits solutions of the form $\mathbf{q}e^{\lambda t}$, where λ is a complex number and \mathbf{q} is a vector of length n . Substituting this *ansatz* into (19) gives

$$[-\lambda I_n + A + Be^{-\lambda\tau_1} + Ce^{-\lambda\tau_2}] \mathbf{q} = 0. \quad (20)$$

For non-trivial solutions, we require that the *characteristic equation* of the linearised system satisfies

$$\Delta(\lambda) = \det [-\lambda I_n + A + Be^{-\lambda\tau_1} + Ce^{-\lambda\tau_2}] = 0. \quad (21)$$

The stability properties of the equilibrium solution \mathbf{x}^* are determined by the roots of the characteristic equation in (21). In particular, we have that the equilibrium solution is stable if all roots have negative real part. However, for delay differential equations, the presence of the terms $e^{\lambda\tau_{1,2}}$ means that there are infinitely many solutions of (21), and so special methods are required to determine stability (see, e.g., the book by Kolmanovskii and Nosov [54]). In practice, stability properties of delay differential equations such as Eq. (18) are determined using numerical bifurcation software packages (such as XPPAUT [55] and DDE-BIFTOOL [56, 57]) that are capable of not only detecting bifurcations of fixed points but can also follow branches of stable and unstable periodic orbits, as well as more complicated dynamical objects such as homoclinic and heteroclinic orbits.

2.2 A Single Time-Delayed Wilson–Cowan Node

We begin by reviewing recent results (see, e.g., [28] and references therein) for a single time-delayed Wilson–Cowan node of the form

$$\begin{aligned}\frac{du}{dt} &= -u(t) + f(au(t - \tau_1) + bv(t - \tau_2) + P), \\ \frac{dv}{dt} &= -v(t) + f(cu(t - \tau_2) + dv(t - \tau_1) + Q).\end{aligned}\quad (22)$$

As before, u and v represent the synaptic activity of two neural populations; however, both populations are now subject to the fixed delays τ_1 and τ_2 .

Fixed point solutions of Eq. (22) are, of course, independent of the delays τ_1 and τ_2 . Just as in the case with no delays, we wish to not only determine fixed point (and periodic) solutions of (22), but we would also like to monitor their stability, as well as to infer the effect of perturbations to important model parameters. To begin, we compute the linearisation of (22) about the fixed point (u^*, v^*) :

$$\frac{d}{dt} \begin{pmatrix} u \\ v \end{pmatrix} = A \begin{pmatrix} u \\ v \end{pmatrix} + B \begin{pmatrix} u(t - \tau_1) \\ v(t - \tau_1) \end{pmatrix} + C \begin{pmatrix} u(t - \tau_2) \\ v(t - \tau_2) \end{pmatrix}, \quad (23)$$

where

$$A = \begin{pmatrix} -1 & 0 \\ 0 & -1 \end{pmatrix}, \quad B = \begin{pmatrix} a\beta u^*(1 - u^*) & 0 \\ 0 & d\beta v^*(1 - v^*) \end{pmatrix}$$

and

$$C = \begin{pmatrix} 0 & b\beta u^*(1 - u^*) \\ c\beta v^*(1 - v^*) & 0 \end{pmatrix}.$$

It follows that the characteristic equation of (22) is given by

$$\begin{aligned}\Delta(\lambda) &= \det[-\lambda I_n + A + Be^{-\lambda\tau_1} + Ce^{-\lambda\tau_2}] \\ &= \det \begin{pmatrix} -\lambda - 1 + a\beta u^*(1 - u^*)e^{-\lambda\tau_1} & b\beta u^*(1 - u^*)e^{-\lambda\tau_2} \\ c\beta v^*(1 - v^*)e^{-\lambda\tau_2} & -\lambda - 1 + d\beta v^*(1 - v^*)e^{-\lambda\tau_1} \end{pmatrix}.\end{aligned}$$

To establish the stability of the fixed point requires the determination of the roots, or eigenvalues, of $\Delta(\lambda)$. Note that the roots of $\Delta(\lambda)$ depend continuously on the delays τ_1 and τ_2 , as well as the matrices A , B and C , and so the number of roots of $\Delta(\lambda)$ with positive real part can only change if a root passes through the imaginary axis.

To find the parameter values where the above characteristic equation has eigenvalues with zero real part, we substitute $\lambda = i\omega$, where $\omega \in \mathbb{R}$. Setting

$$\kappa_1 = a\beta u^*(1 - u^*), \quad \kappa_2 = d\beta v^*(1 - v^*) \quad \text{and} \quad \kappa_3 = bc\beta^2 u^* v^* (1 - u^*)(1 - v^*),$$

we obtain

$$\Delta(i\omega) = (-i\omega - 1 + \kappa_1 e^{-i\omega\tau_1}) (-i\omega - 1 + \kappa_2 e^{-i\omega\tau_1}) - \kappa_3 e^{-2i\omega\tau_2} = 0, \quad (24)$$

which upon equating real and imaginary parts gives

$$\begin{aligned} \operatorname{Re} \Delta(i\omega) &= (1 - \kappa_1 \cos(\omega\tau_1)) (1 - \kappa_2 \cos(\omega\tau_1)) \\ &\quad - (\omega + \kappa_1 \sin(\omega\tau_1)) (\omega + \kappa_2 \sin(\omega\tau_1)) - \kappa_3 \cos(2\omega\tau_2) = 0, \end{aligned} \quad (25)$$

and

$$\begin{aligned} \operatorname{Im} \Delta(i\omega) &= (1 - \kappa_1 \cos(\omega\tau_1)) (\omega + \kappa_2 \sin(\omega\tau_1)) \\ &\quad + (\omega + \kappa_1 \sin(\omega\tau_1)) (1 - \kappa_2 \cos(\omega\tau_1)) + \kappa_3 \sin(2\omega\tau_2) = 0. \end{aligned} \quad (26)$$

Nonzero values of ω that simultaneously solve Eqs. (25) and (26) are typically taken as the definition of a Hopf bifurcation, although in practice the transversality condition

$$\frac{d}{dt} (\operatorname{Re} \lambda) \neq 0$$

should also be satisfied to guarantee that the eigenvalue crosses the imaginary axis. Note that in the case when $\omega = 0$, the above reduces to

$$(1 - \kappa_1)(1 - \kappa_2) - \kappa_3 = 0,$$

which is the same as the saddle-node condition considered earlier.

The two main tools at our disposal for analysing systems of delay differential equations are direct simulation and numerical bifurcation techniques. For illustrative purposes, as well as guidance when choosing parameter values when simulating BNMs with delay in the next section, we repeat the numerical bifurcation analysis performed in [28]. All simulations were performed in MATLAB using the DDE-BIFTOOL [56, 57] toolbox. More specifically, we analysed the behaviour of the system in (22) as the parameters P and $\tau_1 = \tau_2 = \tau$ were varied. The remaining parameters were set as

$$Q = 0.5, \quad \beta = 60, \quad a = -1, \quad b = -0.4, \quad c = -1 \quad \text{and} \quad d = 0.$$

Typical results are shown in Figure 5, which displays the saddle-node (solid line) and Hopf (dashed line) bifurcation sets as well as saddle-node bifurcations of periodic orbits (line with circles). Figure 6 shows a cross section of Fig. 5 for the following values of the delay: $\tau = 0.5$, $\tau = 0.2$ and $\tau = 0.09$. For $\tau = 0.5$, we see from Fig. 6a that for increasing P a branch of stable periodic orbits is created connecting the Hopf bifurcations on the lower and upper branches of fixed points at approximately $P = 0.43$ and $P = 0.97$, respectively. For $\tau = 0.2$, we find regions of parameter space in which stable and unstable periodic orbits coexist due to the creation of

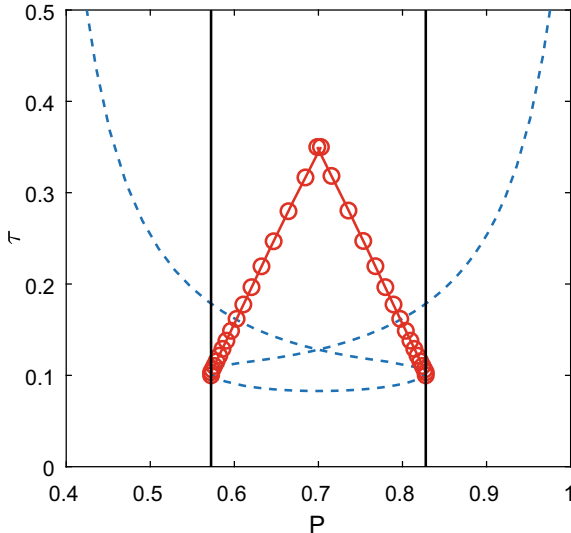


Fig. 5 Bifurcation diagram. Solid line—saddle-node bifurcation of fixed points; dashed line—Hopf bifurcation; line with circles—saddle-node bifurcation of periodic orbits. The parameter values where as in [28]: $Q = 0.5$, $\tau_1 = \tau_2 = \tau$, $\beta = 60$, $a = -1$, $b = -0.4$, $c = -1$ and $d = 0$

saddle-node bifurcations of periodic orbits. And finally, for $\tau = 0.09$ we observe the creation of a branch of unstable periodic orbits via a Hopf bifurcation on the unstable branch of fixed points (For further details see [28]).

2.3 Time Delays in a Network of Wilson–Cowan Masses

In this section, we consider a network of time-delayed Wilson–Cowan masses and explore, via numerical simulations, the effect of network structure using model architectures as well as a BNM constructed using the cortical connectivity of the Macaque monkey.

The general model we consider is of the form

$$\begin{aligned} \frac{du_i}{dt} &= -u_i(t) + f(au_i(t - \tau_1) + bv_i(t - \tau_2) + P + \epsilon \sum_j w_{ij}u_j(t - \tau_3)), \\ \frac{dv_i}{dt} &= -v_i(t) + f(cu_i(t - \tau_2) + dv_i(t - \tau_1) + Q), \end{aligned} \quad (27)$$

for $i = 1, 2, \dots, N$. Here, $W \in \mathbb{R}^{N \times N}$ is the scaled adjacency matrix (see Eq. (16)), the within population delays are given by τ_1 , τ_2 , and the delay between populations, or brain regions, is given by τ_3 . All other parameters are as defined previously in

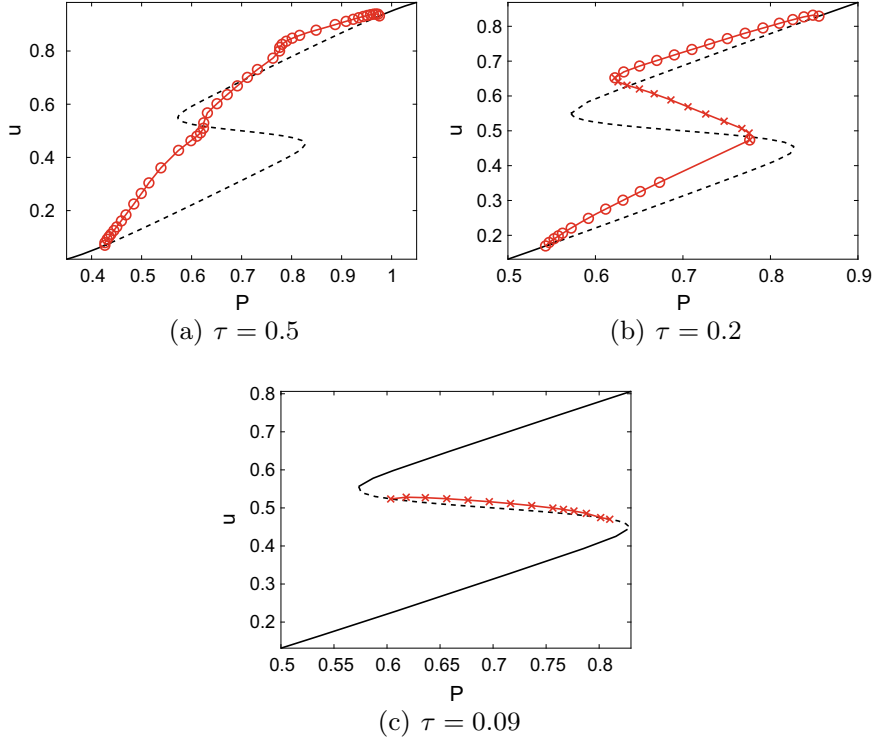


Fig. 6 Cross sections of Fig. 3.1 from horizontal slices at varying τ values. Solid line—stable fixed points; dashed line—unstable fixed points; circles—stable periodic orbit; crosses—unstable periodic orbit

Sect. 2.2. Note that more general forms of delay are possible, for example, we could define heterogeneous intra-delays $\tau_{1,i}$ and $\tau_{2,i}$, or internode delays that are distance dependent $\tau_{i,j}$ (here the delay depends on the distance between brain regions i and j). However, for simplicity, as well as for comparative purposes with the study in [24], we restrict to three delays (two intra and one inter) in our work.

Importantly, the model in (27) reduces to that of Coombes and Laing [28] as ϵ tends to zero and so each node behaves as in the previous section. To investigate the effect of the coupling term on the resultant network dynamics, we set the parameters

$$Q = 0.5, \quad \beta = 60, \quad a = c = -1, \quad b = -0.4 \quad \text{and} \quad d = 0,$$

as in the previous section, choose $\tau_1 = \tau_2 = 0.5$ and set $P = 0.65$. As can be seen in Fig. 6a, such a choice of parameter values ensures the existence of stable oscillations for small values of ϵ . In the following, we investigate the dynamical behaviour of the BNM in (27) as the coupling strength ϵ and internodal delay τ_3 are varied.

We solve the model in (27) using the built-in MATLAB routine `dde23`, which deploys Runge–Kutta methods capable of solving systems of delay differential equations with constant delays [58]. The method requires as input a routine that evaluates the right side of the system in (27), a vector containing the delays and a history function. In our experiments, the history function $\mathbf{x}(t) = \phi \in \mathbb{R}^{2N}$ was chosen to be a constant vector with elements drawn at random from the uniform distribution on $[0, 1]$. All simulations shown were integrated for $T = 250$ using `dde23` with absolute and relative tolerances both set to $1e - 6$.

To quantify synchronisation transitions for the coupled WC nodes, we compute the following synchronisation parameter, introduced in [59], for the excitatory variables $u_i(t)$:

$$R = \frac{\langle \bar{u}(t)^2 \rangle - \langle \bar{u}(t) \rangle^2}{\frac{1}{N} \sum_{i=1}^N (\langle u_i(t)^2 \rangle - \langle u_i(t) \rangle^2)}, \quad (28)$$

where

$$\bar{u}(t) = \frac{1}{N} \sum_{i=1}^N u_i(t). \quad (29)$$

The angular brackets denote averages over time. Clearly, the synchronisation parameter lies in the interval $[0, 1]$ with larger R values indicating greater synchrony between neural units—a value of $R = 1$ is returned in the completely synchronous case.

Network models Before considering the model in (27) on cortical architectures, we deploy a range of model network configurations in order to investigate how network topology influences the Wilson–Cowan dynamics. More specifically, we consider five different network structures: a path network, a cycle network, a star network, a square lattice and a complete network—see Fig. 7 for representations of each network. For the toy network models, we set $N = 16$ as this is both large enough to observe the effects of network structure but also small enough to be computationally efficient (similar results have been observed for $N = 100$ —results not shown). Table 1 shows structural properties for each of the five networks.

Figure 8a shows results for simulations for fixed internodal delay, $\tau_3 = 1$, and two different coupling strengths ($\epsilon = 0.1$ (top row) and $\epsilon = 0.25$ (bottom row)) for each of the network structures shown in Fig. 7. We also display the synchronisation score, R , for each simulation. Note that although these results are for a single initial condition, they are typical in the sense that the patterns observed are robust to changes in the initial data. The first point of interest is that for weak coupling, all structures are regularised to some extent, in the sense that they tend towards a more synchronised state. The complete network and the star network are fully synchronised (i.e., $R = 1$), whilst the cycle, lattice and path networks are synchronised to a lesser extent: $R = 0.83164, 0.68131$ and 0.33643 , respectively. In our experiments, we find that the complete network and the star network are the most stable in that the synchronised state is rapidly recovered regardless of the initial state. Whilst slightly less stable, the cycle network typically results in stable patterns with high synchronisation scores, again, independent of the initial state. The path and lattice networks are in general

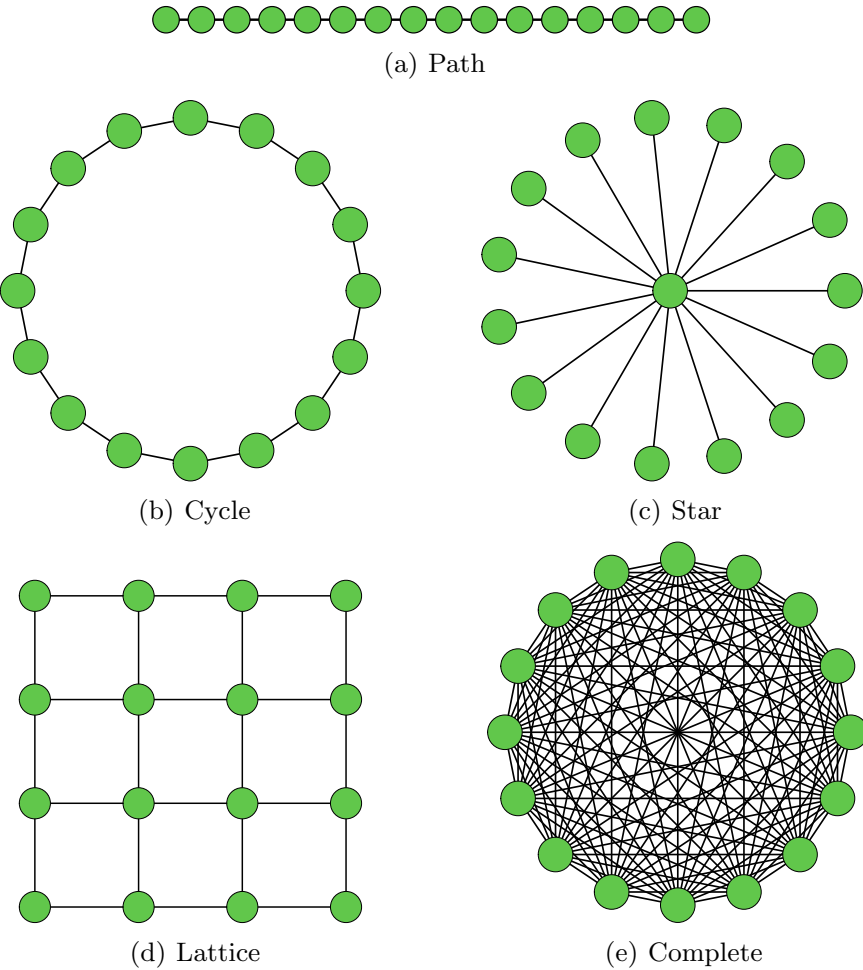


Fig. 7 Illustrations of the toy network models used in our numerical simulations for $N = 16$. We consider **a** path network; **b** cycle network; **c** star network; **d** lattice network and **e** complete network

Table 1 Structural properties for the toy network architectures considered in this chapter

Networks	N	M	$\langle k \rangle$	ρ	$\langle l \rangle$	$\langle C \rangle$	σ
Path	16	15	1.875	0.125	5.667	0	0.0021
Cycle	16	16	2	0.1333	4.2667	0	0
Star	16	15	1.875	0.125	1.875	0	1
Lattice	16	24	3	0.2	2.667	0	0.0041
Complete	16	120	15	1	1	1	0

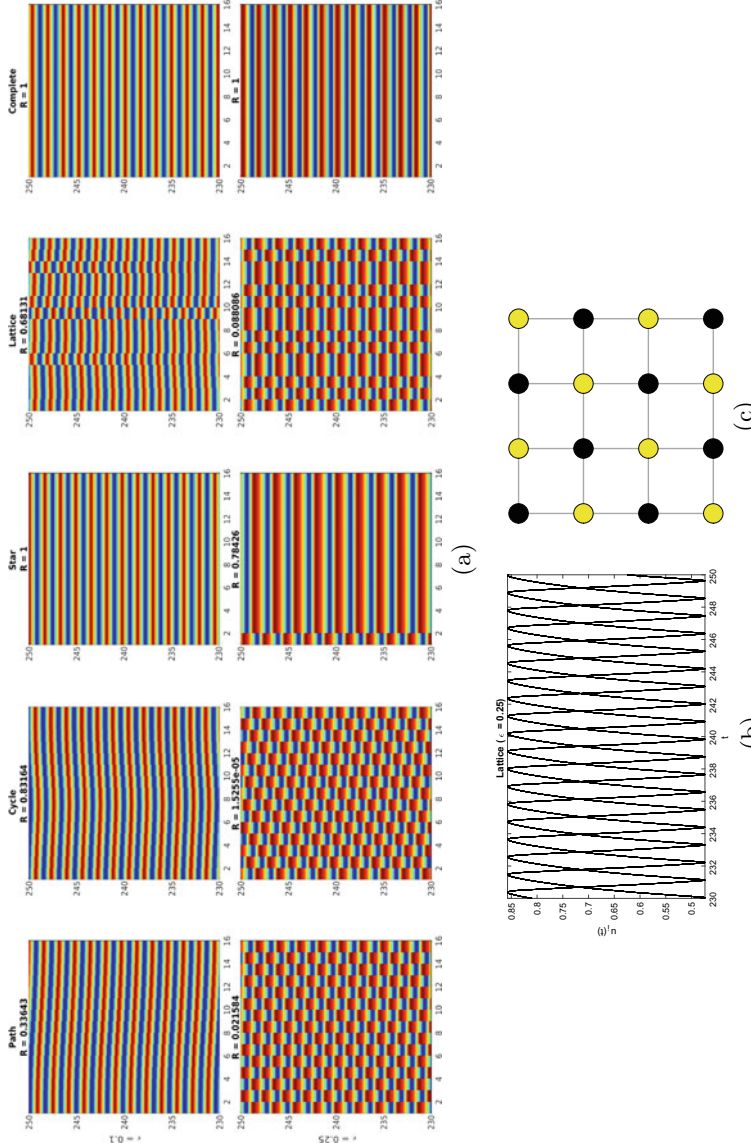


Fig. 8 **a** Illustration of the coupling patterns observed when simulating the Wilson–Cowan equations in (27) for the toy network structures shown in Fig. 7. Results are shown for two different coupling strengths: $\epsilon = 0.1$ (top row) and $\epsilon = 0.25$ (bottom row). **b** Illustration of the anti-phase synchronisation patterns observed for the lattice network. **c** Anti-phase dynamics induces checkerboard patterns in which neighbouring nodes are out of phase as illustrated here in the case of the lattice graph

more difficult to synchronise for the values of coupling strength considered here. Note that whilst our setup is slightly different to the one in [24] (we use random initial data and some parameter values differ), we obtain similar results in that we find regular and/or densely connected networks (i.e., networks with homogeneous degree distributions) appear to induce more stable dynamics.

The second row in Fig. 8a shows the effect of increasing the coupling strength whilst retaining the internodal delay. Interestingly, in this case the dynamics becomes less stable in all networks except for the complete network, which is again fully synchronised. Rather, we find that the path, cycle, star, and lattice networks tend towards an anti-phase synchronised state. Figure 8(b, c) shows the time course of the excitatory variables, u_i , for $T = 230$ to $T = 250$, and the checkerboard pattern induced by the anti-phase synchrony dynamics, respectively, for the lattice network. Note that as can be seen in both plots, the network nodes are grouped into two classes, such that nodes within the same class are completely synchronised, whilst nodes in different classes are out of phase. Similarly, the nodes of the star network are partitioned into two: a set of peripheral nodes that are fully synchronised and the central hub node, which maintains independent dynamics—this type of hub-driven synchrony has also been reported in brain networks [60]. Finally, the path and cycle networks can also be seen to split into subsets of nonadjacent nodes that preferentially synchronise, although to a lesser extent than the other networks considered here. This type of *remote synchronisation*, in which non-neighbouring nodes synchronise, is common in networks with symmetry such as those considered here and has been previously reported for star networks [61] and cycles [62]. It is important to note mind that we have not observed the anti-phase dynamics reported here in the non-delay case.

Cortical networks The BNM that we consider is composed of WC nodes coupled according to the adjacency matrix A describing the corticocortical connectivity of the Macaque monkey brain [63]—see Fig. 9 for a plot of the network structure with nodes labelled according to the standard anatomical atlas. Structural properties of the Macaque monkey network are given in Table 2, and it is immediately obvious that its structure is wildly different to any of the toy networks considered previously. It is clearly a small-world network since it has both a high level of clustering and a low average path-length. Moreover, it is significantly more dense than the toy models (complete network aside) and has a slightly higher level of heterogeneity than all but the star network. An important network property that we do not consider in this chapter is that of network modularity [40], which measures the strength of division of a network into modules (i.e., sets of nodes such that nodes within the same set are highly connected, whilst connections between nodes in different sets are sparse). Like most biological networks, it is well known that cortical networks display high levels of modularity (see, e.g., the cortical connectivity of the Macaque monkey in Fig. 3) and this is likely to have a strong effect on network dynamics; however, the modularity structure of the brain is strongly influenced by spatial constraints and so a proper exploration of these effects should incorporate distant-dependent delays, and so is outside the scope of the current work.

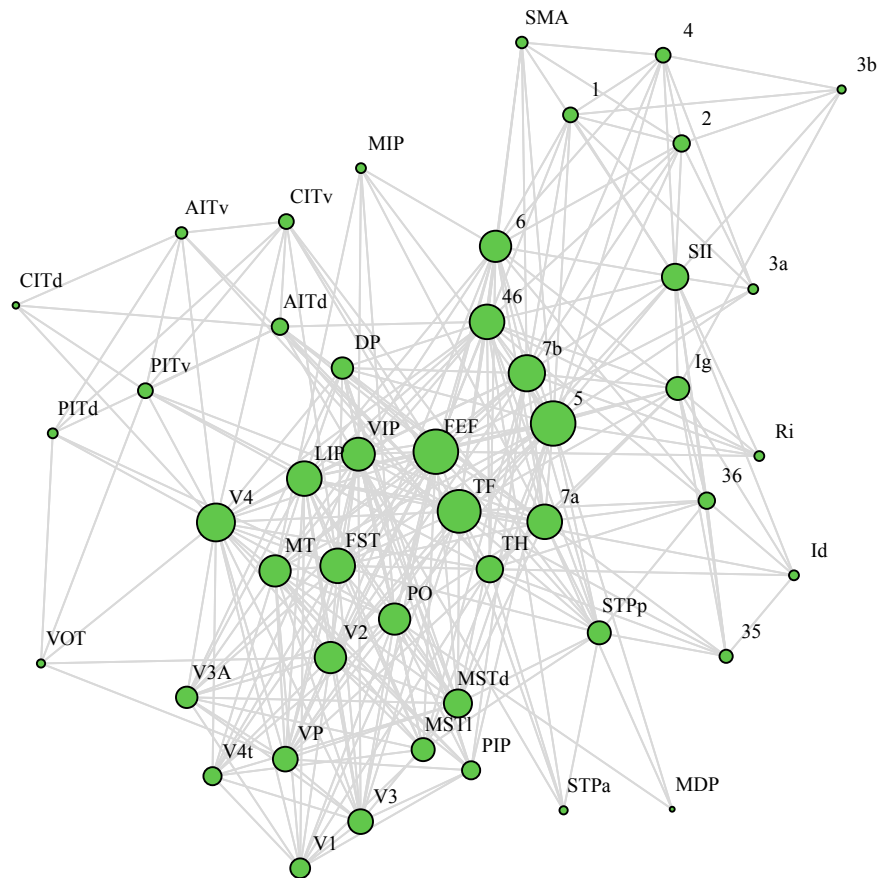


Fig. 9 Structural connectivity network of the Macaque monkey. Node (47 regions of interest) sizes are proportional to degree. Nodes are labelled using standard anatomical abbreviations (see [63] and references therein for further details)

Table 2 Structural properties of the Macaque cortical network

Networks	N	M	$\langle k \rangle$	ρ	$\langle l \rangle$	$\langle C \rangle$	σ
Macaque network	47	313	13.3191	0.2895	1.8501	0.6412	0.0867

Figure 10 shows results of simulations for three different values of coupling and internode delay:

$$\epsilon = \{0.01, 0.1, 0.25\} \quad \text{and} \quad \tau_3 = \{0.01, 1, 10\},$$

respectively. As before, these results are for a single set of random initial conditions but from our experiments appear largely independent of the initial starting point. Simulations are displayed from $T = 230$ to $T = 250$. As well as displaying the time series for the excitatory variable, $u_i(t)$, each panel has a synchronisation score, R , which quantifies the level of synchrony present. Starting with the top row of panels, we see that the weakly coupled system ($\epsilon = 0.01$) does not converge to a synchronised state regardless of the delay time, although the synchronisation parameter is maximised in this row for the greatest delay time ($\tau = 10$). For intermediate coupling strength ($\epsilon = 0.1$), we find that the ‘undelayed’ (i.e., negligible delay $\tau_3 = 0.01$) system tends towards an asynchronous state—interestingly, comparing the synchronisation parameter with that of the undelayed system with $\epsilon = 0.01$ shows a reduction in synchronisation levels. The addition of a delay in this case induces synchrony in the system and so can be seen to have a regularising effect. The final row of plots shows the case of strong coupling ($\epsilon = 0.25$). For this level of coupling the undelayed system converges to the synchronous state. However, the addition of delays now has a variety of effects, leading to asynchronous, possibly chaotic, solutions (Fig. 10—bottom row, middle column), approximate anti-phase oscillations (not shown) and periodic, synchronised solutions (Fig. 10—bottom row, right column), depending upon the length of the delay. For the asynchronous case, the synchronisation parameter $R = 0.0538$, which is the lowest score of any of the solutions shown despite the relatively strong level of coupling in this case.

Our results suggest that dynamical behaviour of the system in (27) can be controlled via a delicate balance between coupling strength and internode delay times. We have seen that varying these two parameters can result in a plethora of dynamic states, including complete synchrony, approximate anti-phase synchrony and ‘chaos’. Early experiments (work not shown) suggest that between these ordered and disordered regions of parameter space there exist regions of metastability, in which the nodal dynamics continuously migrate between various synchronous states [64]. Alongside criticality, metastability is popularly believed to play a crucial role in the brains ability to process temporal information and generate temporal patterns [65] making this finding particularly interesting. Another important point to make, is that internode delay times can be seen to have a regularising effect on network dynamics, even in the case of weak coupling strength, which is typically assumed in the brain [29]. We would hypothesise that the extension of the model in (27) to heterogeneous, distant-dependent delays, would likely lead to delay-induced chimera states [66], as opposed to the global synchrony observed here. Finally, we note that for larger coupling strengths the inclusion of delays more frequently deregularises network dynamics leading to irregular (possibly chaotic) states, which are undesirable from a biological point-of-view.

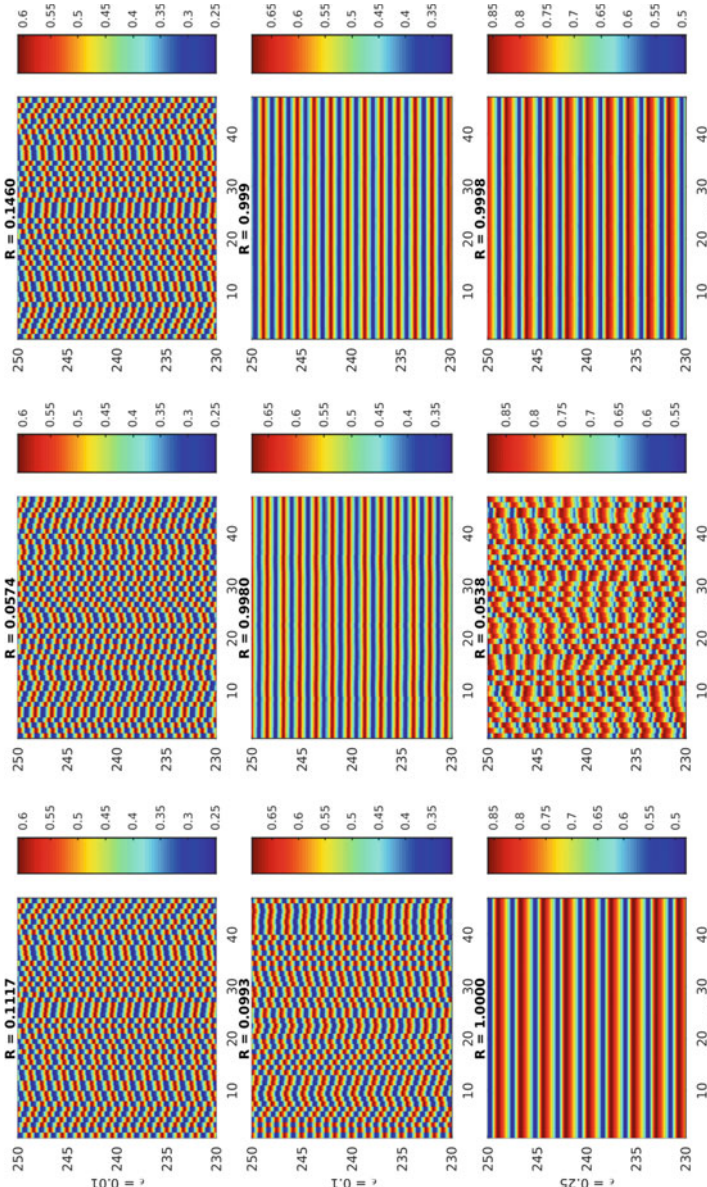


Fig. 10 Comparison of numerical solutions to the Wilson–Cowan model in (27) with network structure given by the anatomical connectivity of the Macaque cortex. The nine panels show results for various combinations of coupling strength ($\epsilon = \{0.01, 0.1, 0.25\}$) and intermode delay times ($\tau_3 = \{0.01, 1, 10\}$). The remaining parameter values are $P = 0.65$, $Q = 0.5$, $\beta = 60$, $a = c = -1$, $b = -0.4$, $d = 0$ and $\tau_1 = \tau_2 = 0.5$

To summarise, the above results suggest that the introduction of internodal delays can promote multi/metastable-like behaviour in a BNM, such as that in (27), even in the weakly coupled case, which is advantageous as it would appear to reduce the likelihood of the system attaining undesirable (irregular, possibly chaotic) brain states, which in our experiments were more frequently observed as the coupling strength increased.

3 Summary and Conclusions

In this chapter, we have considered the effect that time delays can have on a brain network model consisting of coupled Wilson–Cowan nodes. We started with an analysis of a single WC node in the absence of delays, before extending this analysis to the case of a WC node with two distinct discrete delays, outlining in the process some of the tools available for analysing such systems. To determine the effect that network topology has on the dynamics of a coupled, time-delayed WC model, we deployed both artificial and experimental network structures whilst varying important model parameters—coupling strength and internodal delay time. Importantly, we found that network delays induced regularity in all the toy network structures we considered. In particular, we found further evidence (building on the results in [24]) that networks with homogeneous network degrees are more stable in the sense that they synchronise more quickly and for a greater range of parameter values. We also observed delay-induced remote synchronisation in the toy network models in which the networks were grouped into nonadjacent but preferentially synchronised nodes. For the cortical network, we found that the BNM in (27) exhibited a range of dynamics depending upon the balance between coupling strength and delay time, including global synchrony, (approximate) anti-phase synchronisation and irregular, chaotic-like, solutions. Importantly, we found that irregular dynamics occurred more frequently as coupling strength was increased (in the presence of delays). Our results suggest that the incorporation of delays in a weakly coupled system, such as the brain network considered here, provide a potential mechanism for avoiding undesirable (disordered) states, whilst allowing the system to retain a sufficiently rich repertoire of network behaviours.

There are a number of possible extensions of the work presented in this chapter:

1. Deploying human connectivity data, both healthy and diseased, is an important next step in order to test and validate the model used in this section, which to date has only been considered on toy networks [24] as well as the primate connectome considered in this chapter.
2. Incorporating spatial information (i.e., white matter tract length which is available via MRI technologies) in order to consider heterogeneous internodal delays is considered particularly important for BNMs [23] and is thus an important extension of the work considered here.

3. Using more physiologically realistic neural mass models such as those proposed by Jansen and Ritt [30], Liley et al. [31] and Coombes and Byrne [32] is also of great importance, especially given the recent paper by Forrester et al. [67], which found that structure–function relations are influenced by multiple factors, including nodal dynamics, network topology and coupling strength.
4. We have considered fixed intra-delays ($\tau_1 = \tau_2$) in our BNM, and so it would be interesting to consider the effect of varying the node dynamics (i.e., allow different subpopulations to communicate on different timescales) on the overall network behaviour.
5. The addition of noise to the model considered here is an important next step as neural activity is believed to be a combination of anatomical structure, node dynamics *and* noise. Such stochastic models are considered essential if the true dynamic (or metastable) behaviour of functional connectivity and its relation to structure is to be revealed.

References

1. Sporns O (2010) Networks of the brain. MIT Press, Cambridge
2. Coombes S (2010) Large-scale neural dynamics: simple and complex. NeuroImage 52(3):731–739
3. Kaiser M (2011) A tutorial in connectome analysis: topological and spatial features of brain networks. Neuroimage 57(3):892–907
4. Rubinov M, Sporns O, van Leeuwen C, Breakspear M (2009) Symbiotic relationship between brain structure and dynamics. BMC Neurosci 10(1):55
5. Deco G, Ponce-Alvarez A, Romani Mantini D, GL, Hagmann P, Corbetta M (2013) Resting-state functional connectivity emerges from structurally and dynamically shaped slow linear fluctuations. J Neurosci 33(27):11239–11252
6. Breakspear M (2017) Dynamic models of large-scale brain activity. Nat Neurosci 20(3):340
7. Hlinka J, Coombes S (2012) Using computational models to relate structural and functional brain connectivity. Eur J Neurosci 36(2):2137–2145
8. Vértes PE, Alexander-Bloch AF, Gogtay N, Giedd JN, Rapoport JL, Bullmore ET (2012) Simple models of human brain functional networks. Proc Natl Acad Sci 109(15):5868–5873
9. Sporns O (2014) Contributions and challenges for network models in cognitive neuroscience. Nat Neurosci 17(5):652
10. Bansal K, Nakuci J, Feldt Muldoon S (2018) Personalized brain network models for assessing structure–function relationships. Curr Opin Neurobiol 52:42–47
11. Sanz Leon P, Knock SA, Marmaduke Woodman M, Domide L, Mersmann J, McIntosh AR, Jirsa V (2013) The virtual brain: a simulator of primate brain network dynamics. Front Neuroinform 7:10
12. Yahata N, Kasai K, Kawato M (2017) Computational neuroscience approach to biomarkers and treatments for mental disorders. Psychiatry Clin Neurosci 71(4):215–237
13. Lydon-Staley DM, Bassett DS (2018) Network neuroscience: a framework for developing biomarkers in psychiatry. Biomarkers in psychiatry. Springer, Berlin, pp 79–109
14. Stefanovski L, Triebkorn P, Spiegler A, Diaz-Cortes M-A, Solodkin A, Jirsa V, McIntosh AR, Ritter P, Alzheimers Disease Neuroimaging Initiative, et al (2019) Linking molecular pathways and large-scale computational modeling to assess candidate disease mechanisms and pharmacodynamics in alzheimers disease. BioRxiv, p 600205

15. Sporns O, Tononi G, Kötter R (2005) The human connectome: a structural description of the human brain. *PLoS Comput Biol* 1(4):e42
16. Bassett DS, Siebenhühner F (2013) Multiscale network organization in the human brain. *Multiscale Anal Nonlinear Dyn*, pp 179–204
17. Friston KJ (2011) Functional and effective connectivity: a review. *Brain Connectivity* 1(1):13–36
18. Ramirez-Beltran ND, Montes JA (2002) Neural networks to model dynamic systems with time delays. *IIE Trans* 34(3):313–327
19. Campbell SA (2007) Time delays in neural systems. In: *Handbook of brain connectivity*. Springer, Berlin, pp 65–90
20. Stepan G (2009) Delay effects in brain dynamics
21. Rahman B, Blyuss KB, Kyrychko YN (2015) Dynamics of neural systems with discrete and distributed time delays. *SIAM J Appl Dyn Syst* 14(4):2069–2095
22. Muldoon SF, Pasqualetti F, Gu S, Cieslak M, Grafton ST, Vettel JM, Bassett DS (2016) Stimulation-based control of dynamic brain networks. *PLoS Comput Biol* 12(9):e1005076
23. Petkoski S, Jirsa VK (2019) Transmission time delays organize the brain network synchronization. *Philos Trans R Soc A* 377(2153):20180132
24. Conti F, Van Gorder RA (2019) The role of network structure and time delay in a metapopulation Wilson-Cowan model. *J Theor Biol*
25. Pinotsis D, Robinson P, Friston K et al (2014) Neural masses and fields: modeling the dynamics of brain activity. *Front Comput Neurosci* 8:149
26. Wilson HR, Cowan JD (1972) Excitatory and inhibitory interactions in localized populations of model neurons. *Biophys J* 12(1):1–24
27. Garcia-Rill E, Onofrio S, Luster B, Mahaffey S, Urbano FJ, Phillips C (2016) The 10 Hz frequency: a fulcrum for transitional brain states. *Transl Brain Rhythmicity* 1(1):7
28. Coombes S, Laing C (2009) Delays in activity-based neural networks. *Philos Trans R Soc A: Math Phys Eng Sci* 367(1891):1117–1129
29. Hoppensteadt FC, Izhikevich EM (2012) Weakly connected neural networks, vol 126. Springer Science & Business Media, Berlin
30. Jansen BH, Rit VG (1995) Electroencephalogram and visual evoked potential generation in a mathematical model of coupled cortical columns. *Biol Cybernetics* 73(4):357–366
31. Liley DTJ, Bojak I, Dafilis MP, van Veen L, Frascoli F, Foster BL (2010) Bifurcations and state changes in the human alpha rhythm: theory and experiment. In: *Modeling phase transitions in the brain*. Springer, Berlin, pp 117–145
32. Coombes S, Byrne Á (2019) Next generation neural mass models. In: *Nonlinear dynamics in computational neuroscience*. Springer, Berlin, pp 1–16
33. Kale P, Zalesky A, Gollo LL (2018) Estimating the impact of structural directionality: How reliable are undirected connectomes? *Network Neurosci* 2(02):259–284
34. Ernesto Estrada (2012) *The structure of complex networks: theory and applications*. Oxford University Press, Oxford
35. Nishikawa T, Motter AE, Lai Y-C, Hoppensteadt FC (2003) Heterogeneity in oscillator networks: are smaller worlds easier to synchronize? *Phys Rev Lett* 91(1):014101
36. Motter AE, Zhou C, Kurths J (2005) Network synchronization, diffusion, and the paradox of heterogeneity. *Phys Rev E* 71(1):016116
37. Jalili M (2013) Enhancing synchronizability of diffusively coupled dynamical networks: a survey. *IEEE Trans Neural Networks Learn Syst* 24(7):1009–1022
38. Estrada E (2010) Quantifying network heterogeneity. *Phys Rev E* 82(6):066102
39. Watts DJ, Strogatz SH (1998) Collective dynamics of small-world networks. *Nature* 393(6684):440
40. Mark N (2018) *Networks*. Oxford University Press, Oxford
41. Bassett DS, Bullmore ED (2006) Small-world brain networks. *The Neuroscientist* 12(6):512–523
42. Bassett DS, Bullmore ET (2017) Small-world brain networks revisited. *The Neuroscientist* 23(5):499–516

43. Wu Y, Shang Y, Chen M, Zhou C, Kurths J (2008) Synchronization in small-world networks. *Chaos: Interdiscip J Nonlinear Sci* 18(3):037111
44. Qian Y (2014) Time delay and long-range connection induced synchronization transitions in Newman-Watts small-world neuronal networks. *PLoS ONE* 9(5):e96415
45. Crofts JJ, Forrester M, O'Dea RD (2016) Structure-function clustering in multiplex brain networks. *EPL (Europhys Lett)* 116(1):18003
46. Kötter R (2004) Online retrieval, processing, and visualization of primate connectivity data from the cocomac database. *Neuroinformatics* 2(2):127–144
47. Kloeden PE, Platen E (2013) Numerical solution of stochastic differential equations, vol 23. Springer Science & Business Media, Berlin
48. Rubinov M, Sporns O, Thivierge J-P, Breakspear M (2011) Neurobiologically realistic determinants of self-organized criticality in networks of spiking neurons. *PLoS Comput Biol* 7(6):e1002038
49. Stam CJ, Van Straaten ECW, Van Dellen E, Tewarie P, Gong G, Hillebrand A, Meier J, Van Mieghem P (2016) The relation between structural and functional connectivity patterns in complex brain networks. *Int J Psychophysiol* 103:149–160
50. Shew WL, Plenz D (2013) The functional benefits of criticality in the cortex. *The Neuroscientist* 19(1):88–100
51. Erneux T (2009) Applied delay differential equations, vol 3. Springer Science & Business Media, Berlin
52. Smith HL (2011) An introduction to delay differential equations with applications to the life sciences, vol 57. Springer, New York
53. Breda D, Maset S, Vermiglio R (2014) A numerical approach with MATLAB. Stability of linear delay differential equations. Springer, Berlin
54. Kolmanovskii VB, Nosov VR (1986) Stability of functional differential equations, vol 180. Elsevier
55. Ermentrout B (2002) Simulating, analyzing, and animating dynamical systems: a guide to XPPAUT for researchers and students, vol 14. SIAM
56. Engelborghs K, Luzyanina T, Samaey G (2000) Dde-biftool: a matlab package for bifurcation analysis of delay differential equations. *TW Report*, 305
57. Engelborghs K, Luzyanina T, Roose D (2002) Numerical bifurcation analysis of delay differential equations using dde-biftool. *ACM Trans Math Software (TOMS)* 28(1):1–21
58. Shampine LF, Thompson S (2009) Numerical solution of delay differential equations. In: Delay differential equations. Springer, Berlin pp 1–27
59. Gonze D, Bernard S, Waltermann C, Kramer A, Herzel H (2005) Spontaneous synchronization of coupled circadian oscillators. *Biophys J* 89(1):120–129
60. Vlasov V, Bifone A (2017) Hub-driven remote synchronization in brain networks. *Sci Rep* 7(1):10403
61. Bergner A, Frasca M, Sciuto G, Buscarino A, Ngamga EJ, Fortuna L, Kurths J (2012) Remote synchronization in star networks. *Phys Rev E* 85(2):026208
62. Minati L (2015) Remote synchronization of amplitudes across an experimental ring of nonlinear oscillators. *Chaos: Interdiscip J Nonlinear Sci* 25(12):123107
63. Bakker R, Wachtler T, Diesmann M (2012) Cocomac 2.0 and the future of tract-tracing databases. *Front Neuroinform* 6:30
64. Niebur E, Schuster HG, Kammen DM (1991) Collective frequencies and metastability in networks of limit-cycle oscillators with time delay. *Phys Rev Lett* 67(20):2753
65. T Gili, V Ciullo, and G Spalletta (2018) Metastable states of multiscale brain networks are keys to crack the timing problem. *Front Comput Neurosci* 12
66. K Bansal, JO Garcia, SH Tompson, T Verstynen, JM Vettel, SF Muldoon. Cognitive chimera states in human brain networks. *Sci Adv* 5(4):eaau8535, 2019
67. Forrester M, Coombes S, Crofts JJ, Sotiropoulos SN, O'Dea R (2020) The role of node dynamics in shaping emergent spatial functional connectivity patterns in the brain. *Network Neurosci* 4(2):467–483

Chapter 8

Biophysics of Consciousness: A Scale-Invariant Acoustic Information Code of a Superfluid Quantum Space Guides the Mental Attribute of the Universe



Dirk K. F. Meijer, Igor Jerman, Alexey V. Melkikh, and Valeriy I. Sbitnev

1 The Challenges in Current Consciousness Studies

Before we delve into a spectrum of theories that have been proposed to find some solid grounds for the understanding of consciousness, it stands to reason to try to obtain a better overview as to the largely varying definitions that have been put forward for this phenomenon. First of all, as is crucial in scientific endeavor, we should formulate a proper question in this respect, since this alone could bring a part of the required solution. So, what do we really want to know on this very subject? It is quite evident that in the past, a large part of the scientific community, the item of discussing consciousness was unpopular, since it was regarded as a nonpalatable item that easily escapes pure scientific treatment and even adequate philosophical reasoning. At best, it was seen as a subject of metaphysics since it touches upon subjective perceptions or even esoteric reasoning of a diffuse subject

D. K. F. Meijer (✉)

University of Groningen, Groningen, The Netherlands

e-mail: meij6076@planet.nl

I. Jerman

Bion Institute, Ljubljana, Slovenia

A. V. Melkikh

Ural Federal University, Yekaterinburg, Russia

V. I. Sbitnev

St. Petersburg B.P. Konstantinov Nuclear Physics Institute,
Kurchatov NRC, Gatchina, Russia

Department of Electrical Engineering and Computer Sciences,
University of California, Berkeley, USA

Proper mind set for consciousness studies ?

-Most people definitely prefer the permanence of a problem they cannot explain, to an explanation they cannot understand (Balfour)

-The difficult part is not knowing the truth, but replacing it with error (Haeckel).

-The biggest problem is not what we do not know, but what is not true in what we are certain to know (Mark Twain)



Fig. 1 Warnings in the scientific endeavor in consciousness studies

with ever vanishing horizons. Thus, the proper mindset of mainstream scientists was often quite preoccupied and exhibited mild forms of spaceflight [see a treatment of the science process perse in Meijer [1–3] (Fig. 1)].

Yet, there was a remarkable paradigm change in the last four decades in which it was envisioned that executing science can only be realized by *having* consciousness and that deeper penetration into the fabric of reality requires a better understanding of what we are ourselves. Scientific endeavor clearly should be conceived as a product of our consciousness in which, in fact, we, as a part of nature investigate another part in full detail [4]. While consciousness can be simply described as everything that you experience, or better as sentience of awareness of internal and external existence, it was often solely pictured as a product of brain activity. This especially in studying the neuronal correlates of consciousness defined as the minimal neural processes jointly sufficient for any specific conscious state. However, it should be stressed here that we should clearly distinguish here between *consciousness versus self-consciousness*, the latter being coupled to reportability, intentionality, and introspection, thereby introducing a virtual distance or rather an additional dimension.

Through the famous “observer effect” in quantum physics, a special place was inferred for consciousness, as being instrumental in the collapse of the wave function and soon the so-called “idealistic” variant among the many interpretations of quantum physics was conceived (see [5] and later [6–8]). Here, the picture was drastically reversed: human consciousness now was perceived as an integral part of a supposed universal consciousness or knowledge field. The concept of a Universal Knowledge Field was previously framed as Universal Consciousness, Cosmic Consciousness, Universal Mind, Universal Memory, Universal Intelligence, Holographic Memory, Collective Consciousness, Implicate order and the Plenum, among many other terms. Thus, the concept that information can take a universal character, implying that all information is present in a general knowledge field was earlier treated from a number of backgrounds and perspectives [2, 4]. This was often regarded as being

related to the concept of the Bohmian implicate order [9]. In the present framework, the *evolutionary* aspect of consciousness was included, connected to the idea that it is expressed, not only in all living matter but even in non-animate material (panpsychism).

Consciousness was earlier defined by us as “a state of a semi-stable system that has developed in a cooperative and cyclic operating mode so that it has become “causally self-observant” [1]. Thereby, consciousness can not only predict aspects of the local environment but also can integrate memorized information and future-directed projections into a personal worldview that serves individual survival, development, and social communication [10, 11]. Rovelli [12] made clear that Darwin’s theory offers how function and purpose can emerge in biology, but falls short in bridging the gap between physics and meaning. He emphasized the aspect of *meaningful information* by postulating: Meaning = Information + Evolution. Yet, is meaning not rather a mental modality? We postulate that the mental aspect of consciousness is closely related to the fundamental aspect of information. It addresses the question of how mental experience arises through a physical basis and how we can experience archetypes, memes, and subjective qualia (the latter framed as the hard problem in consciousness studies by Chalmers [13]). Pereira and Ricke [14] defined consciousness as both arising from the integration of information (resembling the later important attempt of quantifying consciousness by Tononi et al. [15]) and regarded consciousness as taking part in dynamic action/perception cycles in natural, social and cultural environment. Thus, information integration also requires information *differentiation* in order to become meaningful for life.

Information about the outer world travels the optic pathways of cranial nerves and brain: 3 lb in weight, 2 billion neurons, and upwards of 500 trillion synapses. What is thought to be the likely neural correlate of consciousness today? Neuroscience assumes that, in humans, the cerebral cortex is the “seat of consciousness,” while the midbrain reticular formation and certain thalamic nuclei may provide gating and other necessary functions of informing the cortex and vice versa. However, even if we could describe the function of every neuron, the enigma would remain. Is a subjective phenomenon explainable by science, “which aims at nothing but making true and adequate statements about its object”? How can one be objective about the subjective?

Today, it is thought that seven salient features of human consciousness exist [16]:

1. Consciousness involves short-term memory.
2. Consciousness may occur independently of sensory inputs.
3. Consciousness displays steerable attention.
4. Consciousness has the capacity for alternative interpretations of complex or ambiguous data.
5. Consciousness disappears in deep sleep.
6. Consciousness reappears in dreaming, at least in muted or disjointed form.
7. Consciousness harbors the contents of several basic sensory modalities within a single unified experience.

A current idea is that some communicating systems may connect areas of the cerebral cortex to the intralaminar nucleus of the thalamus. Ascending and descending pathways spread out to form a large recurrent network, being instrumental in storing short-term memory. Llinás used magnetoencephalography and found 40-Hz neural oscillations all over the cerebral cortex. Most interesting is the fact that this “oscillation pattern” *was phase related as if all the neurons were guided by a common orchestral conductor*. During normal consciousness, the 40-Hz activity was overlaid with non-periodic variations. During sleep, the 40-Hz oscillations continued at minimal amplitude and the thalamic neurons were inactive. Furthermore, during rapid eye movement sleep, the activity returned but was not correlated with changes in the environment. Of note, bilateral damage to the intralaminar nucleus of the thalamus produces profound and irreversible coma, but large areas of the cerebral cortex may be destroyed without consciousness being lost. In a review of visual consciousness, Zeki and Bartels [17] suggested the existence of brain nodes belonging to different parallel processing systems. Microconsciousness may occur within, and normal visual perception results from the binding together of these nodes. Yet, anatomical evidence fails to demonstrate any final integrator station in the brain.

Higher planes of consciousness may have to do with the ability to generate ideas, which are not directly related to existing levels of knowledge (intuition, serendipity, channeling), that ultimately can transform our societies hopefully to more advanced levels of civilization. Therefore, we should improve our insight into the mechanisms that underlie consciousness, not only by penetrating into its biological nature but also taken into account its inherent cosmic connections.

In this review, an attempt is made to integrate the various concepts of the authors in a comprehensive treatment of the physics of consciousness, realizing that life in the cosmos cannot exist without fine-tuned collective modality of information.

2 The Fundamental Character of Information

The observable universe consists fundamentally of matter, as we observe it directly, in addition to energy and information. Information should be conceived as a central aspect of the increasingly complex biological and cultural evolution. Information can, in the first instance, be understood as a form of ordering linked to pattern recognition [18]. In biological and cultural evolution, information takes on a broader meaning with its design, processing, and dissemination. Information can be transferred in different ways and levels. In the living cell, these are chemical and electrical signals, but also specific spatial forms (proteins, DNA) and also the sequence of their building blocks (for example the nucleotides in DNA). At the level of human communication, there is transfer in the form of wave and vibration patterns (in light and sound) or electromagnetic waves (in radio, telephone, TV, and cosmic background radiation). Information transfer not only involves complex patterns, but also specific sensors for them. Information only becomes meaningful after reception, perception, and representation. An important question in this context is how the very diverse information

that reaches our brains through our senses (sensory) or in an extrasensory manner, and how it is selected, stored and then transferred again [18, 19].

The universe, as it appears to us, seems to be ingeniously constructed and therefore, from ancient times, was regarded as a “symphony of vibrations”. The basis of this is a very specific system of nature constants that must have an exact value: the symphony therefore may have a mathematical foundation! The origin of life, and also of the appearance of man, appears to have been precisely adjusted, a minor deviation in each of the 25 nature constants established would have made the creation of biological life impossible! [20]. This includes macro-parameters such as the distance from the Earth to the sun (light and temperature), the influence of the moon (life cycles), and the position of our solar system in the Milky Way (shielded from the large black hole in the center!).

Perceived in an anthropic context, life had to develop in this Universe in such a way that it produced intelligent life and thus created its own observers: we humans! This is called the “Anthropic principle”: man exposed the laws of nature, but in fact discovered the underlying processes of biological evolution. In fact, you could say that we humans are part of a universal system of information, and this Universal consciousness may act as the program on which our universe runs! [2, 20]. Where did this exact and coherent information actually come from? It is good to realize that, according to the second law of thermodynamics, the Universe is subject to entropy: the continuous process of decay from order to less order and greater chaos. This implies that more and more information is needed to describe the Universe (order is described more simply than disorder and chaos [18]). At the same time, certainly in our part of the Universe, there is the opposite process known as negative entropy also called neg-entropy or syntropy. The very process of science as it arose from intelligent life, in fact, creates an ever-progressing organizational process of compressing and organizing information [4]. An example of this is the formulation of laws such as the natural laws and in a more biological context, the coherent organization of life processes in cells and organisms. The contemporary pursuit of a “Theory of Everything” would represent an extreme example of information compression. In fact, such a theory does not really imply a *reduction* of information but rather a *better overview and insight* into the information in question! In this respect, some see evolution as an unfolding of ordered information, in addition to bringing together increasingly complex information through supposed “emergent” processes [21–23].

Can information be reduced to matter/energy, and return us to only those single elements, or can energy and matter be defined as modalities of information? Matter and energy were once considered two separate and distinct elements until Einstein proved they were the same thing as expressed in the $E = mc^2$ equation. Using Einstein’s established mass-energy equivalence formula, the relationship between the frequency of light and photon energy, which is observed in the photoelectric effect displayed a maximum rate at which any system can compute based on $E = mc^2$, 2×10^{47} bits/s/g (Fig. 2).

Information is a form of energy [24, 25]. It was elegantly demonstrated that information can be converted to energy [26, 27]. Toyabe and colleagues observed

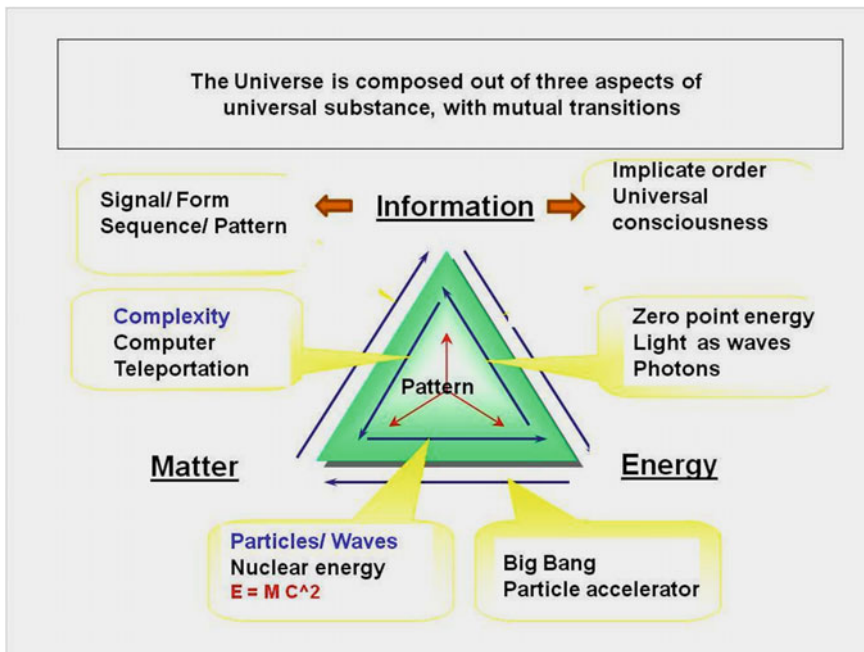


Fig. 2 The triad of energy/matter/information [18]

this energy-information equivalence by varying an electric field so that it represents a kind of spiral staircase. The difference in electrical potential between successive steps on the staircase is kT , meaning that a thermally fluctuating particle placed in the field will occasionally jump up a step but more often than not it will take a step downwards. What the researchers did was to intervene so that whenever the particle does move upwards, they place the equivalent of a barrier behind it, preventing the particle from falling beyond this point. Repeating the process allows it to gradually climb the staircase. The experiment consisted of a $0.3 \mu\text{m}$ -diameter particle made up of two polystyrene beads that were pinned to a single point on the underside of the top of a glass box containing an aqueous solution. The shape of an applied electric field forced the particle to rotate in one direction or, in other words, to fall down the potential energy staircase. Buffered by the molecules in the solution, however, the particle every so often rotated slightly in the opposite direction, allowing it to take a step upwards.

Evolution of our universe gave rise to the processing of the abovementioned, three building blocks, that are currently described in the plethora of elementary particles in the so-called “standard model” and, in more general terms, as waves/particles in quantum physics. The interactions of subatomic waves/particles subsequent to the Big Bang created a dynamic network of quantum information that finally also enabled the formation of highly complex macromolecular structures. The history of these particular wave/particle interactions is supposed to be stored in an all-pervading

quantum field, as it was inherited from the initial information matrix [28]. Each step in the unfolding evolution implied an inherent potential for change and, ultimately, the ability to generate biological life.

Generally speaking, the concept of information seems closely related to notions of news, constraint, communication, control of data, form, instruction, knowledge, meaning, mental stimulus, repeating patterns, perception of experience, as well as representation of observations and pattern recognition [18].

Since “Information”, is often no more than a container term, it seems important to differentiate information in its very nature into, at least, four interrelated layers:

- a. **Intrinsic** physical information, such as the microphysical properties of the constituent elementary particles and, for instance, the basic genetic information;
- b. **Observed** (measured) information: the type of information that is produced in our brain and represents explicit information that was extracted from nature, and subsequently translated and stored as scientific representations, percepts, concepts and/or models;
- c. **Cultural** information, that is, for example, processed in socio-cultural publications, internet, and other media, by which it obtains the significance of societal meaning;
- d. **Sub-numinous** (mostly non-conscious) information that extends to feelings, qualia, intuition, and subjective human experience and that is only partially explicit in category B.

The verb “to inform”, as employed in the common daily language, can be originally related to the expression “to model according to a form”. In fact, “to inform” derives from the Latin term “in-form are”, that means “to give a form”. Aristotle wrote: “Information” (*translated in current terminology*) is a truly more primitive fundamental activity than energy and matter. So this seems to imply that information does not have an immediate meaning, such as the word “knowledge”, but rather it encompasses a modality that precedes every physical form. But how is information organized and integrated into nature? Although a reductionist scheme on the dynamic flow of information in nature from the micro to the macro-scale, seems intellectually satisfactory, such a scheme evidently lacks the aspect of integration and consistency that enables nature to act as a whole at the different levels indicated.

The unfolding and creation of information, as well as the processing of it, can be pictured as an act of composing symphonic music: in addition to the interpretation by the maker and the musicians, it obtains significance through the subjective emotion of the listener. Unfolding can also be pictured as the growth of a huge tree from an extremely small seed (a priori information) that unfolds during maturing. During the growth of the tree, intrinsic (morphogenetic) information is used and new information is collected from the environment, resulting in steadily rising complexity as well as modulation of the basic recipe, resulting in the manifestation of life and survival.

The increasing complexity in nature was earlier defined as a neg-entropic [29] or as a syntropic process [30, 31]. This phenomenon is partly explained by, so-called, “emergent” processes in which completely new properties are claimed to arise spontaneously from building blocks that themselves do not display that particular

property. An often-used example is the wetness of water that, according to this theory, cannot be derived from its building blocks: the very nature of H₂O molecules. However, one could argue that the well-known electrical dipole of the water molecule largely predicts its ordering within the water fluid as well as its behavior on surfaces [32, 33]. For this, and other reasons, the physical background and proof of emergent phenomena are presently debated. In general, supposed emergent processes are often an explanation in retrospect and adequate models to predict emergent phenomena remain to be developed. Alternatively, the induction of novel complexity in time can be seen as a process of “backward causation”. Two different mechanisms may play a role here [34, 35]. Ellis treated the theoretical potential of backward causation (also called retrocausality), while Aharonov’s team experimentally showed retrocausal effects in so-called soft stimulation quantum measurement.

A universal information field also has been connected to the phenomenon of a time-reversed flow of antimatter, that started through symmetry breaking and quantum fluctuation in the quantum vacuum at the Big Bang, following the process of creation of matter/antimatter as related to particle symmetry (see Vannini [30, 31]). The energy/momentum/mass equation states that, following the Big Bang, there was exactly the same amount of matter and antimatter. A major question that physicists ask is: why do we live in a universe mostly made of matter and what has happened actually to antimatter?

If we accept the negative, backward in time, solution of the energy/momentum/mass equation as valid (see Fig. 3), antimatter is described as moving backward in time. As mentioned above, at the moment of the Big Bang, the same amount of matter and antimatter was created. In the concept of Vannini, [30, 31] antimatter immediately started to move backward in time, while matter and energy started to move forward, avoiding any interaction and annihilation.

Consequently, according to this equation, the universe consists of the same amount of matter and antimatter. Yet, these two aspects of reality move in opposite directions that come into contact only indirectly through a supposed central point of time reversal (see Fig. 3). More recently, Boyle et al. [36], proposed that the present universe, after the Big Bang, is the CPT (charge parity-time) mirror-image of the universe before it. They submit, in fact, that at the Big Bang a universe-anti-universe pair was created that explains the relative lack of antimatter (baryon asymmetry) in our universe, suggesting a perfect vacuum isometry under time reversal (see Fig. 3). This idea is also compatible with the boundary conditions that are responsible for the quantum fluctuations seen in the acoustic oscillations of the CMB power spectrum. The presence of matter-antimatter asymmetry in our early universe has been experimentally shown by finding a distinct time reversal violation in the behavior of subatomic particles in so-called pear-shaped nucleus of rare isotopes [37]. The item of negative matter and energy in cosmology was recently discussed by Chang [38], in relation to cosmic inflation, gravitation, and Higgs mechanism.

According to this interpretation, all that is divergent is governed by the laws of entropy, whereas all that is convergent is governed by the law of syntropy. The energy that comes from the future (syntropy) is differentiated and is assumed to be structured in the form of complex attractors, that are hierarchically organized and articulated,

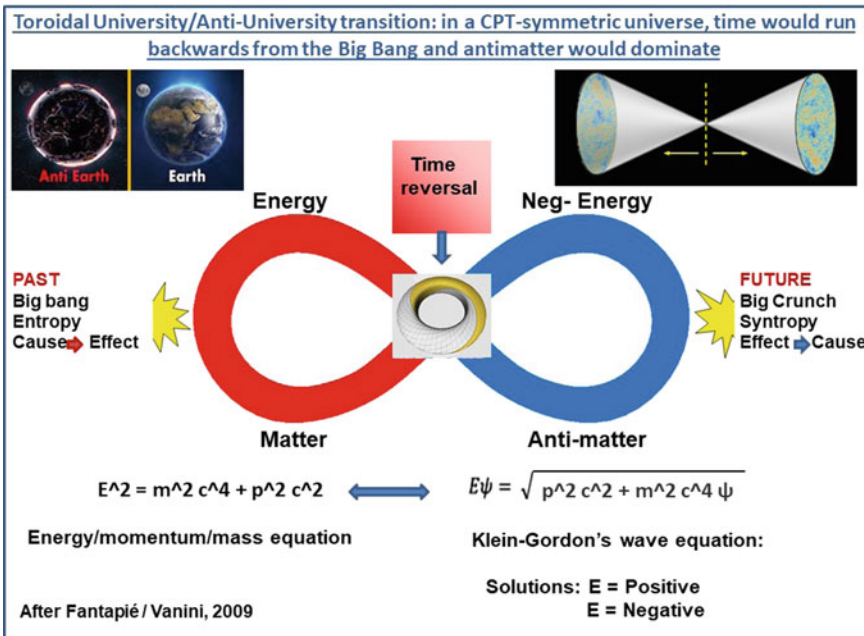


Fig. 3 Graphical representation of the cosmological interpretation of the energy/momenta/mass equation (after Vannini [30, 31])

with their starting point in the “Big Crunch” (see also Fig. 41). Life may, in this manner, be a physical manifestation of these attractors and would represent the organization of a supposed transcendental universe. Since a final Big Crunch is implicit in this theory, a cyclic model of birth and death of our universe is implied (see sect. 9). Consequently, in this model, that includes a transcendental domain, different parts of the brain can, non-locally, decode messages from other distant parts of the universe, without having to wait for classical electrical and chemical signal keys for sensory input and motor output, that move slower than light. The particular (coherent order) parameter landscape is phase- and amplitude-locked into the distributed pattern of the electrical and chemical signals in a set of creative feedback control loops. According to this theory, the imprinting action of the electrical and chemical signal patterns on the postulated, intrinsically mental, landscape can thereby induce our inner conscious qualia and explains the “binding phenomenon” that enables the conscious mind to induce an undivided wholeness.

Bidirectional time was also highlighted in the theory of Vannini as treated above. On the basis of the original work of Fantappiè, as early as 1931, Vannini [30, 31] proposed the following: In 1925, Oskar Klein and Walter Gordon formulated a probability equation which turned out to be very instrumental in quantum mechanics. In 1926, Schrödinger simplified Klein–Gordon’s equation in his famous wave equation

(ψ) in which only the positive solution of Klein–Gordon’s equation was considered, which treats time in an essentially classical and unidirectional way, with a well-defined before and after the collapse of the wave function. In 1927, Klein and Gordon reformulated their Eq. (2) again as a combination of Schrödinger’s wave equation (quantum mechanics) and the energy/momentum/mass equation of special relativity (1). (see [30, 31] and Fig. 3).

$$\begin{aligned} E^2 &= m^2 c^4 + p^2 c^2 \\ \text{Energy/moment/mass equation} \end{aligned} \quad (1)$$

where E is the energy of the object, m the mass, p the momentum, and c the constant of the speed of light ($p \geq 0$).

$$\begin{aligned} E\psi &= \sqrt{p^2 c^2 + m^2 c^4}\psi \\ \text{Klein-Gordon's wave equation} \end{aligned} \quad (2)$$

The Klein–Gordon wave equation depends on square root and, in principle, yields two solutions (Eq. 2 and Fig. 3): the positive solution describes waves which diverge from the past to the future (retarded waves); the negative solution describes waves which diverge from the future to the past (advanced waves). Yet, the negative solution seemed to introduce the final causes and teleological tendencies in science. Therefore, traditional scientists considered it to be unacceptable. However, these ideas were challenged through the discovery of the particle/antiparticle symmetry. The antiparticle of the electron was experimentally observed in 1932 by Carl Anderson in cosmic rays and was named positron. Thereby Anderson became the first scientist to prove the existence of the negative energy solution and this concept, subsequently, was no longer a mathematical absurdity. The Dirac equation also predicted a universe made of matter which moves forwards in time and antimatter which moves backward in time (see Fig. 3).

In computational science, this is called “forwards and backward chaining” in which one can determine both backward (following inheritance) and forwards as to what an object represents. The concept of time symmetry versus our common linear perception of the time invited further considerations on the very nature of consciousness. The duality of time, that started with Dirac’s famous equation of the electron, has been used more recently by King to describe his concept on brain structures [39, 40]. King stated that these structures face continuous bifurcations which derive from the encounter of information which comes from the past (diverging waves, causes) and information that comes from the future (converging waves, attractors).

A number of earlier considerations underline the concept of a bidirectional character of time:

- According to Wheeler and Feynman’s [41] electrodynamics, emitters coincide with retarded fields, which propagate into the future, while absorbers coincide with advanced fields, which propagate backward in time. This time-symmetric

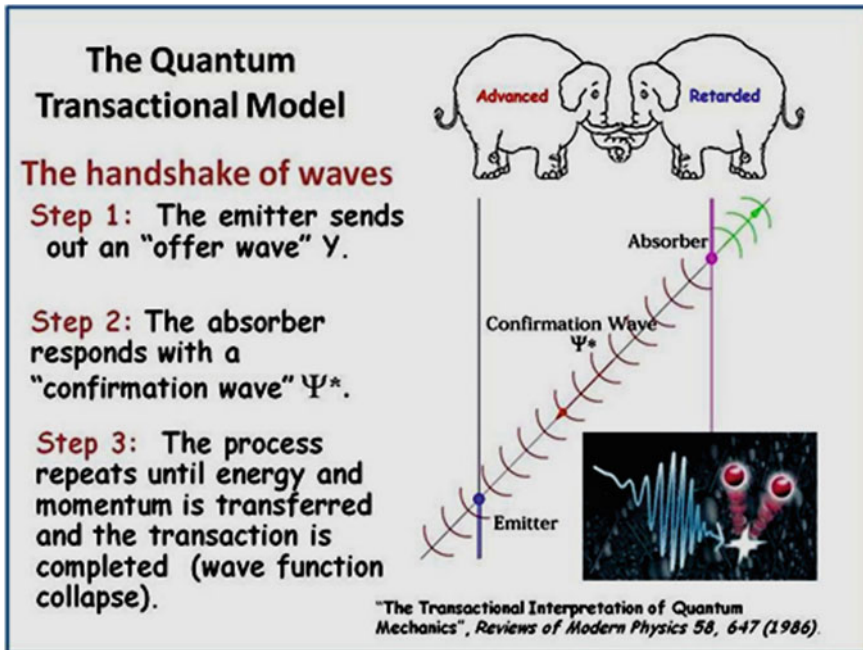


Fig. 4 The Transactional interpretation of Quantum mechanics by John Cramer

model leads to predictions identical to those of conventional electrodynamics. For this reason, according to these theories, it is impossible to distinguish between time-symmetric results and conventional results.

- In his *Transactional Interpretations of Quantum Mechanics* (see Fig. 4), Cramer [39, 42] stated that:

“Nature, in a very subtle way, may be engaging in backwards in time handshaking” (see also above). “The transaction between retarded waves, coming from the past, and advanced waves, coming from the future, gives birth to a quantum entity with dual properties of the wave/particle. Thus, the wave property is a consequence of the interference between retarded and advanced waves, and the particle property is a consequence of the point in space where the transaction takes place. The transactional interpretation requires that waves can really travel backwards in time. This assertion seems counterintuitive, as we are accustomed to the fact that causes precede effects. It is important to underline, however, that unlike other interpretations of QM, the transactional interpretation takes into account special relativity theory which describes time as a dimension of space, as mentioned earlier. Of note, the completed transaction erases all advanced effects, so that no direct advanced wave signaling is possible: The future can affect the past only very indirectly, by offering possibilities for transactions” [39, 42].

Aharonov's team and various collaborating groups [34, 43], studied whether the future events can influence the past, by sophisticated quantum physics technology. Aharonov concluded that a particle's past does not contain enough information to fully predict its fate, but he wondered if the information is not in its past, where could it be? After all, something must regulate the particle's behavior. In 1964, Aharonov, then in New York, proposed a new framework called time-symmetric quantum mechanics. Quantum experiments in about 15 other laboratories around the world seem to actually confirm the notion that the future can influence results that happened before those measurements were even made. Generally, the protocol included three steps: a "pre-selection" measurement carried out on a group of particles; an intermediate measurement; and a final, "post-selection" step, in which researchers picked out a subset of those particles on which to perform a third, related measurement.

To find evidence of backward causality, information flowing from the future to the past, the effects of, so-called, weak measurements were studied. Weak measurements involve the same equipment and techniques as traditional ones but do not disturb the quantum properties in play. Usual (strong) measurements would immediately collapse the wave functions in superposition to a definite state. The results in the various cooperating groups were amazing: repeated post-selection measurement of the weak type changed the pre-selection state, clearly revealing an aspect of non-locality.

Thus, according to Aharonov and associated research teams, it appears that *the universe might have a destiny that interacts with the past, in order to bring the present into view*. On a cosmic scale, this idea could also help explain how complex life arose in the universe against very high odds, supporting the idea that the required knowledge was inherited from a common information pool. It follows also that the idea that quantum uncertainty only is relevant for micro-events, but would not be important with regard to macro events, maybe incorrect). The implication would be that the particles that existed at the time of the early universe, were situated so precisely that, 14 billion years later, human beings would exist and scientists would be looking for the origin of life and even for a "theory of everything" (see also Barrow and Tipler [20]).

It was the Nobel laureate Wilczek [44], who claimed that fabric of reality comes about by *harmonic relations of discrete wave frequencies* displaying beautiful patterns, among others reflected in the color spectrum. Yet, knowledge on the discrete values of the crucial quantum wave frequencies at stake remained scattered, and it was a meta-analysis of biomedical literature, treated in the present paper, that revealed qualitative and quantitative properties. In relation to this, life processes should not only be related to aspects of genomics and proteomics but also to the inherent feature of electromics [45].

2.1 The Architecture of Reality in Relation to Information

The Construction of Reality, depicted in the diagram of Fig. 5, is presented as the unfolding of basic information, which, initially, was present in a quantum information field (black), which consisted of quantum energy, exhibiting an implicate and symmetric order. This field can also be seen as Universal consciousness, containing highly compressed information about all the available data from the present and the future (four-dimensional information from all-time). In the integral scheme in Fig. 5, the unfolding of this information is expressed in a “dual” process consisting of the following:

- the processing of wave information in a transcendental superfluid quantum space (left column);
- the unfolding of information in the 3-D organization of a material world (right column).

These separated processes do not imply the introduction of a kind of “Cartesian dualism”, because they are strictly correlated, assuming that any form of matter

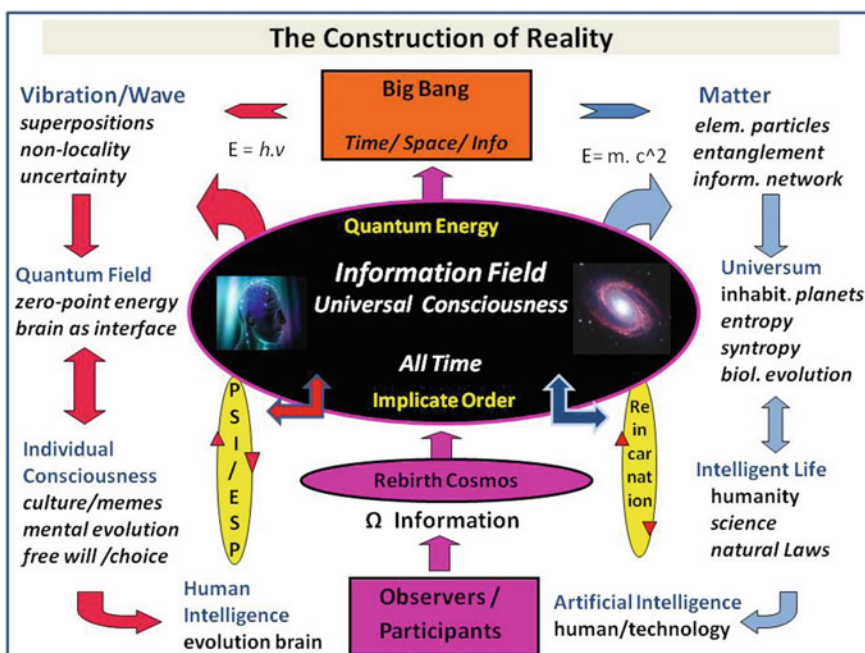


Fig. 5 An integrated scheme depicting the Construction of Reality, with its material (right part of the figure) and mental (left), aspects. This concept assumes a central quantum information field, that provides the very basis for creation of our universe and dynamically evolves further through cyclic feed-back processes from the present reality, in which natural (among others human) and artificial intelligence play crucial roles in observation and participation (see text for further explanation)

also contains mental information, as exemplified in the wave/particle principle, as a basis for the description of nature. More classically, this duality of substance was conceived as panpsychism (see [46–49]). Yet, in our view, Universal consciousness rather implies a dynamic field of information, with a continuous and bidirectional flow of generated information that originates from the entire universe, including our own world [2, 19].

Active information is also central in the work of Bohm [50, 9] with regard to his ontological interpretation of quantum mechanics in which a metaphysical view is coupled to the concept of an implicate order, implying that consciousness may supervene the material world [51]. The implicate order is seen as a configuration space with a guidance function that can express entangled states of a whole complex system, thereby containing more information than can be inferred from its individual parts only. The implicate order with its pilot wave function is, in this view, foundational for both matter and consciousness providing a link between mind and matter (neutral monism), in fact possessing a rudimentary form of mentality housed in a multi-dimensional qualia space. Bohm applied his concept of enfolding and unfolding of information in the context of listening to music. He pictured the series of notes as enfolded in our subconscious memory domain that then can mesh with a future, anticipated, series of notes that may be hidden, but can become unfolded in a total experience of musical awareness, collectively suggesting being part of a greater whole. Such a phenomenon may even play a role in the relation between meditation practice and neuroplasticity as a token of guiding psychokinetics.

Finally, at least one important question remains: if our Universe restarts itself through recurrent symmetry breaking, seemingly producing a division of mind and matter, what would be the potential role of information in this astounding process? It stands to reason that only the perspective for the evolution of intelligence afforded the *potential for the Universe to observe itself* in greater detail in a self-learning mode, [19].

3 The Generalized Music (GM) Biophysical Principle that May Underly Nature

The semi-harmonic EM frequency pattern found by Geesink and Meijer [52–57], was initially discovered by meta-analysis of 500 scientific biomedical publications and this pattern recognition was subsequently extended to a number of purely physical systems [55, 56, 58, 33, 59], in which he authors consistently found this frequency pattern in both animate and non-animate systems (Table 1).

For example, the particular EM frequency pattern was recently found in the electromagnetic frequencies that promote the degree of quantum entanglement (also called EPR effect), according to the famous thought experiment of Einstein, Podolsky, and Rosen [55] and in the frequency spectrum of all elementary particles in the “Standard model” of particles, (see further on in the text and in Geesink and Meijer [56]).

Table 1 In brackets (nr.): Reference to own publications: (1) Geesink and Meijer [52, 60]; (2) Meijer and Geesink [61]; (3) Meijer and Geesink [62, 1]; (4) Meijer and Geesink [1]; (5) Meijer and Geesink [63]; (6) Geesink and Meijer [55]; (7) Geesink and Meijer [56]; (8) Geesink and Meijer [58]; (9) Geesink, Jerman and Meijer[33], Geesink Meijer and Jerman, [32, 59]; (10) Geesink [64, 32]

Biophysical GM-principle in Animate and Non-animate Systems: EMF semi-harmonic frequency patterns	
Animate systems	Non-animate systems
- Biomedical research (1)	- Entanglement in EPR-experiments (6)
- Cancer research (2)	- Energy distribution elementary particles (7)
- Neurological studies *0	- Coherence behavior in superconductors (8)
- Albumin vibr. resonances *1	- Sound induced vibration patterns of Chladni, *4
- RNA synthesis catalysis *2	- Clays and Phyllosilicate semi-conductor materials (11) *5
- Brain function and Consciousness (3, 4)	- Zero-point energy EM frequencies *6
- Protein folding in intact cells (5)	- Gravitational waves *7
- Superconduction in life systems (8)	- EMF absorption Spectrum of pure Water (9)
- Oligo-nucleotides in solution *3	- Nucleotide sequence in DNA *8
- Ir-spectra of proteins, lipids, DNA (10)	

(nr): Own GM-scale papers *= EMF frequency values extracted from related international literature.
In brackets (nr.): reference to own publications : (1) Geesink and Meijer, 2016; (2) Meijer and Geesink, 2018a; (3) Meijer and Geesink, 2016; (4) Meijer and Geesink, 2017; (5) Meijer and Geesink, 2018; (6) Geesink and Meijer, 2018b; (7) Geesink and Meijer, 2018b; (8) Geesink and Meijer, 2019a; (9) Geesink, Jerman and Meijer, 2020; (10) Geesink, 2020; (11) Geesink, Meijer and Jerman, 2020
Supporting research of others: *0: Hamblin et al, 2017; *1: Nardeccia et al, 2017; *2: Ferris, 2006; *3: Tang et al, 2018; *4: Chladni, 1980; *5: Adamatzky, 2013/Hashizume, 2012; *6: Irikura, 2007; *7: Rezzolla et al, 2003; *8: Selvam, 2007

* indicates EMF frequency values that were extracted from related international literature: Supporting research by others: *0: Hamblin et al. [65]; *1: Nardeccia et al. (2017); *2: Ferris [66]; *3: Tang et al. (2018); *4: Chladni [67]; *5: Adamatzky [68], Hashizume [69]; *6: Irikura [70]; *7: Rezzolla et al. [210]; *8: Selfham [72]

These observations of series of discrete frequency values are fully in line with the theory of standing waves that arise from constructive interference of waves in a wave field, for example when a string is connected between two fixed points.

In quantum mechanics, these can only occur in very specific values (eigenvalues, in music that are tones!). If you want to represent these standing waves in relation to each other, you need the musical theory of harmonic resonance that was in fact already thought up by the ancient Greeks. These harmonic patterns occur throughout physics, for example in frequency values of the color spectrum and more recently in the vibration values of strings in the various versions of string theory (united in the so-called M theory). Wherever electromagnetic fields are applied, you can expect a “fit” with interference patterns from standing waves.

Combinations of EM waves form electromagnetic force fields, which according to classical physics are in fact composed of light particles (photons), but which can also be seen as light waves (within quantum physics). These wave/particles have very different energy and so their vibration values (frequencies) are also very uneven. The

discrete frequencies are directly related to the frequencies and are easy to calculate from the known equations of Einstein and Planck, at least if the relevant energies are known from the literature:

$$E = mc^2 = h\nu \text{ (cf. 1)}$$

(E: Energy; m: mass; c light velocity; h: Planck's constant; ν: frequency).

This means that for a given energy, the frequency depends on the mass and that for a given mass, energy and frequency are related. If the mass follows a quantized scale (because it consists of quantized particles), it follows that the frequency also follows a similar scale [56]. Unfortunately, the current quantum mechanics (QM) theory is currently strong against the interpretation of Bohr and Heisenberg (1925), who assumed that the theory mainly indicates the *probability values* of a quantum state (the so-called uncertainty principle) and not its actual form. Geesink and Meijer [54] concluded, however, that quantum states appear to be partly determined and certainly adopt discrete values. Realizing that Einstein once said that “God does not play dice” seems to be confirmed by the present data.

3.1 The Mathematical and Music-Theoretical Basis of the GM-Scale

In their concept, Geesink and Meijer [52], used a 12-layer system (a so-called octave, see Fig. 7), also known from music theory, for the representation of the frequency band pattern, with the value of 1 as the first number. Why this reference value? You can easily calculate it via the meta-analysis of the biomedical studies and also the various physical experiments done by the authors (the analysis of EPR experiments, elementary particles, or superconductors). For example, if you take the measured discrete energies in the EPR wave/particle entanglement experiments, it turns out that there are also 12 discrete energies and equivalent octaves. Planck has found the Planck constant, so divide this series of energies by this constant, and you end up at 12 discrete frequencies, and octaves thereof. The first frequency is then exactly at 1 Hz. So not difficult. The frequencies are easy to calculate with an equation known from music theory, which was in fact already known to Pythagoras.

The full scale of frequencies is therefore much more extensive than the core region of 12 frequencies: connecting uniform scales with either a higher frequency range or lower values can be easily calculated by multiplying the series of 12 by two or dividing it by two. This gives you a total range in the range of Hz, Kilo-Hz, Mega-Hz, Giga-Hz, and Tera-Hz that runs from 0.2 Hz to 500 THz. The so-called far-infrared (Terahertz) area is also important here because these are central to the Einstein Podolsky Rosen (EPR) experiments (see Fig. 6).

It should be realized that this frequency pattern reflects experiments in which the life systems were exposed to *external* EMF radiations, but it became clear to us

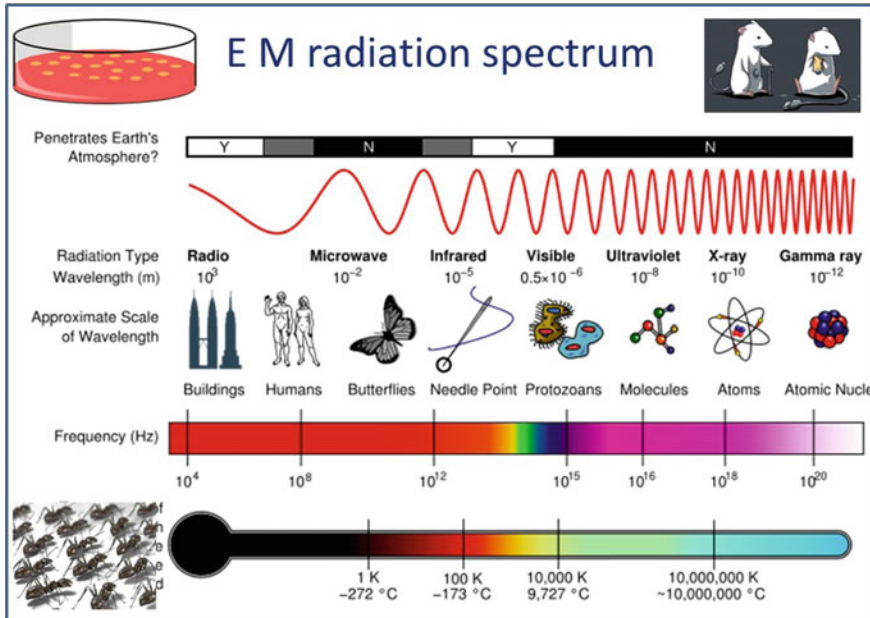


Fig. 6 The electromagnetic frequency spectrum of externally applied EMF radiation in cell lines, and various animal species (see insets)

that the *external* frequencies resonate with *endogenous* EM frequencies, long postulated by Frölich (1968). We inferred therefore that the experimental coherent EMF pattern is effective because it mimics *internal* oscillations within the organism and its constituting cells. In other words, such radiations act through resonant communication, as extensively discussed in literature by many other authors [45, 64, 73] (Hammerslag et al. 2016). Our studies should, therefore, be seen in the light of the rapidly expanding areas of *Biofield Research*, including that of *Quantum Biology*, as adequately reviewed by Huelga et al. [74–76], Marais et al. [77, 78].

A later, more detailed, mathematical analysis [54] shows that the derived arithmetical scale exhibits a sequence of unique products of integer powers of 2, 3, and a factor $\sqrt{2}$. These discrete eigenfrequency values can be related to supposed bio-resonance of solitons or polaron quasi-particles in life systems. Bio-solitons are conceived as self-reinforcing solitary waves, that constitute local fields, being involved in intracellular geometric ordering and patterning, as well as in intra- and intercellular signaling. The discrete pattern of EM wave frequencies is mathematically expressed as follows:

$$E_n = \hbar\omega_{\text{ref}} 2^n 3^m (2^p)$$

E_n : Energy distribution, ω_{ref} : Reference frequency 1 Hz, \hbar : Reduced Planck's constant,

n : Series of integers: 0, 0.5, 2, 4, 5, 7, 8, -1, -3, -4, -6, -7,

m : series of integers: 0, 1, 2, 3, 4, 5, -1, -2, -3, -4, -5,

p : Series of integers: <-4, -4, -3, -2, -1, 0, 1, 2, 3, 4, 5, 6, > +52).

The complete range of EM frequencies (lying between 0.2 Hz to 500 THz, see Geesink and Meijer [52, 60]), on basis of the 12 core frequencies, is depicted in Fig. 7. See for statistical analysis and validation of the frequency pattern the recent paper of Sonderkamp et al. [79]. The entire fractal frequency band pattern can be easily calculated by expanding to lower and higher frequency ranges by multiplication or division by a factor 2. This provides an octave hierarchy of self-similar extensions of the scale. Multiplying this value with the octave hierarchy of 2, up to the THz range (10^{12} Hz), a range can be found where the biophysics of ordering of water molecules, relevant for life conditions, is at stake [33]. It is of interest that the boundaries of the GM frequency spectrum, lies in the far-infrared EM region, that occupies a middle ground between microwaves and infrared light waves, known as the "terahertz gap". Tera-Herz EMF frequencies take a special position in the frequencies of life [80], as well as in the treatment and detection of diseases [81]. Interestingly, infrared frequencies have recently been related to long-range universal metric fluctuations near null surfaces in the entire cosmos. Very similar harmonic quantum oscillation phenomena, including an identical mathematical background, were independently found earlier in fractal and global scaling concepts of Muller [82], Thut [83], and recently discussed in the framework of quantum coherence in life conditions by [84]. These scale-invariant space-time fluctuations may have a longitudinal character, and on the Planck level, may even explain quantum gravity in a holographic context [85].

The Fröhlich/Davydov concept [86–89] on soliton influence on protein vibration has been elaborated and further improved by Pang et al. [88], taking into account that solitons can be largely stabilized, and their life-time increased due to mutual

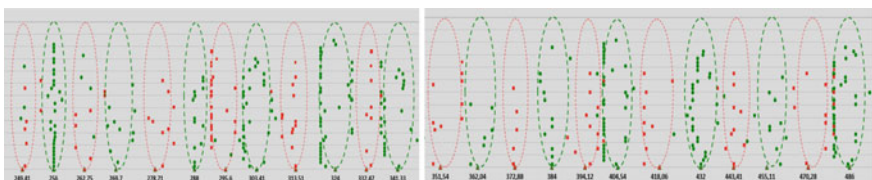


Fig. 7 Measured frequency data of living cell systems that are life-sustaining (green points) and detrimental for life (in red squares) versus calculated normalized frequencies. Biological effects measured following exposures or representing endogenous effects of living cells in vitro and in vivo at frequencies in the bands of Hz, kHz, MHz, GHz, THz, PHz. Green triangles plotted on a logarithmic x-axis represent calculated life-sustaining frequencies; red triangles represent life-destabilizing frequencies. Each individual point in the graph is taken from published biological data and represents a typical frequency employed in one of the reported biological studies. For clarity, points are randomly distributed along the Y-axis

interaction of the particles with lattice vibrations. The important point here is that the soliton transport should be regarded as a concerted action of both the vibration of the quasiparticle and that of the protein backbone lattice in interaction. Solitons/polarons, as quasiparticles, are widely observed physical phenomena that behave like solitary waves but possess many features of particles. They are able to suppress an harmonicity (the deviation of a system from being a harmonic oscillator) by the excitation to higher quantum levels, a process that facilitates the crossing of potential barriers and the transfer of a molecule to a new conformational state [53, 61, 90].

If we come to contemporary life, we may say that each living cell is radiating or resonating in the field of coherent EM energy coupled to its biochemical substrate. If each cell is emitting such a field, then the whole living system is, in effect, a resonating field, being a ubiquitous nonlocal field. Moreover, since biophotons are the entities through which the living system communicates, there exists a near-instantaneous intercommunication throughout the organism. And this, claimed Popp et al. [91, 92], is the basis for coherent biological organization, referred to as quantum coherence. This discovery led Popp to state that the capacity for evolution rests not only on aggressive struggle and rivalry but also on the capacity for communication and cooperation. In this sense, the built-in capacity for species evolution is not based on an individual, but rather on living systems that are interlinked within a coherent whole: living systems are thus neither only subjects, nor are they isolated objects, but simultaneously, as subjects and objects, function in a mutually communicating universe of meaning in a quantum domain [93, 63, 94].

These relatively new developments in biophysics may imply that all biological organisms are constituted from a liquid crystalline medium, whereby body cells are involved in an instantaneous fractal communication via the emittance of biophotons. Furthermore, DNA itself may act as a liquid-crystal, lattice-type of gel-structure. This implies that all living biological organisms continuously emit light, although in an ultra-weak manner, which thereby forms a coherence field for live communication [89].

3.2 *EMF-Guided Three-Dimensional Protein Folding*

Recently, the potential long-range resonant influence was further worked out in a study of three-dimensional protein folding in the intact cell [61, 63, 95]. This process can be largely influenced by the formation of coherent oscillation domains in the cell water interacting with the protein backbone (Fig. 8).

We argued in earlier work that the current geometric and thermodynamic approaches in protein folding studies do not provide a definite solution to understanding mechanisms of folding of biological proteins in the whole cell. A major problem in the understanding of this process is that the protein is first synthesized as a linear molecule that subsequently must reach its native configuration in less than 1 s [90].

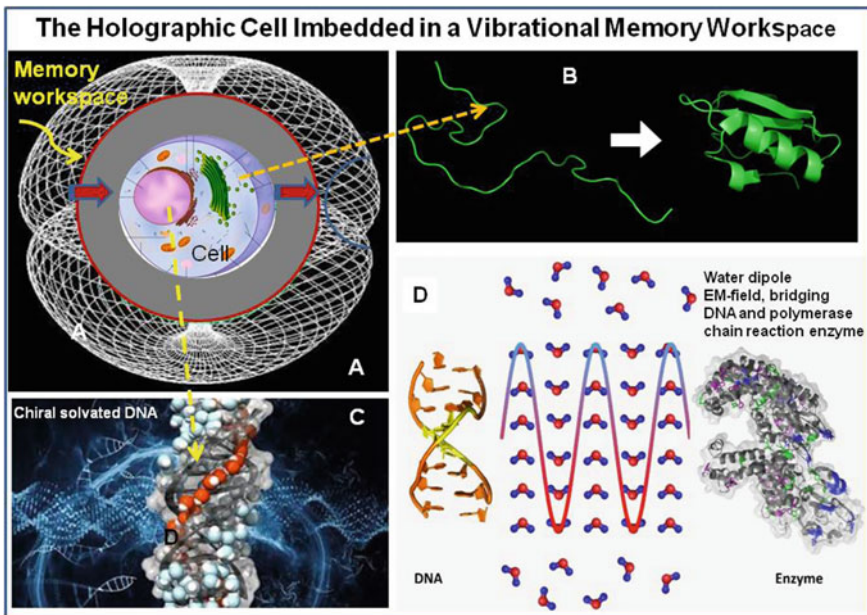


Fig. 8 The life cell in a toroidal setting showing a holographic memory workspace called event horizon (red circle in **a**), that contains information for cell function and survival in the particular environment (**a**, upper inset left), guiding 3-D protein folding (**b**), wave resonance of DNA with associated water (**c**). Structured water-dipoles in coherent state provide an information imprint that stably stores DNA-polymerase chain reaction activity (after [96])

3.3 Superconductive Conditions in Animate and Non-animate Systems

Our recent meta-analysis of the data of different superconductors gaps/frequencies from 1981 to 2018 [58] revealed that the reported values can be positioned on GM-pointer states and fit with the derived equation of coherent frequencies: an adapted Pythagorean scale. The discrete values of these frequencies, thus, could again be positioned on a reference coherent THz-scale, that is expressed in 12 discrete coherent reference THz-frequencies:

1.0995, 1.1583, 1.2370, 1.3031, 1.3915, 1.4660, 1.5549, 1.6493, 1.7376, 1.8554, 1.9547, 2.0873 Thz

As pointed out in our earlier studies [95, 62], both lattice and wave conditions are envisioned in a fractal structure of life systems, being much in line with recent proposals of Turner and Nottale [97, 98]. It is envisioned that the result of these processes will finally exhibit a prominent coherent high-temperature conductor (HTSC)-system, fully guided by coherent wave domains, that can be described by toroidal geometry and numerically expressed by the GM-scale frequency pattern. This implies that phonon- or photon lasing with the proper combination of coherent

wave frequencies, decoherence could be suppressed, leading to stable pointer states. Such a mechanism of light amplification was also proposed by Marjeh et al. [99]. As an alternative, apart from this dominant influence of coherency in HTC superconductivity, some extent of decoherency may play a decisive role either by matrix disturbances (vibrations) that may facilitate the overall rate of charge transfer, as have been suggested in recent studies on photosynthesis [74]. This aspect was also attributed to fractal disordered selection of coherent spin states as suggested by Turner and Notale [97, 98], while also the adding of general noise may promote the formation of polaron and polariton quasi-particles that, as mentioned before can be instrumental in Cooper-pair electron formation.

The overall picture is that superconductor materials can be seen as a multi-cavity network on which an energy valley of electromagnetics is superposed that produces 3-D resonance chains of EM activity, yet contain characteristic energy gaps. This reminded us of the work of Hunt [100] on consciousness and brain function, postulating that EMF *resonance chains* may explain certain aspects of consciousness. Such a type of superconductivity may indeed play a role in information processing in the brain as also proposed in the work of Bandyopadhyay (see an interview with him by Hunt [101], see also Sect. 5.9) as well as the superconduction-inducing properties of hydrated protons in aqueous brain compartments as proposed by us (Sect. 7). Our observations on these discrete energy gaps in presently available superconductor materials, highlight a potential quantum bridge between superconducting properties in physics and biology. This also focuses attention on the fact that any material superconductor is permanently embedded in a zero-point energy field. Consequently, the intrinsic vibratory character of such fields should be taken into account as was realized in a number of previous papers on holographic aspects of superconductivity (references in [58]).

It is envisioned that the result of these processes will tend to exhibit a prominent coherent high-temperature superconductive system, fully guided by coherent wave domains. This can be described by toroidal geometry and numerically expressed by the GM-scale frequency pattern, as revealed in the present study. This implies that phonon- or photon lasing with the proper combination of coherent wave frequencies, decoherence can be suppressed, leading to stable pointer states. As an alternative, apart from this dominant influence of coherency in high-temperature superconductivity, some extent of decoherency may play a decisive role (see above) either by matrix disturbances (vibrations) that may facilitate the overall rate of charge transfer, as have been suggested in recent studies on photosynthesis or to fractal disordered selection of coherent spin states as suggested by Turner, while also the adding of general noise may promote the formation of polaron and polariton quasi-particles that, as mentioned before can be instrumental in Cooper-pair electron formation

All this should be very much related to the conceptualization of space-time, that in case of a quantum system should be seen as also being *quantized*. We argued earlier, in this respect, that space-time might be build up from energy vortices that connect through wormhole short cuts [1], which even provides the known quantum foam modality at the Planck scale. It is also of interest that recently wormholes can be seen as instrumental in the attain superconductive properties in the framework of M-brane

geometry [102], in which the wormhole structure can be interpreted as a characteristic part of torus geometry. In a more generalized model, we postulated the geometry of the double torus as a basic building block of reality, implicitly introducing the potential of 4-D rotations. In this respect, we predict a holographic feature in which the 3-D wave structure of superconductors is rather a shadow of a 4D-representation. The underlying AdS-Conformal Field Theory introduces the manifestation of gravity in the 4D domain at the brink of 3D/4D space-time. Holographic superconductor models have been adequately reviewed [103, 660]. This also focuses attention on the fact that any material superconductor is permanently embedded in a zero-point energy field. Consequently, the intrinsic vibratory character of such fields should be taken into account as was realized in a number of previous papers on holographic aspects of superconductivity [103, 660] as well as considerations on ZPE excitations (Turner and Nottale [97, 98]).

Of note, there is recent evidence that superconductive conditions can be experimentally demonstrated in brain tissue [106]. In this paper, in order to extract information from a quantum object (brain slice) by a classical measurement system, a graphene mediator was used that behaves quantum-mechanically at room temperature. This provided direct evidence for superconductive properties that were suggested to be generated in neuronal microtubuli.

Superconductor quantum features of life were proposed by Cope as early as in 1975 [107] and have been demonstrated in current *quantum biology*: in olfaction, long-distance magnetic navigation of various animal species and in particular in photosynthesis (reviewed by [74, 75, 77, 78]; Lloyd [76]). It should be realized here that life material is build up from elementary particles and that essential macromolecule such as proteins and DNA have an inherent vibrational property that can show coherent features, as supported by many other studies reviewed in [45, 58, 33, 64, 73, 86, 88, 89, 90, 108, 109, 110].

3.4 EMF Frequencies of Water Reflect Coherent Quantum Information of the GM-Scale

Water is quantum coherent under ordinary conditions, according to a quantum electrodynamics field theory that may explain many of its most paradoxical properties including life itself [111–113]. Quantum fluctuations and coupling between matter and electromagnetic field in Quantum Electro Dynamics (QED), predicts quantum coherence for liquid water even under ordinary temperatures and pressures, according to Del Giudice and Tedeschi [114, 115]. This theory suggests that interaction between the vacuum electromagnetic field and liquid water induces the formation of large, stable coherent domains (CDs) of about 100 nm in diameter at ambient conditions, and these CDs may be responsible for all the special properties of water including life itself (Fig. 8). Such cellular vibrations of macromolecules were spectroscopically shown by Lundholm et al. [116], Nardechia et al. [117, 118]. A recent study

demonstrating that polymerization of actin in cells is directly activated by terahertz irradiation indicated the potential long-range steering of protein function by EMF [119].

Even if it is still not known how life emerged from inanimate matter, there is a consensus that this should happen in water. Even nowadays organisms still maintain their watery internal milieu, and the multitude of organisms still find their habitat in water. Within organisms, water provides a medium in which all biochemical reactions take place. Water possesses many unique properties due mostly to the polarity (dipole character) of its constituent molecules and in particular to the ability to form hydrogen bonds internally and with other molecules. Moreover, contemporary quantum field theory maintains that all liquids including water have special electromagnetic properties involving potential coherence. Namely, in quantum electrodynamics (QED) the theorem can be proven [87, 120], according to which all molecules fluctuate in unison between two individual configurations, in tune with the enveloping vacuum electromagnetic field. The collective dynamics spans over a region (coherence domain, CD) whose size is the wavelength $\lambda = hc/\Delta E$ of the EM mode, whose frequency in the free space is $\nu = \Delta E/h$; h is the Planck constant and c is the speed of light. Further QED considerations demonstrate that within the CD photons acquire an imaginary mass so that they are unable to propagate themselves and rather appear as the cohesion energy of water molecules. The CD thus becomes a self-produced cavity for the vacuum electromagnetic field, which fuses with the matter field of an ensemble of excitable molecules, hence giving rise to a unique field describing the collective dynamics of the molecules that behave as a single (quantum-like) object.

Stability of the coherent configuration is kept by its lower energy level, namely by the existence of an *energy gap*, the difference in energy between an independent (non-coherent), and correlated (coherent) molecular configuration. This means that the coherent state is stable (low energy) and at the same time ordered state, having low entropy; thus, *no energy is required for the maintenance of order* [113]. In this stabilized order, quantum vacuum field is essential. At any given temperature that allows liquid water there is some proportion of water molecules in coherent domains and another in the non-coherent ones; at room temperature, a molecule of water spends around 30% of time in a coherent domain [121]. In this view and contrary to the established one, where water is considered as a passive solvent medium, here water is seen as an *active medium* where the principle of coherent information can emerge even in inanimate liquid systems and can be developed up to highly organized organisms [87]. The coherent regime in water has the potential of organizing countless biochemical as well as biophysical processes. Thus, water does not play an active and essential role only in contemporary living systems but should be seriously taken into account in any feasible origin of life scenario [33].

Nowadays, it is expected in the biological community that life originated in water and that the multitude of organisms found their habitat in it. Water provides the medium in which all biochemical reactions take place. The importance of water to living organisms originates from its peculiar features including the solvent properties, its high specific heat capacity, as well as its high latent heat of vaporization. Water owes these unique properties to the polarity (dipole character) of its constituent

molecules and in particular to the ability to form hydrogen bonds internally and with other molecules. In this view, water is seen as an active medium where the principle of coherent information starts from inanimate liquid systems up to highly organized organisms [87]. Namely, contemporary quantum field theory does not only unveil life as a profoundly electromagnetic phenomenon, it maintains that all liquids including water have special electromagnetic properties involving potential coherence. Of course, even if the coherent water regime gives a huge potential for coordination and organization of complex biochemical and biophysical processes, a crucial question remains as to how water with its CDs, will behave in an actual living cell, i.e., in the cytoplasm where abound many types of macromolecules, inorganic and organic ions, etc.

The solution for this is likely not to collect individual frequencies of various isolated proteins, DNA/RNA strands, channel proteins, tubulin proteins, etc., because those values depend on the composition of the environment in which the particular spectroscopic measurements have been performed. Rather, the entire integral cell should be taken into consideration, including cytoplasm, organelles, plasma membrane, etc. [63].

3.5 The Combined Patterned Appearance of Coherent and Decoherent EMF Frequencies

It is important to note that in our earlier life studies a regular pattern of *both coherent and decoherent* frequencies was found (Fig. 7). The coherent part of the GM-scale was defined by us as semi-harmonic since it is not only based on integer numbers, as in classic harmonics, but also on imaginary (broken)numbers, according to an adapted Pythagorean scale, that implies a toroidal (rotational) aspect in the mathematical background. Importantly, only coherent and no decoherent values were detected in the purely physical studies on entanglement and elementary particle studies as well as in the present superconductor studies. What could be the reasons that the decoherence aspect seems absent in the latter studies? Needless to say, in the case of EPR and superconductors studies, this is likely to be due to the selection of materials that have been made by the investigators in relation to an optimal function related to coherence and entanglement, yet, in principle, not excluding decoherent frequency values. Combinations of coherent and decoherent states according to the GM-scale, in principle would be found in all kinds of atoms/molecules, and it may be that decoherent states are created through interactions in complex structures as an implicit feature. *We have earlier speculated that the combination of coherent and decoherent wave frequencies in the life systems could reflect a potential regulatory mechanism [53, 57, 61]. Alternatively, they could be related to entropy-forced repair mechanisms to remove corrupted cells from the organism by, for instance, the crucial process of cell apoptosis.*

It has been suggested that the balance of coherent and decoherent states may be more dynamic than earlier thought and that creation of a coherent or decoherent state by interaction with the environment, does not lead to information loss, and thus, in principle, could be a reversible process [122]. Consequently, it would be justified to think in terms of dynamic states of coherence/decoherence in a cycling mode [1, 61]. *Life, including its quantum superconductivity, would thereby operate at the edge of chaos, in a so-called poised realm, that allows the choice between two states in equilibrium, and thereby enabling fast responses essential for the cell ecology and survival.* Of note, for instance, wave/particle duality may occur in a domain in which wave and particle modes are present at the same time. In fact, such a poised condition could be conceived as a thermodynamic balance between entropic and syntrophic (neg-entropic) aspects of reality. In fully physical systems such opposing conditions would have a more implicit character as for instance in matter/antimatter annihilation and forces such as gravity and dark energy. All this would imply a general aspect of symmetry and/or duality [61] (Fig. 9).

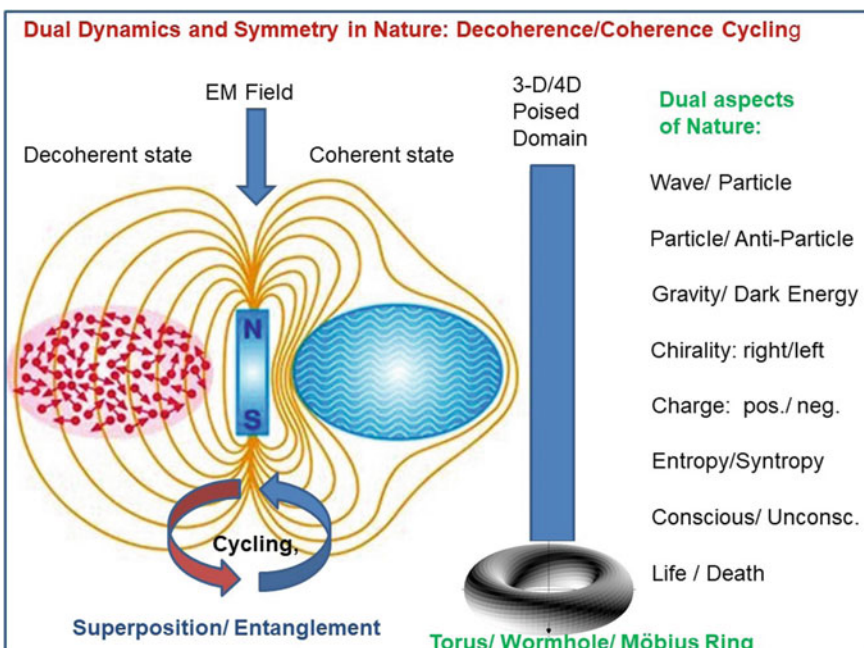


Fig. 9 Hypothetical cycling of quantum coherent and decoherent states (left). Dynamic duality may play a general role in the fabric of reality (right). Middle: 3D/4D poised domain that allows choice between two quantum states in equilibrium in which all of the depicted processes may operate on the brink of 3D and 4D spacetime. Middle below: 3-D Torus can perform 3D to 4-D rotations, that can be compared by closed movement on a Möbius strip (inside is outside), which may imply restoration of non-duality. Right: Other well-known dual processes in nature

In a world seemingly filled with chaos, physicists have recently discovered new forms of synchronization and are learning how to predict and control them [123]: “Neurons in our brains fire in synchronous patterns to operate our bodies and minds, and pacemaker cells in our hearts sync up to generate the beat. Objects with rhythms naturally synchronize. Kuramoto’s model described a population of oscillators and showed why coupled oscillators spontaneously synchronize. In the original model, an oscillator can be pictured as an arrow that rotates in a circle at some natural frequency. When a pair of arrows are coupled, the strength of their mutual influence depends on the sine of the angle between their pointing directions. Thus, the arrows will drift until they find this state of synchrony. Even oscillators that have different natural frequencies, when coupled, reach a compromise and oscillate in tandem”.

Abrams and Strogatz [124], reproduced the peculiar mix of synchrony and asynchrony in their computer simulations and explored the conditions under which it arises. Strogatz dubbed it the “chimera” state. Many researchers suspect chimeras arise naturally. The brain itself seems to be a complicated kind of chimera, in that it simultaneously sustains both synchronous and asynchronous firing of neurons. Last year, researchers found qualitative similarities between the destabilization of chimera states and epileptic seizures. But the chimera state is still not fully understood. Kuramoto worked out the math verifying that the state is self-consistent, and therefore possible, but that doesn’t explain why it arises. Scientists speculate that brain function and even consciousness can be understood as a complicated and delicate balance of synchrony and asynchrony. Building on previous work, they showed that networks break up into “clusters” of oscillators that synchronize. A special case of cluster sync is “remote synchronization,” in which oscillators that are not directly linked nonetheless sync up, forming a cluster, while the oscillators in between them behave differently, typically syncing up with another cluster. In 2017, Motter’s group [122] discovered that oscillators can remotely synchronize even when the oscillators between them are drifting incoherently. This scenario “breeds remote synchronization with chimera states”. They hypothesize that this state could be relevant to neuronal information processing since synchronous firing sometimes spans large distances in the brain. The state might also suggest new forms of secure communication and encryption. D’Souza et al. reported a menagerie of new synchronous states in a network of “nanoelectromechanical oscillators, that made clear that synchronization is a direct manifestation of symmetry—and the way it breaks.

Synchronization seems to spring from symmetry, and yet scientists have discovered that asymmetry helps stabilize synchronous states. Motter and Yang [125] reported that introducing asymmetry into a cluster actually strengthens its synchrony. For example, making the coupling between two oscillators in the cluster unidirectional instead of mutual not only doesn’t disturb the cluster’s synchrony, it actually makes its state more robust to noise and perturbations from elsewhere in the network. “A variety of tasks can be achieved by a suitable combination of synchrony and asynchrony,” Kuramoto observed “Without a doubt, the processes of biological evolution must have developed this highly useful mechanism.

The importance of both coherent and de-coherent aspects in mechanisms of superconductivity was stressed by Turner and Notalle [97]: “One of the aspects of HTSC materials lies in their disordered structure, indicating that HTSC is favored by complex fractal systems and that macroscopic quantum coherence phenomena such as HTSC is dependent on a *disordered* spatial distribution of charges/dopants/holes”. A clear picture emerges that we need to understand HTSC in terms of the underlying physics of a *macroscopic quantum process*. Essentially one has to create the equivalent of a “complex path integral “in order to induce macroscopic quantum coherence. They proposed that the disordered distribution in HTSC’s is not a chaotic, but a partially rotational distorted structure, against the background of an ordered tetrahedral network structure, that thereby can be accommodated by toroidal geometry. The same complex structure has been found in Smectite minerals and in pure water molecules that are ordered in a partially distorted tetrahedral geometry [57] (Fig. 20). Of note, it was suggested earlier that ring-shaped Bose-Einstein condensates trapped in a toroidal geometry may undergo self-interference, resulting in alternating vortex/anti-vortex dark soliton patterns [126]. Thus, the coherence/decoherence pattern could represent an interference phenomenon, similar to those observed in classical double split experiments that also operate in life conditions.

An essential role for decoherent noise in superconductive biology has also been concluded from recent studies in quantum biology, in particular for the process of photosynthesis [127, 128, 129]. It was concluded that the wave character of particles allows excitons to pass through the plant matrix in a broad front, enabling intracellular traffic of many parallel pathways that speed up the process of reaching the reaction centers. However, a second mechanism is involved to explain the high efficiency of this process: incoherent quantum noise of the conducting lattice facilitates smooth passage of these charged units, in the process of energy transport (Plenio and Huelga 2008) [74]. A very similar concept on a crucial role of de-coherence processes [97], was proposed in relation to superconductive modes, as mentioned above. When energy levels reach a critical point, *destructive interference* effects (which we associate with observed quasiparticle interference in HTSC) will cancel out most frequencies, leaving those matching the resonant frequencies dictated by the geometry of the fractal network to form a complex velocity field and an associated macroscopic quantum potential (MQP), leading to the establishment of coherent standing waves. We note that a very similar view on decoherence (taking a different approach and using different terminology) has been expressed by Dolce [130], who consider gauge symmetry breaking in terms of the competition between quantum recurrence and thermal noise”.

3.6 ZPE/SFQS-Field Effects and the Organization of Water Molecules in Life Conditions

Quantum field theory explicitly recognizes an extended quantum vacuum field, (“zero-point field or superfluid quantum space”), interacting with matter, as well as quantum fluctuations, whereby energy in the vacuum field in the form of photons can be captured by matter. When energy is absorbed from the vacuum field, the particles will begin to oscillate between two configurations. In particular, all particles coupled to the same wave length of the fluctuations will oscillate in phase with the EM field, that is, they will be coherent with the EM field. According to calculations performed by Preparata [131] and colleagues, the renormalized (physically observable) frequency of the trapped EMF in the CD corresponding to 0.26 eV is 6.24×10^{13} Hz, which is in the far-infrared region. Del Giudice et al, also argued that water CDs can be easily excited, and are able to collect small external excitations to produce single coherent vortices whose energy is the sum of all the small excitation energies, turning the originally high entropy energy into low entropy coherent energy, which is trapped stably in the water CDs.

It stands to reason that if cell water is exposed to an EM field in the form of quantum states in the frequencies detected by us, it will lead to a “geometric imprinting” that resembles the geometric Chladni patterns in [67] at a much smaller scale and thereby exerts a coherent ordering of cell plasma, including the associated macromolecules. Similar, GM-like discrete EMF, effects were recently reported by Sheldrake and Sheldrake [132], inducing superficial geometric (Faraday) patterns in water. It is of interest that a new quantum state of water molecules was discovered with a six-fold rotational symmetry (Figs. 8 and 26), in which the water dipole molecules are arranged in a kind of superposition, that is, if they are placed in tiny channels in tiny spaces of the type that also occur in living cells. Johnson [133, 134], Kolesnikov et al. [135], Maret [84]. The particular water clusters possess unique terahertz frequency vibrational modes in the 1–6 THz range and are supposed instrumental in cellular architecture, protein folding, structuring of DNA/RNA, in addition to EM phonon coupling and specific absorption of gravitational active virtual photons from vacuum fluctuations. Of note, in an astrophysical context, the *structured water in cosmic dust* may contribute to cosmic background radiation and is a candidate for the baryonic dark matter [133, 134]. This is important for life since water is seen as a fundamental substance for organizing biochemical processes [86, 87, 115, 136, 137, 138].

There is recent evidence that quantum zero-point fluctuations of a discrete wave frequency character can be experimentally observed and are clearly manifest in mesotropic structure in water [139, 70, 140, 141]. The ZPE field acts on all mesoscopic surface water layers to form coherent phases of water with domains of the length of 100–300 nm and also may influence interfacial layers on macromolecules such as proteins and DNA. Such an effect was modeled by Sen et al. [140]. In relation to such processes in chemistry in general, it is quite relevant to mention the zero-point NMR study of Thayer and Pines [142], which revealed four zero-point frequency

regions with peaks at 35, 111 and 132 kHz, that almost exactly fit our GM-scale values.

The crucial question is how to strike a balance between *internal* (endogenous) and *external* energetic EMF influences. Turner [97, 98] and personal communication), suggested that all molecules in the cell drive the cell water to certain vibrations, but in our opinion, it may be rather a symmetrical (bidirectional) process with mutual aspects. In other words, water is functioning as the primary antenna (mirror) of external EMF influences and is able to transmit those vibrations to other dissolved substances in such a way that, in unison, coherent vibration domains of cell compartments are formed.

As mentioned in Sect. 3.5, it has been postulated that the balance of coherent and decoherent states may be more dynamic than earlier thought and that creation of a coherent or decoherent state could in principle be a reversible process [122, 143, 144, 145, 146]. Consequently, it would be justified to think in terms of dynamic states of coherence/decoherence in a cycling mode [145, 146]. Life would thereby always operate at the edge of chaos in a, so-called, poised realm that allows the choice between two states in equilibrium thereby enabling fast responses essential for the cell ecology and survival, as reviewed by Moldonado [147].

It is of interest that many of the discrete frequencies influencing life molecules are situated in the infrared/far-infrared EMF region [80, 148], and have also been implicated in scale-invariant quantum fluctuations [85] that could arise from interferences of dual gravity and dark energy fields in a wormhole connective context.

Conclusion The cell and its components are always under the influence of active wave fields of internally ATP induced EM oscillations and are at the same time driven in concert by pilot waves of the quantum vacuum or implicate order (the Broglie/Bohm concept). Pilot wave mechanisms have now also been convincingly demonstrated in hydrodynamic experiments [149]. As mentioned above, water may therefore also play a general role as a *cosmological conduit* since it is present in cosmic dust in the form of metal-doped phyllo-silicates that pervade galactic spaces in the universe [137, 150, 151]. Biological systems exhibit macroscopic quantum properties, and superconductive properties [57, 97, 98]. The particular spectral patterns of water, that show multiple discrete absorption bands arise from the NIR and the mid-infrared region and perfectly fit the GM-scale frequency pattern [59]. Possibly, this knowledge can be applied for defining appropriate biomarkers for the diagnosis of healthy and diseased states, which is researched in aquaphotonics [152].

4 Torus Operators Mediate Information Flux in a Super-Fluid Quantum Space by Forming a Wormhole Communication Network

When light confines itself through electromagnetic-gravitational-interaction, confinement has been created with a changing boundary layer where the equilibrium between the attractive confining electromagnetic-gravitational forces and the repulsive scattering electromagnetic-gravitational forces changes within an area of the confinement [153], see added reference list. The author summarizes as follows:

In the Tri-Unity concept, the particle aspect, the wave aspect and the mass aspect are the three aspects of the same origin: confined light of one single frequency. In this concept, a particle does not remain a particle with its own mass. The particle has a flexible dimension, frequency and mass and changes during a transition from a lower to a higher energy level. The corresponding frequency and the corresponding mass changes during this transition. The “de Broglie wave” represents a real confined electromagnetic wave with a single frequency that describes the energy level of the confinement. In the example of an electron in a spherical orbit around the nucleus in a hydrogen atom, the electron is a spherical single-harmonic electromagnetic confinement around the nucleus. Because of the spherical confinement, the mass of the confined electromagnetic radiation will be divided in a spherical orbit around the nucleus.

These material waves, discovered by Louis de Broglie and mathematically described by Schrödinger could never be solutions of the well-known four linear equations of Maxwell. The material waves are spherical and elliptical solutions of confinement and not compatible with the solutions of the linear Maxwell Equations, since superposition is possible but electromagnetic interaction and electromagnetic confinement can only be described by a set of non-linear differential equations.

What are the fundamental boundaries which are required for a stable electromagnetic field configuration in which light can exist? There is only one boundary condition: the electromagnetic field has to be in a perfect equilibrium (balance) with itself and its surrounding and when an electromagnetic field interacts with a gravitational field, exactly the same boundary condition is required. It is a real electromagnetic wave in which the real part is the solution for the electric part and the imaginary part is the magnetic part.

The exact solution for a gravitational electromagnetic confinement van even results in diameters much smaller than Planck’s Length (1.616229×10^{-35} [m]). The fundamental question is: How it is possible to create confinements from “visible light” (with a wave length between 3.9×10^{-7} [m] until 7×10^{-7} [m]) within dimensions smaller than Planck’s Length? This is only possible when the wave length of the confined radiation is smaller than the dimensions of the confinement. This requires extreme high frequencies. The transformation in frequency from visible light into the extreme high frequency of the confinement is possible because of the Lorentz transformation during the collapse of the radiation when the confinement has been formed (implosion of visible light).

We hold that such confinement of light is operating through fractal toroidal geometry, that in the whole cosmos is scale-invariant, and may be instrumental on the brink of the Planck-scale domain and a phase space beyond the Planck scale that provides mathematical and geometric semi-harmonic information.

It is of interest that toroidal wormholes may support electromagnetic and magnetic flux [154–156], and at the same time can scatter electromagnetic waves [157, 158].

This latter aspect was also proposed for superluminal photon flux in neuronal microtubuli [159]. We speculate that the coherent set of discrete EMF frequencies revealed by us is instrumental in creation of such super-radiance conditions. This idea is supported by the findings that a similar pattern of EMF frequency bands promotes the creation of entangled conditions [55], is instrumental in the production of superconductivity [58], as well as shows an almost perfect fit with the pattern of the energy distribution of elementary particles [56], see Table 1).

One essential understanding here is that nature inherently includes information feedback loops in such systems that enable a “self-reflective” process in which the system learns from its environment, adjusts accordingly to maintain balance and well-being for itself, and communicates these data back to its environment, creating new patterns and behaviors that registers these adjustments and in turn again informs the living system as a whole (see further Sect. 6). We hold that the recurrent process that underlies this process can be successfully modeled by toroidal geometry (Fig. 10). This geometric process of spiral *information enfolding and unfolding* can be literally observed and discerned conceptually in many natural systems, in metabolic processes, in the function of certain blood cells, as well as in the resource exchange

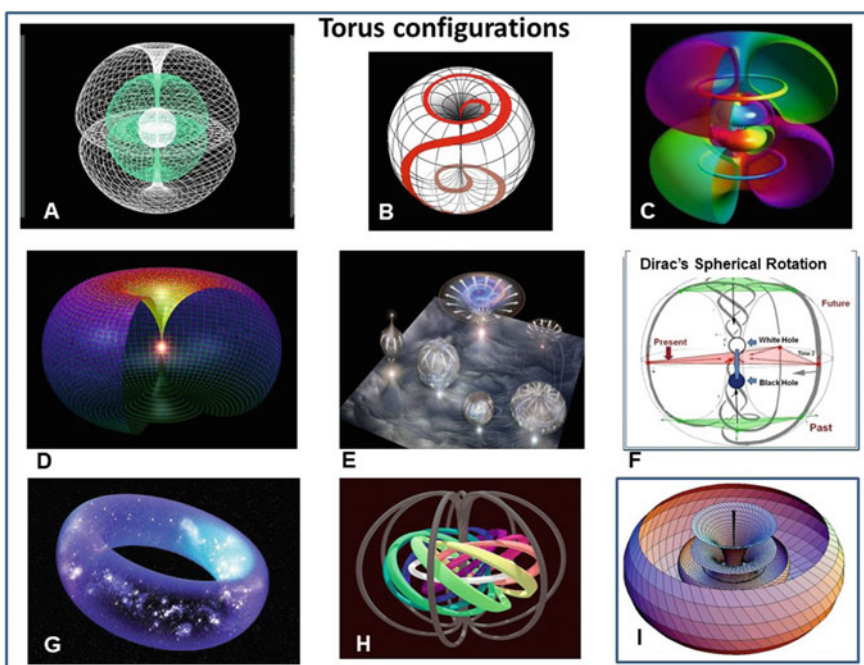


Fig. 10 Various modalities of toroidal geometry: **a** Nested torus structure, **b** Torus trajectory (red), **c** Atomic structure as double torus, **d** Filled space-time structure with singularity, **e** Torus network, **f** Dirac spherical rotation showing toroidal trajectories in relation to time, **g** Donut model of the universe, **h** Knot structure in torus as metaphor for attractor/standing wave, **i** cartoon of a twistor as a supposed space-time unit

of plants and animals within their environment. It is also evident outwardly in the macrocosmic realms of planets, stars, and galaxies, and inwardly in the micro-cosmic elemental and atomic realms (Fig. 10). Thus, the synergetics of torus geometry and recurrent toroidal energy flow patterns seem to be fundamental to all cosmic creation [160].

5 Brain Function and Consciousness Studies

5.1 *Modeling as a Holofractal Flux of Information with Toroidal Geometry*

Consciousness, in a cosmological context, can be defined, as a state of a semi-stable system that has developed in a cooperative and cyclic operating mode, so that it became “causally self-observant”. According to Dehaene et al. [161], individual human consciousness can be envisioned as the processing of information that not only makes meaningful information available for global broadcasting in the brain but also offers self-monitoring and quality control. Thereby, it cannot only predict aspects of the local environment but also can integrate memorized information and future-directed projections into a personal worldview that serves individual survival, development, and social communication [10, 11]. Yet, in the present paper, an even wider context for consciousness is offered, in which our individual mind is seen as a part of a larger universal consciousness, itself being instrumental in the entire fabric of reality [2]. In other words, each conscious element in nature and thus each individual is implicitly part of universal consciousness, for humans: *we are in consciousness*, implying the position of Idealist ontology, albeit based on the fundamentals of quantum-(bio) physics and cosmology. This concept integrates a non-material mental framework, submitting that information represents a basic building block of nature [19], an idea that was earlier framed as protopos by Görnitz [162, 163]. This concept is also based on our earlier consideration of brain that is encompassing an extended mind [164] and the earlier treated observation that life processes are sustained by a generalized biophysical principle of a discrete pattern of electromagnetic wave frequency bands [1, 62].

Consciousness, therefore, is not only a human faculty and implies a reflexive state that both involve information integration as well as subjective “feeling” of past and future events. It requires a graded complexity of life systems to deal with the requirements of multi-tasking and ecological maintenance. A central item in brain research is the question whether consciousness should be conceived solely as an *emergent* phenomenon, as related to the extreme neurological complexity of the brain or rather that the central nervous system is embedded in a much wider context in which it also *receives* (quantum) wave information, partly unrelated to the known senses. However, it remains an open question of how humans develop self-consciousness and obtain the basic knowledge of the type called qualia [13].

The *hard problem of consciousness* is the problem of explaining how and why we have qualia or phenomenal experiences and how sensations acquire characteristics, such as colors and tastes. A very interesting treatment of the quantum models of consciousness research, as reviewed by Meijer and Raggett [165], was given by Wolf-Meyer and Cochran [166], in the framework of the anthropology of science in general.

Kozyrev [167], considered that all life forms might be drawing information from a spiraling source of energy. He suggested that life could not be formed in any other way, because it is actively drawing off this spiraling vortex-like energy to sustain itself. In this sense, we can think of the living system as possessing efficient resonators for tuning into geometrically organized energy, most likely in the form of toroidal flux patterns. There are recent proposals for toroidal models in the functioning of specific brain cells, neuronal networks, functional parts of the brain as well as the whole brain [168, 169]. The natural candidate for such a toroidal information flux is the spatially embedded network of the so-called human connectome: a comprehensive map of neural connections in the brain, that may be thought of as its “wiring diagram”. More broadly, a connectome would include the mapping of all neural connections within an organism’s nervous system and represents a non-stationary, highly dynamical structure characterized by complex topological geometry [170]. Toroidal information flux (see Fig. 10), was also postulated by us to provide the basis for the existence of consciousness at different scales of the Universe. There are distinct reasons to choose the multidimensional symmetrical aspects of the double vortex torus, a geometry that may mimic a combination of transversal, longitudinal and circular waves [4, 171, 172].

The nature of electromagnetic toroidal excitations, as developed in physics, was reviewed by Papasimakis et al. [173], and their interactions with the inorganic matter by Tsytovich et al. [174]. In this manner, toroidal operators integrate quantum information and store it on the edge of each fractal unit, a 2-D hypersphere that in the case of the black hole was called the “event horizon”. Thus, quantum information, like energy, is retained in this manner. Verlinde [175], used the holographic principle for his entropic gravity theory. The holographic theory was invented by the Nobel laureate ‘t Hooft [176, 177], (see for holography aspects of the cosmos [24, 178, 179]). *The leading principle of holography is that every object is fully described with information gathered on a screen around the object (the event horizon).* It follows that also galaxies, suns, planets and likely the entire universe and even life systems are also to be regarded as toroidal organized information fields each projecting digital information on their respective event horizons.

According to classical information theory, information always arises through *interactions of wave-particles* and, entropy of information represents the *potential* to ask yes/no questions in such an event with regard to a particle system [180, 18]. According to these concepts, information is in fact the sum of *expected* information obtained from such yes/no questions. An example is DNA in our cells which in itself contains a lot of *potential* information (digitally expressed in Bits), but this can only be clearly expressed in the cell with the help of RNA to produce the gene products: the proteins. The intrinsic (hidden) information of each object is therefore

the result of the entanglement of the stored (individual) information from its various constituting particles, providing a sort of global information store of it. This information is fed back to a universal information matrix, that, therefore, is dynamic in time [181–183]. The zero-point energy field [184–187], was considered to be an obvious candidate for such information storage. In the latter framework, the aforementioned background may be related to the concept of *quantum foam at the Planck scale as a persistent storage matrix* ([180, 188, 189]; Ford and Roman 2000, see also Wikipedia/quantum foam). For example, it is assumed that information entering a black hole from the outside is never lost, but, as mentioned above, is rather being projected on its outer screen, called the “*event horizon*”, that may take a similar physical form [180, 190, 191, 192, 193].

5.2 Consciousness as a Scale-Invariant Phenomenon in the Cosmos

Consciousness has often been approached as a phenomenon of cosmic dimensions. This view has a long history, from ancient cults to Hermetic wisdom and Greek philosophers. Also, after the emergence of modern science and physics, there are persistent attempts to liberate the study of consciousness from a purely human neurological context and to search for a much broader or deeper fundament. Among others, this led to the recognition that conscious states arise through permanent interactions with the environment, even in a genetic context as revealed in the recent studies of epi-genetics. It became also clear that in animals, dependent on the species involved, clear signs of consciousness and even self-consciousness can be detected. This aspect seems related to the open question if in biological evolution all life systems should possess some form of (proto)- consciousness or awareness that is intrinsically required for problem-solving, survival, and defense of self. In this respect, the extremely complex brain was even conceived by some as mirroring the very universe, combined with the idea that cosmic processes such as electromagnetism, gravity, and dark energy are likely to influence life processes. Since any organism is embedded in such cosmic force fields, it is obviously preferable to envision each individual as being part of a dynamic wholeness, or even better as an active participant in the further evolution of our planet and the entire universe [194]. In the latter framework, some recent studies focused on this aspect, apart from extensive treatment of the item of *universal consciousness* (see for instance an integral overview of this subject by Meijer [2]).

All this is based on the central idea that the information perse may represent an essential fundament of reality and may act as a connecting principle in describing both nature at the micro- to macro-level [19], at the same time touching upon mind/matter relations. In astrophysics, in an article in nature, this even led to the ultimate vision that the universe, in the deepest sense, is not material but rather mental [195]. In a relevant essay on: “Quantum Mind: the Matrix of the Universe” [196], further

emphasizes this point by saying that information is a closed book until someone opens it and starts reading. This is certainly referring to the works on the information of David Bohm, John Wheeler, Seth Lloyd, Paul Davies, and that of Vlatko Vedral on "Decoding Reality", collective concepts that may provide a final vision upon a theory of everything. Here, Smetham [196] argues that Stephen Hawking in his recent work with Mlodinow [197], backed away from the essential impact of consciousness in the fabric of reality, probably in an outspoken fear for notions of intelligent design and strong anthropic reasoning.

Transpersonal aspects of brain function were extensively treated by Mays and Mays [198], Desmond [199] Kowal and Deshpande [200], Darmos [201], all implying a type of "Unified Field Science", as also central in the work of Amaroso [202]. The latter authors are implying that one can say that consciousness belongs to the organism, but that there is ample reason to rather say that organism belongs to consciousness, in line with the earlier formulated "Monistic Idealism" of Amit Goswami [5]. In most of these articles, holographic models along with toroidal (Riemann geometry) and cosmic information horizons play a significant role.

It was considered in this respect that the origin and nature of time as well as conscious experience cannot be satisfactorily approached in material terms without running into explanatory gaps and hard problems [203]. He stated that radiant fields involved are in effect spherical standing waves that follow a double helix spiral vortex Möbius/Klein path with both compressing (Gravity) and expanding (EMF/dark energy) aspects. In this view, information is resonantly related to spin momentum as carried by harmonic fields in the ZPE, a field that may also empower scale-invariant black hole/white hole information transmission.

A recent theory [190, 192], claims that information can pass through the black hole structure, via a connecting wormhole (a sort of short cut in space-time) to arrive in an intrinsic "white hole", that instead has an anti-gravitational character. Some believe that the final fusion of all black holes will yield a giant one that can disperse the stored integral information into a new version of our universe (see inset F in Fig. 10), in a rebounce or cyclic operating mode of the Universe. This model for the final fate of our Universe (the so-called Big Bounce [164]), might predict that information of a newly formed universe is integrated into a *nested* configuration with the preceding one ([190, 204], see Fig. 10). The nested torus structure therefore can be seen as a fundamental aspect of quantized spacetime. Interestingly, twistor geometry (Fig. 10), which was intended to unify quantum mechanics and general relativity by unraveling the phenomenon of gravitation, can also be used for solving non-linear Schrödinger equation to obtain solutions for *soliton wave phenomena* [205]. As earlier treated, Haramein et al. [154], postulated a collective wormhole background on the Planck scale (see Fig. 18), that may underly our reality. The presence of apriory information could explain the partially directed character of biological and cosmic evolution, as have also be indicated by Khrennikov and Melkikh [206] see also Sect. 6.

Most investigators agree that maps of the universe clearly indicate that the visible cosmos is fractal [24, 207, 641], Linden 2017; Gaite 2018) although the discussion on this subject goes on (see also Wikipedia, Fractal Cosmology). A fractal is a *self-similar* geometric pattern, meaning that the whole pattern is always exactly contained

within its parts, as in a hologram and similar patterns recur at progressively smaller scales. By zooming in on a massive cluster of galaxies, the self-similar structure of the universe becomes evident. Most fascinating is how certain snapshots of the far universe look similar to the fractal structure of a brain cell network [160, 209].

Fractals, as mathematical entities, are infinite and this is clearly demonstrated in the case of computer-generated fractals. We emphasize that the information processing involved should be seen in a scale-invariant holographic context. This is supported by the increasing evidence for a holographic universe [210] in which, at the black hole level, a distinct discretization of spacetime may be observed [211]. The holographic approach was also highlighted in the work of Haramein as to electron and proton mass computations and Planck scale quantum oscillations [154, 188, 212]. As mentioned earlier, at the other extreme scale of the cosmos, EMF-oscillations were measured associated with black holes with frequencies that were fully compatible with our GM-scale values [52, 60, 213]. Inspecting nature as a whole, fractal geometry can be observed not only in the macro-cosmos but also in many natural forms such as trees, plants, lightning, clouds, rivers, crystals, blood vessels, veins, mountains, the brain, snowflakes, shorelines, lungs, and other parts of the animal and human anatomy [160].

We submit that in an information grounded universe the existence of a fundamental background field containing wave information in the form of discrete acoustic oscillations could explain a general guiding role in the architecture of reality, including biological evolution [3, 19]. In this respect, the sound power spectrum of Cosmic Microwave Background (CMB) could provide one interesting framework, since CMB-features exhibit acoustic standing waves that even reveal a fundamental with harmonics. In this case, we should take into account the CMB integer fractional frequency relationship, that resembles an octave-like distribution and that, on an exponential frequency scale, allows a piano keyboard to be directly superposed [214]. Luminet [215], stated that the CMB temperature fluctuations can be decomposed into a sum of spherical harmonics. He compared these vibrations in primordial plasma with the well-known Chladni patterns that can be induced by sound on a sand-covered drumhead, as was also treated by the first author in previous work on phonon-guided biology [62]. CMB radiation is conceived as emission of uniform, blackbody energy coming from all parts of the sky and such oscillating sources push down a quantum superfluid substance resulting in alternating density fluctuations [216]. It is assumed that decay of the vacuum (zero-point) energy, also seen as dark energy/dark matter, results in CMB-background photons [217].

It was suggested, in this respect, that dark matter may interact electromagnetically with ordinary matter through either electric or magnetic anapoles that are related to toroidal dipole moments [218]. How could this type of physics be related to life systems and brain function? It is of great interest that recently a 5-D model theory was proposed for the creation of life forms [219]. In this theory, a Boson-Einstein, condensed, *monopole boson field* was proposed to be instrumental in the creation of life matter (this in relation to the creation of carbon 12) and in particular in the formation of DNA/RNA. Of note, not only the energy distribution of a variety of elementary particles [56] but also a variety of boson modalities remarkably fit the GM-scale

frequency pattern described in Sect. 3.1 (Dr. K. W. Wong, personal communication), see further in Sect. 5.3 and Fig. 13. The special position of C12 reminds us of the unique Hoyle state of the carbon atom that may represent an anthropic feature, as was earlier proposed by Fred Hoyle. He revealed the special resonance state of carbon in its production from the fusion of three helium nuclei, in which the highly unlikely stable ground eigenstate is formed through an enhancement effect with exactly the right excited energy resonance state [220]. Hoyle's intuition was conceived by him in retrospect as a token of intelligent design that later formed the basis for his support for the so-called anthropic principle. The latter concept proclaims that the universe must have certain properties (fundamental forces, particles, and discrete natural constants in the law of physics) because otherwise, our own existence would not be possible.

The major influence of macro long-distance forces is quite explicit in the known influence of time-varying geomagnetic activity such as Schumann resonances on the nervous system [221]. This aspect is also central in the quantum model studies of Kozwolski and Marciak-Kozwolski [222] and Persinger and St-Pierre [223]. These authors, conceived the physical basis of consciousness both in the non-local excess correlation with regard to entanglement as well as in the cosmic transposition of zero-point photon energy as dominant factors in brain function, as later also hypothesized by Keppler [181, 182, 183, 224] (see Fig. 11).

Interpretation of the ZPF “Phase Locking” Mechanism

- Filtering: quantum systems filter their sets of resonance frequencies selectively out of the full ZPF spectrum: the formation of an attractor corresponds to “a chord played on the guitar of the zero-point field”.
- Information: quantum systems leave characteristic fingerprints in the ZPF : the formation of an attractor imprints an information state on the ZPF.
- Following the hypothesis that the ZPF is the substrate of consciousness, it is claimed that:
 - Every ZPF information state is associated with a conscious state,
 - Universal mechanism that provides such systems with the ability to acquire not only their physical properties, but also their phenomenal qualities.

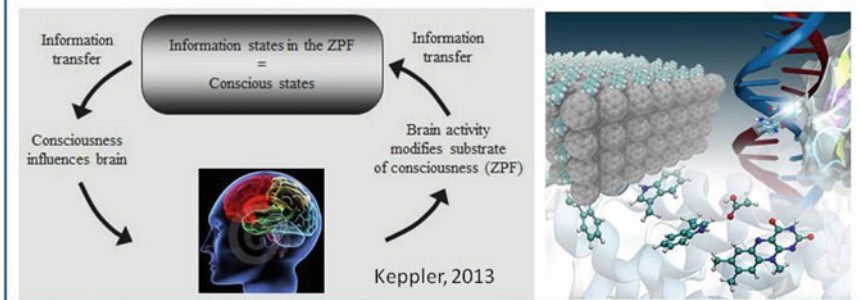


Fig. 11 Filtering of resonance frequencies from the ZPE field (modified from Keppler [182]), by a phase-locking mechanism yields the qualia for our brain function. In reverse, the quantum brain leaves fingerprints in the ZPE field and the resulting dynamic and permanently updated ZPE constitutes the very substrate for consciousness and life processes (inset below right)

Dynamical systems in the physical world tend to arise from dissipative (actively spreading) systems, a process that always includes some kind of driving force that maintains its motion. The dissipating driving force tends to balance the initial transients and settle the system into a typical, future-directed, behavior, known as an *attractor* [181, 182], Fig. 11). An attractor can even constitute a complex set with a *fractal* structure, known as a *strange attractor*. The latter aspect promotes a *collective and coherent* behavior that can lead to flux-maximization. In the framework of our model for brain function, both the subjective unconscious and conscious aspects [225–229] can, in principle, be modeled as information flow and recurrent storage as taking place in a nested toroidal setting, since the human brain organization clearly shows functional *circuits* and obvious *fractal* properties [230, 231].

More precisely, our concept is that the brain is embedded in such an information storing field, that can be described by hypersphere geometry. This model may help to solve long-standing questions concerning our psychological activities such as mind-wandering, memory retrieval as well as the ability to connect past, present, and future events [168]. The human brain exhibits the unique ability to connect past, present, and projected future events in a single, coherent, toroidal screen, glued together in a mental kaleidoscope. Interestingly, these authors see the model of the brain hypersphere as a starting point for further evaluation of a brain-associated fourth spatial dimension (see for this aspect Sect. 5.3). In this extra spatial dimension, mental operations may take place both in physiological and pathological conditions. The connectivity patterns at rest might constitute a “signature of consciousness”, reflecting a stream of ongoing cognitive processes. Tozzi and Peters [168], speculate that conscious moments might be correlated with specific trajectory states in a “Clifford torus” structure. In this framework, it has been proposed that features of EEG brain signals with spectral peaks in preferred bands (alpha, beta gamma EEG waves) originate from such feature vectors in a 4-D Euclidean space. One example of a recurrent toroidal type of brain activity might be found in the periodically repeating pattern of so-called grid cells in the brain. These patterns have therefore been related to a supposed toroidal architecture of brain wave attractors [232].

Many scientists have earlier suggested that basic information reaches our brain *from outside* [226, 233, 234, 235], since the nervous system may also function as a *receiver* of subliminal signals. One could regard this process as a physically defined “extrasensory perception”. Evidently, we have to take into account a “sixth” sense in the form of a *vibrational, resonance sensitive macromolecular apparatus* in each of our cells [236]. The particular cellular sensors are composed of flexible three-dimensional structures of proteins, oligonucleotides, and elements of the cell skeleton, that mutually communicate through discrete wave resonances and are sensitive to fluxes of photons, phonons, excitons and related quasiparticles such as polarons (solitons) and polariton. These receivers act at the same time as receptors and emitters of quantum information and operate as resonant oscillators with specific resonance frequencies, coupled with a natural quantum field [73]. This bio-sensing apparatus, situated in an apparently (bio)electromagnetic cell, was tentatively called the *electrome of the cell* [45], being under the continuous influence of naturally occurring internal as well as external electromagnetic fields [1, 62]. In this respect,

it is worthwhile to mention that, based on quite solid evidence, the brain has been described as an electromagnetic workspace [237–239].

5.3 *Multi-dimensional Space-Time Including an Extra (4th) Spatial Dimension*

Two difficult problems remain to be solved before consciousness can be explained. First, there is the “phenomenal problem”. The redness of the rose that one sees, exists in a private domain. We cannot communicate to anyone else what redness is like: redness and other qualia are subjective phenomena that cannot be described to outsiders. Second, there is the “binding problem”. How can multiple memories and afferent impulses combine simultaneously to produce a moment of lucid conscious awareness when the data are scattered throughout the brain and there appears to be no central station to coordinate the information? Carlson [240], pointed out that we do not perceive physical space and that in fact we are restricted in conceiving it. This, in fact, provides the purpose of science: to build a predictive causal framework for our scattered perceptions. The author approached the 4D-manifold by the causal set theory in which any change of space-like interval is a purely structural consequence of the stepping action of time. Using a time fork, followed by two-step converging time series and forming a reconverting sequence, a time triangle is created. In this manner, spacetime and dimensionality can be build up from such triadic patterns formed by temporal successions.

Time has been designated to the position of a fourth dimension, so we live our everyday lives in three dimensions plus 1: time together forming space-time. Although our brains can imagine objects only in the three spatial dimensions, some concept of higher dimensions is, in principle, possible. For example, a hypercube of four spatial dimensions may be appreciated by examining its three-dimensional shadow. It has been proposed that light is a vibration in the fifth dimension.

An interesting study in this respect, as to brain function, was performed by Walling [241, 242], in which EEG patterns were recorded in different stages of recovery from deep general anesthesia. The availability of powerful computers for data analysis resulted in an approach in the field of nonlinear dynamics. The signals were analyzed according to non-linear dynamics and showed distinct patterns with attractor dimensions that invariably went point, periodic, and toroidal before the chaotic brain pattern emerged. The smallest attractors registered (1.3–2.0 dimensions) all involved subjects that were meditating or at prayer. Under these conditions, the conscious mind is closed to the senses while the subject concentrates on the prayer or meditates. In contrast, the highest number of dimensions was detected at multitasking (Fig. 12).

Thus, each signal inhabits its own dimensional manner to move from one dimension to another. In this way, the signals are separate but bound together at the same time. In other words, sensory binding has been accomplished, while the perception of vision and hearing are kept separate. The layers are deposited at about 40 Hz and

the higher-dimensional, apparently seamless percept may represent content of more than three dimensions. Thus, by employing nonphysical perceptual space, the percipient is freed from the constraint imposed by the event horizon of three-dimensional physical space. In humans, the authors have shown that nonlinear dynamics may exist in the form of higher-dimensional fractal attractors up to a value of 4.8 dimensions. A 4.8-dimension attractor may combine more than four variables in phase space (Fig. 12 a).

The team has also shown evidence of nonlinear dynamic activity in the brains of animals, an activity that seems to increase in complexity among various species in a logical progression. To look for signs of nonlinear dynamics, the team again manipulated data from electroencephalographs of 11 different fauna: anemone, starfish, earthworm, moth larva, crayfish, minnow, perch, catfish, frog, dog, and human. This was done in order to see whether an increase in mathematical sophistication across species correlated with preconceived notions regarding evolutionary ranking in the central nervous systems of the animals. The electroencephalograph correlation dimensions from the six animals were plotted against their age as estimated from the fossil record: anemone, 700 million years; crayfish, 650 million years; bony fish, 490 million years (mean of perch, catfish, and minnow, $D_2 = 2.65$); frog, 245 million years; dog, 65 million years; and human, estimated at 30 million years. They showed that the greatest attractor dimensions for these species increased steadily during the period of animal evolution (Fig. 12a). The shape of the curve took the form of a logarithmic spiral, obviously being self-similar. The authors noted that such a typical pattern may be seen throughout nature, from the arms of spiral galaxies to the arcing shape of the shell of the chambered nautilus.

Thus, the more variables there are in a nonlinear system, the more dimensions are needed to accommodate them. Conversely, the higher the dimension of the fractal attractor, the greater the number of variables that are required to represent it. Consequently, the fractal attractor Walling et al. observed could be evidence of a repository for the information required for higher-dimensional brain activity. The attractors may, in fact, represent the "knot" where the "binding" of information occurs. In conclusion: all investigated species, including humans, showed evidence of fractal attractors in brain EEG activity and demonstrated increasing fractal dimensions commensurate with their status in evolutionary development (Fig. 12a). If such curves achieved more significance by the addition of corroborating data, it would be quite possible that a better understanding of the evolution of the brain is attained.

Kaluza's theory [243] derived the electromagnetic field extending throughout the first three dimensions of a 4D-space. It was postulated that only a $4 + 1$ space-time structure (thus with an extra spatial dimension), allows a unity of relativistic and quantum physical reality [244], including time-symmetric operation and backward causation [19, 164]. This also allows causal and tensed-time modalities that are essential for self-consciousness and reflection [245]. Quantum information mechanisms were recently used to model human consciousness as well as the unconscious in relation to conscious perception [246], in which various modalities of non-locality were discussed. Of note, entanglement and non-locality may not only apply to spatial separation but also a temporal one. It was proposed by Martin et al. [246], Baaque

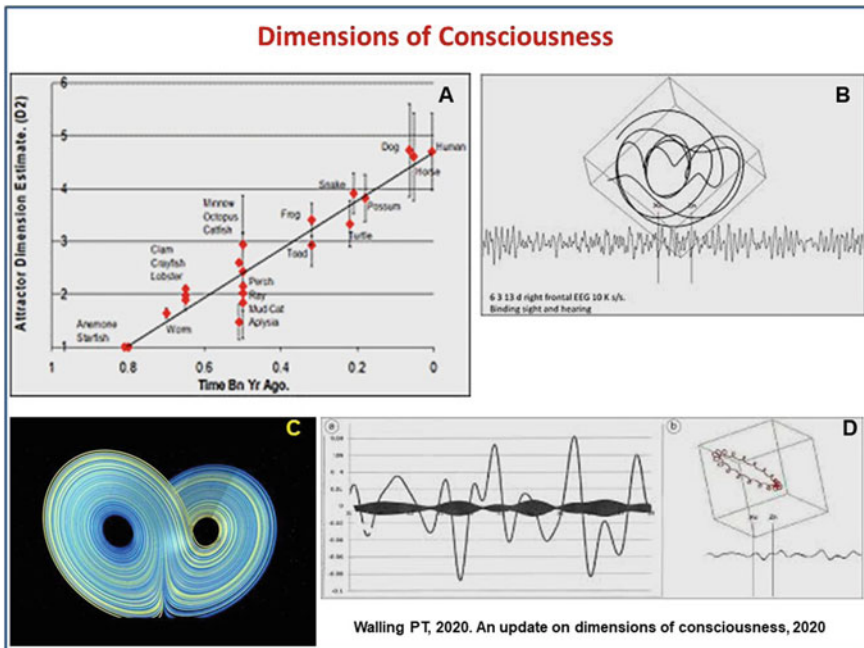


Fig. 12 **a** The highest recorded attractor dimension observed in various species investigated, plotted against the time of each species first appearance billions of years ago. **b** Frontal EEG with its associated attractor above it. **c** Cartoon of a Lorenz attractor generated by an equation of turbulence. **d** Two carrier functions of about 1 and 20 Hz during metronome ticking/flashing, showing how hearing and vision can be simultaneously received and yet remain separate qualities. Left inset: the same two frequencies isolated from the EEG (being a degraded version of the corresponding attractor), and recombined in three dimensions as depicted in inset **d**

and Martin [247] that archetypical information can be stored as quantum information in appropriate fields and that consciousness may be controlled by quantum entanglement from *outside the* classical 3 + 1-D space-time configuration, in an extra 4th spatial dimension [179, 245, 248, 249, 250, 251].

An extra spatial dimension is also assumed in the hypersphere brain model of Tozzi and Peters [252, 253], Tozzi and Peters 2019b; see later) and in the elegant Globotoroid space theories of Samardzija [254]. Interestingly, a 5D model theory of life was recently proposed by Wong et al. [219], in which the creation of life was conceived as a process of symmetry breaking from a homogeneous 5 D spacetime manifold to a continuous 4D one, which should include the formation of separate torus-like manifolds. These, in turn, create magnetic monopole bosons of a diagonal long-range order, thereby exhibiting a Bose-Einstein condensed space. In life forms, such a monopole boson field could be formed through resonances of carbon 12 nucleus hard sphere (which is a component of all life forms) in DNA and RNA. The build up of the genetic material is accomplished through quantum tunneling of one hexagon onto another in an adjacent hexagon layer, creating RNA, while interaction

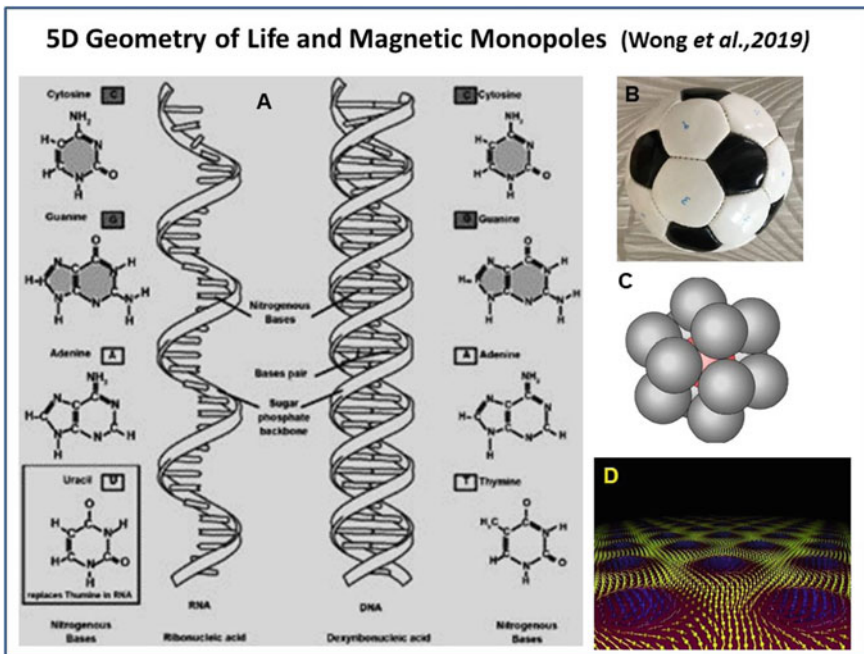


Fig. 13 **a** Images of DNA and RNA with base to base separation gaps in which a monopole boson field tunnels from one layer of nitrogenous base to the next if exceeding the wavelength of the space gaps. **b** fractal picture of hexagon/pentagon model of C1. **c** C12 hardsphere dense packing model. **d** Cartoon of a magnetic monopole bosonic field

with the pentagonal nitrogenous bases set can be seen as forming the surface of a Buckyball, by which a standing wave of the bosonic monopole is realized (see Fig. 13). Thus, this type of symmetry breaking may explain the creation of life structures at the atomic scale.

Interestingly, Hut [255], envisioned that symmetry breaking could even be the basis for the poorly understood relation of mind/matter. Instead of seeing information as a derivative of matter, we should see information expressed in mind and consciousness as an equally fundamental aspect of reality. In electromagnetism, we see electrons as carriers of the material, but we never see the carrier of magnetic fields, such as the hypothetical magnetic monopoles. However, such a natural duality should be present in a unified theory of electromagnetism and only symmetry breaking would show this. Hut suggests that a similar situation may be manifest in a potential unified modality of mind/matter, in which mind is hidden as a sort of panpsychism entity and cognition and matter have an unexpected intimate connection.

Another major finding, in relation to this, is that physical information should be seen as a modality of energy and that information and energy can be mutually converted to each other [26, 27, 256], confirming previous ideas on three fundamental building blocks for the fabric of reality [19]: matter, energy, and information, (see

Sect. 2). A study by Aharonov et al. [257], even indicates that information can be physically separated from the matter it describes.

5.4 *Biophysics and Brain Signaling, the Function of Bio-Photons and Solitons*

Introduction

The possibility that quantum physical aspects play a non-trivial role in brain function and consciousness was reviewed earlier by Vannini [31], Atmanspacher [258] and Meijer and Raggett [165], Schwarz et al. (2004), as well as more recently by Adams and Petruccioni [259] and Keppler [183]. A large variety of theories is presently available, (see Table 2, in Sect. 8), all deal with the question if quantum effects can occur in the brain, and if so, how such mechanisms could be involved in, or even be a prerequisite for the generation of conscious states. An essential question that was raised from the beginning is related to the question if coherent quantum states can persist long enough in the warm and wet organism to be able to do work and guarantee the faceful transmission of quantum information [260]. A potential answer to this was found in the field of quantum biology, in which it was demonstrated that quantum coherence under such conditions can occur in processes such as enzyme function, photosynthesis, olfaction and navigation in migration of various animal species, (reviewed by Marais et al. [75, 77, 78], Lloyd [76], Huelga and Plenio [74]). The ongoing dialogue was centered around questions like: can a quantum state be protected against local decoherence (by interactions with the environment). This requires either effective shielding of the quantum state within the cell (by gel states of water [261] or compartmental enclosure such as resonating ions inside ion-channels [262] or through the influence of repeated attention in cognitive processes [263]). The alternative quantum mechanism is that the brain is rather embedded in a quantum field that enables non-locality, entanglement, and other well-known features of quantum physics that are instrumental in brain binding and information transfer [111, 264].

In addition, are quantum effects manifest only in modulating the well-known neurotransmission mechanisms or do alternative modalities of neural communication play a role? One candidate for the latter is photo/phonon mediated communication as proposed by several authors [234, 266, 267].

Table 2 Current neurological and neural correlate models (left) and quantum/spacetime models (right)

Current models of human consciousness	
Neuro-correlate models	Quantum/Spacetime models
Global workspace model— Baars/Dehaene	Wholeness/implicate order model— Bohm
Multiple drafts theory— Dennett	Quantum field model— Jibu/Yasue
Dynamic Core/Neural Darwin, model— Edelman	Quantum brain dynamics — Umezawa
Information interaction theory— Tononi/Koch	Dissipative brain model— Vitiello
Thalamic cortical rhythms model— Llinas	Holonomic mind model— Pribram
Coalitions of neurons model— Crick/Koch	Attention quantum zeno effect model— Stapp
Field models— Kinsbourn/McFadden/Pockett	Psychon brain dynamic model— Beck/Eccles
Subcortical models— Penfield/Merker/Ward	Ion-channel coherence model— Bernroider
Internal and world simulation model— Revonsuo	Orch. Obi. Quant. Reduct.— Hameroff/Penrose
Retinoid model— Trehub/Metzinger	Spin-mediated Consc. Model— Hu/ Wu
Self-model theory— Metzinger/Hesslow/Grush	EM field models— McFadden/Pockett
Sensimotor Theory model— O'Regan/Noe	Holographic resonance model— Mitschell
Supramodular interaction theorv— Morsella	Hierarchical model consciousness— Kaivariainen
Multilevel feedback model— Haikonen	Dual-time Supercausality model— King
Intermediate level theory— Jackendorf	Topological Geometro Dyn. Mode 1— Pitkanen
Radical plasticity thesis— Cleeremans	Poised state quantum model— Kauffman
Corollary discharge attention model— Taylor	Photon Med. Consc.— Bokkon/Dotta/Persinger
Attention to memories theory— Izhikevich	Noetic field theory— Amoroso/DiBiase
Bicameral mind model— Jaynes	Zero-point energy model— Keppler/Cagliuiri
Operational architectonics model— Fingelkarts	Neural field theory— Robinson
Self comes to mind model— Damasio	Infinite spiral staircase model— Hardy
Free energy unified brain theory— Friston	Nuclear spin neural Qbit model— Fisher
Triple aspect monism model— Pereira	Oscillating agent quantum model— Plikynas

References to the neuro-correlate models can be found in Seth [265] and for the Quantum brain models, see Meijer and Raggett [165] and other references in the present paper

5.5 Bio-Photon and Soliton-Mediated Information Transfer in Brain

Wang et al. [268], presented a clear experimental proof of the existence of spontaneous biophoton emission and visible-light-induced delayed ultra-weak photon emission in brain, as recently reviewed by Rahnama et al. [269] (Fig. 14).

In their experiments, they used *in vitro* freshly isolated rat's whole eye lens, vitreous humor, and retina. As a consequence of their findings, they proposed that the photochemical source of retinal discrete noise, as well as retinal phosphenes, may originate from natural bioluminescent photons within the eyes [266, 270]. Thus, a potential candidate is a photon/phonon-instrumented messaging network, that may operate parallel with neuronal transmission apparatus, as described extensively by Dotta [267] and Bókkon and D'Angiulli [266] and on an electromagnetic basis.

Georgiev and Glazebrook [271], presented a detailed analysis of the molecular structure of the synapse and concluded that the best candidate for the regulation of exocytosis is a group of three proteins collectively referred to as "Soluble NSF Attachment Receptor" ("SNARE") proteins. They showed that the conformation of these proteins at the neural synapse facilitates the creation of a quantum quasiparticle called a *Davydov soliton*. They further proposed a model based on quantum

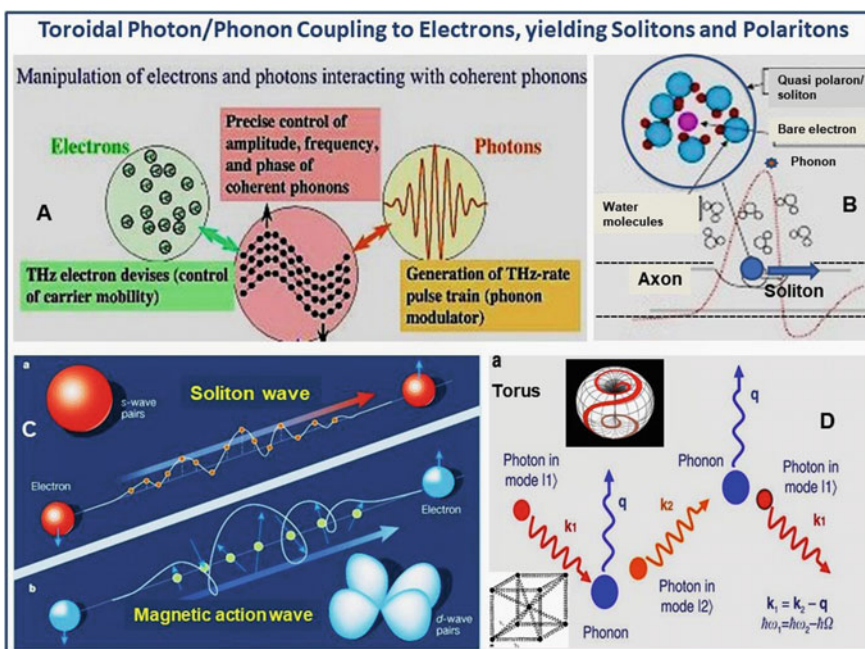


Fig. 14 The formation of phonon/electron quasi-particles such as polarons (solitons) and photon-electrons like polaritons and their interactions (a). b Polariton propagation along neuronal axons in brain. c Phonon dressing of electrons. d Phonon/photon interaction in matrix

tunneling of this soliton across a potential energy barrier and shows that the model is able to reproduce the experimentally determined exocytosis probability *and may thereby promote entanglement of neuronal structures*. Bessler [272], in a transparent analysis of this work, links this mechanism to the innovative studies of Flohr [273], who showed that impairment of consciousness by anesthetic agents always involves the N-methyl-D-aspartate (NMDA) receptor, a glutamate receptor which has also been shown to play a pivotal role in exocytosis and thereby in the creation of extensive neural networks. He suggested that this work of Flohr could well be related to the quantum entanglement aspect of the earlier mentioned Georgiev, as a top-down process of exocytosis mediated neural integration. Thus, *solitonic information transfer*, operating in a top-down model could guide the related cortical template to higher coordination of reflection and action as well as network synchronicity, as required for conscious states.

A few years ago [52, 60] we stated: electromagnetically seen, we may be living in a “diluted plasma” with natural coherent quantum resonances, that can be approached by equations for standing waves”. In this respect, the potential role of solitons (polarons, being electrons dressed with phonons) was highlighted [62]. Soliton waves exhibit remarkable resistance to distortions and noise interference, keeping shape and velocity even after collision with each other by which they can penetrate into materials without losing their identity. Therefore, they can function as information carriers in the entire universe, and were present at the beginning of life. They can also be regarded as energy-informational systems in whole organisms, in the brain as well as its components such as proteins, DNA, and bioplasm [61, 63, 95, 90, 274]. Soliton interactions with macromolecules result in self-trapping of electrons in localized soliton states. Due to these properties, they can guide protein folding and also can pass outside the brain in a sort of extra-cranial communication [274] and references therein). Phonon waves can, therefore, be considered as photon activity expressed as sound vibrations within a solid matrix and the physical similarity between both types of energy are described above. Photon-like waves are permanently present in our body through resonance, since the organism is embedded in the zero-point energy field and are also generated in the brain as so-called, bio-photons.

Photons are intrinsically quantum objects and, by their nature, long-distance carriers of information. Annila [275], stressed their importance in relation to consciousness. It seems clear that the properties of a molecule cannot be inferred from properties of its constituent atoms alone since they also rely on photons that couple them to their surroundings. The ultra-rapid brain responses, discussed in a previous publication [276], were seen as being related to photon/phonon mediated communication, in line with the findings of Bókkon and D’Angiulli [266], Dotta [267] and Persinger et al. [234]. Yet, in this context, the role of the earlier mentioned 4D-mental holographic domain coupled to the concept of a *universal consciousness field* (defined as the implicate order by Bohm [277, 9]) should be taken into account [2]. In this respect, a ZPE stochastic electro-dynamic field as postulated by Laszlo [184], Keppler [182], and Caligiuri [278], should be seen as the crucial “steering” modality that mutually communicate with the *whole nervous system of the organism*, including its neuronal networks with their conscious and non-conscious aspects. It

is of interest that Simon [279] related spin/photon-mediated quantum entanglement in the brain to the qualia aspects of consciousness and that photons being constantly generated in neuronal tissue may represent a primary evolutionary value for cells to detect potential dangerous reactive oxygen species, and later in evolution evolved in a general communication system in the neural context.

5.6 *The Concept of a Field-Receptive Workspace, Associated with the Brain*

Bidirectional communication between the brain and an intrinsic mental workspace was proposed to occur by toroidal integration of the above-mentioned information spectrum in both the physical and mental domains [1], see Fig. 15). It was postulated that the mutual communication process between the proposed mental workspace and the associated neuronal/cavity landscape is being instrumented by magnetic flux and/or photon/phonon/soliton-mediated wave resonance and/or phase conjugation.

It was postulated earlier [1], that consciousness in the entire universe arises through, scale-invariant, nested toroidal coupling of various energy fields, that may include quantum error correction. Such a toroidal process may cause the coupling of gravitational, dark energy, and zero-point energy fields, as well as that of Earth magnetic fields (Fig. 15). Through the supposed field-receptive workspace, wave information may be exchanged with the brain tissue, which thereby becomes instrumental in conscious and sub-conscious information processing. We proposed that the latter, crucial process, also generates self-consciousness which is conceived to be operating from a 4th spatial dimension (hyper-sphere). As treated before, the torus is envisioned as a basic unit (operator) of energy flow in space-time, among others collecting the array of discrete GM-frequencies that in concert represent an algorithm for coherent life processes [62]. The implied integral memory structure, associated with the brain is functionally implied by us as supervening as well as executing error correction of brain function. The reported time delay between experimentally induced actions of individuals and their 0.5 s delayed conscious perception of the event [280], could be related to the protective activity of the supposed mental workspace. This may be related to its central role in organizing action against the background of the integral self also in relation to its global connections with the entire world. This may represent an evolutionary inherited advantage in order to avoid surprise and counter-productive brain reactions in the broadest context.

It is of considerable interest that Alzheimer's models showing memory loss in the hippocampus area can be reactivated by photonic pulses into the corresponding cortical cells, using the technique of optogenetics. This procedure results in restoration of the retrieval of the particular lost information from the engram cells, likely due to the formation of new dendritic connections and related protein synthesis, possibly via light-sensitive proteins called channel rhodopsins,[281]. This technique

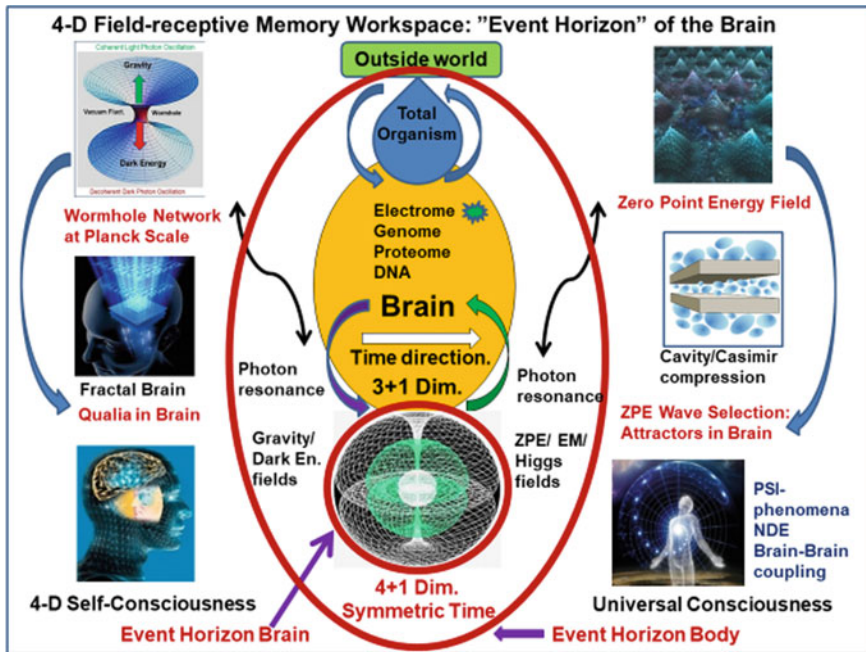


Fig. 15 Modeling of brain/mind relation in a $4 + 1$ -dimensional space-time framework. $4 + 1$ implies four spatial dimensions and one single dimension of time, on the basis of energy trajectories in a nested toroidal geometry. The opposing forces of Dark energy (diverging force) and Gravity (converging force) as well as discrete wave frequencies of electromagnetic fields, are instrumental in the generation and compression of individual life information. The human brain may receive quantum wave information directly derived from the Planck space-time level (left above) through quantum gravity mediated wave reduction, as well as through resonance with the ZPE field (right above). Our brain can perceive only $3 + 1$ dimensions with the one-directional arrow of time. The material brain and its $4 + 1$ -D supervening field-receptive mental workspace should be seen as an integral whole, until bodily death of the organism. The 4th spatial dimension allows individual self-consciousness since an extra degree of freedom is required for self-observation and reflection, while in the mental context the time dimension is symmetrical, allowing to integrate past and future-anticipating events. The 4th spatial dimensions is also assumed to accommodate the bidirectional flow of information between the domains of self-consciousness and universal consciousness. The bottom-up information flow from the Planck scale, combined with top-down information conjugation from the ZPE field, constitutes the event horizon of the brain, also integrating gravitational and dark energy related force fields, supervening the physical brain. Event horizons of the brain and the whole body are depicted in the red ellipse and circle respectively

may mimic the supposed photonic communication from the 4-D mental workspace as proposed in the present paper.

The importance of the concept of the universe as a cosmic hologram has been earlier reviewed in a comprehensive study of Curriwan [282] and was recently elegantly reviewed by Lefferts [160]. It was physically described in more detail by St. John [283] and related to a fractal 5-D holofractal structure by Linden [284]. In the brain, the proposed holographic workspace collects active information in its

“*brain event horizon*”, and is supposed by us to produce an internal and fully integral model of the self. This brain-supervening workspace is equipped to convert integrated coherent wave energies into attractor type/standing waves that guide the related cortical template to higher coordination of reflection and action. It may as well promote brain network synchronicity, known to be required for inducing conscious states. Here we find a striking similarity with the earlier conceptualized 3-D brain as a “personal universe” [164]. That the brain, with regard to information processing, may mirror a hyperspherical universe, in which the present universe is nested in a surrounding toroidal hypersphere, was earlier derived from Einstein’s relativity theory on the basis of a re-interpretation of the Klein–Gordon equation, as performed by the famous Italian mathematician Fantappié (see Sect. 2 and [285, 286]).

In relation to its scale-invariant global character of consciousness, extensive literature support was found for a universal (cosmic) information matrix [2, 287]. The presence of a field-receptive resonant workspace associated with the brain, being an integral part of a universal information field, may also provide an interpretation framework for the widely identified transpersonal conscious states ([1], see Sect. 5.7). A field type of information was also discussed in relation to an algorithmic origin of life [61, 63, 94, 95, 90, 62], see Sect. 6). In general, the potential reflection of universal consciousness in our individual brains points out the deep connection of mankind with the cosmos and our collective responsibility for the future of our planet.

5.7 *The PSI-Framework of Consciousness and Transcendental Aspects*

We hold that our collective knowledge field concepts may constitute an interpretation framework for poorly understood mental states such as intuition, telepathy, far distance observation as well as near-death experiences [244, 270, 288] and other Psi phenomena [227, 288, 289], to mention only some of the many studies available on this topic. In addition, the subjective experiencing of qualia as well as transpersonal and extra-sensory events such as clairvoyance and near-death experiences (NDE), seems compatible with our model [226]. The NDE aspect is documented in thousands of international reports and nowadays open to scientific inquiry [228, 270, 290, 291]. NDE’s can occur in life-threatening situations close to dying (asphyxia, near-drowning, traffic accidents, and stroke). They can even be induced by deep meditation, that is with full awareness of one’s own body [292]. In cases of stroke and heart failure, the specific components of this experience, often with a long-lasting psychological impact on the recovered patient, include so-called out of the body experiences, tunnel visions, and a remarkably clear and holistic state of awareness, verbally reported by the particular patients, albeit in retrospect. This conscious state is claimed to occur in the apparent absence of the cortical activity and is clearly different from a general dream state since in that case abundant EEG activity is observed in the cortical area.

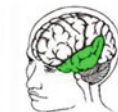
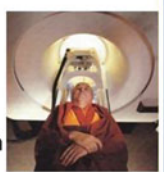
The typical descriptions of a felt dissociation from the body, in addition to a *total life panorama* [228, 290, 291, 293], as reported by a part of the NDE cases. This may imply an access to a wealth of detailed information of non-neuronal origin, that only can be imagined assuming a radiant and resonant mind field [18, 287], as proposed above. Such an external source of information seems to resemble the concept of a “personal double” as earlier proposed by [113]. The availability of such “external” information that somehow persists while other brain functions seem defective is characteristic. This overall picture of NDE may, therefore, imply the presence of a supervening field that is not directly dependent on normal cortex activity and the detailed verbal reports following consciousness recovery may indicate that information was obtained from another, seemingly timeless dimension (see Fig. 16).

In addition, other subjective phenomena such as intuition and serendipity, that frequently were envisioned as crucial elements in major scientific breakthroughs and/or technological innovations (Meijer 2017a), should be taken into account in this context. Breaking the barriers between the brain and a normally hidden information space can also be interpreted as a distortion of the normal “filtering” between conscious and unconscious workspaces [287]. Partial removing of filter function of the brain is also widely discussed in relation to the potential effects of meditation and induced dream states on such phenomena [225–228]. A recent paper of Tononi

**The Science of Self-transcendence and Neurotheology, How to Promote
Mystical Experiences and Perception of Universal Consciousness**

Self-transcendence correlates with brain function impairment
B. Kastrup, 2017, J. Cognition and Neuroethics, 4, 33-42 and Sc. Am.



- Cerebral Hypoxia: Holotropic Breathwork, program. hyperventilation
- Deep Meditation: Long-term meditation practizing by monks
- Physiological Stress: Near Death experiences, G-force, fainting
- Electromagnetic inhibition: Transcranial magnetic stimulation
- Trance- induced inhibition : Psychografic imaging by media
- Chemical inhibition: Psychedelics : DMT, Psilocybine, and Ayahuasca
- Stroboscopic light therapy inducing release of de DMT in the pineal gland (ajna light/ lucia N 03)



Fig. 16 The feeling of the reality of a cosmic (universal) consciousness, was suggested to be promoted by a number of procedures, of which the listed examples have been experimentally tested/and or investigated (see Kastrup [7, 226])

et al. [15], reviewing the earlier mentioned “integration of information concept” in consciousness, mentioned an interesting view of Sullivan [294] that *another type of consciousness* becomes manifest in meditative states that in fact can be considered as rather *information content-less*, and could reveal a normally hidden part of consciousness that is normally masked or filtered away by the busy default activity of our brain [226, 227, 228, 246].

In these brain states, biophotonic information transmission also could play a role. Generally, neurologists are hesitant to accept bio-photons as an extra messenger system along with the prevailing assumptions of the “neuron doctrine”. Yet, in physics, the photon is generally recognized as the faceful carrier of information between atoms and molecules and (not only for this reason) perfectly fits into the context of a versatile and dynamic brain structure. This is certainly the case if photonic wave information would be protected against decoherence in the brain environment through the influence of low-frequency phonons, realizing that a dominant aspect of de-coherence is via phonon coupling with the environment and that an acoustical mismatch between the immediate and wider environment of the quantum system could largely prolong coherent states at low frequencies [75, 77, 78, 93, 295].

Any organism (and also the brain) is considered as an open energy system, implying a continuous interaction with the environment. Yet, such interaction must occur in a noise protected manner, that requires capabilities of feedback control. Indeed, James, Bergson and Huxley, and more recently, Jahn and Dunne [226] as well as Kastrup [7, 8] speculated that part of the brain acts as a “filter” or “reducing valve”, by selectively blocking out external information so that only the registration and expression of a narrow band of perceivable reality is manifest. Possibly, in the course of evolution, the brain was adapted to eliminate most of those extra-sensory perceptions, being incompatible with the urgent needs of everyday survival.

One hypothesis suggested a dual development of the brain, namely an evolutionary improvement of technical and logical abilities, at the cost of loss of contemplative/spiritual potential [296]. Of note, in Kastrup’s studies the important suggestion was made that the normal filtering aspect of brain function can be largely decreased in a variety of special conditions that can be characterized as an evident *reduction* in overall brain activity (see Fig. 16). Carhart-Harris and Friston [297], in a lucid review on the potential mechanisms of brain actions of psychedelics, state that such agents relax the activity of a so-called *high level controlling summary system* that normally compresses information flow from lower centers, leading to ego-dissolution and liberation of compressed information due to an elevated entropic state. Such conditions lead to feelings of increased insight, cosmic unitive experience, and interconnectedness as well as therapeutically relevant elevated self-knowledge and social openness, by some claimed as the basis of an awakening to the true depths of being. Even several directed procedures (listed in Fig. 16) can be created to increase self-transcendental experiences and mystical states and open the doors to the perception of universal consciousness (recently treated in [287]).

5.8 Discrepancy Between Cerebral Structure and Cognitive Functioning

The implicit suggestion of a *non-material* and *extra-corporal* mental workspace, that may supervene and complement our neural system is indirectly supported by observations in fNMR studies that *long-term memory is not correlated with scaled sizes of the brain*. For instance, Savants, that usually have normal brain size, can demonstrate a huge, almost disproportional memory capacity: entire novels and even complete contents of telephone books are memorized in detail in such cases. Even more impressive are the observations with regards to so-called hydrocephalic patients that have only about 5% of normal brain volume (called microcephaly) and can show quite normal intelligence and social behavior [298–300]. Other striking examples are patients with a largely destroyed forebrain that maintain a quite normal life (Sasal et al. 2016). Even the known split-brain patients that seem to develop two different types of consciousness probably related to the isolated, right and left *halves* of the brain, in fact, show this aspect. Noticeable, split-brain patients with disconnected hemispheres can even perform better at some cognitive tests (see Sasal et al. 2016).

Nahn et al. [301], reviewed quite a number of striking cases involving brain dysplasias (abnormal cell development) and brain lesions (cell damage) indicating that large amounts of brain mass and its organic structures, even entire hemispheres, can be drastically altered, damaged, or even absent without causing a substantial impairment of the mental capacities of the affected persons. These exceptional individuals thus display a notable discrepancy between the condition of their cerebral structures and the quality of their cognitive functioning. This includes cases of gross hydrocephalus having global IQ between 100 and 130 and verbal IQ up to 140. In some cases, they were married, having a job, while in one case such individuals even spoke seven languages. Thus, the macro- and microanatomy of the brain and its tissue layers differ drastically in people with severe hydrocephalus compared with people with normally developed brains. For example, brain structures such as the thalamus, the amygdala, and the corpus callosum were not visible at their usual positions in the scans obtained from the patient, described by Feuillet et al. [298], but were most likely pressed toward the cranium together with the layers of the 0.5–1 cm cortical mantle, see later Fig. 24.

Often, such malformations result in impaired mental and motor skills, but apparently, this is not always the case. *The central question is if partial recovery from such conditions is due to plasticity of the remaining cells or, alternatively, is this related to the increased volume of the quantum informed, aqueous brain compartments. The latter would provide extra “antennas” for receiving quantum information as a compensatory factor* (see also Sect. 7).

Another case is presented in cases of *hemispherectomies*, how can we explain that the remaining brain structures and its neural activities can “know” that a “language center” is missing now, and how the remaining neurons induce and guide the duplication of this function in the still present hemisphere. Majorek [302] argued that this activity requires the existence of a “higher control center” that would be

able to detect this gap in function and to initiate steps that lead to its mending, and to imagine where such a control center could be located.

On the basis of these different cases of discrepancy between cerebral structure and cognitive functioning discussed above, some authors doubt that the brain serves as a sole comprehensive memory store, arguing that its function more closely resembles that of a receptor or transmitter of memory and allied cognitive processes [299]. Cleeremans [303], in his “radical plasticity thesis” put the question: “how the brain learns to be conscious”. The author implies that consciousness arises as a result of the brain’s continuous attempts to predict not only the consequences of its actions on the world and on other agents but also the consequences of this activity in one cerebral region on activity in other regions. Therefore, the brain continuously *learns to redescribe its own activity to itself*, in this way developing systems of *meta-representations* that characterize and qualify the target first-order representations. Such learned redescriptions, enriched by the emotional value associated with them, form the basis of conscious experience in interaction with the world, as a sort of signal detection of the mind. Cleeremans [303] stated: “Any theory of consciousness has to be able to explain why a person who’s missing 90% of his neurons, still exhibits normal behavior.

In the opinion of the present authors, the consensus concerning the crucial thalamocortical mediated consciousness, under normal conditions, still holds in spite of the abovementioned observations, but these observations also may indicate that consciousness can be *learned or received*, even when only the brain stem remains. The postulate of a supervening integral memory workspace in the present paper is very much in line with this idea. It is tempting to suggest that not only some sort personal brain is created within our organism, but that somehow, at the same time, an extra-neuronal personal information source is produced, that may be associated with the personal brain but is not reducible to it (see also [304, 305]). Both aspects of knowledge acquisition may operate in the framework of biological evolution and personal survival [287]. The human brain should, in that case, be rather viewed upon as an *information interfacing* system not only *connecting* individual and universal consciousness but seeing our consciousness as *directly derived from* a realm outside our organism. Such a modality forms the very basis for the concept of an “*extended mind*” that is founded in the philosophy of so-called Idealism [5, 6, 7, 8, 306].

It should be realized that, according to this concept, consciousness can be conceived as a part of “cosmic thinking”, and in this sense, quantum properties of the universe are also involved in such a thinking process. In Melikh [307, 308], a model was constructed, according to which the essential quantum properties of biologically important neuronal molecules may provide one potential basis of thinking. In particular, the strength of synaptic connection can be described based on the following equation [307]:

$$\frac{\partial p_n(\xi_{X12})}{\partial t} = \sum_m^{m_{\max}} W_{mn}(\xi_{X12}) p_m(\xi_{X12}) - \sum_m^{m_{\max}} W_{nm}(\xi_{X12}) p_n(\xi_{X12}).$$

Here X is a collection of innate behavioral programs whose physical realization is the quantum state of biologically important molecules. Indexes 1 and 2 relate to neurons between which synaptic contact is established. The variable ξ , stands for the internal degrees of freedom of the reacting molecules, as well as for their spatial position. The quantities p_n characterize the probabilities of finding the system in state n , and W_{nm} the frequency of transitions between states. The particular collective quantum-entangled state in the brain is open for quantum resonance through the cosmic force fields in which the life organism is embedded and requires a supervening field sensitive workspace (Sect. 7)

5.9 *The Generalized Music Principle as Created from Cosmic Harmonics*

The role of musical sound in discrete wave frequencies in the induction of very complex geometric patterns was earlier treated by us [1, 52, 60] on the basis of the famous experiments of Chladni,[67] (see also Rossing 1982), as well as the experimentations in cymatics of Jenny (1974) and Waller (1955). In these studies, sounds create clearly mathematical defined, distribution patterns of fragmented material on a flexible surface (see for this the illustrations of [160]). These intriguing observations, made quite long ago now, are still broadly mentioned in more recent physics.

In *Music and the Making of Modern Science*, Pesic [309], even claims that the art of harmonics shaped today's science in line with the science philosophical study on Science and Art of the present first author [4]. Music resonates, it pulses, it leaps into our psyches. From a wide array of scientific research in music cognition, neurophysiology, genetics, acoustics, quantum physics, and own calculations and experiments, Pesic developed a set of principles and mathematical models to explain how we recognize and enjoy music. The theory proposes that life grows as a balance between resonance and damping, just like a vibrating string and that music perception is a built-in pattern matching between the harmonic geometry of sound and identical structures in the ear and brain. It is from this organic pattern matching process that the musical qualities of consonance, dissonance, tension, and resolution can be defined mathematically and then visualized geometrically as crystalline and quasi-crystalline structures, (see also [160]).

In quantum mechanics and quantum field theory, the ability of energy to travel freely through space is referred to as vacuum permittivity or the permittivity of free space and defined by the “electric constant” (see Fig. 17). Each point (or quark) in the lattice requires a little extra space in order to oscillate and resonate, in which Phi provides in the phase-conjugate spacing of sinusoidal waves. Thus, the more harmonic and in phase the vibration, the more the so-called Phi gap comes into play and the more stable and coherent music and matter becomes (see Fig. 17c). [160] made clear that the aspect of damping creates the stillness that is required to really discern the individual tones within an octave, and that the perception of music rather

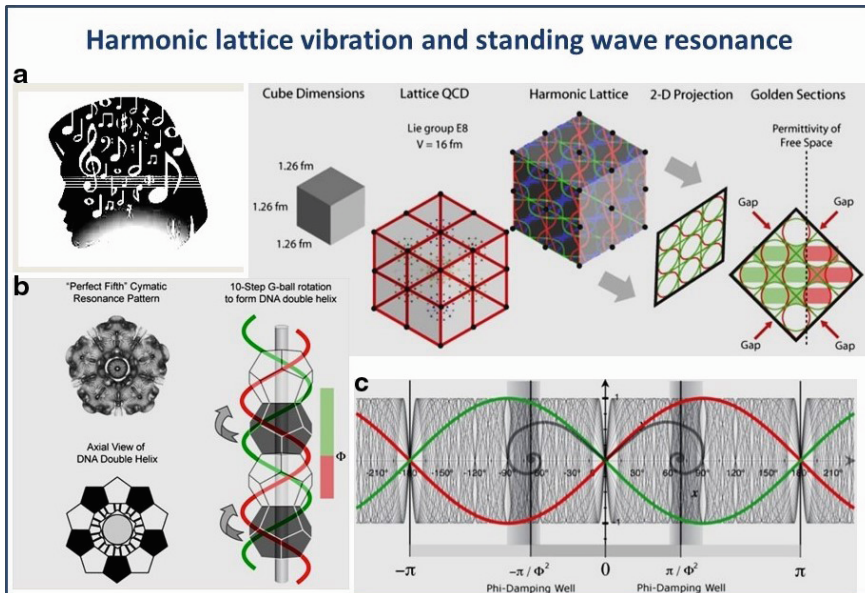


Fig. 17 **a** Permittivity of free space as a function of the golden ratio. **b** DNA double helix modeled as G-ball dodecahedron resonating up around a central axis. **c** Harmonic standing wave sharing energy inside Phi-damping tat provides the very separation of notes

becomes manifest *between* the notes. The study of these in phase states is thus based on quantum coherence and this aspect is fully expressed in theoretical science behind such phenomena as lasers, superconductivity, and superfluidity.

In general, the *Harmonic Interference Theory* of Merrick [310, 311], offered a unified natural philosophy that merges ancient Pythagorean harmonic science with the quantum holographic model of Bohmian physics and holonomic brain theory. One of the key principles of Harmonic Interference Theory is the idea that coherent wave interference of any kind is recursive in space and time, nesting the same pattern inside itself synchronously in order to maintain coherence.

The colors used in the various harmonic models are based on the simple idea that the visible color spectrum represents an octave frequency range just like a musical octave. Just as a musical octave is a frequency doubling of x to $2x$, such as A-440 to A-880 Hz, the color octave is also a frequency doubling from 370 THz to 740 THz. As a result, the Newton 12-step color wheel may be assigned as isomorphic spectral proportions to each of the tones in a musical octave using the Harmonic Center (D in the key of C) as a polar axis. Harmonic Interference Theory indeed proposes that it is the flow of energy across these two "Phi-damping locations" that account for perceived qualities in music, such as consonance, dissonance, tension, and resolution (Fig. 17c).

But what has music to do with brain function? Modern scanning studies have revealed a major influence of musical sound on brain activity and particularly in overall brain binding and connectivity.

In this musical framework, it is of great interest that music is increasingly used in the therapy of brain disorders and cognition studies. Music engages much of the brain and coordinates a wide range of processing mechanisms. This naturally invites consideration of how music processing in the brain might relate to other complex dynamical abilities.

Sanyal et al. [312], stated: the tremendous ability that music has to affect and manipulate emotions and the brain is undeniable, and yet largely inexplicable. The study of music cognition is drawing an increasing amount of research interest. Like language, music is a human universal, involving perceptual discrete elements organized into hierarchically structured sequences. Music can thus provide the study of brain mechanisms, underlying complex sound processing, and also can provide novel insights into the functional and neural architecture of brain functions. The change in the structure and form of music does clearly bring a change in the neural dynamics, inviting studies on the correlation of cognitive processes and a spectrum of musical modalities. Perlovsky (2009) made a very interesting analysis of its relation with musical emotions, suggesting an evolutionary split in proto-humans into one of language, offering the potential for *differentiation*, with an implicit loss of wholeness of the primordial unity of the psyche and another of music as a compensation for this. Music is rather directed at increasing the sense of communication-*shared intentionality* and *synthesis* in order to reconcile these cultural aspects in a new balance. Music, therefore, restores the deeper meaning of knowledge as an inborn instinct of harmony that, interestingly, is already manifest in babies beyond 4 months.

Of note, music is seen now as an important instrument in the rehabilitation of disorders of consciousness, (for example Alzheimer's) and is likely associated with neuroplasticity. In this respect, significant effects of personally- liked music on the brain level of certain neurotrophic factors, as well as on dopamine release and reward circuitry including endorphins, have been reported [313]. It is of great interest that recently striking results were reported on the treatment of Alzheimer's model in mice showing a clear reduction in amyloid plaques and improved cognitive performance, especially following a combination of visual (photonic) and 40 Hz acoustic brain stimulation. In this study the mice were treated with trains of tones repeating at various frequencies for one hour per day during seven days [314], demonstrating the potential healing effect of such therapeutic music guided approaches that may have a toroidal geometric background.

According to Koelsch [315], a number of studies demonstrated that music listening, (and even more so music production), activates a multitude of brain structures involved in cognitive, sensorimotor, and emotional processing. It is likely that the engagement of these processes by music can have beneficial effects on the psychological and physiological health of individuals. In addition, neuroscientific studies, in which music was used in order to investigate emotion and social cognition are reviewed, including illustrations of the relevance of these domains for music therapy

Many examples of distinct EM frequency bands of brain cells, neurons, and different glands have been identified (see Persinger 2016; [316, 317]), that largely resemble some of the individual eigenfrequencies of the geometric/acoustic pattern revealed in our studies. This supports the notion that communication of life information through coherent EM radiation is a widely spread phenomenon and that this aspect deserves further detailed investigation (see further Sect. 7).

We propose, therefore, that the pro-life EM frequency bands, identified in our studies may literally act in concert as “tonal octave-based symphony” to provide living systems, including the brain, with information embedded in such harmonic-like resonance patterns (see also [170], as discussed later). Such “tonal” projections, that , may organize synchronicity, both spatially and temporally in essential organs in the body (heart and brain). This “tuning” of life processes may originate from the proposed supervening resonance field, which in the brain imposes a coherent vibrating 3-D imprint in the cortical region, producing an *integral* modality of consciousness [1, 61]. The relation between music, harmonics, and consciousness was also treated by Pitkänen [318], and Heyning [319], interestingly both from the point of view of Pythagorean harmonics and modern physics. Pitkänen [318] discussed the GM-scale theory as treated above in Sect. 3 and stressed the importance of zero energy ontology and holography, also stipulating the importance of fractal hierarchy for brain function. Fractality and power-law scaling are considered to be a crucial aspect in both organization of life systems in general [320] and in neurodynamics in general [209].

It is of major importance in this respect, that recently a brain model was proposed on the basis of a fractal information theory, derived from a geometric musical language that enables the brain to perform intelligent hypercomputing [321]. It is based on the concept that any living system is part of music that is played in the universe, and involves chains of resonances in the fractal brain structure, with at all levels a specific micro-clock in a nested configuration ranging from macromolecules down to atoms. Such a type of fractal information processing in the brain was earlier proposed by us [276]. Interestingly, and in accordance with our concept, the group of Bandyopadhyay [100, 321, 322, 323] found evidence for firing *below the synaptic threshold* in EMF-guided information processing in the brain. The particular oscillatory activities are supposed to be generated not only in microtubuli but also in many other protein complexes in the cell, that is, clearly in a fractal setting that is expressed in circular and periodic modes in 12 fractal memory layers. The authors developed an innovative technique of atomic resolution scanning dielectric microscopy enabling the observation of the operation of a resonating single protein [324]. The multi-layer memory may operate on the basis of 3-D resonance chains that also contain un-occupied elements that can be filled up by electromagnetic oscillator activity to produce proper information processing in the required integrated time cycles (resembling the concepts for superconductors in Sect. 3.3).

In the brain, Bandyopadhyay et al. identified 350 different classes of cavities in the nested (fractal) 12 layers and described each *cavity resonator as an octave musical flute* that together with silence periods collectively generates the known

brain rhythms. Their fundamental basis is fractally organized, geometric information that finally becomes expressed in the EEG. They identified 12 discrete resonance frequencies, among others with a solitonic (quasi-wave-particle) frequencies, very much resembling the mathematics of our GM-scale EMF pattern [53]. These discrete frequencies are integrated with many other factors in so-called “*fractal frequency wheels*”. As mentioned above, we submit that the periodic circular/spiral energy trafficking in the brain is organized according to in nested toroidal geometry, in which each oscillation returns to itself in a self-referential manner, thereby tentatively explaining the aspect of self-consciousness. Of note Bandyopadhyay et al., mentioned two types of memory loops they could not physically define, called by them “hyperspace memory” and/or “assembly of reality sphere”, that we may have defined in our present work on an event horizon memory workspace (see Sect. 5.7). This aspect has also been approached earlier by toroidal computing [62, 252, 253, 325, 326, 327, 328].

So, what can we learn from the role of a potential *musical master code* that likely operates scale-invariant in the Universe? In our first papers on the generalized music principle and phonon-guided biology [52, 62]. As mentioned above, we suggested that “electromagnetically seen, we may be living in a “diluted plasma” with natural coherent quantum resonances, (see also Van de Bogart 2019). Now we indeed see the growing importance of *acoustic cosmology* [329, 330] that is manifest on the macro-scale in a plasma universe (Peratt 2013). On the micro-scale there is also rising interest in distinct musical patterns steering on the level of whole organisms and cells [3]. This is valid for various components of cells such as microtubuli in the group of Anirban Bandyopadhyay [322, 323, 324, 331], DNA [332, 333], Pi-electrons of lipids [334] and also the sound tapestry of single proteins and their networks studied in the MIT group of Buegler [335, 336]. All this, points at a resonant vibrational matrix that guides life and possibly entire nature, using a distinct musical code [3]. This may also be true with regard to brain dynamics, as discussed in the present paper, for which even a novel brain ontology of *neural resonance and acoustics* was earlier proposed [133, 134].

5.10 Universal/Cosmic Consciousness and Brain Function

The presence of a “steering” functional mind field may provide an interpretation framework for those phenomena that still seem to escape current scientific verification. A most important aspect is the, often mentioned, modality of Universal consciousness also called Cosmic Consciousness. This concept, that information can take a universal character and that all information is stored in a general knowledge field or universal consciousness, can be treated from a number of backgrounds and perspectives (reviewed recently by [4]). As mentioned before, the concept is well-known from the work of Bohm ([9], 1987), who coined the term implicate order and László [184], who introduced the so-called Akashi field concept. The latter author particularly linked his concept with the physics of the zero-point energy field (ZPE)

that, as previously mentioned, was later also applied in stochastic electrodynamic models for consciousness by Refs. [6, 7, 8, 224, 278, 337].

Such an all-pervading cosmic field can in principle exchange information with the supposed 3-D and 4-D workspaces associated with the brain (see Fig. 18). An important study from Princeton showed that two, and possibly more, brains can become interconnected, looking at the brain f-MRI scans of speaker and listener. It was shown that the brain activity patterns of such a communicating couple are clearly correlated in a sort of wave resonance, mirroring, effect [338–343]. This study also invites further investigation into mechanisms of telepathy and so-called synchronicity [226, 227, 228, 233].

Hardy [344], takes a space-time approach by positioning individual consciousness and the Self in a *hyper-dimension* in which death is just the severing of the link between this domain and the brain/body, leading to an independent holographic semantic field on a personal basis. This aspect was further worked out recently by Meijer [287]. The latter phenomenon resembles the proposal of Irwin [345], seeing consciousness as a quantized space-time language that can be described

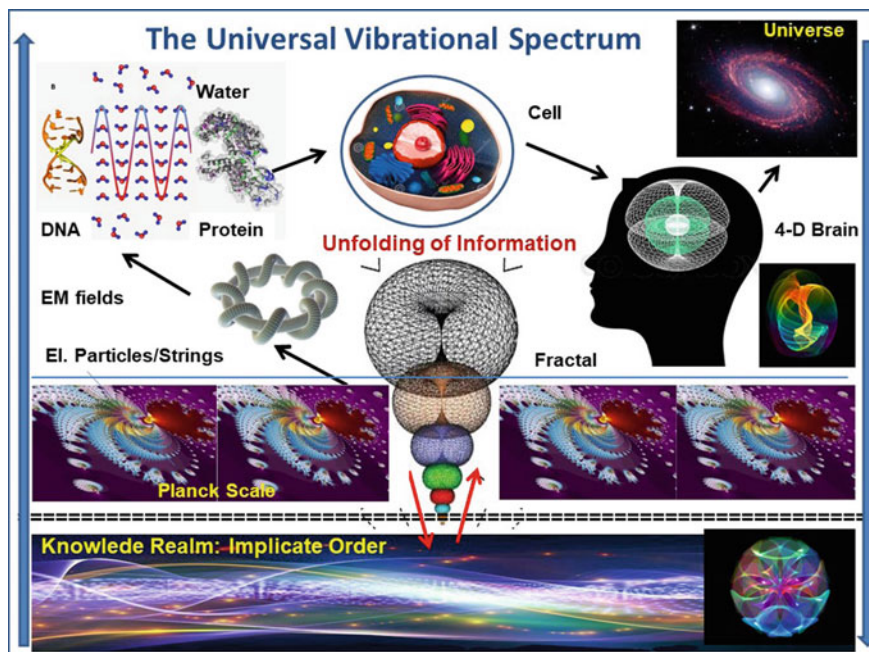


Fig. 18 The flow of information in the whole universe from micro- to macro-levels (bottom to top) conceived as a nested toroidal operation that is fractal and scale-invariant and is initiated in a knowledge realm underlying the known wormhole matrix (quantum foam) at the Planck scale. Supposed quantized string activities produce elementary particles, atoms, molecules and life systems. The latter contain dedicated holographic memory spaces at the cellular and organ level. The human brain integrates, internally and externally, guided conscious states. Further fractal and self-similar properties in a quantum fluid universe provide the architecture of cosmic macro-structures

by quasicrystal mathematics of the E8 geometry. It was also suggested that self-consciousness could continue outside the body but remains at the level of Planck-scale geometry, as related to the generation of biophotons in which visual imageries are coupled to long-term visual memory. This is supported by a strong indication that NDE is driven by visual processes [270].

In more general terms, the aspect of non-material mental aspects of consciousness has been thoroughly pursued from neurological [346], biophysical [182], philosophical [6], quantum physical/cosmological [195] and evolutionary viewpoints [22, 347].

As mentioned above, Penrose [348], proposed that spin networks could be fundamental in the description of space-time, that is, in a background (string)-lacking manner, (see for the latter also Rovelli 1996; Smolin 2004). In the brain, spin networks were pictured as electron-unpaired electron spins that represent pixels, collectively forming a “mind screen” that is known to be highly sensitive to fluctuating internal magnetic fields and action potentials. Such perturbations were considered to modulate neural dynamics, but also could enhance synchronization and stochastic resonance as have been noticed in the brain (Hu and Wu 2004). The particular spin physics, bridges classical neural activity, serving as input via the magnetic influences on biochemical processing.

Spin network dynamics may enable a quantum decoherence-resistant entangled modality of wave collapse since, through tunneling, they are rather insulated from the environment in decoherence-free subspaces, while repeated attention/intention (the so-called Zeno effect, see [263]), may help in promoting coherent quantum states (Hu and Wu 2004).

Finally, we want to emphasize again that general ordering of the functional architecture of cells is obviously not sufficient to explain the fine-tuning of life: clearly, deeper, more subtle, levels of dynamic organization are required. It was recently pointed out by Görnitz [163], that we do know very little of the fabric of reality from the size of the electron down to the Planck scales, and that it is a *misunderstanding that going smaller makes understanding simpler*. This is also true for explaining life: Grandpierre (2011), postulated that “DNA works with the help of a factor that is utterly beyond DNA or any other material life system physical capabilities. This something is immaterial yet effective and belongs to science and is called by him the first principle of biology that acts as a deeper intelligence of the “vacuum”. This, in the sense that it virtually maps all the possible histories, summarizes the results of this mapping on its own basis and then decides about the biological endpoint and from there, and finally “chooses” the optimum physically realizable path”. This may also account for the fact that intelligence is a highly convergent feature in different evolutionary lines of animals that may have highly different brain structures (see also [349, 350]; Horic et al. 2012).

Conclusion: In the present essay, it is considered that the brain and mental aspects are somehow coupled to the universe, probably via its superfluid domains (Fig. 15), meaning that apart from neurobiological QM processes, cosmological QM-ones also affect brain transitions and dynamics. A unified theory of mind and matter has been postulated earlier on the basis of *information*, viewed upon as the most

fundamental element for the description of the fabric of reality [18, 19, 23, 245, 351, 352] (Grandpierre et al. 1997). In other words: life, with its potential energy and isoenergetic character, exhibits the ability to screen and collect useful information, counteracting the destructive tendency of ever-increasing entropy and at the same time may employ (entropic) gravity mechanisms to materialize essential knowledge. Perhaps this bimodal modality has been foreseen by Schrödinger (1986), as the potential contribution of quantum processes in creating mental dimensions.

6 Prominent Roles of EM Fields in Biological Evolution and First Life

6.1 *Introduction*

The development of science is not a linear way of steady progression; it is more akin to a living organism and knows not only ebb and flow but also critical bifurcation points, as aptly described in the seminal book about revolutions in science by Kuhn [353]. These are the points of major decisions in which a current scientific discipline radically changes its outlook, its paradigm, and its understanding of laws. It, therefore, separates itself from a part of previous achievements as they are no more in harmony with the newly chosen paradigm and insights [4].

In biology and related sciences, the situation is even more complicated (than for instance in physics) since biology still lacks the actual definition of its very object of research, namely, life. The majority in consensus science would say that life is a highly organized and complex biochemical process, which pivots around DNA or RNA. However, this outlook seems quite limited, since it cannot satisfactorily explain various phenomena, especially the ones discovered in the field of bioelectromagnetics by some called the “electrome”. This aspect is connected to the generally recognized electromagnetic signature of a spectrum of organisms and also includes the consistent finding of effects of externally applied EMF radiation on various organisms *in vitro* and *in vivo*, according to the GM-scale frequency patterns discussed above. Thus, a supplementary outlook should be adopted, based upon a biofield concept, sometimes framed as a morphogenetic field [64, 89, 354, 355, 356, 357].

The basic principle that hovers behind life, should come into expression at its origin. In other words, to understand the essential nature of life, one should understand the processes of its very emergence. Since an increasing number of uncovered exo-planets, resembling the Earth, are being discovered almost daily, the question of life and its origin cannot be limited only to the known life on the Earth but should be extended to that in the whole universe. If life is indeed widespread in the cosmos, it may drastically differ from the chemistry known on the Earth (DNA-RNA/proteins). Also, it could possess characteristics and capabilities that may fundamentally differ from the situation on Earth since adaptive changes would be dictated by other planetary conditions. On Earth, contemporary life, even in its simplest forms, exhibits high

complexity and order. In terms of informational theory, it has a relatively high informational content that should be stably reproduced from generation to generation, still allowing adaptive changes for survival. In this respect, the processing of chemicals that could be reproduced in simple primeval Earth-simulating conditions (like ammonium ion, formaldehyde, hydrogen, etc.) would still lack a clear, persuasive, and stable explanatory scenario for the formation of the essential building blocks of life. Thus, it seems unlikely that this approach, of starting with similar precursors to finally obtain macromolecules capable of accurate duplication, would easily lead to endproducts similar to those in contemporary organisms [19, 63, 358]. Even Miller, the famous scientist that simulated the pre-biotic Earth conditions, resigned from his primary optimism when he realized that it is almost impossible to achieve the synthesis of, for instance, the RNA world in such a spontaneous way [359]. Anyway, the RNA world perse would be unlikely to solve the major origin of life problem, namely the known DNA—protein dichotomy.

Disillusioned by the possibility that life and its origin can be explained solely by chemical processes, a novel concept was formulated by Walker and Davies [94]. Their starting point for the emergence of life was envisioned in the establishment of causal powers from the side of *organized information over molecules*. Here, the information in living systems is not seen as coded in a linear process (as through DNA), but in a diffuse, quantum wave-like, non-localized manner (Fig. 21). In this concept, the dispersed, organized, and operational (active) information only partially resides in DNA. It is rather widespread as if diffused in the whole living state of the organism. This aspect is known from the experiments with *Acetabularia mediterranea*, which can reproduce its cap even without the nucleus, therefore with no DNA is needed [87, 356, 360].

Consequently, and in line with Walker and Davies, we may transcend our understanding of organisms only as *trivial duplicators with errors* and assume a much more advanced point of view that was implicit even in von Neumann's work [361]. In contemporary computer science, the principle of self-organizing potential is well-known as related to any informational system. Various types of artificial intelligence have been shown and, among others, can be expressed in attempts to design the evolution of artificial life [362]. Therefore, in this more advanced view, organisms are perceived as systems that process self-organized information with a high degree of flexibility (variability, adaptability). Accordingly, life can be defined basically as a dynamic and highly (self)-organized form of information processing [18, 19]. In a more comprehensive framework, such dynamic and highly organized information, expresses itself through molecular systems and that are capable of further, potentially limitless, enrichment of their content, (leading to higher complexity) and fractal levels of organization. The origin of life then could be envisioned as the enrichment with problem-solving information, combined with a further sophistication of biochemical/metabolic instrumentation [360]. Therefore, in our attempts to understand the possible origin of life as well as its continuation, we may try to identify those essential vital factors that

- (a) should play an essential role in biological processes in ensuring the enrichment with holographically dispersed information that contains meaning for useful adaption and survival,
- (b) should maintain a high level of orderliness and stability, even in highly diversified chemical systems (even systems without intrinsic “memory” molecule or genetic codes),
- (c) should be able to increase its informational content (complexity) through time in an evolutionary context,
- (d) should be capable of specific interactions with a wide range of molecules, with capabilities to direct their transformations in a catalytic way (effectiveness),
- (e) should at least be feasible, if not probable, under the supposed conditions of the pre-biotic world.

Contrary to the conventional biological expectation that these vital factors should solely be expressed in molecular features, or in the function of biochemical networks, one should transcend *short-range chemical reactions* but should rather take into account *long-range signaling* as it is provided in the area of (bio)physics, in the realm of bio-fields. A promising path in this direction was taken by the already mentioned British biophysicist Herbert Fröhlich, who made a great discovery in the sixties of the last century. Seeking an integrative principle working in living cells, he found that the living state, at the level of cells, rests on rhythmic and coherent oscillations of polar (macro) molecules [148]. He found that these synchronized oscillations could bring higher orderliness in cells and even into the cellular biochemistry. Fröhlich’s ideas were later elaborated by an Italian group of quantum physicists [113, 131, 138] from the standpoint of quantum field theory. This theory, called quantum bio-electrodynamics, argues that life at the cellular level (biochemistry, molecular movements) is highly organized through coherent (laser-like) electromagnetic (EM) fields that can guide formation of organized water molecular clusters (coherent water domains or CD’s) and also the oscillation of particles of various mass (Sect. 3.1 and 3.2). If the frequency of a coherent EM domain resonantly matches a neighboring molecule, the latter is attracted to its outer surface and oriented at the same time. The field is also important from the thermodynamic standpoint, namely the output energy of a chemical reaction is not dispersed since it continues traveling as a longitudinal wave, i.e., as a *soliton* being a quasi-particle of phonon covered electrons. Hence, in an extended coherent region, i.e., the region that comprises many CDs and in which the diffusive, Brownian motion of molecules is replaced by a selective dynamic oscillating regime, where molecules recognize and interact with one another via *frequency matching*. Since the excitable spectrum of a CD is very rich [363]), a variety of extended domains—domains of domains—may emerge, assuming fractal (nested) architecture, as analyzed by Vitiello [113, 364].

Extended coherent domains involve two important features, namely, a defined size of the coherent system and the appearance of geometrical shape [114]. To have a precise frequency matching, the relative positions of reacting molecules must assume a specific spatial configuration, corresponding to the biological structures involved. Taking into account the assumed primordial conditions on planet Earth, the coherent

characteristics of water treated in Sects. 3.1 and 3.2, as well as the findings of Fröhlich in relation to the quantum field theoretical extensions, we may have identified the above-listed elements of the vital factor. All of the five required characteristics of a partially coherent and hierarchically ordered field of polar oscillations in an aqueous medium, including dissolved molecules, are present (see Fig. 19). According to the previously formulated definition of life, we hold that such organized systems cannot stay alive and reproduce if they lack stable and long-range trajectories in evolutionary phase space to attain even higher complexity for meaningful adaption.

Without such dynamic features for the coupling between coherent modes (existing on the field level) and bio-chemistry (existing at the substance level), they would be similar to various autocatalytic cycles and only, by appearance, resemble cellular structures. One example is Oparin's coacervate [365], representing tiny bodies that strongly resemble living organisms. Their multiplication indicates that they do possess *active organized information* on a certain level but since they lack a genetic memory, distinctive for ordinary living beings and even viruses, cannot be considered as living beings. It seems therefore that only specifically organized information, through a close and mutual interplay of the coherent EM fields with the spectrum of

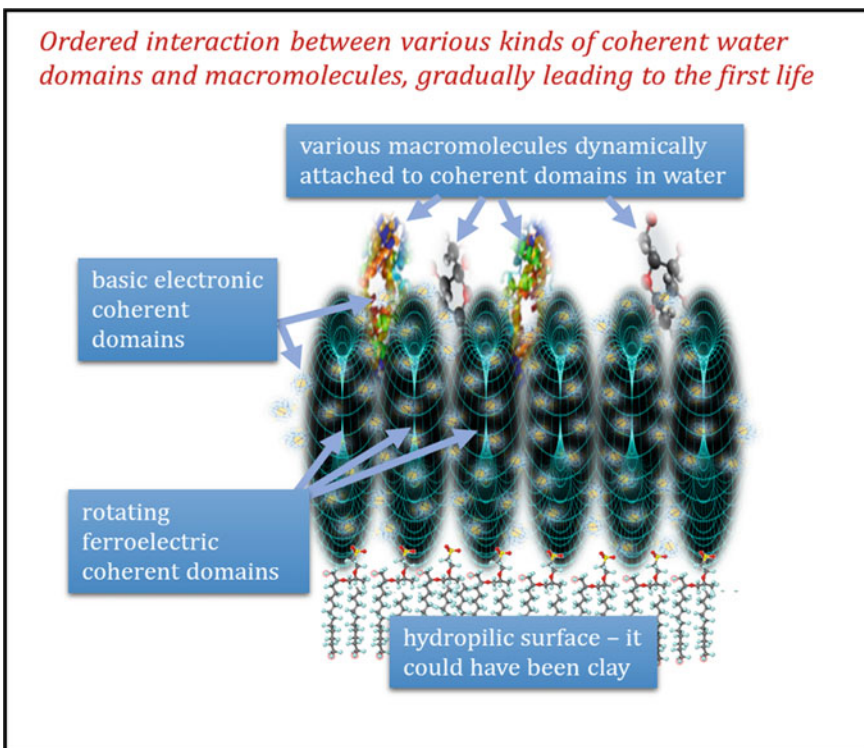


Fig. 19 Ordered interaction between various kinds of coherent water domains and macromolecules, gradually leading to conditions for first life

molecular network interactions ensures the successful transition from the prebiotic stage to the first life.

The intrinsic order of coherent modes of pre-living vesicles of organic and inorganic substances in primordial water solutions (in oceans, lakes, pools, etc.) probably functioned as a dispersed systemic memory that could sustain active organized information without the contemporary function of DNA or RNA. No genetic code was therefore initially needed, instead, a code of resonant matching between coherent field oscillations and molecular reactions was sufficient. Presumably long after the first living organisms appeared, natural selection together with the laws of the living state dynamics, resulted in the transfer of dispersed memory contained in coherent oscillations into compartmentalization of molecular ordering of sequence information, as based on DNA and RNA that allowed persistent information storage and retrieval.

6.2 *Creation of First Life and the Role of Phyllosilicates (Clay Materials)*

In addition to our considerations that connect the coherent EM field considerations that deal with the origin of life, we can add some more chemical considerations that are closely connected with the already discussed coherent field. It was Cairns-Smith that first proposed a comprehensive theory of the origin of life, based on clays [366]. Further research in this direction found additional important points supporting the original hypothesis that, in a certain prebiotic phase, clays played an important role in the process of the formation of life. Namely, some of us found that coherent natural and permanently operating wave pattern phenomena are present in typically selected clay minerals, that have semi-conductor like properties [52, 53, 60, 62]; identical EM field eigenvalues could be measured by Ir. J. H. Geesink, The Netherlands (Fig. 20). Of note, these types of clay minerals are, apart from being present in the soil of our planet, are also abundantly suspended in the whole universe, in the form of, so-called, cosmic or extraterrestrial dust. This versatile material can contain some water and has been suggested to provide a semi-conductive medium that produces selective EM wave patterns following solar excitation and exposure to other external energy sources, providing conductive properties on a cosmic scale.

Interestingly, such silicates have been reported being among candidates for the facilitation of oligonucleotide synthesis in the creation of first life in the biological evolution [1, 52, 60, 90, 62, 68, 69]. The selected silicates probably act as quantum replicators. They specifically emit EM radiation at GM-like coherent frequencies in the surroundings of ordered water molecules. Therefore, such silicate quantum replicators may have been instrumental in the initiation of first replicating cells, somewhere towards the end of the pre-biotic evolution [22, 94, 347, 68, 69, 367]. We hold that the organization of precursor molecules for building the first life macromolecules fits into a discrete coherent pattern of resonances, and can be described by

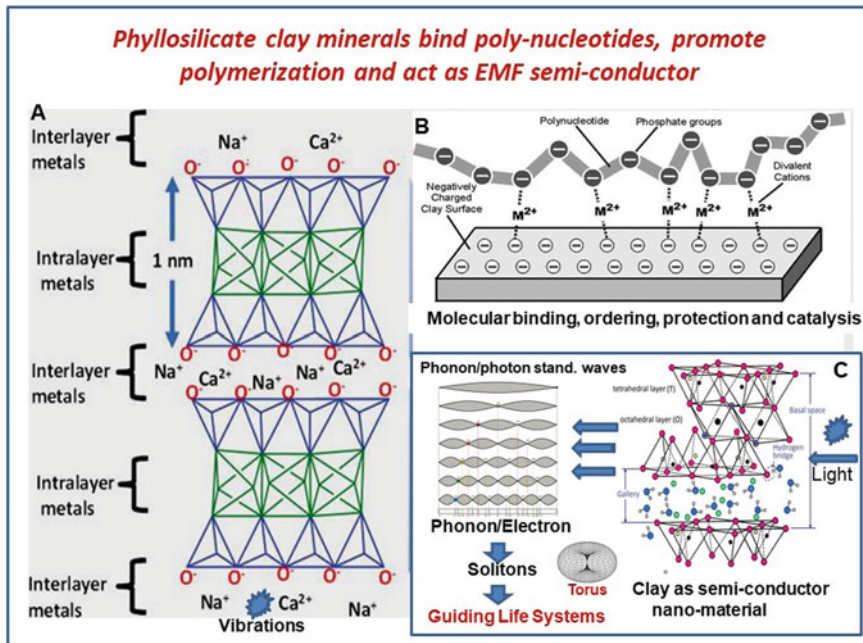


Fig. 20 Phyllosilicate clay mineral with stabilized ion/water clathrates. **a** The metal ion-doped silicate structure exhibits platonic geometries (After G. Sposito). **b** Surface structure of a clay mineral offers binding sites for negatively charged polynucleotides as assisted by positively charged metal ions. **c** Clay a semiconductor: EMF wave function, guiding the ordering principle in life processes as an acoustic, standing wave, system, generated by transmitting exposed light to discrete EMF wave frequencies

the proposed semi-harmonic quantum wave equation, see Sect. 3). Another item is the number of possible spatial configurations of replicators. As was shown in [308], the complication of replicators sooner or later leads to the impossibility of simple enumeration of their conformations. This entails the need to take into account the quantum properties of biologically important molecules (see also Sect. 6.2).

In general, quantum processes, working on the field level, creating the potential of atomic resonance producing organic shapes and geometric folding of carbon-containing molecules ([22, 94, 219, 347, 367], in Sect. 5.3 and Fig. 13). This basic mechanism should have paralleled the lattice type of organization of dipole water molecules as mentioned before. Together they should have formed a harmonic-like matrix resembling fluid crystals in which life can be viewed as a crystallized (stabilized) form of quantum oscillations. This concept invites us to see the cosmos as a partially guided incubator for life as treated in Sect. 6.4. Very likely, syntropic (i.e., neg-entropic) wave information from the zero-point energy field [70, 187, 368], selected in resonance with the electrome [45] of the proto-cells, played a crucial role in the morphogenesis and building up of functional biochemical networks during pre-biotic processes [224, 369, 370, 371].

Conclusion: elements in the universe have apparently assembled themselves in such a way that the organization of matter resulted in the ability to acquire sufficient life-sustaining information from the environment and the quantum vacuum. Over time, highly complex neg-entropic structures arose that could collect, store, retrieve, and communicate essential information to maintain stability and survivability. Such pattern recognition ability may have been directed by combinations of EM radiation frequencies through inducing morphic resonance with coherent vibrational elements (structured water, proteins, oligonucleotides) of proto-cells [3, 63, 90]. Here, the 3-D conformation of macromolecules is crucial in attaining a versatile functional state, as treated in the following.

6.3 Long-Distance Guiding of Cellular Processes in Life

According to Wolynes (2015), the integral 3-D protein folding process includes random mutations, potential misfoldings/unfoldings, recombinations, and selection by successful competition with less optimal protein species, in which the protein finally obtains sufficient stability in subsequent generations of cells. As such the proteins were seen by the author as non-linear elements in cellular networks that *arise from a sort of information spaces* that, unfortunately, were not further defined. One could also question the supposed random character of this self-organizing process. In other words, how can the selection of non-functional precursors of the particular protein be envisioned? Moreover, by what physical mechanism is a specific function assigned to the particular protein? As argued by Grandpierre (2001), life functions of proteins cannot arise by chance, they can only be assigned by their host cell itself. Yet, such a cell cannot arise without these functions being already assigned and present.... We propose therefore that a primordial biological principle (a register of rules) was operating, which acts as a “recipe for life” [19]. This type of a-priority information must have preceded the development of first life and we postulate that all known force fields, that were present from the birth of the universe, should be taken into account (see more on this aspect in Sect. 9). In addition, as treated before, quantum processes have probably played an essential role in facilitating the various steps that gave rise to the first life and initiation of the first replicating cells [63, 94].

One of the unsolved problems of cell functioning is the problem of protein folding (Levinthal’s paradox). Despite several decades of attempts, this problem is still unsolved. In [90, 372], this problem is generalized to arbitrary interaction between biologically important molecules in the form of a *generalized* Levinthal’s paradox. The particular paradox is formulated as follows:

The number of degrees of freedom (mainly conformational) of molecular machines and other molecules in the cell is exponentially large, but only a small fraction of them are permissible during the functioning of the cell. On the other hand, the interaction potentials between atoms, based on their interaction mainly with their nearest neighbors, do not allow us to distinguish precisely these degrees of freedom.

To solve the paradox, a model of interaction between biologically important molecules was proposed, including long-range quantum interaction between them. According to the model, the general form of reaction-diffusion equations between substances u and v will be as follows:

$$\frac{\partial u(\xi)}{\partial t} = \gamma f(u, v, \xi) + D_u \Delta u.$$

The presence of the variable ξ in this equation means that a *certain* reaction between these substances will substantially depend on their conformations. Only at a certain value of ξ can a reaction be considered to be completed. For all other values, it can be said that substances are eliminated from the “game” because they are not able to perform useful work (the probability that the substances are useful will be small). The problem of the accuracy of reactions between biologically important molecules is important for any cell, from protocells to protein sorting in modern cells [373, 374].

England et al. [375], on the basis of conventional thermodynamics, derived a mathematical formula they believe is capable to explain the capacity for creating life conditions. The formula, based on established physics (more precisely, the 2nd law of thermodynamics of entropy), indicates that when a group of atoms is driven by an external source of energy (like the sun or chemical fuel) and surrounded by a heat bath (like the ocean or atmosphere), it will often gradually restructure itself in order to dissipate increasingly more energy.

This could mean that under certain conditions, matter inexorably acquires the key physical attribute associated with life. Consequently, according to this hypothesis, as particles in a system move around and interact, they will, through sheer chance, tend to adopt configurations in which the energy is spread out. Eventually, the system arrives at a state of maximum entropy called “thermodynamic equilibrium,” in which energy is uniformly distributed. It is known that the phenomenon of quantum coherence, assumed to be present in prebiotic systems, may enhance photosynthesis because it simultaneously excites two kernels in the system by the appearance of two interrelated quantum-entangled excited states [376].

England [375], stated that: “Living entities are self-assembled and self-replicating wet and warm, stochastically moving, supramolecular systems where quantum entanglement can be continuously generated and destroyed by non-equilibrium effects in an environment where no static entanglement exists. Quantum entanglement involves the biomolecules inside one living or between other neighboring living entities”.

However, a number of fundamental questions can be raised with regards to the proposed mechanism of emergence of cellular life by England et al., especially with regard to the item of self-organization:

- The present authors maintain that such an emergent process will exhibit countless potential solutions to which the evolutionary time would be insufficient to make proper choices for ones that lead to the first life [90].
- It speaks for itself that in this manner molecules could in principle be formed that are suicidal for the overall process, as it has already been demonstrated for Eigen’s

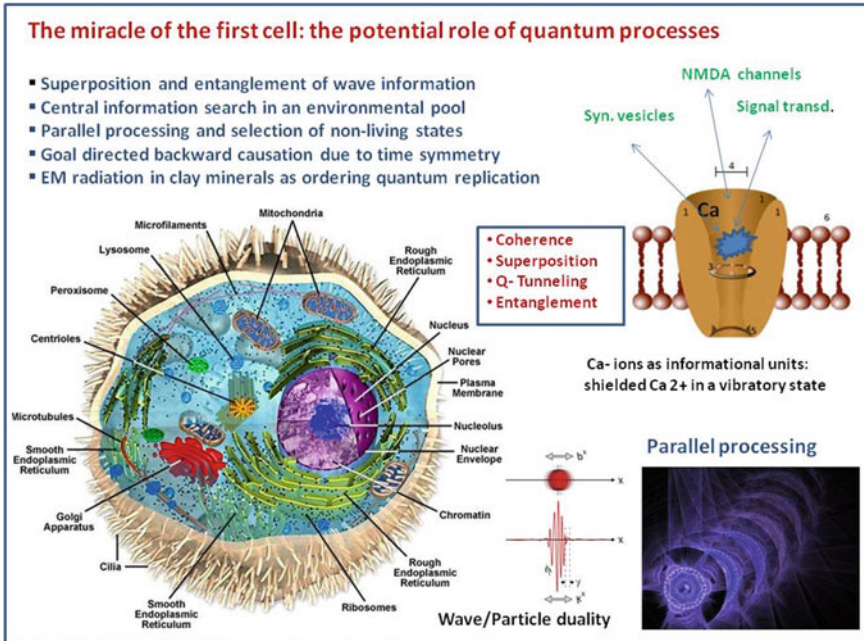


Fig. 21 Potential role for quantum processes in biological evolution (listed left above) and the initiation of first life, showing various essential processes. Inset on the right above depicts a Ca^{2+} channel protein with Ca^{2+} -ion in a decoherence protected vibratory quantum information state. Inset right below indicate the process of parallel processing of pre-biotic life information as enabled through environmental search of various quantum states

autocatalytic hypercycles that would be sooner or later destroyed by parasitic autocatalytic (hyper)cycles [377].

- The scheme of England does not take into account that a potential top-down information flux of future states can in principle operate since local quantum processes allow symmetrical time modalities (Fig. 21). This item was touched upon also by Stuart Kauffman in his concept of adjacent possible concept [378].
- We postulated above that primordial information is required, and assume life to be guided by long-distance discrete EMF frequencies as a form of *partially directed* evolution [3, 63, 90], as treated in the following section.

6.4 Biological Evolution is a Partially Directed Process

In the present paper, we assume a long-distance wave/particle influence on brain function in relation to consciousness. Such a long-range aspect was earlier described by some of us for a potential soliton-guided protein folding [90]. All this is based on the conjecture that a background field, such as a zero-point energy field or a

superfluid quantum space (see Sect. 7.1), plays a crucial guiding role regarding the biological macromolecules and their countless interactions within organisms. A part of this quantized vacuum field could be represented by the generalized music scale biophysical principle [3, 63], which was revealed in both animate and non-animate systems (see Sect. 3). How does the proposed directed evolution relate to human consciousness? In various papers [379, 307, 206, 380, 381], it was shown that thinking (and thereby implicitly also consciousness) is the natural product of a *partially directed* evolution of the universe and that, consequently, new knowledge should, at least partly, explain the already existing knowledge at a much deeper level. Jerman et al. [87, 356, 382], in the foregoing, strongly advocated the significance of a guiding biofield in biological evolution, together with the laws of complex biological systems [357]. Such a steering modality exhibits non-linear properties with feed-back amplification and refers to the earlier mentioned coherent field postulated by Fröhlich [148], at frequencies from 10^{11} to 10^{12} Hz, as well as the biophotonic field of Popp et al. [92], two aspects that even can be mutually connected. This also implies a conceptual extension of the Neo-Darwinian theory, in which the environment is not merely considered as a contingently changing source of selective pressures, but rather as an integrative and formative system with its own dynamic physical laws [356]. Miller et al. [383], stipulated that for a self-referential observer physical data can become biological information and that the real question is how any sender/receiver resonant cell gains sufficient coherence to become a problem-solving entity. Such collective qualities of recurrent information processing and related memory in a cell, may be conceived as learning the language of life and thus the defense of self and ultimately may evolve into a form of proto-consciousness.

In Melkikh [308, 206, 380, 384, 385], the above-mentioned theory of directed evolution was proposed. The main motivation of the proposed theory is the impossibility of enumerating gene variants during the life of the universe under conditions of a priori undirected evolution. In addition, the work [308] showed that the formation of new species is a directed process. The consequences of this directivity modality are such properties of organisms as the existence of sexes and horizontal gene transfer, aging and death, symbiosis and neutrality. Consequently, the role of selection, random mutations, and genetic drift in evolution seem to be rather secondary. In this case, the origin of species can only occur, taking into account the recognition by the organism of the state of the environment. As an extension of this, it was shown in [308] that the emergence of complex forms of *animal and human behavior* can also be seen as a directed process within the framework of directed evolution of life. In particular, one of the important items of behavior and thinking is the problem of *knowledge acquisition* [386]. The central feature here is that any interaction of an animal or human with the environment is inevitably accompanied by *recognition*. In this case, a dilemma arises: either the image from the external environment is recognized, but then it is not new, or it is not recognized, but then there is no reason to believe that adequate behavior is possible in relation to it. Therefore, it is not clear how a human (animal) in general conceives something as new.

To solve this problem of knowledge acquisition in his work [387], the concept of quantum *metalanguage* was introduced. This is seen as a higher level language

that implicitly supervenes a spectrum of known languages. Only some operations within this metalanguage can be used to generate entirely new languages from given languages, including replenishing them with new terms, symbols, etc. According to Melkikh et al. [387], the physical basis of the proposed quantum metalanguage is the collective nonlocal long-range interaction between biologically important molecules (see above). Such a collective interaction provides the evolutionary rise in information capacity of molecules, as well as that of the whole cell. The total required integral information can not only be related to overall genetic coding, the latter being orders of magnitude to low to ensure the evolutionary complexity of life. Thus, we hold that the physical basis for this is the non-local quantum field, embedding the biologically important molecules. We propose that these molecules or rather their collective wave fields are involved in the organization and work of innate life programs and that this is based on the related language programs.

The superfluid quantum/ZPE space, as treated in the present paper in Sect. 7.1, seems an excellent modality for defining the semantic basis for such an underlying metalanguage of nature. As treated above, we see the generalized process of *thinking (memorizing, memory retrieval, and perception of meaning, that determine pro-life decision making)* as essential. This seems similar to the already mentioned adjacent possible concept of Kauffman [378], Kauffman (2008, 2009), as a natural stage in the directed evolution of life. Such an evolution, in our opinion, also contains a priori *information about the future states of the evolving system* (see for this aspect Sect. 9). At the same time, genetic and epigenetic events are, at least partly, controlled by long-range quantum forces [206, 380, 381]. We, therefore, argue that in a hidden form of force fields, this type of “thinking” existed at any stage of evolution. Such properties of living systems therefore should be implicit in describing the topological states of the universe, even before the Big Bang (in cosmology called the Big Bounce).

The proposed model of the evolution of the universe [379] and the further emergence of life in it, demonstrates the great similarity of the universe with the features of an organism. Such similarity of the universe with living organisms in many respects is not accidental and suggests that the universe itself can be considered alive. A similar idea was previously put forward by Lovelock’s Gaia concept in relation to our planet Earth. The process of bounce (scattering of the universe) seems largely deterministic (predictable). In this sense, it is in many ways similar to gene exchange between living organisms or cell division. As shown earlier [380], gene exchange is a largely deterministic process in which randomness plays a secondary role, and mutations seem rather controlled. The assumption that the universe was in a pure quantum state until a Big Bounce, allows us to solve the basic paradoxes of the standard cosmological model [379, 308], without any additional assumptions: the problem of the predominance of matter over antimatter (see Sect. 2), the problem of the absence of monopoles, the problem of flatness of the universe, and the horizon problem.

To summarize, in the studies of Melkikh [379], the hypothesis of *directed evolution of life* in the Universe was put forward, which can be formulated in the form of the following provisions:

1. Before the Big Bounce (scattering process), the universe was in a pure quantum state. In this state, after scattering, the properties of the universe (field constants, particle masses, etc.) were encoded. This state itself arose by the mechanism of quantum phase transition.
2. At the initial stage of expansion, the universe was still in such a pure quantum state. As a result of an ongoing entropic decay (decoherence) it became hot. Yet, at the same time, some of its subsystems, weakly interacting with others, could even remain in a pure quantum state for a longer time.
3. Further, expansion of the universe was somehow controlled by a gradual change in the parameters of dark energy and/or dark matter. The collective values of the constants and fields were expressed in macro-parameters determining the evolving architecture of the Universe and, for instance, allowing stars and galaxies to be formed later. Other parameters, related to force fields created the necessary conditions for the emergence of life at later stages.
4. At a certain stage, given the presence of all of these necessary conditions and following the appearance of atoms and molecules in certain complex systems, *quantum laws* governing the spatial structure and the evolution of replicators began to play an important role. Of note, these laws were also ultimately determined by the state of the Universe before the Big Bounce (by scattering). The presence of anti-matter was largely directed to a supposed adjacent universe (see Boyle and Turok [36]).
5. Subsequently, the proposed partially directed evolution went in the direction of increasing the complexity of organisms, in relation to their ongoing adaptation to various environmental conditions. It should be realized, therefore, that the particular laws of partially directed evolution, were ultimately the result of the collective laws of physics as well as the initial conditions that characterized the initial forming of the Universe. However, the laws of physics as understood here do not only concern the known 5% of matter in the universe, but also the rest of its mass and the quantum vacuum.

Conclusion: the here proposed model of a partially directed evolution of the universe, including the further emergence of life in it, demonstrates a striking similarity of the becoming of the universe with that of the evolution of living organisms. Because of this striking similarity, we may infer that our universe itself can be considered as a *living modality*. In this case, all existing lifeforms, with respect to the universe, can in fact be regarded as endo-symbionts of a cosmic super-organism.

7 Quantum Consciousness Is Steered by Hydrodynamic Mechanisms from a Superfluid Quantum Space

7.1 ZPE/SFQS-Field and Interactions with Life Organism and Brain

The vacuum is filled with scalar fields that serve as order parameters for superfluidity, being quantum phase-coherent over macroscopic distances. Superfluid quantum space (SFQS) concepts have been developed by Fedi [388, 389] and Sbitnev [390] and recently reviewed by Sbitnev [390], in the framework of plasma physics. A hypothesis has been formulated, according to which, space is a quantum superfluid and fermions absorb space's quanta (SQ), generating an attractive force, which corresponds to gravity. According to Fedi [388, 389], the mechanism of absorption is based on the description of fermions as vortices in a superfluid quantum space (SFQS), similarly to nano-vortices occurring in superfluid helium-4, i.e., as dynamic topological defects of SFQS. To compensate this absorption, emission of virtual photons would occur, capable of explaining the existence of charged particles.

Superfluid quantum space theory (SFQS-T), sometimes known as the BEC vacuum theory, is an approach in theoretical physics and quantum mechanics where the fundamental physical vacuum (non-removable background) is viewed as superfluid or as a Bose-Einstein condensate (BEC). An ultimate goal of this approach is to develop scientific models that unify quantum mechanics (describing three of the four known fundamental interactions) with gravity, making this theory a candidate for defining of quantum gravity and describing all known interactions in the Universe, at both microscopic and astronomic scales, as different manifestations of the same entity, superfluid vacuum.

As early as in 1945 [391], Dirac published two papers where he pointed out that we should take into account quantum fluctuations in the flow of the aether. His arguments involve the application of the uncertainty principle to the velocity of aether at any space-time point, implying that the velocity will not be a well-defined quantity. In fact, it will be distributed over various possible values. At best, one could represent the aether by a wave function representing the perfect vacuum state for which all aether velocities are equally probable. An observer who resides inside such vacuum and is capable of creating or measuring the small fluctuations would observe them as relativistic objects . If the energies and momenta are below the excitation threshold then the superfluid background behaves like the ideal fluid, therefore, the Michelson–Morley-type experiments would observe no drag force from such aether.

According to the approach, the curved spacetime itself is the small collective excitation of the superfluid background, therefore, the graviton would be in fact the “small fluctuation of the small fluctuation”, which does not look like a physically robust concept. As a result, it may be not just a coincidence that in general relativity the gravitational field alone has no well-defined stress–energy tensor. SFQS-T does

not a priori forbid an existence of the non-localized wave-like excitations of the superfluid background. Thus, the usage of the Higgs boson (or any other elementary particle with predefined mass) alone is not the most fundamental solution of the mass generation problem but only its reformulation ad infinitum.

Thus, SFQS-T has its own idea of the fundamental mass generation mechanism, elementary particles acquire mass due to the interaction with the vacuum condensate, similar to the gap generation mechanism in superconductors or superfluids. Consequently, the Higgs boson, even if it exists, would be a by-product of the fundamental mass generation phenomenon rather than its cause. In this model, the physical vacuum is conjectured to be strongly-correlated quantum Bose liquid, whose ground-state wavefunction is described by the logarithmic Schrödinger equation. It was shown that the relativistic gravitational interaction arises as to the small-amplitude collective excitation mode, whereas relativistic elementary particles can be described by the particle-like modes in the limit of low energies and momenta.

Recently, Sorli (2019) stated: Today, mainstream science considers that the observer and all observed physical phenomena exist in time and space. Nonetheless, recent research shows that the time measured with clocks is merely a *mathematical parameter of material change*, i.e., motion which runs in space. In this picture, the existence of past, present, and future is merely a mathematical one. As regards EPR-type experiments, observer and observed phenomena exist only in space which originates from a fundamental quantum vacuum which is an immediate medium of quantum entanglement. Fedi [388, 389] has developed a model of the vacuum as a shear-thickening (dilatant) fluid (the Newtonian fluid, see Fig. 22). In his model relativistic energy of the proton can be seen as accelerated proton thickens the vacuum ahead of it. Important is that both models see the relativistic energy of the proton as the energy of the vacuum which is absorbed or is thickening ahead of the proton. Proton does not gain its relativistic energy because of the motion in an empty space.

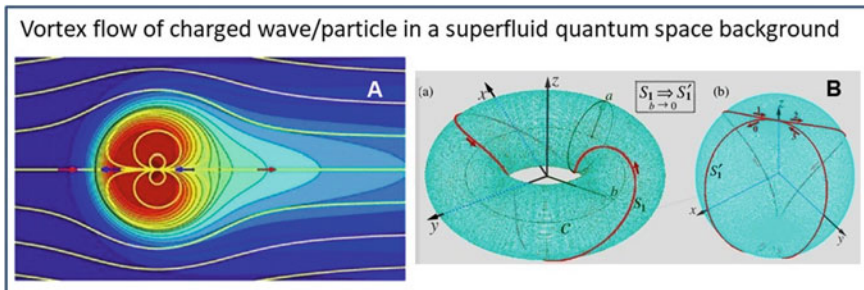


Fig. 22 **a** Steady vortex avenue confined by transfer flow with a dipole source inside and a uniform background flow outside. Yellow streamlines outside of the vortex area represent possible Bohmian trajectories. **b** Transformations of torus shown in **a** to the tori when the radius b tends to the radius a , or to the double surface sphere shown in **b** when the radius b tends to zero. Pilot waves of Bohm can be envisioned as motion of vortices guiding a particle along the optimal trajectory, in which the torus bears a wave pattern that accommodates all the information about the environment by reflection and therefore can fully simulate the particle until its final destination

Proton relativistic energy is vacuum energy which is interacting with the proton due to its motion in a vacuum. Some theoretical research speculates the vacuum might be a four-dimensional reality: It is a general trend in modern theoretical physics to consider extended objects, like strings and membranes. Usually, one applies these ideas to hypothetical, high-dimensional completions of the four-dimensional world. However, lower-dimensional structures might also exist in four dimensions.

Sorli [392] proceeded: at the present time, there is no well-developed theory that would predict such structures. However, there is accumulating evidence obtained within the lattice QCD that there are lower dimensions objects percolating through the vacuum of four-dimensional Yang–Mills theories. Some other researchers predict the vacuum could be a four-dimensional reality. If the vacuum actually is four-dimensional, we cannot apply a classical understanding of vacuum density, which works only in the three-dimensional domain. The superfluid quantum vacuum model with the variable density is the development of the electromagnetic quantum vacuum model (QED) which is one of the most successful theories. With giving electromagnetic vacuum variable density, we can describe Higgs potential and also the origin of gravity. The perspective of further research on the variable density of vacuum is to integrate QED with the Higgs mechanism model and quantum gravity model. Recent research of Sbitnev on the hydrodynamics of the physical vacuum opens the new perspective where elementary subatomic particles could be seen as the vacuum vortices. In the Sbitnev model, the vortex is periodically exchanging energy with the vacuum via vacuum fluctuations. According to Sorli, Sbitnev model is enhancing the model of vacuum fluctuations presented with clear insight, namely, we cannot study subatomic particles without considering their active relatedness with the vacuum.

According to the brain model presented in this chapter, a given vortex is in active relation with the vacuum. When accelerated the vortex is “dragging” with the vacuum and absorbing some of its energy which is its relativistic energy. Considering that vacuum is 4-dimensional, and so proton is 4-dimensional vacuum vortex, we are limited in the proton observation with the 3-dimensional apparatuses and 3-dimensional sensorial sense (sight). Taking into account that atom is three-dimensional, the subatomic world could be four and more dimensional. We have to be aware that higher dimensionality of the subatomic world may also represent the limitation of our scientific endeavor.

The exchange of SQ occurring between two adjacent vortices would, moreover, justifies the strong interaction leading to the complete unification of the four fundamental forces. The reasons for considering fermions and other particles as superfluid vortices of SQ are several. One could, for instance, explain the appearance of particle-antiparticle pairs from the quantum vacuum as a perturbative phenomenon analogous to that described in a so-called Kármán vortex street, where pairs formed by a right- and a left-handed vortex occur due to a perturbation of the flow. In our case, the flow may be represented by the gravitational field and the disturbance by other particles or stochastic perturbations of SFQS. The trigger to the formation of vortex-antivortex pairs in the fluid quantum space, corresponding to matter and antimatter within our analogy, might be a phase transition similar to the fluid vortices providing a new basis to describe the wave equations of fundamental fermions. In this direction, Sbitnev

[369, 370, 371, 393, 394, 395, 396, 397] considers quantum vacuum as a superfluid and applies quantum considerations to Navier–Stokes equations (see Sect. 7.2).

Sbitnev describes vortex objects (vortex balls) that, unlike Hill’s spherical vortices, show intersected streamlines (Fig. 19) and satisfactorily reproduce fermions’ spin by varying their orientation at each revolution. When a photon is described as a phonon in SFQS, the energy it carries would be justified within the quantum phenomenon of second sound, occurring in this case in SFQS.

Conclusion: the physical definition of SFQS and ZPE field are closely related, yet it should be realized that the ZPE concept mainly reflects the frequency of quantum fluctuations of the field, while the superfluid quantum space defines the total overall dynamic field structure that may underlie the fabric of reality in which also our world is embedded.

7.2 Does the Brain Exhibit Two Different Mechanisms for Information Transfer?

In the following section, we will pay attention to the question of how our brain may communicate with cosmic fields such as Zero-point energy/Superfluid quantum space, as previously treated in Sect. 7.1. We argue that consciousness is partly received from quantum wave information derived from these fields in a bi-directional interaction with our organism and here we address the potential physical mechanisms involved. This implies that we should identify the potential field-receptive medium in and around brain tissue, according to quantum mechanical principles. This serves two major problems in current understanding in neurology and brain physiology: the origin of so-called qualia and the supposed broadcasting functions of neural networks that may explain the binding of distant brain nuclei [398]. The assumed broadcasting mechanism should afford an instantaneous integration of the various sensory input that underlies our integral observation of the world around us. However, the physiological or biophysical process responsible for such broadcasting has not been identified until now, although a field type of mechanism seems plausible.

As mentioned earlier, we hypothesize the permanent involvement of photon- and phonon-dressed fermions such as electrons and protons (the quasi-particle soliton is one example). We hold that these are crucial in the function of our entire organism, with special reference to our brain [1, 3, 62]. The necessity to involve such a special mechanism has various backgrounds: (a) to be able to deal with the ultra-rapid brain responses that are not compatible with the relatively slow synaptic process of neurotransmission [399], (b) in order to explain the abovementioned binding and synchronicity phenomena in brain function (c) to understand the unexpected cognition capabilities of patients with severe brain damage (see Sect. 5.8) and (d) to address the presently unexplained subjective experiences in the category of Psi phenomena (Sect. 5.7). All of these phenomena point to some kind of *ultra-rapid communication*

at a distance in brain tissue and/or between different individuals. This may also be related to a non-local connection of humans to some kind of information domain that may explain phenomena such as precognition and near-death experiences.

We stipulate nevertheless that our hypothesis does not deny current models of neuronal transmission: it is rather meant as a complementary but essential aspect. Alternatively, the structures that underlie neuronal function may be involved in brain function in another manner than the classical neural mechanisms generally assume. As mentioned before [271] presented an intriguing model of synaptic communication, in which quantum tunneling on the basis of solitonic interactions with SNARE protein complexes at synaptic vesicles is essential. The latter seems a modern version of the earlier presented model of Beck and Eccles [400]. We hold that biological evolution may have selected all available biophysical processes for intra- and inter-cellular communication. In this respect, a “Two-Brain hypothesis” was postulated earlier by Goodman et al. [401]: postulating one electro-ionic modality related to the well-known neuro-humoral transmission and another that may be rather electromagnetic field-based. The latter could be related to (bio)photon transmission that is *extrinsic* to classic neuronal brain circuitry. Implicit in the latter photon mechanism, is the particular speed of the process with inherent rates that are many orders of magnitudes higher than that of chemical neurotransmission. Also, it remains in principle possible that the quantum field type of transmission uses material elements that are also instrumental in classical circuitry. For example, it has been proposed that connective tissue/water assemblies may afford superconductive properties [402] and that myelin-based white matter in the brain may function as optical waveguide [403].

In any event, we should also take into account that the study of mental aspects of brain function and consciousness may require aspects of entanglement, non-locality, and wave coherence, not offered by classical physics. Of note, such phenomena are experimentally demonstrated now in various cellular processes in Quantum Biology (Sect. 3.3), and thus open the potential for top-down and retro-causal elements, as well as wave mediated action at a distance. They also invite a less reductionistic and more holistic top-down approach in the study of life in a cosmic context [404]. One example is the peculiar notion that consciousness and reality have a “mobius-strip” type of relation: consciousness may itself be instrumental in quantum wave collapse producing the material world, versus the view that such a wave collapse, may only occur through gravitational (orchestrated) reduction of wave information at the Planck scale, thereby *producing* conscious moments as proposed by Penrose [405].

As soon as the “Orch OR” consciousness model of Hameroff and Penrose was published, it was severely criticized by Tegmark [406], whose primary remarks concerned the following egregious discrepancies: (a) the collapse of the wave function is much shorter than that of relevant dynamic timescales of neuron firings; and (b) wet warm brain, working at room temperature, cannot provide supporting quantum computations. Thermal noise of the brain would, in his opinion, completely exclude such delicate computations. This criticism, however, was later extensively and quite satisfactory addressed [261].

It is important to note that the microtubule hypothesis in brain function of Hameroff and Penrose -[407, 408](#)] was experimentally supported by the innovative studies in Anirban Bandyopadhyay's group [[322, 323, 331](#)]. In the latter studies, it was shown in life visualizations that self-assembly of tubular proteins can be obtained under the influence of discrete EMF frequencies in the kHz, MHz, and GHz ranges and that many of the registered resonance peaks of tubulins seem compatible with the earlier treated fractal GM-scale revealed by us [[3](#)]. It is of great interest that Anirban Bandyopadhyay's group found clear evidence for a fractal information theory-derived geometric musical language, that may guide brain-inspired hypercomputing as a basic phenomenon underlying consciousness, (see Sect. [5.9](#)), a concept that is very much in line with the concepts in of the present paper.

Taking into account the earlier mentioned criticisms, let us look at the Hameroff-Penrose theory from another side: the side mentioned by Tuszynski [[409](#)]. By inspecting the Hameroff-Penrose solution on the central role of oscillating microtubular proteins, an enormous matrix of oscillating tubular elements is occupying the whole brain, especially if other organelles such as mitochondria and nuclear DNA are involved at the same time This entire vibratory machinery is embedded everywhere in the brain in the intracellular water.

The present study, emphasizes the importance of cerebral and interstitial fluids, that in concert with coherent water domains in the cells, could be involved in the guiding of consciousness originating from realms outside the brain. Interestingly, microtubuli in this context are not only 'scaffolding' instruments of cells but may also serve as a warehouse for memory and memristors [[410](#)] (Chua 1971), as instrumented by heavy ions, such as *calcium ions*. In the past [[164](#)], but also more recently, a number of attractive quantum brain models, have been proposed (see later, Table [2](#) and [3](#)), that are at least partially compatible with the present "event horizon model" (see Fig. [13](#)).

To emphasize the place of proton in brain consciousness functions, we show a rough diagram of brain organization, shown in Fig. [23](#). A conditional diagram of brain organization consists of three levels (Tarlaci 2010): (a) a 'water basin' containing all the other levels; (b) a level consisting of many neurons and glial cells, which organize the electrical activity of the nerve cells against a background of the neurochemical medium prepared by special nuclei and cells; and (c) a level expressing higher cognitive functions, which provide adequate behavior of a living organism in the social environment [[411](#)].

It is noticed earlier, that the thermal action parameter $k_B T \delta \tau$ and the Planck constant are almost equal to each other. Here k_B and $T \approx 310$ K are the Boltzmann constant and temperature of human body and $\delta \tau \approx 2 \times 10^{-13}$ s is the average lifetime of proton mobility in water [[412, 413](#)]. The above equality means, that exchange of the hydrogen ion energy with the vacuum zero-point energy can be available as well. It should be noted in this regard, that the quantum mechanical zero-point energy is mentioned also by Beck and Eccles [[400](#)], in an article entitled "quantum aspects of brain activity and the role of consciousness".

The mass of the quasi-particle, which they adopt in this article, is the mass of the hydrogen atom. The vacuum zero-point energy fluctuations happen on the surface of

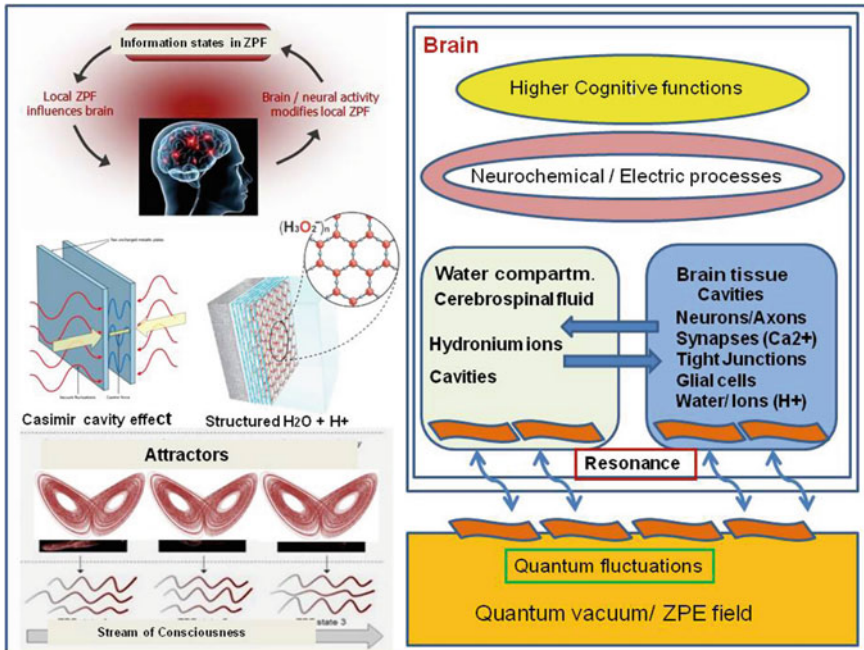


Fig. 23 Model for wave-coherence-mediated conscious states: The brain water compartment functions as a receiver and conduit for discrete quantum wave frequencies via (i) excitation of hydronium ions in brain fluids that promote coherent domains in structured water (inset middle right) and other interacting cavity modalities or (ii) through cyclotron EM wave activity resulting in perturbation of delocalized ions such as Ca^{2+} in dedicated channel proteins, that through vibratory states can become quantum-entangled. Both these events are leading to syntropic flow of information and increased functional binding and synchronization of neuronal centers that are known to promote conscious states. Information is, apart from the known senses, obtained by quantum resonance with the vacuum (zero-point energy field) and in the non-linear organized brain produced attractors that are the building blocks of conscious states (see Fig. 23, left)

a vast ocean of energy called by the dark energy, or more specifically the “superfluid quantum space”, the name proposed by the earlier mentioned Fedi [388, 389]. It contains virtual particle-antiparticle pairs, which are created and annihilated again and again by staying in a continuous vortex dance. The pairs possess integer spin and therefore form the Bose-Einstein condensate covering the entire Universe [414]. Thus, the hydrogen ion (proton) has the possibility of tunneling through the space on huge distances. Let us look at the proton migration mechanism from the perspective of the de Broglie-Bohm theory [415, 416]. In this case, the ‘water wires’ look like the Bohmian trajectories forming every time the need arises. But first, we shall show the hydrodynamical equations describing the motion of hydrogen ions in the water medium. In fact, the balanced equation for electrical processes occurring in nervous tissue [417] is written down initially, which leads further to the Naveir-Stokes equation and the continuity equation (see Fig. 30).

7.3 Water Configurations as Quantum Wave Antenna: The Role of Protons in Hydronium Ions

Living brain is a biological organ that operates in a slightly salty liquid environment at room temperature. Most widespread chemical substance in the living body is liquid water [287, 418].

Water is the main liquid medium in the brain, where important events, related to consciousness occur. Although dendrites and axon terminals of neurons of the brain penetrate through all brain space densely, there are spaces relatively free of the nervous filaments. These spaces are ventricles of the brain filled by the cerebral liquid. As treated in Sect. 5.8, in medical practice, there is a peculiar case in which a 44-year-old patient with postnatal hydrocephalus of an unknown cause [298]. Magnetic resonance imaging (MRI) showed that his brain had hypertrophied brain ventricles, Fig. 24d. The deficit of the filamentous organization demonstrates a massive enlargement of the lateral, third, and fourth ventricles, with a very thin cortical mantle and a posterior fossa cyst. Surprisingly, however, this patient possesses quite normal social functions and exhibited an intelligence quotient (IQ) of around 75. This example

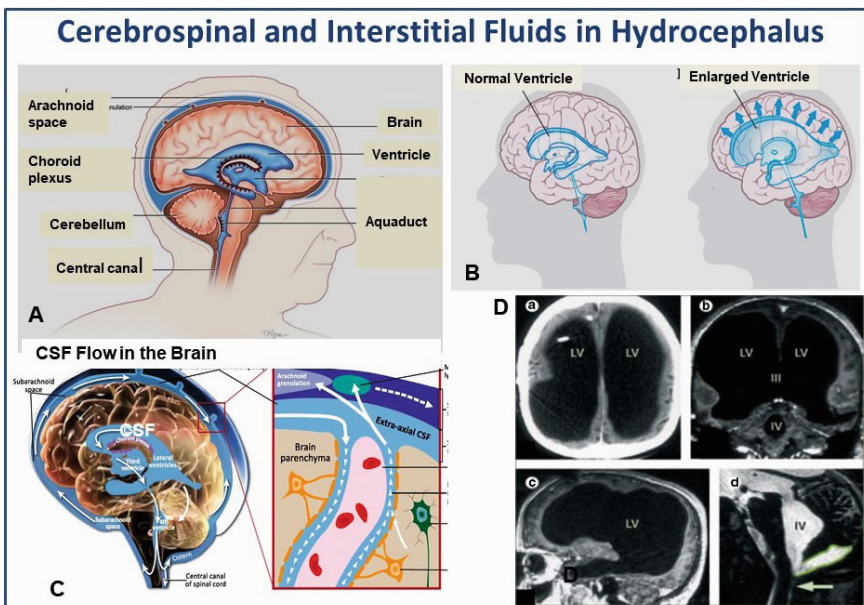


Fig. 24 **a** Cerebrospinal fluid compartments within and surrounding brain. **b** Enlarged ventricle compresses brain tissue. **c** Circulation of cerebrospinal fluid and contact with interstitial fluid. **d** Massive ventricular enlargement, in a patient with normal social functioning: **a–c** MRI with gadolinium contrast at different cross-sections; **d** T2-weighted MRI. LV = lateral ventricle. III = third ventricle. IV = fourth ventricle. Arrow points to Magendie foramen. The posterior fossa cyst is outlined in **d**. The figure is taken from Feuillet et al. [298] (see also Sect. 5.8)

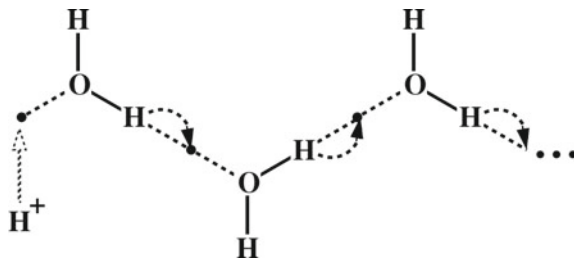


Fig. 25 Diagram illustrating the hydrogen-bonded chain mechanism for proton migration (Grotthuss mechanism, [420]): a proton enters the chain from the left side and then, as a result of the series of proton hops indicated by the arrows, a proton exits the chain on the right side. This chain represents a hydrogen-bonded 'water wire' [418]

provides an indirect hint that the cerebral liquid, slightly brackish water, may have a direct relationship to cognitive functions of the brain.

We assume that the proton plays an important role in the transport of subcritical information through the brain liquid. At room temperature, the liquid water consists of many fluctuating hydrogen-bonded clusters [418]. The hydrogen bond is strong enough to maintain the coupling of atoms during some time under thermal fluctuations. As treated above, water can be depicted as consisting primarily of a mixture of clusters of water molecules with different degrees of hydrogen bonding in an equilibrium. Under thermal fluctuations, some hydrogen couplings are broken but other arise [419, 32].

On average, the equilibrium distribution of different cluster sizes is maintained. Figure 25, illustrates the hydrogen-bonded chain mechanism [420], called the Grotthuss mechanism, by means of which protons tunnel from one water molecule to the next via hydrogen bonding [418, 421]. Consciousness may arise through information transfer to this water from the ZPE field. It can be shown that the *thermal action parameter* of a proton

$$b = k_B T \delta\tau, \quad (3)$$

in which k_B = Boltzmann constant = $1.38 \cdot 10^{-23} \text{ J/K}$, T = the room temperature = 298 K , $\delta\tau$ = lifetime of a hydronium ion = 2^{-13} s , and we get $b = 8.2 \cdot 10^{-34} \text{ J s}$. One can see that h = Planck constant = $6.6 \cdot 10^{-34} \text{ J s}$, is in the same order of magnitude as the thermal action parameter, b [369–371].

In the fluid medium, as a basic speed of matter transfer, we choose the speed of sound rather than the speed of light proposed by Brady and Anderson [422]. In a saline water solution at room temperature, $T = 298 \text{ K}$, the speed is equal to $c_s = 1508 \text{ m/s}$. The speed is taken from the formula of Wilson [423]. Observe that

$$m_* = \frac{k_B T}{c_s^2} \approx 1.81 \times 10^{-27} \text{ kg} \quad (4)$$

is slightly larger than the proton bare mass $m = 1.6726 \times 10^{-27}$ kg.

This means, that the hydrogen ion may behave as a particle exchanging its energy permanently with the vacuum zero-point energy and not only with water. In other words, the hydrogen ion can act as an intermediary between the physical vacuum (i.e., the superfluid quantum space) and the water environment of the brain [369–371]. The quantum mechanical zero-point energy is also mentioned by Beck and Eccles, in their article [400] entitled “Quantum aspects of brain activity and the role of consciousness”.

The mobility of the hydrogen ion in water leads to an average lifetime of 2×10^{-13} s [412, 413]. Hydrogen ion, that is proton, is considered here as a bit of information transmitted across the cerebral liquid of the brain by the Grotthuss mechanism [418] (see Fig. 25).

The mass of the quasi-particle, which Beck and Eccles assumed in their article [400], was in the range of the mass of the hydrogen atom. Besides, they [400] noted that *the thermal energy* $k_B T$ of the external environment ($T = 298$ K) expressed in units of the electron-volt

$$E_e = k_B T/e \approx 26 \text{ mV}. \quad (5)$$

lies in the range of voltages where neurons operate. It means that thermal noise may have an impact on the electric activity of nerve cells. It is instructive, to draw attention in this article, to the time of the metastable instability of electronic transition, τ , evaluated by the authors to be about 10^{-13} to 10^{-14} s. Their estimation shows a relatively good agreement with the average lifetime of the hydrogen ion, $\delta\tau = 2 \times 10^{-13}$ s.

In the transport of protons, the so-called exclusion zone (EZ) phase of water could play a significant role, Fig. 26. This special “fourth phase” of water arises near hydrophilic surfaces that abound in living tissues. Water molecules are ordered into a hexagonal lattice, Fig. 26 and the exclusion zone (EZ) water [424] expels any foreign inclusions so that EZ water molecules are more constrained. An assembly of EZ water molecules is more stable. EZ has a negative charge, which is friendly to the resting membrane potential of neural cells. EZ absorbs light at the wavelength around 270 nm. These unique properties make the water a perfect conductor of the hydrogen ions through itself by the Grotthuss mechanism [425], see Fig. 25) [426], see Fig. 27a).

Here we will try to understand what pathways are available for the moving protons. As was noted above, the main mechanism is the Grotthuss one that can be effective when water is in the “fourth phase” as expected to exist near the countless subcellular structures and the cellular membrane of neurons as well as in the brain fluid molecular material. In that case, water molecules are predominantly arranged according to the hexagonal symmetry, see Figs. 26 and 27. As shown in Fig. 27a the hexagonal symmetry can provide an eightfold path for the hydrogen ion entering on a hexagon assembled from water molecules. In the beginning, the hydrogen ion enters the right hexagon at the node a and hops along with it around central point A clockwise. Then, upon reaching node a , the hydrogen ion begins to hop along with the left hexagon

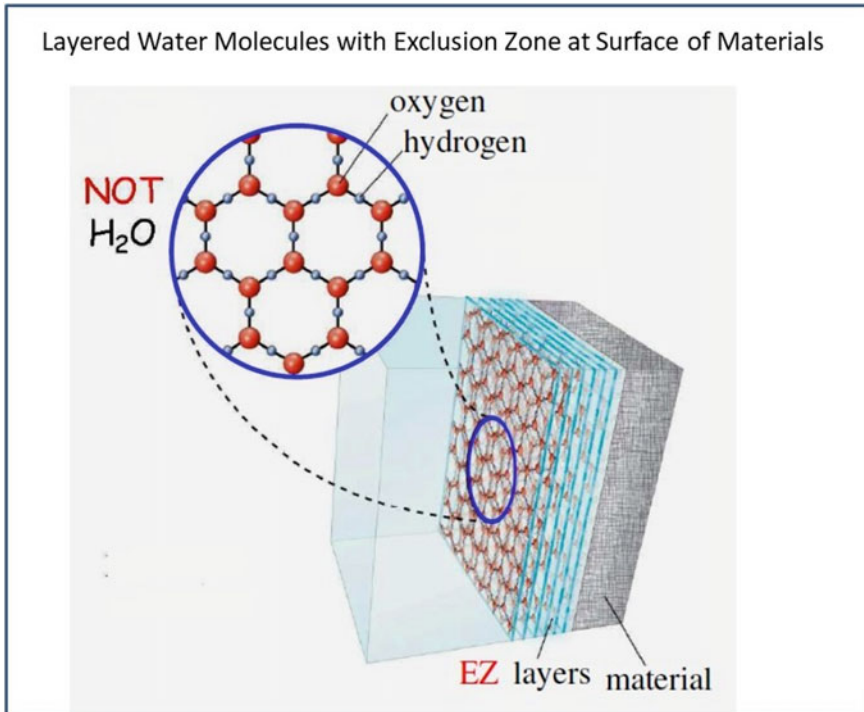


Fig. 26 From Pollack [424]. The hexagonal water lattice can work as an interferometric device acting as a receiving and transmitting antenna

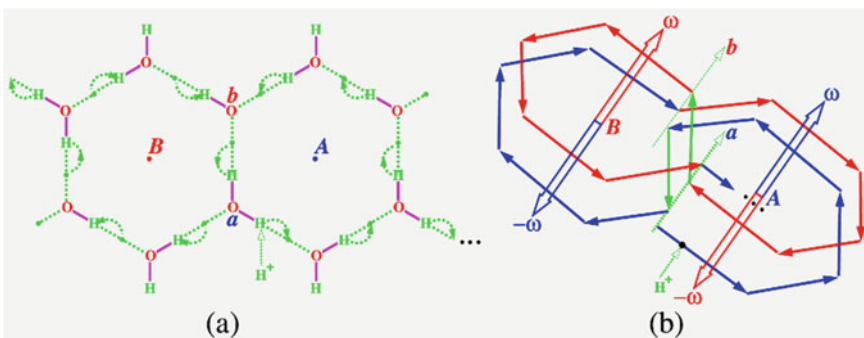


Fig. 27 Hydrogen ion hopping along two EZ water hexagonal structures: **a** a general organization of EZ water consisting of two hexagons; **b** dynamics of the hydrogen ion hopping along two hexagons. According to the righthand law, currents about the closed circuits induce magnetic fields, oriented perpendicular to these circuits—along either red arrow or blue arrow depending on orientation of the current in the circuit—either counterclockwise or clockwise. Such currents synergistically flowing along the water hexagons on the hexagonal lattice (see Fig. 26) lead to cumulative effect either of radiating information to subtle worlds or of receiving information from these worlds

around center point B in a counterclockwise manner. Upon reaching node b , the hydrogen ion re-enters the right hexagon, and so forth.

Each eightfold path corresponds to two oppositely-oriented vorticities $\vec{\omega}$ that change the orientation after the completion of each cycle, see Fig. 27b. This illustration shows the following sequence of changing the vorticity sign. Initially, the hydrogen ion hops along with the left hexagon in a clockwise manner. The vorticity $\vec{\omega}$ is represented by the blue arrow. At the transition to the left hexagon at the node a , the hydrogen ion begins to hop in a counterclockwise way. The vorticity $\vec{\omega}$ corresponding to this motion gets the opposite orientation (the same blue arrow oriented in the opposite direction). After completing the motion along with the left hexagon, the hydrogen ion in node b enters again the right hexagon and begins to hop along with it. The vorticity orientation remains (red arrow). After completing the motion on the right hexagon, the hydrogen ion, in node a , again passes to the left hexagon. The orientation of the vorticity changes sign in the opposite direction (the same red arrow oriented in the opposite direction).

As a result, we have the following pattern: (a) the eightfold path along EZ water molecules consist of oscillating dipoles in time due to the change of vorticity. (b) we note that arrows drawn on tips of the green dotted lines in Fig. 27b point to flow of these dipoles by time. (c) the dipoles exchange the orientations in the tact with oscillations that fluctuate in time. (d) if the EZ water contains many such eightfold paths working synchronously, then this EZ water plate can work as a multi-slot emitter-receiver of the electromagnetic field (multi-slot interferometer).

The hydronium ion can obtain a *soliton character* since when moving along some surface it scrolls a mass of matter composed of a substrate along with it during this moving. In other words, the soliton can obtain a torque mode. If its core carries a charge, for example, the positive charge of the hydrogen ion, then due to the torque it is covered by a coat of negative charges. In particular, due to this coat, the soliton lives longer than that with a naked charge. Surprisingly, excess protons can create their own pathways, ‘water wires’, before protons can migrate along [426].

Grotthuss shuttling of an excess proton charge defect through hydrogen-bonded water networks, shows the interesting avalanche-like mechanism of the hydrogen ion transport through it, Fig. 28. It turns, there is a related process in which water molecules move (“shuttle”) through a hydrated excess proton charge defect in order to wet the path ahead for subsequent proton charge migration. Surprisingly, before the proton enters the nanotube, it starts “shooting” water molecules into the otherwise dry space via Grotthuss shuttling, effectively creating its own water wire where none existed before. As the dry nanotube gradually becomes wet when the proton charge defect enters it, the free energy barrier of proton permeation through the tube via Grotthuss shuttling drops significantly. This finding suggests that an important wetting mechanism may influence proton translocation in biological systems, i.e., one in which protons “create” their own water structures (water “wires”) in hydrophobic spaces (e.g., protein pores) before migrating through them.

In their motion, there are several ways through which protons can transfer their information or energy. Let us consider some typical Feynman diagrams (i) of elastic scattering of a hydrogen ion on a hole (it is a vacant place for the hydrogen ion) and

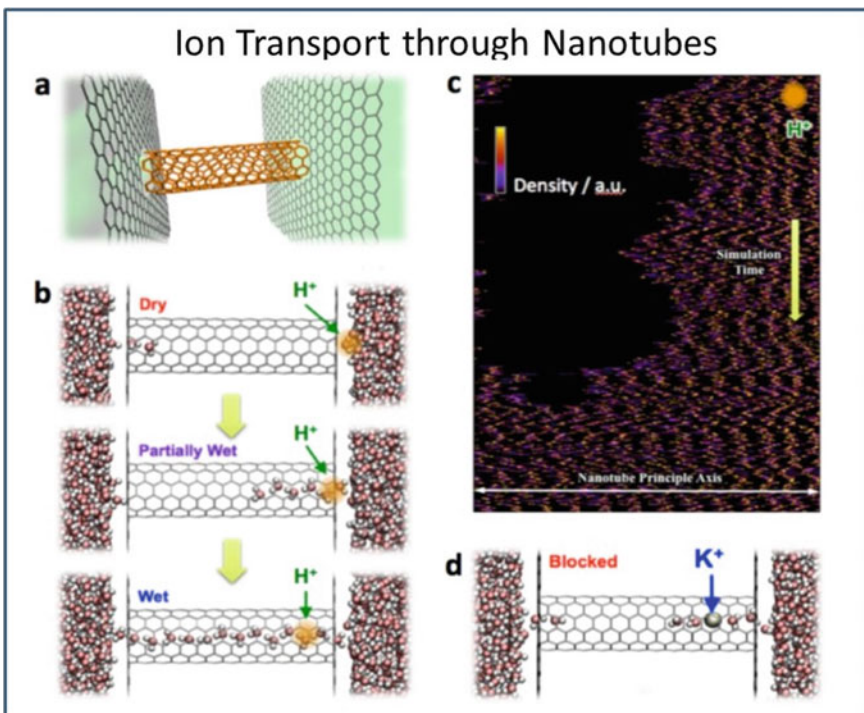


Fig. 28 The ion transport through an originally “dry” nanotube [426]: **a** The armchair-type (6) single walled carbon nanotube (CNT) is assembled between two graphene single layers that separate the bulk water. **b** Simulation of the proton induced wetting process along with the motion of the excess proton from bulk-tube interface. **c** Simulation in real-time of densities traces of the channel water molecules starting from a partially dry nanotube at the existence of the excess proton (time runs from the above to down). **d** Simulation with the potassium ion K^+ inside the nanotube, which remains mostly dry

(ii) tunneling of a hydrogen ion through some obstacle. These processes are shown in Fig. 29 a, b, respectively.

Two processes shown on these figures, illustrate the elastic scattering of a hydrogen ion on a hole and tunneling of a hydrogen ion through an obstacle. The first figures (a) show ideal processes without loss of energy. While the second figure (b) shows processes with loss of the energy that is dissipated into heating the water. Causes of this dissipation can be the presence of “mind contaminants” that dissipate phonons generated in the course of these processes. It means that for avoiding the dissipations we need to have clear water, which is the case in the EZ-phase.

It should be noted that the mobility of the hydrogen ion is highest among many other ions, such as K^+ and Na^+ [427] that are important ions for neuronal communications. These ions have individual ion pumps, while special water wires are prepared each time when a problem regarding the transport of hydrogen ions, protons, arises. One can assume that the aqueous proton transport [428] is set each time along most

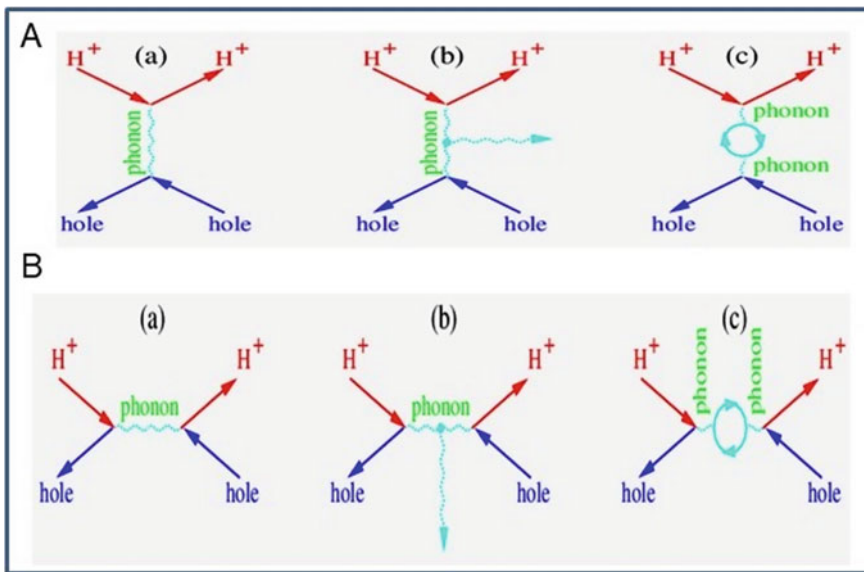


Fig. 29 Interaction of a hydrogen ion with a hole (vacant seat of hydrogen ion): **a** Elastic scattering (a) of a hydrogen ion, H^+ , on a hole; (b) scattering of a hydrogen ion with the energy dissipation because of radiation of a thermal phonon; (c) elastic scattering of a hydrogen ion on a hole accompanied by creation/annihilation of two virtual particles. **b:** Tunneling: (a) of a hydrogen ion, H^+ , occurs by its annihilation with a hole and radiation of the phonon. This, after a while, generates pair of a hydrogen ion and hole; (b) generation of pair is preceded by scattering of the phonon on a mud with loss of energy; (c) tunneling of a hydrogen ion is accompanied by creation/annihilation of virtual particle-antiparticle pair

optimal paths, like the Bohmian trajectories of particles in the physical quantum space.

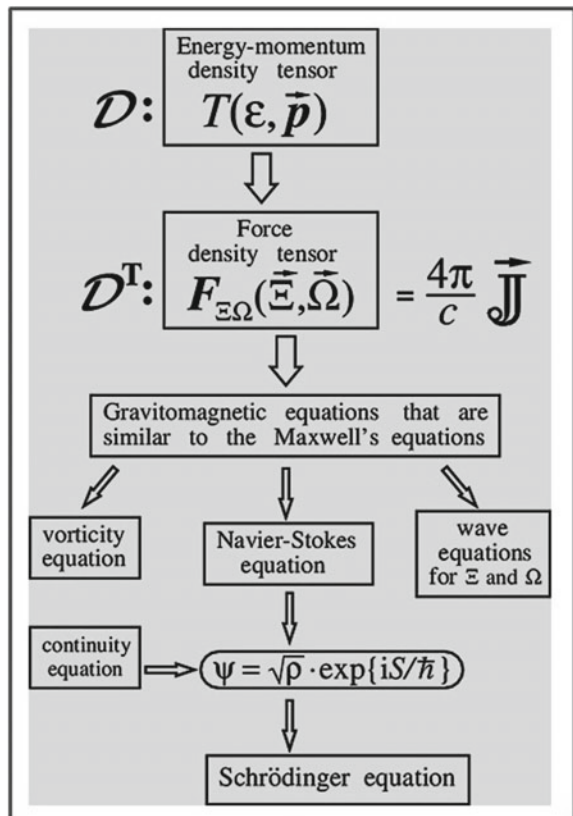
7.4 Flows of Hydrogen Ion Ensembles in Water and the Motion Equations

Our goal is to come to the Schrödinger equation by leaning on the above facts relating to the movement of the proton in water.

We begin from general equations that describe (a) the *conservation law of the mass density distribution* and (b) the *velocity field of the hydrogen ions in water* (see Fig. 30).

These two equations are basic and independent from the matter under consideration. First, we define two real functions—*the mass density distribution* $\rho_M(\vec{r}, t)$ and *the velocity field* $\vec{v}(\vec{r}, t)$. Here $M = N m_{H^+}$ is a total mass of the hydrogen ions (m_{H^+} is the mass of a single hydrogen ion, that is the mass of proton) in the unit volume

Fig. 30 Diagram showing the generalized quaternion differential operators D and DT on the energy-momentum and force density tensor, leading to emergence of the vorticity equation, Schrödinger equation and the wave equations



ΔV , so

$$\rho_M(\vec{r}, t) = \frac{M}{\Delta V} = m_{H^+} \frac{N}{\Delta V} = m_{H^+} \rho(\vec{r}, t) \quad (6)$$

Take your attention to the equality $\rho_M(\vec{r}, t) = m_{H^+} \rho(\vec{r}, t)$, binding the mass density distribution to the density distribution $\rho(\vec{r}, t) = N/\Delta V$ by multiplying the latter by the mass of hydrogen ion. Here N is the amount of hydrogen ion within the unit volume ΔV . Running ahead, we note that the density distribution $\rho(\vec{r}, t)$ together with the phase shift, are the main terms in the wave function.

The first equation is *the continuity equation*. It reads:

$$\frac{\partial \rho_M(\vec{r}, t)}{\partial t} + (\nabla \rho_M(\vec{r}, t) \cdot \vec{v}(\vec{r}, t)) = 0 \quad (7)$$

The second equation is an equation akin to *the second Newton law* that says that the acceleration of a body multiplied by its mass is equal to forces acting on this body $\vec{a} \cdot m = m \cdot d\vec{v}/dt = \vec{F}$. In our case, the body is a deformable fluid volume. Therefore,

the forces acting on this fluid volume lead to its deformations. At the consideration of deformable media instead of the total derivative in time, (a) we will go to the partial derivatives in order to have a possibility to consider spatial deformations of the body. It is important to emphasize that (b) the external forces cause, as response, opposite acting internal forces, manifested in (c) emergence of the pressure gradients in the body and (d) its heating because of the viscosity. This task is solved by invoking the Navier–Stokes equation that, in fact, is a generalization of the Newton second law. The Navier–Stokes equation reads [369–371]:

$$\rho_M(\vec{r}, t) \underbrace{\left(\frac{\partial \vec{v}}{\partial t} + (\vec{v} \cdot \nabla) \vec{v} \right)}_{(a)} = \underbrace{\vec{f}(\vec{r}, t)}_{(b)} - \underbrace{\rho_M \nabla(P/\rho_M)}_{(c)} + \underbrace{\mu(t) \nabla^2 \vec{v}}_{(d)} \quad (8)$$

Here the term embraced by bracket (b) is the *external force density* $\vec{f}(\vec{r}, t) = \vec{F}(\vec{r}, t)/\Delta V$ containing, in particular, the Lorentz force: $\vec{f}_1 = \rho_q \vec{E} + [\vec{J}_q \times \vec{B}]$. Here $\rho_q = q/\Delta V = eN/\Delta V$ is the charge $q = eN$ per the unit volume (e is the electron charge), $\vec{J}_q = q\vec{v}/\Delta V$ is the density current. \vec{E} and \vec{B} are external electric and magnetic fields, respectively. Brace (c) covers the modified pressure gradient. One can rewrite down this term in more detail

$$\rho_M \nabla(P/\rho_M) = \rho \nabla(P/\rho) = \nabla P - P \nabla \ln \rho. \quad (9)$$

In this formula, the first term, ∇P , is well-known from *the original Navier–Stokes equation* that is acceptable in the case of consideration of the classical fluid motion. The extra term, $P \nabla \ln \rho$ is small enough in the classical sector and for that reason, it can be omitted. However, this term turns out to be important in the case of transition to the quantum realm. It turns out that the term (P/ρ) represents itself the quantum potential Q , which plays an important role by supporting entanglement, in the words of Einstein, “spooky action at a distance”. If we recall that the barotropic liquid is incompressible, then a slight pressure on one its edge is instantly transferred to the other edge. In a real viscous fluid, such an instantaneous transmission is impossible since any impact on it is scattered into the heat. However, a superfluid can provide such a transmission. Let us prove that the pressure P divided by the density distribution ρ is the quantum potential Q .

7.5 Quantum Potential

Let the pressure P can be represented by sum of two pressures P_1 and P_2 . As for the pressure P_1 we begin with Fick’s law which says that the diffusion flux, \vec{J} , is proportional to the negative value of the mass density gradient, $\vec{J} = -D \nabla \rho_M$. Here D is the diffusion coefficient. Since the term $D(\nabla \cdot \vec{J})$ has dimension of pressure, we define the first pressure as follows:

$$P_1 = D(\nabla \cdot \vec{J}) = -D^2 \nabla^2 \rho_M \quad (10)$$

Here D is the diffusion coefficient. In quantum mechanics, in particular, it is equal to $\hbar/2m$.

Observe that the kinetic energy of the diffusion flux of the fluid medium is $(M/2)\left(\vec{J}/\rho_M\right)^2$. It means that one more pressure exists as averaged momentum transfer per the unit volume:

$$P_2 = \frac{M}{2\nabla V} \left(\frac{\vec{J}}{\rho_M} \right)^2 = \frac{D^2}{2} \frac{(\nabla \rho_M)^2}{\rho_M}. \quad (11)$$

One can see that the sum of the two pressures, $P_1 + P_2$, divided by ρ [we remark that $\rho_M = m_{H^+} \rho$, see Eq. (4)], gives the *quantum potential*:

$$Q = \frac{P_2 + P_1}{\rho} = m_{H^+} D^2 \left(\frac{1}{2} \left(\frac{\nabla \rho}{\rho} \right)^2 - \frac{\nabla^2 \rho}{\rho} \right). \quad (12)$$

7.6 Definition of the Diffusion Coefficient D

Now we need to define the diffusion coefficient D for the hydrogen ions in the physiological solution. This coefficient for the Brownian motion of a particle in the viscous liquid is described by the Stokes-Einstein formula [429]:

$$D = \frac{k_B T}{6\pi \mu r_1}. \quad (13)$$

Here the denominator $6\pi \mu r_1$ is the Stokes drag coefficient for the diffusing particles of radius r_1 in the fluid with the viscosity μ . Since the particle has a charge, it drags a cloud of oppositely charged particles. Therefore, there is an added drag coefficient, which is as follows:

$$\frac{R}{r_2} \cdot \frac{e^2}{2\pi \epsilon_w r_2^2}. \quad (14)$$

Here R is the linear resistance (its dimension is Ohm m), e is the particle charge, r_2 is a cross-section size of the cloud, and $\epsilon_w = 81$ is the relative dielectric constant of seawater. Of great value for the dielectric constant are the peculiarities of the chemical structure of the H₂O molecule [418]. It is connected to the fact that water is a polar liquid and therefore has a soft orientation degree of freedom (rotation of molecular dipoles). Water possesses a large shielding effect. It means that two ions placed in

the water lose electric sensibility towards each other through a shorter distance than in a vacuum. The cross-section of the shielding cloud is temperature-dependent.

Following to the above observation, we define the *diffusion coefficient* as follows:

$$D = k_B T \left(\frac{1}{6\pi \mu r_1} + \left(\frac{Re^2}{2\pi \varepsilon_w r_2^3} \right)^{-1} \right). \quad (15)$$

Observe that, in this equation, we sum inverse values of the drag coefficients. By adopting the parameters from Table 1 given in [369–371], one can choose the cloud radius r_2 , such that the diffusion coefficient D would give the value shown in the same table. For $r_2 = 691$ pm we get $D = 5.61 \times 10^{-9}$ m²/s for $T = 273$ K. For $r_2 = 609.7$ pm we get $D = 9.31 \times 10^{-9}$ m²/s for $T = 298$ K. From here, it follows that the cloud radius r_2 represents a temperature-dependent parameter. The size of the cloud is decreased as the temperature rises. One can guess that the decreasing size of the cloud occurs because of the thermal chaotization of the polar groups of water molecules.

Now we need to *define the diffusion coefficient D in terms related to the quantum mechanics problems*. E. Nelson considered these problems in his monographs [46, 430]. According to Nelson [431], Brownian motion of a sub-particle in the vacuum is described by the Wiener process with a diffusion coefficient that is equal to $\hbar/2m$. In accordance with definition given in Penrose and Hameroff [432], we write down the diffusion coefficient as follows

$$D = \hbar/2m_* \quad (16)$$

Here $\hbar = b/2\pi$ is the reduced thermal action parameter (1), like the reduced Planck constant $\hbar = h/2\pi$ and m_* is an effective ion mass. We may evaluate the effective ion mass by equating expressions (12) and (13). We obtain

$$m_* = \frac{\delta\tau (2\pi)^{-1}}{2 \left(\frac{1}{6\pi \mu r_1} + 2\pi \frac{\varepsilon_w r_2^3}{Re^2} \right)}. \quad (17)$$

Here $\delta\tau$ is 2×10^{-13} s for the average lifetime of the hydronium ion H₃O⁺ [433]. From here, we find that $m_* \approx 2.44 \times 10^{-27}$ kg for $T = 273$ K and $m_* \approx 1.83 \times 10^{-27}$ kg for $T = 298$ K. Comparison with the proton mass shows that the first effective mass is in about 1.5 times larger and the second is 1.1 times larger than the proton bare mass, kg. Compare the calculated values of the mass m_* done at room temperature by the formulas (2) and (15). A strikingly good coincidence of numbers is impressive.

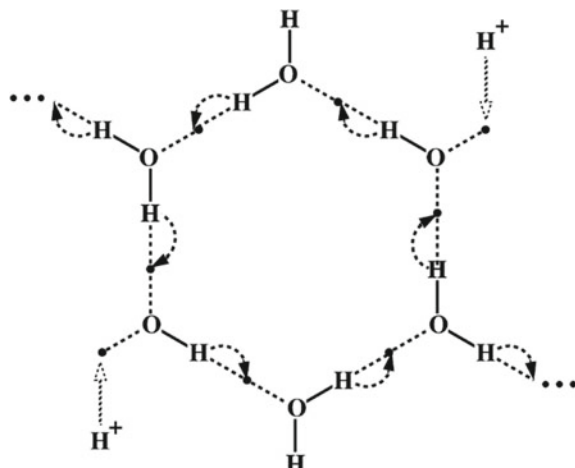
7.7 Viscosity Term

Presence of the viscosity term in Eq. (6) that is enveloped by a bracket (d) leads to a thermal scattering of the energy of hydrogen ions. Such energy losses and consequently the related information losses would be counterproductive. Let us consider some typical Feynman diagrams (i) of elastic scattering of a hydrogen ion on a hole (it is a vacant place for the hydrogen ion) and (ii) tunneling of a hydrogen ion through some obstacle. These processes are shown in Fig. 29a, b, respectively. Two processes shown on these figures illustrate the elastic scattering of a hydrogen ion on a hole and tunneling of a hydrogen ion through an obstacle. The first figures (a) show ideal processes without loss of energy. While the second figures (b) show processes with loss of the energy that is dissipated into heating the water. Causes of this dissipation can be the presence of mud that dissipates phonons generated in the course of these processes. It means that for avoiding the dissipations we need to have clear water.

This special kind of water arises near hydrophilic surfaces that abound in living tissues and is called: the fourth phase of water. Water molecules are ordered into a hexagonal lattice, Figs. 26 and 31. It is also called the exclusion zone (EZ) water [424] since it expels any foreign inclusions so that EZ water molecules are more constrained. An assembly of EZ water molecules is more stable. EZ has a negative charge which is friendly to the resting membrane potential of neural cells. EZ absorbs light at the wavelength around 270 nm. These unique properties make the water a perfect conductor of the hydrogen ions through itself by the Grotthuss mechanism [425], see Fig. 31).

In biology, protons are widely used to transmit signals and energy. They are transported through both protonated residues and buried water molecules by means of the Grotthuss mechanism [426]. The explanations for proton transfer in biological systems usually started with the assumption that proton follows water routes, along so-called “water wires”. Figure 28 shows simulations of ion transport through an

Fig. 31 The hexagonal lattice provides a perfect space for the Grotthuss mechanism



originally “dry” nanotube. The wetting process of the nanotube induces the motion of the excess hydrogen ions along the nanotube, Fig. 28b. As a result, it can remind an avalanche-like process shown in Fig. 28c. A remarkable point in this simulation is that the carbon plate hexagonal symmetry is the same as the hexagonal symmetry of the fourth phase of water (compare Figs. 26 and 28a).

It follows, that the results of this simulation can be useful in discussing the transport of hydrogen ions in the EZ water.

$$m v(t) \nabla^2 \vec{v}(\vec{r}) - \nabla U(\vec{r}) = m \nabla^2 \vec{v}(\vec{r}) \left(\frac{v(t) - \overbrace{(m \nabla^2 \tilde{v}(\vec{r}))^{-1} \nabla U(\vec{r})}^{\text{additive}}}{\tilde{v}(t)} \right). \quad (18)$$

Now the renormalized viscosity coefficient $\tilde{v}(t)$ in the average is zero, but its dispersion is not zero, namely:

$$\langle \tilde{v}(t) \rangle = 0_+, \quad \langle \tilde{v}(t), v(0) \rangle > 0 \quad (19)$$

7.8 Transition to the Schrödinger Equation

Let us now rewrite the modified Navier–Stokes Eq. (9) in the following representation:

$$m_* \left(\underbrace{\frac{\partial \vec{v}}{\partial t} + \frac{1}{2} \nabla v^2}_{(a)} + [\vec{\omega} \times \vec{v}] \right) + \underbrace{\left(\frac{\partial \vec{A}}{\partial t} + \nabla \phi \right)}_{(b)} + e[\vec{B} \times \vec{v}] + \underbrace{\nabla(Q + U)}_{(c)} - \underbrace{m_* \tilde{v}(t) \nabla^2 \vec{v}}_{(d)}. \quad (20)$$

In this equation, instead of the mass density $\rho_M = m_* \rho$, we write the mass m_* represented as the main multiplier at the first brackets, since the equation we divided on the density distribution ρ . The term captured by curly bracket (a) comes from $(\vec{v} \cdot \nabla) \vec{v}$. The vector $\vec{\omega} = [\nabla \times \vec{v}]$ is called vorticity. The vorticity is perpendicular to the plane of rotation of the fluid [434]. It corresponds to the axis about which a vortex rotates. The term given to curly bracket (b) is the *Lorentz force*. Here, we adopted the SI unit. In addition, we rewrite $[\vec{J}_q \times \vec{B}] = -[\vec{B} \times \vec{J}_q]$.

It should be noted, that the mobility of the hydrogen ion is highest among many other ions, such as K^+ and Na^+ [427] that are important ions for neuronal communications. These ions have individual ion pumps, while special water wires are prepared each time when a problem regarding the transport of hydrogen ions, protons, arises. One can assume that the aqueous proton transport [428] is set each time along most optimal paths, like the Bohmian trajectories of particles in the physical quantum space.

From the above, we may conclude that EZ water represents a water space where the Grotthuss mechanism has a minimal loss of the energy at the hydrogen ion hoppings. Observe that the Grotthuss mechanism, along with the relative lightness and small size of the proton, possesses an unusually high diffusion rate of the proton in an electric field, relative to that of other common cations [427]. Therefore, we will assume that along the water wires the water viscosity vanishes (theoretically, we will assume the viscosity inside the water wires in the average is zero).

Let $v(t) = \mu(t)/\rho_M$ be the kinematic viscosity coefficient of water at the normal phase fluctuating in time [$\mu(t)$ is the dynamic viscosity coefficient]. On the other hand, we assume that there is potential energy due to which a surprising phenomenon is revealed. Namely, an excess proton charge defect creates its own aqueous transport pathway by shuttling water molecules through it into the hydrophobic nanoconfined space [426].

The gradient $\nabla(Q + U)$ enclosed by curly bracket (c) determines a *generalized force of Newton's second law* in the *Bohmian mechanics* (Benensey et al. 2014) [435], due to presence of the quantum potential Q added to the external potential U . The latter is due to the abundant presence of the microtubules in neural cells, and other cell elements in the brain tissues.

Together with it, the viscosity of this transport pathway becomes as small as possible. Let $U(\vec{r})$ be potential energy, providing formation of the water wire and the proton transport along with it. Following this remark, we write down an expression that provides decline of the viscosity within the water wire in the average to zero: as it is written in Eq. (17).

The term captured by curly bracket (d) describes the renormalized viscosity, as shown in Eqs. (16) and (17), within the proton water wire. One can see that on average through time the viscosity is close to zero but its dispersion does not vanish. This fluctuating chaotic activity describes the energy exchange with the deep superfluid quantum medium (with the quantum ether) and as believe can be a source of revelations.

7.9 Irrotational and Orbital Vector Fields. Derivation of the Schrödinger Equation

The fundamental theorem of the vector calculus, Helmholtz's theorem, states that any vector field can be expressed through the sum of irrotational and solenoidal

fields [436]. Further, instead of the term “solenoidal” we will use the term “orbital” [216] since it has roots in the Stokes’s theorem computing a circulation about a closed orbital contour. The velocity \vec{v} can be represented as consisting of two components—irrotational and orbital

$$\vec{v} = \vec{v}_S + \vec{v}_O, \quad (21)$$

where subscripts S and O point to the existence of scalar and vector (orbital) potentials, underlying the emergence of these velocities. These velocities relate to vortex-free and vortex motions of the fluid medium, respectively. They satisfy the following equations

$$\begin{cases} (\nabla \cdot \vec{v}_S) \neq 0, [\nabla \times \vec{v}_S] = 0 \\ (\nabla \cdot \vec{v}_O) = 0, [\nabla \times \vec{v}_O] = \vec{\omega} \end{cases}. \quad (22)$$

One can trace parallels between these equations and the *Maxwell equations for electric and magnetic fields* [437, 438]. In this key, we may represent the kinetic momentum $\vec{p} = m_* \vec{v}$ and the kinetic energy by the following expressions

$$\begin{cases} \vec{p} = m_*(\vec{v}_S + \vec{v}_O) = \nabla S - e\vec{A} \\ m_* \frac{(\vec{v}_S + \vec{v}_O)^2}{2} = \frac{1}{2m_*} (\nabla S - e\vec{A})^2 \end{cases} \quad (23)$$

Here S is a scalar function called the *action*, the gradient of which determines the irrotational velocity \vec{v}_S , whereas the vector potential \vec{A} underlies the determination of the orbital velocity $-\vec{v}_0$.

Taking into account $m_* \vec{v} = \nabla S - e\vec{A}$ let us rewrite Eq. (18) in more detail

$$\begin{cases} \vec{p} = m_*(\vec{v}_S + \vec{v}_O) = \nabla S - e\vec{A} \\ m_* \frac{(\vec{v}_S + \vec{v}_O)^2}{2} = \frac{1}{2m_*} (\nabla S - e\vec{A})^2 \end{cases} \quad (24)$$

First, one can see that the both terms $e\partial\vec{A}/\partial t$ in this expression cancel each other out. In addition, the term $m_*[\vec{\omega} \times \vec{v}]$ can be transformed to $e[\vec{B} \times \vec{v}]$ with sign minus as soon as instead of $\vec{\omega}$ we substitute its representation by $[\nabla \times \vec{v}_O] = -e/m_*[\nabla \times \vec{A}]$. The latter expression one can rewrite in a more compact form: $\vec{v}_O = -(e/m_*)\vec{A}$.

Now we can rewrite Eq. (22) in a more compact form

$$\nabla \left\{ \frac{\partial}{\partial t} S + \frac{1}{2m_*} (\nabla S - e\vec{A})^2 + e\phi + \tilde{v}(t)m_* \frac{\partial \ln(\rho)}{\partial t} + (Q + U) \right\} = 0 \quad (25)$$

The term $\partial \ln(\rho)/\partial t = -(\nabla \cdot \vec{v})$ [369–371] comes from the continuity equation of the mass density, Eq. (5), as soon as we rewrite it for the density distribution:

$$\frac{\partial \rho}{\partial t} + (\nabla \cdot \vec{v})\rho = 0 \quad (26)$$

The expression enclosed in curly brackets in Eq. (23) is the Hamilton-Jacobi-like equation

$$\frac{\partial}{\partial t} S + \frac{1}{2m_*} (\nabla S - e\vec{A})^2 + e\phi + \tilde{v}(t)m_* \frac{\partial \ln(\rho)}{\partial t} + Q + U = C \quad (27)$$

loaded by the extra terms Q and $\tilde{v}(t)m_* \partial \ln(\rho)/\partial t$. From the left C is the integration constant.

Equations (24) and (25) stem from the following nonlinear Schrödinger equation

$$i\hbar \frac{\partial \Psi}{\partial t} = \frac{1}{2m_*} (-i\hbar \nabla - e\vec{A})^2 \Psi + \underbrace{e\phi \Psi + U(\vec{r})\Psi + \tilde{v}(t)m_* f(\rho)\Psi - C\Psi}_{(28)}$$

It should be noted that in this equation the reduced thermal action parameter, \hbar , is presented, not the reduced Planck constant \hbar . In the above equations, C is the integration constant that arises at extracting solution from Eq. (23).

We arrived at a single equation, the Schrödinger-like equation, describing flows of the hydrogen ions in water by their representations through the complex-valued function—the wave function $\Psi(\vec{r}, t)$. Observe that $\rho(\vec{r}, t)$ deals with the probability of detection of the hydrogen ion in the vicinity of point \vec{r} in the moment of time t , and the action $S(\vec{r}, t)$ points to its mobility in the vicinity of this point. Substituting in Eq. (26) the *wave function represented in the polar form*:

$$\Psi = \sqrt{\rho} \exp\{\mathbf{i}S/\hbar\} \quad (29)$$

and after *separating the real and imaginary parts* of this equation, we come to the Eqs. (25) and (24), respectively.

From the above, we may conclude that EZ water represents a water space where the Grotthuss mechanism has a minimal loss of the energy at the hydrogen ion hoppings. Observe that the Grotthuss mechanism, along with the relative lightness and small size of the proton, possesses an unusually high diffusion rate of the proton in an electric field, relative to that of other common cations [427]. Therefore, we will assume that along the water wires the water viscosity vanishes (theoretically, we will assume the viscosity inside the water wires in the average is zero). On the other hand, we assume that there is potential energy due to which a surprising phenomenon is revealed. Namely, an excess proton charge defect creates its own aqueous transport pathway by shuttling water molecules through it into the hydrophobic nanoconfined space [426]. Such superconductivity is described in [369–371], where the average viscosity coefficient declines to zero. This also could in part explain ultra-rapid brain response.

7.10 The Path Integral: Gap Junction Channels

There are rigorous mathematical proofs concerning the extraction of the Schrödinger equation out of the Feynman path integral [439, 440], as well as solutions of the Schrödinger equation by applying the same path integral technique [395]. Following this statement, the Schrödinger wave equation can be resolved by heuristic writing of a solution by using the Huygens Principle [393, 394], which mathematically appears as:

$$|\Psi(\vec{r}, t)\rangle = \int K(\vec{r}, \vec{\xi}, t) |\Psi(\vec{\xi}, 0)\rangle d\vec{\xi}. \quad (30)$$

The propagator $K(\vec{r}, \vec{\xi}, t)$ bears information about the neuron tissue that is contained in the terms covered by the curly bracket in the Schrödinger Eq. (26). Here the integral summarizes all paths coming from a source of radiation to a point of observation (receiving information). Between the source and the endpoint of receiving information, there can be placed many biological agents such as microtubules, gap junctions, etc. They are represented in the Schrödinger equation by the potential energy term U and, consequently, interfere with the wave function.

The microtubules, for example, can play a role not only of a component of the cellular skeleton and to provide transportation of biological molecules on long distances, but also may serve as a sort of memory, as it was suggested by Hameroff and Penrose [408, 441, 442]. As was shown recently by Tuszyński et al., the microtubules possess memristive properties [443], which makes them suitable for long-term storage of memory.

The gap junctions, in turn, are specialized intercellular connections between different cells directly connecting the cytoplasm of two cells; see the insert in Fig. 32. The gap junction, also named electrical synapses, exists in every major area of the central nervous system [444–446]. Gap junctional intracellular communications are formed into ordered arrays showing predominantly hexagonal packing, (Fig. 32), with about 6–9 nm center-to-center spacing [447, 448].

Such ordered arrays represent slit gratings for the ion beams passing through them and reproduce an interference effect behind them. In fact, it is an ideal interference device for ensuring information processing. A wave function describing the interference pattern from a grating containing N slits and placed in the 2D space is

$$|\Psi(x, z)\rangle = \frac{1}{\sqrt{1 + i \frac{\zeta \lambda_{dB}}{2\pi s^2}}} \cdot \sum_{n=0}^{N-1} \exp \left\{ -\frac{(x - (n - \frac{N-1}{2})d)^2}{2\xi^2(1 + i \frac{\zeta \lambda_{dB}}{2\pi s^2})} \right\}. \quad (31)$$

Here, ζ is a width of the slit, d is the distance between slits, and n is the sequence number of the slit. Here $\lambda_{dB} = b/c_s m_* \approx 0.3$ nm is the de Broglie wavelength of the hydrogen ion, and b is the thermal action parameter (1). The slits are placed along the x -axis, with equidistant spacing between them, and the z -axis is perpendicular

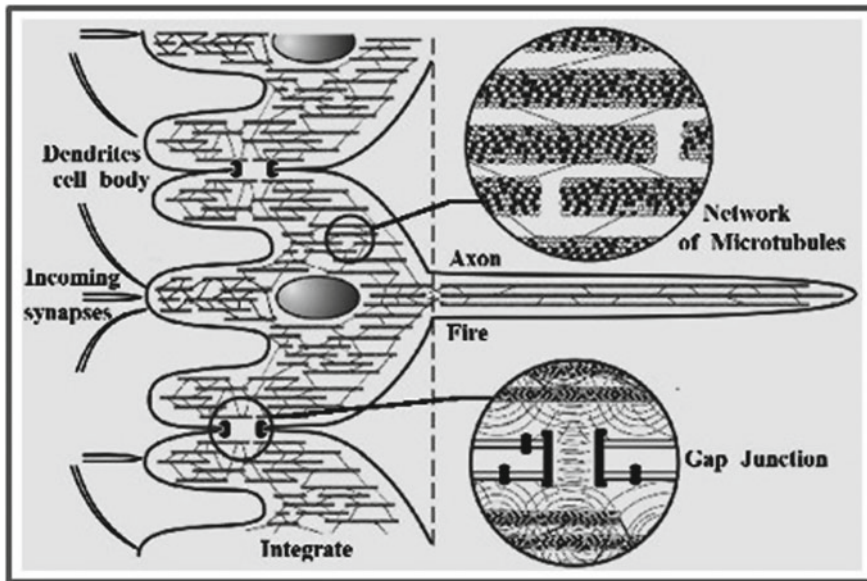


Fig. 32 An “integrate-and-fire” brain neuron and parts of other such neurons are shown schematically with gap junction and internal microtubules interconnected by microtubule-associated proteins [449]

to the grating position. The density distribution of this wave function $p(x, z) = \langle \Psi(x, z) | \Psi(x, z) \rangle$ is shown in Fig. 34.

The gap junctions are observed predominantly on the glial cells, which number is much larger than the number of neurons in the brain. They are often strong enough to mediate close synchronization of subthreshold and spiking activity among clusters of neurons [444, 450]. The gap junctions are a ubiquitous, yet underappreciated, a feature of neural circuits of the mammalian brain. They may contribute to the cognitive processes in both aspects, namely, perception and attention [451]. Particularly impressive work in this range is the article by Richard Maxwell [452] devoted to connections of a subtle world through chakras with the body organs by means of intercellular gap junction connections.

The latter mechanism provides a physiological modality underlying subtle energy systems. Here we have come close to understanding the importance of gap junctions, in connecting a lower level of the brain with a higher level. In addition, we highlighted proton transport through intracerebral fluid and the Grothuss mechanism, picturing the water interface between the brain and the superfluid quantum medium (the quantum ether).

To show a place of the human consciousness in the Universe we give a conditional cartoon of the brain in Fig. 34. Two figures show the brain in two states—the awake brain, Fig. 35a, and the brain in REM dream, Fig. 35b. In both cases, the brain has a connection with the vacuum zero-point fluctuations due to protons of water.

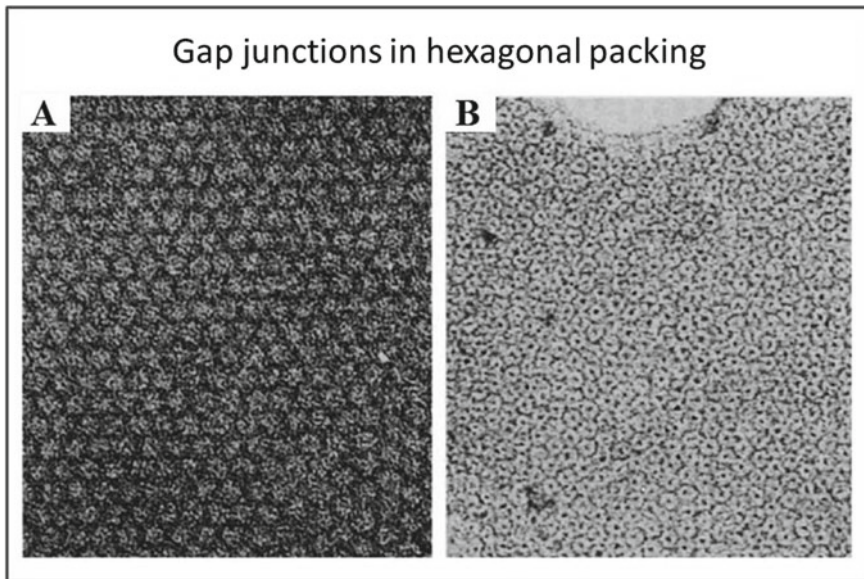


Fig. 33 Gap junctions stained with **a** phosphotungstic acid, $\times 580,000$; **b** and uranyl acetate, $\times 470,000$. Well visible is the hexagonal packing. Photos are borrowed from Zampighi [448]

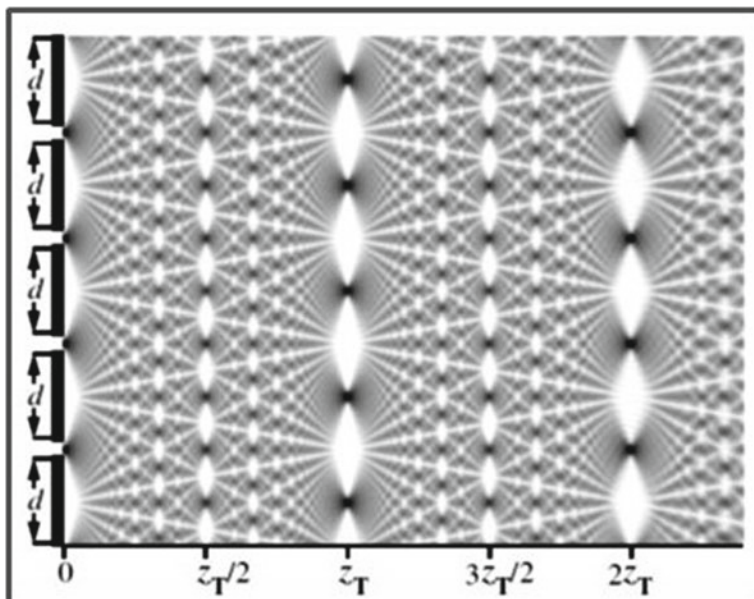


Fig. 34 The density distribution of the wave function (8). Here $z_T = d^2/\lambda_{dB}$ is the Talbot length adopted unit of length in the interferometry

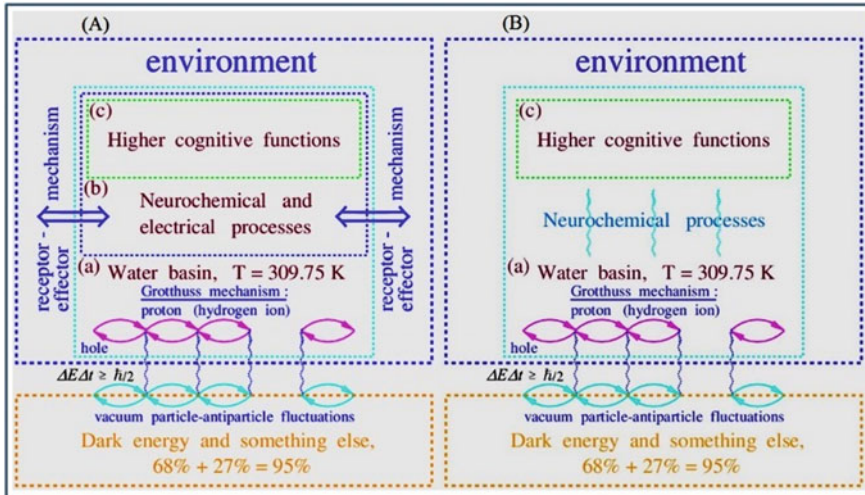


Fig. 35 Conditional cartoon of a living being: **a** three-level diagram of brain organization in awake state: (a) a water basin containing all the other levels; (b) nervous tissue and glial cells, supporting electrical activity of the receptor–effector mechanism; and (c) higher cognitive functions creating consciousness as a paradox [411]. All of this is backed by a dark substance—the “superfluid quantum space” [216, 390]; **b** three-level diagram of brain organization in REM dream state: here the nervous tissues regulating the receptor–effector mechanism are in a deep rest

In the first case, however, because of a huge noise conditioned by the operation of receptor–effector mechanism of connecting us with the environment, we do not sense tiny zero-point fluctuations. In the second case, the case of REM dream, the nervous tissues regulating the receptor–effector mechanism are in deep rest and, therefore, there is no huge noise drowning out a faint stream from the depths of consciousness. In this state, we may experience dreams.

Perhaps, there are people that can have a perception of tiny fluctuations, coming from deeper layers of the consciousness, related to the dynamics of the Universe. These people, as a rule, are somehow in borderline states of their consciousness. For that reason, their psyche can be very sensitive to such tiny fluctuations (see Sect. 5.8 and 5.9). These borderline states of the consciousness represent bifurcation conditions, according to a term from brain pathology such as in epilepsy [453, 454] and even in schizophrenia [455, 456].

7.11 Extra-Sensory Perception at the Cognitive Level

There is a lot of evidence that people exist with psychic abilities who somehow can register a type of super-weak radiation information. Such radiations can either have an electromagnetic or a gravity-torsion nature. These radiations are described

by solutions of the wave equations that stem from the equations for the electro-magnetic and gravity-torsion fields. They have different orientations of the torsion and magnetic fields [457], but this difference is not of major importance. There is, however, a significant difference with the gravitomagnetic field, being several orders of magnitude weaker than the electromagnetic field. Yet, while the latter field can be shielded by a Faraday cage, for example, the gravity-torsion field is rather all-pervading. For that reason, many scholars believe that the torsion field can have some relation to a spiritual emanation and Cosmic Consciousness [458].

The wave equation for the weak torsion field $\vec{\Omega}$ is as follows [216]:

$$\frac{\partial^2 \vec{\Omega}}{c^2 \partial t^2} - \nabla^2 \vec{\Omega} = -\frac{4\pi}{c} [\nabla \times \vec{\mathfrak{J}}] \quad (32)$$

and the wave equation for the weak gravitational field $\vec{\Xi}$ looks as follows:

$$\frac{\partial^2 \vec{\Xi}}{c^2 \partial t^2} - \nabla^2 \vec{\Xi} = -4\pi \left(\nabla \wp + \frac{\partial \vec{\mathfrak{J}}}{c^2 \partial t} \right). \quad (33)$$

Here, \wp and $\vec{\mathfrak{J}} = \vec{v}_\wp$ are the density distribution of gradient from all external and internal forces acting on a body as immersed in the superfluid quantum ether and the 3D current density, respectively. The vorticities of hydrogen ions, during hopping along the EZ water hexagonal complexes (see Figs. 26, 27), give a contribution to the 3D current density $\vec{\mathfrak{J}}$ and, consequently, they are sources of the torsion field.

Based on the Wheeler-Feynman absorption theory [459], Cramer put forward the transaction interpretation of quantum mechanics [460], see also Sect. 2). According to the formulation of this interpretation, the retarded (forward in time) and advanced (backward in time) waves were considered as real physical objects. The idea is as follows: a source generates a retarded offer wave, which travels to an absorber, forcing the absorber to generate an advanced confirmation wave, which moves back along the path to the source. In that key, the advanced wave is an echo-wave of confirmation due to which the “spooky action at a distance” gets implementation as soon as a standing wave between the source and the absorber is established. Cramer [460] writes: “the exchange (between the offer and confirmation waves, V.S.) cyclically repeats until the net exchange of energy and other conserved quantities satisfies the quantum boundary conditions of the system, at which point the transaction is complete”.

In relation to this mechanism, one can put a question: “can an extra-sensitive person foresee the future on the basis of this mechanism?” Historical documentation that provides biographies of individuals with clairvoyance type of capabilities [see, for example, Edgar Cayce (Cayce, wiki) and Baba Vanga (Vanga, wiki)] may suggest a reading (feeling) of future events. In an altered state of consciousness of the person, the echo-waves coming from different sources can in principle create a quantum interference pattern that provides a sense of foreseeing. Yet, the particular foresight experience will always contain some intrinsic uncertainty as to the sought prediction

due to the uncertainty principle, according to which it is impossible to predict an exact location and the dynamics of a specific event at the same time.

Inspecting Fig. 36 we may ask: how can the perception of super-weak emanations reach such a high level of cognitive function? Note that the supposed super-weak emanations can become manifest through signaling the limbic system that plays a crucial role in these types of emotional experience. Here we consider the functions of the hippocampus as a versatile part of the limbic system Fig. 36, left shows the hippocampus (colored in blue), which has a direct contact with the cerebral fluid through hippocampal fimbria that are adjacent to the vascular plexuses of the lateral ventricles. The two parts of the hippocampus symmetric (left and right), have the shape of curved tubes. The hippocampus consists of an anterior and posterior part (in primates) joined at the stems by the commissure of fornix Fig. 36, right, located under the corpus callosum, shows a diagram of the fornix originating from the hippocampus. The hippocampal commissure together with the fornix act as the major output tract of the hippocampus through the corpus callosum on to the entorhinal cortex. Pay your attention as the back part of the hippocampus fits from the bottom on the corpus callosum by forming a tight contact by fornix, Fig. 36, right part.

As one can see in this figure two hippocampal pillars, together with the hippocampal commissure and body of the fornix form a closed chamber where the thalamus supports the third ventricle as seen from below. In the medial part of this chamber, the pineal gland, (epiphysis), adjoining to the third ventricle is located. We remark that the pineal gland has a size of about 6–8 mm in length and 4 mm in cross-section and contains in itself many sand-like crystals. Sand crystals, shown to be present in the brain of several species, possess so-called piezoelectric properties [461]. This property may imply that these crystal structures may function

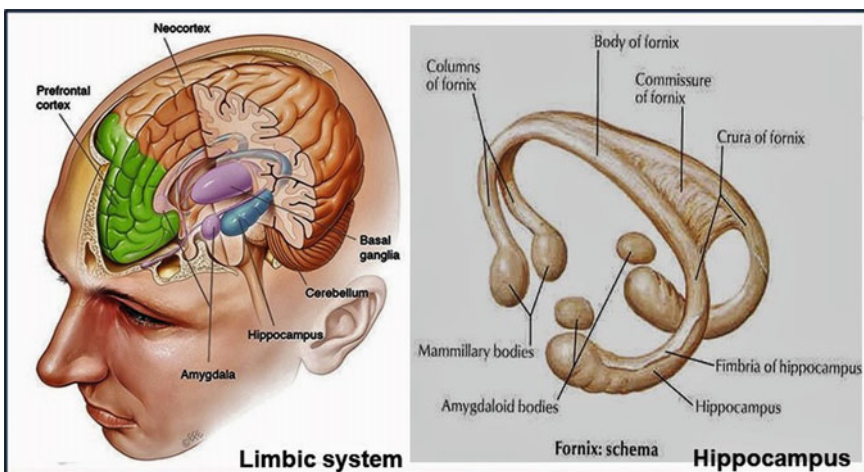


Fig. 36 Some tissues belonging to the limbic system (colored in red) shown from the occipital side: (a) hippocampus; (b) lateral ventricles (dark blue indicates the cerebral aqueduct); (c) commissure of the fornix; (d) corpus callosum; (e) diagram of the fornix originating from the hippocampus

as solid-state clock generators, representing the so-called “biological clock” [462]. The particular wave frequencies have been claimed to be related to the standard brain biorhythm harmonics, such as alpha-, beta-, gamma-, and delta rhythms. These rhythms play an important role in the organization of the functional activity of the hippocampus both at the awake state (predominantly alpha and beta rhythms) and in the dream state (predominantly gamma and delta rhythms). In order to evaluate this role, let us glance at the inner organization of the hippocampal tissues in the cross-section of the hippocampus slice presented in Fig. 37. Here the left figures show the cross-section hippocampal slices and the right figures represent the linking pathways between the entorhinal core and the hippocampus through intermediaries the dentate gyrus (DG) and subiculum, also the Shaffer collaterals and the mossy fibers. All

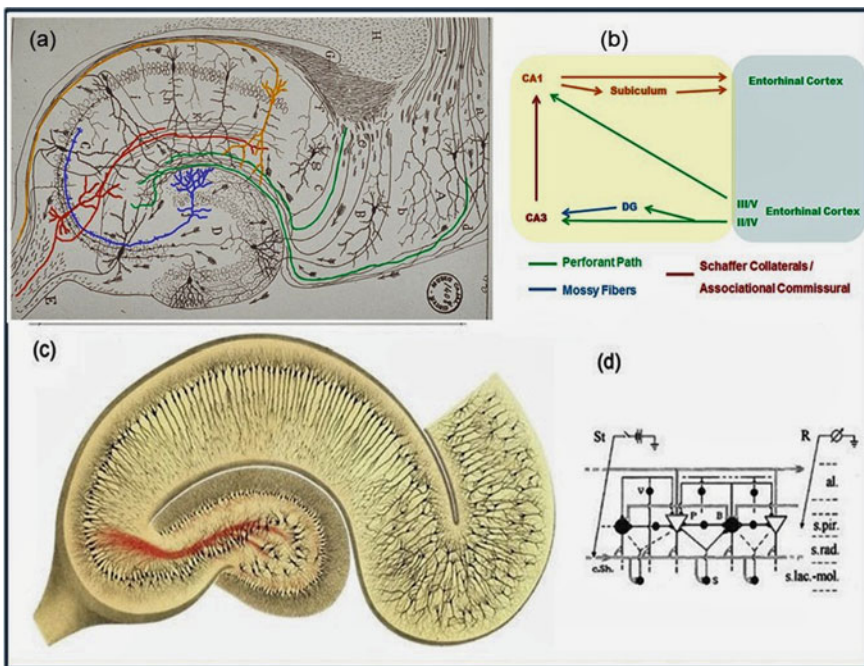


Fig. 37 A cross-section of hippocampus. The figure **a** is modified original drawing of Santiago Ramón y Cajal's in 1911 and **b** schematic diagram of the rodent hippocampal circuitry. The picture shows the flux of excitatory projections (arrows) from entorhinal cortex (EC) neurons (green) directly to CA₁ (orange) or CA₃ (red) hippocampal pyramidal neurons or indirectly through projections to the dentate gyrus (DG, blue) through the perforant pathway. DG granule neurons project along the mossy fibers to CA₃ pyramidal neurons [465]. The figure **c** shows principal cells of the hippocampus drawing by Camillo Golgi in 1894 [466]. Figure **d** shows principal types of neurons, pathways and synaptic connections in the field CA₁ of the hippocampus (according to Lacaille and Schwartzkroin [467] and Williams et al. [468]). Black circles are inhibitory neurons, and white triangles are pyramidal cells. Single lines show axonal pathways from the inhibitory neurons and dendrites; double lines represent both axons from the pyramidal cells and the Shaffer collateral pathway [417]

these pathways support working the hippocampus at recognition and accumulation of new data in the long-lived memory [463, 464].

The hippocampus is seen to receive incoming streams of impulses from the entorhinal cortex (through the dentate gyrus) and the results of their processing are sent back to the entorhinal cortex (through the subiculum). Along the way, information is filtered by pyramids of hippocampal fields CA3, CA2, CA1 in the clock cycle with rhythms) alpha, about 7 Hz, or gamma, about 4 Hz and delta, 2 Hz and smaller) coming along the Shaffer collaterals from the dentate gyrus.

Figure 37c shows a very remarkable drawing of principal (pyramidal) cells made by Camilio Golgi in 1894 from a cross-section of the hippocampus. This structure is very similar to the retina of the human eye with well-oriented principal cells. However, unlike the eye receiving the light and converting it into chemical energy, these well-oriented principal cells of the hippocampus receive the impulse flow from the entorhinal cortex and sort them in accordance with the rhythm coming from the same dentate gyrus. One can guess that the involuntarily saccades typically for rapid eye movements may also be inherent in the left and right lobes of the hippocampus.

In this framework, the hippocampal processing of spatial information is playing a primary and central role, which underlies the Cognitive Map Theory [463]. The hippocampus is connected to the rest of the brain in such a way that it is ideal for integrating both spatial and nonspatial information. Connections from the postrhinal cortex and the medial entorhinal cortex provide spatial information to the hippocampus. Connections from the perirhinal cortex and lateral entorhinal cortex provide nonspatial information. The integration of this information in the hippocampus makes it instrumental in cognitive mapping, which necessarily involves combining information about an object's location and its other features [469]. Note that, pyramidal cells are involved and function as the neuronal basis for cognitive maps within the hippocampal system.

The epiphysis or pineal gland is one of the central organs of the endocrine system. It regulates all processes that occur in the body rhythmically, as well as circadian rhythms. It is supposed to modify the functional activity of organs during the day, biorhythms «sleep-wake». During wakefulness, all receptor and effector organs are active. For that reason, the brain loses its sensitivity to weak emanations of the subtle world because the brain is subjected to a very noisy manifestation of the environment. During sleep, all receptor and effector organs rest, in which the brain activity is undergoing qualitative changes. Instead of day's alpha and beta rhythms (7–20 Hz) in the hippocampus slow rhythms, gamma, and delta (4–2 Hz and smaller), appear. This rhythm aspect was also treated by [100], in his resonance theory of consciousness that was related by him to gamma synchrony combined with lower frequencies as the potential neuro correlates of consciousness. Bandyopadhyay [470], in an interesting interview of him by Hunt, emphasized the importance of resonance chains in the setting of nested frequency fractals that correspond with various modalities of memory.

We propose that the hippocampus performs the same function as a pair of eyes for light perception, a pair of ear snails for sound perception, or a pair of nostrils for smell perception. The only difference is that a pair of hippocampal arcs are located

in the temporal lobes of the brain (Fig. 36). Wilder Penfield, a revolutioner in the understanding of the human brain [471], discovered that stimulation of the temporal lobes provoked hallucinations, dream, startlingly vivid recollections, up to out-of-body experiences [472, 473]. All these serve to proof of the physical basis of memory [474].

In relation to our concepts of the quantum wave processing of the brain treated before, we hypothesize that the pair of hippocampal arcs may work as a sort of two-slit interferometer. Such a mechanism of cognitive interference was also suggested in the study of Deli [475]. This interferometer manifests itself especially at the state of the dream, the REM dream, when most of the neural receptors and effectors are disabled, Fig. 35b. In this state a new channel may open, connecting the brain with the subtle domain of transpersonal entities. Working frequencies, in this case, are about 4 Hz (theta rhythm) to 2 Hz and below (delta rhythm). It should be noted that such an altered state of consciousness (see also Sect. 5.7) can be achieved in several ways (see Fig. 16) but in particular by special meditative states induced by monotonous chants or monotonous recitation of prayers. All these meditative techniques aim to bring the brain rhythms to the lower frequency range as indicated above.

The transpersonal efforts to foresee potential future events should evidently be accompanied by the ability to bring such, often sub-conscious, experiences up to the level of emotionally attached recurrent dream states that thereby finally may surface as a reportable conscious moment. The transcendental experience is often associated with a fearless feeling of being part of a timeless universal consciousness [2]. Here we come to an “inversed” form of the so-called anthropic principle: the very reason that we can reflect on something like the processing of information in the human brain is that only something as complex as a field embedded brain can produce such deliberations.

Summarizing this section: here we tried to understand what mechanisms may be responsible for the exchange of wave information with the oscillating and superconducting quantum ether. As was noted above, a major transmission mechanism is represented by the Grotthuss process that can be effective when water is in the fourth phase. This process can be expected to exist near countless subcellular structures, including the cellular membranes and intracellular organelles of neurons and probably other cell types, in permanent vibratory contact with the fluid constituents of the brain. A dedicated receiver of information coming from the subtle world is represented by the hippocampus localized in the limbic system. Both lobes of the hippocampus, located in the temporal lobes of the brain, may function like a two-slit interferometric device that registers ultra-weak emanations under tuning on the frequency range of *Theta* and *Delta* rhythms.

7.12 *The Crucial Informational Role of Ca²⁺ Ions in Brain Function*

Through the prism of the above description, we may now consider the consciousness evolving in the wet, warm, and noisy brain system. It interacts with a massive volume of memory stored in a deeper, finer-grained scale of a memristive system [410]; Chua 1971). The interaction manifests itself through the destructive and constructive interference effects, like the effect of a vote. The memristive system by itself is based on the cellular organelles involved in the sequestration of calcium ions (networks of the granulated units of Ca²⁺), including the calcium-calmodulin-dependent protein kinase II (CaMKII), which is implicated in the strengthening of active neural connections [476].

Ca²⁺ takes a crucial position in the integration of the distributed information within the brain, not only due to its specific atom electronic properties (empty atomic electron shells) and thereby its potential for entanglement and superposition, but also since it affects at least ten different cellular processes that have been shown to correlate with modalities of conscious perception (reviewed by Pereira [477, 478], Pereira and Furlan [479], see also Fig. 38). Interaction of general anesthetics with NMDA receptor/channel function have been shown to induce the loss of consciousness [273], but has also be related to high affinity for tubulin proteins, thereby blocking their Tera-Herz oscillations in microtubules (Craddock et al. 2017). Earlier it was shown that electromagnetic fields may influence cell function via activation of voltage-gated Ca-channels in the plasma membranes and that this can both lead to beneficial and adverse effects in the exposed cells [480]. In addition, phonon patterns affect trapped Ca²⁺ ions in astrocytes, a process that is instrumental in the formation of quantum information states that in the proposed astroglial/neuronal “protectorate” may survive decoherence [477, 478]. This special fractal scaled Ca²⁺ behavior supports the premise that astrocytes support functions added to the normal neuronal mechanisms. In fact, they may contribute directly to cognitive functions and resultant behavior [479, 481]. Of note, grafted human astrocytes in mouse brain have a higher rate of Ca²⁺ flux and are much larger and more complex than normal mouse cells and, interestingly, showed enhanced learning, memory, and plasticity [482].

It has been shown that Ca²⁺ ions are also hydrated, and, in principle, their behavior can be described by similar hydrodynamics and path integral approaches, as described in the previous for hydronium ions. Thus, just as there is a wide variety of intercellular Ca²⁺ waves in different cell types, so there is a corresponding variety in their mechanism of extra-cellular propagation. Nevertheless, two basic mechanisms are predominant: propagation by the diffusion of an extracellular messenger and propagation by the diffusion of an intracellular messenger through gap junctions. Sometimes both mechanisms operate in combination to drive an intercellular wave. Of note, Ca²⁺ waves can exhibit spiral patterns [483] and are also influenced by external cyclotron EMF resonances (Meijer and Geesink 2015), both supporting our concept of toroidal flux mediation in the brain. Nunn [484], also stipulated the importance of

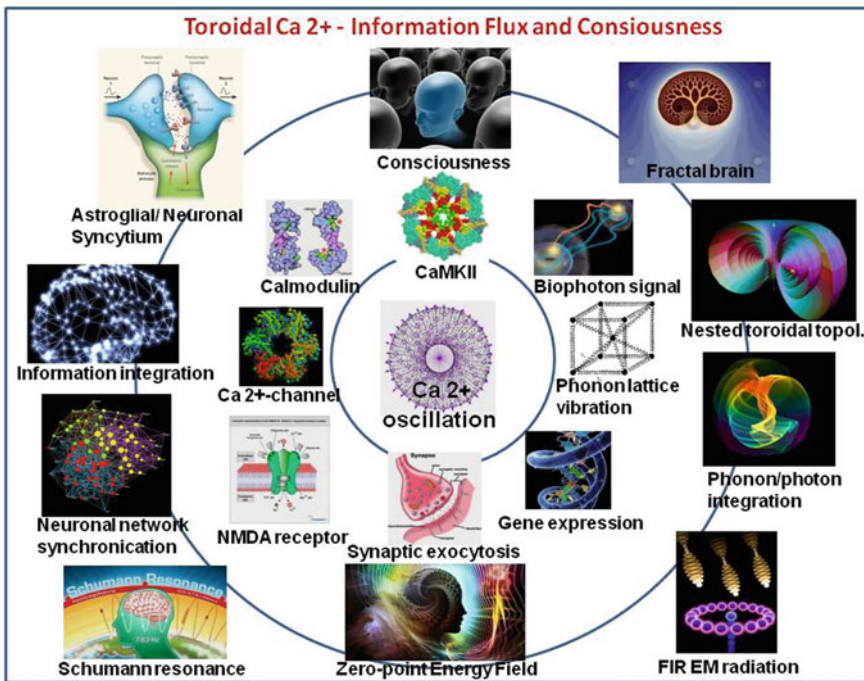


Fig. 38 The fractal organization of Ca^{2+} mediated cellular mechanisms related to conscious perception. The pivotal role of Ca^{2+} ions, as the second informational messengers in brain function is indicated at micro- and macro-levels. The inner circle is depicted anti-clockwise: Neuron/astrocyte mediated Ca^{2+} flux leads to activation of calmodulin-associated kinases (CMKII), calmodulin, NMDA-receptor/channel proteins and quantum resonance within Ca-channels that may stimulate synaptic neurotransmitter exocytosis. Outer circle macro-scale: Ca^{2+} flux in syncytia of neurons/astrocytes leads to phonon/photon-mediated information storage and integration as well as neuronal assembly and neuronal network synchronization. The Ca^{2+} messenger function may be influenced by Schumann and cyclotron resonances by far-infrared (FIR) radiation resonance as well as Zero-point energy (ZPE). The resulting phonon and photon scalar waves in the brain are integrated and protected against decoherence through toroidal processing. Topological integration on the brain macro-scale is realized by torus nesting and self-similar fractal representation. This integral process may contribute to the creation of awareness and conscious perception in relation to the external world.

fractal patterns of re-entrant calcium waves in order to map brain attractors that could even represent a bridge between the realm of physical laws and a timeless platonic realm (phase space) of mathematical objects as pictured in Fig. 15.

Interestingly, calcium may also play an unexpected role in nuclear quantum spin-mediated brain communication in the brain. Fisher [485] identified the so-called “Posner molecule”, $\text{Ca}_9(\text{PO}_4)_6$, as a unique molecule that through shielding the phosphate group (Fig. 39a) can protect the spin-mediated neural qubits for very long times and thereby may serve as a (working) *quantum-memory*. A central requirement for quantum-processing is *quantum entanglement across the brain*. It was argued that

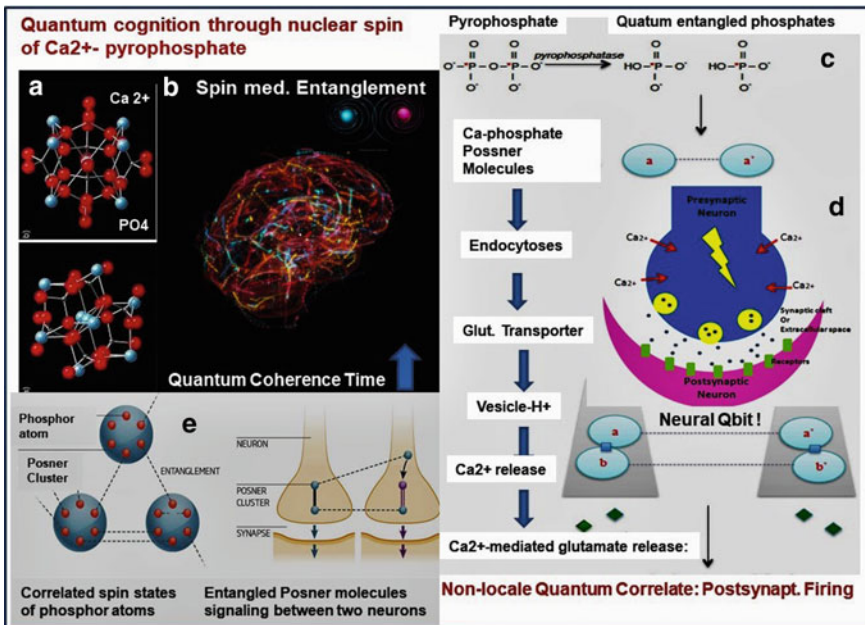


Fig. 39 The potential role of quantum-entangled Ca -phosphates (a) in brain (b), that protect spin-entangled neural Qbits and after endocytosis of Posner molecules in neurons, release Ca^{2+} - ions that influence neuronal glutamate release (d) and thereby induce post-synaptic firing in spin-entangled neurons (e) throughout the brain

the phosphatase enzyme that breaks a pyrophosphate ion into two phosphate ions can form quantum-entangled pairs of qubits (Fig. 39c). A mechanism for transporting Posner molecules into presynaptic neurons during vesicle endocytosis was than proposed. This endocytic process is supposedly coupled to a glutamate transporter in the plasma membrane and in intracellular vesicles. Quantum measurements throughout the brain, due to the generated spin-entangled state of multiple neurons, can then occur. When a pair of Posner molecules, engulfed into the neurons fall apart it releases a burst of intracellular calcium ions, that then can trigger further neurotransmitter release and enhance the probability of post-synaptic neuron firing of the quantum spin-entangled neurons (Fig. 39d). This is one example of a well thought out multi-step quantum brain mechanism. Yet it remains to be experimentally demonstrated at any of the abovementioned steps.

7.13 Conclusions in Relation to Sect. 7

- We submit that consciousness states are, at least partly, received from the superfluid quantum space/zero-point energy field and the information flux is likely

bidirectional (back reaction). Consequently, a field-type of cosmic connectivity is attained, necessary for global synchronization in the brain and of the brain with the cosmos.

- The fractal water compartments in the brain function as superconductive antennas for the ZPE/superfluid quantum space wave information [58]. This aspect extends to interstitial spaces and non-neuronal cell types, in which spiral Ca^{2+} wave fluxes, that mediate multiple bio-information mechanisms in the brain, play a crucial role.
- For wave information transfer in the brain, one needs two separate mechanisms operating in brain water: the intermolecular jump of hydrated protons (Grot-thuss mechanism) for superconductive states as well as a different mechanism of wave/particle diffusion. The latter propagation process in the whole brain is facilitated by quasiparticle formation of solitons (rotating electrons or protons that become dressed with phonons/photons). Hydrated protons have been shown to be quasiparticles with solitonic solutions.
- It could be shown that mass-energy and dynamics of movements of protons exhibit a quantum wave character that obeys the non-linear Schrödinger wave equation. Since the Klein–Gordon mass-energy equation, as a starting point (Fig. 3), has a dual solution including negative mass/energy, by which anti-particles may travel from future to past, allowing the reversed flow of time and retro-causality. This aspect may explain some known Psi phenomena as earlier discussed in Sect. 5.7.
- The solitonic solutions implicitly introduce the aspect of vortex-like rotation and toroidal geometry of energy trajectories (Fig. 9). Rotatory mediated toroidal flux is likely important for information integration and error correction of various forms of wave energies.
- Holographic memory storage and retrieval can be understood from a 4-D situated event horizon workspace that is associated with the brain but not reducible to it (Fig. 15). The cerebrospinal and interstitial water compartments are equipped with, and sensitive to internally generated and also external resonating solitonic excitations. In conscious states in the brain and the entire cosmos, resonating wave activities can function as the communication conduit between zero-point superfluid space and modalities of life organisms.
- Current observations on the relative intelligence of hydrocephalic patients, life panorama aspects of NDE experiences, and pre-cognition PSI phenomena (see Sects. 5.7 and 5.8) can be better understood through the present superfluid and superconduction model.

8 Comparison of the Present Model with Other Current Models of Consciousness

Definition of our hypothetical model

Graded states of consciousness in the universe (dream states/primary awareness/(sub)-conscious states/transpersonal experience/universal consciousness) are

scale-invariant and are guided by a pattern of semi-harmonic quantum waves (meta-language of the GM-scale principle). The latter originates from a superfluid quantum space/zero-point energy field (SFQS/ZPEF), creating pilot wave-induced resonance and cosmic connectivity. The steering of life processes is realized through semi-harmonic tuning of fractally structured water, in a dynamic relation with vibrating macro-molecules, such as hydrated proteins and DNA, in several cell types of the human brain and in its aqueous compartments. Conscious states arise through solitonic communication with a field-receptive, workspace, that is associated but not reducible to the brain. It implies a holographic memory workspace (“event horizon”), that supervenes brain function and is organized according to toroidal geometry. Collective pilot waves, including their backreaction lead to a conformal cosmic information field, representing the mental attribute of reality also expressed in human individuals.

In which aspects does our present model differ from earlier proposed concepts on consciousness and its supposed neural correlates?

Global workspace models

These models are often inspired by “Global workspace theories” of Baars et al. [398], Dehaene et al. [161] and Dehaene et al. [486], Table 2, left column. The various postulated concepts cannot be treated in detail here (see Seth 2007, for a short but an adequate review). Interestingly, many of these models are also based on an *internal self-model* in the framework of a supposed global workspace. In the latter models the unresolved problem of instantaneous binding of distant brain nuclei, in relation to our *integral* observation and sensing of our world, is approached by assuming multiple “broadcasting” hot spots in the neural networks of the brain, that according to the present authors may communicate via resonance of standing waves, phase coupling or even in a spiral (toroidal) mode. Some even consider the integrating activity of this broadcasting of information as the very process of realization of consciousness [398, 486, 487], in which *consciousness is just brain-wide sharing of information* that is in the global workspace.

However, some aspects remain to be established: what is the physical mechanism behind this supposed broadcasting phenomenon (multi-synaptic, electromagnetic, holographic, or (bio)photonic), in what form is the particular information sent and also how is the received information in the cortex integrated to conscious moments with meaning? In the present work, we propose that such a complex phenomenon requires an information-integrating, workspace, in which the broadcasted information can be put into the context of the entire memory content of the organism. Dehaene et al. [161] assume two types of information processing: a selection of information for “global broadcasting”, sharing it across modules, and holding it over time, in order to make it available for computing and reporting. In addition, he assumes a self-monitoring of this information in relation to reflexive aspects and error correction as a *sort of meta-cognition*. Prefrontal cortex neuronal circuits or even parallel circuits that are operating on the same sensory data are supposed to entertain error correction and differentiation between self-generated versus externally driven representations.

Yet we question, if such synaptic mechanisms are rapid enough or, *alternatively*, that phonon/photon/soliton-mediated communication should also play a role. This should also account for potential extra-sensory information such as NDE, blindsight and inter-personal data sharing is integrated into this concept (see Sect. 5.7). It has been argued by Rizvi [488] and many others, that synaptic transmission and axonal transfer of nerve impulses are too slow to organize a coordinated activity in large areas of the central nervous system. The duration of a synaptic transmission is at least 0.5 ms, thus the transmission across thousands of synapses takes about hundreds or even thousands of milliseconds. The transmission speed of action potentials varies between 0.5 m/s and 120 m/s along an axon. More than 50% of the nerve fibers in the corpus callosum are without myelin, thus their speed is reduced to 0.5 m/s. How can these low velocities (i.e., classical neurophysiological signals) explain the fast processing in the nervous system?

A more meta-cognitive form of consciousness rather will contain a graded modality of hierarchically as well as referential ordered and bodily determined working structure, which is essential for fully coordinated action, and was earlier called “individuated information utilized in action” [653]. Interestingly, such a conscious state space (Bekovich-Ohana and Glicksohn 2014), [490], was modeled by a geometry of two concentric spheres (not unlike our torus model), representing a phenomenological space with three dimensions: time, awareness and emotion.

As mentioned above, we tentatively add to this configuration a fourth space-time dimension (Sect. 5.3), in relation to self-consciousness in continuous contact with an extended consciousness or awareness continuum that is defined by us and many others as *universal consciousness*. The latter aspect rejects the usual framing of a mental workspace as a dualistic concept, since we envision our proposal of the extended brain as being *derived* from universal consciousness, as the very source of all that exists [2, 5, 6]. In a similar manner, we previously treated life as originated and thereby *extended* from the quantum vacuum from its substance, behavior, and laws.

Multi-dimensional models. Our model is, at least to some extent, related to earlier proposed quantum/spacetime models of Pribram [491] and Mitchell and Staretz [492], on the holonomic brain, as well as to the electromagnetic field brain theories of McFadden [238] and Pockett [239]. It also bears some resemblance to the orchestrated objective quantum reduction model of Hameroff and Penrose [408, 441, 442], the TGD universe framework of Pitkänen [318], and relates to the so-called dissipative information brain model of Vitiello [113], (see Table 2, right column), as previously reviewed by Meijer and Raggett [165].

An interesting series of studies was reported by Irwin et al. (2016) and [345, 493, 494, 495, 496], in which consciousness is approached according to a quasi-crystalline quantized language of primitive units, representing mathematical operators that also bear geometric features. Reality is conceived as composed of pixels of change (time) and length (space) on the Planck scale, processed according to an underlying algorithm that acts as a conscious operator, instrumental in the actualization of potential information into physical information as if it “observes” reality into existence. A similar mechanism was recently described in a paper on a generalized interpretation

of quantum physics on the basis of resolution of quantum indeterminacy, emerging from an integral and simultaneous change of physical relationships at the Planck scale [497].

The quasi-crystalline symbolic code is supposed to be related to shape number theory of 3D-simplex integers converted into 4D forming supercluster-cells in which nature accomplishes the dual task of creating new information and in turn, transferring (processing) such information further. The 3-simplex code resembles that of the building blocks of the universe in the, so-called, causal tri-angulation program of Loll et al. [498], in an attempt to build the universe from “scratch”.

According to Irwin [496], the universe, as a whole, operates similar to a non-deterministic neural network that allows binary choices and thus free will. All this implies that the aspect of quantum observation and measurement is intrinsic on the micro-scale level as a sort of gravity code acting as a “quantum viewer”. The authors stipulate the central role of the golden ratio and recursive fractal patterns as well as toroidal cycling in the generation of an *information-theoretic universe*. This dynamical pattern should also be expressed in the semi-harmonic energy signature of elementary particles as indeed confirmed by us before [54–57]. The scale-invariant, self-organized recursive modality of the cosmos would even enable a self-stimulation (creation) of the universe, that is if error correction and retrocausality aspects would be included [495]. In such a process a strange loop-like flux of information from the future results in a nested hierarchy of thoughts or a musical symphony in which the universe becomes the mind itself after a long run-time and our human experience of linear time should, therefore, be conceived as an illusion.

Implicitly, a major difference with the abovementioned models is that it is not solely related to the known neuronal/astroglial based central neural system, but that *an additional* modality of an associated mental workspace in a 4-D context is introduced [244, 245, 289, 499]. This workspace mirrors our total of experiences and is sensitive to relevant information derived from various force fields of nature such as geomagnetism, gravity, Higgs field, as well as zero-point and dark energy. We presume, as stated before, that it also comprises an even larger connecting principle in the sense of *universal consciousness*, as it is inferred by some of us [4]. In this sense, our model supports that of Haramein and Rauscher [188, 500], (dual toroidal/wormhole geometry in physics and cosmology), as well as the model of Hameroff and Penrose [408, 441, 442]. The latter addressed quantum gravity mediated communication with information on the Planck scale. The holonomic models mentioned in Table 2, of Pribram [491], Mitchell and Staretz [492], and Amoroso [501], largely stimulated our present concept. Reports on the crucial role of consciousness in the proper functioning of the brain were emphasized by Darmos [201], and on the unitary relation of brain and cosmos from an energetic point of view by Persinger and St-Pierre [223], both supported our ideas on the extended brain in relation to the whole universe.

Of particular interest are the studies of Atasoy et al. [502, 503], which revealed a distinct presence of harmonic brain waves as related to the connectome. The researchers used data from two imaging techniques—magnetic resonance imaging (MRI) and diffusion tensor imaging (DTI)—to create three-dimensional maps of the structure of the brains of a group of individuals. The MRI-data yielded the structure

of the cortex and the DTI yielded an anatomical map of the underlying connections of the white matter in the brain. The team then analyzed these brain maps using the mathematical framework of Laplace Eigenmodes, or harmonic waves, which describe natural vibrations of a system where all parts move together at the same frequency. See for this aspect also the adequate paper of Joye [504]. Thereby, they could ask the question: how these harmonic patterns, or connectome harmonics, actually *make up* the fMRI data. The collective data indicate that a new language emerged to describe both the spatial and temporal elements of neural activity. Namely, the patterns tell which regions should be synchronized with each other at a particular frequency, and allow them to characterize the fMRI data as a combination of these patterns.

Atasoy et al. (2015), interestingly, suggest a *musical analogy*, since the patterns can be compared to musical notes composing a complex musical piece, very much in line with the present paper (Sect. 5.9), indicating that functional networks of the human brain are probably predicted by semi-harmonic patterns, ubiquitous throughout nature. Therefore, the model of Atasoy about human brain networks may have a direct relation with the proposed GM-scale: both models make use of eigenfrequencies, coherent behavior, connected harmonic patterns, overlap between different state networks, harmonics corresponding to different frequencies (wavenumbers) and based upon a general physical principle of self-organization. This aspect is very much in line with the studies of Deli [505] and Deli et al. [475], describing the syntactic coding for projecting information between brain structures through oscillating rhythms of standing waves. This pattern produces a holographic mental landscape that obtains cosmic features of toroidal information processing in a “black hole/white hole” type of memory conservation. Deli et al. [475], in a follow-up study, see these oscillations operating through the interplay of short and fast brain frequency timescales that determine the direction of information flow and taking the form of standing sound-waves that exhibit harmonic musical features. These could even be seen as a form of nerve pulse propagation through the solitonic sound waves as described by Andersen et al. [506], that can travel without loss of energy and can provide repetitive patterns of movements, thoughts or memories.

Atasoy et al. [502], in this respect, refer to the classical Chladny vibration patterns that were re-calculated earlier by us [52, 60], showing a perfect fit with the frequencies of the GM-scale. The introduced framework of harmonic brain modes, therefore, not only establishes a relation between the spatial structure of correlation patterns and temporal oscillations (linking space and time in brain dynamics) but also enables a new dimension of tools for understanding fundamental principles underlying brain dynamics in different states of consciousness. Atasoy et al. [170], see Fig. 40), more recently examined the minds of 12 people treated with placebo or on LSD, and listening to music. They recorded their brain activity through the lens of the brain’s underlying connectome harmonics. What they found was that under the influence of LSD, more of these harmonics were contributing to brain activity and their strength of activation was also increased. The brain was essentially activating more of its harmonics simultaneously and in new combinations. Apart from combinations of harmonic EMF *frequencies* also the aspect of *wave amplitudes* should be taken into consideration. Kraikivsky [507], postulated the importance of the amplitude of

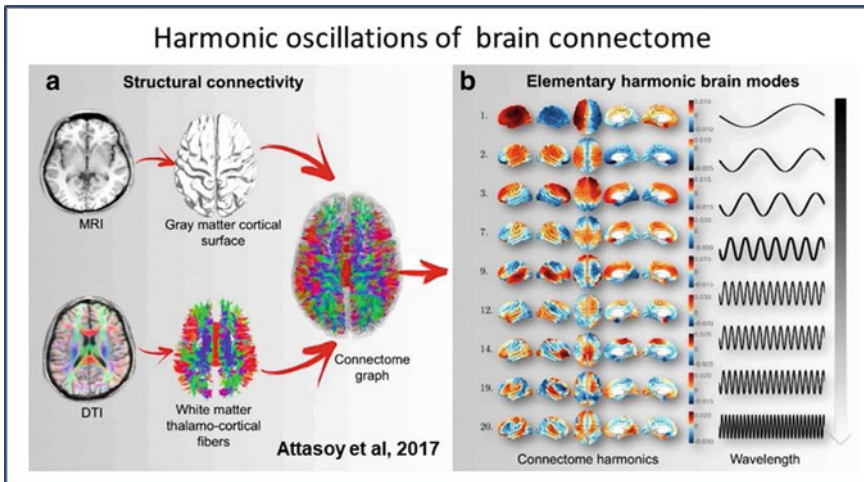


Fig. 40 **a** Structural connectivity of the human brain defined as the combination of local cortical, gray matter connections. **b** Elementary harmonic brain modes defined as fully synchronous patterns of neural activity are estimated as the harmonic modes of structural connectivity; i.e., connectome harmonics (after [170])

coupled oscillators for the creation of conscious percepts. Interestingly, the author postulates the functionality of an *operational map isomorphic to a distance matrix with space-like properties* that would serve as a timeless linking (integrating) unit, allowing a rapid selection of a repertoire of functional states, encoded in amplitude patterns of oscillatory processes.

This, very much, resembles the concept of a guiding/supervening holographic memory workspace as envisioned in the present study. The latter is also true for the Fractal-like Information Integration Theory of Bandyopadhyay [470] as discussed in Sect. 5.9, although we prefer the use of nested toroidal geometry for describing self-referential information flow and also added the aspect of an extra 4-D spatial dimension to arrive at a cosmic mental workspace concept by which we integrated mind/matter aspects in the consciousness framework.

It is striking indeed that many related and recent studies on consciousness contain the suggestion that a supervening memory workspace is required to understand an integral operation of the brain on the brink of chaos, as a sort of quality controlling and updating system. Such ideas take quite different forms but, at least partly, support our present concept (see Table 3). This is certainly true for the very elegant consciousness model of Fingelkurt et al. [508], Fingelkurt, and Fingelkurt [509], called nested operational architectonics of the brain. In this model, it was postulated that an electromagnetic brain field [510], for a fractal representation) connects a mind-subjective space-time to a distant physical space-time. Meta-cognitive aspects of consciousness on the basis of current physics and cosmology were also proposed by Pereira et al. [511], postulating a matrix of reality being an N-dimensional combinatorial state space of eternal self-organizing elementary energy forms. This is seen as the ground

Table 3 Literature compatible with and/or supporting the present memory space supervening brain model concept

Scientific subject	Author(s)	Congruent aspect
Global workspace model	Baars/Dehaene	Long dist. broadcasting commun. brain
Information integration theory	Tononi/Koch	Information core concept
Orchestrated objective. Red. theory	Hameroff/Penrose	Q-coherent oscillatory tubular proteins
Projective mind hypothesis	Williford et al.	Virtual projective integrate brain
Toroidal brain hypothesis	Tozzi and Peters	4D-Toroidal brain inform. domain
Human connectome and harmonic brain modes	Atasoy et al.	Harmonic frequency modes in brain
Glutamate-induced biophotonics in neural circuits	Tang et al.	Physics of biophotonic brain comm.
Biophotonics redshift activity in brain	Wang et al.	Biophotons higher brain functions
Fractal Information geometric musical theory	Bandyopadhyay et al.	Fractal musical brain language
Operational Architectonics theory	Fingelkerts et al.	Operation of a mental brain domain
The consciousness and cosmos framework	Pereira et al.	Universal field of consciousness
Intuition as a holographic phenomenon of	Bradley	Intuition from holographic memory
Spin-mediated consciousness	Hu and Wu	Spin as mind-pixel in consciousness
Water as conduit in cosmic entanglement	Carniello et al.	Universal role of H ₂ O in cosmol. order
Qualia: interaction with proto-Consciousness	Tressoldi et al.	Proto-consciousness domain
The Pribram-Bohm Holoflux theory of consciousness	Joye	Holofield theory and implicate order
Brain and neg-entropic entanglement	Poznanski	Consc. guiding encoded in ZPE field
Genomic consciousness in neurons	Cacha/Poznanski	Solitonic interactions with DNA
Physical bases to consciousness	Persinger/St- Pierre	Unified, non-local cosmic brain energy
Quantum gravity and role of consciousness	Darmos	Role of consciousness in physics
Two-brain hypothesis	Goodman et al.	Electro-ionic/electromagnetic brain

(continued)

Table 3 (continued)

Scientific subject	Author(s)	Congruent aspect
Nonsynaptic model of longterm memory	Cacha et al.	Engrams as phys. waves in interfacial water
Quantum physics of synaptic transmission	Georgiev et al.	Q. tunneling in neurotransm. release
Systems of oscillators for conscious percepts	Kraikivski	Distant space-time matrix as operational. map
Holoinformational model of consciousness	Di Base	Superimpose order in organizing Mind
Nature of mind and consciousness	Greyson	Is consciousness only produced by the Brain?
Integral relativity of awareness	Neal	Role of photon/phonon symphonic resonance.
DNA resonance code as neural code	Savelyev et al.	Proton oscillations in DNA morphogenic Field

of reality as a universal field, potentially encompassing all possible manifestations, either material or mental, connected via a transitional zone to a manifest world with its informational and qualia endowed aspects.

Poznanski et al. [512, 513] present a related theory in which brain consciousness is guided by hidden dynamics of dipole associated electrons, modeled by ZPE field/de Broglie/Bohm type of active information of oscillating waves, as touched upon in our studies. The same group emphasized the importance of biophotonic/electromagnetic information transfer [399, 514] and in relation to this suggested the concept of a “Two-brain hypothesis”: one brain with an electro-ionic character and a simultaneously acting electromagnetic brain [401].

These aspects of the theory are in striking agreement with the present model. Both the aspects of macro-quantum equation and error correction, on the basis of negentropic entanglement, are mentioned but lack the toroidal geometrics and the essential photon/phonon/soliton coupling of electrons as an optical guiding mechanism. We hold that a total acoustic semi-harmonic scaling of frequency patterns should be included, describing a balance of *coherent* but also *decoherent* modes, in order to construct the long-range order of phase synchrony in the consciousness code (see Sect. 3).

Further congruence with our model is noted from the studies of Tressoldi et al. [515], who conceive consciousness as emergence of qualia through an interaction with a *supposed non-local proto-consciousness or proto-mind*, acting as an interpreter and decision-maker, constantly redescribing its own activity enriched with the emotional value. A projective consciousness model was hypothesized by Williford et al. [516] that combines a projective geometrical model of a perspectival phenomenological structure of the field of consciousness with a free energy minimization model of interference. This process acts as a *4-D projective transformation*, that is instrumental in the integration of perception, emotion, and memory as well

as in reasoning and imagination, in order to control behavior as well as to optimize resilience and preference satisfaction. Irwin [345], postulated that a first principles theory of everything has yet to be achieved but that a derived code of quantized spacetime should meet the following suggested requirements:

- (1) First principles explanation of time dilation, inertia, the magnitude of the Planck constant and the speed of light.
- (2) First principles explanation of conservation laws and gauge transformation symmetry.
- (3) Must be fundamentally relativistic with nothing that is invariant being absolute.
- (4) Pursuant to the deduction that reality is fundamentally information-theoretic, all information must be generated by observation/measurement at the simplest Planck scale of the code/language.
- (5) Must be non-deterministic.
- (6) Must be computationally efficient.
- (7) Must be a code describing “jagged” (quantized) waveform, a waveform language.
- (8) Must have a first principles explanation for preferred chirality in nature.

The particular projective space proposed is virtual and outside our 3-D space as an extra parametric dimension active in creating a world model for the sake of selfhood, as a viewer or transcendental ego (our double or daemon unveiled) that provides a global availability and multi-modal information integration. This resembles the cosmological approach of Pletcher [517], that pictures consciousness as an interactive process of polarizing an observed source of a *higher-dimensional* ($4 + 1$) space on to a cognitively modeled collapsed ($3 + 1$) space. All this supports our concept of the requirement of a reflexive 4-D workspace in a superfluid quantum space with rotatory geometry. Of note, [518, 280], rightfully stated that the ultimate scientific challenge lies to produce experimental evidence for the two-way interaction between the conscious mind field (also called the stored mental map in a cognitive space) and the physical brain, as attempted in the present study.

Aspects of the quantum holographic theory were also applied by Bradley [519] and Di Biase [520], in relation to an intuitive perception of the future, based on interaction with non-local information through unfolding and harmonic resonance. This phenomenon, according to the authors, is not restricted solely to the brain but works also via information input in the cardiac system in the form of quanta of energy. These may arise from zero-point energy guiding that can overlap with the future (most probable potentials in the implicate order domain) and can lead to intuition, synchronicity, clairvoyance, and telepathy (see also Sect. 5.7).

The importance of a new scientific framework for the (re)-union of science and spirituality, was treated by the physicist Faggin [521], (the designer of Intel’s first microprocessor), arguing that death is not final but rather necessary to dissolve the identification of consciousness with the body, freeing it to recognize its own true nature. The latter aspect was also treated in a very recent paper of the first author [2, 287].

Conclusions of Sect. 8

(Self)-Consciousness is generally considered to arise from the brain's thalamocortical recurrent neuronal activity. Yet, we hold that consciousness is at least partly *received* from a qualia space (superfluid quantum space/ZPE information field) to a sub-Planckian space-less and timeless dimension, bearing geometric patterns with mathematical relations [432]. Communication from these fields takes place with photons/phonons/solitons through a holoflux of active information (as described by [522]). This guiding process, in the brain, is, among other factors, mediated through its water compartments (cerebrospinal, interstitial, and intracellular spaces) in the form of freely moving protons, creating a superconducting medium. Hydrated protons are converted to and serve as antennas for electrons covered with phonons (phonon-dressed electrons or solitons) that exercise shaping effects on proteins and organelles. This can occur with the help of structured water, in which the information from the aforementioned fields is mirrored in fractal frequency wave patterns. This life in-formation is not only stored by interaction with proteins and DNA but also, holographically, in a memory sphere (event horizon) around each cell that can be physically imagined in the vicinity of the plasma membrane with its complex array of intrinsic proteins and aqueous layers [61]. All this takes place in a fractal-like manner in the cell at the micro-level (down to the level of elementary particles) as well as at the macro level. This implies entangled conditions in the whole brain and in the entire organism with its various organs and connective systems.

This concept is in line with the holofractal and semi-harmonic vibrations proposed by us that, as earlier mentioned, have been demonstrated in the brain by Atasoy et al., [170, 502], with scanning techniques, and also showed by Tozzi et al. [252, 253, 523] as a holographic domain that operates from a 4th spatial dimension, projecting into our 3D world. Both the *semi-harmonic* character of the EMF frequency pattern and the here proposed superfluid state, indicate vortex dynamics and toroidal geometry. Ca²⁺ ions and their transmembrane gradients, as quantum information carriers, are envisioned by us as playing a crucial role in the cells and the integration of neuronal activity in various parts of the brain. Their quantum state is protected against the environment (decoherence) by being partially being enclosed in water gels or confinement within shielded Ca-channel proteins. Ca²⁺ ions influence a spectrum of biochemical and biophysical processes in the brain (Fig. 38) and, partly, by astroglial fluxes promote cerebral binding and synchronicity of brain activity [479]. These, have been related to EEG signals with typical alpha-, beta-, gamma- and delta-frequency ranges. Therefore, water is seen as very central as a superconducting and phonon-antenna containing matrix that drives the balance of coherence/decoherence of wave information to the left.

The consciousness theory of Atasoy et al. [502], was confirmed by brain scanning in the abovementioned studies and is supported by the fact that certain hydrocephalic patients and other conditions with greatly reduced neuronal brain tissue may have an unexpected level of consciousness and intelligence (see also Greyson [524], Sect. 5.8). We, therefore, present the concept of a *non-material, field-receptive,*

resonant, mental workspace that is part of a *universal* mechanism of rotational information flow. This may represent an Idealist ontology, placing Universal Consciousness (UC) as a central factor at the origin of life and in the conscious experience of biological beings. Yet we emphasize that the UC concept that we submit is, for the first time, physically defined in relation to a superfluid quantum space and moreover we propose a plausible mechanism for its communication with the brain through hydronium superconductivity and resonance in brain water.

Of note, the present authors hold that Darwinism provided a very prominent view on biological evolution, yet with regard to cosmic evolution should be completed with reference to universal consciousness as a guiding principle. In particular, we confirm the importance of Darwin's approach in offering insight in the selection of information for problem-solving, aimed at evolutionary survival, but state that the theory falls short in addressing the gap between physics and meaning. Rather, a partially directed evolution is envisioned (Sect. 6.4), through the involvement of apriory information and harmonically directed guidance of first life. As to the latter respect, we postulate that following the emergence of first life, guided coherency as well as quantum downward (top-down) causation also played a crucial role in later stages of evolution involving the higher cellular and species complexity.

Testability The present GM-EMF frequency scale concept is experimentally based, since it evolved from meta-analyses of more than 1000, mostly peer-reviewed, articles, consistently showing the particular frequency band pattern in a variety of disciplines such as biomedical/biophysical studies, quantum entanglement studies, the energy distribution of elementary particles, superconductor studies, clay material EMF properties and water absorption frequencies (see Table 1).

Our consciousness hypothesis can further be experimentally tested by exposing various types of brain tissues *in vitro* or *in vivo* to externally applied combinations of discrete EMF frequencies and/or selective shielding of such external EMF radiation modalities. This, through the use of advanced radiation technologies and/or specific EMF frequency modulating materials and probing of responses of the electric activity or performing scanning of tissue slices or whole brain with various high-tech methods. The more transcendental aspects could be tested in further detailed analyses of a spectrum of known subjective experiences under the influence of discrete musical frequency bands and their combinations.

9 The Construction of Reality: An Integral Model

From the abovementioned phenomena, it is obvious that a “final theory” in physics in the future, should describe *both* the *material* and *mental* aspects of reality and consequently must integrate a testable model of consciousness and self-consciousness. Such a comprehensive model of the whole should also be based on a solid mathematical and geometric framework and be compatible with a *completed theory of*

quantum mechanics. It should thus include an integral description of the cosmos at the micro- and macro-scale. The hypothesis that gravitational integration and compression leads to a universal memory space of which individual human self-consciousness is a discrete part should be further investigated (see for more information on this aspect [154, 525]).

The present hypothesis on brain function, may for some readers imply that a part of our memory is *localized externally from our organism* (non-neuronal and even non-material). However, it should be realized that the present authors situate this mental workspace in an extra (fourth) spatial dimension, which is not visible to humans, so that differentiation between extra- and intra-neuronal is trivial, while the supposed mental modality is, in fact, quantum physically defined. In addition, in the present work, we emphasize that aqueous compartments inside and surrounding the brain neuronal tissues may play a much more central role in the creation of (self)-consciousness than traditionally thought. We hold that these cerebrospinal and interstitial water compartments can function as an important part of dedicated antenna domains for receiving external and internally produced EMF signals.

We stipulate that the information dissipating brain, as earlier described [113] may create our integral and universal memory, coined by the latter author as “*our double unveiled*”. Consequently, as mentioned above, we consider our concept to be compatible not only with present neurological concepts but also with trans-personal observations such as the unexpected brain to brain connections as recently experimentally demonstrated by Hasson et al. [338], Wackermann et al. [343], Radin [340], Richards et al. [341], Standish et al. [342], as well as Pizzi et al. [339]. In a similar vein, we should take into account the many cases of personal life panorama’s reported in stunning detail by the many registered near-death cases (for a critical discussion on the latter item [526], in which astounding transpersonal information states of consciousness states are experienced in the absence of neuronal processing and fluxes of information in brain cortex [287]).

In the light of the superb treatment by McGillchrist [527] of the very different features of and crosstalk between right and left-brain hemispheres, as well as its socio-psychological implications, one should ask how this very crosstalk is organized, and what determines its outcome, memory storage and retrieval. A personal supervening and integrating memory workspace, that, among others, is mirrored in the water compartments inside and surrounding the brain, as postulated in the present paper, could be envisioned as a “third hemisphere” in a 4D context, that earlier was framed as our “Double” and long ago by Greek philosophers as our “Daemon”.

It is shown in the present paper that the consciousness aspect of bottom-up panpsychism can be reconciled with the “top-down aspect” of a retro-causally driven guiding field of thoughts and qualia (see a stimulating discussion on that in Kastrup [7]). We submit that this occurs due to their physical relation, being a two-way recurrent information flux that can be modeled by the self-referential toroidal geometry, in which consciousness returns to itself in an everlasting dynamic mode. Nature thus seems to unfold itself through the operation of natural laws within a matrix of semi-harmonic relations, as guided by a *musical master code*, creating an overwhelming symphony that we experience as a vivid dream of a concealed reality. Humans, in this respect,

are not only observers but also active participants in this cosmic endeavor: the evolution of conscious entities has been woven into the cosmic code from the beginning. We hold that *the ZPE/SFQS domain is instrumental in these events and that we may, for the first time, have identified, at least a part, of its EMF frequencies*.

These resonance patterns may also represent a pilot wave aspect of the “hidden” implicate order as proposed long ago by Bohm and De Broglie. In this sense we also touched upon, what is called, the “Hard Problem” of consciousness studies of Chalmers [13], since our model, apart from the aspects of Chalmer’s (relatively) “Easy problem” of neurological/behavior correlations, the present study also treats the “Hard problem” aspect, through its considerations on mind/matter relations and the potential origin of qualia. The present model also highlights the basic notions of top-down causation and potential retrocausal quantum influences on life processes. The main thesis of this chapter on the nature of space, time, and consciousness is that in science and philosophy the dominant paradigm of materialism should be considered as incomplete for explaining the whole of reality. This, in spite of the recent claim that “consciousness is a state of matter” [260]. For this peculiar concept, Tegmark did make a special invention: that of a supposed “perceptronium”, being a hypothetical *substance* that *feels* subjectively *self-aware* and stores and processes information……, and, ultimately, may turn out as Tegmark’s own “discovery of mind”.

In various parts of the review, we refer to *primordial or apriory information, as well as partially directed evolution*, so what is meant here? We hold that the architecture of reality is so astoundingly complex, and at the same time seems so fine-tuned in all of its physical relations that it is highly unlikely that the universe started from zero information. Although the Anthropic principle lacks explanatory power and even can be seen as some biased pre-selection of data, its very content of discrete natural constants combined with the macro-cosmic features, of the planet we happen to live on, is undeniable. We believe that often heard multiverse arguments that are used to explain the anthropic context away, are speculative since this constellation is unproven and, even worse, untestable. Scientifically acceptable hypotheses that presume potential primordial information are the theories of Steinhardt and Turok [528] and, independently, that of Penrose [529], on the circular character of our universe, framed in cosmology as the rebound Universe (see Fig. 41). In this vein, our present universe may be viewed upon as a previous modality of the present one, in which at least some information was preserved as a recipe for its evolution. The latter can also be seen as an unfolding of information in the Bohmian context, in addition to the “it from a bit” context in the participatory universe of John Wheeler [164].

An intriguing hypothesis for the relationship between the mind and the brain was put forward by Kastrup [6–8] which seems entirely consistent with current neuroscience data and increasingly supported by the latest scientific evidence. The author deserves credit for highlighting the crucial aspect of *Idealism* again in science philosophy (see for a splendid dialogue with some renowned materialists [306]). The particular hypothesis explains not only why brain states are, ordinarily, tightly correlated to mind states, but also how, under extraordinary conditions, subjective

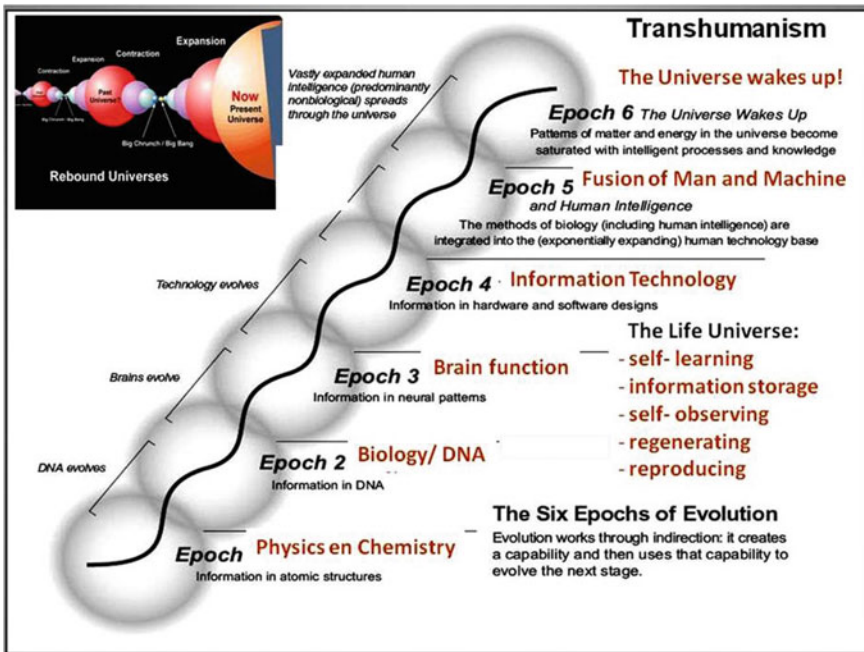


Fig. 41 The sequential epochs in the evolution of our universe (modified after [530]), depicting the present and future evolution of a “living” Universe (see text on its features in the middle). A cyclic (rebound) universe model (top left) in which the present universe is reborn through operating in a cyclic mode [528, 529] is shown

experience can occur in the absence of brain function. The theory offers a rational, evidence-based, yet fundamentally different perspective on the nature of consciousness, life, identity, and death than that offered by materialism. As mentioned above [13, 531], asked how can something immaterial like subjective experience and self-consciousness arise from a material brain? Yet, we may rephrase this question: if consciousness is indeed the most fundamental aspect of reality [19, 21, 532, 533], we may wonder how consciousness can be instrumental in the manifestation of matter. The, so-called, panpsychism (every material object contains specific information), at first sight, maybe a logical solution to Chalmers question, as put forward, for example, in the information integration concept of Tononi and Koch [534], Tononi et al. [15]. Yet the latter may rather be seen as a reductionist approach in the line of current materialistic physics since one fails to envision the issue from the point of view of consciousness as *primary* [5, 6, 7, 8, 224, 181, 182, 183, 535, 536].

Finally, Schwarz [404], in a lucid report postulated: “In mind/body research particularly, the issue of consciousness has attained a new prominence, as evidenced by the growing number of placebo studies, research on meditation, mindfulness and its effects on the brain, and its practical use in things like posttraumatic stress disorder (PTSD); studies on the role of psychophysical self-regulation in healing; This

includes prospective research on near-death experiences (NDE); studies suggesting the reality of reincarnation and immortality [2, 287] as well as research into the relationship of genius and spirituality". In his thesis on the beginning and end of our Universe, [537] stated: "But how can we imagine to seriously care for such an issue as cosmological immortality? We can summarize five steps towards it. The first is to realize that your individual death is normal and inevitable in the long term. The second is to develop psychologically and fulfill all your needs to grow the hierarchy of needs up to the need for self-transcendence. You then surpass yourself to become compassionate and identify with the process of cosmic evolution. Even if you accept individual death, you still refuse death as a whole, namely the idea that nothing would continue to evolve after the predictable death of your body, society, species, Sun, galaxy, and universe. You then set the immortality of the evolutionary process as a goal".

Here our journey into deeper levels of the fabric of reality ends, at least for now, yet we will remember the wide vistas and beautiful horizons exposed to our exploring eyes: will we ever oversee the splendid integral landscape so secretly hidden from us by nature?

The late John Wheeler (revisited by the first author [164]), expressed all this with his famous prophecy of hope:

Someday we'll understand the whole thing as one single marvelous vision, that will seem so overwhelmingly simple and beautiful that we may say to each other: 'Oh, how could we have been so stupid for so long? How could it have been otherwise!'

Acknowledgements We are largely indebted to Ir. Hans Geesink, who through his consistent meta-analysis of the literature from a spectrum of disciplines in the past 5 years, provided the very basis for revealing the generalized musical (GM)-EMF-frequency scale as treated in the present chapter.

We are grateful for all the work of Dr. Trudi Sonderkamp as to detailed text control and professional suggestions for improvement of the manuscript.

We thank Marshall Lefferts for elegantly placing our concepts in a cosmometric context in his book on Cosmometry, A Unified Model of Cosmic Geometry, Physics, Music, and Consciousness.

References

1. Meijer DKF, Geesink JH (2017) Consciousness in the Universe is scale invariant and implies the event horizon of the human brain. NeuroQuantology 15:41–79 https://www.researchgate.net/publication/320267484_Consciousness_in_the_Universe_is_Scale_Invariant_and_Implies_an_Event_Horizon_of_the_Human_Brain
2. Meijer DKF (2019a) Universal consciousness. Collective evidence on the basis of current physics and philosophy of mind. ResearchGate. https://www.researchgate.net/publication/328538224_Universal_Consciousness_Collective_Evidence_on_the_Basis_of_Current_Physics_and_Philosophy_of_Mind_Part_1
3. Meijer DKF, Geesink JH (2019b) Life and consciousness are guided by a semi-harmonic EM background field. NeuroQuantology 17(Issue 4):37–44. <https://www.neuroquantology.com/index.php/journal/article/view/2074>

4. Meijer DKF (2018) Processes of science and art modeled as a holoflux of information using toroidal geometry. *Open J Philos* 8:365–400. https://pdfs.semanticscholar.org/cddd/d1975ad29ee4cbbe653a933f204f5120f640.pdf?_ga=2.106736387.1244523350.1576662063-1419431810.1574855531, <https://doi.org/10.4236/ojpp.2018.84026>
5. Goswami A (1990) Consciousness in quantum physics and the mind-body problem. *J Mind Behav* 11(1):75–96
6. Kastrup B (2018) The Universe in consciousness. *J Conscious Stud* 25:125–155
7. Kastrup B (2017a) There is an unconscious, but it may well be conscious. *Eur J Psychol* 1841–0413
8. Kastrup B (2017b) Making sense of the Mental Universe. *Pilos Cosmol* 19:33–49
9. Bohm D (1980) Wholeness and the implicate order. Routledge & Kegan Paul, London
10. Forshaw SD (2016) Memory of a universal mind. Galactic structures and their existence as cognitive operators in an emerging universally conscious machine. *Research Gate* 309209078
11. Forshaw SD (2016) The third state. Towards a quantum theory of consciousness. *NeuroQuantology* 14:49–61
12. Rovelli C (2016) Meaning = Information + Evolution. [arXiv:1611.02420v1](https://arxiv.org/abs/1611.02420v1) [physics.hist-ph]
13. Chalmers D (1995) Facing up to the problem of consciousness. *J Conscious Stud* 2(3):200–219. <http://consc.net/papers/facing.pdf>
14. Pereira A, Ricke H (2009) What I consciousness. Towards a preliminary definition. *J Conscious Stud* 28–45(16). https://www.researchgate.net/profile/Alfredo_Pereira_Junior/publication/233663656_What_is_Consciousness_Towards_a_Preliminary_Definition/links/0046352182781aa05700000/What-is-Consciousness-Towards-a-Preliminary-Definition.pdf
15. Tononi G, Boly M, Massimini M, Koch C (2016) Integrated information theory: from consciousness to its physical substrate. *Nat Rev Neurosci* 1–12
16. Churchland (1995) The engine of reason, the seat of the soul: a philosophical journey into the brain. MIT Press, Cambridge. ISBN 0262531429
17. Zeki S, Bartels A (1999) Toward a theory of visual consciousness. *Conscious Cogn* 8(2):225–259
18. Meijer DKF (2013) Information: what do you mean? *Syntropy J* 3:1–49. https://www.researchgate.net/publication/275017053_Information_What_Do_You_Mean
19. Meijer DKF (2012) The information universe. On the missing link in concepts on the architecture of reality. *Syntropy J* 1:1–64. https://www.researchgate.net/publication/275016944_Meijer_D_K_F_2012_The_Information_Universe_On_the_Missing_Link_in_Concepts_on_the_Architecture_of_Reality_Syntropy_Journal_1_pp_1-64
20. Barrow JD, Tipler FJ (1988) The anthropic cosmological principle. Oxford University Press
21. Davies PCW (2007) The implications of a cosmological information bound for complexity. *Quantum Inf Nat Phys Law*. <http://power.itp.ac.cn/~mli/pdavies.pdf>
22. Grandpierre A (2014) Biologically organized quantum vacuum and the cosmic origin of cellular life. In: Phenomenology of space and time book 1. The forces of the cosmos and the ontopoietic genesis of life. *Analecta Husserliana* 116:107–133
23. Grandpierre A et al (2013) Multidisciplinary approach to mind and consciousness. *NeuroQuantology* 11:607–617
24. Alfonso-Faus A (2011) Cosmology, holography, the brain and the quantumvacuum. <https://arxiv.org/ftp/arxiv/papers/1102/1102.0443.pdf>
25. Alfonso-Faus A (2013) Fundamental principle of information-to-energy conversion. <https://arxiv.org/ftp/arxiv/papers/1401/1401.6052.pdf>
26. Bérut AB, Arakelyan A, Petrosyan A, Ciliberto S, Dillenschneider R, Lutz E (2012) Experimental verification of Landauer's principle linking information and thermodynamics. *Nat Lett* 483:187–190
27. Toyabe S et al (2010) Experimental demonstration of information-to-energy conversion and validation of the generalized Jarzynski equality. *Lett Nat Phys* 1 Vol 6, December
28. Zizzi P (2006) Consciousness and logic in a quantum-computing universe. In: The emerging physics of consciousness. The frontiers collection. Springer, Berlin, pp 457–481, chapter 14, https://doi.org/10.1007/3-540-36723-3_14

29. Schrödinger (1967) What is life? Cambridge Press. Cambridge. https://archive.org/details/WhatIsLife_201708
30. Vannini A (2009) A syntropic model of consciousness. *Syntropy J* 1:109–169
31. Vannini A (2008) Quantum models of consciousness. *Quantum Biosyst* 1(2):165–184
32. Geesink HJ (2020) Informational code of biomolecules and its building blocks: quantum coherence versus decoherence, submitted to *Quantum Biosystems*
33. Geesink HJ, Jerman I, Meijer DKF (2019b) Water: the cradle of life in action, water in cells is guided by coherent quantum frequencies as revealed in pure water. In the press in *Water Journal*. https://www.researchgate.net/publication/331976119_Water_the_cradle_of_life_in_action_cellular_architecture_is_guided_by_coherent_quantum_frequencies_as_revealed_in_pure_water
34. Aharonov Y, Popescu S, Tollaksen J (2010) A time-symmetric formulation of quantum mechanics. *Phys Today* 27–32
35. Ellis GFR (2012) Top down causation and emergence: some comments on mechanisms. *J Roy Soc Interface Focus* 2:126–140
36. Boyle L, Finn K, Turok N (2018) CPT-symmetric universe. *Phys Rev Lett* 121:251301
37. Gaffney L, Butler P, Scheek M et al (2013) Studies of pear-shaped nuclei using accelerated radioactive beams. *Nature* 497:199–204. <https://doi.org/10.1038/nature12073>
38. Chang Y-F (2007) Negative matter, repulsion force, dark matter, phantom and theoretical test. <arXiv:0705.2908> [physics.gen-ph]
39. Cramer J (1988) An overview of the transactional interpretation. *Int J Theor Phys* 27:227
40. King CC (2003) Chaos, Quantum-transactions and Consciousness, *NeuroQuantology* 1(1):129–162
41. Wheeler JA, Feynman (1994) At home in the universe, New York Institute of Physics
42. Cramer J (2005) A farewell to copenhagen? *Analog*, December
43. Merali Z (2010). Back from the future, *Discover Magazine*, August 26, 2010
44. Wilczek F (2008) The lightness of being. Mass, ether, and the unification of forces. New York: Basic Books
45. De Loof A (2016) The cell's self-generated "electrome": the biophysical essence of the immaterial dimension of life? *Commun Integr Biol* 9(5):e1197446
46. Nelson E (1967) Dynamical theories of Brownian motion. Princeton University Press, Princeton
484. Griffin DR (1997). Parapsychology, philosophy, and spirituality: A postmodern exploration, (SUNY Series in Constructive Postmodern Thought), State University of New York Press
48. Skrbina D (2017) Panpsychism in the west MIT press Ltd ISBN13 9780262534062
49. Strawson G (2009) Mental reality (2nd ed.). Cambridge, MA: MIT Press. <http://dx.doi.org/10.7551/mitpress/9780262513104.001.0001bina>
50. Bohm DF, Hiley BJ (1993) The undivided universe. An ontological interpretation of quantum theory
51. Williams GR (2019) Quantum mechanics, metaphysics and Bohm's implicate order. *Mind Matter* 17:155–185
52. Geesink JH, Meijer DKF (2016a) Quantum wave information of life revealed: an algorithm for electromagnetic frequencies that create stability of biological order, with implications for brain function and consciousness. *NeuroQuantology* 14:106–125. file:///C:/Users/Dick/Documents/911-2447-1-PB.pdf
53. Geesink JH, Meijer DKF (2017) Electromagnetic frequency patterns that are crucial for health and disease reveal a generalized biophysical principle: the GM scale. *Quantum Biosys* 8:1–16. https://www.academia.edu/35199978/Electromagnetic_Frequency_Patterns_that_are_Crucial_for_Health_and_Disease_reveal_a_Generalized_Biophysical_Principle_the_GM_scale
54. Geesink JH, Meijer DKF (2018a) Evidence for a guiding principle in quantum physics. *Quantum Biosyst* 9:1–7. [http://www.quantumbiosystems.org/admin/files/QBS%209%20\(1\)%201-17%20\(2018\).pdf](http://www.quantumbiosystems.org/admin/files/QBS%209%20(1)%201-17%20(2018).pdf)

55. Geesink JH, Meijer DKF (2018b) A harmonic-like electromagnetic frequency pattern organizes non-local states and quantum entanglement in both EPR studies and life systems. *J Modern Phys* 9:898–924. https://www.academia.edu/36384076/A_SemiHarmonic_Frequency_Pattern_Organizes_Local_and_Non-Local_States_by_Quantum_Entanglement_in_both_EPR-Studies_and_Life_Systems
56. Geesink JH, Meijer DKF (2018c) Semi-harmonic scaling enables calculation of masses of elementary particles of the standard model. *J Modern Phys* 9:925–947. <https://pdfs.semanticscholar.org/e576/b8da181ff3e598618dfe440bb5c5904f61a2.pdf>
57. Geesink JH, Meijer DKF (2018d) Mathematical structure of the GM life algorithm that may reflect Bohm's implicate order. *J Modern Phys* 9:851–897. <https://www.scirp.org/journal/PaperInformation.aspx?PaperID=83681>
58. Geesink JH, Meijer DKF (2019a) Superconductive properties in animate and inanimate systems are predicted by a novel biophysical quantum algorithm. *Quantum Biosyst*. https://www.academia.edu/38224924/Superconductive_properties_in_animate_and_inanimate_systems_are_predicted_by_a_novel_biophysical_quantum_algorithm
59. Geesink JH, Meijer DKF, Jerman I (2019c) Clay minerals: primordial biofield and fractal quantum information network? submitted to *Quantum Biosystems*
60. Geesink JH, Meijer DKF (2016b) Bio-soliton model that predicts non-thermal electromagnetic frequency bands, that either stabilize living cells. *Electromagn Biol Med* 36(4):357–378. <https://doi.org/10.1080/15368378.2017.1389752>
61. Meijer DKF, Geesink JH (2018a) Favourable and unfavourable EMF frequency patterns in cancer: perspectives for improved therapy and prevention. *J Cancer Ther* 9:188–230. <https://www.scirp.org/journal/PaperInformation.aspx?PaperID=82944>
62. Meijer DKF, Geesink JH (2016) Phonon guided biology. architecture of life and conscious perception are mediated by toroidal coupling of phonon, photon and electron information fluxes at discrete eigenfrequencies. *NeuroQuantology* 14(4):718–755. <http://www.neuroquantology.com/index.php/journal/article/view/985>
63. Meijer DKF, Geesink JH (2018b) Guided folding of life's proteins in integrate cells with holographic memory and GM-biophysical steering. *Open J Biophys* 8:17–154. https://file.scirp.org/pdf/OJBIPHY_2018071615175972.pdf
64. Muehsam D, Ventura C (2014) Life rhythm as a symphony of oscillatory patterns: electromagnetic energy and sound vibration modulates gene expression for biological signaling and healing. *Glob Adv Health Med* 3(2):40–55. <https://doi.org/10.7453/gahmj.2014.008>
65. Hamblin MR (2017) Photobiomodulation for traumatic brain injury and stroke. *J Neurosci Res* 96:731–743. <https://doi.org/10.1002/jnr.24190>
66. Ferris, Andrew J, Olsen Murray K, Cavalcanti Eric G, Davis Matthew J (2008) Detection of continuous variable entanglement without coherent local oscillators. *Phys Rev A* 78:060104
67. Chladni EFF (1980) *Entdeckungen über die theorie des klanges* [Discoveries in the Theory of Sound], Leipzig, 1787:pp. 78,Reprint, Leipzig
68. Adamatzky A (2013) Game of life on phyllosilicates: gliders, oscillators and still life. *Phys Lett* 377:597–1605
69. Hashizume H (2012) Role of clay minerals in chemical evolution and the origins of life. *Life Phys Lett* 377:597–1605. <https://doi.org/10.5772/50172>
70. Irikura KK (2007) Experimental vibrational zero-point energies: diatomic molecules. *J Phys Chem Ref Data* 36(2):389
72. Selfham AM (2007) Universal spectrum for DNA base C + G frequency distribution in human chromosomes 1 to 24. *World Journal of Modeling and Simulation*; and on ResearchGate
73. Rouleau N, Dotta BT (2014) Electromagnetic fields as structure-function zeitgebers in biological systems: environmental orchestrations of morphogenesis and consciousness. *Front Integr Neurosci* 8:84
74. Huelga SF, Plenio MB (2013) Vibrations, quanta and biology. *Int J Mod Phys B* 10:1735–1754
75. Lambert N, Chen YN, Cheng YC, Li CM, Chen GY, Franco N (2013) Quantum biology. *Nat Phys* 9(1):10–18. <https://doi.org/10.1038/nphys2474>

76. Lloyd S (2011) Quantum coherence in biological systems. *J Phys.: Conf Ser* 302:012037. <https://doi.org/10.1088/1742-6596/302/1/012037>
77. Marais A, Adam B, Ringsmuth AK, Ferretti M, Gruber JM, Hendrikx R, Schuld M, Smith Samuel L, Sinayskiy I, Kru TPJ, Petruccione F, van Grondell R (2018) The future of quantum biology. *J R Soc Interface* 15:20180640. <https://doi.org/10.1098/rsif.2018.0640>
78. Marais A et al (2018) The future of quantum biology. *J R Soc Interface* 15:0640
79. Sonderkamp T, Geesink JH, Meijer DKF (2019) Statistical analysis and prospective application of the GM-scale, a semi-harmonic EMF scale proposed to discriminate between “coherent” and “decoherent” EM frequencies on life conditions. *Quantum Biosyst* 10(2):33–51. <https://www.quantumbionet.org/quantumbiosystems/>
80. Hand K, Yates E (2017) Teraherz: dictating frequencies of life. Do macromolecular vibrational modes impose thermal limitations on terrestrial life? *J R Soc Interface* 14:073
81. Siegel PH (2004) Teraherz technology in biology and medicine. *IEEE transactions on microwave theory and techniques*, vol 52, no 10
82. Muller H (2017) Chain systems of harmonic quantum oscillators as a fractal model of matter and global scaling in biophysics. *Progr Phys* 13:231–233
83. Thut WK (2020) Water frequencies and resonance. <https://www.slideshare.net/Magazineonth eSpot/water-frequencies-and-resonantie-walter-thut>
84. Maret K (2020) Microwaves and radiofrequency radiation affect coherence in living organisms, available from the Dove Health Alliance through maret@cruzio.com
85. Verlinde EP, Zurek KM (2019). Observational signatures of quantum gravity in interferometers. <https://arxiv.org/abs/1902.08207>
86. Bischof M, Del Giudice E (2013) Communication and emergence of collective behavior in living organisms. A quantum approach. *Mol Biol Int* 1. <https://doi.org/10.1155/2013/987549>
87. Jerman I (2016). The origin of life from quantum vacuum, water and polar molecules. *Am J Modern Phys.* 5(4–1):34–43. <http://article.sciencepublishinggroup.com/html/10.11648.j.ajmp.s.2016050401.16.html>
88. Pang XF, Chen S, Wang X, Zhong L (2016) Influences of electromagnetic energy on bio-energy transport through protein molecules in living systems and its experimental evidence. *Int J Mol Sci* 17(8):1130
89. Preto J (2016) Classical investigation of long range coherence in biological systems. *Chaos*
90. Melkikh AV, Meijer DKF (2018) On a generalized Levinthal's paradox: the role of long- and shorrange interactions in complex bio-molecular reactions, including protein and DNA folding. *Progr Biophys Molecular Biology.* 132:57–79. <https://www.sciencedirect.com/science/article/pii/S0079610717300846>
91. Popp FA, Quao G, Ke-Hsuen L (1994) Biophoton emission: experimental background and theoretical approaches. *Modern Phys Lett* 8:21, 22
92. Popp FA, Chang JJ, Herzog A, Yan Z, Yan Y (2002) Evidence of non-classical (squeezed) light in biological systems. *Phys Lett A* 293(1, 2):98–102
93. Davies PCW (2014) Does quantum mechanics play a non-trivial role in life? *BioSystems* 2014(78):69–79
94. Walker SI, Davies PCW (2013) The algorithmic origin of life. *J R Soc Interf* <https://royalsocietypublishing.org/doi/pdf/10.1098/rsif.2012.0869>
95. Meijer DKF, Geesink JH (2018c) Is the fabric of reality guided by a semi-harmonic, toroidal background field? *Int J Struct Comput Biol.* <https://pdfs.semanticscholar.org/43a5/dbabe7ce98c06d45451e2329a19327c42dbc.pdf>
96. Montagnier L, Aïssa J, Capolupo A, Craddock TJA, Kurian P, Lavallee C, Polcari A, Romano P, Tedeschi A, Vitiello G (2017) Water bridging dynamics of polymerase chain reaction in the gauge theory paradigm of quantum fields. *Water* 9:339
97. Turner P, Notalle A (2016) New Ab initio approach to the development of high temperature superconducting materials. *J Supercond Nov Magn.* 29(12):3113–3118. <https://doi.org/10.1007/s10948-016-3756-z>
98. Turner P (2019) New insights into the physical processes that underpin cell division and differentiation, submitted

99. Marjieh R, Sabag E, Hayt A (2016) Light amplification in semiconductor-superconductorstructures. *New J Phys* 023019
100. Hunt T, Schooler JW (2019) The easy part of the hard problem: a resonance theory of consciousness. *Front Hum Neurosci* 13:378. <https://www.ncbi.nlm.nih.gov/pmc/articles/PMC6834646/>
101. Hunt T (2017) How deep is the neuron? A conversation with Anirban Bandyopadhyay about new advances in neuroscience. Society for the Advancement of Metadarwinism. <http://metadarwinism.com/how-deep-is-the-neuron/>
102. Sepehri HG (2017) A mathematical model for DNA. *Int J Geometric Methods Mod Phys* 14(11): 1750152
103. Hameroff S, Tuszynsky J (2010) Quantum states in protein assemblies: The essence of Life?. <http://www.quantumconsciousness.org/sites/default/files/PaperIntlSocOptEngineeringQuantumStatesinProteinsandProteinAssemblies.pdf>
104. Wigner EP (1983) Remarks on the mind-body problem. In: Wheeler J, Wojciech Z (eds) *Quantum theory and measurement*. Princeton University Press, Princeton, p 99
106. Mikheenko P (2018) Possible superconductivity in brain. *J Supercond Novel Magn* 32:1121–1134
107. Cope FW (1975) A review of the applications of solid state physics concepts to biological systems. *J Biol Phys* 3(1):1–41. https://drive.google.com/file/d/1ZWecGBR9NyIR_rNmycangi5T0rKgnuxM/view?usp=sharing
108. Brizhik L (2015) Biological effects of pulsating magnetic fields: role of solitons; arxiv.org/pdf/1411.6576
109. Fröhlich F, McCormick DA (2013) Endogenous electric fields may guide neocortical network activity. *Neuron* 67:129–143. <https://doi.org/10.1016/j.neuron.2010.06.005>
110. Hammerschlag R, Levin M, Mc Craty R, Bat BA, Ives JA, Lutgendorf SK, Oschman JL (2015) Biofield physiology: a framework for an emerging discipline. *Glob Adv Health Med* 4:35–41. <https://doi.org/10.7453/gahmj.2015.015.suppl>
111. Jibu M, Yasue K (1993) Introduction to quantum brain dynamics. In: *Nature, Cognition and System* ed, Carvall
112. Umezawa H (1993) Advanced field theory. The American Institute of Physics Press, New York
113. Vitiello G (2001) My double unveiled: the dissipative quantum model of brain. John Benjamins Publishing
114. Del Giudice E, Tedeschi A (2009) Water and autocatalysis in living matter. *Electromagn Biol Med* 28:46–52
115. Del Giudice E, Spinetti PR, Tedeschi A (2010) Water dynamics at the root of metamorphosis in living organisms. *Water* 2:566–586
116. Lundholm IV, Rodilla H, Wahlgren WY, Duelli A, Bourenkov G, Vukusic J, Friedman R, Stake J, Schneider T, Katona G (2015) Terahertz radiation induces non-thermal structural changes associated with Fröhlich condensation in a protein crystal. *Struct Dyn* 054702. <http://dx.doi.org/10.1063/1.4931825>
117. Nardecchia I, Torres J, Lechelon M, Giliberti V, Ortolani M, Nouvel P, Gori M, Donato I, Preto J, Varani L, Sturgis J, Pettini M (2017) Out-of-equilibrium collective oscillation as phonon condensation in a model protein. <https://arxiv.org/pdf/1705.07975.pdf>
118. Nardecchia I, Spinelli L, Preto J, Gori M, Floriani E, Jaeger S, Ferrier P, Pettini M (2014) Experimental detection of long-distance interactions between biomolecules through their diffusion behavior: numerical study. *Phys Rev E* 90. Article ID: 022703. <https://doi.org/10.1103/PhysRevE.90.022703>
119. Yamasaki et al (2018) Actin polymerization is activated by teraherz irradiation. *Nat Sci Rep* 8:9990
120. Plankar M, Jerman I, Krasovec R (2011) On the origin of cancer: can we ignore coherence? *Prog Biophys Molecul Biol* 106:380–390
121. Yannon TA, Elia V (2013) Dynamics in perturbed very dilute aqueous solutions: theory and experimental evidence. *Int J Mod Phys B* 27(05):1350005

122. Vattay G, Kauffman SA (2015) Quantum criticality at the origin of life. [arXiv:1502.06880](https://arxiv.org/abs/1502.06880) [cond-mat.dis-nn]
123. Wolchover N (2019) The universal law that aims time's arrow <https://www.quantamagazine.org/the-universal-law-that-aims-times-arrow-20190801>
124. Abrams DM, Strogatz SH (2004) Chimera states for coupled oscillators. *Phys Rev Lett* 93:174102
125. Motter AE, Yang Y (2017) The unfolding and control of network cascades. *Phys Today* 70(1):32. <https://doi.org/10.1063/pt.3.3426>
126. Toykka LA (2014) Self-interference of a toroidal Bose-Enstein condensate. *New J Phys* 16:043011
127. Collini E, Cathy Y, Wilk K E, Curmi PMG, Brumer, Scholes PGD (2010) Coherently wired light-harvesting in photosynthetic marine algae at ambient temperature *Nature* 463(7281):644–7, 2010 Feb 4, <https://doi.org/10.1038/nature08811>
128. Engel GS (2011) Quantum coherence in photosynthesis. *Science Direct, Procedia Chem* 3(2011):222–231
129. Romero E, Augulis R, Novoderezhkin VI, Marco Ferretti M, Jos Thieme J, Zigmantas D, van Grondelle R (2014) Quantum coherence in photosynthesis for efficient solar energy conversion. *Nat Phys* 10(9):676–682. <https://doi.org/10.1038/nphys3017>, 2014 Sept 1
130. Dolce D (2017) Introduction to the quantum theory of elementary cycles: the emergence of space, time and quantum. [arXiv:1707.00677v1](https://arxiv.org/abs/1707.00677v1) [physics.gen-ph]
131. Preparata G (1992) Coherence in QCD and QED In: Bressani T, Minetti B, Zenoni A (eds) *Common problems and ideas of modern physics*. World Scientific, Singapore, p 3
132. Sheldrake M, Sheldrake R (2017) Determinants of Faraday wave patterns in water samples oscillated vertically at a range of frequencies from 5–200 Hz. *Water* 9:1–27
133. Johnson K (2009) Water buckyball. Terahertz vibrations in physics, chemistry, biology, and cosmology. <https://arxiv.org/ftp/arxiv/papers/0902/0902.2035.pdf>
134. Johnson M (2009) Toward a new ontology of brain dynamics: neural resonance + neuroacoustics. Qualia Research Institute. Available from: <https://opentheory.net/2009/11/toward-a-new-ontology-of-brain-dynamics-neural-resonance-neuroacoustics/>
135. Kolesnikov LA, Anovitz I, Mamontov E, Podlesnyak A, Ehlers G (2014) Strong anisotropic dynamics of ultra-confined water. *J Phys Chem B* 118(47):13414–13419. <https://doi.org/10.1021/jp505355b>
136. Arani R, Bono I, Giudice ED, Preparata G (1995) QED coherence and the thermodynamics of water. *Int J Mod Phys B* 9:1813–1842
137. Carniello TN, Vares DAE, Persinger MA (2015) Quantitative support for water as the conduit of interaction for universal entanglement. *J Consciousness Explor Res* 6(9):738–749
138. Del Giudice E, De Ninno A, Fleischmann M, Mengoli G, Milani M, Talpo G, Vitiello G (2005) Coherent quantum electrodynamics in living matter. *Electromagn Biol Med* 24:199–210
139. Ganeshan S, Ramirez R, Fernandez-Serra MV (2013) Simulation of quantum zero point effects in water using frequency dependent thermostat. <https://arxiv.org/abs/1208.1928>
140. Sen S, Gupta K, Coey JMD (2015) Mesoscopic structure formation in condensed matter due to vacuum fluctuations. *Phys Rev B* 92:155115
141. Sen S, Gupta KS (2017) Observable consequences of zero-point energy. *Mod Phys Lett A* 32:1750217
142. Thayer AM, Pines A (1987) Zero-field NMR. Accounts of Chemical Research, pp 47–53, 20 February
143. Bouchard F et al (2015) Observation of quantum recoherence of photons by spatial propagation. *Nat Sci Rep* 5:15330
144. Chin AW et al. (2013) The role of non-equilibrium vibrational structures in electronic coherence and re-coherence in pigment-protein complexes. *Nat Phys*
145. Kauffman SA (2008) Reinventing the sacred: a new view of science, reason, and religion. Basic Books
146. Kauffman SA (2009) Towards a post reductionist science. The Open University. Kastrup B (2017) Self-transcendence correlates with brain function impairment. *J Cognit Neuroethics* 4(3):33–42. <https://philpapers.org/rec/KASSCW>

147. Moldonado CE (2018) A quantum coherence-recoherence-based model of reality. *NeuroQuantology* 16:44–48
148. Fröhlich H (1968) Long-range coherence and energy storage in biological systems. *Int J Quantum Chem* 2:641–649
149. Bush JWM (2015) Pilot wave hydrodynamics. *Annu Rev Fluid Mech* 47:26992
150. Brown PA (2019) Water: the new science behind the universal conduit. http://www.laserpetcare.com/wp-content/uploads/2014/10/Brown_Water-The-New-Science-Behind-the-Universal-Conduit_AHVMA_09_14.pdf
151. Brown W (2019) Unified physics and the entanglement nexus of awareness. *NeuroQuantology* 17:40–52
152. Tsenkova R, Muncan J, Pollner B, Kovacs Z (2018) Essentials of aquaphotonics and its chemometrics approaches. *Front Chem*. 6, 1 August, Article 363 www.frontiersin.org
153. Vegt W (2015) The world beyond superstrings. The origin of electric charge and magnetic spin. <https://osf.io/6e847/> <https://www.amazon.com/Beyond-Superstrings-Origin-Electric-Magnetic/dp/9402179631>
154. Haramein N, Brown WD, Val Baker A (2016) The unified spacememory network: from cosmogenesis to consciousness. *NeuroQuantology*. 14(4):657–671. <https://doi.org/10.14704/nq.2016.14.4.961>
155. Jensen K, Karch A (2013) The holographic dual of an EPR pair has a wormhole. www.mpp-mpg.de/conf/ggd2013/files/slides/jensen.pdf
156. Zagorskin AM, Chipoline A, Il'ichev E, Johansson JR, Nori F (2015) Toroidal qubits: naturally-decoupled quiet artificial atoms. *Nat Sci Rep* 5:16934
157. Kirillov AA, Savelov EP (2012) On scattering of electromagnetic waves by a wormhole. *Phys Lett B* 710(4, 5):516–518
158. Marquet P (2012) Traversable space-time wormholes sustained by the negative energy electromagnetic field. <http://zelmanov.ptep-online.com/papers/zj-2012-05.pdf>
159. Musha T, Caliguri LM (2015) Possible existence of superluminal photons inside microtubules and the resulting explanation for brain mechanisms. *Am J Opt Photonics*. 3(5):54–57
160. Lefferts M (2019) Cosmometry. Exploring the holofractal nature of the cosmos. Cosmometria Publishing, New York
161. Dehaene S, Lau H, Koulder S (2017) What is consciousness, and do machines have it? *Science* 358:486–492
162. Görnitz T (2012) Quantum theory as universal theory of structures. Essentially from Cosmos to Consciousness. <http://cdn.intechopen.com/pdfs-wm/28316.pdf>
163. Görnitz T (2016) A century of quantum theory-time for a change in thinking, versus the popular belief that material building blocks are the basis of the reality. https://www.researchgate.net/publication/301895324_A_century_of_quantum_theory_-time_for_a_change_in_thinking_Versus_the_popular_belief_that_material_building_blocks_are_the_basis_of_the_reality
164. Meijer DKF (2015) The universe as a cyclic organized information system. An essay on the worldview of john wheeler. *NeuroQuantology* 1:1–40. <http://www.neuroquantology.com/index.php/journal/article/view/798/693>
165. Meijer DKF, Raggett S (2014) Quantum physics in consciousness studies. The Quantum Mind Extended. review, 180 pp. <http://quantum-mind.co.uk/wp-content/uploads/2014/11/Quantum-Ph-rev-def-2.pdf>
166. Wolf-Meyer M, Cochran C (2015) Minor science. Unifying minor sciences and minor literatures: Reproduction and revolution in quantum consciousness as a model for the anthropology of science. *Anthropological Theor* 15:407–433. <https://journals.sagepub.com/doi/abs/10.1177/1463499615615739>
167. Kozyrev SV (1997) Ultrametric space of free coherent states. *TMF Theoret Math Phys* 110(2):265–266
168. Tozzi A, Peters JF (2015) Brain activity on a hypersphere. *Quant Biol Neuron Cognit arXiv: 1512.00036* [q-bio.NC]

169. Knierim JJ, Zhang K (2012) Attractor dynamics of spatially correlated neural activity in the limbic system. *Ann Rev Neurol*. <https://doi.org/10.1146/2012/062111-150351>
170. Atasoy S, Deco G, Kringsbach ML, Pearson J (2018) Harmonic brain modes: a unifying framework for linking space and time in brain dynamics. *Neuroscientist*. 24(3):277–293. <https://doi.org/10.1177/1073858417728032>. Epub Sep 1. 2017
171. Amiot E (2013) The torii of phases. In: Yust J, Wild J, Burgoyne JA (eds) Mathematics and computation in music. MCM 2013. Lecture Notes in Computer Science, pp 7937
172. Bjerke A (2016) The fractal-holographic universe. <http://holofractal.net/the-holofractographic>
173. Papasimakis N, Fedotov VA, Savinov V, Raybould TA, Zheludev NI (2016) Electromagnetic toroidal excitations in matter and free space. *Nat Mater* 15:263–271. <https://doi.org/10.1038/nmat4563>
174. Tsytovich VN, Morfill GE, Fortov VE, Gusein-Zade NG, Klumov BA, Vladimirov SV (2007) From plasma crystals and helical structures towards inorganic living matter. *New J Phys* 9
175. Verlinde EP (2011) On the origin of gravity and the laws of newton; JHEP. arXiv:1001.0785 Bibcode:2011JHEP...04..029 V. [https://doi.org/10.1007/jhep04\(2011\)029](https://doi.org/10.1007/jhep04(2011)029)
176. 't Hooft GA (2007) Mathematical theory for deterministic quantum mechanics. *J Phys: Conf Ser* 67
177. 't Hooft GA (2016) Fundamental theories of physics. The cellular automaton interpretation of quantum mechanics, pp 185
178. Batiz Z, Milovanovic D (2017) Quantum holography and agency: toward a formalism of schema QD. *NeuroQuantology* 15:45–59
179. Sieb RA (2016) Human conscious experience is four-dimensional and has a neural correlate, modeled by einstein's special theory of relativity. *NeuroQuantology* 14:630–644
180. Lloyd NJ (2007) Black hole computers. <https://www.scientificamerican.com/.../black-hole-computers-2007>
181. Keppler JA (2013) A new perspective on the functioning of the brain and the mechanisms behind conscious processes. *Front Psychol Theor Philos Psychol* 1–6
182. Keppler JA (2016) On the universal mechanism underlying conscious systems and the foundations for a theory of mind. *Open J Philos* 6:346–367
183. Keppler JA (2020) The common basis of memory and consciousness: understanding the brain as a write-read head interacting with an omnipresent background field. *Front Psychol* 10:2968
184. László E (2007) The Akashic Field. Dutton, New York
185. László E (2012). Cosmic symphony: a deeper look at quantum consciousness. http://www.huffingtonpost.com/ervin-laszlo/cosmic-symphony-a-deeper_b_532315.html
186. Nation P, Jahansson J, Blencowe M, Nori F (2012) Stimulating uncertainty: amplifying the quantum vacuum with superconducting circuits. *Rev Modern Phys* 81(1):1
187. Setterfield B (2002) Exploring the vacuum. *J Theor*. <http://www.setterfield.org/exploringvacuum.htm>
188. Haramein N, Rauscher EA (2016) Collective coherent oscillation plasma modes in surrounding media of black holes and vacuum structure—quantum processes with considerations of spacetime torque and coriolis forces. The Resonance Project Foundation. www.the-resonanceproject.org
189. Loll R (2011) Quantum gravity at the planck scale: getting a hold on spacetime foam. <http://physics.technion.ac.il/~conf/Waves/RenateLoll.pdf>
190. Haggard HM, Rovelli C (2014) Black hole fireworks: quantum-gravity effects outside the horizon spark black to white hole tunneling, 6 Jul 2014. arXiv:1407.0989v2 [gr-qc]
191. Maldacena J, Susskind K (2013) Cool horizons for entangled black holes. *High Energy Phys Theor* (hep-th). doi: <http://arxiv.org/pdf/1306.0533v2.pdf>
192. Pourhasan R, Afshordi N, Mann RB (2013) Out of the white hole. The holographic origin for the big bang. arXiv:1309.1487v2 [hep-th]. 22 Sep
193. Susskind I (2016) Copenhagen vs Everett, Teleportation, and ER = EPR
194. Wheeler JA, Feynman (1994) At home in the Universe. New York Institute of Physics, New York

195. Henry RC (2005) The mental Universe. *Nature* 436(7):29
196. Smetham GP (2010) Quantum mind matrix of the Universe. *J Conscious Explor Res* 1:864–887
197. Hawking S, Mlodinow L (2010) The grand design. Bantam Press, New York
198. Mays RG, Mays SB (2011) The theory of mind and brain that solves the hard problem of consciousness. <https://www.selfconsciousmind.com/TheoryOfMindAndBrain-12052011.pdf>
199. Desmond T (2014) Psyche = singularity: a comparison of Carl Jung's transpersonal psychology and Leonard Susskind's holographic string theory. Thesis Publ ProQuest, UMT Press
200. Kowal JP, Deshpande BP (2016) It's the other way around: matter is a form of consciousness and death is the end of illusion of life in te world. *J Conscious Explor Res* 7:1154–1208
201. Darmos SOA (2019) Quantum gravity and the role of consciousness in physics. https://www.academia.edu/34051559/Quantum_Gravity_and_the_Role_of_Consciousness_in_Physics
202. Amoroso RL, Di Biase F (2016) Unified field mechanics & its application: elucidating the objective character of experience. *God J* 7:59–81
203. Maurer LH (2010) How unconditioned consciousness, infinite information, potential energy and time created our univese. *J Conscious Explor Res* 1:610–624
204. Popławski NJ (2010) Radial motion into an einstein-rosen bridge. *Phys Lett B* 687(2, 3):110. <https://doi.org/10.1016/j.physletb.2010.03.029>
205. Dunajzki M (2009) Twistor theory and differential equations. *J Phys A: Math Theor* 42:404004
206. Melkikh AV, Khrennikov A (2017) Quantum-like model of partially directed evolution. *Prog Biophys Mol Biol* 125:36–51
207. Anjamrooz et al (2011) The cellular universe: a new cosmological model based on the holographic principle. *Int J Phys Sci* 6:2175–2183
209. Werner G (2010) Fractals in the nervous system: conceptual implications for theoretical neuroscience. *Front Physiol* 1, art 15. <https://www.ncbi.nlm.nih.gov/pmc/articles/PMC3059969/pdf/fphys-01-00015.pdf>
210. Afshordi N et al (2017) From planck data to planck era: observational tests of holographic cosmology. *Phys Rev Lett* 118(4):041301. [arXiv:1607.04878](https://arxiv.org/abs/1607.04878) [astro-ph.CO]
211. Picato D (2017) A spacetime discretization and black holes properties in a holographic representation. [arXiv:1703.10795](https://arxiv.org/abs/1703.10795) [hep-th]
212. Val Baker AK, Haramein FN, Airol O (2019) The electron and the holographic mass solution. *Phys Essays* 32:2
213. Rezzolla L, Yoshida S, Maccarone TJ, Zanotti O (2003) A new simple model for high-frequency quasi-periodic oscillations in black hole candidates. *Mon Not R Astron Soc* 344(3):L37–L41
214. Whittle M (2010) Big bang acoustics: sound from the newborn Universe. http://people.virginia.edu/~dmw8f/BBA_web/index_frames.html
215. Luminet JP (2007) Geometry and topology in relativistic cosmology. [arXiv:0704.3374](https://arxiv.org/abs/0704.3374) [astro-ph]
216. Sbitnev VI (2019) Quaternion algebra on 4D superfluid quantum space-time: gravitomagnetism. *Found Phys* 49(2):107–143. <https://arxiv.org/pdf/1901.09098.pdf>
217. Opher R, Pelinson A (2005) Decay of vacuum energy into cosmic microwave background photons. *Mon Not Astron Soc* 362:167–170
218. Ho CM, Scherrer RJ (2013) Anapole dark matter. *Phys Lett B* 722:341–346. <https://www.sciencedirect.com/science/article/pii/S0370269313003286>
219. Wang KW, Fung PCW, Chow WK (2019) 5D model theory for the creating of life forms. *J Modern Phys* 10:1548–1565
220. Thorvaldsen S (2014) Unique hoyle state of the carbon atom. Proceedings of the Conferences on the Dialogue between Science and Theology November, pp. 6–11
221. Mc Craty R et al (2017) Synchronization of human nervous system rhythms with geometric activity in human subjects. *Int J Environ Res* 14:770. *Public Health*

222. Kozwolski M, Marciak-Kozwolski J (2017) Quantum model of consciousness. *J Conscios Explor Res* 8:1–17
223. Persinger MA, St-Pierre LS (2015) The physical bases to consciousness: implications of convergent quantifications. *J Syst Integr Neurosci* 1:55–64
224. Keppler JA (2012) Conceptual framework for consciousness based on a deep understanding of matter. *Philos Stud* 2(10):689–703
225. Bernstein P (2015) Intuition: what science says (so far) about how and why intuition works. In: Buccheri R et al (eds) *Endophysics, time, quantum and the subjective*. World Scientific Publishing, Singapore
226. Jahn RG, Dunne BJ (2004) Sensors, filters, and the source of reality. *J Sci Explor* 18(4):547–570
227. Rousseau D (2011) Understanding spiritual awareness in terms of anomalous information access. *Open Inf Sci J* 3:40–53
228. Schwartz JM, Stapp H, Beauregard M (2005) Quantum physics in neuroscience and psychology: a neurophysical model of mind–brain interaction. *Phil Trans R Soc B* 360:13091327
229. Tammietto M, de Gelder B (2010) Neural basis of the non-conscious perception of emotional signals. *Nat Rev Neurosci* 1–13
230. Bieberich E (2012) Introduction in the practicality principle of consciousness and the sentyon postulate. *Cognit Comput* 4:13–28
231. Gardiner J, Overall R, Marc J (2010) The fractal nature of the brain: EEG data suggests that the brain functions as a “quantum computer” in 5×8 Dimensions. *NeuroQuantology* 8:137–141
232. Zheng J-m, Wei-Chun C, Khijniak E, Khijniak EJ, Pollack GH (2006) *Adv Colloid Interface Sci* 127:29
233. Grof S (1987) Beyond the brain; birth, death and transcendence in psychotherapy. State University of New York Press, New York
234. Persinger MA, Murugan NJ, Karbowski LM (2015) Combined spectral resonances of signalling proteins’ amino acids in the ERK-MAP pathway reflect unique patterns that predict peak photon emissions and universal energies. *Int Lett Chem Phys Astron* 43:10–25
235. Persinger MA (2008) On the possible representation of the electromagnetic equivalents of all human memory within the earth’s magnetic field: implications for theoretical biology. *Theor Biol Insights* 1:3–11
236. Hameroff S, Tuszynsky J (2010) Quantum states in protein assemblies: The essence of Life <http://www.quantumconsciousness.org/sites/default/files/PaperIntlSocOptEngineeringQuantumStatesinProteinsandProteinAssemblies.pdf>
237. John ER (2001) A field theory of consciousness. *Conscious Cogn* 10:184–213
238. McFadden J (2007) Conscious electromagnetic (CEMI) field theory. *NeuroQuantology* 5(3):262–270
239. Pockett S (2012) The electromagnetic field theory of consciousness: a testable hypothesis about the characteristics of conscious as opposed to non-conscious fields. *J Conscious Stud* 19(11, 12):191–223
240. Carlson CR (2020) A frequency ratio account of temporal atomism. https://www.researchgate.net/publication/340065335_A_Frequency_Ratio_Account_of_Temporal_Atomism_revised
241. Walling PT (2020) An update on dimensions of consciousness. *Proc Bayl Univ Med Cent* 33(1):126–130
242. Walling P, Hicks KN (2003) Dimensions of Consciousness. *BUMC Proc* 16:162–166
243. Gabella M (2006) The Randall-Sundrum Model. <https://www.thphys.physics.ox.ac.uk/people/MaximeGabella/rs.pdf>
244. Beichler JE (2012c) The neurophysical basis of mind and consciousness: an electromagnetic model of the neuron. A presentation at the annual spring meeting of the OSAPS. Ohio State 68 University. <http://www.neurocosmology.net>
245. Carter PJ (2014) Consciousness and perception in higher-dimensional quantum space-time. *NeuroQuantology* 12:46–75

246. Martin F, Carminati F, Carminati G (2013) Quantum information theory applied to unconscious and consciousness. *NeuroQuantology* 11:16–33
247. Baquie BE, Martin F (2005) Quantum psyche. Quantum field theory of the human psyche. *NeuroQuantology* 1:7–42
248. Luminet JP (2016) The holographic Universe. <https://arxiv.org/abs/1602.07258>
249. Sirag SP (1993) Consciousness, a hyperspace view. <http://www.williamjames.com/Theory/Consciousness.pdf>
250. Smythies J (2003) Space, time & consciousness. *J Conscious Stud* 10(3):47–5
251. Wesson PS (2014) Looking for the fifth dimension. *Phys Int* 5:5–7
252. Tozzi A, Peters JF (2016) Symmetries, information and monster groups before and after the big bang. *Information* 7:73
253. Tozzi A, Peters JF (2016) Towards a fourth spatial dimension of brain activity. *Cogn Neurodyn* 10(3):189–199 PMID: 27275375
254. Samardzija N (2018) From spheroids to globotoroids. *Int J Sci Eng Investig* 7:99–102
255. Hut P (2017) Mind and magnetic monopoles: matter, mind and magic. <https://www.yhousenyc.org/yhouse-blog/all-posts/2017-09-11/mind-and-magnetic-monopoles>
256. Peterson JPS, Sarthour RS, Souza AM, Oliveira IS, Goold J, Modi K, Soares-Pinto DO, Céleri LC (2016) Experimental demonstration of information to energy conversion in a quantum system at the Landauer limit. *Proc R Soc A-Math Phys Eng*. <https://royalsocietypublishing.org/doi/10.1098/rspa.2015.0813>
257. Aharonov Y, Popescu S, Rohrlich D, Skrzypczyk P (2013) Quantum cheshire cats. *New J Phys* 15:1–8
258. Atmanspacher H (2011) Quantum approaches to consciousness. *Stanford Encycl Philos* 1–33
259. Adams B, Petruccioni (2019) Quantum effects in the brain: a review. [arXiv:1910.08423](https://arxiv.org/abs/1910.08423) [q-bio.NC]
260. Tegmark M (2015) Consciousness as a state of matter. [http://arxiv.org/abs/1401.1219](https://arxiv.org/abs/1401.1219)
261. Hagan S, Hameroff SR, Tuszyński JA (2002) Quantum computation in brain microtubules: Decoherence and biological feasibility
262. Bernroider G (2003) Quantum neurodynamics and the relationship to conscious experience. *NeuroQuantology* 1:163–168
263. Stapp H (2012) Reply to a critic: mind efforts, quantum zeno effect and environmental decoherence. *NeuroQuantology* 10(4):601–605
264. Hu H, Wu M (2013) The relationship between human consciousness & universal consciousness. *Sci GOD J* 4:209–225
265. Seth A (2018) Consciousness: the last 50 years (and the next). *Brain and Neurosci Adv* 2, pp. 1–6. ISSN 2398-2128
266. Bókkon I, D'Angiulli A (2009) Emergence and transmission of visual awareness through optical coding in the brain: a redox molecular hypothesis on visual mental imagery. *Biosci Hypotheses* 2:226–232. <https://doi.org/10.1016/j.bihy.2009.01.009>
267. Dotta BT (2013) Ultraweak photon emission in cells: coupling to molecular pathways, applied magnetic fields, and potential non-locality, thesis
268. Wang CH, Bokkon I, Dai J, Antal I (2010) Spontaneous and visible light-induced ultra-weak photon emission from rat eyes. *Brain Res* <https://doi.org/10.1016/j.brauinres.2010.10.077>
269. Rahnama M, Tuszyński J, Bokkon I, Cifra M, Sardar P, Salari V (2011) Emission of biophotons and neural activity of the brain. *J Integr Neurosci* 10(1):65–88. <https://doi.org/10.1142/s0219635211002622>
270. Bókkon I, Mallick BN, Tuszyński JA (2013) Near death experience: a multidisciplinary hypothesis. *Front Hum Neurosci* 7:1–11
271. Georgiev DD, Glazebrook JF (2018) The quantum physics of synaptic communication via the SNARE protein complex. *Prog Biophys Mol Biol* 135:16–29
272. Bessler P (2019) Some macroscopic applications of Georgiev's quantum information model. *NeuroQuantology* 17:29–35
273. Flohr H (1998) On the mechanism of action of anaesthetic agents. In Hameroff SR, Kaszniak AW, Scott AC (eds) *Toward a science of consciousness II*. MIT Press, pp 2–459

274. Adamski A (2019) The historical aspect of the development of quantum consciousness at the beginning of the XXI century. *Gerontol Geriatrics Stud* 4. GGS.000588.2019
275. Annila A (2013) On the character of consciousness. *Front Syst Neurosci*. [arXiv:1308.4802v3](https://arxiv.org/abs/1308.4802v3) [hep-th] 7
276. Meijer DKF (2014) The extended brain: cyclic information flow. In A quantum physical realm. *NeuroQuantology* 12:180–200. <http://www.neuroquantology.com/index.php/journal/article/view/754/651>
277. Bohm D, Hiley BJ (1993) The undivided universe. An ontological interpretation of quantum theory. Routledge, London
278. Caligiuri LM (2015) Zero-point field, QED coherence, living systems and biophoton emission. *Open J Biophys* 5:21–34
279. Simon C (2019) Can quantum physics help solve the hard problem of consciousness? A hypothesis based on entangled spins an photons. *J Conscious Stud* 26(5, 6):204–218
280. Libet B (1994) A testable field theory of mind-brain interaction. *J Conscious Stud* 1:119–126
281. Tonegawa S, Pignatelli M, Roy DS, Ryan TJ (2015) Memory engram storage and retrieval. *Current Opin Neurobiol* 35:101–109
282. Curriav J (2017) The cosmic hologram. Information at the Center of Creation. Inner Traditions, Rochester Vermont, USA
283. St. John TJ (2018) The holomorphic process—understanding the holographic nature of reality. *Arch Phys Res* 9:17–44
284. Linden RFJ (2009) The universe as a multi-dimensional fractal. <https://bruceleeeowe.files.wordpress.com/2009/10/fractal-universe.pdf>
285. Chiatti L (2007) Fantappié–Arcidiacono theory of relativity versus recent cosmological evidences: a preliminary comparison. <https://arxiv.org/ftp/physics/papers/0702/0702178.pdf>
286. Galloni GM (2012) The heresy of Fantappié and Teilhard and the converging revolution. *Syntropy* 2(1):79–84
287. Meijer DKF (2019b) Anticipation of afterlife as based on current physics of information. Available on ResearchGate, https://www.researchgate.net/publication/336531043_The_Anticipation_of_Afterlife_as_Based_on_Current_Physics_of_Information
288. Radin D (1997) The conscious Universe. The Scientific Truth of Psychic Phenomena, New York, HarperEdge
289. Beichler JE (2012b) The neurophysics of mind and consciousness: a theoretical model of emergence, evolution, psi and survival. A presentation made at the SMN/SSE conference at An Grianan AEC, Ireland. <http://www.neurocosmology.net>
290. Greysen B (2010) Seeing dead people not known to have died: “peak in darien” experiences. *Anthropol Hum* 35(2):159–171
291. Lake J (2015) The near-death experience: implications for a more complete theory of consciousness. *Quantum Biosys* 6:131–138
292. Van Gordon et al (2018) Meditation-induced near-death experiences: a 3-year longitudinal study. *Mindfulness* 9:1794–1806
293. Pereira C, Reddy JSK (2016) Near-death cases, non-locality/disembodiment via quantum mediated consciousness. *J Conscious Explor Res* 7:951–968
294. Sullivan PR (1995) Contentless consciousness and information processing theories of mind. *Philos, Psychiatry & Psych* 2:51–59
295. Davies PCW (2009) The quantum life. *Phys World* pp 24–28
296. Bitbol M, Luisi PL (2004) Autopoiesis with or without cognition: defining life at its edge. *J R Soc Interface* 1(1):99–107 [PubMed: 16849156]
297. Carhart-Harris RL, Friston KJ (2019) REBUS and the anarchic brain: towards a unified model of brain action of psychedelics. *Pharmacol Rev* 71:316–344
298. Feuillet L, Dufour H, Pelletier J (2007) Brain of a white-collar worker. *The Lancet* 370(9583):262
299. Forsdyke DR (2014) Long-term memory: scaling of information to brain size. *Front Hum Neurosci* 8:1–4

300. Mashour GA, Alkira M (2013) Evolution of consciousness: phylogeny, ontogeny and emergence from general Anesthesia. PNAS 110:10357–10364
301. Nahn et al (2017) Discrepancy between cerebral structure and cognitive functioning: A review. J Nerv Mental Dis 205(12):967–972
302. Majorek MB (2012) Does the brain cause conscious experience? J Consciousness Stud 19(3)
303. Cleeremans A (2011) The radical plasticity thesis: How the brain learns to be conscious. Front Psychol 2, Pp. 86. <https://www.ncbi.nlm.nih.gov/pmc/articles/PMC3110382/>
304. Wolf FA (1989) On the quantum physical theory of subjective antedating. J Theor Biol 136:13–19
305. Wolf FA (1985) The quantum physics of consciousness: towards a new psychology. Integr Psychiatr 3(235):4–25
306. Kastrup B (2019) Conflating abstraction with empirical observation: the false mind-matter dichotomy. Constr Found 13(3):341–360
307. Melkikh AV (2019) Thinking as a quantum phenomenon. Biosystems 176:32–40
308. Melkikh AV (2020) Theory of directed evolution. Lambert Academic Publishing
309. Pesic P (2014) Music and making modern science. MIT Press. <https://mitpress.mit.edu/books/music-and-making-modern-science>
310. Merrick RS (2009) Interference: a grand scientific musical theory (self-published). Fairview, Texas. ISBN 978-0-615-20599-1
311. Merrick RS (2010) Harmonically guided evolution. In: Proceedings of the natural philosophy alliance, vol 7
312. Sanyal S, Banerjee A, Sangupta, Ghosh D (2016) Chaotic brain, musical mind—a nonlinear neurocognitive physics based study. J Neurol Neurosci 7(63):1–10
313. Kotchoubey B, Pavlov YG, Kleber B (2015) Music as research and rehabilitation od disorders of consciousness: physiological and neurophysiological foundations. Front Psychol 6:1763
314. Martorell AJ, Paulson AL, Suk HJ, Abdurrob F, Drummond GT, Guan W, Young JZ, Kim DN, Kritskiy O, Barker SJ, Mangena V, Prince SM, Brown EN, Chung K, Boyden ES, Singer AC, Tsai LH (2019) Multi-sensory gamma stimulation ameliorates Alzheimer's-Associated pathology and improves cognition. Cell 177(2):256–271.e22. Epub 14 Mar 2019
315. Koelsch S (2009) The neuroscientific perspective on music therapy. Ann NY Acad Sci 1169:374–384
316. Hartwich K, Pollak T, Klausberger T (2009) Distinct firing patterns of identified basket and dendrite-targeting interneurons in the prefrontal cortex during hippocampal theta and local spindle oscillations. J Neurosci 29(30):9563–9574
317. Gramowski-Vöb A, Schwertle HJ, Pielka AM, Schultz L, Steder A, Jügelt K, Axmann J, Pries W (2015) Enhancement of cortical network activity in vitro and promotion of GABAergic neurogenesis by stimulation with an electromagnetic field with a 150 MHz carrier wave pulsed with an alternating 10 and 16 Hz modulation. Front Neurol 6:158. <https://doi.org/10.3389/fneur.2015.00158>
318. Pitkänen M (2016) What could be the physical origin of Pythagorean Scale? http://tgdttheory.fi/public_html/articles/geesinkscale.pdf
319. Heyning EC (2017) Star music, The ancient idea of cosmic music as a philosophical paradox. Thesis, Canterbury Christ Church University. https://www.academia.edu/35078706/Star_Music_The_ancient_idea_of_cosmic_music_as_a_philosophical_paradox
320. Auffray C et al (2020) Progress in integrative systems biology, physiology and medicine: towards a scale relative biology. Eur Phys J A 56:88. <https://link.springer.com/article/10.1140/epja/s10050-020-00090-3>
321. Agrawal et al (2018) Fractal information theory (FIT) derived geometry musical language (GML) for brain-inspired hypercomputing. In: Soft computing: theories and application, Advances in intelligent systems and computing, vol 584. Springer Nature, Singapore Pte Ltd
322. Sahu S, Ghosh S, Ghosh B, Aswani K, Hirata K, Fujita D, Bandyopadhyay A (2013) Atomic water channel controlling remarkable properties of a single brain microtubule: Correlating single protein to its supramolecular assembly. Biosens Bioelectron 47(2013):141–148. <https://doi.org/10.1016/j.bios.2013.02.050>

323. Sahu S, Ghosh S, Fujita D, Bandyopadhyay A (2015) Live visualizations of single isolated tubulin protein self-assembly via tunneling current: effect of electromagnetic pumping during spontaneous growth of microtubule. *Sci Rep* 4(1). <https://doi.org/10.1038/srep07303>
324. Agrawal L, Sahu S, Ghosh S, Shiga T, Fujita D, Bandyopadhyai A (2016) Inventing atomic resolution scanning dielectric microscopy to see a single protein complex operation live at resonance in a neuron without touching or adulterating the cell. *J Integr Neurosci* 15:435–462
325. Purwins H, Blankertz B, and Obermayer K (2007) Toroidal models in tonal theory and pitchclass analysis tonal theory for the digital age. *Comput Musicol* 15:73–98
326. Tozzi A, Peters JF (2017) A symmetric approach elucidates multisensory information integration. *Information* 8:4
327. Tozzi A, Peters J (2017) Plasma-like brain: collective movements in the extracellular nervous spaces. https://www.researchgate.net/publication/304777768_PLASMALIKE_BRAIN_COLLECTIVE_MOVEMENTS_IN_THE_EXTRACELLULAR_NERVOUS_SPACES
328. Van De Bogart WG, Forshaw S (2015) Re-constructing memory using quantized electronic music and a “Toridion byte” quantum algorithm: creating images using zero logic quantum probabilistic neural networks (ZLQNN). <https://www.researchgate.net/publication/281480809>
329. Handler G (2012) Asteroseismology, Copernicus Astronomical Center/arXiv.org, 23 Sept 2019. Available from: <https://arxiv.org/pdf/1205.6407.pdf>
330. Stark G (2017) Adventures in acoustic cosmology. Royal Astronomical Society. Available from: <http://www.binarydust.org/author/admin/>
331. Agrawal L, Chhajed R, Ghosh S, Ghosh B, Kanad R, Sahu S, Daisuke Fujita D, Bandyopadhyay A (2017) Fractal Information Theory (FIT)-derived geometric musical language (GML) for brain-inspired hypercomputing. *Adv Intell Syst Comput* 584:343–372. https://doi.org/10.1007/978-981-10-5699-4_33
332. Savelyev IV et al (2019) On the existence of the DNA resonance code and its possible mechanistic connection to the neural code. *NeuroQuantology* 17:106–121
333. Savelyev I, Myakishev-Rempel M (2019b) Possible traces of resonance signaling in the genome. <http://vixra.org/pdf/1908.0282v2.pdf>
334. Crawford MA, Thabet M, Wang Y (2018) An introduction to the theory on the role of pi-electrons of docosahexanoic acid in brain function. *Quantum Brain OCL* 25:A402
335. Giesa T, Spivak DI, Buehler MJ (2011) Reoccurring patterns in hierarchical protein materials and music: the power of analogies. *BioNanoScience* 1(4)
336. Qin Z, Buehler MJ (2019) Analysis of the vibrational and sound spectrum of over 100,000 protein structures and application in sonification. *ScienceDirect* Available from: <https://www.sciencedirect.com/science/article/pii/S2352431618302414>
337. De la Peña L, Cetto AM (1994) Quantum phenomena and the zero-point radiation field. *Found Phys* 24:6:917–48
338. Hasson U, Ghazanfar AA, Galantucci B, Garrod S, Keysers C (2012) Brain to brain coupling: a mechanism for creating and sharing a social world. *Trends Cogn Sci* 16:114–212
339. Pizz R, Gelain F, Vescovi A (2004) Nonlocal correlations between separated neural networks. *Proc SPIE Int Soc Opt Eng* 5436:107–111
340. Radin DI (2004) Event-related electroencephalographic correlations between isolated human subjects. *J Altern Complement Med* 10(2):315–323
341. Richards TL, Kozak L, Johnson LC, Standish LJ (2005) Replicable functional magnetic resonance imaging evidence of correlated brain signals between physically and sensory isolated subjects. *J Altern Complement Med* 11(6):955–963
342. Standish LJ, Kozak L, Johnson LC, Richards T (2004) Electroencephalographic evidence of correlated event-related signals between the brains of spatially and sensory isolated human subjects. *J Altern Complement Med* 10(2):307–314
343. Wackermann J, Seiter C, Keibel H, Walach H (2003) Correlations between brain electrical activities of two spatially separated human subjects. *Neurosci Lett* 336(1):60–64
344. Hardy CH (2016) ISS theory: cosmic consciousness, self, and life beyond death in a hyperdimensional physics. *J Conscious Explor Res* 7(11):1012–1035

345. Irwin K (2014) A new approach to the hard problem of consciousness: a quasi-crystalline language of primitive units of consciousness in quantized spacetime. *J Conscious Explor Res* 5:483–497
346. Nagel T (2012) Mind and cosmos: why the materialist neo-Darwinian conception of nature is almost certainly false. Oxford New York: Oxford University Press, ISBN 9780199919758
347. Grandpierre A (2014) Does the universe have a physical, biological, or psychological nature? In: brain, mind, cosmos: the nature of our existence and the universe. Sages and Scientists Book
348. Penrose R (1989) The Emperor's New Mind: Concerning computers, minds, and the laws of physics. Oxford University Press
349. Seed A, Emery N, Clayton N (2009) Intelligence in corvids and apes: a case of convergent evolution? *Ethology* 115(5):401–420
350. Roth G (2015) Convergent evolution of complex brains and high intelligence. *Philos Trans R Soc B: Biol Sci* 370:20150049. (The article itself). <https://www.ncbi.nlm.nih.gov/pmc/articles/PMC4650126/pdf/rstb20150049.pdf>
351. Levin M (2012) Molecular bioelectricity in developmental biology: new tools and recent discoveries: control of cell behavior and pattern formation by transmembrane potential gradients. *BioEssays* 34:205–217
352. Samal S, Geckeler KE (2001) Unexpected solute aggregation in water on dilution. *Chem Commun (Camb)* 21:2224–2225
353. Kuhn T (1970) The structure of scientific revolutions, 2nd edn. The University of Chicago Press, ISBN: 0-226-45803-2
354. Goodwin BC (1985) Developing organisms as self-organising fields. In: Mathematical essays on growth and the emergence of form. The university of Alberta Press, pp 185–200
355. Cifra M, Fields JZ, Farhadi A (2010) Electromagnetic cellular interactions. *Progr Biophys Mol Biol* 1–24. <https://doi.org/10.1016/j.pbiomolbio.2010.07.003>
356. Jerman I, Krasovec R, Leskovar RT (2009a) Deep significance of field concept in contemporary biomedical medicine. *Electromagn Biol Med* 28(1):61–70. <https://doi.org/10.1080/15368370802711060>. https://www.researchgate.net/publication/321686137_Evidence_for_biofield
357. Tzambazaki A (2015) The evolution of the biological field concept. https://emmind.net/open_papers_repos/Endogenous_Fields-Mind/General/EM_Various/2015_The_evolution_of_the_biological_field_concept.pdf
358. Jerman I (2017) What nanobacteria and nanovesicles may tell us about the origin of life? *Open Access Libr J* 4(1):1–13
359. Larralde R, Robertson MP, Miller SL (1995) Rates of decomposition of ribose and other sugars: implications for chemical evolution. *Proc Natl Acad Sci* 92(18):8158–8160
360. Jerman I (2018) Emergence of organisms from ordered mesotropic states of water (liquids). Physical instead of chemical origin of life. https://www.researchgate.net/.../Manuscript_18_Jerman_Emergence
361. von Neumann J (1966) The theory of self-reproducing automata. University of Illinois Press, Champaign
362. Aguilar W, Santamaría-Bonfil G, Froese T, Gershenson C (2014) The past, present, and future of artificial life. *Front Robot AI* 1:8
363. Del Giudice E, Preparata G (1998) Electrodynamical like-charge attractions in metastable colloidal crystallites. *Mod Phys Lett B* 12:881–886
364. Vitiello G (2020) Symmetries and metamorphoses. *Symmetry* 12(6):907
365. Oparin AI, Gladilin KL (1980) Evolution of self-assembly of probiotics. *BioSystems* 12:133–145
366. Cairns-Smith AG (2009) An approach to a blueprint for a primitive organism. In: Waddington CH (ed) The origin of life: towards a theoretical biology, vol 1. Aldine Transaction, pp 57–66, ISBN 978-0-202-36302-8
367. Tranter GE (1985) Parity-violating energy differences of chiral minerals and the origin of biomolecular homochirality. *Nature* 318:172–173

368. Sarfatti A (2015) Bohm Pilot wave post quantum theory. https://www.academia.edu/27132022/Bohm_Pilot_Wave_Post-Quantum_Theory
369. Sbitnev VI (2016a) Dark matter is a manifestation of the vacuum Bose-Einstein condensate. <https://arxiv.org/pdf/1601.04536.pdf>
370. Sbitnev VI (2016b) Quantum consciousness in warm, wet, and noisy brain. *Modern Phys Lett B* 30. <https://arxiv.org/abs/1606.00258>
371. Sbitnev VI (2016c) Hydrodynamics of the physical vacuum: I. Scalar quantum sector. *Found Phys* 46(5):606–619. <https://arxiv.org/abs/1504.07497>
372. Melkikh AV (2014) Congenital programs of the behavior and nontrivial quantum effects in the neurons work. *Biosystems* 119:10–19
373. Melkikh AV, Sutormina MI (2019) Protocells and LUCA: transport of substances from first physicochemical principles. *Prog Biophys Mol Biol* 150:184–202
374. Melkikh AV, Sutormina MI (2020) Intra- and intercellular transport of substances: models and mechanisms. *Prog Biophys Mol Biol* 150:184–202
375. England JL, Park S, Pande VS (2008) Theory for an order-driven disruption of the liquid state in water. *J Chem Phys* 128:044503
376. Tamulis A, Grigalavicius M (2011) Quantum entanglement in photoactive prebiotic systems. *Orig Life Evol Biosph* 41:51–71
377. Cronhjort MB, Blomberg C (1997) Cluster compartmentalization may provide resistance to parasites for catalytic networks. *Physica D: Nonlinear Phenomena* 101(3, 4):289–298
378. Kauffman SA (2000) Investigations. Oxford University Press
379. Melkikh AV (2018) The universe as a superorganism. *Int J Astrobiol Aerobiosc Technol. IJAAAT-104*. <https://doi.org/10.29011/ijaat-104> 100004
380. Melkikh AV, Khrennikov A (2017b) Molecular recognition of the environment and mechanisms of the origin of species in quantum-like modeling of evolution. *Progr Biophys Mol Biol* 130(Part A):61–79
381. Melkikh AV, Mahecha DS (2017) On the broader sense of life and evolution: its mechanisms, origin and probability across the universe. *J Astrobiol Outreach* 5(3):1–13
382. Jerman I (1998) Electromagnetic origin of life. *Electro Magnetobiol* 17(3): 401–413. https://www.researchgate.net/publication/232054835_Electromagnetic-Origin_of_Life
383. Miller WB, Tordy JS, Baluska F (2019) Biological evolution of defense of self. *Prog Biophys Mol Biol* 142:54–74. <https://doi.org/10.1016/j.pbiomolbio.2018.10.002>, <https://pubmed.ncbi.nlm.nih.gov/30336184/>
384. Melkikh AV (2014) Quantum information and the problem of mechanisms of biological evolution. *BioSystems* 115:33–45
385. Melkikh AV (2015) Paradoxes of early stages of evolution of life and biological complexity. *Orig Life Evolut Biosph* 45(1):163–171
386. Melkikh AV (2014) The no free lunch theorem and hypothesis of instinctive animal behavior. *Artif Intel Res* 3(4):43–63
387. Melkikh AV, Khrennikov A, Yampolsky R (2019) Quantum metalanguage and the new cognitive synthesis. *Neuroquantology* 17(1):50–74
388. Fedi M (2016) A superfluid theory of everything. <https://hal.archives-ouvertes.fr/hal-01312579v2/document>
389. Fedi M (2016) Gravity as a fluid dynamic phenomenon in a superfluid quantum space. *Fluid Quantum Gravit Relativ.* <https://hal.archives-ouvertes.fr/hal-01248015v4>
390. Sbitnev VI, Fedi M (2017) Superfluid quantum space and evolution of the universe. In: Souza AJCD (eds) Trends in modern cosmology, Rijeka, InTech, pp 89–112. https://www.researchgate.net/publication/317419096_Superfluid_Quantum_Space_and_Evolution_of_the_Universe
391. Dirac PAM (1945) On the analogy between classical and quantum mechanics. *Rev Mod Phys* 17:195
392. Šorli AS (2019) Mass–energy equivalence extension onto a superfluid quantum vacuum. *Nat Sci Rep* 9:11737

393. Sbitnev VI (2012) chap. 15. In: Pahlavani MR (ed) Theoretical concepts of quantum mechanics. InTech, Rijeka, pp 313–334
394. Sbitnev VI (2012) Bohmian trajectories and the path integral paradigm—complexified lagrangian mechanics. In: Pahlavani MR (ed) Theoretical concepts of quantum mechanics. InTech, Rijeka, pp 313–334
395. Sbitnev VI (2013a) Generalized path integral technique: Nanoparticles incident or slit grating matter wave interference. In: Bracken P (ed) Advances in quantum mechanics. InTech, Rijeka, chap. 9, pp 183–211
396. Sbitnev VI (2015) Chapter 12. In: Pahlavani MR (ed) Selected topics in applications of quantum mechanics. InTech, Rijeka, pp 345–373
397. Sbitnev VA (2017) Hydrodynamics of superfluid quantum space: de Broglie interpretation of quantum mechanics. <https://arxiv.org/abs/1707.08508>
398. Baars BJ, Franklin S, Zoëge Ramsoy T (2013) Global workspace dynamics: cortical “binding and propagation” enables conscious contents. *Front Psychol* 4:200
399. Cacha LA, Poznanski RR (2014) Genomic instantiation of consciousness in neurons through biophoton field theory. *J Integr Neurosci* 13:253–292
400. Beck F, Eccles JC (1992) Quantum aspects of brain activity and the role of consciousness. *Proc Natl Acad Sci USA* 89(23):11357–11361
401. Goodman G, Poznanski RR, Cacha L, Bercovich D (2015) The two-brains hypothesis: towards a guide for brain-brain and brain-machine interactions. *J Integr Neurosci* 14:1–13
402. Ho MW (2012) Super-conducting liquid crystalline water aligned with collagen fibres in the fascia as acupuncture meridians of traditional Chinese medicine. *Forum Immunopathol Dis Ther* 3:221–236
403. Kumar S et al (2016) Possible existenc of optical communication channels in the brain. *Nature Scientific Reports* 6:36508
404. Schwartz SA (2013) Crossing the threshold: non-local consciousness and the burden of proof. *Explore* 9:77–81
405. Penrose R (2014) On the gravitization of quantum mechanics 1: quantum state reduction. *Found Phys* 44:557–575
406. Tegmark M (2000) The importance of quantum decoherence in brain processes. *Phys Rev E* 61:4194
407. Hameroff S, Penrose R (2011) Consciousness in the universe: neuroscience, quantum space-time geometry and orch or theory. *Cosmol Conscious Quantum Phys Neurosci Mind* 14:51–102
408. Hameroff S, Penrose R (2014) Consciousness in the universe: a review of the ‘Orch OR’ theor. *Phys Life Rev* 11(1):39–78
409. Tuszyński JA (2014) The need for a physical basis of cognitive process: comment on “Consciousness in the universe. A Review of the ‘Orch OR’ theory” by Hameroff and Penrose. *Phys Life Rev* 11:79
410. Chua LO (2011) Resistance switching memories are memristors. *Appl Phys A* 102:765–783
411. Allakhverdov VM (2000) Consciousness as a paradox. Experimental psychologic. St.-Petersburg, Russia: Publ. DNK
412. Bell RP (1973) The proton in chemistry, 2nd edn. Springer USA, p 21
413. Bell RP (1959) The proton in chemistry. Cornell University Press, Ithaca
414. Albareti FD, Cembranos JAR, Maroto AL (2014) The large scale structure of tha vacuum. *Int J Mod Phys D* 23:7 (1442019)
415. Bohm D (1952) Wholeness and the implicate order. Routledge & Kegan Paul, London
416. De Broglie L (1987) Interpretation of quantum mechanics by double solution theory. *Annales de la Fondation Louis de Broglie* 12:1
417. Dudkin AO, Sbitnev VI (1998) Coupled map lattice simulation of epileptogenesis in hippocampal slices. *Biol Cybern* 78:479
418. Chaplin M (2016) Water structure and science: Grotthuss mechanism. Available: <http://www1.lsbu.ac.uk/water/grotthuss.html#r2116>. Accessed 16 Mar 2016

419. Messori C (2019) Deep into water: exploring the hydro-electromgnetic and quantum-electrodynamic properties of interfacial water in living systems. *Open Acces Library J* 6:e5435
420. DeCoursey TE (2003) Voltage-gated proton channels and other proton transfer pathways. *Physiol Rev* 83(2):475–579
421. Hassanali A, Giberti F, Cuny J, Kühne TD, Parrinell M (2013) Proton transfer through the water gossamer. *PNAS* 110(34):13723–13728
422. Brady R, Anderson R (2014) Why bouncing droplets are a pretty good model of quantum mechanics. <http://arxiv.org/abs/1401.4356>
423. Wilson WD (1960) Speed of sound in sea water as a function of temperature, pressure, and salinity. *J Acoust Soc Am* 32(6):641
424. Pollack GH (2013) The fourth phase of water: beyond solid, liquid, and vapor. Ebner and Sons Publ., Seattle, pp 98105
425. Agnon N (1995) The Grotthuss mechanism. *Chem Phys Lett* 244(5–6):456–462
426. Peng Y, Swanson JMJ, Kang SG, Zhou R, Voth GA (2015) Hydrated excess protons can create their own water wires. *J Phys Chem B* 119(29):9212–9218
427. Atkins P, de Paula J, Friedman R (2009) Quanta, matter, and charge: a molecular approach to physical chemistry. W. H. Freeman, New York
428. Brewer ML, Schmitt UW, Voth GA (2001) The formation and dynamics of proton wires in channel environments. *Biophys J* 80(4):1691–1702
429. Miller CC (1924) The Stokes-Einstein law for diffusion in solution. *Proc R Soc Lond. Ser A* 106(740):724–749
430. Nelson E (1985) Quantum fluctuations. Princeton University Press, Princeton
431. Nelson E (1966) Derivation of the Schrodinger equation from Newtonian Mechanics. *Phys Rev* 150:1079–1085
432. Penrose R, Hameroff S (2011) Consciousness in the Universe. *J Cosmol* 14. <http://journalofcosmology.com/Consciousness160.html>
433. Tarlaci S (2013) What should a consciousness-mind-brain theory be like? Reducing the secret of the rainbow to the colours of a prism. *NeuroQuantology* 11(2):360–377
434. Lighthill MJ (1986) An informal introduction to theoretical fluid mechanic. Oxford University Press, Oxford
435. Benseñy A, Albareda G, Sanz AS, Mompart J, Oriols X (2014) Applied Bohmian mechanics. *Eur Phys J D* 68:286–328
436. Kundu P, Cohen I (2002) Fluid Mechanics. Academic Press, San Diego
437. Martins AA, Pinheiro MJ (2009) Fluidic electrodynamics: approach to electromagnetic propulsion. *Phys Fluids* 21:097103
438. Martins AA (2012) Fluidic electrodynamics: on parallels between electromagnetic and fluidic inertia. 21 February. Available: <http://arxiv.org/abs/1202.4611>
439. Derbes D (1966) Feynman's derivation of the Schrodinger equation. *Am J Phys* 64(7):881–884
440. Feynman RP, Hibbs A (1965) Quantum mechanics and path integrals. McGraw Hill, New York
441. Hameroff S, Penrose R (2014) Reply to seven commentaries on “consciousness in the universe: review of the ‘Orch OR’ theory. *Phys Life Rev* 11(1):94–100
442. Hameroff S, Penrose R (2014) Reply to criticism of the ‘Orch OR qubit’—‘Orchestrated objective reduction’ is scientifically justified. *Phys Life Rev* 11(1):104–112
443. Tuszyński JA et al (2019) Microtubules as sub-cellular memristors, submitted for publication
444. Connors BW, Long MA (2004) Electrical synapses in the mammalian brain. *Ann Rev Neurosci* 27:393–418
445. Söhl G, Maxeiner S, Willecke K (2005) Expression and functions of neuronal gap junctions. *Nat Rev Neurosci* 6:191–199
446. Meier C, Dermietzel R (2006) Electrical synapses—gap junctions in the brain. In: Eckart D, Seidenbecher C, Schraven B, Gundelfinger (eds) Cell communication in nervous and immune system. Springer, Berlin, pp 99–128
447. Berg JM, Tymoczko JL, Stryer L (2002) Biochemistry, 5th edn. W. H. Freeman, New York

448. Zampighi G (1987) Gap junction structure. Cell-to-Cell communication. Plenum Press, New York, pp 1–28
449. Hameroff S (1998) Quantum computation in brain microtubules? The Penrose-Hameroff ‘Orch OR’ model of consciousness. *Phil Trans R Soc Lond A* 356:1896–1896
450. Volman V, Perc M, Bazhenov M (2011) Gap junctions and epileptic seizures—two sides of the same coin? *PLoS ONE* 6(5):e20572
451. Nagy JI, Dudek FE, Rash JE (2004) Update on connexins and gap junctions in neurons and glia in the mammalian nervous system. *Brain Res Rev* 47:191–215
452. Maxwell RW (2009) Neurobiology of chakras and prayer. *Zygon* 44(4):807–824
453. Jin M-M, Zhong C (2011) Role of gap junctions in epilepsy. *Neurosci Bull* 27(6):389–406
454. Nemani VM, Binder DK (2005) Emerging role of gap junctions in epilepsy. *Histol Histopathol* 20:253–259
455. Mitterauer BJ (2014) Pathophysiology of Schizophrenia based on impaired Glial-Neuronal interactions. *Open J Med Psychol* 3(2):126–140
456. Wang X-J (2010) Neurophysiological and computational principles of cortical rhythms in cognition. *Physiol Rev* 90(3):1195–1268
457. Ciufolini I, Wheeler JA (1995) Gravitation and inertia. Princeton University Press, Princeton, New Jersey
458. Nader T (2015) Consciousness is all there is. *Int J Math Conscious* 1:1
459. Wheeler JA, Feynman RP (1945) Interaction with the absorber as a mechanism of radiation. *Rev Mod Phys* 17:157–181
460. Cramer JG (1986) The transactional interpretation of quantum mechanics. *Rev Mod Phys* 58:647–688
461. Baconnier S, Lang SB (2004) Calcite microcrystals in the pineal gland of the human brain: second harmonic generators and possible piezoelectric transducers. *IEEE Trans Dielectr Electr Insul* 11(2):201–209
462. Golubev SN, Golubev SS (2009) Sight at the physical microcosm from the position of the biologist. (Dalnauka, Vladivostok; in Russian). http://www.chronos.msu.ru/old/RREPORTS/golubevy_mikromir.pdf
463. Kryukov V (2008) The role of the hippocampus in long-term memory: is it memory store or comparator. *J Integr Neurosci* 7(1):117–84. <https://doi.org/10.1142/s021963520800171x>
464. Vinogradova OS (1975) The hippocampus and memory. Nauka, Moscow
465. Saura CA, Parra-Damas A, Enriquez-Barreto L (2015) Gene expression parallels synaptic excitability and plasticity changes in Alzheimer’s disease. *Front Cell Neurosci* 25 August 2015; doi: <https://doi.org/10.3389/fncel.2015.00318>
466. iNeuronLab (2017) Hippocampal circuits. CC Attribution-Share Alike 4.0 International
467. Lacaille J-C, Schwartzkroin PA (1988) Striatum lacunosum-molecular interneurones of hippocampal CA1 region. 2. Intrasomatic and intradendritic recordings of local circuit synaptic interactions. *J Neurosci* 8:1411–1424
468. Williams S, Samulack DD, Beaulieu C, Lacaille J-C (1994) Membrane properties and synaptic responses of interneurons located near the stratum lacunosum-moleculare/radiatum border of area CA1 in whole-cell recordings from rat hippocampal slices. *J Neurophys* 71:2217–2235
469. Manns JR, Eichenbaum H (2009) A cognitive map for object memory in the hippocampus. *Learn Mem* 16:616–624. <https://doi.org/10.1101/lm.1484509>
470. Bandyopadhyay A (2019) Resonance chains and new models of the neuron. <https://medium.com/@aramis720/resonance-chains-and-new-models-of-the-neuron-7dd82a5a7c3a>
471. Eccles J, Feindel W (1978) Wilder Graves Penfield, 26 January 1891–5 April 1976. *Biogr Mem Fellows R Soc* 24:472–513. <https://doi.org/10.1098/rsbm.1978.0015>
472. Blom JD (2009) A dictionary of hallucinations. Springer Science & Business Media. pp 1–51. <https://doi.org/10.1007/978-1-4419-1223-7>
473. Tong F (2003) Out-of-body experiences: from Penfield to present. *Trend Cognit Sci* 7(3):104–106. [https://doi.org/10.1016/s1364-6613\(03\)00027-5](https://doi.org/10.1016/s1364-6613(03)00027-5)
474. Penfield Wi (1952) Memory mechanisms. *Archives of neurology and psychiatry* 67(2):178–198. <https://doi.org/10.1001/archneurpsyc.1952.02320140046005>

475. Deli E, Tozzi A, Peters JF (2017) Relationship between short and fast brain timescales. *Cogn Neurodyn* 11:539–552
476. Craddock TJA, Tuszyński JA, Hameroff S (2012) Cytoskeletal signaling: is memory encoded in microtubule lattices by CaMKII phosphorylation? *PLoS Comput Biol* 8:e1002421
477. Pereira A (2007) Astrocyte-trapped calcium ions: the hypothesis of a quantum-like conscious protectorate. *Quantum Biosyst* 2:80–92
478. Pereira A (2007) Astrocyte-trapped calcium ions: the hypothesis of a quantum-like conscious protectorate. *Quantum Biosystems* 2:80–92
479. Pereira A, Furlan FA (2007) Biomolecular information, brain activity and cognitive function. *ARBS Ann Rev Biomed Sci* 9:12–29
480. Pall ML (2013) Electromagnetic fields act via activation of voltage-gated calcium channels to produce beneficial or adverse effects. *J Cell Mol Med* 17:958–965
481. Bull C, Freitas KC, Zou S, Poland RS, Syed WA, Urban DJ, Minter SC, Shelton KL, Hauser KF, Negus SS, Knapp PE, Bowers MS (2014) Rat nucleus accumbens core astrocytes modulate reward and the motivation to self-administer ethanol after abstinence. *Neuropsychopharmacology* 39:2835–2845 [PubMed: 24903651]
482. Han X et al (2013) Forebrain engraftment by human glial progenitor cells enhances synaptic plasticity and learning in adult mice. *Cell Stem Cell* 12(3):342–353. 7 Mar 2013, <https://doi.org/10.1016/j.stem.2012.12.015>, <https://www.ncbi.nlm.nih.gov/pmc/articles/PMC3700554/>
483. Tang A, Wang S (2009) Transition of spiral calcium waves between multiple state patterns can be triggered by single calcium spark in the fire-diffuse-fire model. *CHAOS* 19:037114
484. Nunn C (2010) Landscape of mentality, consciousness and time. *J Conscious Explor Res* 1:516–528
485. Fisher MPA (2015) Quantum cognition: the possibility of processing with nuclear spin. 29 Aug 2015. [arXiv:1508.05929v2](https://arxiv.org/abs/1508.05929v2) [q-bio.NC]
486. Dehaene S, Sergent C, Changeux, JP (2003) A neuronal network model linking subjective reports and objective physiological data during conscious perception. *Proc Natl Acad Sci* 14: 8520–8525
487. Tononi G (2008) Consciousness as integrated information: a provisional manifesto. *Biol Bull* 215:216–242
488. Rizvi SIM (2018) Quantum mechanics of ‘conscious energy’. *Int J Mind Brain Cogn* 9(1, 2):132–160
489. Verlinde EP (2016) Emergent gravity and dark Universe. <https://arxiv.org/abs/1611.02269>
490. Brandenburg JE, Hardy CH (2016) Entropic gravity in pre-spacetime & the ISS theory of a cosmic information field. *Pre-spacetime J* 7:828–838
491. Pribram KH (2014) Consciousness reassessed. *Mind Matter* 2:7–35. philpapers.org/rec/PRICR
492. Mitchell ED, Staretz R (2011) The quantum hologram and the nature of consciousness. *J Cosmol* 14:1–35
493. Irwin K (2017) Eight things as first principles theory of everything should posses. <https://www.semanticscholar.org/paper/Eight-Things-a-First-Principles-Theory-of-Should-Irwin/bc0b5a9dc19466a27151399fdf24b257d8bb121>
494. Irwin K (2017) Quantum walk on a spin network and the golden ratio as the fundamental constant of nature. https://www.researchgate.net/publication/316554631_Quantum_Walk_on_a_Spin_Network_and_the_Golden_Ratio_as_the_Fundamental_Constant_of_Nature
495. Irwin K (2020) The self-simulation hypothesis interpretation of quantum mechanics. *Entropy* 22(2):247. <https://doi.org/10.3390/e22020247> <https://www.mdpi.com/1099-4300/22/2/247>
496. Irwin K (2019) Towards the unification of physics and number theory. *Rep Adv Phys Sci* 3:1950003
497. Brueck DL, Meijer DKF (2020) A new premise for quantum physics, consciousness and the fabric of reality, submitted for publication
498. Loll R, Ambjorn J, Jurkiewicz J (2005) The Universe from Scratch. [arXiv:hep-th/0509010](https://arxiv.org/abs/hep-th/0509010)
499. Bechler JE (2012a) The evolutionary imperative of consciousness. *J Biol Phys* 38:113–120

500. Haramein N, Rauscher EA (2007) Spinors, twistors, quaternions and the spacetime torus topology. *Int J Comput Anticip Syst*, pp 1–18
501. Amoroso RL (1999) An introduction to the noetic field theory: the quantization of mind. *Noetic J* 2:18–37
502. Atasoy S, Donnelly I, Pearson J (2016) Human brain networks function in connectome-specific harmonic waves. *Nat Commun* 7:1–10. <https://doi.org/10.1038/ncomms10340>
503. Atasoy S, Roseman L, Kaelen M, Kringlebach ML, Deco G, Carhart-Harris R (2017) Connectome-harmonic decomposition of human brain activity reveals dynamical repertoire reorganization under LSD. *BioRxiv*, 1–55. <http://doi.org/10.1101/163667>
504. Joye SR (2016) The Pribram-Bohm holoflux theory of consciousness: an integral interpretation of the theories of Karl Pribram, David Bohm and Pierre Teilhard de Chardin. *Cosmos and History: J Nat Soc Philos* 12(2):2016
505. Deli E (2017) Consciousness, a cosmic phenomenon—a hypothesis. *God J* 8:24–42
506. Andersen SSL, Jackson AD, Heimburg T (2009) Towards a thermodynamic theory of pulse propagation. *Progr Neurol* 88:104–113
507. Kraikivsky P (2019) Systems of oscillators designed for a specific conscious percept, <https://arxiv.org/abs/1903.02594>
508. Fingelkurts AA, Fingelkurts AA, Neves CFH (2010) Emergent monism, biological realism, operation and brain-mind problem. *Phys Life Rev* 7:264–268
509. Fingelkurts AA, Fingelkurts A (2014) Present moment, past and future: mental kaleidoscope. *Front Psychol*
510. Kida T, Tanaka E, Kakigi R (2016) Multi-dimensional dynamics of human electromagnetic brain activity. *Front Human Neurosci* 9:1–20
511. Pereira A, Nunn C, Pregnolato M, Nixon G (2018) Consciousness and cosmos. Building an ontological framework. *J Conscious Stud* 25(3, 4):181–205. https://www.researchgate.net/publication/319632327_Consciousness_and_Cosmos_Building_an_Ontological_Framework
512. Poznanski RR, Cacha LA, Latif AZ, Salleh SH, Ali J, Yupapin P, Tuszynski JA, Tengku MA (2019) Theorizing how the brain encodes consciousness based on negentropic entanglement. *J Integr Neurosci* 18(1):1–10
513. Poznanski RR, Cacha LA, Latif AZA, Salleh SH, Ali J, Yupapin P, Tuszynski JA, Tengku MA (2018) Spontaneous potentiality as formative cause of thermo-quantum consciousness. *J Integr Neurosci* 17:371–385
514. Cacha LA, Ali J, Rizvi ZH, Yupapin PP, Poznanski RR (2017) Non-synaptic plasticity model of long-term memory. *J Integr Neurosci* 16:493–509
515. Tressoldi P, Facco E, Lucangeli D (2016) Emergence of qualia from brain activity or from an interaction of protoconsciousness with the brain: which one is the weirder? Available evidence and a research agenda https://www.scienceopen.com/document_file/582a2cc6-0249-43b1-ae9f-91dcd27ae34a/ScienceOpen/3752_XE510976944243037072.pdf
516. Williford K, Bennequin D, Friston K, Rudrauf D (2018) The projective consciousness model and phenomenal selfhood. *Front Psychol* 9, article 2571
518. Pletcher AE (2019) Quantum cosmology and the role of consciousness. *NeuroQuantology* 17(01):104–111. <https://doi.org/10.14704/nq.2019.17.01.1934>
518. Libet B (1996) Conscious mind as a field. *J Theor Biol* 178:223–224
519. Bradley RT (2018) The psychophysiology of intuition: A quantum-holographic theory of nonlocal communication. *World Futur* 63(2):61–97 <https://philpapers.org/rec/BRATPO-2>
520. Di Biase F (2009) Quantum-Holographic informational consciousness *neuroQuantology* 7(4). <https://doi.org/10.14704/nq.2009.7.4.259>
521. Faggin F (2014) A framework for the union of science and spirituality. <http://www.fagginfofoundation.org/articles-2/a-conceptual-framework-for-the-union-of-science-and-spirituality-2/>
522. Bohm D, Peat FD (2008) Science, order and creativity, 2nd edn. Routledge, London (transferred to digital printing, Routledge): ISBN 0-415-17182-2
523. Tozzi A, Peters JF, Jaušovec N (2017) Repetitive modular oscillation underlies human brain electric activity. <http://biorxiv.org/content/biorxiv/early/2016/08/31/072538.full.pdf>

524. Greyson B (2013) Nature of mind and consciousness. Is consciousness produced by the brain? http://sfm.scienceformonks.org/SciencePrograms/MonasticGraduates/Conference/CosmologyAndConsciousnessI/Resources/Text_Is_Consciousness_Produced.pdf
525. Carr BJ (2017) Quantum Blackholes as the link between microphysics and mactophysics. *Proc Phys* 208:85–94. [arXiv:1703.08655](https://arxiv.org/abs/1703.08655) [gr-qc].
526. Lichfiled (2015) The science of near-death experiences. Empirically investigating brushes with afterlife. <https://www.theatlantic.com/magazine/archive/2015/04/the-science-of-near-death-experiences/386231/>
527. McGillchrist I (2009) The master and his emissary: the divided brain and the making of the western world. Yale University Press, New Haven. See for interview and discussion also: Divided Brain, Divided world, why the best part of us struggles to be heard. RSA Centre Brain Project
528. Steinhardt PJ, Turok N (2002) Cosmic evolution in a cyclic universe. *Phys Rev D* 65(12):126003. Bibcode:2002PhRvD.65l6003S, [arXiv:hep-th/0111098](https://arxiv.org/abs/hep-th/0111098). <https://doi.org/10.1103/physrevd.65.126003>
529. Penrose R (2010) Cycles of time: an extraordinary new view of the universe. The Bodley Head, London. ISBN 978-0-224-08036-1
530. Kurzweil R (2005) The singularity is near: when humans transcend biology, 1st edn., Kindle edition. Penguin Books, p 965, 22 Sept 2005
531. Chalmers DJ (2018) The meta-problem of consciousness. *J Conscious Stud* 25:6–61
532. Zeilinger A (2003) Quantum teleportation. *Scientific Am.* 8–16 Feb. Update: <http://www.univie.ac.at/qfp/publications3/pdffiles/2003-24.pdf>
533. Zeilinger A (2003) Why the quantum? It from bit? A participatory universe? Three far-reaching, visionary challenges from John Archibald wheeler and how they inspired a quantum experimentalist. Harper, Templeton Foundation Press, Charles L
534. Tononi G, Koch C (2015) Consciousness: here, there and everywhere? *Philos Trans R Soc* 370
535. Pereira C (2015) Electromagnetic radiation, a living cell and the soul, a collated hypothesis. *NeuroQuantology* 13:426–438
536. Pagnolato M, Pereira A (2016) On the possible existence of quantum consciousness after death. *J Conscious Explor Res* 7:969–991
537. Vidal C (2014) The beginning and the end: The meaning of life in a cosmological perspective. https://www.researchgate.net/publication/282286323_The_Beginning_and_End_The_Meaning_of_Life_in_a_Cosmological_Perspective
538. Adey WR (1993) Biological effects of electromagnetic fields. *J Cell Biochem* 51: 410–416
539. Akhmet MA, Fen MO (2014) Generation of cyclic/toroidal chaos by Hopfield Neural Networks. *Neurocomputing* 145:230–239
540. Atwood D (1999) Graviton production by two photon and electron-photon processes in Kaluza-Klein theories with large extra dimensions. <http://arxiv.org/abs/hep-ph/9909392>
541. Auletta G, Ellis GFR, Jaeger L (2008) Top-down causation by information control: from a philosophical problem to a scientific research programme. *J R Soc Interface* 5(27)
542. Aurich R, Janzer HS, Lustig S, Steiner F (2008) Do we live in a small universe? *Class Quant Grav.* arxiv.org/abs/0708.1420
543. Baez J, Vicary J (2014) Wormholes and entanglement. *Class Quantum Gravity* 31:11
544. Beck F (2008) Synaptic quantum tunnelling in brain activity. *NeuroQuantology* 6:140–151
545. Belousov LV, Opitz JM, Gilbert SF (2004) Life of Alexander G. Gurwitsch and his relevant contribution to the theory of morphogenetic fields. *Int J Dev Biol* 41(6):771–777
546. Berkovich-Ohana A, Glicksohn J (2014) The consciousness state space (CSS)—a unifying model for consciousness and self. *Front Psychol*
547. Bérut A et al (2012) Experimental verification of Landauer's principle linking information and thermodynamics. *Nature* 483:187–190
548. Bono I, Del Giudice E, Gamberale L, Henry M (2012) Emergence of the coherent structure of water. *Water* 4:510–532

549. Burke RC, Persinger MA (2013) Convergent quantitative solutions indicating the human hippocampus as singularity and access to cosmological consciousness. *Neuroquantology* 11:1–7
550. Chai S, Pollack GH (2010) Solute-free interfacial zones in polar liquids. *Phys Chem B* 114:5371
551. Campbell RJ, Bickhard MH (2010) Physicalism, emergence and downward causation. <http://www.lehigh.edu/~mhb0/physicalemergence.pdf>
552. Carhart-Harris RL, Friston KJ (2010) The default-mode, ego-function and free energy: a neurobiological account of Freudian ideas. *Brain* 133:1265–1283
553. Cayce E. Wiki. https://en.wikipedia.org/wiki/Edgar_Cayce
554. Chaplin MF (2000) A proposal for the structuring of water. *Biophys Chem* 24, 83(3):211–21
555. Couder Y, Fort E (2006) Single-particle diffraction and interference at a macroscopic scale. *Phys Rev Lett* 97:154101
556. Craddock TJA, Friesen D, Mane J, Hameroff S, Tuszyński J (2014) The feasibility of coherent energy transfer in microtubules. *J R Soc Int* 11. Article ID: 2014067
557. Craddock TJA, Friesen D, Mane J, Hameroff S, Tuszyński J (2014) The feasibility of coherent energy transfer in microtubules. *J R Soc Interf* 11. Article ID: 2014067
558. Daywitt WC (2009) The planck vacuum. *Progr Phys* 1:20–26
559. DeliE TA, Peters JF (2017) Relationship between short and fast brain timescales. *Cogn Neurodyn* 11:539–552
560. Dirac PAM (1933) The lagrangian in quantum mechanics. *Physikalische Zeitschrift der Sowjetunion* 3:64
561. Dupays A, Lamine B, Blachard A (2013) Can dark energy merge from quantum effects in a compact extra dimension? *Astron Astrophys*. <https://arxiv.org/pdf/1301.1763.pdf>
562. Eddi A, Sultan E, Moukhtar J, Fort E, Rossi YM, Couder J (2011) From bouncing to floating: noncoalescence of drops on a fluid bath. *Fluid Mech* 674:433
563. England JL (2015) Dissipative adaptation in driven self-assembly. *Nat Nanotechnol* 10:919–923
564. Ehresmann B, Burmeister S, Wimmer-Schweingruber R, Reitz G (2011) Influence of higher atmospheric pressure on the Martian radiation environment: implications for possible habitability in the Noachian epoch. *J Geophys Res (Space Phys)* 116(A15):10,106
565. Fedi M, Sbitnev VI (2017) Superfluid quantum space and evolution of the universe. Sbitnev VI, Fedi M (eds). <http://dx.doi.org/10.5772/68113> <https://cdn.intechopen.com/pdfs/54849.pdf>
566. Feynman RP (1948) Space-time approach to non-relativistic quantum mechanics. *Rev Mod Phys* 20:367
567. Finkelkurts A, Finkelkurts A, Neves Carlos FH (2009) Phenomenological architecture of a mind and operational architectonics of the brain: the unified metastable continuum. *J New Math Nat Comput* 5(1):221–244
568. Fiscaletti D (2012) The geometrodynamical nature of the quantum potential. *Ukr J Phys* 57:560
569. Freeman WJ, Vitiello G (2006) Nonlinear brain dynamics as macroscopic manifestation of underlying many-body field dynamics. *Phys Life Rev* 3:93–118
570. Fremling M (2013) Coherent state wave functions on a torus with a constant magnetic field. *J Phys A: Math Theor* 46(27)
571. Frohlich F (2014) Endogenous and Exogenous electric fields as modifiers of brain activity: rational design of non-invasive brain stimulation with transcranial alternating current stimulation. *Dialogues Clin Neurosci* 16:93–102
572. Graham TM, Bernstein HJ, Wei TC, Junge M, Kwiat PG (2014) Superdense teleportation using hyperentangled photons. *Nat Commun* 6:7185. <https://doi.org/10.1038/ncomms8185>
573. Green BR, Levin J (2007) Dark energy and stabilization of extra dimensions. [arXiv:0707.1062v2 \[hep-th\]](https://arxiv.org/abs/0707.1062v2)
574. Gregorcic A, Jerman I (2009) On the structure of the theoretical evolutionary space in relation to biological laws. https://www.researchgate.net/publication/44658843_On_the_structure_of_theoretical_evolutionary_space_in_relation_to_biological_laws

575. Grygiel WF (2018) On the adequacy of qualifying Penrose as a complex Pythagorean. zfn.edu.pl/index.php/zfn/article/download/439/462/
576. Hameroff S (2014) Consciousness, microtubules, & ‘Orch OR’: a ‘space-time odyssey’. *J Conscious Stud* 21:126
577. Hameroff S (2012) How quantum brain biology can rescue conscious free will. *Front Integr Neurosci* 6:1–17
578. Haramein N, Val Baker A (2019) Resolving the vacuum catastrophe: a generalized holographic approach. *J High Energy Phys Gravitat Cosmol* 5:412–425
579. Hawking S (1988) A brief history of time. https://www.goodreads.com/book/show/3869.A_Brief_History_of_Time
580. Hodgkin AL, Huxley AF (1952) A quantitative description of membrane current and its application to conduction and excitation in nerve. *J Physiol (London)* 117:500
581. Heine L et al (2012) Resting state networks and consciousness. *Front Psychol* 3:1–12
582. Hiller J (2019) Space, time and consciousness. https://www.nderf.org/NDERF/Articles/space_time.pdf
583. Ho M-W (2015) Illuminating water and life: in Emilio Del Giudice *Electromagn Biol Med*, Early Online: 1–10 Informa Healthcare USA, Inc. <https://doi.org/10.3109/15368378.2015.1036079>
584. Hu H, Wu M (2007) Spin-mediated consciousness: theory, experimental studies, further developments & related topics. arXiv.org>quant-ph. [arXiv:quant-ph/0208068](https://arxiv.org/abs/0707.1081)
585. Huang K (2013) Dark energy and dark matter in a superfluid universe. <https://arxiv.org/abs/1309.5707>
586. Jackiw RV, Nair P, Pi S-Y, Polychronakos AP (2004) Perfect fluid theory and its extensions. *J Phys A* 37:R327
587. Jerman I, Dovc P, Ratajc P, Krapez V (2009b) Existence, nature and significance of biological field (the biofield). <https://www.researchgate.net/project/Existence-nature-and-significance-of-biological-field-the-biofield>
588. Jishi RA (2013) Feynman diagram techniques in condensed matter physics. Cambridge University Press, Cambridge; Jung CG (2008) Synchronicity: an causal connecting principle. Routledge, East Sussex
589. Johnson K (2019) Cosmic water nanoclusters: a possible common origin of dark matter and dark energy. https://www.researchgate.net/publication/331903636_Cosmic_water_nanoclusters_a_possible_common_origin_of_dark_matter_and_dark_energy
590. Jumper CC, Scholes GD (2014) Life—warm, wet and noisy? *Phys Life Rev* 11:85
591. Kim D, Bowman C, Bonis-O'Donnell JTD, Matzavinos A, Stein D (2017) Giant acceleration of DNA diffusion in an array of entropic barriers. *Phys Rev Lett* 118:048002. Published 27 January 2017
592. Kira M, Hoyer W, Stroucken T, Koch S (2001) Exciton Formation in Semiconductors and the Influence of a Photonic Environment. *Phys Rev Lett* 87(17):176401. <https://doi.org/10.1103/PhysRevLett.87.176401>
593. Kozlowska JM (2015) Consciousness and biological dark matter. https://www.researchgate.net/publication/309668098_Consciousness_and_Biological_Dark_Matter
594. Kriegl JM, Niehaus GU (2004) Structural, dynamic, and energetic aspects of long-range electron transfer in photosynthetic reaction centers. *Proc Nat Acad Sci USA* 1:12312–12318
595. Lambert J-F (2015) Origin of life: From the mineral to the biochemical world. *Web Conf* 4:00012
596. Lamoreaux GK (2007) Casimir forces: still surprising after 60 years. *Physics Today*, pp 40–45
597. Lanczos C (1970) The variational principles of mechanics. Dover Publ., Inc., New York
598. Landau LD, Lifshitz EM (1987) Fluid mechanics. Pergamon Press, Oxford
599. Lehar S (2003) Harmonic resonance theory: an alternative to the “neuron doctrine” paradigm of neurocomputation to address gestalt properties of perception. *Perception*. 32:423–448. <http://cns-alumni.bu.edu/~slehar/webstuff/hr1/hr1.html>
600. Leroy CC, Robinson SP, Goldsmith MJ (2008) A new equation for the accurate calculation of sound speed in all oceans. *J Acoust Soc Am* 124(5):2774–2782

601. Levin M (2016) Reading and writing the morphogenetic code. Foundational White Paper of the Allen Discovery Center at Tufts University
602. Liboff AR (1985) Geomagnetic cyclotron resonance in living cells. *J Biol Phys* 13
603. Linton O (2015) Consciousness as a meta-phenomenon. <http://quantum-mind.co.uk/consciousness-as-a-meta-phenomenon/>
604. Lodish H, Berk A, Zipursky SL, Matsudaira P, Baltimore D, Darnell J (2000) Molecular cell biology, Sect. 16.2 electron transport and oxidative phosphorylation, , 4th edn. W. H. Freeman, New York
605. Lou SY et al (2013) Interactions between solitons and other non-linear Schrödinger waves. [arXiv:1208.5314v2](https://arxiv.org/abs/1208.5314v2) [nlin.SI]
606. Manousakis E (2006) Founding quantum theory on the basis of consciousness. *Found Phys* 36. 13 Apr 2006. [arXiv:quant-ph/0604100v1](https://arxiv.org/abs/quant-ph/0604100v1)
607. Mavromatos NE, Mershin A, Nanopoulos DV (2002) QED-cavity model of microtubules implies dissipationless energy transfer and biological quantum teleportation. *Int J Mod Phys B* 16:3623
608. Mc Naughton BL, Battaglia FP, Jensen O, Moser EI, Moser MB (2006) Path integration and the neural basis. *Neuroscience* 7(8):663–678
609. Merker B (2007) Consciousness without a cerebral cortex: a challenge for neuroscience and medicine. *Behav Brain Sci* 30(1):63–81. discussion 81–134. <https://www.ncbi.nlm.nih.gov/pmc/articles/PMC1747503>
610. Moreva E, Brida G, Gramegna M, Giovannetti V, Maccone L, Genovese M (2013) Time from quantum entanglement: an experimental illustration
611. Minds NT, Cosmos (2012) Why the materialist neo-darwinian conception of nature is almost certainly false. Oxford University Press, New York
612. Neal L (2018) Integral relativity of awareness and energy—the continuum of consciousness, energy, mind and matter. *NeuroQuantology* 16:48–68
613. Ozil JP, Markoulaki S, Toth S, Matson S, Banreza B, Knott JG, Schultz RM, Huneau D, Ducibella T (2005) Egg activation events are regulated by the duration of a sustained [Ca²⁺]cyt signal in the mouse. *Dev Biol* 282:39–54
614. Ozols M (2007) Geometry of a Qubit. ID 20286921. [http://home.lu.lv/~sd20008/papers/essays/Geometry%20\[paper\].pdf](http://home.lu.lv/~sd20008/papers/essays/Geometry%20[paper].pdf)
615. Pan JZ, Xi J, Eckenhoff MF (2008) Inhaled anesthetics elicit region-specific-changes in protein expression in mammalian brain. *Proteomics* 8(14). <https://doi.org/10.1002/pmic.200800057>
616. Pekar S (1963) Research in electron theory of crystals. Tech Rep AEC-tr-5575. United States Atomic Energy Commission, Washington, DC
617. Pereira Jr. A, Jonathan CW, Lehmann DE, Nunn C, Trehub A, Max Velmans, Understanding consciousness a collaborative attempt to elucidate contemporary theories. <https://pdfs.semanticscholar.org/83c5/3ff7dbb3d7c668af7a30b841113b29b2ff22.pdf>
618. Perlovski L (2010) Musical emotions: functions, origins evolution. *Phys Life Rev* 7:2–27
619. Persinger MA, Lavallee CF (2010) Theoretical and experimental evidence of macroscopic entanglement between human brain activity and photon emissions: implications for quantum consciousness and future applications. *J Cons Explor Res* 1:785–807
620. Persinger MA (2014) Relating casimir to magnetic energies results in spatial dimensions that define biology systems. *Int Lett Chem Phys Astron* 39:160–165
621. Pitkänen M (2017) What music could teach you about consciousness. https://pdfs.semanticscholar.org/a519/9ca490fb0244b0a0163e601710b3d135a0b7.pdf?_ga=2.56050478.424886245.1592225
622. Pnevmatikos SN, Tsironis G (1989) Protonic conductivity: a new application of solute theory. *J de Phys HAL* Id: jpa-oo229440
623. Pockett S (2013) Field theories of consciousness. *Scholarpedia* 8:4951
624. Pollack GH (2001) Cells, gels and the engines of life. Ebner and Sons Publ., Seattle
625. Rajna G (2018) The magnetic field of the electric current and the magnetic induction. http://academia.edu/3833335/The_Magnetic_field_of_the_Electric_current

626. Reddy JSK, Pereira C (2016) On science & the perception of reality. *J Conscious Explor Res* 7:333–336
627. Reimers JR, McKemmish LK, McKenzie RH, Mark AE, Hush NS (2014) *Phys Life Rev* 11:101
628. Roy A (2005) Discovery of parity violation. *Resonance* 10(12):164–175. <https://doi.org/10.1007/bf02835140>
629. Rovelli C, Smolin L (1990) Loop space representation of quantum general relativity. *Nucl Phys B* 331:80–152
630. Savelyev I, Myakishev-Rempel M (2005) Evidence for DNA resonance signaling via longitudinal hydrogen bonds. <https://vixra.org/pdf/2005.0157v1.pdf>
631. Sbitnev VI (2009) Bohmian trajectories and the path integral paradigm: complexified lagrangian mechanics. *Int J Bifurcation Chaos* 19:2335. <https://doi.org/10.1142/S0218127409024104>
632. Sbitnev VI (1996) Matter waves in the Talbot-Lau interferometry (2010). <http://arxiv.org/abs/1005.0890>
633. Sciré A (2020) A mesoscopic model for the collective dynamics of water coherence domains. [arXiv:2004.07545](https://arxiv.org/abs/2004.07545)
634. Sengupta B, Laughlin SB, Niven JE (2013) Balanced excitatory and inhibitory synaptic currents promote efficient coding and metabolic efficiency. *PLoS Comput Biol.* [PMC free article] [PubMed]
635. Sheehan D (2011) Frontiers of time: quantum retro-causation, theory and experiments. *AIP Conf Proc* 1408:255–278. <https://www.amazon.com/Frontiers-Time-Retrocausation-Experiment>
636. Shea N, Boldt A, Bang D, Yeung N, Heyes C, Frith CD (2014) Supra-personal cognitive control and metacognition. *Trend Cognit Sci* 18(4):186–193. <https://doi.org/10.1016/j.tics.2014.01.006>
637. Shoup R (2011). Understanding retrocausality. Can a message be send to the past?; https://www.researchgate.net/publication/234885500_Understanding_Retrocausality_Can_a_Message_Be_Sent_to_the_Past
638. Sporns J (2013) Network attributes to segregation and integration in the human brain. *Curr Opin Neurobiol* 23:162–171
639. Stretsov A, Singh U, Dhar HS, Bura MN, Adesso G (2015) Measuring quantum coherence with entanglement
640. Sunhammer J, Sulyok G, Bernroider G (2018) Quantum dynamics and non-local effects behind ion transition states during permeation in membrane channel proteins. *Entropy* 20:558
642. Tang M et al (2015) Terahertz spectroscopy of oligonucleotides in aqueous solution. *J Biomed Opt* 20:0950091–0950095
643. Tenen S (2002) The shape of information. *Noetic J* 3:173–182. <http://www.meru.org/Noetic/ShapeofInfoA3HiTOC.pdf>
644. Tielrooy KJ (2010) Molecular motions of water: th effect of charged and hydrophobic solutes. Chapter 7: Structure and dynamics of the hydrated proton, pp 87–96
645. Tiller WA (1999) Towards a predictive model of subtle domain connections in the physical domain of reality. *J Sci Explor* 13:41–67
646. Torday S, Miller WB (2017) A systems approach to physiologic evolution: from micelles to consciousness: systems evolutionary physiology. https://www.researchgate.net/publication/312644789_A_Systems_Approach_to_Physiologic_Evolution_From_Micelles_to_Consciousness_Systems_Evolutionary_Physiology, <https://arxiv.org/ftp/arxiv/papers/1401/1401.6052.pdf>
647. Toyabe S (2015) Supplementary information for information heat engine: converting information to energy by feedback control. [arXiv:1009.5287v2](https://arxiv.org/abs/1009.5287v2) [cond-mat.stat-mech]
648. Van De Bogart WG (2017) Consciousness and electronic music applied to xenolinguistics. Available from. https://www.researchgate.net/publication/317328554_Consciousness_and_Electronic_music_applied_to_xenolinguistics_New_alternatives_in_extraterrestrial_communication_by_orchestrating_the_harmonic_building_blocks_of_the_universe_to_create_space_music

649. Van De Bogart WG (2017) Creating Sonic Topologies using Electronic Music to develop a new. Cosmol Model Conscious. <https://www.researchgate.net/publication/336243136>
650. Vanga, wiki. https://en.wikipedia.org/wiki/Baba_Vanga
651. Van Horik JO, Clayton NS, Emery NJ (2012) Convergent evolution of cognition in corvids, apes and other animals. In: The Oxford handbook of comparative evolutionary psychology, pp 80–101
652. Van Raamsdonk (2010) Building up spacetime with quantum entanglement. Gen Relativ Gravit 42:2323. <https://arxiv.org/pdf/1005.3035.pdf>
654. Vasiliev BV (2013) Superconductivity and superfluidity. <http://arxiv.org/abs/1008.2691>
655. Vasiliev BV (2015) Superconductivity and superfluidity. Science Publ. Group, New York
656. Vitello G (2015) The aesthetic experience as a characteristic feature of brain dynamics. Aisthesis. Pratiche, linguaggi e saperi dell'estetico [S.I.] 8(1):71–89. ISSN 2035-8466
657. Wang Z, Wang N, Li Z, Xiao F, Dal J (2016) Human intelligence is involved in spectral redshift of biophotonic activities in the brain. PNAS 113:8753–8758
658. Webber (2018) Surfism. The fluid foundation of consciousness. www.danwebberblog.wordpress.com
659. Weingarten CP, Doraiswami PM, Fisher MPA (2016) A new spin on neural processing: quantum cognition. Front Hum Neurosci 10. art.541
661. Williamson JG, van der Mark MB (1997) Is the electron a photon with toroidal topology? Annales de la Fondation Louis de Broglie 22(2):133
662. Witten E (2003) Perturbative gauge theory as a string theory in Twistor space. Commun Math Phys 252:189–258. arXiv:hep-th/0312171, Bibcode:2004CMaPh.252..189W, <https://doi.org/10.1007/s00220-004-1187-3>
663. Wolf FA (2006) Why nerve cells work faster than the theories allows. <https://www.mpg.de/535717/pressRelease20060418>
664. Wongjun (2013) Casimir dark energy, stabilization of extra dimensions and Gass-Bonet term
665. Wyatt RE (2005) Quantum dynamics with trajectories: introduction to quantum hydrodynamics. Springer, Berlin
666. Yang Y, Qin Y, Ding Q, Bakhtina M, Wang L, Tsai MD, Zhong D (2014) Ultrafast water dynamics at the interface of the polymerase—DNA binding complex. Biochemistry 53:5405–5416
667. Yepez O (2004) Matter and light in flatland, general physics, (physics.gen-ph). <http://arxiv.org/pdf/physics/0401153.pdf>
668. Yoo H, Paranjri R, Pollack GH (2011) Impact of hydrophilic surfaces on interfacial water dynamics probed with NMR spectroscopy. J Phys Chem Lett 2:532
669. Yu CH, Qin Z, Martin-Martinez FJ, Buehler MJ (2019) A self-consistent sonification method to translate amino acid sequences into musical compositions and application in protein design using artificial intelligence. ACS Nano 13(7):7471–7482. 2019 Jul 23, <https://doi.org/10.1021/acsnano.9b02180>. Epub Jun 26
670. Zhao C, Deng W, Gage FH (2008) Mechanisms and functional implications of adult neurogenesis. Cell. 132(4):645–60. <https://doi.org/10.1016/j.cell.2008.01.033>
671. Zhang L, Yang Y, Kao YT, Wang L, Zhong D (2009) Protein hydration dynamics and molecular mechanism of coupled water—protein fluctuations. J Am Chem Soc 131:10677–10691